

BULGARIAN CHEMICAL COMMUNICATIONS

2017 Volume 49 / Special Issue G

Proceedings of 10th Chemistry Conference are dedicated to the 55 Years of Education in Chemistry at the University of Plovdiv and 25th Anniversary of the Faculty of Chemistry Plovdiv, 9-11 October, 2016

*Journal of the Chemical Institutes
of the Bulgarian Academy of Sciences
and of the Union of Chemists in Bulgaria*

Preface

Dear reader,

This special issue of the 'Bulgarian Chemical Communications' contains most of the studies, presented during the 10th Chemistry Conference (10CC) that was held on 9-11 October 2016, in Plovdiv, Bulgaria. The conference was organized by the Faculty of Chemistry at the Plovdiv University "Paisii Hilendarski". The program included plenary lectures of two of the Doctor Honoris Causa of the University of Plovdiv - Prof. Dr. Antonio Canals from the University of Alicante, Spain and Corresponding member of the Bulgarian Academy of Science Prof. DSc Dimitar Tzalev, from the Sofia University "St. Kliment Ohridski". Plenary lectures had also invited speakers from the University of Oxford, UK - Prof. Mark Moloney, from the Technical University, Vienna, Austria - Prof. Erwin Rosenberg, from the University of Alicante, Spain - Prof. Francisco Alonso, from the IAEA Environment Laboratories – Dr. Emilia Vassileva and from Sofia University "St. Kliment Ohridski" Prof. Vasil Simeonov. The presentations of the invited keynote speakers in different research fields along with the participation of prominent Bulgarian scientists working together with colleagues from leading International Institutes was highly appreciated by all present.

The conference was attended by 167 participants from 6 countries – Bulgaria, Turkey, Spain, UK, Austria, and Monaco. There were presented 26 oral presentations in three different sections: Section I – Analytical chemistry, Theoretical chemistry and Physical chemistry (9); Section II – Organic chemistry and Food chemistry (8); Section III - Inorganic chemistry, New methods and materials, Chemistry and education (9). There were 87 poster presentations also. The significant attendance of more than 50 young scientists, researchers and PhD students indisputably added to the one of the most important conference mission. The continuous communication during the session days, also, provided valuable opportunities to the attendees to share knowledge and exchange experience and confer on the latest developments in the field of chemistry research and technologies in the corresponding areas of interest.

The Organizing Committee of the conference thanks this journal for the help in publishing the full text articles and for the chance given to the conference's participants to meet the wide audience.

Chair of the Organizing committee
Assoc. Prof. G. Antova

Guest Editor
Prof. I. Ivanov

Determination of heavy metals in mushroom samples by atomic absorption spectrometry

L. Dospatliev^{1*} and M. Ivanova²

¹*Department of Pharmacology, Animal Physiology and Physiological Chemistry, Trakia University, Stara Zagora 6000, Bulgaria*

²*Department of Informatics and Mathematics, Trakia University, Stara Zagora 6000, Bulgaria*

Received October 27, 2016; Revised December 2, 2016

The concentrations of heavy metals in the mushroom samples collected from the Batak mountain, Bulgaria have been determined by flame and graphite furnace atomic absorption spectrometry after dry ashing, wet ashing and microwave digestion. The study of sample preparation procedures showed that the microwave digestion method was the best. Good accuracy was assured by the analysis of standard reference materials. In all cases, quantitative analytical recoveries ranging from 92 to 104% were obtained. Results obtained are in agreement with data reported in the literature.

Keywords: Atomic absorption spectrometry, Digestion, Heavy metals, Mushroom

INTRODUCTION

Edible mushrooms are homely food for people in eastern and central Europe, while in western and northern European countries wild edible fungi are less popular [1-3]. Many studies have confirmed the high and balanced nutritional value of mushrooms [4-10], since they are rich sources of digestible proteins, vitamins B, D and K and in some cases vitamins A and C [11-15]. Carpophores are a good source of minerals, particularly K, P, Ca, Mg and Na [16-23]. Mushrooms are considered not only as spice and taste ingredients, but also as a nutritional supplement in the human diet and can also play a role as functional foods [24-29]. It is worth stressing here that many studies have focused on the medicinal properties of mushrooms [30-34]. They have also been reported to show anti-inflammatory, antibacterial, antiviral and antioxidant potential [35-36].

Mushroom has been used as a bioindicator by various researchers to determine the heavy metal pollutions [37-40]. Compared to green plants, mushroom can build up large concentrations of some heavy metals such as Pb, Cd, Hg, and a great effort has been made to evaluate the possible danger to human health from the ingestion of mushrooms [41-43].

Decomposition of solid samples is an important step in combined analytical methods. In most cases, when using highly sensitive measuring methods, such as flame atomic absorption spectrometry (FAAS), graphite furnace AAS, ICP-OES, ICP-MS, the sample is measured in an aqueous solution [44-

46]. Combined analytical methods are favoured for multi element analysis of environmental and biological samples at very high speed. Sequential and simultaneous determinations of the elements can be made using the above analytical techniques [47-50].

In this study, the levels of heavy metals in wild edible mushrooms (*Lactarius deliciosus*) from the Batak mountain, Bulgaria were determined by flame and graphite furnace AAS after various digestion methods.

EXPERIMENTAL

Sampling

One hundred and fifty mushroom samples were collected in 2014 and 2015 from the Batak mountain by the authors themselves.

Mushroom samples were washed with distilled water and dried at 105°C for 24 h. The dried samples were ground, then homogenized using an agate pestle and stored in polyethylene bottles until analysis.

Reagents

All reagents were of analytical reagent grade unless otherwise stated. Double deionized water (Milli-Q Millipore 18.2 MΩ cm resistivity) was used for all dilutions. HNO₃, H₂SO₄, H₂O₂, HF, HClO₄ and HCl were of suprapur quality (E. Merck). All the plastic and glassware was cleaned by soaking in dilute HNO₃ (1+9) and rinsed with distilled water prior to use. The element standard solutions used for calibration were prepared by diluting a stock solution of 1000 mg l⁻¹ (Pb, Cd, Co, Cr,

* To whom all correspondence should be sent.
E-mail: lkd@abv.bg

Table 2. Operating conditions for mushroom samples in microwave digestion system

Steps	Time (min)	Power (W)
1	2	250
2	2	0
3	6	250
4	5	400
5	8	550

Vent: 8 min

Analytical procedure

Detection limit is defined as the concentration corresponding to three times the standard deviation of ten blanks. Detection limit values of elements as microgram per liter in flame AAS were found to be 0.025 for Cd, 0.127 for Co, 0.083 for Cr, 0.072 for Cu, 0.111 for Fe, 0.058 for Mn, 0.145 for Ni, 0.450 for Pb and 0.021 for Zn. The concentrations of Cu, Zn and Fe were determined in the plant samples using FAAS. The other elements (Cd, Pb, Co, Cr, Mn and Ni) were below the corresponding detection limits of FAAS. These elements in plant samples were determined using graphite furnace AAS by autosampler. During analyses, internal argon flow rate through the graphite tube was 250 ml min⁻¹; gas flow was interrupted during atomization. Sample volume, ramp and hold times for the drying, ashing, atomization and cleaning temperatures were optimized before analysis to obtain maximum absorbance and minimum background. Matrix modifiers were added 0.050 mg NH₄H₂PO₄ + 0.003 mg Mg(NO₃)₂ for Pb, 0.050 mg NH₄H₂PO₄ + 0.003 mg Mg(NO₃)₂ for Cd, 0.015 mg Mg(NO₃)₂ for Co, 0.005 mg Pd + 0.003 mg Mg(NO₃)₂ for Mn, 0.015 mg Mg(NO₃)₂ for Ni and 0.015 mg Mg(NO₃)₂ for Cr. Most of the matrix was removed before the atomization step and less interference occurred during atomization.

Each graphite furnace AAS analysis calls for 20 µl of solution and 5–10 µl of the matrix modifier. As Table 1 shows, matrix modifier was used for all 6 elements determined by GFAAS. Characteristic mass for 0.0044 absorbance was found to be 1.3 pg for Cd, 17.0 pg for Co, 7.0 pg for Cr, 20.0 pg for Ni, 6.3 pg for Mn and 30 pg for Pb.

Statistical processing

SPSS (Statistical Package for Social Science) program for Windows was used for statistical data processing.

RESULTS AND DISCUSSION

It is desirable to use a higher ashing temperature in graphite furnace in order to remove the matrix efficiently for many analytes in food, biological and environmental samples. The ashing and atomization temperatures of heavy metals were increased using different chemical modifiers.

SPSS was used in this study. The comparison of dry, wet and microwave digestion methods showed no statistically significant differences in results. Therefore, the microwave digestion procedure was preferred because this procedure is more proper with respect to both time and recovery than dry and wet digestion. The disadvantage of the method consists in its expensiveness and need of some experience.

The standard deviations of the dry and wet digestion methods are higher than those of the microwave digestion method. The accuracy of the method was evaluated by means of heavy metals determination in CRM. The achieved results were in good agreement with certified values. The results from the analysis of CRM were all within the 95% confidence limit.

Table 3. Observed and certified values (µg g⁻¹) of element concentrations in the CRM (CTA-VTL-2) as average ± S.D.

Element	Certified value	Observed value					
		Dry ashing	Recovery (%)	Wet ashing	Recovery (%)	Microwave digestion	Recovery (%)
Pb	22.1 ± 1.2	22.5 ± 1.1	101.8	21.0 ± 1.3	95	23.0 ± 0.8	104
Cd	1.52 ± 0.17	1.44 ± 0.08	94.7	1.45 ± 0.09	95.4	1.50 ± 0.05	98.7
Ni	1.98 ± 0.21	1.89 ± 0.1	95	1.91 ± 0.06	96	1.94 ± 0.02	98
Cr	1.87 ± 0.16	1.87 ± 0.22	100	1.78 ± 0.13	95	1.91 ± 0.11	102
Mn	79.7 ± 2.6	76.4 ± 2.1	95.9	75.1 ± 2.0	94.2	77.5 ± 1.2	97.2
Co	0.429 ± 0.026	0.408 ± 0.009	95	0.408 ± 0.02	95	0.433 ± 0.006	101
Cu	18.2 ± 0.9	17.6 ± 0.8	96.7	18.9 ± 0.9	104	18.1 ± 0.7	99.4
Zn	43.3 ± 2.1	42.3 ± 3.0	97.7	43.9 ± 2.6	101.4	44.1 ± 1.6	101.8
Fe	1083 ± 33	1050 ± 48	96.9	996.36 ± 49	92	1160 ± 44	103

Table 4. Concentration of heavy metals in mushroom samples (*Lactarius deliciosus*) collected from Batak mountain, Bulgaria (n = 15)

	Pb	Cd	Ni	Cr	Mn	Co	Cu	Zn	Fe
\bar{X} mg kg ⁻¹	0.81	0.33	0.16	0.08	0.88	0.10	6.41	61.32	88.52
SD mg kg ⁻¹	0.11	0.08	0.05	0.01	0.83	0.01	1.64	6.07	10.64
Min	0.63	0.21	0.08	0.06	0.18	0.08	4.11	51.72	74.56
Max	0.94	0.42	0.22	0.11	2.76	0.12	8.93	69.26	105.13
95% Confid. Level	0.06	0.04	0.03	0.01	0.46	0.01	0.91	3.36	5.89

According to this study, the edible wild mushroom *Lactarius deliciosus* could be used in human nutrition due to its good parameters. Heavy metal content of samples indicated that the Batak mountain was an ecologically pure region of Bulgaria, and therefore the mushrooms collected from this location could be consumed without any risk for human health.

CONCLUSIONS

The dry and wet digestion methods are more time-consuming and complicated than microwave digestion method without any advantage in terms of digestion efficiency. The use of microwave digestion system in mushroom samples provides a better, safer and cleaner method of sample preparation. The accuracy of the method was checked and confirmed by CRM.

From the obtained concentrations of heavy metals one can say that the locality Batak mountain is ecologically clean area and very suitable for collecting wild edible mushrooms that we can use in our daily menu.

REFERENCES

- I. Druzhinina, J.M. Palma-Oliveira, *J. Environ. Radioactiv.*, **74**, 83 (2004).
- J. Árvay, J. Tomáš, M. Hauptvogel, M. Kopernická, A. Kováčik, D. Bajčan, P. Massányi, *J. Environ. Sci. Health. B*, **49**, 815 (2014).
- M. Drewnowska, J. Falandysz, *Ecotox. Environ. Safe.*, **113**, 9 (2015).
- E. Dadáková, T. Pelikanova, P. Kalač, *Eur. Food Res. Technol.*, **230**, 163 (2009).
- A. Cayır, M. Coskun, M. Coskun, *Biol. Trace Elem. Res.*, **134**, 212 (2010).
- F.A. Ayaz, H. Torun, A. Colak, E. Sesli, M. Millson, R.H. Glew, *Food. Nutr. Sci.*, **2**, 53 (2011).
- A. Chojnacka, G. Jarzyńska, M. Lewandowska, I.C. Nnorom, J. Falandysz, *Fresen. Environ. Bull.*, **22**, 2707 (2013).
- K. Chudzyński, G. Jarzyńska, J. Falandysz, *Food Addit. Contam. B*, **6**, 249 (2013).
- R. Ashrafi, M. Rahman, M. Jahiruddin, M. Mian, *Progressive Agriculture*, **25**, 1 (2014).
- M. Mleczek, P. Niedzielski, P. Kalač, A. Budka, M. Siwulski, M. Gąsecka, P. Rzymiski, Z. Magdziak, K. Sobieralski, *Environ Sci Pollut Res.*, in press.
- R. Sanmee, B. Dell, P. Lumyong, K. Izumori, S. Lumyong, *Food Chem.*, **82**, 527 (2003).
- N. Durkan, I. Ugulu, M.C. Unver, Y. Dogan, S. Baslar, *Trace Elem. Electroly.*, **28**, 242 (2011).
- J. Falandysz, J. Borovička, *Appl. Microbiol. Biotechnol.*, **97**, 477 (2013).
- M. Ali Karimi, S. Zia Mohammadi, A. Hatefi-Mehrjardi, A. Mohadesi, J. Yarahmadi, *JAST*, **6**, 25 (2015).
- A. Zosel, M. Stanton, *J. Clin. Toxicol.*, **6**, 1 (2016).
- P. Mattila, K. Könkö, M. Euroala, J.M. Pihlava, J. Astola, L. Vahteristo, V. Hieraniemi, J. Kumpulainen, M. Valtonen, V. Piironen, *J. Agr. Food Chem.*, **49**, 2343 (2001).
- L.M. Cheung, P. C.K. Cheung, V. E.C. Ooi, *Food Chem.*, **81**, 249 (2003).
- A. Kaya, H. Bag, *Asian J. Chem.*, **22**, 1515 (2010).
- P. Kalač, *Food Chem.*, **122**, 2 (2010).
- E. Guillamón, A. Garcia Lafuente, M. Lozano, M. D'Arrigo, M.A. Rostagno, A. Villares, J.A. Martínez, *Fitoterapia*, **81**, 715 (2010).
- A.K. Kojta, G. Jarzyńska, J. Falandysz, *J. Geochem. Explor.*, **121**, 76 (2012).
- Q. Huang, Y. Jia, Y. Wan, H. Li, R. Jiang, *J. Food. Sci.*, **80**, 1612 (2015).
- A. Zosel, M. Stanton, *J. Clin. Toxicol.*, **6**, 1 (2016).
- P.C. Cheung, *Mushrooms as functional foods*. A John Wiley, Hoboken, New Jersey, 2008.
- M. Gućia, G. Jarzyńska, A.K. Kojta, J. Falandysz, *J. Environ. Sci. Health. B*, **47**, 81 (2012).
- G. Gramss, K-D. Voigt, *Biol. Trace. Elem. Res.*, **154**, 140 (2013).
- P. Niedzielski, M. Mleczek, Z. Magdziak, M. Siwulski, L. Kozak, *Food Chem.*, **141**, 3571 (2013).
- D. Qin, H. Jiang, S. Bai, S. Tang, Z. Mou, *Food Control*, **50**, 1 (2015).
- M. Kosanic, B. Rankovic, A. Rancic, T. Stanojkovic, *JFDA*, **24**, 477 (2016).
- M.S. Mantovani, M.F. Bellini, J.P.F. Angeli, R.J. Oliveira, A.F. Silva, L.R. Ribeiro, *Mutat. Res.*, **658**, 154 (2008).
- S.P. Wasser, *Appl. Microbiol. Biot.*, **89**, 1323 (2011).
- K. Biswas, D. Paul, S. N. Sinha, *FEM*, **1**, 39 (2015).

33. K.M. Mohiuddin, M. Mehediul Alam, M. Taufique Arefin, I. Ahmed, *Asian J. Med. Biol. Res.*, **1**, 495 (2015).
34. M. Mleczek, P. Niedzielski, P. Kalač, M. Siwulski, P. Rzymiski, M. Gąsecka, *Food Addit. Contam. A*, **33**, 86 (2016).
35. L. Robles-Hernandez, A. Cecilia-Gonzalez-Franco, J.M. Sota-Parra, F. Montes-Dominguez, *Tecnociencia Chihuahua*, **2**, 95 (2008).
36. Y. Liu, D. Chen, Y. You, S. Zeng, Y. Li, Q. Tang, G. Han, A. Liu, C. Feng, C. Li, Y. Su, Z. Su, D. Chen, *Food Chem.*, **211**, 83 (2016).
37. M. Tüzen, M. Ozdemir, A. Demirbas, *Food Chem.*, **63**, 247 (1998).
38. E. Sesli, M. Tüzen, *Food Chem.*, **65**, 453 (1999).
39. L.M. Cheung, P. Cheung, V. Ooi, *Food Chem.*, **81**, 249 (2003).
40. S.P. Therkelsen, G. Hetland, T. Lyberg, I. Lygren, E. Johnson, *Plos One*, **11**, 1 (2016).
41. M.A. Garcia, J. Alonso, M.I. Fernandez, M.J. Melgar, *Arch. Environ. Contam. Toxicol.*, **34**, 330 (1998).
42. M.S. Khan, M.T. Shah, I. Ud-din, A. Ahmed, *Pak. J. Bot.*, **47**, 133 (2015).
43. M. Nadhim Owaid, S. S. S. Al-Saeedi, I. Ali Abed, *GIDA*, **40**, 319 (2015).
44. C.H. Gast, E. Jansen, J. Bierling, L. Haanstra, *Chemosphere*, **17**, 789 (1988).
45. M. Tüzen, *Food Chem.*, **80**, 119 (2003).
46. M. Mleczek, M. Siwulski, P. Mikołajczak, M. Gąsecka, I. Rissmann, P. Goliński, K. Sobieralski, *J. Environ. Sci. Health B*, **50**, 659 (2015).
47. G. Knapp, *Microchim. Acta*, **2**, 445 (1991).
48. M. Tüzen, M. Ozdemir, A. Demirbas, *Z. Lebensm. Unters. Forsch. A*, **206**, 417 (1998).
49. M. Gucia, G. Jarzyńska, E. Rafał, M. Roszak, A.K. Kojta, I. Osiej, J. Falandysz, *Environ. Sci. Pollut. Res.*, **19**, 416 (2012).
50. C. Sarikurkcü, B. Tepe, M.S. Kocak, M.C. Uren, *Food Chem.*, **175**, 549 (2015).

ОПРЕДЕЛЯНЕ КОЛИЧЕСТВОТО НА ТЕЖКИ МЕТАЛИ В ПРОБИ ОТ ГЪБИ ЧРЕЗ АТОМНА АБСОРБЦИОННА СПЕКТРОСКОПИЯ

Л. Доспатлиев¹, М. Иванова²

¹Катедра “Фармакология, физиология на животните и физиологична химия”, Ветеринарно-медицински факултет, Тракийски университет, Стара Загора

²Катедра “Информатика и математика”, Стопански факултет, Тракийски университет, Стара Загора

Постъпила на 27 октомври 2016 г.; приета на 2 декември 2016 г.

(Резюме)

Концентрациите на тежки метали в проби от гъби, събрани от Баташката планина в България са определени чрез атомноабсорбционна спектрометрия в пламък и графитна пещ след сухо опепеляване, киселинна минерализация и микровълнова минерализация. Проучването на процедурите за подготовка на проби показва, че методът на микровълновата минерализация е най-добрият. Добрата точност е доказана чрез анализ на сертифициран референтен материал. Във всички случаи на пробоподготовка се получават количествени извличания на елементите вариращи от 92 до 104 процента от сертифицираната стойност. Получените резултати са в съгласие с данните, докладвани в литературата.

Ключови думи: Атомна абсорбционна спектроскопия, разтваряне, тежки метали, гъби

Determination of Cd, Cr, Cu, Ni, Pb and Zn in compost: evaluation of different approaches for sample preparation and instrumental analysis (MP-AES as an alternative to ICP-OES)

V. Y. Zapryanova^{1,2*}, K. K. Simitchiev¹ and E. N. Piskova²,

¹Department of Analytical Chemistry and Computer Chemistry, University of Plovdiv "Paisii Hilendarski",
24 Tzar Assen Str., 4000 Plovdiv, Bulgaria

²Laboratory for Testing of Solid Biofuels and Compost, Energy Agency of Plovdiv, 139 Ruski Blvd, office 403,
4000 Plovdiv, Bulgaria

Received November 12, 2016; Revised December 19, 2016

In the Bulgarian legislation are stated maximum acceptable concentrations for several elements (Cd, Cr, Cu, Ni, Pb and Zn) in treated biowaste such as compost. The prescribed limits correspond to the soluble fraction of the elements extracted with nitric acid or aqua regia using procedures described in EN 16173:2012 and EN 16174:2012, respectively. In the current work it was compared the elemental transfer into solution when the two eligible reagents (nitric acid or aqua regia) were used. The acid extractions were carried out under microwave irradiation in closed vessels. The soluble fractions of the elements were measured by two alternative instrumental techniques i.e. inductively coupled plasma optical emission spectrometry (ICP-OES) and microwave plasma atomic emission spectroscopy (MP-AES). The results show that MP-AES is an adequate alternative to ICP-OES which fits the analytical purpose to monitor Cd, Cr, Cu, Ni, Pb and Zn in compost. Several samples from different manufacturers were studied and it was found that the extraction of Cd, Cr, Pb and Zn was not influenced by the applied acid treatment. On the opposite, the extraction of Cr and Ni was significantly higher when aqua regia was used in comparison to the solely application of nitric acid.

Key words: elemental analysis of compost; microwave-assisted acid extraction of elements; inductively coupled plasma optical emission spectrometry (ICP-OES), microwave plasma atomic emission spectroscopy (MP-AES).

INTRODUCTION

The intensive farming and the inadequate land management leads to a reduction of the needed for agriculture organic substances in soils [1]. Possible solution of the latter problem can be found in the application of compost as a source of organic matter. Various types of compost have been obtained from resources, such as municipal solid waste, green waste, food processing waste, animal manures, sewage sludge [2, 3].

Since the compost is a product from reutilized materials it can be a source of pollutants, in particular heavy metals, which will be deposited by its use in the environment. The contamination with toxic elements is a hazard to the human health and the animal populations because these pollutants can be taken up directly by humans and animals through inhalation of dusty soil or they may enter the food chain as a consequence of absorption by plants or infiltration to the groundwater and contamination of the drinking waters [4]. For this reason, monitoring of the toxic chemical elements in agricultural soils and soil improvers, such as compost, is needed. In Bulgaria the quality requirements for compost are

prescribed in a regulatory document called "Ordinance on treatment of biowaste" [5]. In the latter document are stated maximum acceptable levels for the soluble fractions of Cd, Cr, Cu, Ni, Pb and Zn extracted from compost with nitric acid or aqua regia following procedures described in EN 16173 [6] and EN 16174 [7], respectively. No preference is given to any of the suggested sample preparation approaches. Hence the aim of the current work was to assess if there is any significant difference in the soluble fractions of the listed elements extracted with each eligible reagent – nitric acid or aqua regia.

Inductively coupled plasma optical emission spectrometry (ICP-OES) is one of the recommended instrumental techniques for elemental detection in treated biowaste [8]. A relatively new instrumental technique which can be used for multi-elemental analysis with lower operational costs than ICP-OES is microwave plasma atomic emission spectroscopy (MP-AES) [9]. To the best of our knowledge MP-AES was not previously used for determination of Cd, Cr, Cu, Ni, Pb and Zn in compost samples and this motivated us to test the applicability of this technique for the intended purpose.

* To whom all correspondence should be sent.

E-mail: vzapryanova@uni-plovdiv.net

EXPERIMENTAL

The reagents used for extraction of soluble fractions of elements from compost were hydrochloric acid ($\text{HCl} \geq 37\%$, Fluka, grade p.a.) and nitric acid ($\text{HNO}_3 \geq 65\%$, Fluka, grade p.a.). Ultrapure water with $2 \mu\text{S cm}^{-1}$ electroconductivity (Ultrapure Water System Adjarov Technology Ltd.) was used throughout this work for preparation of solutions and rinsing the vessels. Standard solutions were prepared from a multi-element standard solution (ICP Multi-element Standard Solution IV 1000 mg L^{-1} - Ag, Al, B, Ba, Bi, Ca, Cd, Co, Cr, Cu, Fe, Ga, In, K, Li, Mg, Mn, Na, Ni, Pb, Sr, Tl, Zn, Merck KGaA) by dilution with acidified ultrapure water (5% w/w HNO_3).

The analysed compost samples were produced by three different manufacturers reutilizing green waste from Bulgaria. Samples were dried in an oven at 40°C for 16 hours, after that they were quartered to provide about 200 g sub-sample which was homogenized with grinder for 2 minutes.

Acid extractions were accomplished according to EN 16173 (reagent - nitric acid) [6] and EN 16174 (reagent - aqua regia) [7]. Sample with mass 0.5 g was weighed into microwave vessels and 10 mL nitric acid or 8 mL aqua regia (6 mL hydrochloric acid and 2 mL nitric acid) were added. The following microwave program for heating was used: 20 min ramp to $175 \pm 5^\circ\text{C}$, hold on $175 \pm 5^\circ\text{C}$ for 10 min. After cooling to room temperature the digests were filtered through filter paper and diluted with ultrapure water to 50 g. Blank samples were proceeded for each extraction procedure.

A Microwave Digestion System (MARS 6, CEM Corporation) with closed vessels was used to perform the microwave-assisted extraction.

Inductively coupled plasma optical emission spectrometer ICP-OES Agilent 720 and microwave plasma atomic emission spectrometer MP-AES Agilent 4200 were used for elemental detection with operating parameters indicated on Table 1.

RESULTS AND DISCUSSION

Compost samples from three different Bulgarian manufacturers (represented in the text as *Manufacturer 1*, *Manufacturer 2* and *Manufacturer 3*) were studied in the current work. Samples with diverse origin were included in the research aiming to subject to analysis varying compost matrices with different analyte concentrations.

Inductively coupled plasma optical emission spectrometry (ICP-OES) is a well-established instrumental method for elemental analysis of sludge, treated biowaste and soils [8]. For the

reason it was used as a primary technique for detection of Cd, Cr, Cu, Ni, Pb and Zn in compost. A second instrumental method for analysis which applicability for the intended purpose has been checked was the microwave plasma atomic emission spectroscopy (MP-AES). Both element specific detection techniques were tested in view of the arising spectral and non-spectral interferences when sample solutions after microwave-assisted digestion with nitric acid or aqua regia were analysed.

When an instrumental technique based on emission spectrometry is used for elemental analysis several issues should be considered for selection of analyte lines which will be measured. In the current study the set criteria for spectra registration in priority order (for both ICP-OES and MP-AES) were as follows: i) analyte lines free from spectral interferences, ii) low background noise and iii) high sensitivity of the measured lines. The studied emission lines (nm) in compost matrices for ICP-OES were Cd II 214.439, Cd II 226.502, Cd I 228.802, Cr II 267.716, Cr II 283.563, Cr I 357.868, Cu II 224.700, Cu I 324.754, Cu I 327.395, Ni II 221.648, Ni II 230.299, Ni II 231.604, Ni I 341.476, Pb II 220.353, Pb I 283.305, Zn II 202.548, Zn II 206.200 and Zn I 213.857. The respective ones for MP-AES were Cd II 214.439, Cd II 226.502, Cd I 228.802, Cr I 357.868, Cr I 425.433, Cr I 520.844, Cu I 324.754, Cu I 327.395, Cu I 510.554, Ni I 231.096, Ni I 341.476, Pb I 283.305, Pb I 405.781, Zn II 202.548, Zn II 206.200, Zn I 213.857 and Zn I 481.053. The selected emission lines and the corresponding instrumental conditions for measurements are presented on Table 1.

For all compost samples analysed by ICP-OES, spectral interferences were registered for the lines Cd II 214.439, Cd II 226.502 and Pb I 283.305. When ICP-OES was used for analysis of the compost produced by *Manufacturer 3* spectral interference from Fe I 213.859 over Zn I 213.857 was also found due to the high concentration of iron (*ca.* 0.8%) in this sample. For this reason when MP-AES was used for measurements the most sensitive zinc line (Zn I 213.857) was also not preferred.

In order to compensate for the effect of non-spectral interferences the method of standard addition was used as calibration strategy in any combination between final solution media (nitric acid or aqua regia) and used detection technique (ICP-OES or MP AES).

The obtained methodological detection limits when using ICP-OES and MP-AES are given on Table 2.

Table 1. Operating parameters for ICP-OES and MP-AES

	Agilent 720 ICP-OES	Agilent 4200 MP-AES
Incident power, kW	1	1
Plasma gas, L min ⁻¹	15	20
Auxiliary gas, L min ⁻¹	1.5	1.5
Nebulizer Flow	200 kPa	0.55 - 1.0, L min ⁻¹ ^a
Nebulizer type	OneNeb®	OneNeb®
Sample flow rate, mL min ⁻¹	1.2	0.9
Optics viewing position	axial	axial
Integration time, s	0.05	3
Number of readings	3	3
Selected analyte lines for measurement, nm	Cd I 228.802, Cr II 267.716, Cu I 324.754, Ni I 341.476, Pb II 220.353, Zn II 202.548	Cd I 228.802, Cr I 357.868, Cu I 324.754, Ni I 341.476, Pb I 405.781, Zn I 481.053

^a varying for the different analyte lines (integrated software optimization was applied)

Table 2. Methodological detection limits obtained by ICP-OES and MP-AES for analysis of compost after digestion with different acid mixtures (dilution factor of 100 was applied)

Acid media	ICP-OES		MP-AES	
	Measured line	MLOD mg kg ⁻¹	Measured line	MLOD mg kg ⁻¹
Nitric Acid	Cd I 228.802	0.14	Cd I 228.802	0.30
	Cr II 267.716	0.20	Cr I 357.868	0.46
	Cu I 324.754	0.21	Cu I 324.754	0.21
	Ni I 341.476	0.47	Ni I 341.476	0.67
	Pb II 220.353	1.1	Pb I 405.781	2.0
Aqua Regia	Zn II 202.548	0.27	Zn I 481.053	39
	Cd I 228.802	0.14	Cd I 228.802	0.30
	Cr II 267.716	0.21	Cr I 357.868	0.44
	Cu I 324.754	0.22	Cu I 324.754	0.21
	Ni I 341.476	0.50	Ni I 341.476	0.69
	Pb II 220.353	1.1	Pb I 405.781	2.0
	Zn II 202.548	0.29	Zn I 481.053	41

It should be emphasized that independently from the applied instrumental technique the achieved detection limits for the final solutions containing nitric acid or aqua regia were comparable. A clear advantage of ICP-OES over MP-AES are the lower detection limits of the analytes which can be reached by the former method. However, looking at the maximum acceptable levels for the target elements in compost, according to the Bulgarian legislation (Figure 1), it is obvious that for all elements (except Cd) the achieved methodological detection limits by MP-AES are at least 10 times lower than the regulated levels (the lower ones corresponding to the post transitional period). The latter fact reveals the potential of MP-AES to be applied for control analysis of Cr, Cu, Ni, Pb and Zn in compost samples digested and diluted with factor of 100. In order to lower the methodological LOD of Cd when using MP-AES an analysis with

dilution factor of 50 was also carried out. This was possible due to the utilization of the OneNeb® nebulizer which allows high dissolved solids to be introduced into the spectrometer without clogging. Under these conditions the loss of sensitivity for Cd due to non-spectral interference was *ca.* 20% and no substantial detonation of the background noise was observed. As a result, the methodological LOD of Cd for MP-AES was lowered to 0.18 mg kg⁻¹ with corresponding limit of quantification 0.60 mg kg⁻¹. The last value is more than two times lower than the prescribed limit of 1.3 mg kg⁻¹Cd.

A comparison of the results between ICP-OES and MP-AES was carried out for the compost sample produced by *Manufacturer 1*. To eliminate any artifact from sample heterogeneity six replicate samples were dissolved and each solution (DF = 100) was measured by both ICP-OES and MP-AES. For each individual replicate it was calculated the difference $\langle \text{Diff.} = C_{MP-AES} - C_{ICP-OES} \rangle$ and the corresponding relative difference $\langle \text{Rel.} = (C_{MP-AES} - C_{ICP-OES}) / C_{ICP-OES} \rangle$ between the concentrations obtained by MP-AES and ICP-OES as an assessment of the compliance of the two instrumental methods. On Table 3 are presented the calculated mean difference and the related standard deviation from the analysis of the six replicate samples when the compost sample was digested with nitric acid and on Table 4 the ones corresponding to the analysis of the soluble fraction of elements in aqua regia. The concentrations of the analysed elements in the compost sample produced by *Manufacturer 1* can be seen on Figure 1.

The paired t-test was applied as formal statistical tool to detect any significant difference (p -value < 0.05) between the concentrations measured by MP-AES and ICP-OES.

Even though in many cases the paired t-test resulted in statistically significant deviation, generally the relative difference of the results was in the range from -5% to 5% which can be accepted

as good compliance between the instrumental techniques. The highest relative difference was observed for the analysis of Cd which can be explained with its low concentrations in the sample solution and inevitably deteriorated repeatability of the instrumental measurement under these conditions. An emphasis can also be put on the analysis of Cr for which the results obtained by MP-AES are averagely elevated with 6.5% in comparison to ICP-OES for solutions containing only nitric acid (Table 3). On the opposite when Cr was measured in the aqua regia soluble fraction the MP-AES results were lower than the ones registered by ICP-OES (Table 4). Summarizing the results from Tables 2, 3 and 4 it can be concluded that MP-AES can be used as an acceptable alternative to ICP-OES for analysis of Cr, Cu, Ni, Pb and Zn in compost samples. The analysis of Cd by MP-AES is problematic due to the insufficient detection power of the instrumental technique. The following analysis of compost samples produced by Manufacturer 2 and 3 was accomplished by final measurement with ICP-OES.

According to the Bulgarian legislation for each target element are prescribed two maximum acceptable concentrations in compost i.e. Cd – 1.30

Table 3. Comparison of the results obtained by ICP-OES and MP-AES for compost (*Manufacturer 1*) dissolved with nitric acid (DF = 100)

	Cd		Cr		Cu		Ni		Pb		Zn	
	Diff. ^a , mg kg ⁻¹	Rel. ^b , %	Diff. ^a , mg kg ⁻¹	Rel. ^b , %	Diff. ^a , mg kg ⁻¹	Rel. ^b , %	Diff. ^a , mg kg ⁻¹	Rel. ^b , %	Diff. ^a , mg kg ⁻¹	Rel. ^b , %	Diff. ^a , mg kg ⁻¹	Rel. ^b , %
Mean ^c	0.01	0.7	3.8	6.5	9.2	5.9	0.5	1.6	0.4	0.3	36	5.2
SD ^d	0.16	11.5	1.5	2.6	4.1	2.6	1.2	4.3	2.9	2.2	7	0.9
p-value ^e	0.90		0.002		0.003		0.39		0.74		<0.001	

^a Difference between the concentrations obtained by MP-AES and ICP-OES;

^b Relative difference between the concentrations obtained by MP-AES and ICP-OES normalized to the result achieved by ICP-OES;

^c Mean value of the differences obtained from 6 replicate samples;

^d Standard deviation of the differences obtained from 6 replicate samples;

^e Obtained by the paired t-test.

Table 4. Comparison of the results obtained by ICP-OES and MP-AES for compost (*Manufacturer 1*) dissolved with aqua regia (DF = 100)

	Cd		Cr		Cu		Ni		Pb		Zn	
	Diff. ^a , mg kg ⁻¹	Rel. ^b , %	Diff. ^a , mg kg ⁻¹	Rel. ^b , %	Diff. ^a , mg kg ⁻¹	Rel. ^b , %	Diff. ^a , mg kg ⁻¹	Rel. ^b , %	Diff. ^a , mg kg ⁻¹	Rel. ^b , %	Diff. ^a , mg kg ⁻¹	Rel. ^b , %
Mean ^c	-0.11	-8.5	-3.7	-4.0	6.6	4.2	0.1	0.2	-4.3	-3.4	32	4.7
SD ^d	0.25	18.5	1.1	1.6	0.6	0.3	0.4	1.0	0.6	0.4	4	0.8
p-value ^e	0.32		<0.001		<0.001		0.54		<0.001		<0.001	

^a Difference between the concentrations obtained by MP-AES and ICP-OES;

^b Relative difference between the concentrations obtained by MP-AES and ICP-OES normalized to the result achieved by ICP-OES;

^c Mean value of the differences obtained from 6 replicate samples;

^d Standard deviation of the differences obtained from 6 replicate samples;

^e Obtained by the paired t-test

and 2.00 mg kg⁻¹; Cr – 60 and 100 mg kg⁻¹; Cu – 200 and 250 mg kg⁻¹; Ni – 10 and 80 mg kg⁻¹; Pb – 130 and 180 mg kg⁻¹; Zn – 600 and 800 mg kg⁻¹[5]. The higher limit is a requirement to the compost production for the first 7 years from the launch of a new manufacturing plant (transition period) and the lower more rigorous limit corresponds to the next ongoing time of biowaste treatment. The legal limits are in regard to the soluble fraction of elements extracted from the compost samples by two eligible procedures i.e. extraction with nitric acid (EN 16173:2012) or aqua regia (EN 16174:2012). Since in the official regulatory document [5] no preference is given to any of the sample preparation approaches it is supposed that both extraction schemes should be accomplished and the obtained results in each case should be compared to the maximum acceptable concentrations.

In our study the solid compost sample was subjected to preliminary homogenization, before acid treatment, which efficiency was tested by analysis of several separately dissolved replicates. On Table 5 are presented the results obtained from the analysis of 11 replicates of compost (*Manufacturer 3*) treated with nitric acid.

Table 5. Assessment of sample homogeneity - results for compost from *Manufacturer 3*

Element	Min	Max	Mean	SD	mg kg ⁻¹ ^a			RSD, %
					Percentiles			
					25-th	50-th	75-th	
Cd	0.53	0.83	0.71	0.08	0.69	0.72	0.75	10.8
Cr	38	45	41	2	40	42	43	4.8
Cu	98	113	106	4	105	108	108	3.9
Ni	22	25	24	1	23	24	24	4.4
Pb	101	119	109	5	106	108	111	5.1
Zn	393	438	423	17	418	432	435	3.9

^a 11 replicate samples were analyzed after extraction with nitric acid.

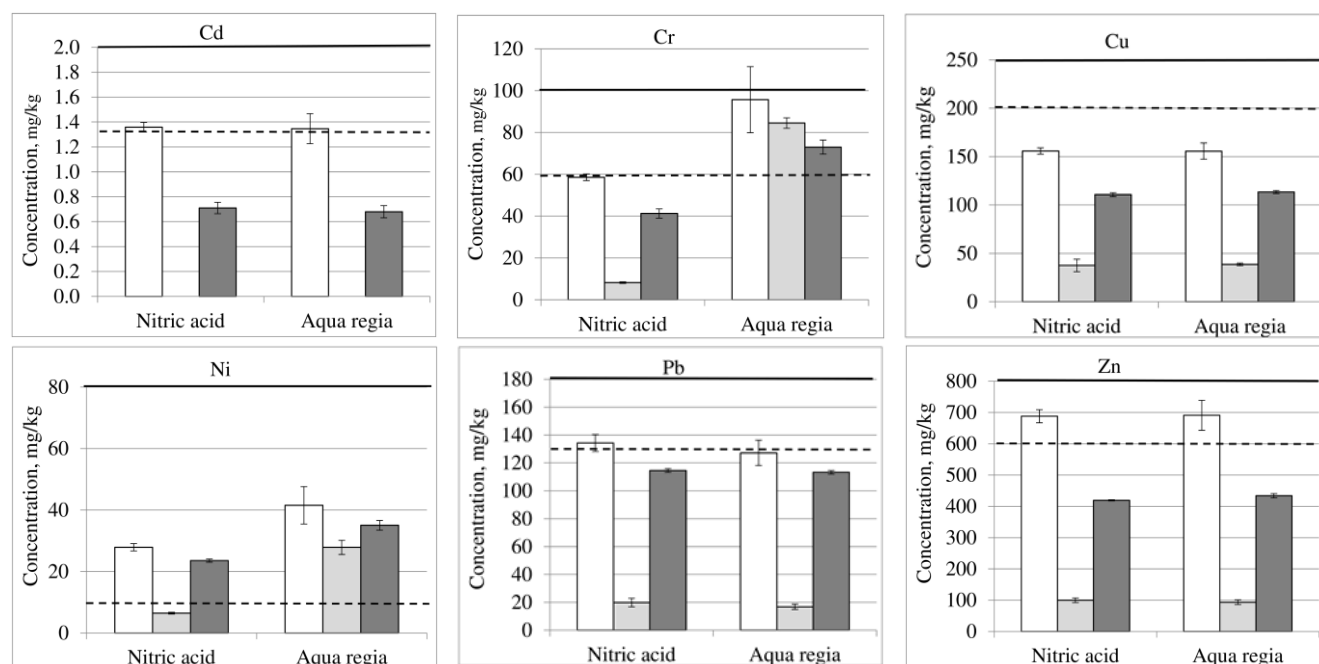


Figure 1. Comparison of the extracted amounts of elements with nitric acid and aqua regia from three different compost samples i.e. white bars - *Manufacturer 1* (6 replicates), light gray bars - *Manufacturer 2* (3 replicates) and dark gray bars - *Manufacturer 3* (3 replicates). The visualized uncertainties correspond to the standard deviation calculated from the analysis of several replicate samples. With solid line is presented the maximum acceptable concentration for the first seven years of compost manufacturing and with dashed line the one which is prescribed for the ongoing years

From the data given in Table 5 it can be derived that the used homogenization procedure is adequate. Only for Cd the relative spread of the concentrations exceeded 5%. However, since the concentration of Cd is much lower than the ones of the other elements, the higher variation range of the Cd content is most likely to be due to the deteriorated reproducibility of the instrumental measurement ($RSD\% > 8\%$) and is less probable to be a consequence of the sample heterogeneity.

Proving that the studied compost samples are homogenous is needed in order to distinguish if there is any difference in the concentration of the soluble fractions of Cd, Cr, Cu, Ni, Pb and Zn when the compost was treated alternatively with nitric acid or aqua regia. The obtained results for all tested compost samples (*Manufacturer 1*, *2* and *3*) are shown on Figure 1.

The concentration of Cd in the compost produced by *Manufacturer 2* is not presented on Figure 1 since it was below the methodological limit of quantification of ICP-OES (0.44 mg kg^{-1}).

It was found that the soluble fractions of Cd, Cu, Pb and Zn were statistically identical when nitric acid and aqua regia were used for sample treatment. This conclusion is valid for the three studied compost matrices. On the opposite for all compost samples it was found that the extracted amounts of Cr and Ni were significantly higher when aqua regia was applied for extraction compared to the treatment with nitric acid. A caution should be paid on this fact since in some samples the concentrations of Ni and Cr extracted with nitric acid are below the maximum acceptable levels but the content of these elements in the soluble

fractions in aqua regia is above the prescribed limits (Fig.1).

CONCLUSIONS

Concerning the sample preparation step for monitoring of elemental impurities in compost it can be concluded that the soluble fractions of Ni and Cr in aqua regia may be significantly higher than the ones extracted with nitric acid. No such difference was observed for Cd, Cu, Ni and Zn. The obtained results by ICP-OES and MP-AES were in good accordance and the achieved methodological limits of quantification with MP-AES were sufficiently low to allow the application of this instrumental technique to test the compliance with the maximum acceptable concentrations in compost for Cr, Cu, Ni, Pb and Zn. MP-AES can also be an adequate technique for monitoring the accordance of Cd concentration with its regulatory limit if sample dilution factor is decreased down to 50.

Acknowledgements: *KS is grateful for financial support of Project Number N115-HF-001 (NPD, University of Plovdiv "Paisii Hilendarski"). VZ and KS acknowledge T.E.A.M. Ltd. for the complimentary supplied spectrometer Agilent 4200*

MP-AES at Faculty of Chemistry, University of Plovdiv.

REFERENCES

1. F. Madrid, R. López, F. Cabrera, *Agric. Ecosyst. Environ.*, **119**, 249 (2007).
2. T. Manios, *Environ. Int.*, **29**, 1079 (2004).
3. E. Meller, E. Niedźwiecki, P. Rogalska, G. Jarnuszewski, D. Wilczyński, *J. Ecol. Eng.*, **16**, 154 (2015).
4. Z. Sharifi, S.M.T. Hossaini, G. Renella, *J. Geochemical Explor.*, **169**, 202 (2016).
5. Ordinance on treatment of biowaste, approved by Government Decree of Republic of Bulgaria № 235 from 15th October 2013.
6. EN 16173, Sludge, treated biowaste and soil - Digestion of nitric acid soluble fractions of elements (2012).
7. EN 16174, Sludge, treated biowaste and soil - Digestion of aqua regia soluble fractions of elements (2012).
8. EN 16170, Sludge, treated biowaste and soil - Determination of elements using inductively coupled plasma optical emission spectrometry (ICP-OES) (2016).
9. C. T. Kamala, V. Balaram, V. Dharmendra, M. Satyanarayanan, K. S. V Subramanyam, A. Krishnaiah, *Environ. Monit. Assess.*, **186**, 7097 (2014)

ОПРЕДЕЛЯНЕ НА Cd, Cr, Cu, Ni, Pb И Zn В КОМПОСТ: ОЦЕНКА НА РАЗЛИЧНИ ПОДХОДИ ЗА ПРЕДВАРИТЕЛНА ПОДГОТОВКА НА ПРОБИТЕ И ИНСТРУМЕНТАЛЕН АНАЛИЗ (MP-AES КАТО АЛТЕРНАТИВА НА ICP-OES)

В. Й. Запрянова^{1,2*}, К. К. Симитчиев¹, Е. Н. Пискова²

¹*Катедра аналитична химия и компютърна химия, Пловдивски Университет „Паисий Хилендарски“, ул. Цар Асен 24, 4000 Пловдив, България*

²*Лаборатория за изпитване на твърди биогорива и компост, Енергийна Агенция Пловдив, бул. Руски 139, офис 403, 4000 Пловдив, България*

Постъпила на 12 ноември 2016 г.; приета на 19 декември 2016 г.

(Резюме)

Съгласно българското законодателство са постулирани пределно допустими концентрации за набор от елементи (Cd, Cr, Cu, Ni, Pb и Zn) в третирани биоотпадъци като компост. Зададените граници са по отношение на разтворимите фракции на елементите, екстрахирани с азотна киселина или царска вода, съгласно процедури описани в БДС EN 16173:2012 и БДС EN 16174:2012. В настоящата работа бе сравнено количеството на извлечените елементи в разтвор при използване на препоръчаните реагенти (азотна киселина или царска вода). Киселинните екстракции са проведени в микровълнова система, ползваща затворени съдове за разтваряне. Разтворимите фракции на елементи са анализирани посредством две инструментални техники - оптико-емисионна спектрометрия с индуктивно свързана плазма (ICP-OES) и атомно-емисионна спектрометрия с микровълново генерирана плазма (MP-AES). Получените резултати показват, че MP-AES може да бъде приложен за мониторинг на Cd, Cr, Cu, Ni, Pb и Zn в компост и методът е адекватна алтернатива на ICP-OES. При изследването на набор от проби компост от различни производители бе установено, че екстракцията на Cd, Cr, Pb и Zn е статистически идентична за различните подходи на киселинно третиране. Заключениеето за Cr и Ni бе противоположно – екстрахираните количества от тези елементи с царска вода са значително по-големи спрямо извлечените при самостоятелната употреба на азотна киселина.

Ключови думи: *елементен анализ на компост; микровълново-подпомогната киселинна екстракция на елементи; оптико-емисионна спектрометрия с индуктивно свързана плазма (ICP-OES), атомно-емисионна спектрометрия с микровълново генерирана плазма (MP-AES).*

Mathematical analysis of the trace element content of Bulgarian fruits

G. Toncheva^{1*}, K. Nikolova², D. Boyadziev¹, G. Antova¹, Z. Jelev¹

¹University of Plovdiv, "Paisii Hilendarski", Plovdiv, 4000 Bulgaria

²Medical University "Paraskev Stoyanov", Varna, 9000 Bulgaria

Received November 13, 2016; Revised December 28, 2016;

The content of 8 essential and toxic elements (Cr, Mn, Fe, Ni, Cu, As, Cd, Pb) in most famous Bulgarian fruits as strawberry, white cherry, peach, apricot, green apple, pear, blackberry, fig, prune, green and blue-black grapes, melon, watermelon, quince and pumpkin were investigated. The highest content of Fe was found in quince ($35.7 \pm 0.2 \text{ mg kg}^{-1}$), followed by green grapes ($16 \pm 0.2 \text{ mg kg}^{-1}$). Strawberry was rich in Mn ($10.5 \pm 0.1 \text{ mg kg}^{-1}$), while green grapes had the highest content of Cu ($921 \pm 2 \text{ } \mu\text{g kg}^{-1}$). The contents of toxic metals Ni, As and Cd were significantly below the maximum levels for contaminants in food. Excessive lead content was observed in strawberry ($369 \pm 1 \text{ } \mu\text{g kg}^{-1}$) and fig ($181 \pm 2 \text{ } \mu\text{g kg}^{-1}$). K-Cluster analysis with three groups ($K = 3$) was carried out. The first cluster was occupied with white grapes, the third cluster included white cherry, melon and watermelon, and all the other fruits were in the second cluster. The differences in metal content of the investigated fruits were proven by application of statistical analysis. Discriminant analysis was used to obtain a model of Bulgarian fruits which contained the following canonical variables ordered by level of significance - Cr, Fe, Mn, Cu, Cd and Pb.

Key words: trace element content, fruits, ICP-MS, discriminant analysis.

INTRODUCTION

Fruits are very vital components of human nutrition. They are good sources of fiber, minerals, carbohydrates, organic acids, enzymes and vitamins, contain more than 20 different minor and trace elements. Most of them like Mn, Cu, Fe and Cr, are mostly cofactors of many enzymes and thus have very important role in several physiological functions of humans, they facilitate normal metabolism and growth. Any deficiency of these essential elements causes disturbances in the whole physiological system [1, 2].

The amount of metals in fruits is normally very small, but their contents can be significantly altered according to soil, air pollution and resulting from manufacturing and packaging processes [3, 4]. Furthermore metals such as Cd, Pb, Cr and Ni may contaminate the environment and thus into fruits at various levels causing health problems [5]. For some metals effects on the human body are cumulative and it is necessary to control their level in the food [6]. Thus for monitoring of fruits quality in manufacture and trade good measurements are always required.

Different techniques have been employed for carrying out the determination of trace elements in fruits across the world namely: stripping potentiometry [7], flame furnace atomic absorption spectrometry [8, 9], flow injection spectrometric methods [10], atomic fluorescence

spectrometry [11], capillary zone electrophoresis [12], inductively coupled plasma mass spectrometry (ICP-MS) [13, 14].

ICP-MS is a methodology which provides a rapid analysis and possibility for simultaneous multi-element analysis. This technology dominates as the most suitable methodology for quantification in fruits according researches by other authors [3, 15]. Our experience to study the wild fruits [16] also shows that it gives satisfactory results.

Because the data on the element composition of traditional Bulgarian fruits are limited, in this work using ICP-MS technique we determined 8 elements in 15 most common Bulgarian fruits. Mathematical model of the composition was developed.

MATERIALS AND METHODS

Plant material

The most popular fruits available in Bulgaria were selected. Foodstuffs as strawberry, white cherry, peach, apricot, green apple, pear, blackberry, fig, prune, green and blue-black grapes, melon, watermelon, quince and pumpkin were analyzed. All products are purchased from retail stores, supermarkets and market squares in Plovdiv areas. Fruits were purchased at the peak of their season. A total of three subsamples weighing 0.2-0.3 kg were obtained of each food item. Randomly from them one sample representing each fruit was arranged. Before analysis all the products were washed with ultrapure water to remove the dust and soil particles and the fertilizers residues.

* To whom all correspondence should be sent.

E-mail: galq_toncheva@mail.bg

The samples for analysis were prepared ready for consumption, i.e. only the edible parts were analyzed.

For element content determination all samples were dried (18 h at 80 °C) and after homogenization were stored at -18 °C. Prior instrumental analysis, the dried fruit (~0.5 g) were treated on hot plate with concentrated HNO₃ (Merck, Darmstadt, Germany) and 30% H₂O₂ (Chimtex Ltd, Dimitrovgrad, Bulgaria) according the procedure described in ref. [16].

Analysis of moisture content and carbohydrate content in fruits

The moisture content of the fruit was determined by weighing the samples before and after drying at 97 °C for 16 h (ISO 712:2009). The content of total soluble carbohydrates and monosaccharides was determined by the method of Schoorl [17].

Determination of element contents in fruits

An inductively coupled plasma quadrupole mass spectrometer (Agilent 7700 Tokyo, Japan), with an octopole reaction system (He collision gas) was used for simultaneous multi-element detection of Cr, Mn, Fe, Cd, Ni, Cu, As and Pb in sample solutions. Operating conditions for ICP mass spectrometer are the same as in our previous publication [16]. The calibrants in concentration range 10-1000 µg L⁻¹ were prepared from ICP multi-element standard solution VI (110580 Merck, Darmstadt, Germany) after appropriate dilution in 0.1 % (v v⁻¹) HNO₃. Rhodium (CPAchem Bulgaria) was used as an internal standard for correction of both matrix effect and instrumental drift.

Statistical analysis

Program "Statistica" was used for the data processing. The data distribution was normal according to the criterion of Kolmogorov - Smirnov [18, 19]. Discriminant analysis with a priori equal probabilities was used for modeling groups of fruits [20, 21]. K-means clustering was applied for comparing the Bulgarian fruits. [22, 23]. This method classifies data through fixed a priori number of clusters [24].

RESULTS AND DISCUSSION

Dry matter, protein and carbohydrate content of fruits

Table 1 shows basic chemical parameters of Bulgarian fruits. Their profiles in the fruits are typical for these types of foods [25, 26]. Slightly higher levels of the protein content in grape, cherry and apple were observed. This difference can be explained by sortable and soil characteristics. A green grape contains the highest carbohydrate content (16.7%±0.1) and proteins (1.1%±0.1).

Correlation between moisture content and trace element composition of the fruit was not established.

Element contents in fruit samples

The element contents with corresponding combined uncertainties (U) - in fresh fruits are summarized in Table 2. The studied fruits green and red grapes have the richest composition in terms of essential elements. These foodstuffs have a high content of Fe, Mn, Cr and Cu. The main trends in Bulgarian fruits are similar to those observed by other authors [3, 4, 27]. The highest content of any elements of all fruits was shown by Fe.

Iron is essential trace element. Iron participates in two important processes in body such as transport of oxygen and electron transfer, due to iron-binding proteins [1]. Iron content in the examined Bulgarian fruits ranges from 1.03±0.02 mg kg⁻¹ to 35.7±0.2 mg kg⁻¹. Similar iron content (from 2 mg kg⁻¹ to 48 mg kg⁻¹) is observed for fruits by Finland and Poland [3, 4]. The investigated grapes, prunes and strawberries accumulate from the soil more Fe than similar English products [27]. The highest Fe content was found in quinces (35.7±0.2 mg kg⁻¹), followed by green grapes (16±0.2 mg kg⁻¹). Daily consumption of 100 g Bulgaria quinces provides approximately 5% of the Recommended Daily Allowance (RDAs) for Fe. This value for consumption of 100g Bulgarian grapes is approximately 2.5% of RDAs [28].

Chromium is a mineral that humans require in trace amounts to enhance the action of insulin. The highest Cr content was found in blue-black grapes (220±3 µg kg⁻¹) and the smallest - in melons (15±0.3 µg kg⁻¹). Bulgarian and Chinese strawberries have similar content of this metal. Bulgarian strawberries have a low content of Cr (54±0.8 µg kg⁻¹) compared to these by China (88.3±4.5 µg kg⁻¹) [15]. Daily consumption of 100 g Bulgaria blue-black grape provides approximately 10% of the Recommended Daily Allowance (RDAs) for Cr.

The amount of the essential elements Mn and Cu is in the range from 0.8 mg kg⁻¹ to 10.5 mg kg⁻¹ for Mn and in the range from 140.0 µg kg⁻¹ to 921 µg kg⁻¹ for Cu.

Bulgarian fruits have approximately the same content of Mn as the analogical products from Finland and Poland, while the content of copper is lower than those analogs [3, 4]. The content of toxic metals Ni, As and Cd were in amount significantly below the maximum levels for contaminants in food. Excessive lead content was observed in strawberry (368.6±10.5 µg kg⁻¹) and fig (180.7 ±20.5 µg kg⁻¹) [29, 30].

Table 1. Dry matter, protein and carbohydrate content in Bulgarian fruits

No	Fruits	Dry matter, %	Protein, %	Total carbo- hydrate, %	Mono- saccharides, %	Total sugar, %
1	Strawberries	8.35±0.19	0.7±0.1	8.2±0.1	6.3±0.1	1.9±0.1
2	Cherries white	17.00±0.12	0.9±0.1	14.5±0.2	13.4±0.2	0.9±0.1
3	Blackberries	15.50±0.10	0.9±0.1	6.3±0.1	6.1±0.1	0.2±0.1
4	Peaches	17.09±0.21	0.7±0.1	8.7±0.1	3.2±0.1	5.5±0.1
5	Apricots	14.24±0.25	0.6±0.1	7.3±0.1	4.4±0.1	2.9±0.1
6	Green apples	13.17±0.13	0.5±0.1	8.8±0.2	6.9±0.1	1.9±0.1
7	Pears	12.14±0.15	0.5±0.1	5.1±0.1	4.9±0.1	0.2±0.1
8	Figs	21.05±0.10	0.9±0.1	13.5±0.1	13.0±0.1	0.5±0.1
9	Prunes	21.56±0.15	0.4±0.1	10.3±0.1	9.1±0.1	1.2±0.1
10	Green grapes	19.30±0.12	1.1±0.1	16.7±0.1	16.6±0.1	0.1±0.1
11	Blue-Black grapes	19.00±0.15	1.1±0.1	14.0±0.1	13.7±0.1	0.3±0.1
12	Watermelons	9.24±0.10	0.6±0.1	6.6±0.1	3.1±0.1	3.5±0.1
13	Melons	7.98±0.10	0.3±0.1	4.9±0.1	2.1±0.1	2.8±0.1
14	Quinces	16.65±0.15	0.4±0.1	9.1±0.1	8.4±0.1	0.7±0.1
15	Pumpkin	23.91±0.14	1.1±0.1	4.4±0.1	1.4±0.1	3.0±0.1

Table 2. Trace element content in Bulgarian fruits

No	Fruits	Cr		Fe		Mn		Ni		Cu		As		Cd		Pb	
		Conc. µg/kg	±U	Conc. mg/kg	±U	Conc mg/kg	±U	Conc µg/kg	±U	Conc µg/kg	±U	Conc. µg/kg	±U	Conc. µg/kg	±U	Conc µg/kg	±U
1	Strawberries	54	0.8	5.08	0.08	10.5	0.1	26.3	0.3	140	1	1.9	0.04	8.2	0.1	369	1
2	Cherries white	57	0.2	1.30	0.01	0.91	0.02	46.9	0.7	631	2	8.2	0.2	0.3	0.02	103	1
3	Blackberries	70	0.5	8.57	0.10	3.19	0.07	99.0	0.2	663	4	5.9	0.3	4.8	0.3	61	0.5
4	Peaches	120	0.2	7.20	0.10	3.90	0.03	163	4	128	1	2.0	0.1	4.4	0.1	64	1
5	Apricots	87	0.6	1.58	0.07	2.48	0.02	152	3	851	9	0.2	0.03	2.7	0.1	68	0.1
6	Green apples	61	0.5	6.87	0.02	2.24	0.03	35.6	0.1	297	2	0.7	0.01	0.4	0.02	28	0.6
7	Pears	87	0.9	13.2	0.2	2.27	0.02	91	2	838	8	3.0	0.2	2.1	0.01	95	1
8	Figs	41	0.3	11.2	0.2	2.85	0.02	169	2	255	2	3.3	0.2	5.9	0.3	181	2
9	Prunes	55	0.5	13.9	0.1	2.32	0.02	90	1	451	3	14.6	0.5	1.9	0.1	110	1
10	Green grapes	126	1	16	0.2	8.2	0.1	146	1	921	2	2.5	0.1	3.2	0.04	58	0.3
11	Blue-Black grapes	220	3	10.6	0.1	5.8	0.1	134	2	751	9	6.0	0.2	4.6	0.05	88	0.5
12	Watermelons	33	1	1.03	0.02	1.01	0.02	42.2	0.4	202	1	2.1	0.1	5.2	0.1	102	1
13	Melons	15	0.3	1.04	0.08	0.99	0.01	40.3	0.4	487	2	0.9	0.07	1.3	0.1	34	2
14	Quinces	128	1	35.7	0.2	2.07	0.02	172	1	287	2	2.3	0.09	6.1	0.1	42	0.2
15	Pumpkin	74	1	9.3	0.2	0.81	0.01	177	1	567	3	6.8	0.2	12.2	0.1	133	2

The Scheffe criterion shows significant statistical differences in the studied fruits. The availability of these differences in mineral content in the fruits provides the reason for a subsequent modeling of its origin. A linear discriminant

analysis was applied with grouping parameter "type of Bulgarian fruit". The obtained model includes the following parameters arranged as Cr, Fe, Mn, Cu, Cd, and Pb. Cluster analysis was applied with the method of K-means clusters. Most suitable was

the grouping in 3 clusters. The fruits included in them had similar values of trace element content, which differentiate them from the products in the other clusters. In Table 3 is shown product participation in each of the 3 clusters and also the percentage distribution of the fruits into the three clusters.

The first cluster contains only green grapes, because this product is the richest of essential elements. The second contains the predominant part of the products. The third cluster contains four fruits, which have almost equal content of the Ni, Fe and Mn - watermelon, melon, apricot and white cherry.

Canonical analysis was performed for a better visualization of the results. The groups of the products are presented in Figure 1. The first two canonical variables are crucial for model. The figure confirms our hypothesis for the presence of significant differences between the separate groups of fruits. The analysis of the Mahalanobis distances (Table 4) between the three groups shows that the second and the third group are close to each other and are relatively far from the group of the white grape. If we trace the projections of the clouds of the various groups upon the first canonical variable (which plays important role in discrimination of the groups) – the white cherry, apricot, melon, watermelon are projected on the positive, while the fruits of the second group are projected close to zero in the negative direction. The white grape is projected in the negative direction.

Table 3. Distribution of type summer fruits in clusters

Fruits in clusters	Number of fruits	Distribution of the fruits, %
1	2	3
Green grapes	1	7.7
Blackberry, peach, apple, pear, black grapes, pumpkin, fig, prune	8	61.5
White cherry, apricot, melon, water melon	4	30.8

Table 4. The mahalanobis distances for different fruits groups

Mahalanobis distances			
Groups	G ₁	G ₂	G ₃
1	2	3	4
G ₁	0.00	83.54	218.69
G ₂	83.54	0.00	58.44
G ₃	263.81	58.44	0.00

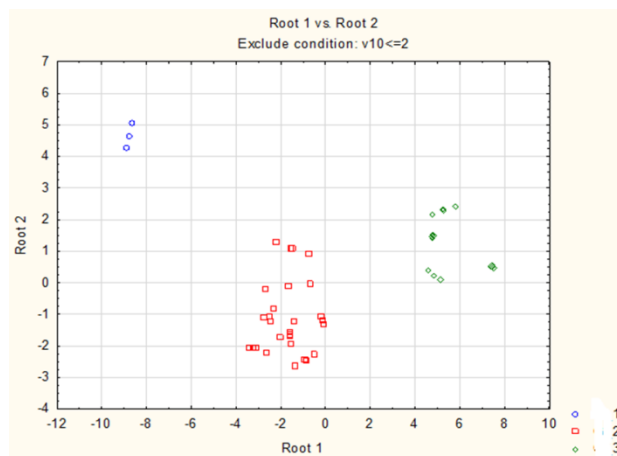


Figure 1. Disposition of the groups of fruits in the plane of the first two canonical variables

CONCLUSION

The highest Fe content in Bulgarian fruits was found in quinces ($35.7 \pm 0.2 \text{ mg kg}^{-1}$), followed by green grapes ($16 \pm 0.15 \text{ mg kg}^{-1}$). Differences in the values of trace element content for different groups of fruits were statistically proven. This makes efficient the use of the discriminant analysis for qualitatively differentiate of various fruits. The content of the elements Cr, Fe, Mn, Cu, Cd and Pb determines the specificity of Bulgarian fruits.

Acknowledgements The authors would like to express their gratitude to the Research Fund of the University of Plovdiv "Paissii Hilendarski" (contract N115-HF001) for the financial support.

REFERENCES

1. E. Ochiai, Chemicals for Life and Living, Springer, Berlin, p. 73, (2011).
2. C. G. Fraga, *Molecular aspects of medicine*, Elsevier, **26**, 235, (2011)
3. P. Ekholm, H. Reinivuo, P. Mattila, H. Pakkala, J. Koponen, A. Happonen, J. Hellstrom, M. Ovaskainen, *J. of Food Composition and analysis*, **20**, 487 (2007).
4. P. Szefer, M. Grembecka, Mineral components in food crops, beverages, luxury food, species, and dietary food, *Taylor & francis Group*, New York, p.231, (2007).
5. L. Järup, *Br. Med. Bull.*, **68**, 167, (2003).
6. N. Khan, S. Jeong, M. Hwang, *Food Chemistry*, **147**, 220 (2014).
7. R. Ratana-ohpas, Kanatharana, W. Ratana-ohpas, Kongsawasdi, *Anal. Chimica acta*, **333**, 115 (1996).
8. S.P Sanchez-Castillo, P.J. Dewey, J.J. Aguirre, R. Lara, R. Vaca, *J. of food composition and analysis*, **11**, 340 (1998).
9. C.C.Nascentes, M.A. Arruda, A.R.Nogueira, J.A. Nóbrega, *Talanta*, **64**, 912 (2004).
10. M.A. Korna, B.Jailson, J.B.de Andrade, D.S. Jesus, V.A. Lemos, *Talanta*, **69**, 16, (2006).
11. L. Ebdon, E. Mike, M. E.Foulkes, S. Roux and R. Muñoz-Olivas, *Analyst*, **127**, 1108, (2002).

12. R. Rodriguez, J. Manes, Y. Pico, *Anal. Chem.*, **75**, 452, (2003).
13. I. Suchara, J. Sucharova, *Anal. Chimica Acta.*, **576**, 163 (2006).
14. S.J.Hill, Inductively Coupled Plasma Spectrometry and its Applications, *Blackwell Publishing*, Plymouth UK, p. 12, (2008).
15. H. Zhang, Z.Y. Wang, X. Yang, H.T. Zhao, *Food Chemistry*, **147**, 189 (2014).
16. G. Toncheva, D. Georgieva, G. Antova, *Scientific works of University of Food Technologies*, **LXI**, part II, 23, (2014).
17. N. Luzkanov, T. Ivanova, I. Pistiiski, A. Koleva, Textbook practical exercises, *Poligrafia*, Plovdiv, (1994).
18. G. McLachlan, Discriminant Analysis and Statistical Pattern Recognition, *John Wiley & Sons, Inc.*, (1992).
19. B. Vandeginste, D. Massart, L. Buydens, S. Jong, P. Lewi, Handbook of Chemometrics and Qualimetric, Part A, Elsevier, Amsterdam, p. 45 (1997).
20. Bondar, A., G. Statuha, Planirovanie eksperimenta v himicheskoj tehnologii, *Высшая школа*, Moscow, p. 97-99, (1976).
21. G. Lakin, Biometry, *Высшая школа*, Moscow, p. 56, (1990).
22. D. Vindev, *Applied Statistics 2*, Sofia, p. 123, (2003).
23. B. Duran, P. Odel, Cluster Analysis, *Statistics*, p. 34, (1977).
24. J. Hartigan, *J. of Classification*, **2**, 63, (1985).
25. A. Jack, *Food composition tables*, New York, p. 24, (2011).
26. R.C. Atkins, New Carbohydrate Gram Counter, *New York: M. Evans and Company*, p. 27, (1996).
27. A.M. Mayer, *British Food J.*, **99**, 207, (1997).
28. Commission Directive (EC), Directive 2008/100/EC, *Official J. of the European Union*, L 285, p. 9, (2008).
29. Commission regulation (EC) №1881/2006 Maximum levels of certain contaminants of food stuffs, (2006).
30. WHO, Trace Elements, World Health Organization, Geneva, p. 1-361, (1996).

МАТЕМАТИЧЕСКИ АНАЛИЗ НА СЪДЪРЖАНИЕТО НА МИКРОЕЛЕМЕНТИ В БЪЛГАРСКИ ПЛОДОВЕ

Г. Тончева^{1*}, К. Николова², Д. Бояджиев¹, Г. Антова¹, З. Желев¹

¹Пловдивски Университет "Паисий Хилендарски", Пловдив, 4000 България

²Медицински Университет "Параскев Стоянов", Варна, 9000 България

Постъпила на 13 ноември 2016 г.; приета на 28 декември 2016 г.

(Резюме)

В състава на най-известните български плодове - ягода, бяла череша, праскова, кайсия, зелена ябълка, круша, къпина, смокиня, синя слива, бяло и черно грозде, диня, пъпеш, дюля и тиква е определено съдържанието на микроелементи (Cr, Mn, Fe, Ni, Cu, As, Cd, Pb). Най-високо съдържание на Fe е установено за дюля ($35.7 \pm 0.2 \text{ mg kg}^{-1}$), следвана от бяло грозде ($16 \pm 0.2 \text{ mg kg}^{-1}$). Ягодата е богата на Mn ($10.5 \pm 0.1 \text{ mg kg}^{-1}$), докато бялото грозде показва най-високо съдържание на Cu ($921 \pm 2 \text{ } \mu\text{g kg}^{-1}$). Съдържанието на токсични метали Ni, As и Cd е в количества значително по-ниски от максимално допустимите нива на замърсители в храни. Наблюдава се завишено съдържание на олово в ягода ($369 \pm 1 \text{ } \mu\text{g kg}^{-1}$) и смокиня ($181 \pm 2 \text{ } \mu\text{g kg}^{-1}$). Направен е К-кълъстерен анализ с три групи ($K = 3$). Първият кълъстер съдържа бяло грозде, третият включва бяла череша, пъпеш и диня, а всички останали плодове са във втория кълъстер. Разликите в съдържанието на микроелементи са проверени с прилагане на дискриминантен анализ. Математическият модел на елементния състав на български плодове включва следните канонични променливи подредени по ниво на значимост: Cr, Fe, Mn, Cu, Cd и Pb.

Ключови думи: съдържание на микроелементи, плодове, масспектрометрия с индуктивно свързана плазма, дискриминантен анализ.

Valorization of waste of *Calendula officinalis* - obtaining of ethanol extracts

N. S. Yantcheva¹, I. N. Vasileva¹, P. N. Denev², P. V. Lutova¹, S. E. Mitov¹, Z. A. Iordanova¹,
M. A. Galabova¹, I. N. Panchev³, A. M. Slavov^{1*}

¹Department of Organic Chemistry, University of Food Technologies, 26 Maritza Blvd., 4002 Plovdiv, Bulgaria

²Laboratory of Biologically Active Substances, 139 Ruski Blvd., 4000 Plovdiv, Bulgaria

³Department of Physics, University of Food Technologies, 26 Maritza Blvd., 4002 Plovdiv, Bulgaria

Received October 28, 2016; Revised December 21, 2016

Valorization of wastes of food industry and agriculture became a priority in the last years. Novel promising waste materials are residues from the essential oils and natural pigment industry. Such underexplored waste is obtained from *Calendula officinalis* (marigold) which is widely used as herbal medicine and industrially for extraction of lutein. The aim of our work was to investigate the possibility for valorization of the waste of marigold. Two kinds of residues were investigated – one obtained after extraction of marigold flowers by freon (1,1,1,2-tetrafluoroethane) and second obtained after steam distillation. The total polyphenols and antioxidant activity of the ethanol extracts were investigated and was found that extraction of the raw materials by freons preserves to a large extent polyphenols – wastes after freon extracted marigold had 1543.8 mg/L total polyphenols compared to 336.5 mg/L for the after hydro-distilled marigold flowers. The same results were confirmed from the data for antioxidant activity – wastes from freon treated flowers showed 15856.2 $\mu\text{mol TE/l}$ (by ORAC method) and 5011.3 $\mu\text{mol GAE/l}$ (by HORAC method) while waste of hydro-distilled marigold flowers showed almost 5 times lower values. The individual phenolic acids and flavonoids were determined by HPLC and the main compounds found were chlorogenic and caffeic acids (from the phenolic acids), and naringin from the flavonoids. By GC-MS were investigated polar metabolites and aroma compounds in the ethanolic extracts. The results from the present investigation showed that the marigold waste could be a valuable source for obtaining of by-products with pronounced antioxidant activity.

Key words: *Calendula officinalis* (marigold), waste valorization, antioxidant activity, polyphenols

INTRODUCTION

Marigold (*Calendula officinalis*) is a very common flower grown across Europe as garden plant. It has been used also as herb, edible plant and it has well known medicinal properties [1]. The flower is found in the wild but also it has an important commercial application due to the facts that its seed oil contains large amounts of calendic acid which is used for coatings, in formulation of cosmetics etc. [1]. Marigold flowers are also a valuable source for commercial production of lutein [2]. Due to the fact that the concentration of active compounds in the plant materials are relatively low after extraction or distillation of the important biologically active substances large quantities of wastes remain. Throwing simply away or using as compost is among the very often used procedures to eliminate these wastes. But they could also serve as initial materials for extraction of valuable by-products. In a previous work of us we have investigated the possibility for extraction of water-soluble pectic polysaccharides from several plant wastes including marigold [3]. The aim of the present work was to explore further the possibilities for valorization of wastes of marigold obtained

after extraction with freons and steam distillation.

MATERIALS AND METHODS

Materials

The waste *Calendula officinalis* mass (steam distilled) was obtained from the region of Chehlare (region of Plovdiv, crop 2015). The *Calendula officinalis* (crop 2015, region of Plovdiv) was extracted by freon (1,1,1,2-tetrafluoroethane, R134a) as described by Nenov [4]. After treatment the residues were cooled down, inspected for elimination of impurities and dried under vacuum at 50 °C. The mass was stored at -18 °C until further treatment. All the solvents used were of analytical grade and purchased from local distributors.

Methods

The 70 % ethanolic extracts from two wastes of *Calendula officinalis* (extracted by freon and steam distilled) were obtained according to Kratchanova *et al.* [5].

The total polyphenol content of ethanolic extracts was determined using the method described by Singleton and Rossi, [6]. The antioxidant activity by ORAC and HORAC assays was measured as described by Číž *et al.* [7].

* To whom all correspondence should be sent.
E-mail: antons@uni-plovdiv.bg

The content of individual phenolic and flavonoid components was analyzed on Agilent 1220 HPLC system (Agilent Technology, USA), equipped with binary pump and UV-Vis detector. Wavelength of $\lambda = 280$ nm was used. Separation was performed using Agilent TC-C18 column (5 μm , 4.6 mm x 250 mm) at 25°C. Mobile phases constituted of 0.5 % acetic acid (A) and 100% acetonitrile (B) at flow rate 0.8 ml/min. The gradient conditions started with 14% B, between 6 min and 30 linearly increased to 25% B, then to 50% B at 40 min. The standard compounds (gallic acid, 3,4-dihydroxy benzoic acid, chlorogenic acid, caffeic acid, p-coumaric acid, ferulic acid, ellagic acid, catechin, epicatechin, rutin, naringin, myricetin, quercetin, naringenin and kaempferol) were purchased from Sigma-Aldrich (Steinheim, Germany).

The individual volatile and non-volatile compounds in the ethanolic extracts were determined according to the following procedures:

1). Non-volatile substances – 0.2 ml ethanolic extract was lyophilized and 50 μL pyridine and 50 μL N,O-Bis-(trimethylsilyl)-trifluoroacetamide (BSTFA) were added. The sample was incubated at 70 °C for 40 min. For analysis 1.0 μL from the solution was injected on gas chromatograph Agilent GC 7890 with mass-selective detector Agilent MD 5975 and column HP-5ms (30 m with diameter 0.32 mm and 0.25 μm thicknesses). The following temperature regimen was used – initial temperature 100 °C (hold for 2 min) then increase to 180 °C with 15 °C/min (hold for 1 min) and increase of the temperature to 300 °C with 5 °C/min (hold for 10 min); injector and detector temperatures – 250 °C, helium was used as carrier gas at 1.0 ml/min. The scanning range of mass-selective detector was $m/z = 50 - 550$ in split-split mode (10:1).

2). Volatile substances – 1.0 ml ethanolic extract was extracted with 1.0 ml dichloromethane (triple). The combined organic layers were dried under vacuum at 30 °C. To the dry residue 100 μL dichloromethane was added. For analysis 1.0 μL from the solution was injected on gas chromatograph Agilent GC 7890 with mass-selective detector Agilent MD 5975 and column HP-5ms. The following temperature regimen was used – initial temperature was 40 °C and then increase to 300 °C with 5 °C/min (hold for 10 min); injector and detector temperatures – 250 °C, helium was used as carrier gas at 1.0 ml/min. The scanning range of mass-selective detector was $m/z = 40 - 400$ in splitless mode.

The individual compounds were identified comparing the retention times and the relative index (RI) with those of standard substances and mass-

spectral data from libraries of The Golm Metabolome Database (<http://csbdb.mpimp-golm.mpg.de/csbdb/gmd/gmd.html>) and NIST'08 (National Institute of Standards and Technology, USA).

RESULTS AND DISCUSSION

Treatment of the wastes with aqueous-ethanolic solutions is usually applied before extraction of polysaccharides from the raw materials. It aims to remove some low-molecular substances (pigments, sugars, etc.) which will hamper the future extraction. In our case it also aimed at obtaining of extracts rich on polyphenolic substances [3, 8]. In previous experiments we have investigated the influence of the ethanol concentration on extractability of polyphenols and subsequent polysaccharide extractions (Slavov, unpublished results). Our findings showed that extraction with 70% ethanol solutions gave the optimum results for possibilities of combined valorization of the waste materials of *Rosa damascena* and for this reason we have decided the treatment of the marigold residues after extraction or steam distillation to be performed with 70 % ethanol. The extracts obtained were subjected to preliminary analysis for their total phenolic substances and antioxidant activity. The results from the analysis are shown in Table 1.

The results from the preliminary experiments suggest that steam distillation led to significant reduction of polyphenols due to their partial extraction. Extraction with freons preserves to a large extent substances which contribute to the antioxidant activity of the ethanolic solutions.

It seems also that this extraction led to better disintegration of the cell walls of the plant materials which is beneficial for the further extractions of biologically active substances. In this respect extraction of the plant materials by halocarbons resembles extraction with supercritical CO_2 although the state of the freons used is above their critical point.

Furthermore we had investigated the polyphenolic profile of the 70 % ethanolic extracts obtained – Table 2.

Table 1. Polyphenols and antioxidant activity of 70 % ethanol extracts of marigold wastes

No	Waste material	Total phenolics, mg/L	ORAC, $\mu\text{mol TE/l}$	HORAC, $\mu\text{mol GAE/l}$
1	Marigold – after freon	1543.8 \pm 84.9	15856.2 \pm 1427.0	5011.3 \pm 267.6
2	Marigold – after steam distillation	336.5 \pm 36.2	3654.2 \pm 211.3	981.2 \pm 79.8

Table 2. Phenolic acids and flavonoids in 70% ethanolic extracts.

Phenolic acids, mg/100 ml	70 % ethanol extracts	
	Marigold – after freon	Marigold – after steam distillation
Chlorogenic acid	3.44±0.42	0.24±0.01
Neochlorogenic acid	1.55±0.10	-
Vanillic acid	1.02±0.03	0.42±0.08
Caffeic acid	3.08±0.89	0.13±0.04
p-Coumaric acid	1.64±0.09	0.09±0.01
Ferulic acid	0.38±0.05	0.01± -
Ellagic acid	0.61±0.03	0.09± -
Cinnamic acid	0.16±0.01	0.07± -
Gallic acid	1.19±0.20	0.31± 0.04
TOTAL, mg/100 ml	13.07±0.90	1.36±0.8
Flavonoids, mg/100 ml		
Quercetin	1.39±0.08	0.46±0.04
Quercetin-3-β-glucoside	1.32±0.40	0.30±0.06
Myricetin	1.67±0.06	-
Kaempferol	0.96±0.08	0.16±0.01
Naringin	40.99±1.20	3.35±0.58
Naringenin	6.69±0.90	2.86±0.09
Catechin	4.43±0.40	2.68±0.10
Epicatechin	-	-
TOTAL, mg/100 ml	57.45±1.20	9.81±0.80

The highest contents of the phenolic acids were observed for chlorogenic and caffeic acids – two compounds which are known for their pronounced antioxidant activities [9]. Other phenolic acids contributing to the higher antioxidant activity of the ethanolic extract from marigold treated with freon were p-coumaric, neochlorogenic, gallic and vanillic acids. Comparing the total amount of phenolic acids could be concluded that ethanolic extract from marigold treated with freon has 10 times more than steam distilled residues. The 70% ethanolic extract of freon treated marigold is also rich of flavonoids (5 times higher) from which almost 85% is due to presence of naringin and naringenin.

In the next analysis were determined by GC-MS the volatile and non-volatile polar compounds present in the 70% ethanolic extracts. The results are presented in Tables 3 and 4.

The results from the analysis showed that even after extraction / distillation a high amount of linoleic and linolenic acids (which also includes amounts of calendic acid – a conjugated linoleic acid) [10] remain in the wastes. The extract from marigold waste (freon) also is rich on malic, quinic, caffeic and syringic acid. The results from the analysis confirm the observation that extraction with freons preserves to a larger extent in the plant material the non-volatile biologically active substances.

Table 3. Polar non-volatile substances in ethanolic extracts. RI - relative index (Kovats retention index); % of TIC - total ion current.

Compounds	RI	% of TIC	
		Marigold – after freon	Marigold – after steam distillation
Succinic acid	1310	0.763±0.012	0.342±0.065
Fumaric acid	1355	0.407±0.015	0.367±0.008
L-Threonine	1390	0.319±0.020	0.192±0.015
L-Homoserine	1446	0.112±0.009	0.088±0.005
Malic acid	1488	2.505±0.090	0.776±0.079
Salycilic acid	1516	0.226±0.089	0.313±0.068
L-Threonic acid	1528	0.677±0.078	0.228±0.072
Vanillic acid	1758	0.241±0.085	0.144±0.079
Protocatechuic acid	1813	0.299±0.056	0.233±0.046
Quinic acid	1843	1.372±0.120	2.615±0.111
Syringic acid	1888	1.310±0.110	1.399±0.099
Gluconic acid	1991	1.762±0.090	1.197±0.068
Glucaric acid	2013	0.722±0.085	0.302±0.078
Caffeic acid	2140	0.693±0.054	0.211±0.045
Linoleic acid	2209	3.113±0.154	3.684±0.132
α-Linolenic acid	2217	2.675±0.123	3.403±0.097
Stigmasterol	3315	0.547±0.045	0.852±0.056
β-Sitosterol	3355	0.693±0.047	1.595±0.095

Table 4. Polar volatile substances in ethanolic extracts. RI - relative index (Kovats retention index); % of TIC - total ion current.

Compounds	RI	% of TIC	
		Marigold – after freon	Marigold – after steam distillation
Hyacinthin	1075	0.205±0.025	0.101±0.021
Benzeneacetic acid	1274	0.188±0.054	0.125±0.065
Syringol	1336	0.333±0.065	0.099±0.066
Eugenol	1358	0.265±0.075	0.142±0.078
2-Methylbenzoate	1372	0.154±0.021	0.076±0.019
α-Copaene	1379	0.317±0.032	0.085±0.026
β-Cubebene	1391	0.296±0.065	0.102±0.059
Methyleugenol	1405	0.144±0.012	1.358±0.025
β-Caryophyllene	1419	0.208±0.016	0.126±0.014
β-Copaene	1431	0.129±0.024	1.283±0.048
γ-Cadinene	1513	1.985±0.089	1.566±0.087
Viridiflorene	1518	2.133±0.087	0.908±0.068
δ-Cadinene	1529	1.922±0.095	0.322±0.069
Veridiflorol	1592	1.511±0.086	0.077±0.008
α-Cadinol	1641	3.180±0.113	0.713±0.063
α-Bisabolol oxide B	1648	3.514±0.124	3.085±0.114
7-Methoxy-coumarin	1737	1.595±0.102	8.747±0.254
α-Bisabolol oxide A	1792	2.221±0.098	5.949±0.168
7-hydroxy-coumarin	1813	0.755±0.085	0.578±0.077

Results from analysis for volatile substances in ethanolic extracts showed that even after the extraction / distillation of the plant materials remain significant amounts of aroma compounds in the residues. The highest quantities of floral aroma substances were found for α -Bisabolol oxide B, α -Cadinol, α -Bisabolol oxide A and viridiflorene. The above-mentioned compounds were found in ethanolic extracts from the two investigated wastes (marigold extracted with freons and steam distilled) in relatively high concentrations and even more some compounds (7-Methoxycoumarin, methyleugenol, α -Bisabolol oxide A, etc.) were preserved to a larger extent due to their insolubility in water in steam-distilled marigold residues.

CONCLUSIONS

The present study focused on valorization of marigold wastes showed that the 70% ethanolic extracts have pronounced antioxidant effects and also were rich on phenolic acids and flavonoids. To a larger extent the extraction with non-polar solvents (halocarbons) led to significant preservation in the wastes of valuable biologically active substances. Steam distillation due to the formation of water phase led to extraction and loss of some of the substances. The investigated approach of treatment of the wastes with ethanol and obtaining of valuable by-products also have the advantage that it could be combined with further

extraction of the plant residues in order to obtain polysaccharides and thus will lead to a better valorization of the wastes.

Acknowledgement: We acknowledge the financial support from the Fund for Scientific Research of the University of Food Technology - Plovdiv, project 6/15-H.

REFERENCES

1. H. Meizer zu Beerentrup, G. Robbelen, *Fat Sci. Technol.*, **6**, 227 (1987).
2. J. Lin, D. Lee, J. Chang, *Bioresource Technol.*, **184**, 421 (2015).
3. A. Slavov, I. Panchev, D. Kovacheva, I. Vasileva, *Food Hydrocol.*, **61**, 469 (2016).
4. N. Nenov, *Sci. works UFT*, **53**, 195 (2005).
5. M. Kratchanova, M. Gocheva, E. Pavlova, I. Yanakieva, D. Nedelcheva, V. Kussovski, A. Slavov, *Bul. Chem. Commun.*, **40**, 561 (2008).
6. V. Singleton, J. Rossi, *Am. J. Enol. Viticult.*, **50**, 3828 (1965).
7. M. Číž, H. Čížová, P. Denev, M. Kratchanova, A. Slavov, A. Lojek, *Food Control*, **21**, 518 (2010).
8. I. Pawlaczyk, L. Czerchawski, W. Pilecki, E. Lamer-Zarawska, R. Gancarz, *Carbohydr. Polym.*, **77**, 568 (2009).
9. Y. Sato, S. Itagaki, T. Kurokawa, J. Ogura, M. Kobayashi, T. Hirano, M. Sugawara, K. Iseki, *Int. J. Pharmaceut.*, **403**, 136 (2011).
10. H.T.H. Cromack, J.M. Smith, *Ind. Crops Prod.*, **7**, 223 (1998).

ОПОЛЗОТВОРЯВАНЕ НА ОТПАДЪЦИ ОТ *Calendula officinalis* – ПОЛУЧАВАНЕ НА ЕТАНОЛНИ ЕКСТРАКТИ

Н. С. Янчева¹, И. Н. Василева¹, П. Н. Денев², П. В. Лютова¹, С. Е. Митов¹, З. А. Йорданова¹, М. А. Гълъбова¹, И. Н. Панчев³, А. М. Славов^{1*}

¹Катедра Органична химия, Университет по хранителни технологии, бул. „Марица“ 26, 4002, Пловдив, България, e-mail: antons@uni-plovdiv.bg

²Лаборатория по биологично активни вещества, бул. „Руски“ 139, 4000 Пловдив, България

³Катедра Физика, Университет по хранителни технологии, бул. „Марица“ 26, 4002, Пловдив, България

Постъпила на 28 октомври 2016 г.; приета на 21 декември 2016 г.

(РЕЗЮМЕ)

Оползотворяването на отпадъците от хранителната индустрия и селското стопанство е един от основните приоритети в последните години. Едни нови и с голям потенциал като източник на биологично активни вещества отпадъци са тези, получени при преработката на етерично-маслени и медицински растения. Недостатъчно изследвани са отпадъците получени при преработка на цветове *Calendula officinalis* (невен) които са широко използвани в козметиката, както и за получаване на лутеин. Целта на настоящата работа е да се изследва възможността за оползотворяване на отпадъците, получени при преработка на невен. На изследвания са подложени два вида материали – получени след екстракция на цветове невен с фреон (1,1,1,2-тетрафлуороетан) и получени след водно-парна дестилация. Общите полифеноли и антиоксидантната активност на екстрактите са изследвани и е намерено, че екстракцията с фреон запазва до голяма степен полифенолните съединения – отпадъците, получени след екстракция с фреон имат 1543.8 mg/L общи полифеноли в сравнение с 336.5 mg/L за отпадъците от невен, получени след водно-парна дестилация. Подобни резултати са получени и при изследване на антиоксидантната активност – отпадъците след екстракция с фреон показват 15856.2 $\mu\text{mol TE/L}$ (чрез ORAC метода) и 5011.3 $\mu\text{mol GAE/L}$ (по HORAC метода), докато екстрактите, получени от отпадъци на невен, дестилирани чрез водно-парна дестилация имат 5 пъти по-малки стойности. Чрез HPLC са определени индивидуалните фенолни киселини и флавоноиди и е показано, че основните компоненти са хлорогенова и кафеена киселини, и нарингин (от флавоноидите). Чрез GC-MS са изследвани полярните нелетливи метаболити и ароматичните вещества в етанолните екстракти. Резултатите показват, че отпадъците от преработката на цветове невен могат да бъдат един добър източник за получаване на вторични продукти с изразена антиоксидантна активност.

Ключови думи: *Calendula officinalis* (невен), отпадъци, оползотворяване, антиоксидантна активност, полифеноли.

Comparison of physicochemical parameters of pectic polysaccharides from different plant materials

D. V. Markova, I. N. Vasileva, N. S. Yancheva and A. M. Slavov*

Department of Organic Chemistry, University of Food Technologies, 26 Maritza Blvd., Plovdiv 4002, Bulgaria

Received October 28, 2016; Revised December 21, 2016

Physicochemical parameters – degree of methoxylation, purity, molecular weight, foaming, emulsifying and stabilizing properties of pectins derived through consecutive fractional extraction from waste rose petals were investigated and compared with properties of eight commercial and non-commercial pectins. All of the investigated pectins were high molecular weight with molecular masses in the range $1.32 \times 10^4 \div 4.08 \times 10^5$ Da. The polyuronic acid content (purity) was above 50 % except for acid extracted rose pectin. It was found that all of the investigated pectins except the one derived from celery had relatively low foaming and foam-stabilizing properties. Emulsions obtained with acid extracted pectin (Rose A) showed higher transmittance index but it was relatively unstable when mechanically treated. The most stable emulsion was obtained using celery pectin. The present data show that waste rose petals could be used as source for obtaining of pectins with physicochemical properties similar to other well-known pectins.

Key words: pectins, waste rose petals, foams, emulsions.

INTRODUCTION

Pectins are complex structural heteropolysaccharides build mainly by 1,4-linked α -D-galacturonic acid units interrupted by single (1 \rightarrow 2) linked α -L-rhamnose residues [1]. They are commonly found in the middle lamellae of higher plants [1, 2]. Pectins were used successfully for many years in the food and beverage industry as a thickener, emulsifier, texturizer, a colloidal stabilizer and as gelling agent in preparation of jams and jellies [1, 3]. Pectin is usually added in fruit juices, fruit drink concentrates, desserts, baking fruit preparations and dairy products [1].

Apple pomace and citrus peels are the raw materials traditionally used for industrial extraction of pectins [4] because they contain high amounts of pectic substances and are available in abundant supply as residues from fruit juice production [5]. Other sources of pectin were also explored as alternative sources – sugar beet pomace [6], sunflower head residues, olive pomace [1] and mango waste [7]. Pectins were also extracted from potato pulp [6], peach pulp [8], pumpkin pulp [9] and linseed residues [10]. In previous experiments Slavov *et al.* [11] investigated the possibility to extract water soluble pectin from waste rose petals.

The aim of the current research was to investigate and compare the degree of methoxylation, purity, molecular weight, foaming, emulsifying and stabilizing properties of pectins obtained through consecutive fractional extraction

of waste rose petals with pectic polysaccharides derived from well-known commercial (apple pomace, citrus peels) and non-commercial sources (sunflower head residues, celery tubers, carrots and grapefruits).

MATERIALS AND METHODS

Materials

The following pectins were used: from waste rose petals (W-water, C-chelate, A-acid extracted; prepared as described [12]), sunflower heads, apple pomace, carrots, citrus peels, grapefruit peels and celery tubers – prepared by acid extraction according to [7]. Three of the investigated pectins were commercial – two apple (obtained from Obipectin, Switzerland; №6 – low-methoxyl pectin and №8 – high-methoxyl pectin; numbering according to Table 1) and one citrus pectin (obtained from CP Kelco, Germany). All solutions were prepared with deionized water from Milli-Q system. Electrolyte 0.15 M NaCl (Merck) was used for preparation of all the pectin solutions.

Methods

1. Physicochemical characterization

1.1. Degree of methoxylation

The degree of methoxylation (DM) of the pectins was determined according to Kratchanova *et al.* [13].

1.2. Intrinsic viscosity and determination of molecular weight

The viscosimetric measurements of pectic solutions were performed as described by Panchev *et al.* [14].

* To whom all correspondence should be sent.

E-mail: antons@uni-plovdiv.bg

2. Foam and emulsifying properties

2.1. Model foam systems

2.1.1. Foam preparation

In order to eliminate the influence of the protein part co-extracted with pectic polysaccharides, pectins were deproteinized by the Sevage method [15]. Pectins were dissolved (0.6 wt %) by stirring at 45 °C. Foam ability and stability were studied by a stirring/shaking method whipping out 20 ml pectin solution for 60 s in a graduated cylinder. The initial foam volume and the subsequent foam decrease during 60 minutes were monitored. The foam ability was characterized by the volume of the trapped air.

The total volume of pectin solution before (V_1) and after (V_2) whipping, the volume of the formed foam ($V_{\text{foam}0}$) were measured immediately after shaking (at $t = 0$). The foam stability was characterized by the volume of entrapped air, still remaining in the foam after a certain period of time, $t > 0$ (V_{foam}) changed with the time t . All foam tests were performed thrice and the data presented as mean values.

2.1.2. Evaluation of foam capacity

Foam capacity was determined as described by Diniz *et al.* [16] with some modification. Foam capacity (FC) was determined by volume increase (%) immediately after whipping and was calculated by the formula:

$$\text{FC}\% = (V_2 - V_1/V_1) \times 100,$$

where V_2 is the volume of pectin solution after whipping and V_1 is the volume of solution before whipping.

2.1.3. Evaluation of foam stability

Foam stability was determined according to Marinova *et al.* [17] with modification. Foam stability was expressed by the parameter percentage volumetric foam stability, FS % which is defined as:

$$\text{FS}\% = (V_{\text{foam}}/V_{\text{foam}0}) \times 100,$$

where $V_{\text{foam}0}$ was the volume of the formed foam; V_{foam} was the volume of the foam changed with time t . Stability of the foams over time was assessed by measuring the foam volume at 1, 2, 3, 4, 5, 6, 7, 8, 9, 10, 15, 20, 25, 30 and 60 min after stirring.

2.2. Model emulsion systems

2.2.1. Emulsion preparation

Pectins were dissolved (0.6 wt %) by stirring at 45 °C. 20 ml solution (6 mg/ml) was homogenized with 20 ml sunflower oil for 5 min at 50 s⁻¹ using homogenizer (Ultra Turrax IKA T18 Basic, Germany). The dispersity was determined measuring the translucency index (T %) after 10 times dilution, on a Camspec-M 107 spectrophotometer at $\lambda=540$ nm.

2.2.2. Evaluation of emulsifying activity and emulsion stability

Emulsifying activity and emulsion stability of the model systems of the studied pectins were determined as described by Kuncheva *et al.* [18].

Microscopic Test – The microstructure of the emulsions was evaluated by microscope system (microscope CarlZeiss, Germany, equipped with a camera connected to a personal computer) at 100 magnification immediately after preparation.

Centrifugal Test – The emulsion stability was evaluated by centrifugation of 10 ml emulsion at 3000×g (Hettich EBA 20, Germany) for 20 min. The height of the emulsified layer and separated phases were recorded. The emulsifying stability was calculated as a ratio of the height of the emulsified layer and the height of the total content of the tube and multiplied by 100.

Temperature Test – 5 ml of each emulsion was placed in tubes and stored at four temperatures: -18 °C (frozen); 4°C (refrigeration conditions); 25°C (room temperature) and 50°C for 48 hours. After that the height of the emulsified layer and separated phases were recorded. The emulsion stability was calculated as a ratio of the height of the emulsified layer and the height of the total content of the tube and multiplied by 100.

RESULTS AND DISCUSSION

1. Physicochemical characterization of the pectins

Important parameters of pectic polysaccharides which determine their possible application in food industry are their degree of methoxylation, purity and molecular weight. For this reason we analyzed the pectic polysaccharides and the results are presented in Table 1.

From the eleven samples two were high-metoxyl, one was medium-metoxyl and the rest – low-metoxyl pectins. All the pectins had polyuronic acid content (purity) above 50% except the pectic polysaccharides obtained by acid extraction from waste rose petals. The ash content of the pectins was in the range from 0.40 to 5.54 %.

2. Characterization of model foam systems

Foams are important two-phase systems present in numerous colloidal products. Food foams very often contain surface-active agent (usually proteins) which improves the foam-forming and foam-stabilizing properties.

In certain cases food polysaccharides could be used as foaming agents or could be added in order to significantly improve physico-chemical properties of the foams [19, 20]. In this regard we examined the foam-forming abilities of the investigated pectins (Fig. 1).

Table 1. Physico-chemical characteristics of the pectins

№	Type of pectin	DM, %	Purity, %	Viscosity $[\eta]$, dm ³ /g	Molecular weight, Da	Ash content, %
1	Rose W	61.70 ± 0.8	53.97 ± 1.3	0.0975	1.03 x 10 ⁵	5.06
2	Rose C	33.20 ± 0.7	68.72 ± 1.6	0.0362	2.65 x 10 ⁴	4.29
3	Rose A	49.50 ± 0.9	46.22 ± 1.1	0.0683	6.32 x 10 ⁴	5.54
4	Carrot	64.13 ± 0.5	62.85 ± 0.5	0.0416	3.20 x 10 ⁴	4.6
5	Sunflower	28.28 ± 0.4	88.94 ± 0.8	0.0218	1.32 x 10 ⁴	3.31
6	Apple*	34.49 ± 0.7	50.78 ± 1.2	0.1755	2.31 x 10 ⁵	1.77
7	Apple	35.06 ± 1.2	56.23 ± 0.6	0.0515	4.29 x 10 ⁴	3.25
8	Apple*	56.26 ± 0.6	71.29 ± 0.9	0.2663	4.08 x 10 ⁵	1.01
9	Citrus*	14.29 ± 1.3	54.14 ± 1.2	0.0449	3.56 x 10 ⁴	1.62
10	Grapefruit	14.00 ± 0.5	78.33 ± 0.8	0.0253	1.62 x 10 ⁴	0.40
11	Celery	36.13 ± 0.9	56.28 ± 0.7	0.1170	1.32 x 10 ⁵	1.90

* - commercial pectins.

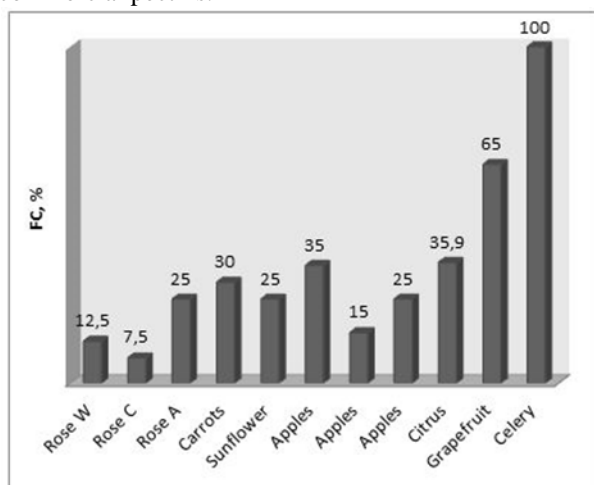


Fig. 1. Foam-forming abilities of the pectins

From the results it could be concluded that with the highest foam-forming ability (> 100 %) is characterized celery pectin, followed by grapefruit – 65 % and citrus pectins (commercial) – 35.9 %. The pectins obtained from waste rose petals showed relatively low foam-forming ability – the one obtained by acid extraction had 25 %, followed by chelate-extracted pectin – 12.5 %. The lowest foam-forming ability showed pectin obtained by aqueous extraction – 7.5 %.

In further experiments, the ability of the polysaccharides to stabilize the resulting foams was investigated and the results for the 30th and 60th minutes are summarized on Fig. 2.

All the investigated pectins showed less than 45 % retained foam volumes after 60 minutes.

The most stable foams were obtained using pectins extracted through consecutive fractional extraction of waste rose petals (Rose W and Rose A samples) – 44.0% after 30 minutes and 1 hour. Nevertheless these results should be interpreted with caution since the initial values of foam ability for these two pectin samples were very low. As a conclusion from the results obtained for the foam

stability it could be said that some of the pectins were able to produce foams but they were not stable over time.

3. Characterization of model emulsion systems

Emulsions are two (or more) phase dispersed colloidal systems. Many foodstuffs exist in the form of emulsions – milk, butter, margarine, mayonnaise etc. In order to avoid the separation between two immiscible phases an emulsifying agent is added. The emulsifying agents have amphiphilic nature (i.e. having both hydrophilic as well as lipophilic moieties) and thus will migrate to, and organize, at the interphase. In practice the most used substances are lecithins, mono- and diglycerides, sucrose esters and polyglycerol esters. Certain biopolymers also possess emulsifying properties – proteins [21], polysaccharides [18] etc. Therefore it was of interest to investigate and compare the emulsifying properties of the pectic polysaccharides from different sources.

Until now there were no data presented about the emulsifying properties of pectins obtained from waste rose petals. Emulsion systems type oil/water (O/W – 1:1) were prepared. The microstructure of the emulsions was monitored by direct observation and comparing the structures of all emulsions it was found that the celery pectin gave the best quality emulsion system (equally dispersed droplets) – Fig. 3.

In the images the oily dispersed phase can be seen as areas of irregular shape (Fig. 3a, b and c) or spheres (Fig. 3d) which suggest that the emulsion prepared with celery pectin is the most stable. Generally emulsions prepared using rose pectins are not stable, with large droplets (Rose A), irregular shapes and even for Rose W pectin with distinct phase separation. Of the three types rose pectins the most stable emulsion is the one made with Rose A pectin.

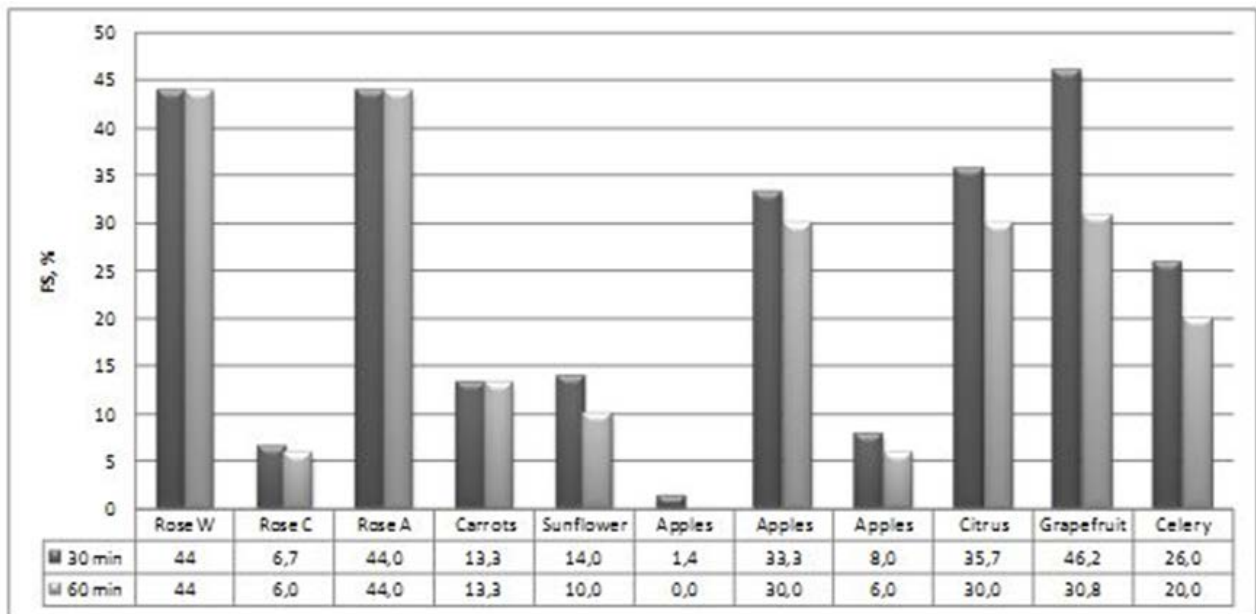


Fig. 2. Foam stabilities

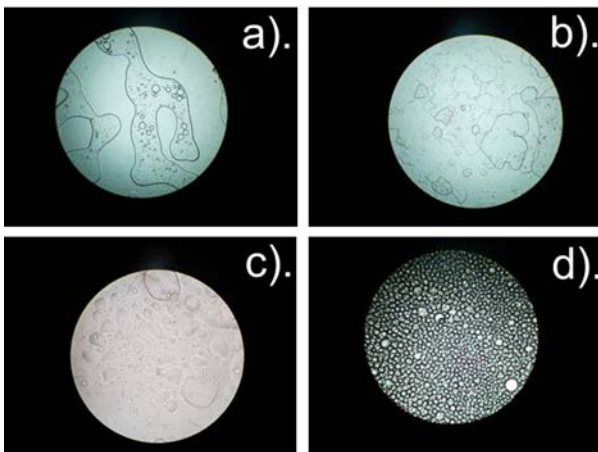


Fig. 3. Images of the structures of model O/W emulsions prepared with 0.6% pectin solutions: a). Rose W; b). Rose C; c). Rose A and d). Celery

Table 2. Emulsion stability and light transmittance of 50 % O/W emulsions

№	Type of pectin	Separated phases, %			T, %
		Oil	Water	Emulsion	
1	Rose W	2.0 ± 0.1	44.5 ± 1.2	53.0 ± 0.6	33.6 ± 1.2
2	Rose C	8.0 ± 0.2	36.5 ± 1.3	55.0 ± 0.8	48.9 ± 2.3
3	Rose A	3.8 ± 0.1	24.0 ± 0.8	72.1 ± 1.1	5.8 ± 0.9
4	Carrot	8.2 ± 0.3	39.8 ± 1.5	52.0 ± 0.6	26.9 ± 2.8
5	Sunflower	2.0 ± 0.1	46.0 ± 0.7	52.0 ± 1.1	98.0 ± 1.9
6	Apple	2.3 ± 0.2	44.4 ± 1.1	53.3 ± 0.9	78.0 ± 2.6
7	Apple	6.1 ± 0.1	40.8 ± 0.9	53.1 ± 1.1	28.6 ± 1.2
8	Apple	4.7 ± 0.3	44.2 ± 1.5	51.2 ± 0.8	19.8 ± 1.3
9	Citrus	4.3 ± 0.2	47.9 ± 1.1	47.9 ± 0.7	76.8 ± 2.4
10	Grapefruit	5.4 ± 0.1	59.5 ± 0.8	35.1 ± 1.3	51.7 ± 1.8
11	Celery	4.9 ± 0.2	42.6 ± 0.7	52.5 ± 0.9	19.6 ± 0.8

Furthermore the quality and stability of the emulsions was examined by measuring the light transmittance index (T, %) and carrying out centrifugal test. The results obtained are presented in Table 2.

All the emulsions subjected to mechanical treatment showed separation to a certain extent and formation of oil and water phases.

The emulsion with the highest retain O/W phase was obtained using Rose A (72.1 %) but from the microscopic observations it is seen that the droplets are not as fine as the emulsion obtained with the celery pectin. The lowest separated oil phase had emulsion with sunflower pectin but it shows also formation of high amount of water phase. This emulsion has the highest light transmittance (98.0%), meaning quickly disrupting emulsion. The emulsion obtained from Rose A pectin has the lowest light transmittance (5.8 %).

An important parameter influencing the stability of emulsions is the temperature of their storage. For this reason they were stored 48 hours (Table 3) at four temperatures (-18° C, 5 °C, 20 °C and 50 °C) which were chosen because they are similar to temperatures usually used for storage of foodstuffs. Storing the emulsions under refrigeration (5 °C) and ambient temperature (20 °C) results in the smallest degree of separation (largest % saved O/W emulsion). When the emulsions were frozen (-18 °C.) and subsequently thawed this often caused phase reversion (O/W in a W/O emulsion) or increased the percentage of water and oil phases. This kind of inversion was observed for emulsions obtained with apple (sample № 7 and 8), citrus and grapefruit pectins. Increase of temperature to 50 °C led in most cases to small increase of disruption of emulsions compared to 20 °C.

Stabilities of emulsions prepared with pectins from waste rose petals and celery were compared. At -18°C the emulsions were the least stable and were disrupted except for the celery pectin emulsion which showed equal stability (over 80%

retained O/W phase). The smallest changes of the investigated rose pectins the highest emulsion emulsions were observed under ambient (20 °C) stability was observed with rose C pectin. and refrigeration (5 °C) conditions. From the three

Table 3. Temperature test of emulsions stored for 48 hours at -18 °C, 5 °C, 20 °C and 50 °C.

Pectin	t_s , °C	Water	O/W emulsion	W/O emulsion	Oil
1. Rose W	-18 °C	44.9 ± 1.3	8.2 ± 1.1	0.0	46.9 ± 1.0
	5 °C	33.3 ± 0.9	66.7 ± 0.7	0.0	0.0
	20 °C	30.6 ± 0.8	67.3 ± 0.9	0.0	2.0 ± 0.3
	50 °C	34.7 ± 1.2	65.3 ± 0.6	0.0	0.0
2. Rose C	-18 °C	76.0 ± 1.5	24.0 ± 1.5	0.0	0.0
	5 °C	22.4 ± 1.0	77.6 ± 0.8	0.0	0.0
	20 °C	20.0 ± 0.8	80.0 ± 0.9	0.0	0.0
	50 °C	37.5 ± 0.7	62.5 ± 0.4	0.0	0.0
3. Rose A	-18 °C	37.7 ± 1.5	54.7 ± 1.7	0.0	7.5 ± 0.9
	5 °C	22.0 ± 1.1	78.0 ± 0.6	0.0	0.0
	20 °C	25.5 ± 0.5	74.5 ± 1.1	0.0	0.0
	50 °C	40.4 ± 0.7	59.6 ± 0.7	0.0	0.0
4. Carrot	-18 °C	47.9 ± 1.3	52.1 ± 1.1	0.0	0.0
	5 °C	33.3 ± 0.9	66.7 ± 0.6	0.0	0.0
	20 °C	29.2 ± 0.6	70.8 ± 1.8	0.0	0.0
	50 °C	36.0 ± 0.9	60.0 ± 0.7	0.0	4.0 ± 0.6
5. Sunflower	-18 °C	42.3 ± 1.2	44.2 ± 1.1	0.0	13.5 ± 1.1
	5 °C	40.4 ± 0.6	44.7 ± 1.3	0.0	14.9 ± 0.7
	20 °C	44.0 ± 0.7	50.0 ± 0.8	0.0	6.0 ± 0.8
	50 °C	46.0 ± 1.0	34.0 ± 0.9	0.0	20.0 ± 0.7
6. Apple	-18 °C	48.0 ± 1.4	40.0 ± 1.4	0.0	12.0 ± 1.3
	5 °C	43.1 ± 0.9	52.9 ± 0.7	0.0	3.9 ± 0.9
	20 °C	45.1 ± 1.1	54.9 ± 0.6	0.0	0.0
	50 °C	46.9 ± 1.1	46.9 ± 0.9	0.0	6.1 ± 0.4
7. Apple	-18 °C	40.0 ± 1.3	0.0	54.0 ± 1.2	6.0 ± 1.6
	5 °C	34.7 ± 0.9	57.1 ± 1.0	0.0	8.2 ± 0.7
	20 °C	34.0 ± 1.2	58.0 ± 0.9	0.0	8.0 ± 0.8
	50 °C	43.1 ± 0.8	51.0 ± 1.2	0.0	5.9 ± 0.6
8. Apple	-18 °C	38.0 ± 1.0	0.0	22.0 ± 1.0	40.0 ± 1.5
	5 °C	8.0 ± 0.7	92.0 ± 1.6	0.0	0.0
	20 °C	29.2 ± 0.6	70.8 ± 0.7	0.0	0.0
	50 °C	28.6 ± 1.1	71.4 ± 0.8	0.0	0.0
9. Citrus	-18 °C	41.5 ± 1.4	58.5 ± 1.4	0.0	0.0
	5 °C	44.2 ± 0.6	3.8 ± 0.9	44.2 ± 0.9	7.7 ± 0.8
	20 °C	45.1 ± 0.8	49.0 ± 0.8	0.0	5.9 ± 0.8
	50 °C	46.0 ± 0.5	54.0 ± 0.9	0.0	0.0
10. Grapefruit	-18 °C	45.1 ± 1.3	51.0 ± 1.4	0.0	3.9 ± 1.0
	5 °C	34.6 ± 0.4	0.0	57.7 ± 0.4	7.7 ± 0.5
	20 °C	37.3 ± 0.6	0.0	58.8 ± 0.9	3.9 ± 0.9
	50 °C	47.1 ± 1.0	0.0	52.9 ± 1.0	0.0
11. Celery	-18 °C	7.8 ± 0.8	92.2 ± 1.4	0.0	0.0
	5 °C	18.0 ± 1.1	82.0 ± 1.2	0.0	0.0
	20 °C	20.0 ± 0.8	80.0 ± 0.8	0.0	0.0
	50 °C	17.6 ± 0.7	82.4 ± 0.9	0.0	0.0

CONCLUSIONS

For the first time to our knowledge we investigated physicochemical properties of pectins derived through consecutive sequential extraction of waste rose petals and compared them with the properties of known commercial and non-commercial pectins. The results from the

experiments showed that rose pectins have (as most of the investigated pectins except for celery pectin) slight foaming and foam-stabilizing abilities. Concerning the emulsifying properties the highest quality emulsion was obtained with celery pectin. From rose-derived pectins the highest emulsifying ability showed acid extracted pectin (Rose A) but its emulsions were relatively unstable. The highest

emulsion stability was observed using celery pectin. The present data showed that waste rose petals are promising source for obtaining of pectins with physico-chemical properties similar to other commercial and non-commercial pectins.

Acknowledgement: We acknowledge the financial support from the Fund for Scientific Research of the University of Food Technology - Plovdiv, project 6/14-H.

REFERENCES

1. J.A. Lopes da Silva, M.A. Rao, in: Food Polysaccharides and Their Applications, IInd edition, A. M. Stephen, G. O. Phillips, P. A. Williams (eds.) Taylor & Francis Group, Boca Raton, 2006, p. 353.
2. A. Slavov, M. J. Crépeau, S. Durand, C. Garnier, J. F. Thibault, E. Bonnin, in: H. A. Schols, R. G. F. Visser, A. G. J. Voragen (eds.) Pectins and pectinases. Wageningen Academic Publishers, Wageningen, 2009, p. 127.
3. M. Jindal, V. Kumar, V. Rana, A.K. Tiwary, *Carbohydr. Polym.*, **93**, 386 (2013).
4. M. F. Sato, D. C. Rigoni, M. H. G. Canteri, C. L. O. Petkowicz, A. Nogueira, G. Wosiacki, *Acta Sci., Agron.*, **33**, 383, (2011).
5. C. D. May, *Carbohydr. Polym.*, **12**, 79, (1990).
6. T. Turquois, M. Rinaudo, F.R. Taravel, A. Heyraud, *Food Hydrocolloids*, **13**, 255, (1999).
7. M. Kratchanova, C. Bénémou, Chr. Kratchanov, *Carbohydr. Polym.*, **15**, 271, (1991).
8. J. Pagán, A. Ibarz, M. Llorca, A. Pagán, G.V. Barbosa-Cánovas, *Food Res. Int.*, **34**, 605, (2001).
9. N. M. Ptitchkina, I. A. Danilova, G. Doxastakis, S. Kasapis, E. R. Morris, *Carbohydr. Polym.*, **23**, 265 (1994). E. I. Díaz-Rojas, R. Pacheco-Aguilar, J. Lizardi, W. Arguëlles-Monal, M. A. Valdez, M. Rinaudo, F. M. Goycoolea, *Food Hydrocolloids*, **18**, 293, (2004).
10. A. Slavov, H. Kyiohara, H. Yamada, *Int. J. Biol. Macromol.*, **59**, 192, (2013).
11. M. Kratchanova, M. Gocheva, E. Pavlova, I. Yanakieva, D. Nedelcheva, V. Kussovski, A. Slavov, *Bulg. Chem. Commun.*, **40**, 561, (2008).
12. M. Kratchanova, A. Slavov, Chr. Kratchanov, *Food Hydrocolloids*, **18**, 677, (2004).
13. I. N. Panchev, A. Slavov, Kr. Nikolova, D. Kovacheva, *Food Hydrocolloids*, **24**, 763, (2010).
14. S. H. Li, Y. X. Sang, D. Zhu, Y. N. Yang, Z. F. Lei, Z. Y. Zhang, *Ind. Crops Prod.*, **50**, 666 (2013).
15. R. S. Diniz, J. S. R. Coimbra, Á. V. N. C. Teixeira, A. R. da Costa, I. J. B. Santos, G. C. Bressan, A. M. C. Rodrigues, L. H. M. da Silva, *Food Res. Int.*, **64**, 157 (2014).
16. K. G. Marinova, E. S. Basheva, B. Nenova, M. Temelska, A. Y. Mirarefi, B. Campbell, I. B. Ivanov, *Food Hydrocolloids*, **23**, 1864, (2009).
17. M. Kuncheva, I. Panchev, K. Pavlova, S. Russinova-Videva, K. Georgieva, S. Dimitrova, *Biotechnol. & Biotechnol. Eq.*, **27**, 5 (2013).
18. A. Svagan, PhD thesis, KTH Chemical Science and Engineering, Stockholm, 2006.
19. J. N. Miquelim, S. C. S. Lannes, R. Mezzenga, *Food Hydrocolloids*, **24**, 398 (2010).
20. V. Norn, Emulsifiers in food technology, 2nd edition, Wiley, Chichester, 2015.

Сравнително изследване на физико-химични параметри на пектинови полизахариди от различни растителни източници

Д. В. Маркова, И. Н. Василева, Н. С. Янчева, А. М. Славов*

Катедра Органична химия, Университет по хранителни технологии, бул. „Марица“ 26, 4002, Пловдив, България, e-mail: antons@uni-plovdiv.bg

Постъпила на 28 октомври 2016 г.; приета на 21 декември 2016 г.

РЕЗЮМЕ

Физико-химичните параметри – степен на метоксилиране, чистота, молекулна маса, пенообразуващи, емулгиращи и стабилизиращи свойства на пектини, получени чрез последователна фракционна екстракция от отдестилирани розови цветове са изследвани и сравнени със свойствата на осем комерсиални и некомерсиални пектинови полизахариди. Всички изследвани проби са високомолекулни полизахариди с молекулни маси от 1.32×10^4 до 4.08×10^5 Da. Полиуронидното съдържание (чистотата) е над 50% с изключение на киселинно-екстрахиран пектин от отпадъчен розов цвят. Намерено е, че всички изследвани пектини с изключение на пектин от целина, имат относително ниски пенообразуващи и пеностабилизиращи свойства. Емулсия, получена с киселинно-екстрахиран пектин от отпадъчен розов цвят, има най-висок индекс на светлопропускливост, но е нестабилна при механични въздействия. Най-стабилни емулсии се получават с пектин от целина. Получените резултати показват, че отпадъчния розов цвят е добър източник за получаване на пектинови полизахариди, чиито физико-химични свойства са сравними с тези на други добре изучени пектини.

Ключови думи: пектини, отпадъчен розов цвят, пени, емулсии.

Synthesis and antibacterial activity of 2-substituted benzothiazoles

Y. Stremski¹, S. Statkova-Abeghe^{1*}, D. Georgiev², P. Angelov¹, I. Ivanov¹

¹University of Plovdiv "Paisii Hilendarski", Department of Organic Chemistry,
24 Tzar Asen Str., 4000 Plovdiv, Bulgaria

²Department of Biochemistry and Microbiology, 24 Tzar Asen Str., 4000 Plovdiv, Bulgaria

Received November 11, 2016; Revised January 01, 2017

Multicomponent amidoalkylation reaction of benzothiazole, alkyl chloroformates and cyclic carbonyl compounds for the synthesis of five 2-substituted benzothiazoles is described. The conditions for chromatographic separation and isolation of the newly synthesized products by column chromatography on silica gel or neutral alumina are established. The isolated crystalline compounds are characterized spectrally and tested for antibacterial activity

Key words: Benzothiazole, Multicomponent reaction, Antibacterial activity

INTRODUCTION

Benzothiazole and its derivatives are important heterocyclic compounds, which are common feature of many natural products and pharmaceutical agents [1]. Benzothiazoles have attracted continuing interest because of their varied biological activities such as anticancer [2], anticonvulsant [3], antiviral [4], antitubercular [5], analgesic [6], anti-inflammatory [7], antidiabetic [8] and other activities. Moreover, 2-substituted benzothiazoles (Figure 1) exhibit activity against both Gram-positive and Gram-negative bacteria [9, 10].

Multicomponent reactions are simple and efficient method in the sustainable and diversity-oriented synthesis of heterocycles with various biological activity [11]. The ease of access to a large number of compounds, combined with high-throughput screening techniques make multicomponent reactions a very important tool in modern drug discovery [12].

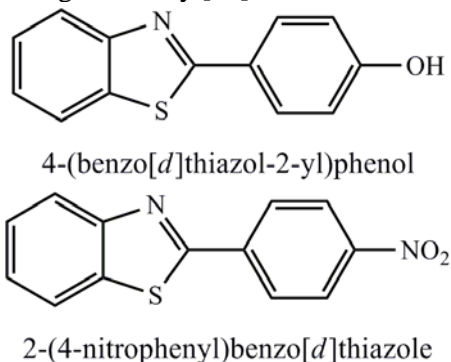
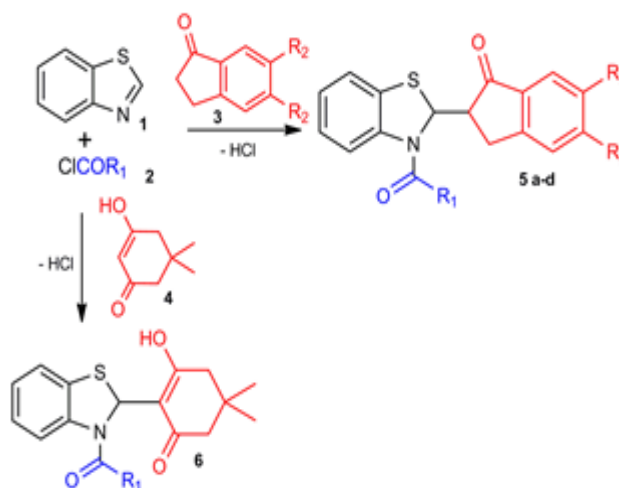


Figure 1. 2-substituted benzothiazoles with antimicrobial activity

This method for performing the reactions offers several advantages, such as simple procedure, short time, clean reaction conditions, simplified purification and good yields [13].

We have previously used N-acyliminium ions derived from various cyclic imines (e.g. 3,4-dihydroisoquinoline, benzimidazole, benzothiazole) and acyl chlorides as electrophilic reagents in intermolecular α -amidoalkylation reactions toward methylene active carbonyl compounds [14–19]. In continuation of our studies on the functionalization of aza-aromatic systems, we herein report a simple and catalyst free method for the direct coupling of cyclic ketones such as 1-indanone, 5,6-methylenedioxy-1-indanone and dimedone with benzothiazole, activated by alkyl chloroformates (Scheme 1).



Scheme 1. One-pot synthesis of 2-substituted benzothiazoles **5 a-d**, **6**

* To whom all correspondence should be sent.
E-mail: stab@uni-plovdiv.bg

EXPERIMENTAL

General information:

Commercial solvents and reagents, such as benzothiazole, alkyl chloroformates and cyclic ketones were purchased from Sigma-Aldrich and were used without further purification. Melting points were determined on a Boetius PHMKO5 hot stage apparatus and are uncorrected. IR and MS spectra were measured on Perkin Elmer 1750 Furie Transform and HRMS "Q-Exative Orbitrap" (Thermo Fisher Scientific, Waltham, MA, USA) spectrometers, respectively. $^1\text{H-NMR}$, $^{13}\text{C-NMR}$ spectra were measured on Bruker Avance AV600 and DRX 300 devices in CDCl_3 and MeOD as solvents. Chemical shifts are given in part per million (ppm) relative to TMS and coupling constants are indicated in Hz. All the NMR spectra were taken at room temperature in CDCl_3 or MeOD. TLC was done on precoated 0.2 mm Merck silica gel 60 plates. Silica gel and neutral alumina were used for column chromatographic separation.

General one-pot procedure for the synthesis of 2-substituted benzothiazoles 5a-d, 6

To benzothiazole (2 mmol) dissolved in 1,2-dichloroethane (5 mL) were added alkyl chloroformate (2 mmol) and the corresponding cyclic ketone (2 mmol). The reaction mixture was stirred for 2 h at 80 °C or 24 h at room temperature (Table 1). After completion of the reaction (monitored by TLC), 30 mL CHCl_3 was added and the mixture was extracted successively with 50 mL 10% HCl, 50 mL 3% Na_2CO_3 and 3x20 mL water. The combined organic layers were dried (Na_2SO_4) and concentrated. After the distillation of the solvent (CHCl_3) the products were purified by column chromatography on silica gel or neutral alumina using mixtures of petroleum and diethyl ether as eluents.

Ethyl-2-(1-oxo-2,3-dihydro-1H-inden-2-yl)benzo[d]thiazole-3(2H)-carboxylate (5 a)

Isolated with eluents petroleum : diethyl ether 8:1, 4:1; Yield: (76 %); M.p.: 127-130 °C;

$^1\text{H-NMR}$ (300 MHz, CDCl_3) (δ , ppm): 1.38 (t, $J = 7.2$, 3H, $\text{CO}_2\text{CH}_2\text{CH}_3$), 3.00 (dd, $^2J = 18$, $^3J = 5.4$, 1H, ArCH_2CH), 3.10 (dd, $^2J = 18$, $^3J = 7.5$, 1H, ArCH_2CH), 3.54 – 3.59 (m, 1H, CH), 4.32 – 4.39 (m, 2H, $\text{CO}_2\text{CH}_2\text{CH}_3$), 6.48 (d, $J = 4.2$, 1H, CH), 6.94 – 7.14 (m, 3H, Ar), 7.34 – 7.40 (m, 2H, Ar), 7.54 – 7.77 (m, 3H, Ar);

$^{13}\text{C-NMR}$ (300 MHz, CDCl_3) (δ , ppm): 14.69, 27.67, 53.75, 62.77, 65.42, 117.54, 122.10, 124.11, 124.38, 125.62, 126.74, 127.71, 123.91, 154.42, 204.41;

m/z $[\text{M}+\text{Na}]^+$ calcd. 362.11, found 362.11; $[\text{2M}+\text{Na}]^+$ calcd. 701.33, found 701.33;

IR (KBr, cm^{-1}): $\nu(\text{C}=\text{O}) - 1703, 1724$, $\nu(\text{C}-\text{O}) - 1268$, $\nu(\text{C}-\text{S}-\text{C}) - 750$, $\nu(\text{Csp}^2-\text{H}) - 2982, 3065$, $\nu(\text{C}\equiv\text{C}) - 1472$

Methyl-2-(1-oxo-2,3-dihydro-1H-inden-2-yl)benzo[d]thiazole-3(2H)-carboxylate (5 b)

Isolated with eluents petroleum : diethyl ether 4:1, 3:1; Yield: (86 %); M.p.: 138-141 °C;

$^1\text{H-NMR}$ (600 MHz, CDCl_3) (δ , ppm): 3.02 (dd, $^2J = 18$, $^3J = 6$, 1H, ArCH_2CH), 3.10 (dd, $^2J = 18$, $^3J = 6$, 1H, ArCH_2CH), 3.58 (br. s, 1H, CH), 3.92 (s, 3H, CO_2CH_3), 6.49 (br. s, 1H, CH), 6.98 – 7.15 (m, 4H, Ar), 7.38 – 7.42 (m, 2H, Ar), 7.58 – 7.79 (m, 2H, Ar);

$^{13}\text{C-NMR}$ (600 MHz, CDCl_3) (δ , ppm): 27.47, 53.42, 117.36, 121.95, 123.96, 124.34, 127.58, 135.06, 136.71, 154.30, 204.50;

m/z $[\text{M}+\text{Na}]^+$ calcd. 348.06, found 348.06, $[\text{M}-\text{H}]^-$ calcd. 324.07, found 324.07;

IR (KBr, cm^{-1}): $\nu(\text{C}=\text{O}) - 1698, 1722$, $\nu(\text{C}-\text{O}) - 1271$, $\nu(\text{C}-\text{S}-\text{C}) - 758$, $\nu(\text{Csp}^2-\text{H}) - 2997$, $\nu(\text{C}\equiv\text{C}) - 1471$

Ethyl-2-(5-oxo-6,7-dihydro-5H-indeno[5,6-d][1,3]dioxol-6-yl)benzo[d]thiazole-3(2H)-carboxylate (5 c)

Isolated with eluent petroleum : diethyl ether 4:1; Yield: (60 %); M.p.: 97-99 °C;

$^1\text{H-NMR}$ (600 MHz, CDCl_3) (δ , ppm): 1.40 (t, $J = 6$, 3H, $\text{CO}_2\text{CH}_2\text{CH}_3$), 2.89 (dd, $^2J = 18$, $^3J = 6$, 1H, ArCH_2CH), 2.97 (dd, $^2J = 18$, $^3J = 6$, 1H, ArCH_2CH), 3.57 (br. s, 1H, CH), 4.33 – 4.40 (m, 2H, $\text{CO}_2\text{CH}_2\text{CH}_3$), 6.06 (d, $J = 6$, 2H, OCH_2O), 6.47 (d, $J = 6$, 1H, CH), 6.77 (s, 1H, Ar), 6.97 – 7.13 (m, 4H, Ar), 7.85 (br. s, 1H, Ar);

$^{13}\text{C-NMR}$ (600 MHz, CDCl_3) (δ , ppm): 14.57, 27.40, 102.35, 102.38, 105.75, 117.33, 124.18, 125.41, 131.40, 148.44, 154.61, 201.96;

m/z $[\text{M}+\text{Na}]^+$ calcd. 406.07, found 406.07;

IR (KBr, cm^{-1}): $\nu(\text{C}=\text{O}) - 1688, 1718$, $\nu(\text{C}-\text{O}) - 1256$, $\nu(\text{C}-\text{S}-\text{C}) - 754$, $\nu(\text{Csp}^2-\text{H}) - 2980, 3056$, $\nu(\text{C}\equiv\text{C}) - 1468$, $\nu(\text{O}-\text{CH}_2-\text{O}) - 2913$

Methyl-2-(5-oxo-6,7-dihydro-5H-indeno[5,6-d][1,3]dioxol-6-yl)benzo[d]thiazole-3(2H)-carboxylate (5 d)

Isolated with eluent petroleum : diethyl ether 4:1; Yield: (81 %); M.p.: 92-94 °C;

$^1\text{H-NMR}$ (600 MHz, CDCl_3) (δ , ppm): 2.79 (dd, $^2J = 18$, $^3J = 6$, 1H, ArCH_2CH), 2.87 (dd, $^2J = 18$, $^3J = 6$, 1H, ArCH_2CH), 3.47 (br. s, 1H, CH), 3.83 (s, 3H, CO_2CH_3), 5.98 (d, $J = 6$, 2H, OCH_2O), 6.36 (br. s, 1H, CH), 6.67 (s, 1H, Ar), 6.88 – 7.04 (m, 4H, Ar), 7.76 (br. s, 1H, Ar);

$^{13}\text{C-NMR}$ (600 MHz, CDCl_3) (δ , ppm): 27.37, 53.42, 102.36, 105.54, 105.75, 111.20, 114.25, 117.31, 120.49, 121.91, 124.30, 125.45, 131.36, 148.45, 154.64, 201.95;

m/z [M+Na]⁺ calcd. 392.06, found 392.06;

IR (KBr, cm⁻¹): ν(C=O) – 1694, 1719, ν(C-O) – 1258, ν(C-S-C) – 747, ν(Csp²-H) – 2954, ν(C=C) – 1472, ν(O-CH₂-O) – 2918

Ethyl-2-(4,4-dimethyl-2,6-dioxocyclohexyl)benzo[d]thiazole-3(2H)-carboxylate (6)

Isolated with eluent petroleum:diethyl ether 4:1; Yield: (67 %); M.p.: 160-161 °C;

¹H-NMR (300 MHz, MeOD) (δ, ppm): 1.04 (s, 6H, 2xCH₃), 1.26 (t, J = 7.2, 3H, CO₂CH₂CH₃), 2.27 (s, 4H, 2xCH₂), 4.17 (q, J = 7.2, 2H, CO₂CH₂CH₃), 6.87 (s, 1H, CH), 6.88 – 6.91 (m, 1H, Ar), 6.96 – 7.03 (m, 2H, Ar), 7.72 (d, J = 7.8, 1H, Ar);

¹³C-NMR (300 MHz, MeOD) (δ, ppm): 14.78, 28.26, 32.89, 58.99, 63.01, 116.41, 117.16, 121.71, 124.10, 125.32, 131.15, 154.37;

m/z [M+Na]⁺ calcd. 370.11, found 370.11, [2M+Na]⁺ calcd. 717.32, found 717.32

IR (KBr, cm⁻¹): ν(C=O) – 1708, ν(C-O) – 1247, ν(C-S-C) – 738, ν(Csp²-H) – 2995, 3064, ν(C=C) – 1472

Antibacterial studies:

The antibacterial effect of the synthesized products against clinically isolated Gram-positive and Gram-negative bacteria – *Bacillus licheniformis* ATCC 14580, *Bacillus cereus* ATCC 11778, *Staphylococcus aureus* ATCC 6538P and *Escherichia coli* ATCC 8739 was studied. For this purpose the method described by Marinova et al. was used [20]. The substance was dissolved in 50 % DMSO solution and added to the growing media in series of twofold decreasing concentrations between 50 – 0.012 ppm. 200 μl of each dilution were inoculated in an amount of 1 × 10⁶ CFU (Colony-forming unit) for various bacteria and transferred in microplates. The plates were cultivated at 37 °C for 18 – 20 h. The growing media used for the cultivation of the test microorganisms was Muller-Hinton broth. The optical density of the samples was read at the end of the cultivation period with (λ = 600 nm) against inoculated media.

RESULTS AND DISCUSSION

Our primary aim was to develop an efficient multicomponent one-pot procedure for the synthesis of benzothiazole derivatives through the reaction of benzothiazole (1), alkyl chloroformates (2) and cyclic ketones (3, 4) and to study their antibacterial activity. The results are shown in Table 1. The reaction conditions were optimized by varying parameters such as solvent, temperature

and time. Using the optimized conditions, the reactions were carried out in dry dichloroethane for 2 h at reflux temperature (80 °C) for the reaction with 1-indanone and 24 h at room temperature for 5,6-methylenedioxy-1-indanone and dimedone, respectively. As shown in Table 1, the reaction worked well with different cyclic ketones and the desired compounds were obtained in good yields. Even though the analysis of the crude products suggests that mixtures of diastereoisomers are formed in these reactions, we only managed to isolate single diastereoisomers by preparative column chromatography (yields given in Table 1). Particularly striking example is **5b** where the TLC of the reaction mixture showed two products in nearly 1:1 ratio, but only one of these was isolated after column chromatography. Most likely this is due to epimerisation process taking place in the chromatography column. Such epimerization is plausible, considering the CH-acidity of the product and the possibility for enolisation at one of the stereogenic centers. The determination of the relative configuration of the isolated products proved difficult and was not accomplished.

The ¹H-NMR spectra of compounds (**5 a-d**) exhibited a distinctive set of two doublet of doublets (dd) in the range of δ = 2.79 – 3.10 ppm for diastereotopic protons from benzylic CH₂ group adjacent to the newly formed stereogenic center.

All products (Table 1) were purified by column chromatography and characterized by IR, ¹H-NMR, ¹³C-NMR and ESI-MS analysis.

The synthesized benzothiazole derivatives were evaluated for antibacterial activity. The antibacterial activity of the compounds was examined via agar diffusion method with concentration of the compounds 100 μg. Effect on Gram-negative bacteria *Escherichia coli* and Gram-positive *Bacillus licheniformis*, *Bacillus cereus*, *Staphylococcus aureus* was measured.

Table 1. Synthesis of benzothiazole derivatives (**5 a-d**, **6**)

Product	R ₁	R ₂	Reaction conditions (Time/ Temperature)	Yields %	M. p. °C
5 a	OEt	H	2 h / 80 °C	76	127–130
5 b	OMe	H	2 h / 80 °C	86	138–141
5 c	OEt	OCH ₂ O	24 h / r.t.	60	97–99
5 d	OMe	OCH ₂ O	24 h / r.t.	81	92–94
6	OEt	-	24 h / r.t.	67	160–161

Table 2. Test results for antibacterial activity of compounds (**5 a-d**, **6**)

Products (5, 6)	Microorganisms (sterile zone, mm)	MIC mg/ml
5 a	<i>Bacillus licheniformis</i> - 19	0.027
	<i>Escherichia coli</i> - 22	0.055
5 b	Shows no activity	-
5 c	<i>Bacillus licheniformis</i> - 18	0.027
	<i>Escherichia coli</i> - 22	0.060
5 d	Shows no activity	-
6	<i>Bacillus cereus</i> - 10	0.031
	<i>Staphylococcus aureus</i> - 12	0.031

The highest activity against *Escherichia coli* and *Bacillus licheniformis* showed compounds (5a, 5c) - MIC 0.027 – 0.060 mg/ml. Compound (6) displayed antibacterial activity against *Bacillus cereus* and *Staphylococcus aureus* – MIC 0,031 mg/ml (Table 2).

CONCLUSIONS

An efficient method for multicomponent synthesis of 2-substituted benzothiazole derivatives is demonstrated. The presented methodology offers several advantages, such as simple procedure, clean reaction and good yields. Three of the newly synthesized compounds showed moderate activity against both Gram-positive and Gram-negative bacterial strains.

Acknowledgements: We acknowledge financial support from the Fund for scientific research of Plovdiv University - NI 15 FC 001. The work was supported by the Bulgarian Ministry of Education and Sciences, Grant DKOF7RP02/20 and EC FP7 REGPOT Project BioSupport. The authors are thankful to Dr. M. Naydenov, University of Plovdiv, Faculty of Biology, Department of Plant Physiology and Molecular Biology, too, for the technical support in the mass spectral characterization

REFERENCES

1. R. S. Keri, M. R. Patil, S. A. Patil, S. Budagumpi, *Eur. J. Med. Chem.*, **89**, 207, (2015).
2. S. T. Huang, I. J. Hsei, C. Chen, *Bioorg. Med. Chem.*, **14**, 6106 (2006).
3. N. Siddiqui, S. N. Pandeya, S. A. Khau, J. Stables, A. Rana, M. Alam, F. M. Arshad, M. A. Bhat, *Bioorg. Med. Chem.*, **17**, 255 (2007).
4. T. Akhtar, S. Hameed, N. Al-Masoudi, R. Loddo, P. Colla, *Acta Pharm.*, **58**, 135 (2008).

5. F. J. Palmer, R. B. Trigg, J. V. Warrington, *J. Med. Chem.*, **14**, 248 (1971).
6. N. Siddiqui, M. Alam, A. A. Siddiqui, *Asian J. Chem.*, **16**, 1005 (2004).
7. B. M. Gurupadaya, M. Gopal, B. Padmashali, V. P. Vaidya, *Ind. J. Heterocy Chem.*, **15**, 169 (2005).
8. S. R. Pattan, C. Suresh, V. D. Pujar, V. V. K. Reddy, V. P. Rasal, B. C. Koti, *Ind. J. Chem.*, **44B**, 2404 (2005).
9. P. Bandyopadhyay, M. Sathe, S. Ponmariappan, A. Sharma, P. Sharma, A. K. Srivastava, M. P. Kaushik, *Bioorg. Med. Chem. Lett.*, **21**, 7306 (2011)
10. P. S. Yadav, Devprakash, G. P. Senthilkumar, *J. Pharm. Sci. Drug Res.*, **3**, 1 (2011).
11. D. M. D'Souza, T. J. J. Müller, *Chem. Soc. Rev.*, **36**, 1095 (2007).
12. (a) J. Zhu, H. Bienayne, (eds.) Multicomponent Reactions; Wiley-VCH: Weinheim, 2005, p. 1; (b) A. Dömling, I. Ugi, *Angew. Chem. Int. Ed. Engl.*, **39**, 3168 (2000); (c) H. Bienaymé, C. Hulme, G. Oddon, P. Schmitt, *Chem. Eur. J.*, **6** 3321 (2000); (d) L. Weber, *Drug Discovery Today*, **7**, 143 (2002).
13. M. T. Maghsoodlou, M. Karima, M. Lashkari, B. Adrom, N. Hazeri, *Bulg. Chem. Commun.*, **48**, 369 (2016).
14. A. Venkov, S. Statkova-Abeghe, *Synth. Commun.*, **26**, 2135 (1996).
15. M. Staykova, S. Statkova-Abeghe, P. Angelov, I. Ivanov, *Arkivoc*, **IV**, 126, (2013).
16. S. Statkova-Abeghe, I. Ivanov, St. Nikolova, *Union of Scientists in Bulgaria – Plovdiv, Scientific session – Technics and Technologies, Natural Sciences and the Humanities*, **5**, 38 (2004).
17. S. Statkova-Abeghe, I. Ivanov, M. Staykova, St. Nikolova, *Annual of University of Shumen "Konstantin Preslavsky"*, *Natural sciences - Chemistry*, **XXB2**, 151 (2010).
18. S. Statkova-Abeghe, D. Georgiev, I. Ivanov, St. Nikolova, *University of Plovdiv "Paisii Hilendarski"*, *Scientific papers - Chemistry*, **34**, 95 (2006).
19. S. Statkova-Abeghe, A. Donova, A. Venkov, *University of Plovdiv "Paisii Hilendarski"*, *Scientific papers - Chemistry*, **31**, 37 (2002).
20. P. Marinova, M. Marinov, Y. Feodorova, M. Kazakova, D. Georgiev, V. Lekova, P. Penchev, N. Stoyanov, *Compt. rend. Acad. bulg. Sci.*, **67**, 513 (2014).

СИНТЕЗ И АНТИБАКТЕРИАЛНА АКТИВНОСТ НА 2-ЗАМЕСТЕНИ БЕНЗОТИАЗОЛИ

Й. Стремски¹, С. Статкова-Абегхе^{1*}, Д. Георгиев², П. Ангелов¹, И. Иванов¹

¹Пловдивски Университет „Паисий Хилендарски”, Катедра Органична химия,
ул. Цар Асен, 24, 4000 Пловдив, e-mail: stab@uni-plovdiv.bg

²Катедра Биохимия и микробиология, ул. Цар Асен, 24, 4000 Пловдив, e-mail: danail_d_g@abv.bg

Постъпила на 11 ноември 2016 г.; приета на 1 януари 2017 г.

(Резюме)

Приложена е мултикомпонентна реакция на амидоалкилиране между бензотиазол, алкилхлороформиати и циклични карбонилни съединения. Успешно са синтезирани пет 2-заместени бензотиазолови производни с добри добиви (от 60 до 86 %). Намерени са условия за хроматографско разделяне и изолиране на новополучените съединения с разпределителна течностно-течна колонна хроматография на силикагел или неутрален алуминиев оксид. Изолираните кристални съединения са спектрално охарактеризирани с инфрачервена, ЯМР-спектроскопия и МАС-спектрометрия.

Изследвана е антибактериалната активност на синтезираните съединения с диск-дифузионен метод срещу четири щама микроорганизми - грам-отрицателни бактерии *Escherichia coli* ATCC 8739 и грам-положителни *Bacillus licheniformis* ATCC 14580, *Bacillus cereus* ATCC 11778, *Staphylococcus aureus* ATCC 6538P.

Ключови думи: Бензотиазол, Мултикомпонентна реакция, Антибактериална активност

Human exposure to some toxic and essential elements through freshwater fish consumption in Bulgaria

K. Peycheva, L. Makedonski, M. Stancheva

Medical University Varna, Department of Chemistry, 84 Tzar Osvoboditel Blv, Bulgaria

Received November 10, 2016; Revised December 15, 2016

Human exposure to As, Cd, Cu, Cr, Mn, Fe, Ni, Zn and Pb through consumption of freshwater fishes (carassius, freshwater bream, common roach and European crap) was estimated by evaluation of target hazard quotient (THQ), target risk (TR), and hazard (HI) indexes. The elements were determined by ICP-OES.

The results from this study show that the THQ for the studied toxic and essential microelements are less than one; signified that a daily exposure at this level is unlikely to cause any adverse effects during a person lifetime. Additionally hazard index of each microelement was also lower than one suggesting that these pollutants pose no hazard to local residents. The TR values were between 10^{-6} and 10^{-4} meaning that there is no important cancer risk associated with the consumption of the examined in the present study fish species.

Key words: toxic/essential elements, freshwater fishes, THQ, HI, Mandra Lake

INTRODUCTION

Fish consumption entails important potential health benefits such as lowering the risk of cardiovascular diseases. However, fish may also be a source of environmental contaminants. Exposure to these contaminants could imply health risks, especially for the more vulnerable consumer groups, such as pregnant women and children [1].

Heavy metals tends to accumulate in advanced organisms through bio-magnification effects in the food chain. Thus, they can enter into human body, and accumulate in the human tissues to pose chronic toxicity. Chronic assimilation of heavy metals is known cause of cancer [2] and can damage vital organ functions. Accumulation of heavy metals in the food web can occur either by accumulation from the surrounding medium, such as water or sediment, or by bioaccumulation from the food source [3]. In the aquatic environment, heavy metals in dissolved form are easily taken up by aquatic organisms where they are strongly bound with sulfhydryl groups of proteins and accumulate in their tissues. The accumulation of heavy metals in the tissues of organisms can result in chronic illness and cause potential damage to the population [4].

Heavy metals can be classified as potentially toxic (arsenic, cadmium, lead, mercury, nickel, etc.), probably essential (vanadium, cobalt) and essential (copper, zinc, iron, manganese, selenium) [5]. The essential metals can also produce toxic effects when the metal intake is excessively elevated. Fish accumulates heavy

metals in its tissues through absorption and human can be exposed to metals via food web. This will cause acute and chronic effect to human [6]. For the estimation of the potential risks to human health of heavy metals in fishes, several ways have been adopted such as calculating the carcinogenic and non-carcinogenic effects. Risk assessment is one of fastest method which is need to evaluate the impact of the hazards on human health and also need to determine the level of treatment which are tend to solve the environmental problem that occur in daily life [7]. Current non-cancer and cancer risk assessment methods do not provide quantitative estimate of the probability of experiencing non-cancer and cancer effects from contaminant exposure. These method are typically are based on the Target Hazard Quotients (THQ) and Hazard Index (HI).

The purpose of this study is to determine the concentration of some heavy metals such as As, Cd, Cu, Cr, Mn, Fe, Ni, Zn and Pb in four freshwater fish species habitat in Bulgarian Mandra lake, which is directly connected with Black Sea basin. By using the target quotient (THQ) and hazard index (HI), health risk associated with heavy metals in these fishes was evaluated.

MATERIALS AND METHODS

Study Sites

Mandra Lake, is a large freshwater lake in South Eastern Bulgaria, located south of Burgas. It is the southernmost of the three Burgas lakes with water surface area of about 1,300 hectares. Its length is 8 km and its maximum width is 1.3 km. It is situated

* To whom all correspondence should be sent.
E-mail: peycheva@hotmail.com

in a well-shaped river valley, oriented perpendicular to the beach and the mouth and the dam are near the southern end of Burgas. Four rivers flow into the lake. This area was selected due to rapid growth of development which are mixed development area comprises residential, commercial, small and medium enterprises and industry.

Field sampling

The freshwater fish samples analyzed in this study are carassius (*Carassius auratus*), freshwater bream (*Abramis brama*), common roach (*Rutilus rutilus*) and European crap (*Cyprinus carpio*). Fish sample was collected from a single fisherman in order to assure regularity in fishing methods. The fish was collected from selected points and transported to the laboratory on the same day in the pre-cleaned polyethylene bags. Total length and weight of the sample brought to laboratory on ice after collection were measured to the nearest millimeter and gram before dissection. All samples were frozen and stored at -18°C immediately upon returning from the field.

Sample Digestion and Instrumental Analysis

Approximately 1.0 g of homogenized muscle tissues sample was digested with 10 cm³ HNO₃ (ultra-pure Merck® Darmstadt, Germany) in a digestion system and diluted to final volume of 25 cm³ with double deionised water. MARS 6 Microwave Sample Preparation System (CEM Corporation, USA) delivering a maximum power and temperature of 800 W and 200 °C, respectively, and internal temperature control, was used to assist the acid digestion process.

One reagent blank for each digestion was included as a representative standard reference, homogeneity and process efficacy in sample replicated. The digested sample was transferred to a marked flask post-cooling.

All fish samples were analyzed for As, Cd, Cu, Cr, Mn, Fe, Ni, Zn and Pb using an Inductively

Coupled Plasma Optical Emission Spectroscopy (ICP-OES). ICP-OES model used in this study was Optima 8000 (Perking Elmer, USA). The instrument working parameters were as follows: plasma gas flow - 10 L/min, auxiliary gas flow - 0.4 L/min, nebulizer gas flow - 0.6 L/min, peristaltic pump flow rate - 1.5 ml/min, spray chamber - cyclonic glass, nebulizer - concentric glass, MEINHARD® Type C. Results were quantified using an calibration curve generated from the responses obtained from multiple dilutions of a multi-element calibration standard prepared (Optima Family Multi-Element Standard, Matrix per Volume: 2% HNO₃). Analytical quality control included analysis of a 2 % ultrapure HNO₃ blank and a sample duplicate from the microwave digestion.

A DORM-2 (NRCC, Ottawa) certified dogfish tissue was used as the calibration verification standard. Recoveries between 90% and 108% were accepted to validate the calibration.

RESULTS AND DISCUSSION

As, Cd, Cu, Cr, Mn, Fe, Ni, Zn and Pb levels in fish species

The concentration of different metals (mg/kg wet weight) in the edible portion of fishes subject to this study are given in Table 1.

There are significant differences on the concentration presents for the heavy metals for Cd, Cr, Cu, Fe, Mn, Ni, Pb and Zn for the different fish species.

Among the heavy metals studied, Zn showed the highest level of accumulation. Tüzen observed a similar trend in his studies about some marine fishes in the Turkish part of Black Sea [8]. In a study performed in the muscle of five common Slovak fish species the lowest mean Zn concentration was detected in Wels catfish (4.61 mg/kg w.w) and the highest mean zinc

Table 1. Mean concentrations (mg/kg w.w) and standart deviation of heavy metals for each species (N is the number of analyzed fish species)

	N	As	Cd	Cr	Cu	Fe	Mn	Ni	Pb	Zn
<i>Carassius</i>	3	n.d	0.041± 0.005	0.044± 0.004	0.17± 0.11	2.23± 1.63	0.19± 0.10	0.09± 0.05	0.27± 0.07	6.98± 0.66
<i>Freshwater bream</i>	3	n.d	0.020± 0.001	0.033± 0.004	0.12± 0.11	5.85± 1.97	0.32± 0.03	0.055± 0.004	0.15± 0.02	1.94± 0.16
<i>Common roach</i>	3	n.d	0.046± 0.007	0.05± 0.05	0.11± 0.03	1.68± 0.96	0.19± 0.16	0.11± 0.03	0.25± 0.06	4.99± 1.12
<i>European crap</i>	2	n.d	0.031± 0.001	0.03± 0.01	0.16± 0.01	1.92± 0.15	0.050± 0.005	0.08± 0.01	0.20± 0.02	3.27± 0.06

concentration in common carp (26.30 mg/kg w.w.) with a significant difference in the bioaccumulation of Zn among different fish species [9]. It is well established that accumulation rate of zinc is higher in omnivorous fish than predatory fish. The results from this study are in accordance with the data from literature.

The lowest mean iron concentration (1.68 mg/kg w.w) was found in common roach and highest mean iron concentration (5.85 mg/kg w.w) in freshwater beam. Similar (2.99–4.38 mg/kg w.w) to our values were found in muscle of five fish species from the Erren River [10]; in five fish species from the Candamo River (Peru) [11] and from 3.70 to 21.10 mg/kg w.w for five common Slovak fish [9].

Higher level of lead in the blood can cause kidney dysfunction and brain damage. The Pb concentration in this study varies between 0.15 mg/kg w.w for freshwater beam up to 0.27 mg/kg w.w for carassius. In a study performed in Věstonice reservoir in Czech Republic the highest lead concentrations were found in tissues of asp (0.12 mg/kg w.w) and carp (0.09 mg/kg w.w) while the lowest lead concentrations were found in pikeperch tissues (0.01 mg/kg w.w) and in pike gonads (0.03 mg/kg w.w) [12]. The mean lead concentration measured in rainbow trout in Western Anatolia, Turkey is 0.08 mg/kg w.w which is less the values found in this study [13]. According to Bulgarian Food Codex, the maximum lead level permitted for fishes is 0.4 mg/kg [14] and our results are below this value.

The cadmium levels found in this study ranged between 0.020 mg/kg w.w in freshwater beam up to 0.046 mg/kg w.w in common roach. Cd levels in the literature varied between 0.005 mg/kg w.w in carp and pikeperch and 0.01 mg/kg w.w in catfish from Serbian part of Danube River [15]; between 0.003 mg/kg w.w and 0.005 mg/kg w.w in fish muscle in the rivers of Lithuania [16]; and around 0.03 mg/kg w.w for common carp from two ponds in Slovak Republik [9]. The Codex Alimentarius limit for cadmium content in fish muscle is 0.05 mg/kg wet weight. This limit was not exceeded.

Chromium concentrations varied from 0.03 mg/kg w.w (European crap) to 0.05 mg/kg w.w (common roach). Similar results were publishes for the muscle tissies of European crap from two southwestern Slovak fish farms [9]. In carp muscles from the five Bohemian ponds chromium concentrations ranged from 0.56 to 0.69 mg/kg wet weight [17]. High variations of chromium concentrations (5.57–197.12 µg/g dry mass) were found in the muscle of *Labeo umbratus* from the Witbank Dam [18]. Chromium content in fish muscle did not exceeded the limit of Codex

Alimentarius (4.0 mg/kg wet weight) in any of the analysed samples.

Copper concentrations ranged from 0.11 mg/kg w.w for common roach to 0.17 mg/kg w.w for caracuss. Higher copper concentrations were reported in fish from the Atatürk Dam Lake [19, 20]. Similar mean copper concentrations to our results was found in the muscle of *Clarias fucus* from the Duy Minh Lake [21], in the muscle of three fish species from four Taimyr Peninsula Lakes [22], and in muscle of marketable carp (*Cyprinus carpio*) from five south and west Bohemian fish ponds [17]. In this study, none of the analyzed muscle samples exceeded the limit for copper allowed by Bulgarian Food Codex (10.0 mg/kg w.w) [14].

Manganese concentrations in the muscle showed a high variation and amount. Concentrations of manganese fluctuated between 0.05 mg/kg w.w. in European crap and 0.32 mg/kg w.w. in freshwater beam. Similar manganese concentrations were found in the muscle of *Lepisosteus platyrhincus* from the Okeechobee Lake (0.394 µg/g wet weight) [23], and in the muscle of *Lisa abu* and *Silurus triostegus* from the Atatürk Dam Lake (0.40 and 0.35 µg/g w.w., respectively) [19]. The limit for manganese in Codex Alimentarius is not defined but our results are in good agreement with the data found in the literature.

Our results for Ni showed relatively low nickel concentrations, fluctuating between 0.055 mg/kg w.w in freshwater beam and 0.11 mg/kg w.w in common roach. Higher levels (more than 40 times greater than our results) of nickel concentrations were found in the muscle of *Labeo umbratus* from the Witbank Dam [18]. In the muscle of *Silurus triostegus* from Atatürk Dam Lake the mean nickel concentration of 0.56 µg/g wet weight was recorded [19]. Results comparable to ours were published for the muscle of common carp (*Cyprinus carpio*) from the five south and west Bohemian ponds [17]. The Bulgairain Food Codex limit for nickel content in fish muscle is 0.5 mg/kg w.w [14]. Our values are lower than the limit.

Health risk assessment

The THQ [24] which is the ratio between the exposure and the reference dose (RfD), is used to express the risk of non-carcinogenic effects. Ratio of less than 1 signifies non-obvious risk. Conversely, an exposed population of concern will experience health risk if the dose is equal to or greater than the RfD. The method for the determination of THQ was provided in the United States EPA Region III risk-based concentration table [24]. The dose calculations were carried out

using standard assumptions from an integrated United States EPA risk analysis.

A THQ below than one implies that the level of exposure is smaller than the reference dose; a daily exposure at this level is believed to cause any adverse effects during a person's lifetime. The models for estimating THQ is expressed as:

$$THQ = \frac{(M_C \cdot I_R \cdot 10^{-3} \cdot EF \cdot ED)}{(RfD \cdot BWa \cdot ATn)}$$

where M_C is the metal concentration in muscle tissues of fish ($\mu\text{g/g}$), I_R is the mean ingestion rate of fish (5.205 g/day), EF is the exposure frequency (53 day/year) or number of exposure events per year of exposure, ED is the exposure duration, total for adult (70 years for females and 63 years for males), RfD is the reference dose (Cu = 0.04, As = 3×10^{-4} , Zn = 0.3, Ni = 0.02, Cr = 3×10^{-3} , Fe = 9×10^{-3} , Cd = 13×10^{-3} , Pb = 4×10^{-3} , Mn = 0.144 $\mu\text{g/g}$ day), BWa is the body weight, adult (60 kg for females and 68 kg for males kg), and ATn is the averaging time, noncarcinogens and it was calculated by multiplying exposure frequency in exposure duration over lifetime (day/year).

The hazard index [24] from THQs can be expressed as the sum of the target hazard quotients of each individual element:

$$HI = THQ_{As} + THQ_{Cd} + THQ_{Cr} + THQ_{Cu} + THQ_{Fe} + THQ_{Ni} + THQ_{Zn} + THQ_{Pb} + THQ_{Mn}$$

In cases where cancerogenic HI did not exceed one, it was assumed that no chronic risks were likely to occur at the site.

Target cancer risk [24] indicates carcinogenic risks. The model for estimating TR was shown as follows:

$$TR = \frac{(M_C \cdot I_R \cdot 10^{-3} \cdot CPSo \cdot EF \cdot ED)}{(Bwa \cdot ATc)}$$

where $CPSo$ is the carcinogenic potency slope, oral (As = 1.5 and for Ni = 1.7 mg/kg bw-day); ATc is the averaging time, carcinogens (day/years) and was calculated by multiplying exposure frequency in exposure duration over lifetime. TR value for intake of As and Ni was calculated to indicate the carcinogenic risk since Cu, Hg and Zn do not cause any carcinogenic effects.

The theoretical and estimated lifetime target hazard quotients (THQs) for As, Cd, Cr, Cu, Fe, Mn, Ni, Pb and Zn to humans due to exposure to consumption of freshwater fishes from Mandra Lake were calculated and presented in Table 2 and 3.

As it can be seen from the Table 3 and Table 4, the THQs of As, Cd, Cr, Fe, Mn, Ni, Pb and Zn did not exceed the safe value of one.

Also the total THQ means HI was less than one for all fish species (between 0.027 and 0.061 for females and between 0.033 and 0.063 for males) and it demonstrated that ingestion of those fishes subject to this research does not result in over exposure of studies metals. Thus, no adverse effect poses to the health of consumers.

Table 2. Risk values of each metal contaminant of the freshwater fish species (females)

Fish samples	Females										Target Risk (TR)		
	Target hazard quotients (THQs)									Hazard Index (HI)	As	Ni	Pb
	As	Cd	Cr	Cu	Fe	Mn	Ni	Pb	Zn				
<i>Carassius</i>	0.00	0.003	0.001	0.0003	0.021	0.00012	0.0004	0.006	0.002	0.034	0.00	$1.33 \cdot 10^{-5}$	$2.27 \cdot 10^{-5}$
<i>Freshwater bream</i>	0.00	0.002	0.001	0.0003	0.054	0.00019	0.0002	0.003	0.001	0.061	0.00	$7.84 \cdot 10^{-6}$	$1.24 \cdot 10^{-5}$
<i>Common roach</i>	0.00	0.004	0.001	0.0002	0.016	0.00011	0.0004	0.005	0.001	0.028	0.00	$1.52 \cdot 10^{-5}$	$2.10 \cdot 10^{-5}$
<i>European crap</i>	0.00	0.003	0.001	0.0003	0.018	0.00003	0.0003	0.004	0.001	0.027	0.00	$1.14 \cdot 10^{-5}$	$1.65 \cdot 10^{-5}$

Table 3. Risk values of each metal contaminant of the freshwater fish species (males)

Fish samples	Males										Target Risk (TR)			
	Target hazard quotients (THQs)										Hazard Index (HI)	Target Risk (TR)		
	As	Cd	Cr	Cu	Fe	Mn	Ni	Pb	Zn	As		Ni	Pb	
<i>Carassius</i>	0.00	0.003	0.001	0.012	0.018	0.0001	0.0003	0.005	0.002	0.042	0.00	1.06.10 ⁻⁵	1.81.10 ⁻⁵	
<i>Freshwater bream</i>	0.00	0.001	0.001	0.009	0.048	0.0002	0.0002	0.003	0.001	0.063	0.00	6.22.10 ⁻⁶	9.85.10 ⁻⁶	
<i>Common roach</i>	0.00	0.003	0.001	0.008	0.014	0.0001	0.0004	0.005	0.001	0.033	0.00	1.21.10 ⁻⁵	1.66.10 ⁻⁵	
<i>European crap</i>	0.00	0.002	0.001	0.012	0.016	0.00003	0.0003	0.004	0.001	0.035	0.00	9.02E-06	1.31.10 ⁻⁵	

Calculated average value of carcinogenic risk (TR) of carassius, freshwater beam, common roach and European crap was performed for As, Pb and Ni, since only those elements from the analysed ones show carcinogenicity (Table 1 and 2). The values are as follows: between 9.02×10^{-6} and 1.06×10^{-5} for Ni for both males and females and between 9.85×10^{-6} and 1.24×10^{-5} for Pb. Since the total concentration of As is below detection limits for this toxic element TR values are equal to zero. In the literature TR for arsenic and nickel was found to be 8.6×10^{-5} (range, 4.7×10^{-5} , *Labeo rohita* to 1.5×10^{-4} , *Catla catla*) and 4.7×10^{-4} (range, 3.0×10^{-4} , *Oreochromis nilotica* to 5.8×10^{-3} , *Catla catla*), respectively for fishes from Kolkata wetland, India [25].; and between 1×10^{-6} to 1×10^{-4} for Cu, Pb, Ni, Cd and Cr except Zn (6.17×10^{-4}) for cultured *P. hypophthalmus* from India [26]. In a previous study related with Black Sea marine fishes the TR values for As and Ni are as follows: 4.3×10^{-5} for As and 3.57×10^{-7} for Ni [27]. Comparing our values with those stated in the literature and the guidelines values, indicates that analysed fish from Mandra Lake are safe for human consumption.

CONCLUSION

In this study, the selected freshwater fish individuals had metal levels below the guideline values established by different environmental agencies. The estimation of noncarcinogenic risk (THQs) conducted in this study showed that adverse health effects may not occur when considering different fish consumption patterns. Hazard index (HI) of each elements were also lower than one suggesting that these pollutants perhaps pose no hazard to local residents. The target cancer risk (TR) due to As, Pb and Ni exposure through freshwater fish consumption from

Mandra Lake do not have the probability of contracting cancer over a long lifetime in future.

REFERENCES

1. S.Jacobs, I.Sioen, S.D.Henauw, N.Tous, A.L.Maulvault, G.Fait, F.C.Pons, W.Verbeke, *Archives of Public Health*, **72**, P8 (2014)
2. A.Nabawi, B. Heinzow, H.Kruse, *Bulletin of Environmental Contamination and Toxicology*, **39**, 889 (1987)
3. T.Tulonen, M. Pihlstrom, L.Arvola, M. Rask, *Boreal Environmental Resarch.*, **11**, 185 (2006)
4. M.N. Amirah, A.S. Afiza, W.I.W. Faizal, M.H. Nurliyana and S.Laili, *Journal of Environment Pollution and Human Health*, **1**, 1 (2013)
5. R. Munoz-Olivas, C. Camara, *The Royal Society of Chemistry*, 331-353 (2001).
6. A.F.Fidan, H. Cigerci, M. Konuk, I. Kucukkurt, R. Aslan, Y. Dundar, *Environmental Monitoring and Assessment*, **147**, 35 (2008)
7. Y. Zhang, B.Zhang, L.Li, Z.Wang, S.Xie, Y.Shen, J. Li, *Journal Of Materials Chemistry*, **22**, 7775 (2012)
8. M. Tüzen, *Food and Chemical Toxicology*, **47**, 1785 (2009)
9. J.Andrej, I.Stranai, M. Kacaniova, Peter Massanyi, M. Valent, *Journal of Environmental Science and Health, Part A: Toxic/Hazardous Substances and Environmental Engineering*, **41**, 1071 (2006)
10. Y.C Chen, C.Y Chen, H.J Hwang W.B Chang, W.J Yeh, M.H. Chen, *Journal of Food Drug Analysis* **12**, 358 (2005)
11. M.A. Arribère, S. Ribeiro Guevara, R.S. Sánchez, M.I Gil, G. Román Ross, L.E Daurade, V. Fajon, M. Horvat, R. Alcalde, A.J. Kestelman, *Science of the Total Environment*, **301**, 187 (2003)
12. R.Kenšová, O.Čelechovská, J.Doubrovová, Z.Svobodová, *Acta Veterinaria Brno*, **79**, 335(2010)
13. M.Yabanl, A.Yozukmaz, Y.Alparslan, Ü.Acar, *Journal of Food, Agriculture & Environment*, **12**, 165(2014)
14. Anonymous, *State Gazette Bulgaria*, 08 October 2004, Issue 88 (2004).

15. S.Subotić, S.Spasić, Ž.Višnjić-Jeftić, A.Hegediš, J.Krpo-Ćetković, B.Mićković, S.Skorić, M.Lenhardt, *Ecotoxicology and Environmental Safety*, **98**, 196 (2013)
16. T.Virbickas, G. Sakalauskienė, *Acta Zoologica Lituanica*, **16**, 271 (2006)
17. Z.Svobodová, V.Zlabek, O. Celechovská, T. Randák, J. Máchová, J. Kolárová, D. Janousková, *Czech Journal of Animal Science*, **47**, 339 (2002)
18. G. Nussey, J.H.J van Vuren, .H.H. du Preez, *Water SA*, **26**, 269 (2000)
19. H. Karadede, S.A. Oymak, E. Unlu, *Environment International*, **30**, 183 (2004)
20. H. Karadede, E. Unlu, *Chemosphere*, **41**, 1371 (2000)
21. A.Wagner, J. Boman, *Spectrochimica Acta*, **B58**, 2215 (2004)
22. S.M. Allen–Gil, J. Ford, B.K Lasorsa, M. Monetti, T. Vlasova, D.H. Landers, *Science of the Total Environment*, **301**, 119 (2003)
23. J.Burger, E.F Orlando, M. Gochfeld, G.A. Binczik, L.J. Guillette, *Environmental Monitoring and Assessment* **90**, 187 (2004)
24. WHO Evaluation of certain food additives and contaminants. Available from: http://www.who.int/ipcs/publications/ehc/ehc_numerical/en/index.html/
25. K. Bhupander, D.P Mukherjee, *Advances in Life Science and Technology*, **2**, 13 (2011)
26. S.C Strivastava, P. Verma, A.K. Verma, A.K Singh, *International Journal of Fisheries and Aquatic Studies*, **1**, 176 (2014)
27. K. Peycheva, V.Panayotova, M.Stancheva, *International Journal of Fisheries and Aquatic Studies* **4**, 41 (2016)

ОЦЕНКА НА ПРИЕМА НА НЯКОИ ТОКСИЧНИ И ЕСЕНЦИАЛНИ ЕЛЕМЕНТИ ЧРЕЗ КОНСУМАЦИЯ НА СЛАДКОВОДНИ РИБИ В БЪЛГАРИЯ

К. Пейчева, Л. Македонски, М. Станчева

Медицински университет Варна, Факултет по химия,
Бул. Цар Освободител 84, 9000 Варна, e-mail: peytcheva@hotmail.com

Постъпила на 10 ноември 2016 г.; приета на 15 декември 2016 г.

(Резюме)

Оценката на експозицията спрямо As, Cd, Cu, Cr, Mn, Fe, Ni, Zn и Pb е съществен елемент от количествената оценка на риска за човешкото здраве. Рискът, свързан с консумацията на някои сладководни риби, е оценен чрез пресмятане на коефициентите за неканцерогенен риск (THQ), индекс на опасност (HI) и канцерогенен риск (TR). Химичните елементи са анализирани чрез ICP-OES.

Резултатите от това изследване показват, че THQ стойностите за токсичните и есенциални микроелементи са под единица, т.е дневната експозиция при това ниво е малко вероятно да причини нежелани ефекти за целия период на човешкия живот. В допълнение, индексът на опасност за всеки един микроелемент е също под единица, което предполага, че тези замърсители не представляват опасност за местните жители. Стойностите за TR са между 10^{-6} и 10^{-4} , което показва, че не съществува риск от ракови заболявания причинени от консумацията на тези видове сладководни риби.

Ключови думи: токсични метали, сладководни риби, THQ, HI, Езеро Мандра.

Synthesis, structure and nonlinear optical properties of tellurium oxide – bismuth oxide – boron oxide glasses

T. R. Tasheva* and V. V. Dimitrov

Department of Silicate Technology, University of Chemical Technology and Metallurgy,
8 Kl. Ohridski Blvd., Sofia 1756, Bulgaria

Received November 7, 2016; Revised January 3, 2017

TeO₂-Bi₂O₃-B₂O₃ glasses are prepared using a conventional melt-quenching method. The polarizability approach based on the Lorentz-Lorenz equation is applied and the optical basicity and the oxide ion polarizability are estimated. The glasses possess relatively high values of the optical basicity (0.734-0.936) and the electronic oxide ion polarizability (1.785-2.276 Å³). The theoretical refractive index of the glasses is also estimated. On this basis the third order nonlinear optical susceptibility of the glasses is established using generalized Miller's rule. The glasses possess comparatively high third order nonlinear optical susceptibility in the 0.64-2.31x10⁻¹³ esu range. The chemical bonding of the glasses is elucidated on the basis of the interaction parameter and the single bond strength of an average cation-oxide ion (M-O) bond. It is found that the glasses possess relatively low values for the average single bond strength (352-254 kJ/mol) and low values of the interaction parameter (0.051-0.028 Å⁻³). These results indicate for the presence of weak chemical bonds which are formed between TeO₄, TeO₃, BiO₆, BO₄ and BO₃ groups confirmed by IR spectral analysis.

Key words: Oxide glasses, polarizability, optical basicity, chemical bonding, IR spectra, nonlinear optical materials

INTRODUCTION

Nonlinear optical materials are attracted much attention because of their importance for the development of optical information processing technology. Since optical nonlinearity is caused by electronic polarization of a material upon exposure to intense light beams, the electronic polarizability is one of the most important properties which govern the nonlinear response of the material. The estimation of the electronic polarizability of ions is subject of the so called polarizability approach which is well known especially in the field of glass science [1]. During the past two decades numerous oxide glasses were investigated by means of the polarizability approach with aim to explain the origin of optical nonlinearity. It was established that bismuthate and tellurite glasses possess high optical nonlinearity and have possible application as nonlinear optical materials [2].

Tellurite glasses have attracted much scientific and practical attention due to their unique combination of properties such as low melting temperatures, chemical durability and stability, high dielectric constant, low phonon energy, broad optical transmission window and high linear and nonlinear refractive indices. In this respect TeO₂-based glasses are promising optical materials for up-conversion lasers and nonlinear optical materials

exhibiting high second and third order nonlinear optical susceptibility [3-6].

Bismuthate glasses are of great interest also because of their potential for the application in the field of optoelectronics and nonlinear optics as photonic switches and third harmonic generation (THG) materials due to their low melting temperatures, extensive glass formation range, physical stability, high refractive index and high nonlinear optical susceptibility [7-9].

Recently, the optical properties and structure of TeO₂-Bi₂O₃-B₂O₃ glasses have been studied [10-12]. Hasegawa [10] has found that the glasses possess high refractive index, high optical basicity and high third order nonlinear optical susceptibility. Zhao *et al.* [11] have applied the polarizability approach and have investigated the structure of the glasses by means of Raman spectroscopy and XPS spectroscopy. Azuraida *et al.* [12] have made comparative studies of bismuth and barium borotellurite glasses and have concluded that the addition of Bi₂O₃ in boro-tellurite glasses improves the optical properties.

The purpose of the present study is to synthesis of novel TeO₂-Bi₂O₃-B₂O₃ glasses and to apply the polarizability approach to them. The structure of the glasses by means of IR-spectroscopy is also investigated.

* To whom all correspondence should be sent.

E-mail: tina.tasheva@gmail.com

EXPERIMENTAL

Glasses in the ternary $\text{TeO}_2\text{-Bi}_2\text{O}_3\text{-B}_2\text{O}_3$ system were prepared using a conventional melt-quenching method. The glass compositions are given in Table 1, column 2. The compositions are divided into three series. Reagent grade commercial powders of TeO_2 , Bi_2O_3 and H_3BO_3 were mixed together and melted in a corundum crucible at 900°C for 20 min in an electric furnace. The melts were poured onto an alumina plate and pressed to a thickness of 1~2 mm by another copper plate. The samples obtained from the third series of compositions were classified as opal glasses. The IR-spectra of the glasses were recorded in the 2000-400 cm^{-1} range by using FT-IR spectrometer Varian 600-IR. The samples for these measurements were prepared as KBr discs. The precision of the absorption maxima was $\pm 3 \text{ cm}^{-1}$.

THEORETICAL BACKGROUND

Recently, the polarizability approach has been applied to different simple oxides, binary and ternary oxide glasses [13-16]. The most familiar and widely used relationship in the polarizability approach is the Lorentz-Lorenz equation which relates the molar refraction (R_m) to the refractive index (n_o) and the molar volume (V_m) of the substance by,

$$R_m = \frac{(n_o^2 - 1)}{(n_o^2 + 2)} V_m \quad (1)$$

Assuming that the molar refraction of a glass with a common molecular formula $\text{A}_x\text{B}_y\text{C}_z\text{O}_n$ is additive quantity it follows that,

$$R_m = 2.52(x\alpha_{iA} + y\alpha_{iB} + z\alpha_{iC} + n\alpha_{o^{2-}}) \quad (2)$$

where $\alpha_{iA}, \alpha_{iB}, \alpha_{iC}$ are the polarizabilities of cations A, B and C and $\alpha_{o^{2-}}$ is the polarizability of the oxide ion, and x, y and z are the numbers of the cations A, B and C and n is the number of the oxide ions in one molecule of glass.

It is possible to calculate the so-called theoretical optical basicity Λ_{th} and the electronic oxide ion polarizability $\alpha_{o^{2-}}$ for ternary oxide glass on the basis of the following equations proposed by Duffy and Ingram [17,18],

$$\Lambda_{th} = X_1\Lambda_1 + X_2\Lambda_2 + X_3\Lambda_3 \quad (3)$$

and

$$\alpha_{o^{2-}} = \frac{1.67}{1.67 - \Lambda_{th}} \quad (4)$$

where X_1, X_2, X_3 are equivalent fractions based on the amount of oxygen each oxide contributes to the

overall material stoichiometry and $\Lambda_1, \Lambda_2, \Lambda_3$ are basicities assigned to the individual oxides.

The third order nonlinear optical susceptibility $\chi^{(3)}$, can be predicted by generalized the so-called Miller's rule [19],

$$\chi^{(3)} = [\chi^{(1)}]^4 \cdot 10^{-10}, \text{ esu} \quad (5)$$

where $\chi^{(1)}$ is linear optical susceptibility calculated in accordance with,

$$\chi^{(1)} = \frac{(n_o^2 - 1)}{4\pi} \quad (6)$$

Based on Sun's fundamental condition of glass formation [20] Dimitrov and Komatsu [21] proposed an approach for calculation of average single bond strength B_{M-O} of oxide glasses using values of single bond strength B_{M-O} for corresponding simple oxides and taking into account the molar part of each oxide in the glass composition. In the case of ternary oxide glass the following equation can be used,

$$B_{M-O} = xB_{A-O} + yB_{B-O} + (1-x-y)B_{C-O} \quad (7)$$

where x, y and $(1-x-y)$ are molar parts of each oxide in the glass composition.

According to the general theory of the dielectric constant of simple ionic crystals based on quantum-mechanical treatment of the complex interaction between neighboring ions proposed by Yamashita and Kurosawa [22] the interaction parameter A of ternary oxide glass could be calculated by using the following equation [23],

$$A = X_1 \frac{(3.921 - \alpha_{o^{2-}})}{2(\alpha_{iA} + 3.921)(\alpha_{o^{2-}} + \alpha_{iA})} + X_2 \frac{(3.921 - \alpha_{o^{2-}})}{2(\alpha_{iB} + 3.921)(\alpha_{o^{2-}} + \alpha_{iB})} + X_3 \frac{(3.921 - \alpha_{o^{2-}})}{2(\alpha_{iC} + 3.921)(\alpha_{o^{2-}} + \alpha_{iC})} \quad (8)$$

where X_1, X_2 and X_3 are equivalent fractions based on the amount of oxygen each oxide contributes to the overall glass stoichiometry, $\alpha_{o^{2-}}$ is oxide ion polarizability of the glass and $\alpha_{iA}, \alpha_{iB},$ and α_{iC} are cation polarizabilities. Pauling's value of 3.921 \AA^3 for the electronic polarizability of the free oxide ion is used.

RESULTS AND DISCUSSION

We have calculated the theoretical optical basicity and oxide ion polarizability of $\text{TeO}_2\text{-Bi}_2\text{O}_3\text{-B}_2\text{O}_3$ glasses by Eq. 3 and 4 using optical basicity data of TeO_2 ($\Lambda=0.975$), Bi_2O_3 ($\Lambda=1.19$) and B_2O_3 ($\Lambda=0.42$) [23]. The molar refraction of the glasses was determined by Eq. 2 taking into account the cation polarizability and oxide ion polarizability. According to [13] the cation polarizabilities are $\alpha_{\text{Te}^{4+}}=1.595 \text{ \AA}^3$; $\alpha_{\text{Bi}^{3+}}=1.508 \text{ \AA}^3$; $\alpha_{\text{B}^{3+}}=0.002 \text{ \AA}^3$.

Table 1 Composition, Molar mass M, density d, molar volume V_m, optical basicity Λ, electronic oxide ion polarizability α_{o²⁻}, molar refraction R_m

	Composition	M, g/mol	d, g/cm ³	V _m , cm ³ /mol	Λ	α _{o²⁻} , Å ³	R _m , cm ³ /mol
Series 1	10TeO ₂ 50 Bi ₂ O ₃ 40B ₂ O ₃	276.79	5.75	48.11	0.857	2.053	19.21
	20TeO ₂ 40Bi ₂ O ₃ 40B ₂ O ₃	246.15	5.43	45.33	0.829	1.986	17.86
	30TeO ₂ 30Bi ₂ O ₃ 40B ₂ O ₃	215.52	5.11	42.20	0.800	1.920	16.55
	40TeO ₂ 20Bi ₂ O ₃ 40B ₂ O ₃	184.88	4.78	38.65	0.768	1.852	15.27
	50TeO ₂ 10Bi ₂ O ₃ 40B ₂ O ₃	154.24	4.46	34.58	0.734	1.785	14.02
Series 2	45.5 TeO ₂ 30.0Bi ₂ O ₃ 24.5B ₂ O ₃	256.05	5.85	43.76	0.891	2.143	18.83
	59.65TeO ₂ 25.0Bi ₂ O ₃ 15.35B ₂ O ₃	222.38	5.89	37.76	0.936	2.274	18.08
	60.2TeO ₂ 20.0Bi ₂ O ₃ 19.8B ₂ O ₃	203.06	5.56	36.54	0.891	2.145	16.90
Series 3	31.2TeO ₂ 45.0 Bi ₂ O ₃ 23.8B ₂ O ₃	276.05	6.21	44.44	0.936	2.274	20.08
	31.0TeO ₂ 40.0Bi ₂ O ₃ 29.0B ₂ O ₃	229.46	5.70	40.25	0.891	2.145	17.86
	45.5TeO ₂ 35.0 Bi ₂ O ₃ 19.5B ₂ O ₃	249.28	6.05	41.18	0.936	2.276	19.09

The molar volume was estimated and the results of V_m, theoretical optical basicity Λ_{th}, oxide ion polarizability α_{o²⁻} and molar refraction R_m are listed in Table 1. It is seen that the glasses possess relatively high optical basicity (0.734-0.936) and electronic oxide ion polarizability (1.785 - 2.276 Å³) which indicate for their basic nature. The results obtained are in good agreement with the data reported by Hasegawa [10] and Zhao *et al.* [11] for other bismuth boro-tellurite glasses. We have estimated the theoretical refractive index of TeO₂-Bi₂O₃-B₂O₃ glasses using Eq. 1. The data are listed in Table 2, column 3. As can be seen the glasses possess high values of refractive index in the 1.713-1.938 range. The third order nonlinear optical susceptibility χ⁽³⁾, was predicted by generalized Miller's rule (see Eqs. 5 and 6). The results are listed in Table 2, column 4. TeO₂-Bi₂O₃-B₂O₃ glasses show relatively high values of the third order nonlinear optical susceptibility in the 0.64-2.31 x 10⁻¹³ esu range which are close to those reported in Refs. 24, 25.

This means that TeO₂-Bi₂O₃-B₂O₃ glasses are probably good candidates for nonlinear optical applications. It was established that third order nonlinear optical susceptibility χ⁽³⁾ of the glasses increases with increasing electronic oxide ion polarizability, that is optical basicity and refractive index.

As can be seen in Table 1 the glasses with high optical nonlinearity possess high electronic oxide ion polarizability, optical basicity and refractive index.

Sun [20] has suggested a bond energy criterion for glass formation and has reported comprehensive data on single bond strength B_{M-O} in kcal per Avogadro bond for various simple oxides based on their dissociation energy E_d. Yamashita and Kurosawa [22] have proposed a general theory of the dielectric constant of simple ionic crystals based on quantum-mechanical treatment of the electronic structure of constituent ions in order to take into account the effect of charge overlapping between neighboring ions.

Table 2 Composition, refractive index n₀, third order nonlinear optical susceptibility χ⁽³⁾, interaction parameter A, single bond strength B_{M-O}

	Composition	n ₀	χ ⁽³⁾ .10 ⁻¹³ esu	A, Å ⁻³	B _{M-O} , kJ/mol
Series 1	10TeO ₂ 50 Bi ₂ O ₃ 40B ₂ O ₃	1.730	0.64	0.036	279
	20TeO ₂ 40Bi ₂ O ₃ 40B ₂ O ₃	1.718	0.58	0.039	297
	30TeO ₂ 30Bi ₂ O ₃ 40B ₂ O ₃	1.713	0.56	0.042	316
	40TeO ₂ 20Bi ₂ O ₃ 40B ₂ O ₃	1.720	0.59	0.046	334
	50TeO ₂ 10Bi ₂ O ₃ 40B ₂ O ₃	1.745	0.70	0.051	352
Series 2	45.5 TeO ₂ 30Bi ₂ O ₃ 24.5B ₂ O ₃	1.807	1.06	0.033	283
	59.65TeO ₂ 25.0Bi ₂ O ₃ 15.35B ₂ O ₃	1.938	2.31	0.028	272
	60.2TeO ₂ 20Bi ₂ O ₃ 19.8B ₂ O ₃	1.893	1.79	0.033	291
Series 3	31.2TeO ₂ 45.0 Bi ₂ O ₃ 23.8B ₂ O ₃	1.864	1.50	0.028	254
	31.0TeO ₂ 40Bi ₂ O ₃ 29.0B ₂ O ₃	1.842	1.32	0.032	274
	45.5TeO ₂ 35.0 Bi ₂ O ₃ 19.5B ₂ O ₃	1.895	1.81	0.028	263

A quantitative measure of this complex interaction is given by the so-called interaction parameter A , which in fact for a chosen cation-anion pair represents the charge overlapping of the oxide ion with its nearest positive neighbor. Therefore, the average single bond strength and the interaction parameter represent the chemical bonding of the glasses based on two different approaches – on the thermodynamics and polarizability, respectively. Both parameters of $\text{TeO}_2\text{-Bi}_2\text{O}_3\text{-B}_2\text{O}_3$ glasses were estimated by using Eqs. 7 and 8. For the calculation of the average single bond strength of the glasses the following values for the corresponding individual oxides were used - 285 kJ/mol for TeO_2 , 103 kJ/mol for Bi_2O_3 and 498 kJ/mol for B_2O_3 (see Ref. 23). The obtained data for both parameters are presented in Table 2. The glasses possess small single bond strength in the 254-352 kJ/mol range and small values of interaction parameter in the 0.028-0.051 \AA^{-3} range. Small interaction parameter means weak interionic interactions resulting in large unshared electron density at one averaged oxide ion. These values of $B_{\text{M-O}}$ and A suggest for the presence of predominantly ionic character of the bonds in the glass structure. Probably Te-O-B , Te-O-Bi and Te-O-Te , along with Bi-O-B and Bi-O-Bi chemical bonds are formed in their structure.

With a view to confirm the presence of such bonds the structure of the glasses in the present study was investigated by means of IR spectroscopy. The IR spectra of $\text{TeO}_2\text{-Bi}_2\text{O}_3\text{-B}_2\text{O}_3$ glasses are shown in Figs. 1-3. In the spectra of the glasses from Series 1 (Fig. 1) it can be seen the presence of two well-defined bands at 1338-1164 cm^{-1} range, a band at 1014-1001 cm^{-1} and two low frequency bands at about 670 cm^{-1} and 440 cm^{-1} . The intensity of the band at about 670 cm^{-1} increases and that of the band at about 440 cm^{-1} decreases with the TeO_2 content increase and Bi_2O_3 content decrease.

In the spectra of the glasses from Series 2 (Fig. 2) it can be seen the presence of two well-defined maxima at 1325-1316 cm^{-1} and 1210-1206 cm^{-1} respectively, weak maxima at 1071-1017 cm^{-1} and strong band at about 658-649 cm^{-1} with a shoulder at 750-742 cm^{-1} .

The spectra of the glasses from Series 3 are similar each other. A broad band in the 1325-1206 cm^{-1} could be observed along with weak band at around 1045-1022 cm^{-1} in the high frequency range. In the low frequency range four or five bands exist, namely at 759-713 cm^{-1} , 658-633 cm^{-1} , 617 cm^{-1} , 562-548 cm^{-1} and 438-433 cm^{-1} . The last band decreases its intensity with Bi_2O_3 decrease.

The change of the tellurium coordination polyhedron from TeO_4 to TeO_3 , the change of boron coordination polyhedron from BO_3 to BO_4 and existence of BiO_6 and BiO_3 groups are well known from structural investigations of different tellurite, borate and bismuthate glasses [7, 25-30]. Arnaudov *et al.* [26] and Dimitriev *et al.* [27] have studied the Te-O stretching vibrations of $\alpha\text{-TeO}_2$ and 16 crystalline tellurites built up by TeO_3 , TeO_4 or combinations of these polyhedra as well as series of tellurite glasses containing similar polyhedra. The characteristic stretching vibrations of these structural groups are located in the 670-635 cm^{-1} range. According to IR- spectral data for large number of bismuthate crystals and glasses collected by Iordanova *et al.* [30] the stretching vibrations of BiO_6 are in the 480-420 cm^{-1} range while those of BiO_3 groups are around 860-840 cm^{-1} .

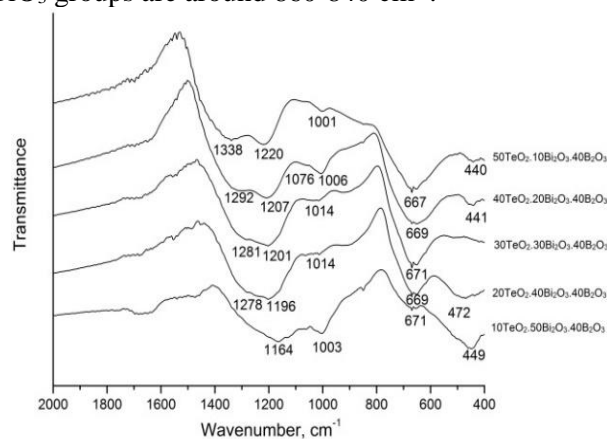


Fig. 1. IR spectra of the $\text{TeO}_2\text{-Bi}_2\text{O}_3\text{-B}_2\text{O}_3$ glasses from Series 1.

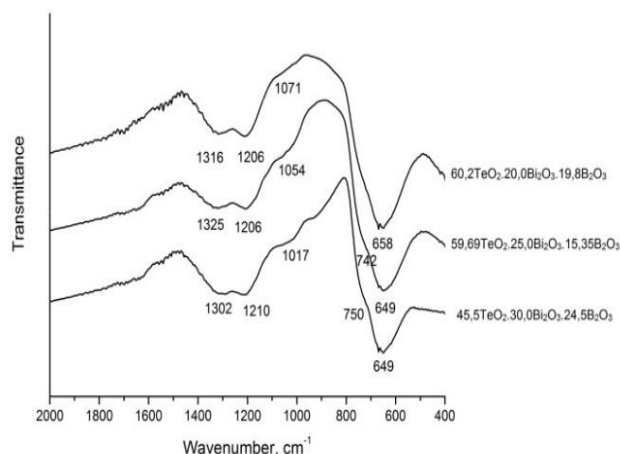


Fig. 2. IR spectra of the $\text{TeO}_2\text{-Bi}_2\text{O}_3\text{-B}_2\text{O}_3$ glasses from Series 2.

The characteristic bands of boron containing crystals and glasses are in the high frequency range of the spectra in which are located the stretching vibrations of BO_3 and BO_4 structural groups.

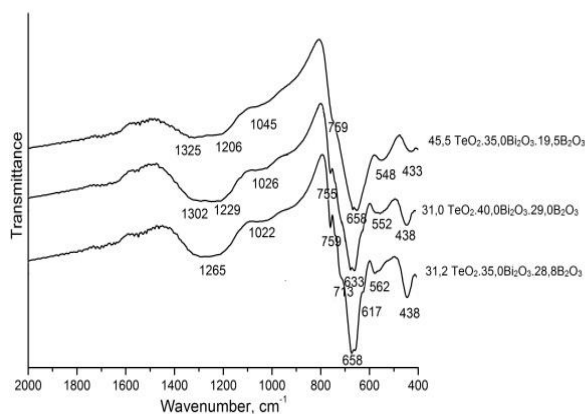


Fig. 3. IR spectra of the $\text{TeO}_2\text{-Bi}_2\text{O}_3\text{-B}_2\text{O}_3$ glasses from Series 3.

According to the review article by Gautam *et al.* [31] on infrared spectroscopic studies of borate glasses with different additives the asymmetric stretching vibrations of B-O bonds of trigonal BO_3 units could be observed in the 1480-1200 cm^{-1} range. The band at about 1345-1235 cm^{-1} is connected with the presence of pyroborate and orthoborate groups. The absorption maxima at about 1015 cm^{-1} gives information of the presence of pentaborate groups containing both BO_3 and BO_4 units. The bands at about 1046-1020 cm^{-1} are assigned to the B-O stretching vibrations of BO_4 units. Similar results about the vibrations of BO_3 and BO_4 units in the structure $\text{ZnO-Bi}_2\text{O}_3\text{-B}_2\text{O}_3$ and $\text{CdO-Bi}_2\text{O}_3\text{-B}_2\text{O}_3$ have been reported also by Saritha *et al.* [32] and Pal *et al.* [33].

On the basis of the discussion mentioned above the following assignment of the bands in the spectra of $\text{TeO}_2\text{-Bi}_2\text{O}_3\text{-B}_2\text{O}_3$ glasses is made. The bands in the 1338-1278 cm^{-1} range and the bands at 1229-1196 cm^{-1} range are assigned to the asymmetrical stretching vibrations of BO_3 units in pyro- and orthoborate superstructural units. The absorption maxima in the 1071-1001 cm^{-1} range is attributed to the stretching vibrations of BO_4 units. The absorption band around 670-650 cm^{-1} is probably due to overlapping between asymmetrical stretching vibrations of axial Te-O bonds in the TeO_4 groups and asymmetrical stretching vibrations of TeO_3 pyramidal groups. The shoulder at 760-713 cm^{-1} could be assigned to symmetrical stretching vibrations of equatorial Te-O bonds in TeO_4 groups or to symmetrical stretching vibrations of TeO_3 groups. The band around 440 cm^{-1} is attributed to the Bi-O stretching vibrations of BiO_6 . The observed structural units namely BO_3 , BO_4 , TeO_3 , TeO_4 and BiO_6 are interconnected in the structure of the $\text{TeO}_2\text{-Bi}_2\text{O}_3\text{-B}_2\text{O}_3$ glasses by B-O-B, B-O-Te, B-O-Bi, Te-O-Te and Bi-O-Bi chemical bonds.

The polarizability approach based on the Lorentz-Lorenz equation has been applied to $\text{TeO}_2\text{-Bi}_2\text{O}_3\text{-B}_2\text{O}_3$ glasses. It was established that the glasses possess high refractive index (1.713-1.938), high electronic ion polarizability (1.785-2.276 \AA^3) and high optical basicity (0.734-0.936). The theoretical third order nonlinear optical susceptibility $\chi^{(3)}$ was determined and it was found that the glasses possess high values of $\chi^{(3)}$ in the $0.64\text{-}2.31 \times 10^{-13}$ range. It was established that the glasses have small single bond strength and interaction parameter, thus suggesting the presence of weak chemical bonds. Such bonds, namely B-O-Te, B-O-Bi, Te-O-Te and Bi-O-Bi probably interconnect TeO_4 , TeO_3 , BiO_6 , BO_3 and BO_4 groups which were confirmed by IR spectral analysis of the glasses. The high polarizability of oxide ions in these bonds accounts to the observed linear and nonlinear optical properties of the glasses.

REFERENCES

1. W. A. Weil, E. G. Marboe, *The Constitution of Glasses*, Wiley, New York, 1962.
2. V. Dimitrov, T. Komatsu, *J. Non-Cryst. Solids* **249**, 160 (1999).
3. M. Yamane, Y. Asahara, *Glasses for Photonics*, Cambridge, University Press, 2000.
4. S. H. Kim, T. Yoko, *J. Am. Ceram. Soc.*, **78**, 1061 (1995).
5. S. Manning, H. Ebendorff-Heidepriem, T. M. Monro, *Opt. Mater. Express* **2** (2), 140 (2012).
6. T. Komatsu, *J. Non-Cryst. Solids* **428**, 156 (2015).
7. T. Maeder, *Int. Mater. Rev.* **58** (1), 3 (2013).
8. T. Hasegawa, T. Nagashima, N. Sugimoto, *Opt. Comm.* **250**, 411 (2005).
9. N. Sugimoto, H. Kanbara, S. Fujiwara, K. Tanaka, K. Hirao, *Opt. Lett.* **21** (20), 1637 (1996).
10. T. Hasegawa, *J. Non-Cryst. Solids* **357**, 2857 (2011).
11. G. Zhao, Y. Tian, H. Fan, J. Zhang, L. Hu, *J. Mater. Sci. Technol.* **29** (3), 209 (2013).
12. A. Azuraida, M. K. Halimah, A. A. Sidek, C. A. C. Azuranim, S. M. Iskandar, M. Ishak, A. Nurazlin, *Chalcogenide Lett.* **12** (10), 497 (2015).
13. V. Dimitrov, S. Sakka, *J. Appl. Phys.*, **79**, 1736 (1996).
14. V. Dimitrov, T. Komatsu, *J. Solid State Chem.* **178**, 831 (2005).
15. T. Tasheva, V. Dimitrov, *J. Chem. Technol. Metallurgy*, **50** (4), 441 (2015).
16. T. Tasheva, V. Dimitrov, *J. Chem. Technol. Metallurgy*, **51** (5), 525 (2016).
17. J.A. Duffy, M.D. Ingram, in *Optical Properties of Glass*, Eds. D. Uhlman, N. Kreidl, Am. Ceram. Soc., Westerville, 1991.
18. J.A. Duffy, *Phys. Chem. Glasses*, **30**, 1 (1989).
19. V. Dimitrov, S. Sakka, *J. Appl. Phys.*, **79**, 1741 (1996).

- T. Tasheva & V. Dimitrov: "Synthesis, structure and nonlinear optical properties of tellurium oxide – bismuth oxide"*
20. K. H. Sun, *J. Am. Ceram. Soc.*, **30**, 277 (1947).
 21. V. Dimitrov, T. Komatsu, *Phys. Chem. Glasses: Eur. J. Glass Sci. Technol. B*, **46**, 521 (2005).
 22. J. Yamashita, T. Kurosawa, *J. Phys. Soc. Japan* **10**, 610 (1955).
 23. V. Dimitrov, T. Komatsu, *J. Univ. Chem. Technol. Metallurgy*, **45**, 219 (2010).
 24. G. V. Prakash, D. N. Rao, A. K. Bhatnagar, *Solid State Comm.* **119**, 39 (2001).
 25. K. Terashima, T. Shimoto, T. Yoko, *Phys. Chem. Glasses* **38**, 211 (1997).
 26. M. Arnaudov, V. Dimitrov, Y. Dimitriev, L. Markova, *Mat. Res. Bull.* **17**, 1121 (1982).
 27. Y. Dimitriev, V. Dimitrov, M. Arnaudov, *J. Mat. Sci.* **18**, 1363 (1983).
 28. T. Sekiya, N. Mochida, A. Ohtsuka, M. Tomokawa, *J. Non-Cryst. Solids* **144**, 128 (1992).
 29. S. Sakida, S. Hayakawa, T. Yoko, *J. Non-Cryst. Solids* **243**, 13 (1999).
 30. R. Iordanova, Y. Dimitriev, V. Dimitrov, S. Kassabov, D. Klissurski, *J. Non-Cryst. Solids* **204**, 141 (1996).
 31. C. Gautam, A. Kunar Yadav, A. Kunar Singh, *Int. Scholarly Res. Network ISRN Ceramics* Article ID 428497 (2012).
 32. D. Saritha, Y. Markandeya, M. Salagram, M. Vithal, A. K. Sigh, G. Bhikshamaiah, *J. Non-Cryst. Solids* **354**, 5573 (2008).
 33. I. Pal, A. Agarwal, S. Sanghi, *Ind. J. Pure & Appl. Phys.*, **50**, 237 (2012).

СИНТЕЗ, СТРУКТУРА И НЕЛИНЕЙНИ ОПТИЧНИ СВОЙСТВА НА ТЕЛУР-БИСМУТ-БОР ОКСИДНИ СЪТЪКЛА

Т. Р. Ташева, В. В. Димитров

*Катедра „Технология на силикатите“, Химикотехнологичен и металургичен университет,
бул. Кл. Охридски 8, София 1756, България, e-mail: tina.tasheva@gmail.com*

Постъпила на 7 ноември 2016 г.; приета на 3 януари 2017 г.

(Резюме)

TeO₂-Bi₂O₃-B₂O₃ стъкла бяха синтезирани посредством рязко охлаждане на стопилки. Беше приложен поляризационния подход, базиран на уравнението на Лорентц-Лоренц. Оптическата основност и кислородната поляризуемост бяха определени. Установено е, че стъклата притежават сравнително високи стойности за оптическата основност (0.734-0.936) и кислородната електронна поляризуемост (1.785-2.276 Å³). Теоретичният показател на пречупване също беше определен. На негова основа беше определена нелинейната оптическа възприемчивост от трети порядък $\chi^{(3)}$ посредством Милеровото правило. Стъклата притежават сравнително високи стойности за $\chi^{(3)}$ (0.64-2.31x10⁻¹³ esu). Химическото свързване е изяснено, на основата на една осреднена катион-кислород (М-О) химична връзка, посредством параметъра на междуйонно взаимодействие и здравината на връзката. Установено е, че стъклата притежават сравнително ниски стойности за здравината на химичната връзка (352-254 kJ/mol) и ниски стойности за параметъра на междуйонно взаимодействие (0.051 до 0.028 Å⁻³). Тези резултати предполагат наличието на слаби химични връзки между TeO₄, TeO₃, BiO₆, BO₄ и BO₃ групите, потвърдени чрез ИЧ спектрален анализ.

Ключови думи: оксидни стъкла, поляризуемост, оптическа основност, химическо свързване, ИЧ спектроскопия, нелинейни оптични материали.

Cloud point extraction of lanthanides with 3-ethylamino-but-2-enoic acid phenylamide from water samples prior to ICP-MS determination

E. K. Varbanova¹, P. A. Angelov², K. K. Simitchiev¹, L. I. Kaynarova¹, V. M. Stefanova^{1*}

University of Plovdiv "Paisii Hilendarski", 24 Tzar Assen str., 4000 Plovdiv, Bulgaria

¹Department of analytical chemistry and computer chemistry

²Department of organic chemistry

Received November 11, 2016; Revised December 16, 2016

A compound representative of the enamines class is studied as a new ligand for Cloud Point Extraction (CPE) of lanthanides (La, Ce, Eu, Gd, Er) from aqueous medium. Extraction parameters such as water phase pH, heating temperature, incubation time, type and quantity of surfactant are optimized. Analyte concentrations are measured by ICP-MS after appropriate dilution of the surfactant-rich phase. The extraction system based on the new ligand showed high efficiency for separation of lanthanides from concomitant alkali and alkaline earth elements, which significantly reduces the risk of spectral interferences in real samples. Selectivity of the tested enamine is compared to the classical ligand 8-hydroxyquinoline. The instrumental drift in sensitivity is corrected by internal standardization with Re. The optimized procedure is applied on water certified reference material and real water samples. Obtained limits of detection are in the interval 0.2-1.3 ng L⁻¹ with 10-fold preconcentration.

Keywords: Lanthanides, Cloud Point Extraction, Enamines, ICP-MS, Water Analysis.

INTRODUCTION

Cloud point extraction (CPE) is a green alternative to classical extraction techniques that doesn't require use of toxic, volatile and flammable solvents [1]. Due to its advantages, CPE has been extensively used in the last decades for separation and preconcentration of organic [2-4] and inorganic [5-7] substances. Extraction of metal ions is principally performed by preliminary formation of water insoluble complexes with variety of ligands: pyridylazo and thiazolylazo derivatives, such as 1-(2-pyridylazo)-2-naphthol (PAN), 1-(2-thiazolylazo)-2-naphthol (TAN), 4-(2-pyridyl-azo) resorcinol (PAR), 2-(5-bromo-2-pyridylazo)-5-(diethylamino) phenol (5-Br-PADAP), ammonium pyrrolidinedithiocarbamate (APDC), diethyldithiocarbamate (DDTC), 2-amino-cyclopentene-1-dithiocarboxylic acid (ACDA), O,O-diethyldithiophosphate (DDTP), 8-hydroxyquinoline (oxine, 8-HQ) and dithizone [8]. Still few authors report procedures for CPE of lanthanide ions (Ln) with ligands as Alizarin Red S and cetyltrimethylammoniumbromide (CTAB) [9], water-soluble calixarenes [10], hydrophobic calixarene platforms [11], 8-hydroxyquinoline [12, 13] and 2-(5-bromo-2-pyridylazo)-5-diethylaminophenol [14].

ICP-MS is considered to be one of the most appropriate techniques for lanthanide analysis in diversity of real samples [15-17]. Nevertheless, the direct determination of these elements is hindered

by spectral interferences caused by barium [18, 19]. Most of the authors recommend separation procedure before the measurement [20].

In this study is presented the potential of enamines (En) as ligands for CPE of lanthanides from water samples.

EXPERIMENTAL

Instrumentation

All measurements are performed with ICP-MS Agilent 7700. The measurements were done using standard plasma operating conditions; Micromist (Glass Expansion) nebulizer, using normal resolution (0.65 amu); 5 replicates per sample; 1 point per mass peak and 0.1s acquisition time. Two isotopes per analyte were monitored ^{140,142}Ce, ^{151,153}Eu, ^{156,157}Gd, ^{166,168}Er with exception of lanthanum where only one isotope is free from isobaric interference ¹³⁹La.

Reagents and standard solutions

All reagents and solvents were analytical grade and used without further purification. Monoelemental solutions of Ce, Er, Eu (1000, mg L⁻¹) were purchased from CPA-spectrTM. Solutions for La and Gd with concentration 1000 mg L⁻¹ were prepared by dissolving of Gd₂O₃ (99,9%, Sigma-Aldrich) and La(NO₃)₃·6H₂O (99,99%, trace metals basis, Sigma-Aldrich) in 1 mol L⁻¹ HNO₃ (p.a., Merck) on heating plate and then diluting with double distilled water. Stock

* To whom all correspondence should be sent.
E-mail: stefanova@uni-plovdiv.net

solution of Re (1000 mg L^{-1}) was obtained from Merck (Darmstadt, Germany). Selectivity test was performed using Multi elemental solution, 100 mg L^{-1} CPA Chem Ref. № B56A.K1.5N.L1. A buffer solution with $\text{pH}=8.3$ was prepared from NH_4OH and NH_4NO_3 (Merck). Certified reference material for surface water SPS Quality Level 1 (Spectrapure standards, Oslo, Norway) was used for method validation. Triton X-100 (TX-100, Merck) and Triton X-114 (TX-114, Fluka AG) were tested as surfactants for CPE. 8-Hydroxyquinoline (Sigma-Aldrich) was used for selectivity comparison.

3-ethylamino-but-2-enoic acid phenylamide (En) was synthesized according to a procedure described by Venkov and Angelov in [21].

Cloud point extraction of lanthanides with tested enaminone

Calibration standards and model solutions were prepared in plastic test tubes as it follows: 40 mL of tested water solution containing target lanthanide ions $1 \mu\text{g L}^{-1}$ (and concomitant elements $10 \mu\text{g L}^{-1}$) was buffered at $\text{pH}=8.3$ by the addition of 5 mL $\text{NH}_4\text{OH}/\text{NH}_4\text{NO}_3$ buffer solution. Then 0.2 mL (0.06 mol L^{-1}) solution of the ligand in ethanol was added and the sample was shaken for 2 minutes. Finally, 5 mL 10% TX-100 were added and test tubes were placed in water bath for 30 minutes at 70°C . After incubation, samples were cooled in freezer. Then the water phase was removed with pipette and surfactant rich phase (SRP) was diluted with 1 mol L^{-1} HNO_3 with internal standard (IS) Re to final volume of 4 mL . Procedural blank was also prepared.

Real samples and Reference material

SPS Water Level 1: Acidified surface water samples were neutralized to $\text{pH}\sim 5$ and then prepared according to the procedure for model solutions.

Cloud point extraction of lanthanides with 8-hydroxyquinoline

The method for CPE with 8-HQ described elsewhere [12] with slight modification - i.e. the SRP was directly diluted with 0.01 mol L^{-1} HNO_3 (with IS Re) after CPE.

RESULTS AND DISCUSSION

Optimization of extraction parameters for CPE with enaminone

The optimization of extraction parameters was started with pH of the initial aqueous solution because it affects both ligand's and analytes' behavior. In our previous studies on liquid-liquid extraction, we found that the highest efficiency of

the reaction between lanthanides and enaminones was achieved in basic medium [22, 23]. The investigated pH range here (from 6 to 9) confirmed that in acidic and strong basic medium the complex formation is suppressed. Expectedly, the highest signals were obtained for $\text{pH}=8$ and for this reason, $\text{NH}_4\text{NO}_3/\text{NH}_4\text{OH}$ with $\text{pH}\sim 8.3$ was used for further experiments.

CPE was tested at the optimum pH value without the addition of ligand because the lanthanides are partially hydrolyzed in basic medium; their hydrophobic hydroxides could be extracted in SRP. Furthermore some authors have reported high yields for lanthanides obtained by CPE in basic ($\text{pH}>9$) [24] and even in acidic media [13] without addition of ligand. The results presented in Figure 1 indicate that ligandless extraction is possible but with low efficiency. The presence of tested enaminone results in a twofold increase in the signals for all elements and ensures higher recoveries.

In addition, it was discovered that the order of mixing the reactants during the sample preparation also influences the signals. Up to 30% lower signals are measured when the surfactant is added before the ligand. This is probably due to the higher solubility of the ligand in a micellar phase formed by surfactant, which decreases its concentration in the aqueous phase before completing the reaction with target ions. Therefore, it is recommended to add firstly the ligand to the sample solution and after vigorous stirring, to introduce the surfactant.

The concentration TX-100 was varied in the interval 0.5-5%, in order to define the minimal amount of surfactant needed for extraction of lanthanides, keeping all other parameters constant. It was established that 1% TX-100 is sufficient for quantitative extraction of the analytes.

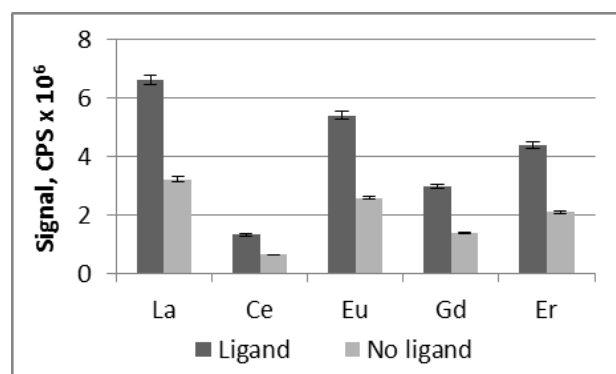


Figure 1. Signals for lanthanides after dilution of SRP with 1 mol L^{-1} HNO_3 with and without ligand. Constant conditions: $\text{pH}=8.3$; $C_{\text{Ln}}=1 \mu\text{g L}^{-1}$; $12 \mu\text{mol}$ Enaminone; 1% TX-100; incubation time of 1 hour, $t=70^\circ\text{C}$; dissolution of SRP - 1 mol L^{-1} HNO_3 .

The incubation time affects both the duration of CPE and its effectiveness, so it is tested on four levels (15, 30, 45 and 75 min.). The signals for all test elements are increased by ~ 25% at an incubation time of 30 minutes in comparison to 15 min. incubation. The extension of incubation time was found unnecessary since it does not improve the efficiency of extraction.

The temperature of the water bath (ranging from 70°C to boiling) showed no significant influence on extraction, so all subsequent experiments were performed at 70°C.

Separation of the water phase and SRP was done after 1 h cooling of the samples in freezer. Preliminary experiments showed that when residual sample solution was separated by the surfactant rich phase by simple decanting, essential decrease of analyte signals was observed. Pipetting the upper phase of aqueous solution allows more precise and reproducible separation, without analyte loss. After separation, the viscous SRP was dissolved with 1 mol L⁻¹ HNO₃ up to 4 mL final volume. Hence, a preconcentration factor of 10 is obtained for the developed CPE procedure of lanthanides with enaminate.

Comparison of CPE procedures with both ligands 3-ethylamino-but-2-enoic acid phenylamide and 8-hydroxyquinoline

The new CPE system for extraction of lanthanides with 3-ethylamino-but-2-enoic acid phenylamide (En) was compared to a published CPE method with a well-known ligand 8-hydroxyquinoline (8-HQ) [12]. The comparison was made in three aspects: 1) affinity towards target lanthanides; 2) co-extraction of concomitant elements; and 3) potential spectral interferences caused by co-extracted elements. For these reasons, extraction was performed under optimal conditions for both ligands with standard solution of lanthanides (Ln 1 µg L⁻¹), and with the same solution spiked with multielement standard (MY) containing 28 elements in concentration 10 µg L⁻¹.

When lanthanides only are subjected to the optimized CPE procedures both ligands show high affinity towards them (Figure 2).

The tested enaminate shows better results, allowing to achieve quantitative recoveries, while the efficiency of the reaction with 8-HQ is lower (R=71-94%).

Both ligands were compared also when the model solution of multielement standard with concentration 10 µg L⁻¹ are subjected to CPE procedures (Figure 3). The experiment showed that alkali and alkaline earth elements are not extracted in both CPE systems. The recoveries for Na, K, Mg

and Ca are less than 5%, so they are not shown in the graph. The extraction degree of Ba is also very low (~5%), but it needs special attention because the most significant risk of spectral interference on lanthanide isotopes is due to the formation of polyatomic barium ionic species as hydrides, oxides, and hydroxides.

8-hydroxyquinoline, as a broad spectrum ligand binds most of the elements in the soliton. Its high affinity to Al is due to the formation of well-known compound Tris (8-hydroxyquinolinato) aluminum. Comparative extraction efficiency for both ligands is observed for Cu, Zn, Cr, and Bi.

3-ethylamino-but-2-enoic acid phenylamide extracts most of the concomitant elements in lower degree (V, Mn, Fe, Co, Ni, Mo, Ag, and Ba). Only for Pb, the tested enaminate shows higher efficiency than 8-hydroxyquinoline.

In this comparison, 3-ethylamino-but-2-enoic acid phenylamide shows better selectivity than 8-HQ, which could be an advantage of the new compound in case of complicated matrices with high concentrations of metals.

Co-extracted elements could worsen the overall performance of the proposed method for lanthanide preconcentration in two aspects: the depletion of ligand could decrease the recovery for analytes and/or the presence of elements in final solution could provoke spectral interferences on selected lanthanide isotopes.

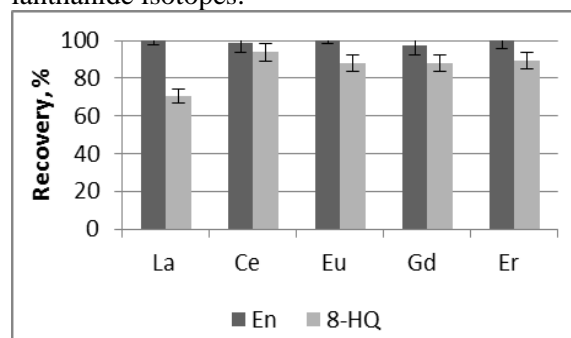


Figure 2. Analytical recovery for lanthanides after CPE with 8-HQ и En; optimal conditions for each ligand.

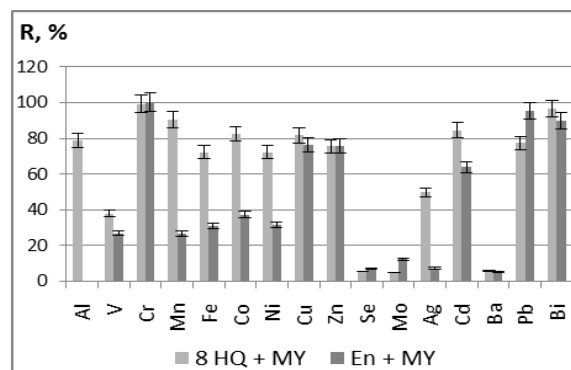


Figure 3. Recovery for concomitant elements (C=10 µg L⁻¹) after CPE with 8-HQ and En.

To study both effects, model solutions of lanthanides only and lanthanides mixed with multi-elemental solution were subjected to the optimized CPEs. In all cases, the concentration of lanthanides was one order of magnitude lower than other elements (1 and 10 $\mu\text{g L}^{-1}$ respectively). Isolated SRPs were diluted and measured by ICP-MS. Figures 4 and 5 show signals for two isotopes per element (with exception of La) after extraction with 3-ethylamino-but-2-enoic acid phenylamide and 8-hydroxyquinoline respectively in the presence and absence of multi-elemental solution.

When the CPE is performed with enaminone, the signals for all tested isotopes are statistically identical independently on the presence of co-extracted elements (Fig. 4) This is evidence that the extraction of target Ln ions is not deteriorated by the concomitant metal ions even if their concentration is higher by 1 order of magnitude. In addition, comparable signals for the two series showed that co-extracted elements do not provoke spectral interference.

When the CPE is performed with the classical reagent 8-hydroxyquinoline, the signals of extracted lanthanides in the presence and absence of concomitant elements are statistically indistinguishable again, with exception of ^{139}La (Fig. 5). The minor increase of average values in the presence of multi-elemental solution is an indication for possible spectral interferences when the content of co-extracted elements in a real sample exceeds too much this of tested lanthanides.

The most significant difference is observed for ^{139}La . It should be noted that the only other isotope of ^{138}La (natural abundance, NA=0.09%) could not be measured because of strong isobaric overlap originated by two other elements: the main isotope of barium (^{138}Ba , NA= 71.7% and co-extraction ~5%) and ^{138}Ce (NA=0.25%, extraction ~94%). It can be seen from Figure 2 that the extraction degree of La with 8-HQ is the lowest among examined lanthanides (R=71%). The observed enhancement in the presence of multi-elemental solution could be due to the synergistic effect originated by the formation of mixed complexes. There are investigations proving that lanthanides are capable of forming some mixed complexes with transition metals such as Co, Ni and Mn [25]. As can be seen from our previous investigations, the extraction degree of these elements with 8-HQ is much higher in comparison to tested enaminone (Fig. 3).

Analytical performance

Both sensitivity and limits of detection of ICP-MS method are highly dependent on natural abundance of selected isotope. Therefore, the final

method includes the isotopes free from isobaric overlap of examined lanthanides which are more abundant - ^{139}La , ^{140}Ce , ^{153}Eu , ^{157}Gd , ^{166}Er .

Non-spectral matrix effect generated by the surfactant phase diluted in the final solution was studied. It was established that the high concentration of surfactant causes suppression of the signals for all tested elements (from 16% for Er up to 22% for La) in comparison to water standards.

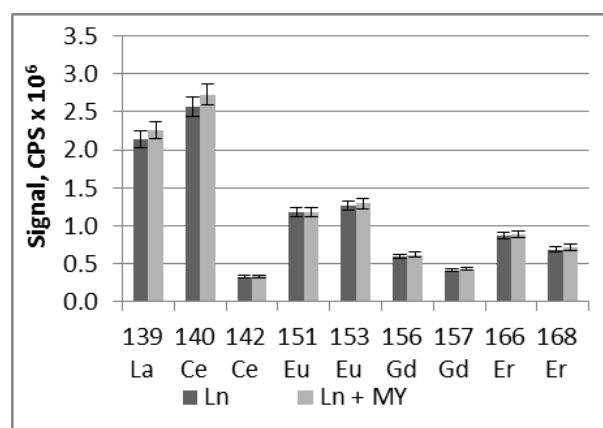


Figure 4. Signals for lanthanides after CPE in presence (Ln + MY) and absence (Ln) of concomitant elements; used ligand - En.

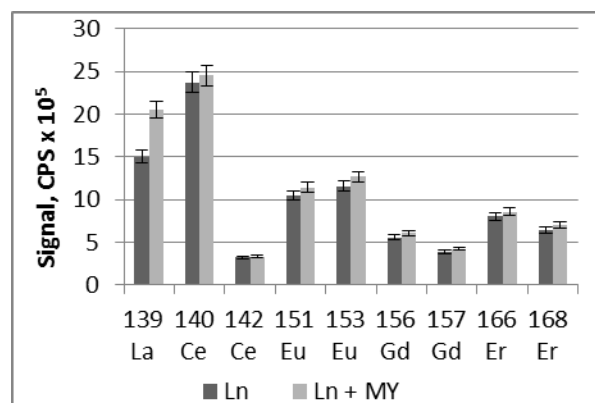


Figure 5. Signals for lanthanides after CPE in presence (Ln + MY) and absence (Ln) of concomitant elements; used ligand - 8-HQ.

Therefore it is recommended that all calibration standards must be subjected to the CPE procedure together with the analyzed samples.

Furthermore, typical for ICP-MS sensitivity drift was also observed although the instrument was conditioned by 20 minutes aspiration of diluted surfactant solution (10% TX-100). Since the signal drift was similar for all analytes, it was assumed that it is due to a change in sample transport and aerosol generation. Several elements were tested as IS candidates (Ge, Rh, In, Te, Re and Tl) in order to overcome this effect. Re was selected as the most appropriate one.

The analytical figures of merit for the CPE procedure for lanthanides with 3-ethylamino-but-2-enoic acid phenylamide as a new ligand are presented in Table 1. Procedural calibration was made by 4 standard solutions and a blank passed through CPE in concentration range 0.05-5 $\mu\text{g L}^{-1}$ with preconcentration factor of 10. Good coefficients of determination ($R^2 > 0.9972$), together with low standard deviations obtained for the calibration slopes, are evidence for the reproducibility of the procedure. Limits of detection (LOD) for all elements are calculated as the concentration, equivalent to three standard deviations of the blank sample ($n=5$), divided by the corresponding slope of procedural calibration.

Analysis of certified reference material and application

Accuracy of the procedure is proved by analysis of certified reference material for surface water SPS

Quality Level 1. Obtained data is presented in Table 2. Analytical recovery was in the range 94-108% and all measured concentrations are statistically identical with the certified values. This good coincidence is clear evidence for the accuracy of the procedure. It should be mentioned that barium is also present in the reference material (in concentration 50 $\mu\text{g L}^{-1}$) and the obtained results are an indication for effective separation of lanthanides from interfering element by CPE procedure with enaminnone.

The CPE procedure was applied for determination of lanthanides in real water sample and results are shown in Table 2. For approval of adequateness of the procedure, samples were spiked with analytes. Recoveries of spiked lanthanides at two levels (100 and 500 ng L^{-1}) were in the range 97-104% for all studied elements (Table 2).

Table 1. Analytical figures of merit obtained by measuring 5 calibration standards passed through the extraction procedure. Standards concentration – 0, 0.05, 0.1, 1, 5 $\mu\text{g L}^{-1}$; internal standard ^{185}Re ; Preconcentration factor of 10.

	Slope, (cpsLn cpsIS ⁻¹ L $\mu\text{g Ln}^{-1}$)	SD slope	Intercept, (cpsLn cpsIS ⁻¹)	SD intercept	R ²	LOD, ng L ⁻¹
¹³⁹ La	1.09	0.02	-0.2	0.5	0.9976	1.3
¹⁴⁰ Ce	1.32	0.02	-0.4	0.5	0.9982	0.4
¹⁵¹ Eu	0.60	0.01	-0.2	0.3	0.9972	0.2
¹⁵⁷ Gd	0.32	0.01	-0.1	0.1	0.9977	0.6
¹⁶⁶ Er	0.45	0.01	-0.2	0.2	0.9975	0.2

Table 2. Certified and measured concentration for lanthanides ($\mu\text{g L}^{-1}$) after CPE with 3-Ethylamino-but-2-enoic acid phenylamide in certified reference material for surface water – SPS quality Level 1, with corresponding uncertainty (U) estimation: * Expanded instrumental uncertainty; ** Uncertainty given in the certificate; Results obtained for lanthanides in real water (ng L^{-1}) sample and R% - recovery of spiked samples.

	Meas., $\mu\text{g L}^{-1}$	U, k=2*	Cert., $\mu\text{g L}^{-1}$	U**	Water 1, ng L ⁻¹	U, k=2*	R, % spike 100 ng L ⁻¹	R, % spike 500 ng L ⁻¹	Water 2, ng L ⁻¹	U, k=2*
La	0.52	0.01	0.50	0.01	68	1	103±1.3	97±1.6	130	10
Ce	0.47	0.03	0.50	0.01	2	0.1	104±0.5	97±1	780	20
Eu	0.52	0.03	0.50	0.01	1	0.2	98±1	95±1.2	390	20
Gd	0.49	0.02	0.50	0.01	1	0.4	102±1.2	101±0.5	2100	30
Er	0.49	0.02	0.50	0.01	2	0.2	98±1.2	99±2.4	420	10

CONCLUSIONS

The proposed procedure for CPE with 3-ethylamino-but-2-enoic acid phenylamide shows high potential for determination of lanthanides in complex environmental samples. The ligand is more selective than classical compound 8-hydroxyquinoline used for separation of lanthanides. The effective separation of lanthanides from concomitant barium by developed CPE

method allows eliminating of spectral interferences. Obtained limits of detection with preconcentration factor of 10 are satisfactory for examination of real waters samples.

Acknowledgements: The current study was accomplished in the frames of the project NI15-HF-001 (NPD, University of Plovdiv "Paisii Hilendarski").

REFERENCE

1. P. Samaddar, K. Sen, *J. Ind. Eng. Chem.*, **20**, no. 4, p. 1209 (2014).
2. E. Ghasemi and M. Kaykhaii, *Spectrochim. Acta Part A Mol. Biomol. Spectrosc.*, **164**, p. 93 (2016).
3. J. Giebułtowicz, G. Kojro, R. Piotrowski, P. Kułakowski, P. Wroczyński, *J. Pharmaceut. biomed.*, **128**, p. 294 (2016).
4. J. I. Cacho, N. Campillo, P. Viñas, and M. Hernández-Córdoba, *Talanta*, **160**, p. 282 (2016).
5. M. Bilal, T. G. Kazi, H. I. Afridi, M. B. Arain, J. A. Baig, M. Khan, and N. Khan, *J. Ind. Eng. Chem.*, **40**, p. 137 (2016).
6. J. M. R. Castor, L. Portugal, L. Ferrer, L. Hinojosa-Reyes, J. L. Guzmán-Mar, A. Hernández-Ramírez, and V. Cerdà, *Food Chem.*, **204**, p. 475 (2016).
7. R. Gürkan, S. Korkmaz, and N. Altunay, *Talanta*, **155**, p. 38 (2016).
8. K. Pytlakowska, V. Kozik, M. Dabioch, *Talanta*, **110**, p. 202 (2013).
9. M. M. Hassanien, I. M. M. Kenawy, M. E. Khalifa, and M. M. Elnagar, *Microchem. J.*, **127**, p. 125 (2016).
10. A. Mustafina, J. Elistratova, A. Burilov, I. Knyazeva, R. Zairov, R. Amirov, S. Solovieva, and A. Konovalov, *Talanta*, **68**, p. 863 (2006).
11. A. Mustafina, L. Zakharova, J. Elistratova, J. Kudryashova, S. Soloveva, A. Garusov, I. Antipin, A. Konovalov, *J. Colloid Interface Sci.*, **346**, no. 2, p. 405 (2010).
12. N. De Jong, M. Draye, A. Favre-Réguillon, G. LeBuzit, G. Cote, and J. Foos, *J. Colloid Interface Sci.*, **291**, p. 303 (2005).
13. Y. Li and B. Hu, *J. Hazard. Mater.*, **174**, no. 1–3, p. 534 (2010).
14. C. Ortega, S. Cerutti, R. a. Olsina, L. D. Martínez, and M. F. Silva, *J. Pharm. Biomed. Anal.*, **36**, no. 4, p. 721 (2004).
15. S. Augagneur, B. Medina, J. Szpunar, and R. Lobinski, *J. Anal. At. Spectrom.*, **11**, no. 9, p. 713 (1996).
16. N. M. Raut, L. S. Huang, S. K. Aggarwal, and K. C. Lin, *Spectrochim. Acta - Part B At. Spectrosc.*, **58**, no. 5, p. 809 (2003).
17. C. Karadaş, D. Kara, A. Fisher, *Anal. Chim. Acta*, **689**, p. 184 (2011).
18. X. Cao, M. Yin, and X. Wang, *Spectrochim. Acta - Part B At. Spectrosc.*, **56**, no. 4, p. 431 (2001).
19. V. L. Dressler, D. Pozebon, A. Matusch, and J. S. Becker, *Int. J. Mass Spectrom.*, **266**, no. 1–3, p. 25 (2007).
20. A. Fisher and D. Kara, *Anal. Chim. Acta*, **935**, p. 1 (2016).
21. A. Venkov and P. Angelov, *Synthesis (Stuttg.)*, no. **14**, p. 2221 (2003).
22. E. Varbanova, P. Angelov, V. Stefanova, *Ecol. Saf.*, **8**, p. 205 (2014).
23. E. K. Varbanova, P. A. Angelov, and V. M. Stefanova, *Talanta*, **160**, p. 389 (2016).
24. A. Ohashi, T. Hashimoto, H. Imura, and K. Ohashi, *Talanta*, **73**, no. 5, p. 893 (2007).
25. E. Harlev, Sh. Bittner, J. Zabicky, Ch. 12, Analytical Aspects of Metal Enolates in The Chemistry of Metal Enolates, J. Zabicky (ed.), Wiley, Chichester, 2009.

ЕКСТРАКЦИЯ ПРИ ТЕМПЕРАТУРА НА КОАГУЛАЦИЯ НА ЛАНТАНИДИ ОТ ВОДНИ ПРОБИ С 3-ЕТИЛАМИНО-БУТ-2-ЕНОВА КИСЕЛИНА ФЕНИЛАМИД И ICP-MS АНАЛИЗ

Е. К. Върбанова¹, П. А. Ангелов², К.К. Симитчиев¹, Л. И. Кайнарова¹, В. М. Стефанова^{1*}

Пловдивски университет „Паусий Хилендарски“, Пловдив, ул. Цар Асен 24

¹Катедра аналитична химия и компютърна химия

²Катедра органична химия

Постъпила на 11 ноември 2016 г.; приета на 16 декември 2016 г.

(Резюме)

Изследван е нов лиганд от клас енаминони за екстракция при температура на коагулация на лантаниди (La, Ce, Eu, Gd, Er) от водни разтвори. Оптимизирани са екстракционните параметри: рН на водната фаза, температура и време на нагряване, вид и количество на използваното повърхностно активно вещество. Концентрацията на анализите е определена чрез ICP-MS, след подходящо разреждане на ПАВ-обогадената фаза. Екстракционната система с новия лиганд притежава висока ефективност за разделяне на лантаниди от съпътстващите алкални и алкалоземни елементи, което значително понижава риска от спектрални пречения при анализ на реални проби. Селективността на изследвания енаминон е сравнена с тази за 8-хидроксихинолин. Инструменталният дрейф на чувствителността е коригиран с вътрешен стандарт рений. Оптимизираната процедура е приложена за анализ на сертифициран референтен материал вода и реални проби. Получените граници на откриване са в интервала 0.02-0.13 ng L⁻¹, при фактор на концентриране ФК=10.

Ключови думи: Лантаниди, Екстракция при температура на коагулация, Енаминони, ICP-MS, Анализ на води

Lipid composition of mustard seed oils (*Sinapis alba* L.)

G. A. Antova¹, M. I. Angelova – Romova¹, Zh. Y. Petkova^{1*}, O. T. Teneva¹, M. P. Marcheva²

¹ University of Plovdiv 'Paisii Hilendarski', Department of Chemical Technology,
24 Tzar Assen Street, Plovdiv 4000, Bulgaria

² Agricultural University - Plovdiv, 12 Mendeleev Blvd., Plovdiv 4000, Bulgaria

Received November 11, 2016; Revised December 5, 2016

Lipid composition of five accessions *Sinapis alba* L. seeds was investigated. The amount of glyceride oil in the seeds was 22.4 – 38.9%. The main components in triacylglycerols were erucic (28.0 – 53.2%), oleic (13.7 – 25.1%), palmitic (3.9 – 5.2%), gadoleic (9.4 – 14.2%) and linoleic acid (4.9 – 17.4%). The total content of phospholipids was 3.6 – 6.9% and the major representatives were phosphatidylcholine, phosphatidylinositol and phosphatidylethanolamine. In the sterol fraction (0.37 – 0.51%) the main component was β -sitosterol (51.9 – 55.9% in free sterols and 52.8 – 59.7% in sterol esters), followed by campesterol (19.1 – 30.5% and 31.1 – 33.5%, respectively) and brassicasterol (11.9 – 22.5% and 3.7 – 8.9%). The fatty acid composition of sterol esters was similar to triacylglycerols with exception of the palmitic acid which amount was found to be higher in esterified sterols. The total tocopherol content was 456 – 1025 mg/kg and the main representatives were α -tocopherol and γ -tocopherol. The oxidative stability of all examined accessions of *Sinapis alba* L. seed oil was 14.8 – 25.1h.

Key words: *Sinapis alba* L., seed oil, fatty acids, phospholipids, sterols, tocopherols

INTRODUCTION

Yellow mustard (*Sinapis alba* L.) is cultivated as an important oil crop and its total production is about 43 million tons per annum, mainly in Bangladesh and India [1, 2]. The oil content in the seeds of species from family *Brassica* ranges from 40.0 to 42.0% [3] and those of mustard seeds is 28.0 – 42.0% [1,4,5]. Only George *et al.*, 1985 [6] established that the oil content of the latter is 26.8%. Mustard seed oil is one of the edible vegetable oils in human diet and has a pungent flavor and aroma as well as high amount of selenium and magnesium which gives it anti-inflammatory properties [7]. It is valuable industrial oil but contains high levels of erucic acid (40.0 – 50.0%) which make it less desirable as a dietary fat [6]. Despite that, significant amounts of linoleic, oleic and linolenic acid were also established [1, 4]. Many researchers have developed the genetic control of fatty acid composition of *Brassica* species and *Sinapis alba* in order to obtain a seed oils with reduced amount of erucic acid [8-12].

There are some studies on biologically active components in mustard seed oils. Phospholipids in the oil are investigated by Parti *et al.*, 2003 [4] and their amount is 6.44% but according to Chhokar *et al.*, 2008 [1] it is 1.32%. Nevertheless, there is no information about the individual composition of phospholipid fraction as well as fatty acid composition. Total sterol content in

mustard oil is about 0.80% where the free sterols consist of 0.32% and esterified sterols are 0.48% [3]. The predominant components of the sterol fraction are β -sitosterol, brassicasterol, campesterol and Δ^5 -avenasterol [2, 3]. Mustard oil contains a high level of tocopherols which amount is 410 mg/kg and γ -tocopherol predominates [13]. α -, β -, γ - and δ -Tocopherols are also established in mustard oil by Mortuza M., 2006 [2].

On the whole, the aim of the study is to be determined the lipid content, fatty acid composition, individual composition of phospholipids, sterols and tocopherols as well as oxidative stability of the oil isolated from five different accessions of mustard seeds.

MATERIALS AND METHODS

Samples

Five accessions of *Sinapis alba* L. with different origin has been analyzed. Two Russian (*Zuzanka* and *Stalingradskaya*), two Bulgarian (*BG431* and *BG290*) and one landrace from Romania (*RO268*) have been evaluated *ex situ* on the experimental field of the Institute of Plant Genetic Resources, Sadovo. Seeds were harvested at 10 % moisture, stored at room temperature and analyzed.

Isolation of glyceride oil and determination of oil content

Mustard oil was extracted from grounded seeds using n-hexane in a Soxhlet apparatus for 8 h [14].

* To whom all correspondence should be sent.
E-mail: zhanapetkova@uni-plovdiv.net

Fatty acid composition

Fatty acid composition of triacylglycerols (TAG) and sterol esters was determined by gas chromatography (GC) [15]. Fatty acid methyl esters (FAMES) were prepared by pre-esterification of the triacylglycerols, esterification of free fatty acids isolated from sterol esters after saponification with sulfuric acid in methanol [16]. Determination of FAMES was performed on HP 5890 gas chromatograph equipped with a 60 m x 0.25 mm x 25 µm capillary DB-23 column and a flame ionization detector. The column temperature was programmed from 130°C (hold 1 min), at 6.5°C/min to 170°C, at 3°C/min to 215°C (hold 9 min), at 40°C/min to 230°C (hold 1 min); the injector and detector temperature were 250°C. Hydrogen was the carrier gas at a flow rate 0.8 mL/min. Identification was performed by comparison of the retention times with those of a standard mixture of FAME subjected to GC under identical experimental conditions.

Determination of phospholipids

Ground seeds were subjected to Folch extraction [17]. Individual phospholipid classes were isolated by two-dimensional thin-layer chromatography (TLC) [18]. Identification was performed by comparing the respective R_f values with those of authentic standards. The quantification was carried out spectrophotometrically at 700 nm after scrapping the phospholipid spot and mineralization of the substance with a mixture of perchloric and sulphuric acid, 1 : 1 (v/v) [19].

Determination of sterols

Free ($R_f = 0.4$) and esterified sterols ($R_f = 0.8$) were isolated from the glyceride oil by TLC with mobile phase n-hexane: acetone, 100: 8 (v/v). Then free sterols were subjected to GC without derivatization while sterol esters were hydrolyzed with 2N KOH in ethanol and sterols were extracted with n-hexane and purified by TLC [20]. Sterol composition was determined on HP 5890 gas chromatograph equipped with a 30 m x 0.25 mm DB - 6 capillary column and flame ionization detector. The temperature gradient was 90°C (hold

2 min) up to 290°C at a rate of change 15°C/min and then up to 310°C at a rate of 4°C/min (hold 10 min); the injector and detector temperature was 300°C and 320°C. Hydrogen was the carrier gas at a flow rate of 0.8 mL/min. Identification was confirmed by comparison of retention times with those of a standard mixture of sterols.

Determination of tocopherols

Determination of tocopherols was carried out by high performance liquid chromatography (HPLC) [21] on 250 mm x 4 mm Nucleosil Si 50-5 column and fluorescent detection at 295 nm excitement and 330 nm emission. The operating conditions were mobile phase of n-hexane: dioxane, 96:4 (v/v) and flow rate 1 mL/min.

Oxidative stability

The oxidative stability (induction period in hours) was determined by Rancimat apparatus Methrom 679 (at 100 °C and an air flow rate 20 L/h) [22].

RESULTS AND DISCUSSION

Total oil content of different accessions of mustard seeds, the quantity of biologically active substances of the oils as well as their oxidative stability were established (Table 1).

Oil content in all examined oils differed in small range (22.4 – 29.4%) apart from accession *Zuzanka* where its quantity was higher (38.9%). Similar results were observed in previous studies where the oil content was 28.0 – 42.0% [1, 4, 5, 6]. Phospholipid content in the oils varied from 3.6 to 6.9% where their amount in *Stalingradskaya* was found to be similar to those presented by Parti *et al.*, 2003 [4] (6.44%).

On the other hand, these values were much higher than results reported by Chhokar *et al.*, 2008 [1] where the amount of phospholipids in mustard oil was significantly lower (1.32%). Total sterol content in all samples was about 0.4 – 0.5% which was lower than data reported by Nagaraj, 2009 (0.8%) [3].

Table 1. Lipid composition of mustard seeds

Compounds	Accessions				
	BG 431	BG 290	RO 268	Zuzanka	Stalingradskaya
Oil content, %	26.7	29.4	26.8	38.9	22.4
Phospholipids, %	3.6	4.4	5.6	4.2	6.9
Sterol content, %	0.51	0.44	0.47	0.37	0.48
- free	0.42	0.34	0.38	0.30	0.38
- esterified	0.09	0.10	0.09	0.07	0.10
Tocopherols, mg/kg	705	465	1025	353	456
Oxidative stability, h	25.1	14.8	16.4	17.0	22.3

Fraction of free sterols was comprised by approximately 80.0 % of total sterols. The amount of free sterols in all samples (0.30 – 0.42%) was approximately four times higher than this of esterified sterols (0.07 – 0.10%). Nonetheless, according to Nagaraj, 2009 [3] the fraction of free sterols was presented in lower quantity (0.32%) than esterified sterols (0.48%). Tocopherol content in seed oil from Romania (*RO 268*) was found to be in high level (1025 mg/kg) followed by Bulgarian accession *BG 431* (705 mg/kg). Tocopherol content of the others seed oils were from 353 to 465 mg/kg which was in a good agreement with Vaidya and Choe, 2011 [13]. Oxidative stability of all seed oils was 14.8 – 25.1h. This results were higher than that observed by Ciubota-Rosie et al., 2013 [23] and Jham et al., 2009 [24] (7h). The seed oils from *BG431* and *Stalingradskaya* were found to be more stable against oxidation than the others samples.

Fatty acid composition of triacylglycerols of mustard seed oils is shown in Table 2.

Table 2. Fatty acid composition of triacylglycerols of mustard oils

Fatty acids, %	Accessions				
	<i>BG 431</i>	<i>BG 290</i>	<i>RO 268</i>	<i>Zuzanka</i>	<i>Stalin-gradskaya</i>
C 12:0	0.2	0.2	0.2	0.3	0.2
C 14:0	0.1	0.2	0.2	0.4	0.2
C 14:1	0.3	0.4	0.4	0.6	0.4
C 16:0	4.0	4.5	4.8	5.2	3.9
C 16:1	0.3	0.3	0.3	0.3	0.2
C 18:0	1.6	2.0	2.3	2.3	1.3
C 18:1	13.7	23.8	20.9	25.1	21.2
C 18:2	11.5	17.4	14.7	13.5	4.9
C 18:3	3.6	5.9	5.4	4.5	2.1
C 20:0	1.3	1.4	1.7	1.1	0.9
C 20:1	9.4	13.9	14.2	11.1	10.6
C 20:2	0.8	0.9	0.7	0.6	0.2
C 22:0	1.8	1.1	1.5	1.0	0.7
C 22:1	51.4	28.0	32.7	34.0	53.2
SFA	9.0	9.4	10.7	10.3	7.2
UFA	91.0	90.6	89.3	89.7	92.8
MUFA	75.1	66.4	68.5	71.1	85.6
PUFA	15.9	24.2	20.8	18.6	7.2

As can be seen, erucic, oleic, linoleic and gadoleic fatty acids were the major components in triacylglycerol fraction in all examined seeds oils. Erucic acid predominated in all of them and varied from 28.0 to 53.2% considering that it was higher in the seed oils from accessions *BG 431* and *Stalingradskaya*. The latter was in a good agreement with results reported by George et al., 1985 [6]. The presence of erucic acid in accession *BG 290* (28.0%) was the same as the data reported

by Vaidya and Choe, 2011 [13]. Moreover, its amount in *RO 268* was almost similar to this in *Zuzanka*. The quantity of oleic acid for all investigated oils was from 13.7 to 25.1%, which was in a good agreement with results reported by Vaidya and Choe, 2011 [13] and Chhokar et al., 2008 [1] apart from accession *BG 431* where it was lower and similar to data observed by Parti et al., 2003 [4]. Linoleic acid was found to be 11.5 – 17.4% in all samples except the oil from *Stalingradskaya* where its amount was lower (4.9%). The data was close to this reported by Parti et al., 2003, Chhokar et al., 2008 and Vaidya and Choe, 2011 [1, 4, 13]. Interestingly, there was higher level of gadoleic acid (9.4 – 14.2%) in all investigated mustard seed oils and the amount of linolenic acid was about 5.0% apart from accessions *BG 431* and *Stalingradskaya* where its quantity was 3.6 and 2.1%, respectively. Unsaturated fatty acids (UFA), especially monounsaturated (MUFA), predominated in all the oil of accessions. The content of UFA was higher in *Stalingradskaya* (92.8%) and lower in *RO 268* and *Zuzanka* (89.7%). The quantity of PUFA varied from 7.2 (*Stalingradskaya*) to 24.2% (*BG 290*) and those of MUFA – from 66.4 (*BG 290*) to 85.6% (*Stalingradskaya*). The higher level of UFA was at the expense of the lower amount of SFA which were presented mainly by palmitic acid.

Composition of free and esterified sterols of different accessions of mustard seed oils is presented in Table 3.

The composition of free sterols and sterol esters was similar in all mustard oils but there were differences in the quantity for all their representatives. β -Sitosterol was the main component in all samples and its amount was approximately the same in both sterol fractions (51.9 – 55.9% in free sterols and 52.8 – 53.9% in esterified sterols) except *Stalingradskaya* where it was found to be 59.7% in esterified sterols.

The percentage of campesterol was higher in sterol esters (31.1 – 33.5 % vs. 19.1 – 30.5 % in free sterols) while the content of stigmaterol was close in both fractions (1.1 – 1.5% in free sterols and 0.9 – 2.1% in esterified sterols). There was low content of cholesterol in both fractions but in the sterol esters it was several times higher than free ones.

Fatty acid composition of sterol esters is shown in Table 4.

Erucic acid was the major component in all samples (26.7 – 46.2%), followed by oleic acid (19.4 – 32.0%).

Table 3. Individual composition of free and esterified sterols of mustard oils

Sterols, %	Accessions									
	BG 431		BG 290		RO 268		Zuzanka		Stalingradskaya	
	free	esteri- fied	free	esteri- fied	free	esteri- fied	free	esteri- fied	free	esteri- fied
Cholesterol	.*	1.0	0.2	0.7	0.2	0.7	-	0.5	-	-
Brassicasterol	22.5	8.9	22.2	7.0	20.7	5.5	19.3	6.1	11.9	3.7
Campesterol	19.5	31.1	19.6	32.5	19.1	31.9	24.2	33.5	30.5	32.2
Stigmasterol	1.5	0.9	1.3	1.0	1.2	1.3	1.5	2.1	1.1	1.5
β - Sitosterol	52.8	53.8	53.5	52.8	55.9	53.6	51.9	53.9	53.8	59.7
Δ⁵ - Avenasterol	0.6	0.9	0.5	1.1	0.4	1.0	0.6	0.3	0.5	0.6
Δ⁷ - Stigmasterol	0.3	0.5	0.3	0.5	0.3	0.9	0.4	0.7	0.3	0.3
Δ⁷ - Avenasterol	2.8	2.9	2.4	4.0	2.2	4.5	2.1	2.9	1.9	2.0

* - Not identified

Table 4. Fatty acid composition of esterified sterols of mustard oils

Fatty acids, %	Accessions				
	BG 431	BG 290	RO 268	Zuzanka	Stalin-gradskaya
C 12:0	0.4	0.4	0.2	1.4	0.9
C 12:1	1.0	1.0	1.0	1.1	1.0
C 14:0	1.0	0.6	0.5	1.8	1.2
C 14:1	1.0	1.2	1.9	1.4	1.8
C 15:0	0.3	0.2	0.2	0.5	0.3
C 16:0	10.9	8.1	9.8	16.7	12.9
C 16:1	0.9	0.5	0.5	1.0	1.2
C 17:0	0.3	0.2	0.2	0.6	0.4
C 18:0	3.2	3.0	4.0	5.5	3.7
C 18:1	19.4	27.8	26.5	27.3	32.0
C 18:2	3.4	7.0	3.5	3.3	3.5
C 18:3	0.2	0.5	0.3	0.1	0.3
C 20:0	1.3	1.6	2.0	1.6	0.9
C 20:1	8.0	13.7	14.7	9.0	8.2
C 20:2	0.3	0.4	0.2	0.4	0.4
C 22:0	2.2	1.2	1.3	1.6	1.0
C 22:1	46.2	32.6	33.2	26.7	30.3
SFA	19.6	15.3	18.2	29.7	21.3
UFA	80.4	84.7	81.8	70.3	78.7
MUFA	76.5	76.8	77.8	66.5	74.5
PUFA	3.9	7.9	4.0	3.8	4.2

The highest amount of erucic acid was established in BG 431 (46.2%) at the expense of lower quantity of oleic acid (19.4%). On the other hand, bigger quantity of oleic acid was found to be in seed oil from accession Stalingradskaya (32.0%). Palmitic acid was presented in smaller amounts in BG 431, BG 290 and RO 268 (8.1 – 10.9%) but it was higher in Zuzanka and Stalingradskaya (12.9 – 16.7%). The quantity of stearic acid in all samples varied from 3.0 to 5.5%. The content of linoleic acid varied from 3.3 to 7.0% and those of linolenic and eicosadienoic acid were found to be less than 0.5%.

The qualitative composition was similar to this of triacylglycerols but there were quantitative differences between all accessions. The amount of erucic acid in BG 431, Zuzanka and Stalingradskaya was lower in esterified sterols (26.7 – 46.2%) than in

triacylglycerols (34.0 – 53.2%). On the other hand, its quantity in BG 290 and RO 268 was higher in sterol esters (32.6 – 33.2%) than in triacylglycerols (28.0 – 32.7%). There were similar differences in the content of other fatty acids such as oleic, palmitic and gadoleic for all investigated seed oils. Considerably higher percentage of SFA was found in sterol esters than in TAG (15.3 – 29.7% vs. 7.2 – 10.7%). On the other hand, the amount of unsaturated fatty acids in sterol fraction was lower (70.3 – 84.7%) than in TAG (89.7 – 92.8%). SFA in seed oil from Zuzanka were found to be 29.7% but the amount of those in other accessions were significantly lower (15.3 – 21.3%). The quantity of MUFA varied from 66.5 to 77.8% while these of PUFA were 3.8 – 7.9% which was lower than in TAG (7.2 – 24.2%). Individual tocopherol composition is given in Table 5.

Table 5. Tocopherol composition of mustard oils

Tocopherols, %	Accessions				
	BG 431	BG 290	RO 268	Zuzanka	Stalingradskaya
α -tocopherol	26.5	26.5	17.4	37.2	16.1
β -tocopherol	-*	-	4.2	-	-
β -tocotrienol	-	-	1.6	-	-
γ -tocopherol	70.7	73.5	60.1	63.8	82.7
γ -tocotrienol	-	-	9.3	-	1.2
δ -tocopherol	2.8	-	7.4	-	-

* - Not identified

Table 6. Phospholipid composition of mustard oils

Phospholipids, %	Accessions				
	BG 431	BG 290	RO 268	Zuzanka	Stalingradskaya
Phosphatidylcholine	51.0	50.2	46.1	37.1	37.2
Phosphatidylinositol	23.8	28.0	29.3	23.7	24.5
Phosphatidylethanolamine	16.8	14.2	17.2	16.5	17.9
Phosphatidic acids	1.1	0.5	0.7	6.0	-*
Phosphatidylserine	0.6	0.2	0.2	3.1	4.2
Sphingomyeline	2.5	3.0	2.6	4.3	5.2
Others	4.2	3.9	3.9	9.3	11.0

* - Not identified

γ -Tocopherol predominated in all investigated mustard oils and it was over 70.0% except in RO 268 and Zuzanka. The amount of α -tocopherol was found to be higher in BG 431 (26.5%), BG 290 (26.5%) and Zuzanka (37.2%), while in seeds oils from RO 268 and Stalingradskaya were established significantly lower quantities (16.1 and 17.4%). There were minor amounts of β - and δ -tocopherol as well as unsaturated derivatives β - and γ -tocotrienol (observed only in RO 268).

Phospholipid composition of mustard seed oils is shown in Table 6.

The major phospholipid components were phosphatidylcholine (37.1 – 51.0%) followed by phosphatidylinositol (23.7 – 29.3%) and phosphatidylethanolamine (14.2 – 17.9%). Accessions Zuzanka and Stalingradskaya were observed to contain lower quantity of phosphatidylcholine at the expense of higher content of the other phospholipids. The quantity of sphingomyeline was considerably higher (2.5 – 5.2%) which made mustard seed oil different from the other vegetable oils (1.0 – 2.0%) [25].

CONCLUSIONS

All investigated seeds of *Sinapis alba* were found to be rich in glyceride oil which contained great amount of biological active substances. There were some differences in fatty acid composition as well as in sterol, phospholipid and tocopherol content as a result of the genotype of the plants, climatic and agrometeorologic conditions. On the whole, it could be summarized that because of the higher quantity of erucic acid all of the examined

seed oils were not suitable for human consumption, but could be used for biodiesel production.

REFERENCES

1. V. Chhokar, V. Beniwal, A. Kumar, J. Rana, *Asian J. Exp. Chem.*, **3**, 6 (2008).
2. M. Mortuza, *Pak. J. Biol. Sci.*, **9**, 1812 (2006).
3. G. Nagaraj, *Oilseeds – properties, processing, products and procedures*. New India Publishing Agency, 2009.
4. R. Parti, V. Deep, S. Gupta, *Plant Foods Hum. Nutr.*, **58**, 1 (2003).
5. C. Damian, *Lucrări Științifice - Zootehnie*, **61**, 39 (2014).
6. L. George, D. Suryavanshi, A. Sipahimalani, V. Srinivasan, *Proc. Ind. Natn. Acad.*, **4**, 511 (1985).
7. A. Khan, P. Sankhyan, S. Kumar, *Asian J. Adv. Basic Sci.*, **1**, 2347 (2013).
8. R. Ecker, Z. Yaniv, *Euphytica*, **69**, 45 (1993).
9. J. Raney, G. Rakow, T. Olson, Proc. 9th Int. Rapeseed Congr., Cambridge, United Kindom, 1995, **2**, 416–418.
10. R. Scarth, J. Tang, *Crop Sci.*, **46**, 1225 (2006).
11. E. Tian, F. Zeng, K. MacKay, V. Roslinsky, B. Cheng, *PLoS ONE*, **9** (5): e97430 (2014).
12. F. Katepa-Mupondwa, R. Gugel, J. Raney, *Can. J. Plant Sci.*, **86**, 1015 (2006).
13. B. Vaidya, E. Choe, *Food Sci. Biotechnol.*, **20**, 193 (2011).
14. ISO 659:2009. *Oilseeds – Determination of oil content*, p. 12 (2009).
15. ISO 5508:2004. *Analysis by gas chromatography of methyl esters of fatty acids* (2004).
16. W. Christie, *Lipid Analysis*. The Oily Press: Bridgwater (3rd Ed.), England, 2003.
17. J. Folch, M. Lees, G.H. Sloane-Stanley, *J. Biol. Chem.*, **226**, 498 (1957).

18. R. Schneiter, G. Daum, In: Yeast Protocol: Second Edition, Methods in Molecular Biology, 313, Edited by: Xiao W., Humana Press Inc., Totowa N. J., 2006.
19. ISO 10540-1:2003. *Determination of phosphorus content – Part 1: Colorimetric method* (2003).
20. ISO 12228:1999. *Determination of individual and total sterols contents - Gas chromatographic method* (1999)
21. ISO 9936:2006. *Determination of tocopherol and tocotrienol contents by HPLC* (2006).
22. ISO 6886:2006. *Determination of oxidative stability* (2006).
23. C. Ciubota-Rosie, J.R. Ruiz, M.J. Ramos, Á. Pérez, *Fuel*, **105**, 572 (2013).
24. G. Jham, B. Moser, S. Shah, R. Holser, O. Dhingra, S. Vaughn, *J. Am. Oil Chem. Soc.*, **86**, 917 (2009).
25. F.D. Gunstone, J.L. Harwood, A.J. Dijkstra, *The Lipid Handbook*, 3rd Ed., CRC Press Taylor and Francis Group, Boca Raton, London, New York, 2007.

ЛИПИДЕН СЪСТАВ НА СЕМЕНА ОТ СИНАП (*Sinapis alba* L.)

Г. А. Антова¹, М. Й. Ангелова-Ромова¹, Ж. Ю. Петкова^{1*}, О. Т. Тенева¹, М. П. Марчева²

¹ ПУ „Паусий Хилендарски”, Катедра „Химична технология”, ул. „Цар Асен” 24, 4000 гр. Пловдив, България

² Аграрен университет - Пловдив, бул. „Менделеев” 12, 4000 гр. Пловдив, България
Постъпила на 11 ноември 2016 г.; приета на 5 декември 2016 г.

(Резюме)

Изследван е липидния състав на семена от пет образци синап (*Sinapis alba* L.). Съдържанието на глицеридно масло в семената е от 22.4 до 38.9%. Основните мастни киселини в триацилглицеролите са ерукова (28.0 – 53.2%), олеинова (13.7 – 25.1%), палмитинова (3.9 – 5.2%), гадолеинова (9.4 – 14.2%) и линолова киселина (4.9 – 17.4%). Общото фосфолипидно съдържание варира между 3.6 и 6.9%, като основните представители са фосфатидилхолин, фосфатидилинозитол и фосфатидилетаноламин. В стероловата фракция (0.37 – 0.51%) основните компоненти са β -ситостерол (51.9 – 55.9% в свободните стероли и 52.8 – 59.7 % в стероловите естери), последван от кампестерол (19.1 – 30.5% и 31.1 – 33.5% съответно) и брасикастерол (11.9 – 22.5% и 3.7 – 8.9%). Маснокиселинният състав на стероловите естери е подобен на този на триацилглицеролите с изключение на палмитиновата киселина, чието количество е по-високо в свързаните стероли. Съдържанието на токофероли е 456 – 1025 mg/kg, като основните представители са α - и γ -токоферол. Оксидантната стабилност на изследваните масла от семена от *Sinapis alba* L. е сравнително висока (14.8 – 25.1 h).

Ключови думи: *Sinapis alba* L., глицеридно масло, маснокиселинен състав, фосфолипиди, стероли, токофероли

Spectral similarity versus structural similarity: Raman spectra

P. N. Penchev*, S. H. Tsoneva, S. R. Nachkova

Department of Analytical Chemistry and Computer Chemistry,

University of Plovdiv "Paisii Hilendarski", 24 Tzar Asen Str., 4000 Plovdiv, Bulgaria,

Received November 13, 2016; Revised November 28, 2016

The study of the relation of spectral similarity and structural similarity shows that the search in Raman spectral libraries gives hitlist compounds structurally similar to the unknown and that the peak search performs equal with the full spectrum search algorithm based on the correlation coefficient. As a result of the study the optimal values for peak search tolerances were found and they are higher than those suited for identity search.

Key words: Raman spectra, spectral similarity, structural similarity

INTRODUCTION

Despite the advance of various 1D and 2D NMR experiments [1] and hyphenated techniques in chromatography [2] the Fourier transform (FT) mid-infrared (MIR) absorption spectroscopy is still the most used routine method in organic labs for the confirmation of structures or identification of known organic compounds (either pure or in mixtures). Nowadays, as an analytical technique, FT-Raman spectroscopy offers many pluses over FT-MIR spectroscopy [3]. The most important of them are the following: (1) little or no sample preparation is required; (2) water as a liquid is a weak scatterer – no special accessories are needed for measuring aqueous solutions; (3) water vapors and carbon dioxide are very weak scatterers – sample compartment purging is unnecessary; (4) Raman bands are narrower and both the overtones and combination bands are generally weak; (5) the spectral range reaches well below 400 cm⁻¹, making the technique applicable to organic compounds containing heavier elements; (6) The symmetric molecular vibrations which appear as low-intensity bands in the IR spectrum exhibit very strong Raman bands. Also here has to be mentioned that the construction of Raman spectral libraries is widely in progress [3].

The current study of ours cast light on the capability of so called *similarity search* in Raman spectral libraries to obtain a list of compounds (called *hitlist*) whose structures are most similar to that of the unknown. The similarity search capability of IR and Raman databases has been extensively explored since late 1970s [4] and has been proven to exist. Later, a practically oriented approach of extracting large and frequent substructures contained in the IR hitlist structures

has been developed [5]. A successful attempt has been made by Varmuza and co-workers to formalize and systematize the study of structure/spectrum relation for IR [6] and low resolution mass-spectra [7]. In the present paper we apply the method of Varmuza *et al.* [6] and extend it to Raman spectra.

SPECTRA AND METHODS

The Raman database used consists of 330 Raman spectra of organic compounds. The Raman spectra are measured in our lab on RAM II (Bruker Optics) with a focused laser beam of Nd:YAG laser (1064 nm) from 4000 cm⁻¹ to 51 cm⁻¹ at resolution 2 cm⁻¹ with 25 scans. The compound structures are represented as connection tables and binary substructure descriptors (0/1) are calculated by software *SubMat* [6] (supplied by Prof. Varmuza) using a set of 500 substructures. The similarity of chemical structures is calculated with these descriptors by the commonly used Tanimoto index [8] as it is done in [6-7].

The comparison of Raman spectra is done by two different spectral similarity measures, SpSim₁ and SpSim₂, given by Eqns. 1 and 2, respectively.

$$\text{SpSim}_1 = 2K / (M + N) \quad (1)$$

$$\text{SpSim}_2 = \frac{\sum_k A_k^U A_k^R}{\|A^U\| \cdot \|A^R\|}, \quad (2)$$

where K is the number of matched bands in the two spectra (U and R) each of them consisting of M and N spectral bands. The two expressions in the denominator of Eqn. 2 are the Euclidean norm of the vector composed of the corresponding peak intensities [9]. In our library search software IRSS [5, 9] the spectral bands are represented with their intensity and wavenumber only. Two peaks are

* To whom all correspondence should be sent.
E-mail: plamen@uni-plovdiv.net

regarded as matched if one falls within the two intervals centered around the other peak. First interval has a width equal to twice the wave number tolerance, $\Delta\nu$, and the second twice the intensity tolerance, ΔI . The peak matching is illustrated in detail in our previous paper [10]. For comparison purpose, a full spectrum search algorithm based on the correlation coefficient is used [5].

The criterion for capability of the similarity search, *grand mean of Tanimoto indices*, $T(h)$, is borrowed from Varmuza et al. [6] (Eqns. 11 and 12 in the cited paper). With 'h' is designated the number of hits which are used for finding the corresponding Tanimoto index average values.

RESULTS AND DISCUSSION

A general opinion among the spectroscopists is that the peak search in IR libraries gives lesser results than full spectrum search: even such was our experience when the maximum common substructure (MCS) concept had been applied to hitlist structures [5]. It has to be mentioned, however, that these findings were produced with both tolerances—in absorbance, ΔA , and wavenumber, $\Delta\nu$ —being small and thus suited for identity search. Furthermore, that was a result of numerous search sessions and intuitive assessment of search performance by a spectroscopist.

The found optimal tolerances for identity IR library search are in the range $\Delta A = 0.4 - 1.0$ a.u. and $\Delta\nu = 4 - 7$ cm^{-1} [11] when SpSim_2 was used. For identity Raman library search these appeared to be $\Delta I = 0.2 - 1.0$ arbitrary intensity units (a.i.u.) and $\Delta\nu = 4 - 11$ cm^{-1} . For both spectral methods as measure of the identity search effectivity the average hit position of 'the unknown' was used as optimum criterion: both tolerances were varied in the intervals 0.1 - 1.0 a.u./a.i.u. and $\Delta\nu = 3 - 50$ cm^{-1} , respectively, and test search sessions with 50 spectra were used.

The proposed by Varmuza et al. method allows to quantitatively estimate similarity search results and find the optimal tolerance values. To find the optimal tolerances for similarity peak search (PS) each Raman spectrum of the spectral library was searched in the same library and the first hit (identical spectrum) was removed thus calculating the grand mean $T(1)$ of Tanimoto indices upon 330 search sessions. Fig. 1 shows $T(1)$ as a function of ΔI and $\Delta\nu$ when SpSim_1 is used, and Fig. 2 when SpSim_2 is applied.

As can be seen from both figures, the highest $T(1)$ values are around 0.60 which compared to the average best structural similarity of 0.80 is neither so low nor so high as one can wish. The average

structural similarity of Raman library is 0.30 which is quite low than the highest $T(1)$ values.

When the full spectrum search algorithm based on the correlation coefficient (CC) is used, the value of $T(1)$ is nearly the same as the above mentioned one: the situation different from the corresponding comparison made for IR spectra where $T_{\text{PS}}(1) = 0.70 < T_{\text{CC}}(1) = 0.74$. It has to be noted here that the statistical distribution of these obviously random variables is unknown and thus an interval estimate could not be made but the curves 'h / $T(h)$ ' for IR spectra are quite distinctive and different from one another which is not the case for Raman spectra (see Fig. 3).

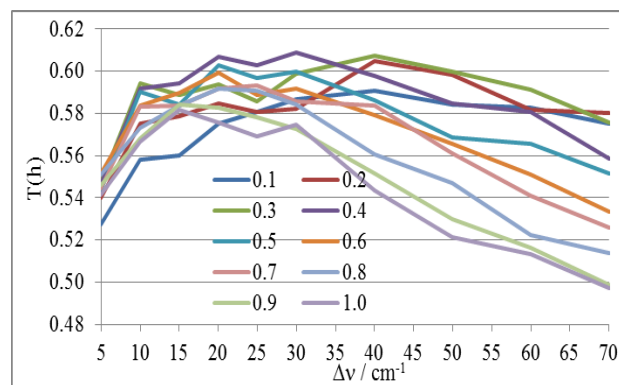


Figure 1. Grand mean of Tanimoto indices as a function of the wavenumber tolerance, $\Delta\nu$, varied by different values of the second tolerance, ΔI . The used spectral similarity measure is SpSim_1 .

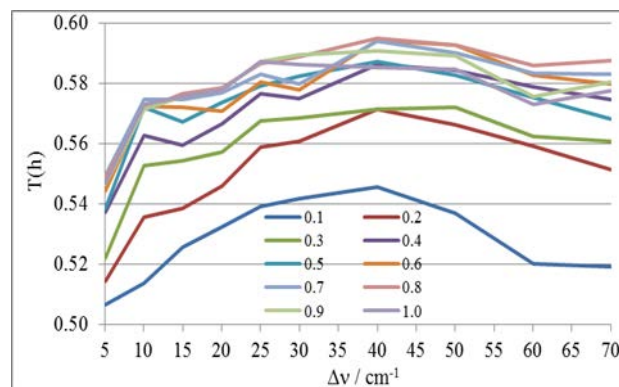


Figure 2. Grand mean of Tanimoto indices, $T(h)$, as a function of the wavenumber tolerance, $\Delta\nu$, varied by different values of the second tolerance, ΔI . The used spectral similarity measure is SpSim_2 .

The last could be attributed to higher variability of the intensity of the characteristic group vibrations in Raman spectra than in IR spectra [12]. As a whole, the discussed results proved that Raman spectra can be used for similarity search and one can derive some conclusions about the unknown structure by a surveying the hitlist structures in some way or the other.

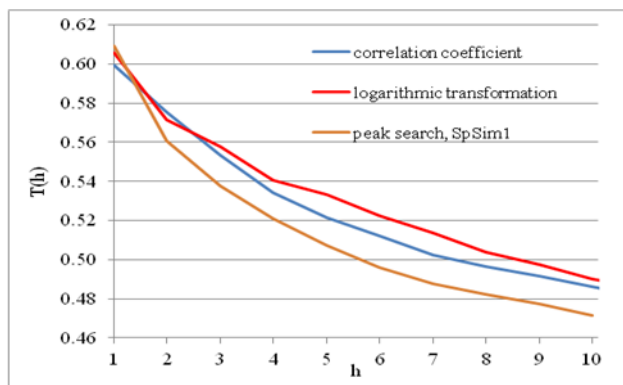


Figure 3. Grand mean of Tanimoto indices, $T(h)$, as a function of the hit position, h , for search in the Raman library. The peak search is done with $SpSim_1$ and $\Delta I = 0.4$ a.i.u. and $\Delta \nu = 30$ cm^{-1} . Logarithmic transformed spectra are compared by full spectrum search algorithm based on the correlation coefficient.

The found optimal values from Fig. 1 are $\Delta I = 0.3 - 0.4$ a.i.u. and $\Delta \nu = 20 - 40$ cm^{-1} and from Fig. 2 $\Delta I = 0.7 - 0.9$ a.i.u. and $\Delta \nu = 30 - 55$ cm^{-1} . As expected, the sensitivity (recall) is lost by small values of both tolerances and the selectivity is lost by their high values and obviously both tendencies lead to the $T(1)$ decrease. The wider optimal tolerance intervals for the second spectral similarity measure are explained with its better selectivity which is achieved by the dot product (scalar product) of peak intensities in the numerator in Eqn. 2. The other facts that support the last assertion are the less steep of the curves in Fig. 2 when the wavenumber increases and that nearly all of the curves are close to each other. A detail view of both figures reveals that the curves are shifted upwards and downwards with the change of ΔI in a systematic way despite the small library size.

As mentioned above, for Raman spectra there is no difference between similarity search capabilities of the full spectrum search and the peak search. This can be clearly seen from Fig. 3 where an additional spectrum transformation—a logarithm of intensities—was tried to improve the similarity search. Since Raman intensities are saved as byte variable (from 0 to 255) in the libraries maintained by our software IRSS, it was hoped that the transformation given by Eqn. 3 will decrease the effect of variability of Raman band intensities, I_k . As seen, the gain in the similarity search capability is only for hits at positions 3 to 10 but the overall structural similarity of hitlist structures to that of the unknown is very important for such methods as MCS and k-nearest neighbors which use all hitlist structures.

$$I_k^{\log} = \log_2(I_k + 1) / 8 \quad (3)$$

The similarity search can be explored also with the distributions of structural similarity of three kinds of pairs as it is shown in Fig. 4.

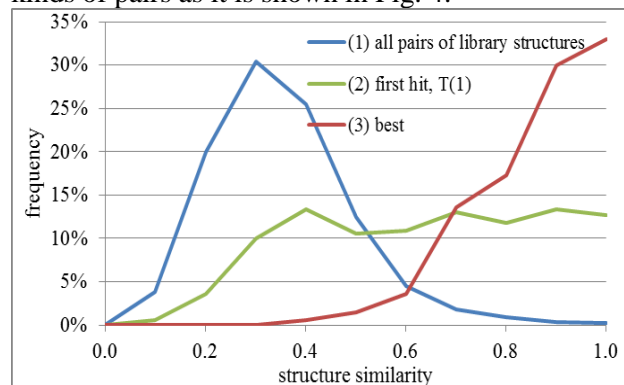


Figure 4. The distribution of structural similarity of three kinds of pairs (see text for explanation).

For (1) all pairs of library structures (altogether $330 \times 329 / 2 = 54,285$ pairs), for (2) 'unknown/first-hit' pairs (330 $T(1)$ values), and for (3) the 'structure/its-most-similar-structure' pairs (also 330 pairs). As can be seen, the distributions of the first two kinds of pairs are different and on average the library search does give a structurally similar first hit. Of course, there is a heavy overlap between them and the middle histogram is not closer the rightmost one which is a perfect case of $T(1)$ distribution.

CONCLUSION

The performed study showed that the search in Raman spectral libraries gives hitlist compounds structurally similar to the unknown and the corresponding hit structures can be used in the structure elucidation process. The peak search performs equal with the full spectrum search algorithm based on the correlation coefficient due to higher variability of the intensity of the characteristic group vibrations in Raman spectra than in IR spectra as the high values of ΔI tolerance compensate the difference in band intensity in structurally similar compounds.

Acknowledgment We thank Prof. Kurt Varmuza for providing the software SubMat and dedicate this paper to him on the occasion of his 75th anniversary (22 February 2017).

REFERENCES

1. M. E. Elyashberg, A. Williams, K. Blinov, Contemporary Computer-Assisted Approaches to Molecular Structure Elucidation, Royal Society of Chemistry, London, 2012.
2. R. Freitag (ed.), Modern Advances in Chromatography. Springer-Verlag, Berlin, 2002.

3. E. Smith and G. Dent, *Modern Raman Spectroscopy – A Practical Approach*, John Wiley & Sons, New York, 2005.
4. H. J. Luinge, *Vib. Spectrosc.*, **1**, 3-18 (1990).
5. K. Varmuza, P. Penchev, H. Scsibrany, *J. Chem. Inf. Comput. Sci.*, **38** (3), 420-427 (1998).
6. K. Varmuza, M. Karlovits, W. Demuth, *Anal. Chim. Acta*, **490**, 313–324 (2003).
7. W. Demuth, M. Karlovits, K. Varmuza, *Anal. Chim. Acta*, **516**, 75-85 (2004).
8. K. Varmuza, P. Filzmoser, *Introduction to Multivariate Statistical Analysis in Chemometrics*, CRC Press, Boca Raton, 2009.
9. P. N. Penchev, N. T. Kochev and G. N. Andreev, *Compt. Rend. Acad. Bulg. Sci.*, **51**, 67-70 (1998).
10. P. N. Penchev, V. L. Miteva, A. N. Sohou, N. T. Kochev, G. N. Andreev, *Bulg. Chem. Commun.*, **40**, 556-560 (2008).
11. P. N. Penchev, Dr.Sc. Dissertation, University of Plovdiv, Plovdiv, 2016.
12. G. N. Andreev, private communication.

ВРЪЗКА МЕЖДУ СПЕКТРАЛНОТО ПОДОБИЕ И СТРУКТУРНОТО ПОДОБИЕ ЗА РАМАН СПЕКТРИ

П. Н. Пенчев*, С. Х. Цонева, С. Р. Начкова

*Катедра „Аналитична химия и компютърна химия“,
Пловдивски Университет „Паусий Хилендарски“, ул. Цар Асен № 24, 4000 Пловдив,
e-mail: plamen@uni-plovdiv.net*

Постъпила на 13 ноември 2016 г.; приета на 28 ноември 2016 г.

(Резюме)

Изследването на връзката между спектрално подобие и структурно подобие показва, че търсенето по подобие в Раман спектрални библиотеки е подходящо за процеса на разкриване структурата на неизвестни съединения. В резултат на изследването са намерени оптималните стойности на толерансите, използвани при пиково търсене и те са по-големи от тези, които са подходящи за търсене за идентификация.

Ключови думи: Раман спектри, спектрално подобие, структурно подобие

Fatty acids, tocopherols and oxidative stability of hazelnuts during storage

S.M. Momchilova^{1*}, S.P. Taneva¹, M.D. Zlatanov²,
G.A. Antova², M.J. Angelova-Romova², E. Blagoeva³

¹ Institute of Organic Chemistry with Centre of Phytochemistry, Bulgarian Academy of Sciences,
Acad. G. Bonchev Str., bl. 9, 1113 Sofia, Bulgaria

² Department of Chemical Technology, University of Plovdiv "Paisii Hilendarski",
24 Tzar Assen Str., 4000 Plovdiv, Bulgaria

³ Agricultural Experiment Station, 1 Minjorska Str., 6600 Kardzhali, Bulgaria

Received November 13, 2016; Revised December 6, 2016

Hazelnuts of three cultivars (*Ata Baba*, *Ran Trapezundski* and *Tonda Gentile*) grown in Bulgaria were stored for 1, 3, 6 and 12 months at different conditions: unshelled (in shell) or shelled (kernels), at 4°C (fridge) or at 20°C (in shadow), and then were analyzed about fatty acids composition, tocopherols and oxidative stability (induction period) of their oil. The results revealed that fatty acids were not practically changed up to 12 months in spite of the different storage conditions whereas the tocopherols amount gradually decreased and that trend was slightly stronger at 20°C than at 4°C as well as for nuts in shell than the kernels. Concerning oxidative stability, the oil from initial hazelnuts had long induction period (40, 47 and 58 hours for *Ata Baba*, *Ran Trapezundski* and *Tonda Gentile* cultivars, respectively). This oxidative stability gradually decreased during the storage period with the same trend, namely the hazelnuts stored at 20°C in shell had slightly shorter induction periods than the corresponding kernels stored at 4°C. All these results indicate that it is possible to store hazelnuts up to 12 months without considerable and harmful changes in their main lipid characteristics. In order to keep their quality at most it is preferable to store them as kernels at 4°C.

Key words: hazelnuts, storage, fatty acids, tocopherols, oxidative stability

INTRODUCTION

Nuts have been known and used as food since ancient times [1] and during the years their health benefits have been clearly recognized [2, 3]. Among all nuts hazelnuts are preferable because of their delicious taste, delicate flavor and beneficial nutritional properties. However, due to high fat content (above 60%) they tend to deteriorate as a result of lipid oxidation. Since the hazelnuts are consumed mainly as kernels the storage conditions are of crucial importance to keep their quality for longer periods. In spite of the significance of that problem, there are not too many publications on the effects of storage conditions on the hazelnut lipid characteristics. Up to now the following have been studied: the storage atmosphere (air or enriched with oxygen vs. inert gases or vacuum [4–8]), temperature (mainly 4–7°C vs. 20–25°C [4, 7–10], in single cases –25°C [8, 11] or even 55°C [12]), the presence of nut shell [4, 5, 9, 10, 13]. The storage periods are usually up to 12 months [4, 5, 7–12, 14], but also periods of two [13] or four [15] years have been tested. The investigated hazelnut characteristics are: textural [6, 11] or sensory [6, 7, 10] attributes, total phenolics [7, 8, 10], acidity and/or peroxide value [4, 7, 10, 13], hexanal content [7, 8], conjugated dienes and trienes [4],

α -tocopherols [12, 13], fatty acids [5, 9, 13–15]. Unfortunately, in these investigations the effects of only single storage condition on particular lipid attribute have been examined. Moreover, some results are contradictory. For that reasons the aim of our work was to study the effects of the two most popular and easy to perform even at home storage conditions, namely the temperature (4°C in fridge and 20°C in shadow) and the presence of nut shell, on the fatty acids, tocopherols and oxidative stability (Induction period in hours) of the oil from hazelnuts stored up to 12 months. Thus, some more general recommendations could be given in order to save the quality of nuts not only as industrial/market product but also as preferable dietary stored at home.

EXPERIMENTAL

Samples

Hazelnut cultivars *Ata Baba* (*Corylus pontica* C. Koch), *Ran Trapezundski* (*Corylus maxima* Mill.) and *Tonda Gentile* (*Corylus avellana* L.) were grown in orchards near the town of Kardzhali, Bulgaria. Fruits of three consecutive crops (2009–2011) were collected and corresponding portions of them were stored as kernels (shelled) or in shell, both types in polyethylene bags, at room temperature (20°C, in shadow) or in refrigerator

* To whom all correspondence should be sent.
E-mail: svetlana@orgchm.bas.bg

(4°C) for 1, 3, 6 and 12 months. Initial portions of hazelnuts were used as respective references (0 months storage).

Reagents

All reagents and solvents were of analytical grade and were used without additional purification. The reference fatty acid methyl esters and tocopherols were from Sigma-Aldrich Chemical Co. (St. Louis, MO, USA).

Extraction of lipids

Hazelnuts (each sample of about 20 g kernels after removing the shell) were ground and the oil was extracted with n-hexane in Soxhlet apparatus for 8 h [16]. The solvent was distilled in rotary evaporator and stock hexane solution of the oil was prepared.

Analysis of fatty acid (FA) composition

Fatty acids were determined by gas chromatography (GC) of their methyl esters (FAME). For the purpose, about 50 mg oil were transmethylated with 1 % sulfuric acid in methanol [17]. Then the FAME were purified by preparative silica gel thin-layer chromatography (TLC) on 20 x 20 cm glass plates developed with hexane-acetone (100:6, v/v) mobile phase. A drop of methyl oleate solution was used as a reference near the edge of the plate. After development, the zones were visualized under UV light (366 nm) after spraying with 0.1 % ethanolic 2',7'-dichlorofluorescein. FAME zone ($R_f \sim 0.7$) was scraped and eluted with diethyl ether in a small glass column. The solvent was evaporated under a gentle stream of nitrogen and the rest was dissolved in hexane to give 1 % solution of FAME. GC was performed on a Trace GC Ultra (Thermo Scientific, Bremen, Germany) gas chromatograph equipped with FID and a DB-225 60 m x 0.25 mm x 0.25 μm column (J&W Scientific, USA). The column temperature was programmed from 150°C to 240°C with 5°C/min and held at this temperature for 20 min. The injector and detector temperatures were 260°C and 280°C, respectively. Helium was the carrier gas at flow rate of 1.0 mL/min. Reference FAME mixture was used for peak identification according to the retention times. The analyses were performed in triplicate. The software package *Xcalibur™ 2.0*, Revision 2.0 SR 1 (Thermo Scientific, Bremen, Germany) was used to record and process the data.

Analysis of tocopherols

Tocopherols were analyzed directly by HPLC on 250 mm x 4 mm Nucleosil Si 50-5 column (Macherey-Nagel), eluted by hexane-dioxane

(96:4, v/v) and fluorescent detection at 290 nm excitement and 330 nm emission [18].

Determination of oxidative stability

Oxidative stability (Induction period in hours) was measured at 100°C (3 g oil sample, air flow 20 L/h) by Rancimat 679 (Metrohm, Switzerland) equipment.

Data processing

Mean values from three consecutive years, each with three parallel measurements, were compared by Student's t-test (Microsoft Excel software) [19].

RESULTS AND DISCUSSION

Fatty acid composition

The main fatty acids in the investigated hazelnuts are oleic (18:1, from 73.3 % to 80.4 % depending on the cultivar, Fig. 1), linoleic (18:2, with values of 7.2 %, 9.8 % and 14.5 % for Tonda Gentile, Ran Trapezundski and Ata Baba cultivars respectively, Fig. 2), palmitic (16:0, in the range 6.8 – 7.8 %, Fig. 3) and stearic (18:0, between 2.3 % and 2.8 %, Fig. 4). Other fatty acids as palmitoleic (16:1), linolenic (18:3), arachidic (20:0) etc. are below 0.2 %. As could be seen (Figs. 1 – 4), the cultivars Tonda Gentile and Ata Baba differ almost twice in their linoleic acid proportion. Nevertheless, fatty acids composition of the investigated hazelnuts in general is similar to that of Turkish [5], Italian, Spanish [12, 20], Croatian, French [21] cultivars. Unlike the available information about fresh hazelnuts the findings published about fatty acids composition of stored nuts are not too many, not systematic and indeed discrepant. Moreover, usually the effect of only single storage condition on fatty acids has been examined. Thus, Koyuncu *et al.* [14] have observed in kernels from three Turkish cultivars slight decrease of 18:2 after the 6th month storage at 21 °C in vacuum bags, without effect of the shell presence or absence on the fatty acids composition [5]. Other authors [9] have noticed increase of 18:0 (from 2.6 % to 3.1 %) after the 8th month and decrease of 18:3 (being 0.1 % in the initial oil) after the 12th month in whole hazelnuts stored at 20 °C but without such changes in kernels stored at 4 °C. Unfortunately, no comparative experiments with whole nuts stored at 4°C and kernels at 20°C were implemented.

On the other hand, Ebrahem *et al.* [13] have shown that 18:1 and 18:2 have not changed in kernels and in whole hazelnuts stored at 0 °C up to 12 months. Similarly, Beyhan *et al.* [15] have stored whole hazelnuts in warehouse up to 4 years practically without differences in their fatty acid composition. In addition to these results, our

experiments confirm that fatty acids have not been changed during hazelnut storage up to 12 months irrespective of different conditions such as temperature (4 °C or 20 °C) and the presence or absence of shell, as well as irrespective of the

differences in the initial fatty acid composition of the three analyzed cultivars (Figs. 1 – 4).

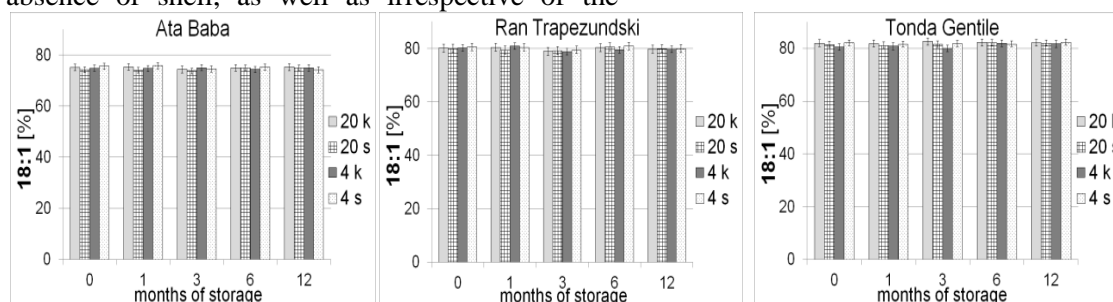


Fig. 1. Oleic acid (9-18:1) content of the oil from three cultivars hazelnuts stored up to 12 months at different conditions: at 20°C or 4°C, as kernels (k) or in shell (s).

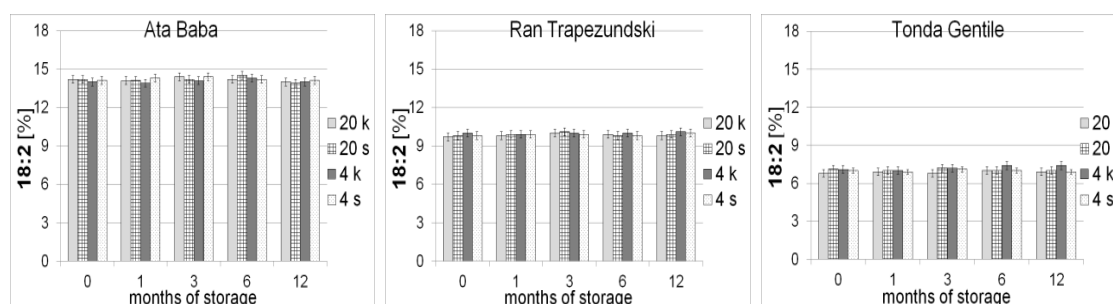


Fig. 2. Linoleic acid (9,12-18:2) content of the oil from three cultivars hazelnuts stored up to 12 months at different conditions: at 20°C or 4°C, as kernels (k) or in shell (s).

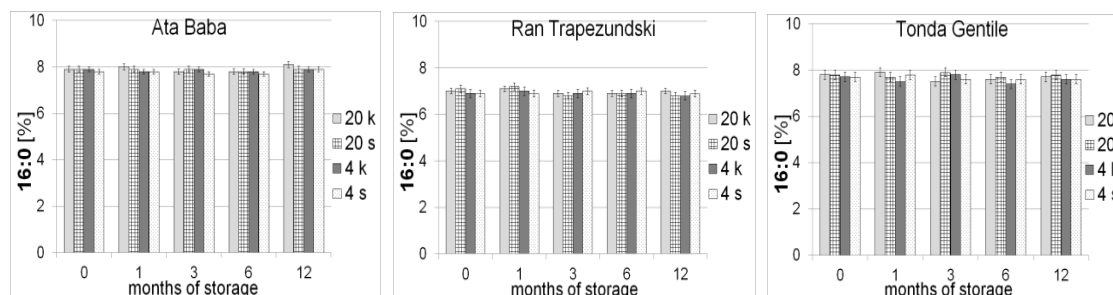


Fig. 3. Palmitic acid (16:0) content of the oil from three cultivars hazelnuts stored up to 12 months at different conditions: at 20°C or 4°C, as kernels (k) or in shell (s).

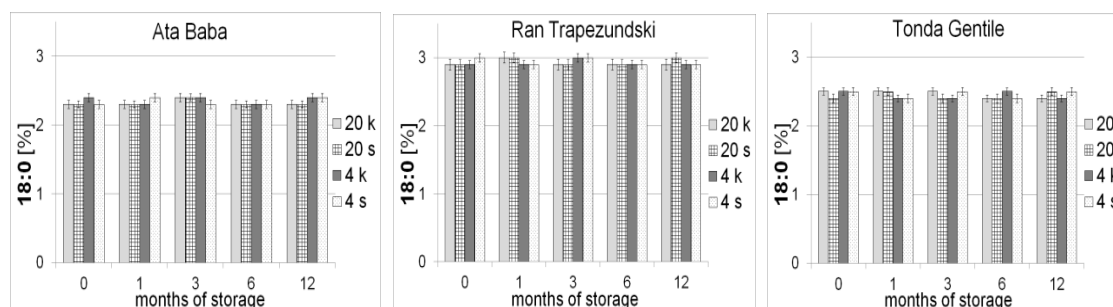


Fig. 4. Stearic acid (18:0) content of the oil from three cultivars hazelnuts stored up to 12 months at different conditions: at 20°C or 4°C, as kernels (k) or in shell (s).

Tocopherols

Tocopherols are important biologically active substances with significant role of strong natural antioxidants. Since their availability prevents the

oils from lipid oxidation higher amount of tocopherols is valuable and desirable virtue. Hazelnut oil from different varieties contains tocopherols in quite wide range: from 115 to

600 mg/kg [12, 20 – 24]. Oils from the three cultivars presented here have quite high initial amounts: 560 mg/kg in *Ran Trapezundski*,

520 mg/kg in *Ata Baba* and 500 mg/kg in *Tonda Gentile* (Fig. 5).

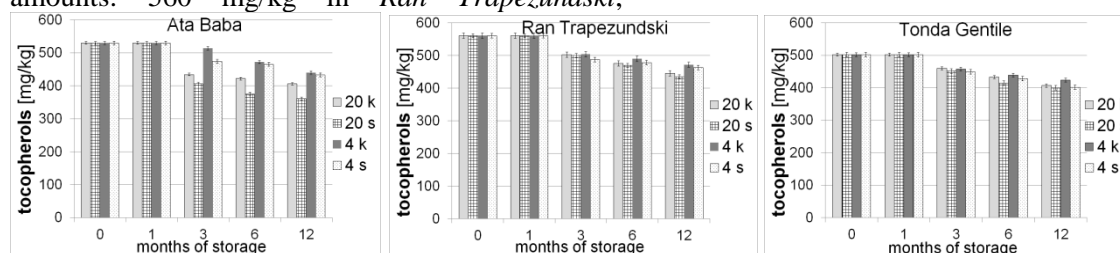


Fig. 5. Total tocopherols in the oil from three cultivars hazelnuts stored up to 12 months at different conditions: at 20°C or 4°C, as kernels (k) or in shell (s).

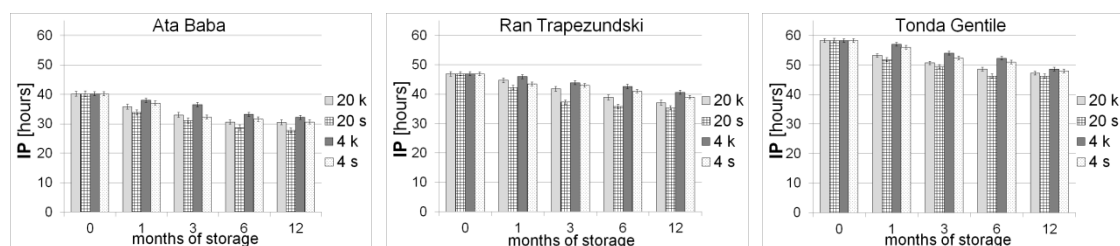


Fig. 6. Oxidative stability (induction period) of the oil from three cultivars hazelnuts stored up to 12 months at different conditions: at 20°C or 4°C, as kernels (k) or in shell (s).

After the first storage month these amounts gradually decrease and that trend is slightly stronger at 20°C than at 4°C as well as for nuts in shell than the kernels. Likewise, respective reducing of the individual α -, β - and γ -isomers is observed (not shown here). As can be seen (Fig. 5) hazelnuts stored at 4°C as kernels contain slightly more tocopherols than that stored at 20°C in shell, irrespective of the differences between the three cultivars. Only two publications were found in the literature concerning determination of tocopherols during hazelnuts storage. They revealed that (i) the remaining amount of α -tocopherol after 9 months storage of kernels was higher at lower temperature (three investigated cultivars) [12], and (ii) hazelnuts stored up to 12 months at 0°C and at 10°C contained slightly higher amount of α -tocopherol as kernels than in shell (one investigated cultivar) [13]. Despite the scarce information, these findings confirm our results that storage of hazelnuts at 4°C as kernels is preferable for keeping their quality for longer period.

Oxidative stability

The oxidative stability of oils is important indicator for their admissible shelf-life. It depends on the fatty acid composition, the availability of natural antioxidants (tocopherols, etc.) as well as on the presence of synergists (e.g. phytosterols). The oxidative stability of hazelnut oil is among the highest for vegetable oils: 16 h of refined [24, 25] or 20 – 40 h of cold-pressed [26] samples (at the same experimental conditions as presented here).

The fresh oils from investigated here three cultivars have even better indexes, i.e. 40 h, 48 h and 59 h for *Ata Baba*, *Ran Trapezundski* and *Tonda Gentile*, respectively (Fig. 6).

During storage of nuts, these values have gradually decreased and some effect of the temperature and shell can be seen, namely the decrease of oxidative stability is stronger at 20°C than at 4°C as well as the kernels have slightly higher stability than nuts in shell. Some reasonable interpretation of these results might be the moisture held by the shell which induces/favors undesirable processes as lipid oxidation and degradation. Comparing the three analyzed cultivars, the highest oxidative stability of *Tonda Gentile* can be explained by the lowest percentage of linoleic acid (Fig. 2) regardless of the lowest amount of tocopherols (as main antioxidant in that oils, Fig. 5). Unfortunately, no data in the literature have been found to compare with these results excepting only partial characteristics of lipid oxidation such as acidity, peroxide value [4, 7, 10, 13], antioxidant capacity (expressed as Trolox equivalent [8]) or conjugated dienes and trienes [4]. Thus, the authors have observed gradual increase during storage of acidity and peroxide values at that in greater extent at higher temperature (25°C vs. 7°C for kernels and whole nuts [4]; or 20°C in shell vs. kernels at 4°C [10]). On the other hand, no significant effects of the storage conditions (temperature and shell) on the antioxidant capacity (as Trolox equivalent, [8])

as well as on the conjugated dienes and trienes [4] have been observed.

CONCLUSION

Fatty acids have not been changed significantly during hazelnuts storage up to 12 months irrespective of different conditions such as temperature (4°C or 20°C) and the presence or absence of shell, as well as irrespective of the differences in the initial fatty acid composition of the three analyzed cultivars. The fresh oils have quite high initial amounts of tocopherols which gradually decrease during storage and that trend is slightly stronger at 20°C than at 4°C as well as for nuts in shell than as kernels. The oxidative stability of the fresh oils decrease similarly during the hazelnuts storage. Thus, it is possible to store hazelnuts up to 12 months without considerable and harmful changes in their main lipid characteristics. In order to keep their quality at most it is preferable to store the hazelnuts as kernels at 4°C.

Acknowledgements: Partial financial support from the Bulgarian Fund for Scientific Research (project DO 02-239) was gratefully acknowledged.

REFERENCES

1. E. Ros, *Nutrients*, **2**, 652 (2010).
2. M. L. Dreher, C. V. Maher, P. Kearney, *Nutr. Rev.*, **54**, 241 (1996).
3. J. Mukuddem-Petersen, W. Oosthuizen, J. C. Jerling, *J. Nutr.*, **135**, 2082 (2005).
4. M. B. San Martin, T. Fernandez-Garcia, A. Romero, A. Lopez, *J. Food Proc. Preserv.*, **25**, 309 (2001).
5. M. A. Koyuncu, *J. Food Qual.*, **27**, 304 (2004).
6. R. Massantini, M. Cortini, M. L. Mordacchini Alfani, M. Guerrieri, D. Monarca, M. Cecchini, *Acta Hort.*, **845**, 635 (2009).
7. D. De Santis, A. Fardelli, F. Mencarelli, *Acta Hort.*, **845**, 693 (2009).
8. D. Ghirardello, M. Bertolino, S. Belviso, B. Dal Bello, M. Giordano, L. Rolle, V. Gerbi, M. Antonucci, N. Spigolon, G. Zeppa, *Postharv. Biol. Technol.*, **112**, 95 (2016).
9. D. Ghirardello, C. Contessa, N. Valentini, G. Zeppa, L. Rolle, V. Gerbi, R. Botta, *Postharv. Biol. Technol.*, **81**, 37 (2013).
10. D. Ghirardello, G. Zeppa, L. Rolle, V. Gerbi, C. Contessa, N. Valentini, R. Botta, *Acta Hort.*, **1052**, 305 (2014).
11. D. Ghirardello, L. Rolle, G. Zeppa, *Acta Hort.*, **845**, 681 (2009).
12. A. S. Pershern, W. M. Breene, E. C. Lulai, *J. Food Proc. Preserv.*, **19**, 9 (1995).
13. K. S. Ebrahim, D. G. Richardson, R. M. Tetley, *Acta Hort.*, **351**, 677 (1994).
14. M. A. Koyuncu, A. Islam, M. Kucuk, *Grasas y Aceites*, **56**, 263 (2005).
15. O. Beyhan, N. Yilmaz, S. Bulut, M. Aktas, E. Ozsoy, *Int. J. Agric. Biol.*, **13**, 741 (2011).
16. ISO 659:2009, Oilseeds – Determination of oil content (Reference method), p. 12 (2009).
17. W. W. Christie, *Lipid Analysis*, The Oily Press, Bridgwater, England, 2003.
18. ISO 9936:2006. Determination of tocopherol and tocotrienol contents by HPLC (2006).
19. ISO 6886:2006. Determination of oxidative stability (2006).
20. P. L. Benitez-Sánchez, M. León-Camacho, R. Aparicio, *Eur. Food Res. Technol.*, **218**, 13 (2003).
21. C. Crews, P. Hough, J. Godward, P. Brereton, M. Lees, S. Guiet, W. Winkelmann, *J. Agric. Food Chem.*, **53**, 4843 (2005).
22. G. P. Savage, D. L. McNeil, P. C. Dutta, *J. Am. Oil Chem. Soc.*, **74**, 755 (1997).
23. C. Alasalvar, J. S. Amaral, G. Satir, F. Shahidi, *Food Chem.*, **113**, 919 (2009).
24. S. R. P. Madawala, S. P. Kochhar, P. C. Dutta, *Grasas y Aceites*, **63**, 143 (2012).
25. S. P. Kochhar, C. J. Henry, *Int. J. Food Sci. Nutr.*, **60**, 289 (2009).
26. H. Ciemniowska-Zytkiewicz, K. Ratusz, J. Brys, M. Reder, P. Koczon, *J. Therm. Anal. Calorim.*, DOI 10.1007/s10973-014-3861-9 (2014).

МАСТНИ КИСЕЛИНИ, ТОКОФЕРОЛИ И ОКИСЛИТЕЛНА СТАБИЛНОСТ НА ЛЕШНИЦИ ПО ВРЕМЕ НА СЪХРАНЕНИЕТО ИМ

С. М. Момчилова^{1*}, С. П. Танева¹, М. Д. Златанов², Г. А. Антова², М. Й. Ангелова-Ромова²,
Е. Благоева³

¹ *Институт по органична химия с Център по фитохимия, Българска академия на науките,
ул. „Акад. Г. Бончев“, блок 9, 1113 София, България*

² *Катедра „Химична технология“, ПУ „П. Хилендарски“, ул. „Цар Асен“ 24, 4000 Пловдив, България*

³ *Опитна станция по земеделие, ул. „Миньорска“ 1, 6600 Кърджали, България*

Постъпила на 13 ноември 2016 г.; приета на 6 декември 2016 г.

(Резюме)

Лешници от три сорта (*Ата Баба*, *Ран Трапезундски* и *Тонда Джентиле*), отглеждани в България, са съхранявани за 1, 3, 6 и 12 месеца при различни условия: с черупки или като ядки, при 4°C (в хладилник) или при 20°C (на сянка), след което са анализирани мастно-киселинния състав, токоферолите и окислителната стабилност (индукционен период в часове) на маслата им. Резултатите показват, че мастните киселини практически не се променят до 12 месеца независимо от различните условия на съхранение, докато количеството на токоферолите постепенно намалява, и тази тенденция е малко по-силно изразена при 20°C, отколкото при 4°C, както и при лешниците с черупки, в сравнение с ядките. Подобно съответно намаляване се наблюдава и при индивидуалните α -, β - и γ -изомери. Относно окислителната стабилност, маслата от изходните лешници имат дълъг индукционен период (40, 47 и 58 часа, съответно при сортовете *Ата Баба*, *Ран Трапезундски* и *Тонда Джентиле*). Тази окислителна стабилност постепенно намалява по време на съхранението по същия начин, както при токоферолите, т.е. лешниците, съхранявани при 20°C с черупки имат малко по-къс индукционен период. Всички тези резултати показват, че е възможно лешниците да бъдат съхранявани до 12 месеца, без да настъпят значителни и вредни за здравето промени в основните им липидни характеристики. За да се запази качеството им в най-голяма степен, е препоръчително те да бъдат съхранявани като ядки при 4°C.

Ключови думи: лешници, съхранение, мастни киселини, токофероли, оксидантна стабилност

Theoretical insights regarding the electronic spectra and proton transfers in a sensor molecule

S.M. Bakalova, J. Kaneti

Institute of Organic Chemistry with CP, Bulgarian Academy of Sciences

Acad. G. Bonchev str., Block 9, 1113 Sofia, Bulgaria

Received November 14, 2016; Revised December 21, 2016

Prototropic tautomerism and possible interpretations of observed electronic absorption and emission spectra are attempted on the basis of time dependent density functional theory (TD DFT) calculations on 2-[2'-hydroxyphenyl]-quinazolin-4-one. Energy differences and excited state proton transfers are studied in the gas phase and in several solvents.

Keywords: 2-[2'-hydroxyphenyl]-quinazolin-4-one, keto-enol tautomerism, electronic absorption and emission spectra, TD DFT, ES IPT transition structures

INTRODUCTION

2-[2'-hydroxyphenyl]-quinazolin-4-one, HPQ, **1**, Fig. 1 is recently being introduced as a valuable sensor for metal ions (mostly divalent) in aqueous solutions thus contributing to the activities against water pollution. The property utilized in this regard is its relatively bright fluorescence in solution, which is quenched by formation of metal ion complexes following the Beer – Lambert law. For example, metal ion fluorescence sensing for Fe³⁺ is possible in the range of 10⁻⁴ to 10⁻⁷ M [1]. Detecting of Hg²⁺ can be done in the same range of concentrations at pH 5.5 – 6.5 [2].

Quantitative and selective detection of Zn²⁺ and Cd²⁺ has also been reported [3].

Compound **1** is fluorescent and solvatochromic in solution. HPQ may be crystallized in two polymorphic forms showing blue, B, or blue-green, BG, fluorescence in the solid state. [4] B and BG forms have different $\pi\cdots\pi$, O...H-C and C=O...C=O dipolar interactions in their respective crystal lattices. This has possibly been the reason to suggest that the actual fluorescent species is an aggregate [3].

As shown on Figure 1, HPQ may exhibit a number of prototropic tautomers, e. g. 1-H and 3-H 4-keto (**2**, and **1**) forms, or 1-H-4-hydroxy-2'-keto vs. 2',4-dihydroxy forms (**6**, **3**) [5]. In addition, twice as many isomers may be generated due to a relatively low barrier to rotation around the C₁ - C₂' single bond, Fig. 1.

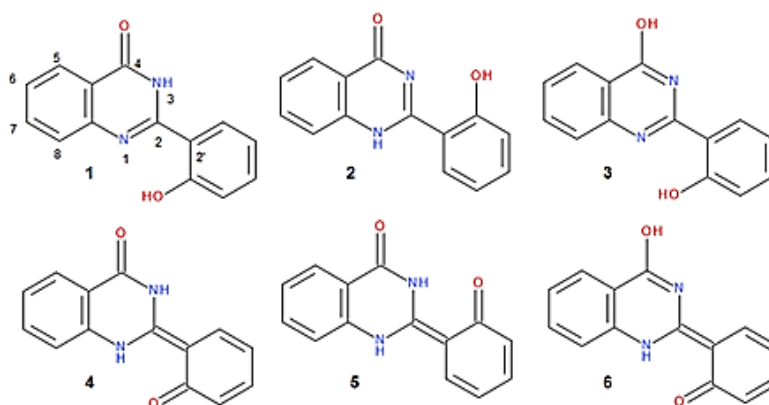


Figure 1. Some possible tautomers of HPQ. Atom numbering is shown with tautomer **1**, which is thus 3-H; Tautomer **2** is 1-H, etc. Pertinent degrees of freedom for prototropic isomerization at each heteroatom, plus a rotation about the C₂ – C₂' bond can give a total of 2⁵, i.e. 32 isomers.

* To whom all correspondence should be sent.

E-mail: bakalova@orgchm.bas.bg; kaneti@orgchm.bas.bg

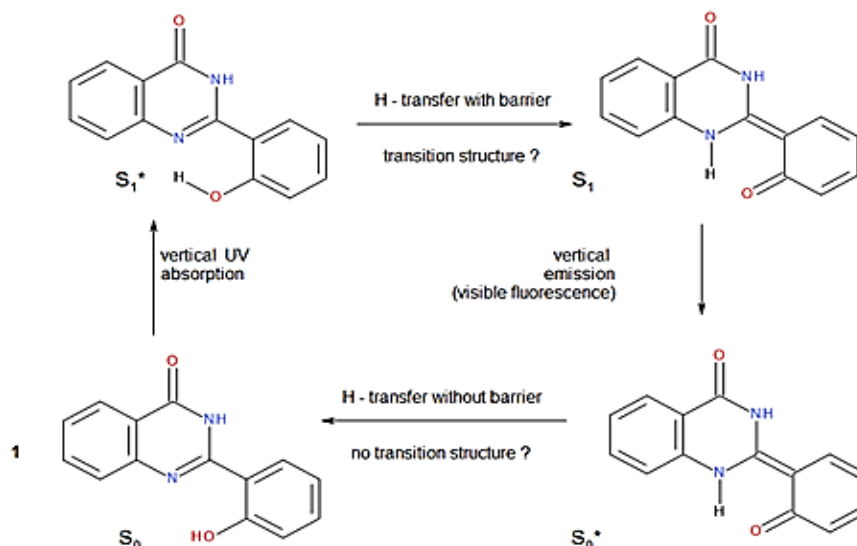


Figure 2. The electronic absorption – emission cycle of HPQ [1 – 4]

Within the manifold of possible prototropic tautomers, the observed fluorescence can be alternatively based on an excited state proton transfer mechanism, ESIPT, [6] which apparently occurs in aqueous solution at pH in the range of 2.0 – 5.5, Fig. 2, as well as in polar solvents.

To understand the structural changes underlying the observed UV light absorption and visible fluorescence emission, we undertake a computational study of electron excitation and structure relaxation in the molecule of **1** and some of its tautomers. This may be conveniently achieved by means of density functional theory, DFT, [7] for the ground electronic states in their equilibrium S_0 . For the excited electronic state(s), S_1 and vibrationally excited S_1^* , we may use the time dependent form of DFT, TD DFT [8]. We use the GAUSSIAN 09 program [9] with default geometry optimization procedures and the 6-31G(d,p) basis set with PBE0, [10] M06-2x [11] and MN12sx [12] functionals for the outlined equilibrium S_0 and S_1 tautomeric structures of **1**, Figure 1, in the gas phase and a series of solvents, using the PCM solvent model [13]. The transition structures for involved intramolecular proton transfers have also been pursued using the standard "Berny" optimization procedure implemented in GAUSSIAN 09 [9]. Solvent effects on the spatial structures of ground S_0 and first excited S_1 electronic states of HPQ are studied within the PCM computational formalism in tetrahydrofuran, dichloromethane, methanol and dimethylsulfoxide. No solvent relaxation effects have been accounted for.

EXPERIMENTAL ELECTRONIC SPECTRA AND ESIPT

The UV and visible electronic absorption spectrum of HPQ show intense absorption at ca. 330 nm, which is barely affected by solvent polarity. In addition, another less intense absorption appears in polar and preferably aprotic solvents as DMSO and DMF, being merely a shoulder in CH_3CN and CH_3OH at about 400 nm. The two solid state fluorescence peaks appear at ca. $460 \div 500$ nm [1]. Solution photoluminescence appears at 492 nm in THF and THF/water, with intensity rapidly increasing with increasing water concentration [2]. The recorded emission profiles are rather sharp, contrary to the observed absorption, and support the notion that solid state HPQ fluorescence is related to severely restricted rotation of the hydroxyphenyl fragment around the connecting C – C bond with quinazolinone [3, 14]. The observed Stokes' shift of fluorescence, ca. $10 \cdot 10^3 \text{ cm}^{-1}$ relative to the "main" absorption peak, suggests a proton transfer mechanism as the source of the emissive excited state structure [6]. The "secondary" longer wavelength absorption could be interpreted as indication of an equilibrium of prototropic isomers even in the ground S_0 electronic state **1** and should be attributed to the *keto*- form **4** [1 – 4].

COMPUTATIONAL MODELING OF PROTOTROPIC ISOMERS AND PROTON TRANSFER

The proton transfer processes shown on Figure 2, which could be the evident source of observed light absorption – emission phenomena of HPQ have been reproduced first in the gas phase using

the three mentioned DFT functionals. Ground S_0 state energy minimizations of 2-(2'-hydroxyphenyl)quinazolin-4-one **1** proceed smoothly to indicate that the structure is a minimum on the potential energy surface, as confirmed also by full vibrational analysis. The comparison of calculated closed shell S_0 thermodynamic free energies ΔG for most tautomers shows that isomer **1** is indeed the most stable, while the remaining possible tautomers, starting with **2**, are at least 4 kcal.mol⁻¹ less stable in DMSO. In less polar solvents, studied here, this energy difference increases and becomes more than 7 kcal.mol⁻¹ in the gas phase. We can therefore safely assume that the main S_0 species existing in solution under standard conditions is 2-(2'-hydroxyphenyl)-3H-quinazolin-4-one **1**.

The minimization of corresponding 2'-keto structure **3** at the S_0 energy surface however behaves differently with the chosen functionals.

The M06-2x models of *keto*-structures **4**, **5**, **6** yield the corresponding enols **1**, **2**, **3** in the gas phase as well as in all solvents studied. PBE0 in addition shows **5** as a minimum in solution, with significant proton transfer from NH to O, but still far of the enol **2**. Still, within the PBE0 model **5** is less stable than corresponding **2** by ca. 3 kcal.mol⁻¹. MN12sx, on the other hand, indicates that *keto*-isomers **4**, **5**, **6** are local minima in all solvents, with minimal effects of solvent polarity. The latter result apparently corresponds to the observed second less intense longer wavelength absorption of HPQ in polar solvents [1 – 4]. Computed TD DFT vertical $S_0 \rightarrow S_1^*$ transition energies are relatively independent of the used functional and choice of solvent. Therefore, we only show the complete manifold of results for PBE0/6-31G(d,p) calculations in Table 1, M06-2x/6-31G(d,p) calculations in Table 2, and MN12sx/6-31G(d) in Table 3.

One may notice that on Figure 1 HPQ tautomers are shown in *keto*-enol pairs according to chosen starting structures. With the three used DFT functionals, geometry optimization of the selected *keto*-enol pairs, at the S_0 potential surface, mostly converge to the respective enols **1**, **2**, **3**. The notable variation of results with the MN12sx/6-31G(d,p) functional, Table 3, is the prediction of the *keto*-form **4** a minimum, somewhat more stable in solution than corresponding enol **1** according to calculated free energy differences $\Delta\Delta G$, ca. 1 kcal.mol⁻¹ depending on the solvent. Nevertheless, calculated vertical $S_0 - S_1$ transition energies are pairwise identical. Note also that computed vertical electron absorptions are practically independent of the solvent. The chosen pairs remain identical also after TD DFT relaxation, with the corresponding

final structures the *keto*-isomers **4**, **5**, **6**. In other words, selected PBE0 (pbe1pbe in GAUSSIAN), M06-2x and MN12sx functionals uniformly predict ESIPT between the hydroxyphenyl and the quinazolin-4-one fragment of HPQ. In the case of ESIPT we also find insignificant solvent dependence with decreasing emission wavelengths in more polar solvents, which reproduces the experiment fairly well, see Figure 3.

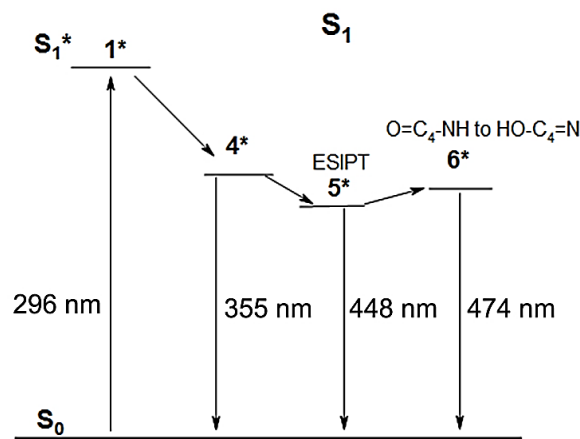


Figure 3. M06-2x/6-31G(d,p) diagram of S_0 and S_1 electronic states of **1** and its possible prototropic conversions in the excited state. Transition energies in THF: absorption is arrow up; fluorescence emissions are given by arrows down; state total energy values for each species in hartrees are as follows: S_0 : -799.2184; S_1^* : -799.0643; S_1 : -799.0789; ESIPT to **2**: -799.0871; **3***: -799.0796. For comparison, corresponding values from TD MN12sx/6-31G(d,p) calculations in DMSO are: S_0 : -798.9443; S_1^* : -798.7991, absorption at 314 nm; S_1 : -798.8128, emissions at 376 nm; ESIPT to **2**: -798.8294, 641 nm; **3***: -798.9005. Excited prototropic structures are marked by asterisks, see also Figure 1.

As far as used computational models suggest an equilibrium between *enol* and *keto*-isomers of HPQ even in the ground electronic state, we attempted several searches for transition structures for proton transfer at the S_0 potential energy surface. However, we met no success in this direction. On the other hand, we verify the identification of ESIPT in HPQ by the location of its transition structure at the S_1 potential energy surface using two computational models, TD M06-2x and TD MN12sx. The resulting structure from the TD MN12sx/6-311(d,p) computation is shown on Figure 4.

TD(nstates=6) MN12sx/6-311G(d,p)

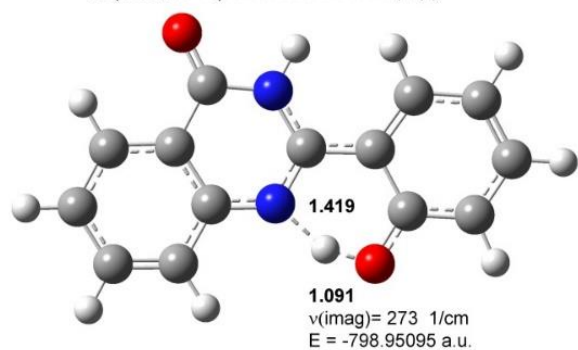


Figure 4. The transition structure for ES IPT on the S_1 -potential energy surface of **1**, TD=(nstates=6) MN12sx/6-311G(d,p). Distances are shown in Å.

Table 1. PBE0/6-31G(d,p) and TD(nstates=6) PBE0/6-31G(d,p) computational results for most stable isomers of HPQ in the ground S_0 electronic state and corresponding S_1 structures. Total energies are in hartrees, $\Delta\Delta G$ in kcal/mol, and wavelengths in nanometers. **f** is the calculated oscillator strength.

Str	E	S_0		S_0 - S_1 vertical		S_1 relaxed	
		ΔG	$\Delta\Delta G$	λ_{abs}	f	λ_{Fl}	f
<i>Tetrahydrofuran</i>							
1	-798.642772	-798.466386	0.00	322.0	0.447	493.0	0.275
4	-798.642772	-798.466385	0.00	322.0	0.447	493.1	0.275
2	-798.635007	-798.460104	3.94	324.3	0.331	494.2	0.301
5	-798.629412	-798.455364	6.92	380.5	0.345	495.6	0.298
3	-798.625260	-798.449889	10.35	337.9	0.171	657.0	0.095
6	-798.625283	-798.449899	10.35	341.3	0.259	656.9	0.095
<i>Dichloromethane</i>							
1	-798.643149	-798.466786	0.00	322.0	0.450	490.4	0.239
4	-798.643149	-798.466783	0.00	322.0	0.451	490.7	0.285
2	-798.635636	-798.460655	3.85	324.4	0.334	491.6	0.311
5	-798.630102	-798.456008	6.76	380.5	0.348	492.4	0.310
3	-798.625749	-798.450342	10.32	337.1	0.176	647.4	0.100
6	-798.625767	-798.450279	10.36	340.7	0.270	647.3	0.100
<i>Methanol</i>							
1	-798.644604	-798.468386	0.00	320.6	0.429	483.4	0.321
4	-798.644604	-798.468383	0.00	320.6	0.429	481.5	0.325
2	-798.638109	-798.462880	3.46	323.2	0.320	484.3	0.349
5	-798.632811	-798.458560	6.17	378.0	0.334	484.1	0.350
3	-798.627638	-798.452189	10.16	333.1	0.174	611.9	0.121
6	-798.627655	-798.452162	10.18	338.5	0.318	611.7	0.122
<i>Dimethylsulfoxide</i>							
1	-798.644782	-798.468597	0.00	321.3	0.448	482.7	0.325
4	-798.644782	-798.468594	0.00	321.3	0.448	481.8	0.328
2	-798.638416	-798.463161	3.41	379.0	0.334	483.5	0.353
5	-798.633148	-798.458876	6.10	323.8	0.347	483.4	0.354
3	-798.627871	-798.452421	10.15	333.2	0.188	607.8	0.124
6	-798.627888	-798.452457	10.12	338.2	0.324	607.5	0.125

Table 2. M062x/6-31G(d,p) and TD(nstates=6) M06-2x/6-31G(d,p) computational results for most stable isomers of HPQ in the ground S_0 electronic state and corresponding S_1 structures. Total energies are in hartrees, $\Delta\Delta G$ in kcal/mol, and wavelengths in nanometers. **f** is the calculated oscillator strength.

Str	S_0			S_0 - S_1 vertical		S_1 relaxed	
	E	ΔG	$\Delta\Delta G$	λ_{abs}	f	λ_{abs}	f
<i>Tetrahydrofuran</i>							
1	-799.218399	-799.042051	0.00	295.6	0.525	355.4	0.704
4	-799.218399	-799.042052	0.00	295.6	0.525	355.5	0.699
2	-799.210472	-799.034316	4.85	293.2	0.390	448.2	0.441
5	-799.210472	-799.034314	4.85	294.2	0.397	448.7	0.439
3	-799.203155	-799.027473	9.15	296.9	0.372	474.0	0.379
6	-799.203166	-799.027530	9.11	301.4	0.500	475.8	0.374
<i>Dichloromethane</i>							
1	-799.218781	-799.042421	0.00	295.6	0.529	356.0	0.721
4	-799.218781	-799.042422	0.00	295.6	0.529	356.0	0.715
2	-799.211098	-799.034990	4.66	293.3	0.394	447.6	0.451
5	-799.211098	-799.034984	4.67	293.3	0.394	492.3	0.310
3	-799.203648	-799.027958	9.08	296.6	0.377	469.9	0.400
6	-799.203660	-799.027973	9.08	301.3	0.512	468.6	0.405
<i>Methanol</i>							
1	-799.220254	-799.043888	0.00	294.3	0.508	358.6	0.781
4	-799.220253	-799.043902	-0.01	294.3	0.508	358.6	0.775
2	-799.213563	-799.037627	3.94	292.2	0.381	446.0	0.488
5	-799.213563	-799.037639	3.92	292.3	0.381	483.2	0.351
3	-799.205569	-799.029879	8.79	294.2	0.362	457.4	0.474
6	-799.205581	-799.029883	8.78	300.9	0.558	457.5	0.476
<i>Dimethylsulfoxide</i>							
1	-799.220434	-799.044076	0.00	295.0	0.528	359.0	0.788
4	-799.220434	-799.044073	0.00	295.0	0.528	359.0	0.782
2	-799.213870	-799.038009	3.81	292.8	0.397	445.7	0.493
5	-799.213870	-799.038044	3.79	292.8	0.398	445.6	0.493
3	-799.205805	-799.030117	8.76	294.6	0.381	456.4	0.482
6	-799.203660	-799.027963	10.11	301.3	0.512	468.6	0.405

Table 3. MN12sx/6-31G(d,p) and TD(nstates=6) MN12sx/6-31G(d,p) computational results for most stable isomers of HPQ in the ground S_0 electronic state and electron transitions to corresponding S_1 structures. Total energies are in hartrees, $\Delta\Delta G$ in kcal/mol, and wavelengths in nanometers. **f** is the calculated oscillator strength.

Str	E	S_0		S_0 - S_1 vertical		S_1 relaxed	
		ΔG	$\Delta\Delta G$	λ_{abs}	f	λ_{Fl}	f
<i>Tetrahydrofuran</i>							
1	-798.942197	-798.764794	1.38	314.5	0.509	371.7	0.833
4	-798.942213	-798.766995	0.00	320.1	0.653	371.6	0.833
2	-798.934143	-798.758373	5.41	312.2	0.328	520.9	0.256
5	-798.926314	-798.752122	9.33	380.9	0.333	520.7	0.257
3	-798.928128	-798.752730	8.95	333.2	0.235	697.6	0.085
6	-798.928128	-798.752687	8.98	333.2	0.235	697.6	0.085
<i>Dichloromethane</i>							
1	-798.942584	-798.765187	1.54	314.5	0.513	372.2	0.845
4	-798.942599	-798.767636	0.00	320.5	0.664	372.3	0.846
2	-798.934774	-798.759028	5.40	312.2	0.332	515.2	0.269
5	-798.927022	-798.752812	9.30	380.7	0.336	515.3	0.268
3	-798.928614	-798.753214	9.05	332.5	0.248	614.4	0.004
6	-798.928614	-798.753220	9.05	332.5	0.248	415.5	0.282
<i>Methanol</i>							
1	-798.944083	-798.766679	0.91	313.1	0.489	375.6	0.894
4	-798.944094	-798.768133	0.00	313.1	0.489	375.7	0.894
2	-798.937180	-798.760097	5.04	312.3	0.324	501.8	0.309
5	-798.929804	-798.755500	7.93	377.6	0.322	501.7	0.310
3	-798.930508	-798.755097	8.18	330.2	0.301	645.6	0.106
6	-798.930508	-798.755125	8.16	330.2	0.301	645.6	0.106
<i>Dimethylsulfoxide</i>							
1	-798.944267	-798.766857	0.92	313.9	0.510	376.1	0.900
4	-798.944276	-798.768323	0.00	322.2	0.713	376.1	0.900
2	-798.937490	-798.760403	4.97	312.9	0.340	500.5	0.314
5	-798.930150	-798.755831	7.84	378.6	0.337	500.4	0.314
3	-798.930742	-798.755371	8.13	330.0	0.307	640.9	0.108
6	-798.930742	-798.755364	8.13	320.0	0.308	640.9	0.108

CONCLUSION

We provide a detailed computational analysis of UV absorption and steady state fluorescence of HPQ by means of TD DFT calculations. This proved to only be possible considering the complete manifold of isomers, mostly prototropic tautomers of the molecule. Suggested ESIPT as the source of observed large Stokes shift of fluorescence is proved computationally.

Acknowledgement: A part of the reported computations has been carried out on the MADARA cluster, IOCCP, acquired under Project RNF01/0110 (2009-2011) of the National Research Fund of Bulgaria.

REFERENCES

1. X.-B. Zhang, G. Cheng, W.-J. Zhang, G.-L. Shen, R.-Q. Yu, *Talanta* **71**, 171 (2007).
2. W.-J. Zhang, J. Peng, L.-M. Lu, J. Zhang, X.-B. Zhang, *Int. J. Envir. Anal. Chem.* **92**, 810 (2012).
3. S. P. Anthony, *Chem. Asian J.* **7**, 374 (2012).
4. M. Gao, S. Li, Y. Lin, Y. Geng, X. Ling, L. Wang, A. Qin, B. Z. Tang, *ACS Sens.* **1**, 179 (2016).
5. S. M. Bakalova, A. G. Santos, I. Timcheva, J. Kaneti, I. L. Philipova, G. M. Dobrikov, V. D. Dimitrov, *J. Mol. Struct. THEOCHEM* **710**(1-3), 229 (2004).
6. D. L. Williams, A. Heller, *J. Phys. Chem.* **74**, 4473 (1970).
7. P. Hohenberg and W. Kohn, *Phys. Rev.*, **136**, B864 (1964). W. Kohn and L. J. Sham, *Phys. Rev.*, **140**, A1133 (1965).
8. R. Bauernschmitt and R. Ahlrichs, *Chem. Phys. Lett.*, **256**, 454 (1996). M. E. Casida, C. Jamorski, K. C. Casida, and D. R. Salahub, *J. Chem. Phys.*, **108**, 4439 (1998).
9. Gaussian 09, Revision **E.01**: M. J. Frisch, G. W. Trucks, H. B. Schlegel, G. E. Scuseria, M. A. Robb, J. R. Cheeseman, G. Scalmani, V. Barone, B. Mennucci, G. A. Petersson, H. Nakatsuji, M. Caricato, X. Li, H. P. Hratchian, A. F. Izmaylov, J. Bloino, G. Zheng, J. L. Sonnenberg, M. Hada, M. Ehara, K. Toyota, R. Fukuda, J. Hasegawa, M. Ishida, T. Nakajima, Y. Honda, O. Kitao, H. Nakai, T. Vreven, J. A. Montgomery, Jr., J. E. Peralta, F. Ogliaro, M. Bearpark, J. J. Heyd, E. Brothers, K. N. Kudin, V. N. Staroverov, R. Kobayashi, J. Normand, K. Raghavachari, A. Rendell, J. C. Burant, S. S. Iyengar, J. Tomasi, M. Cossi, N. Rega, J. M. Millam, M. Klene, J. E. Knox, J. B. Cross, V. Bakken, C. Adamo, J. Jaramillo, R. Gomperts, R. E. Stratmann, O. Yazyev, A. J. Austin, R. Cammi, C. Pomelli, J. W. Ochterski, R. L. Martin, K. Morokuma, V. G. Zakrzewski, G. A. Voth, P. Salvador, J. J. Dannenberg, S. Dapprich, A. D. Daniels, Ö. Farkas, J. B. Foresman, J. V. Ortiz, J. Cioslowski, and D. J. Fox, Gaussian, Inc., Wallingford CT, 2009.
10. J. P. Perdew, K. Burke, and M. Ernzerhof, *Phys. Rev. Lett.*, **77**, 3865 (1996). C. Adamo and V. Barone, *J. Chem. Phys.*, **110**, 6158 (1999).
11. Y. Zhao and D. G. Truhlar, *Theor. Chem. Acc.*, **120**, 215 (2008).
12. R. Peverati and D. G. Truhlar, *Phys. Chem. Chem. Phys.* **14**, 16187 (2012).
13. J. Tomasi, B. Mennucci, and E. Cancès, *J. Mol. Struct. (Theochem)*, **464**, 211 (1999).
14. R. Hu, S. Li, Y. Zeng, J. Chen, S. Wang, Y. Li, and G. Yang, *Phys. Chem. Chem. Phys.*, **13**, 2044 (2011).

ТЕОРЕТИЧНИ ВИЖДЕНИЯ ЗА ЕЛЕКТРОННИТЕ СПЕКТРИ И ПРЕНОСИ НА ПРОТОН В МОЛЕКУЛАТА НА ЕДИН СЕНЗОР

Сн. Бакалова и Х. Канети

Институт органична химия с център по фитохимия, БАН
ул. Акад. Г. Бончев., Бл.9, 1113 София, България

Постъпила на 14 ноември 2016 г.; приета на 21 декември 2016 г.

(Резюме)

Прототропната тавтомерия и възможната интерпретация на наблюдаваните абсорбционни и емисионни електронни спектри на 2-2'-хидроксифенил-хиназолин-4-он са изследвани с помощта на зависимата от времето теория на функционала на плътността. Изследвани са енергиите на електронните преходи и преноса на протон във възбудено състояние в газова фаза и няколко разтворителя.

Ключови думи: 2-2'-хидроксифенил-хиназолин-4-он, кето-енолна тавтомерия, електронни абсорбционни и емисионни спектри, TD DFT, преходни структури за пренос на протон във възбудено състояние

Antioxidant activity of different extracts of dried and frozen fruits of *Schisandra chinensis* (Turcz.) Baill

A. V. Terzieva¹, R. Z. Vrancheva^{2*}, N. D. Delchev²

¹Student of specialty "Analysis and Control of Food Products",
Department of Analytical Chemistry, University of Food Technologies-Plovdiv,
26 Maritza Str., 4000 Plovdiv, Bulgaria

²Department of Analytical Chemistry, University of Food Technologies-Plovdiv,
26 Maritza Str., 4000 Plovdiv, Bulgaria

Received November 10, 2016; Revised January 03, 2017

Schisandra chinensis has been used in traditional Chinese medicine for hundreds of years. In the last decades, the pharmacological and chemical studies of this drug revealed various valuable biological and pharmacological activities, such as antihepatotoxic, antioxidant, detoxificant, anticarcinogenic, tonic and anti-inflammatory effects. The purpose of current study was to assess the antioxidant activity and phenolic profiles of different extracts (water by maceration at ambient temperature; water, 70% and 96% ethanol extracts by heat-reflux extraction at 70°C) of dried and frozen fruits of *Schisandra chinensis* (Turcz.) Baill. Antioxidant potential of investigated extracts was determined by four most applied spectrophotometric methods, namely DPPH, ABTS, FRAP and CUPRAC. The 70% ethanol extracts of dried fruits showed the highest antioxidant activity by all of the tested methods. The highest antioxidant potential of frozen fruits was defined in water extract obtained by heat-reflux extraction at 70°C. Besides, that were the extracts with highest total phenol contents, defined by Folin-Ciocalteu's assay. HPLC analysis of phenol profiles of the investigated extracts revealed the presence of chlorogenic, p-cumaric and sinapic acids.

The established strong antioxidant activity of analyzed extracts of dried and frozen fruits of *S. chinensis* is a prerequisite for their future application as natural preservatives in different food systems.

Key words: *Schisandra chinensis*, antioxidants, phenol acids, biological activity, HPLC

INTRODUCTION

Currently, about 50 000–70 000 plant species are used in food and cosmetic industries, as well as in folk and traditional medicine all over the world. Apart from their better organoleptic impact, the plants also amplify the chemical composition of food with biologically active substances that exhibit high antioxidant, antimicrobial, antiviral, antitumor, immunostimulatory and other valuable activities for human health [1].

Antioxidants are important compounds used against oxidative damages in food systems and free radical induced oxidative stress-associated diseases in humans, such as cancer, atherosclerosis, neurodegenerative diseases and inflammation [2].

In the recent years, there was increased interest in the natural antioxidants with plant origin because of the proved toxic, mutagenic and carcinogenic effects of commercial synthetic ones [3]. Usually, the antioxidant potential of the plant extracts was related to their polyphenolic compounds with strong redox properties (absorbed and neutralized free radicals, quenched singlet and triplet oxygen or decomposed peroxides) [4]. Besides, they exhibit

other valuable biological properties, such as, cardioprotective, antimutagenic, antibacterial, antiviral and anti-inflammatory activities [5, 6]. Considering the important role of phenolic compounds in human health and nutrition, it is mandatory to provide new data on their amounts or variety in medicinal plants and natural foods.

Schisandra chinensis is a traditional Chinese medicine and has been used for hundreds of years [7].

The dried fruits of *Schisandra chinensis* are extensively used in traditional medicine to treat asthma, gonorrhea, enuresis, dysentery, diarrhea, diabetes, atopic dermatitis and others [8]. Fruits of this species also exhibited anti-inflammatory, antiviral, anticancer and neuroprotective effects [9, 10].

Chemical composition of *S. chinensis* consists of amino acid, polysaccharides, sesquiterpenes, vitamins, organic acids, volatile oil, lignans and triterpenoids. Most of the biological activities of this plants were associated with the presence of lignans and triterpenoids that exhibit hepatoprotective, anti-inflammatory, antioxidant, anti-HIV and anticancer activities [11].

Although the fruits of *S. chinensis* have been

* To whom all correspondence should be sent.
E-mail: radka_vrancheva@yahoo.com

used in traditional medicine for many years, their health-promoting properties are still being investigated, and new extraction methods were searched in order to use this fruits in a better way in the food and pharmaceutical industries [12]. The differences in the composition and antioxidant activity of plant extracts were due to the genetic factors, the degree of maturity of plants, cultivation techniques, post-harvest handling, storage conditions and solvents and conditions applied for extractions [13]. Therefore the purpose of current study was comparative analysis of antioxidant activity and phenol profile of different extracts from dried and frozen fruits of *S. chinensis*.

MATERIALS AND METHODS

Plant material

The samples of *Schisandra chinensis* were cultivated in the area of Pleven city (Bulgaria). Part of the fruits was stored in freezer at -18°C. Fresh fruits were dried in shade at ambient temperature and grounded before analysis.

Extraction procedure

Each fresh and frozen sample (1.0 g) was extracted three times with 10 mL of the relevant extraction solvent (96% ethanol, 70% ethanol (v/v) and distilled water) under reflux-heat at 70°C for 20 min. Water extracts obtained by maceration were extracted three times for 24 h with 10 mL distilled water at ambient temperature. The residue of plant material was removed through filter paper filtration and the combined extracts were evaporated to dryness under vacuum. The dried extracts were stored in refrigerator at 4°C in dark and dissolved in appropriate solvent before analyses.

Total phenolics

The total phenolic contents were measured using a Folin-Ciocalteu assay according to the procedure described by Stintzing *et al.* [14] with some modifications. Folin - Ciocalteu reagent (1mL) (Sigma) diluted five times was mixed with 0.2 mL of sample and 0.8 mL 7.5% Na₂CO₃ (Sigma). The reaction was 20 min at room temperature in darkness. After reaction time, the absorption of sample was recorded at 765 nm against blank sample, developed by the same way but without extract. The results were expressed in mg equivalent of gallic acid (GAE) per g dry weight (DW), according to calibration curve, build in range of 0.02 - 0.10 mg.mL⁻¹ gallic acid (Sigma) used as a standard.

HPLC analysis

Qualitative and quantitative determination of phenolic acids was performed by using Elite LaChrome (Hitachi) HPLC system equipped with DAD and ELITE LaChrome (Hitachi) software. Separation of the phenolic acids was performed by Supelco Discovery HS C₁₈ column (5 µm, 25 cm × 4.6 mm), operated at 30°C under gradient conditions with mobile phase consist of 2% (v/v) acetic acid (solvent A) and acetonitrile (solvent B). The gradient program used was: 0-1 min – 95% A and 5% B; 1-40 min: 50% A and 50% B; 40-45 min: 100% B; 46-50 min: 95% A and 5% B. The detection of phenolic acids was carried out at 280 and 320 nm and the flow rate was 0.8 mL.min⁻¹.

Antioxidant activity

Antioxidant activity of the obtained extract was defined by four spectrophotometric methods: DPPH (1,1-diphenyl-2-picrylhydrazyl), ABTS (2,2'-azino-bis(3-ethylbenzothiazoline-6-sulphonic acid)), FRAP (ferric reducing antioxidant power) and CUPRAC (cupric reducing antioxidant capacity), described previously by Ivanov *et al.* [15].

Statistical analysis

Three independent extracts with the relevant solvent (96% ethanol, 70% ethanol (v/v) and distilled water) were prepared from the analyzed samples of fresh and frozen fruits and each extract was analyzed for total phenols, phenolic acid content and antioxidant activity in triple replication. The presented values are means (n = 3) with standard deviations (± SD). Figures were made by Microsoft Office Excel ® 2010.

RESULTS AND DISCUSSIONS

Total phenols

The highest total phenol content was defined in the 70% ethanol extract of dried fruits, as the water extract, obtained by maceration was with the lowest amount of phenols. Water extract obtained under reflux-heat at 70°C showed the highest total phenol content, among the investigated extracts of frozen fruits of *S. chinensis* (Table 1).

Cai *et al.* [16] also reported that alcohol extract (80% methanol) of dried fruits of *S. schinensis* contained about five times higher amount of total phenols (1.05 g for 100 g DW) compared to that in the water extract obtained in the same conditions (in a water bath shaker at 80°C). Pliszka *et al.* [12] found that 80% methanol extract of frozen fruits contain 128.3 ± 5.5 mg GAE for 100 g FW total phenols. This value is close to the total phenol content determined in the water extract under heat-reflux in our study (Table 1).

Table 1. Total phenolic content of extracts of dried and frozen fruits of *S. schinensis*

Extracts	Total phenols in dried fruits, mg GAE.g ⁻¹ DW	Total phenols in frozen fruits, mg GAE.g ⁻¹ FW
96% ethanol	1.08 ± 0.02	0.84 ± 0.03
70% ethanol	2.15 ± 0.06	0.55 ± 0.01
water	0.91 ± 0.01	0.68 ± 0.02
water,70°C	1.76 ± 0.26	1.23 ± 0.02

Considering that water is non-toxic and eco-friendly solvent it is more appropriate solvent for obtaining the extracts with high phenols content compared to the 80% methanol.

HPLC analysis

Provided HPLC analysis of obtained extracts revealed the presence of chlorogenic, *p*-coumaric and sinapic acids (Table 2). The dominant phenolic acid in all of the investigated extracts is chlorogenic acid. That is of great importance because this phenolic acid has been shown to possess multiple beneficial properties, including analgesic, anti-carcinogenic, antioxidant, anti-diabetic, anti-inflammatory, anti-microbial, cardioprotective, hypotensive and neuroprotective effects [17]. Sinapic and *p*-coumaric acids were in highest concentration in the 70% ethanol extract of dried fruits and water extract of frozen fruits, obtained under heat-reflux at 70°C. These phenolic acids also possessed valuable biological activities. It was found that sinapic acid has antiinflammatory effect by suppressing production of some proinflammatory mediators [18]. *p*-coumaric acid could be used against oxidative stress by protecting DNA from oxidative damages [19].

HPLC-UV-MS analysis of extracts of dried fruits of *S. schinensis* revealed the presence of chlorogenic (3.26 ± 0.25 µg.g⁻¹ plant material), *p*-coumaric (<0.02 µg.g⁻¹ plant material) and gentisic acids (<0.02 µg.g⁻¹ plant material) [20].

Table 2. HPLC analysis of phenolic acids of obtained extracts of dried and frozen fruits of *S. schinensis*.

Extract	Chlorogenic acid, µg.g ⁻¹ DW	<i>p</i> -coumaric acid, µg.g ⁻¹ DW	Sinapic acid, µg.g ⁻¹ DW	Chlorogenic acid, µg.g ⁻¹ FW	<i>p</i> -cumaric acid, µg.g ⁻¹ FW	Sinapic acid, µg.g ⁻¹ FW
96% ethanol	297.9 ± 5.2	104.5 ± 1.6	32.6 ± 0.9	32.4 ± 2.1	18.8 ± 0.5	10.4 ± 1.1
70% ethanol	556.2 ± 6.4	157.3 ± 1.4	62.2 ± 2.7	19.2 ± 1.1	14.2 ± 1.4	11.8 ± 1.1
Water	133.5 ± 1.8	77.3 ± 1.1	26.2 ± 0.8	21.4 ± 1.4	16.3 ± 1.4	12.1 ± 1.4
Water, 70°C	265.1 ± 3.1	89.6 ± 1.5	28.9 ± 0.8	55.6 ± 3.5	28.3 ± 2.1	16.5 ± 1.4

Comparing with the results obtained by Mocan *et al.* [20] our samples were with higher concentration of phenolic acids. The differences could be explained with the different extraction method used, as well as genetic factors, geographical and climate conditions, type of soil, season of harvesting, drying and storage of herbs.

Analysis of antioxidant activity

The highest ability to scavenge DPPH· and ABTS⁺ radicals possess 70% ethanol extract of dried fruits of *S. schinensis*. This extract also showed the highest reduction ability defined by FRAP and CUPRAC methods (Fig. 1). Besides, this was the extract with highest total phenol content (Table 1) and highest amount of chlorogenic, *p*-coumaric and sinapic acids (Table 2).

Among the investigated extracts of frozen fruits the highest antioxidant activity defined by all of the tested methods possessed the compounds extracted with water under reflux-heat at 70°C (Fig. 2). The highest antioxidant potential of this extract could be explained with the highest amount of total phenols and phenolic acids compared to the other extracts. The other three extracts (96% ethanol, 70% ethanol, water extracts, obtained at ambient temperature) of frozen fruits showed similar antioxidant potential.

Hot water extracts of dried and frozen fruits of *S. schinensis* were with higher total phenol content and antioxidant activity than the water extracts, obtained by maceration at ambient temperature. Heating the water extracts at 70°C resulted in obtaining the extracts with higher contents of biologically active compounds.

The observed differences in the total phenol content, phenolic acid concentration and antioxidant activity of the investigated extracts could be explained with the different solvent and methods for extraction used, as well as different type of used fruits (dried and frozen).

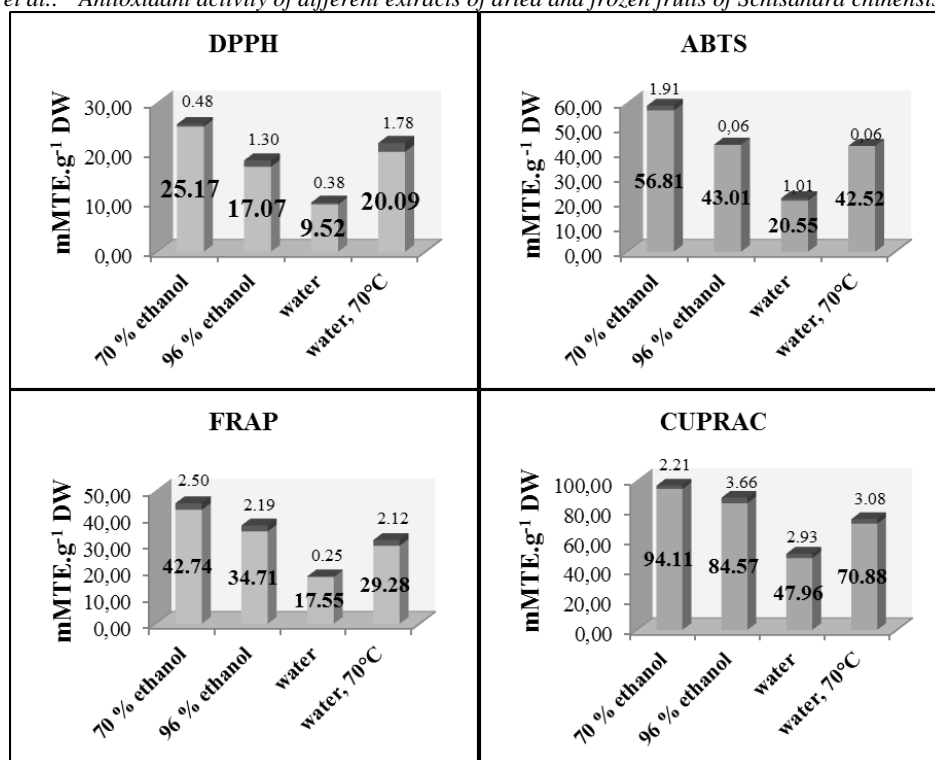


Figure 1. Antioxidant activity of extracts of dried fruits of *S. schinensis* defined by DPPH, ABTS, FRAP and CUPRAC methods.

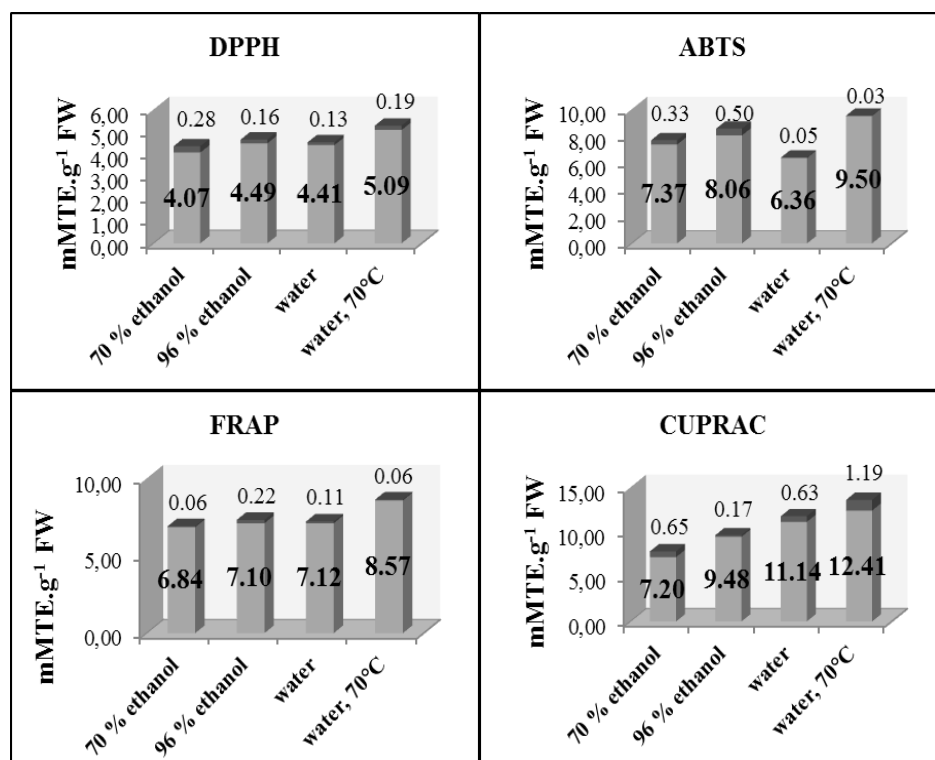


Figure 2. Antioxidant activity of extracts of frozen fruits of *S. schinensis* defined by DPPH, ABTS, FRAP and CUPRAC methods.

CONCLUSION

The present study indicates that the selected solvents are able to obtain extracts from *S. chinensis* fruits with a high antioxidant activity and

high phenolic acids content. This is a base for potentially future application of *S. chinensis* fruits as source of natural antioxidants in different food systems.

REFERENCES

1. N. J. Temple, *Nutrition Research*, **20**, 449 (2000).
2. S. C. Jeong, R. Tulasi, S. R. Koyyalamudi, *Cancers*, **8**, 1 (2016).
3. B. Kaurinovic, M. Popovic, S. Vlasisavljevic, S. Trivic, *Molecules*, **16**, 7401 (2011).
4. D. Benedec, L. Vlase, D. Hanganu, I. Oniga, *Dig. J. Nanomater Biostruct.*, **7**, 1263 (2012).
5. J. Dai, R. J. Mumper, *Molecules*, **15**, 7313 (2010)
6. M. Serafini, R. Bellocco, A. Wolk, A. M. Ekstrom, *Gastroenterology*, **123**, 985 (2002).
7. Y. Lu, D.-F. Chen, *J. Chromatogr. A.*, **1216** 1980 (2009).
8. K.-P. Lee, S. Kang, S.-J. Park, J.-M. Kim, J.-M. Lee, A.-Y. Lee, H.-Y. Chung, Y.-W. Choi, Y.-G. Lee, D.-S. Im, *J. Ethnopharmacol.*, **173** 361 (2015).
9. L. Y. Guo, T. M. Hung, K. H. Bae, E. M. Shin, H. Y. Zhou, Y. N. Hong, S. S. Kang, H. P. Kim, Y. S. Kim, *Eur. J. Pharm.*, **591**, 293 (2008).
10. S. J. Kim, H. Y. Min, E. J. Lee, Y. S. Kim, K. Bae, S. S. Kang, S. K. Lee, *Phytother. Res.*, **24**, 193 (2010).
11. L. Zhang, H. Chen, J. Tian, S. Chen, *Ind. Crops Prod.*, **50**, 690 (2013).
12. B. Pliszka, G. Huszcza-Ciołkowska, E. Wierzbička, *Acta Sci. Pol. Technol. Aliment.*, **15**, 57 (2016).
13. A. Dabija, C. G. C. Pop, A. Buculei, I. Rebenciuc, *Annals and Proceedings of DAAAM International 2011*, **22**, 1003 (2011).
14. F. C. Stintzing, K. M. Nerbach, M. Mosshammer, R. Carle, W. Yi, S. Sellappan, C. C. Acoh, R. Bunch, P. Felker, *J. Agric. Food Chem.*, **53**, 442 (2005).
15. I. Ivanov, R. Vrancheva, A. Marchev, N. Petkova, I. Aneva, P. Denev, V. Georgiev, A. Pavlov, *Int. J. Curr. Microbiol. App. Sci.*, **3**, 296 (2014).
16. Y. Cai, Q. Luo, M. Sun, H. Corke, *Life Sciences*. **74**, 2157, (2004).
17. M. Plazas, J. Prohens, A. Cuñat, S. Vilanova, P. Gramazio, F. Herraiz, I. Andújar, *Int. J. Mol. Sci.*, **15**, 17221 (2014).
18. K. Yun, D. Koh, S. Kim, S. J. Park, J. H. Ryu, D. Kim, J. Lee, K. Lee, *J. Agric. Food Chem.*, **56**, 10265 (2008).
19. F. Guglielmi, C. Luceri, L. Giovannelli, P. Dolara, M. Lodovici, *Br. J. Nutr.*, **89**, 581 (2003).
20. A. Mocan, G. Crişan, L. Vlase, O. Crişan, D. C. Vodnar, O. Raita, A.-M. Gheldiu, A. Toiu, R. Oprean and I. Tilea, *Molecules*, **19**, 15162 (2014).

АНТИОКСИДАНТНА АКТИВНОСТ НА РАЗЛИЧНИ ЕКСТРАКТИ ОТ ИЗСУШЕНИ И ЗАМРАЗЕНИ ПЛОДОВЕ ОТ *Schisandra chinensis* (Turcz.) Baill.

А. В. Терзиева¹, Р. З. Вранчева^{2*}, Н. Д. Делчев²

¹Студент от специалност „Анализ и контрол на хранителните продукти“, катедра „Аналитична химия“, Университет по хранителни технологии-Пловдив, бул. „Марица“ №26, 4000 Пловдив

²Катедра „Аналитична химия“, Университет по хранителни технологии-Пловдив, бул. „Марица“ №26, 4000 Пловдив

Постъпила на 10 ноември 2016 г.; приета на 3 януари 2017 г.

(Резюме)

Китайският лимонник (*Schisandra chinensis*) е използван в традиционната китайска медицина в продължение на стотици години. През последните десетилетия, фармакологичните и химични изследвания на това растение разкриха различни ценни биологични и фармакологични активности, като антихепатотоксична, антиоксидантна, детоксикираща, антитуморна, тонизираща и противовъзпалителна активност. Целта на настоящото изследване е да се определи антиоксидантна активност и фенолния профил на различни екстракти (воден при стайна температура, воден, 70% и 96% етанолен екстракт чрез екстракция на водна баня при 70 °C и обратен хладник) на изсушени и замразени плодове от *Schisandra chinensis* (Turcz.) Baill. Антиоксидантния потенциал на изследваните екстракти е определен чрез четири най-често използвани спектрофотометрични методи, а именно DPPH, ABTS, FRAP и CUPRAC. 70% етанолен екстракт от сушените плодове притежава най-висока антиоксидантна активност, определена чрез всички тествани методи. Най-висок антиоксидантен потенциал на замразените плодове е определен във водния екстракт, получен чрез екстракция на обратен хладник при 70° C. Освен това, тези екстракти са с най-високо съдържание на общо феноли, определени по метода на Folin-Ciocalteu. Чрез HPLC анализ на фенолния профил на изследваните екстракти се установи наличието на хлорогенова, *p*-кумарова и синапова киселина.

Установената висока антиоксидантна активност на изследваните екстракти от изсушени и замразени плодове от *S. chinensis* е предпоставка за бъдещото им прилагане като естествени консерванти в различни хранителни системи.

Ключови думи: *Schisandra chinensis*, антиоксиданти, фенолни киселини, биологична активност, HPLC

Compatibility of measurement results for the active substance Zineb, determined by CIPAC and ICP-OES methods

D. K. Chakarova-Dimitrova*, V. J. Kmetov

*Department of Analytical Chemistry and Computer Chemistry,
University of Plovdiv "Paisii Hilendarski", 24 Tzar Asen Str., 4000 Plovdiv, Bulgaria*

Received November 11, 2016; Revised December 1, 2016

The presented work evaluates the metrological compatibility of the results of the active substances for five batches Zineb, measured by the classical CIPAC25:1993 method in the Accredited Testing Laboratory to Agria S.A., with those measured by a new ICP-OES method. The absolute value of the difference between the measured results for each pair was calculated and was found smaller than twice the standard measurement uncertainty of that difference, which confirmed the compatibility of CIPAC 25 and ICP-OES methods.

The new instrumental ICP-OES method is a faster and "greener" alternative to the classical CIPAC 25 method for determination of the active substance Zineb in biocidal products.

Key words: Zineb, CIPAC, ICP-OES, compatibility

INTRODUCTION

Dithiocarbamates (DTCs) are among the most commonly used classes of organosulfur pesticides. According to the carbon chain DTCs can be divided into the following subsets: DMDs - dimethyl (dithiocarbamates); EBDs - ethylene bis (dithiocarbamates); PBDs - propylene bis (dithiocarbamates) [1]. The object of our study is Zineb - EBD from the so-called "group of Maneb" - Zineb, Maneb, Mancozeb.

Zineb with CAS Number (12122-67-7) has molecular formula $(C_4H_6N_2S_4Zn)_x$, and IUPAC name Zinc ethylene bis (dithiocarbamate). It is a solid, yellowish-white powder with non-characteristic odour.

One of the leading companies in the field of producing, importing and trading with herbicides, fungicides and pesticides is Agria S.A., situated near to Plovdiv, Bulgaria.

Agria S.A. has modern facilities for production, formulation and packaging of plant protection products from the dithiocarbamate group, among them Perozine Marine, which contains Zineb (95% min) as an active ingredient.

Perozine Marine is primarily used as a co-biocide/booster biocide in marine antifouling paints to increase the efficacy of the primary biocide to reduce colonization of biofouling organisms on immersed objects, structures and vessels in the marine environment.

Antifouling paints containing Zineb are applied to the surface of structures to be protected against the build-up of aquatic fouling organisms. This is

achieved via the slow release of the active ingredient over time. These formulations are widely used on the hulls of marine vessels, docks, fishnets and buoys.

Over many years use Zineb has proved to be a very effective partner to the primary biocide in controlling the growth of biofouling organisms. In addition the active ingredient Zineb is considered to be less harmful to the environment than other booster biocides.

In the recent paper [2], Karsaz and Afshar are showing the usefulness of Zineb and Ziram as alternative to the TBT (Tributyltin) which utilization has been stopped since 2003 because of its negative impacts on the marine environment. Comprehensive data about Zineb (product type 21) characteristics and risk assessment of its applications is provided by the European Chemicals Agency (ECHA) in the report published in [3].

For the preparation process of a technical grade pesticide it is very important the active ingredient to be precisely measured and declared.

CIPAC Method 25/TC/M/3 is available to analyze the Zineb content in the Technical Grade of the Active Ingredient (TGAI) [4]. In this paper it will be denoted as CIPAC 25. It is an officially accepted method and is based on the procedure described by D. G. Clarke [5]. The method is set up on the classical titrimetric determination of the carbon disulfide mass fraction produced after thermal degradation of the complex performed by means of an installation called Clarke Apparatus. The testing Laboratory of Agria S.A., which is accredited pursuant to BDS EN ISO/IEC 17025,

* To whom all correspondence should be sent.
E-mail: dilldimitrova@yahoo.com

works with this method since many years. It is recommended for the quality control, the accuracy of the results to be proven either by CRM (Certified Reference Materials) or by inter laboratory comparison with different methods of analysis. Moreover the CIPAC 25 measurement procedure uses H₂SO₄, CdSO₄, etc., needs almost an hour to be accomplished and does not belong to the group of environmentally friendly methods. Therefore the replacement of the classical CIPAC 25 method with better, "greener" methods is highly welcomed.

A new instrumental method based on measurements of Zineb bonded sulfur by ICP-OES has been developed by us. The new method was optimized for maximum precision and reliability.

The analytical task is to quantify the active substance – Zineb in manufactured products in the range between 95÷99 % with target uncertainty $u_c < 1\%$ (expanded uncertainty $U < 2\%$, $k=2$). For both CIPAC 25 and ICP-OES methods uncertainty budget was constructed using Kragten [6] spreadsheet approach. The combined uncertainty u_c was calculated according to the EURACHEM / CITAC GUIDE [7]. All experimental data and uncertainty budget constructed for both methods have been reported on the international seminar "Modern methods for chemical analysis and control", organized by Thermo Scientific, ACM2 Ltd and Plovdiv University in Plovdiv 20.05.2015 and have been submitted for publication in another paper. The experiments showed better precision of the instrumental ICP-OES method with higher sample throughput and environmentally friendly characteristics in comparison to the classical one. The combined uncertainty for the active ingredient Zineb measured (96.6 % w/w) was found 0.46% for ICP-OES and 0.82% for CIPAC 25 method respectively.

Due to the fact, that both methods are indirect and use sulfur determination for quantification of Zineb and because in the manufacturing process the product could suffer from some unknown variations, it is needed compatibility of the CIPAC 25 and ICP-OES methods to be checked for different series of technical material. In this work we evaluate the metrological compatibility of both methods. It must be underlined that there are no CRMs with Zineb higher than 95% available on the market. So the comparison by different methods of analysis seems to be the most applicable procedure for quality control.

In the present work the compatibility of the results from CIPAC 25 and ICP-OES analysis has been evaluated according to the method described in [8].

MATERIALS AND METHODS

Apparatuses

CIPAC 25 method

Apparatus for determination of Zineb according to CIPAC 25 (Clarke installation); calibrated balance Mettler AE200; automatic calibrated burette Brand; beaker 600 mL; magnetic stirrer.

ICP-OES method

Thermo ICP-OES iCAP 6300, calibrated balance Mettler AE200; volumetric flask, class AS V =250 mL; US bath, plastic test tubes 50 mL; syringe filter 0.45 µm.

Reagents

CIPAC 25 method

Merck KGaA iodine solution (titrimetric standard), Sigma-Aldrich products: sodium diethyldithiocarbamate trihydrate, sulphuric acid, tetrasodium salt of ethylenediaminetetraacetic acid (EDTA), potassium hydroxide, cadmium sulphate, acetic acid, phenolphthalein indicator solution, starch; deionized water.

ICP-OES method

Sigma-Aldrich sulfur standard for ICP; Merck KGaA ammonia solution; deionized water.

Procedures

CIPAC 25 method

A set of five different batches of Zineb produced in Agria S.A. have been analyzed. 0.3 g of each sample containing Zineb is dissolved in 30% tetrasodium salt of EDTA solution and is decomposed by boiling with 2 mol/L sulphuric acid to ethylenediamine sulphate and carbon disulphide. The latter is passed through a cadmium sulphate (18.5 g in 100 mL distilled water) scrubber to remove hydrogen disulphide, and then into an absorption train containing 2 mol/L methanolic potassium hydroxide to afford potassium methyl xanthate. The produced xanthate, after neutralization with 10% acetic acid, is titrated with 0.05 mol/L iodine standard.

Calculation of Zineb active ingredient (A.I.)

$$A.I. \% = \frac{(A - B) \cdot M \cdot M_m Zb \cdot K}{m \cdot 1000} \cdot 100 \quad (1)$$

A = volume of iodine used for titration of the sample, mL

B = volume of iodine used for titration of the blank, mL

M = molar concentration of iodine, mol/L

M_mZb = molar mass of Zineb, g/mol

m = sample weight, g

K = factor of apparatus

ICP-OES method

The same set of five different batches of Zineb produced in Agria S.A. has been analyzed by ICP-OES. The optimized instrumental conditions are listed in Table 1. External "bracket" calibration

was used. For that purpose two sulfur standard solutions were prepared - 160 and 200 mg/L S in ammonia medium as follows: (i) for 160 mg/L calibrator - 8 g of standard solution of sulfur 1000 mg/L were weighed in a test tube and dissolved to 50 g with 3.75% ammonia (75 mL 25% ammonia to 500 mL with deionized water) and (ii) 10 g standard solution of sulfur 1000 mg/L was dissolved in the same manner for 200 mg/L calibrator.

Sample: 0.2 g Zineb from each batch was dissolved in 250 mL 7.5% ammonia in a volumetric flask. An ultrasonic bath was used for faster dissolution (dilution factor DF = 1250). Second dilution was made just before the instrumental analysis by mixing 25 g of the above sample solution with 25 g of 3.75% ammonia. The final DF = 2500 ensures that in the prepared Zineb samples solution the S concentration will lie between the bracket standards.

For determination of unbonded sulfur, water extracts have been developed as follows: 0.5 g of each batch Zineb was suspended in 50 g deionized water. The sample solution was filtered through syringe filter 0.45 µm. Second dilution was made just before the instrumental analysis by mixing 25 g of the above sample solution with 25 g of 7.5% ammonia.

Table 1. Instrumental parameters of the ICP-OES determination of sulfur

Parameter	Value
Radiofrequency power	1250 W
Plasma gas flow rate	15 L min ⁻¹
Auxiliary gas flow rate	0.5 L min ⁻¹
Nebulizing/carrier gas flow rate	0.7 L min ⁻¹
Peak processing	3 pixels per peak
Background correction	2 sides one pixel
Number of replicates	4
Replicate read time	10 s
Nebulizer type	OneNeb Flow Blurring® nebulizer
Sample flow rate	1.2 mL min ⁻¹
Spray chamber	Single-pass cyclonic chamber
Viewing mode	Axial
Spectral lines for sulfur	182.624 nm

Calculation of Zineb active ingredient (A.I.) after ICP-OES determination of sulfur

$$A.I. \% = \frac{C_z \cdot V_{pr} \cdot m_{2pr} \cdot M_m Zb.}{m_{pr} \cdot m_{1pr} \cdot 4 \cdot A_m S} \cdot 100 \quad (2)$$

C_z= content of bonded in the Zineb sulfur (measured by ICP-OES), mg/ml

V_{pr} = initial volume for sample dissolution, ml

m_{1pr}= amount of sample solution taken, g
m_{2pr} = final sample weight (for second dilution),g

M_mZb = molar mass of Zineb, g/mol

A_mS = atomic weight of sulfur, g/mol

m_{pr} = sample weight, mg

ICP-OES determination of sulfur after "bracket" calibration

$$C_z \frac{mg}{l} = \frac{C_1 \left(I_2 - \left(I_z - \frac{I_0}{F} \right) \right) + C_2 \left(\left(I_z - \frac{I_0}{F} \right) - I_1 \right)}{I_2 - I_1} \quad (3)$$

I_z = intensity of the sample Zineb, cps

I₀ = intensity of the extracted sample Zineb, cps

I₁ = intensity of the low standard of S, cps

I₂ = intensity of the high standard of S, cps

F = ratio between concentrations of Zineb sample and the extracted one

C₁= concentration of the low standard, mg/mL

C₂= concentration of the high standard, mg/mL

RESULTS AND DISCUSSION

Despite the fact that the manufacturing process of technical Zineb (near 95%) is strictly controlled the final product differs in the active substance content from 95 till 99%. Fit for purpose analysis has to be performed to justify the particular content of the active ingredient. Therefore representative samples from five batches of Zineb, manufactured in different days in Agria S.A. have been collected. For each batch the active substance Zineb was determined by the CIPAC 25 method in the Testing Laboratory of Agria S.A. and by the ICP-OES method in the laboratory of the University of Plovdiv, Department of Analytical Chemistry and Computer Chemistry. Results obtained from both methods are listed on columns (2) and (3) in Table 2. No reference material Zineb was available, hence the reliability of the tests could be concluded if the results from both methods are compatible.

One commonly used approach described in the textbooks [9] for comparing analytical methods is the use of regression lines. In this approach one axis of a regression graph is used for the results obtained by the classical method, and the other axis for the results obtained by applying the new or comparative method to the same samples. It is clear that if each sample yields an identical result with both analytical methods, the regression line will have a zero intercept "a", with a slope "b" and a correlation coefficient "r" - equal to 1. In the current case however the commented above regression approach is inapplicable and can give unreliable estimations.

Working with the sets of data from Table 2 and using the line regression approach (CIPAC25 versus ICP-OES), the calculated parameters are $b = 1.65$; $a = 62.5$ and $r = 0.985$, which are quite far from the ideal case. The reason is that all five

samples tested, contain Zineb in pretty close concentration to the centroid – 96.6 %, and due to the uncertainty attributed to the results it seems we do evaluation of regression with very close to one point of concentration, which is a nonsense.

Table 2. CIPAC and ICP-OES results and their estimators of compatibility (see in the text) for determination of the active substance Zineb in percent (%)

No batch	ICP-OES						
	CIPAC 25 x_c	x_i	$ x_i-x_c $	u_c	u_i	u_d	ku_d
(1)	(2)	(3)	(4)	(5)	(6)	(7)	(8)
1	95.51	95.05	0.46	0.78	0.44	0.90	1.79
2	95.71	95.40	0.31	0.78	0.44	0.90	1.80
3	96.66	97.35	0.69	0.79	0.45	0.91	1.82
4	96.73	97.44	0.71	0.79	0.45	0.91	1.82
5	97.63	98.40	0.77	0.80	0.45	0.92	1.84

Therefore another approach using the model given in [8] was selected as a more reliable estimator of the compatibility of both methods for Zineb quantification. The metrological compatibility of measuring results is defined in [VIM3 2.47] [10] as: "property of a set of measurement results for a specified measurand, such that the absolute value of the difference for any pair of measured quantity values from two different measurement results is smaller than some chosen multiple of the standard measurement uncertainty of that difference". In our case and according to [8] the compatibility could be proved if the absolute value of the difference $|x_i-x_c|$ for each pair of results (ICP-OES – CIPAC25) is smaller than the combined uncertainty of the difference u_d multiplied by the coverage factor $k=2$.

Hence for the data in Table 2 the difference d for each pair (x_i – for ICP-OES method and x_c - for CIPAC 25 method) was found and the absolute value is given on column (4). The combined uncertainty u_d of the difference for each pair of measurement results was calculated according to the propagation law using the equation 4:

$$u_d = \sqrt{u_i^2 + u_c^2} \quad (4)$$

The u_c and u_i from columns (5) and (6) on Table 2 are the combined uncertainties estimated for CIPAC 25 and ICP-OES measurements of Zineb respectively.

The obtained u_d are listed in column (7)

As one can see, all the five values in column (4) are smaller than those in column (8) which is the condition to claim that the results are compatible:

$$|x_i-x_c| < ku_d \quad (5)$$

samples tested, contain Zineb in pretty close concentration to the centroid – 96.6 %, and due to the uncertainty attributed to the results it seems we do evaluation of regression with very close to one point of concentration, which is a nonsense.

Moreover all the five values in column (4) are smaller than those in column (7) which is even more significant proof.

Figure 1 was constructed with the same data from Table 2 but averaged points (from CIAPAC 25 and ICP-OES) have been added for each batch sample tested with dotted line for CIPAC 25 and solid line for ICP-OES. It is important to emphasize that lines are crossed and with a different distance between them. All this is an evidence for the existence of random effects in the measurement shifts rather than a systematical one.

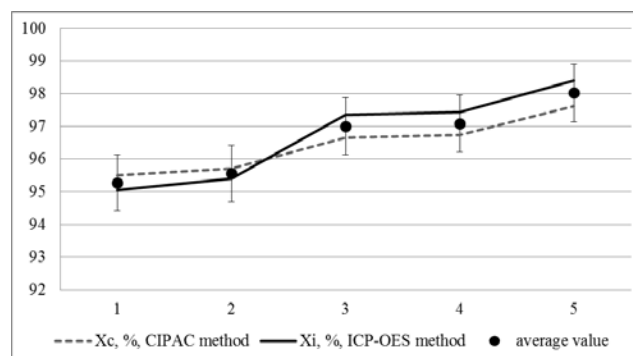


Fig. 1 Plotted results for the active substance zineb (the error bars shows the target uncertainty)

CONCLUSION

The new instrumental ICP-OES method is a faster and "greener" alternative to the classical CIPAC 25 method for determination of the active substance Zineb in biocidal products. The metrological compatibility between the new ICP-OES method and CIPAC method is proved for measuring concentrations near 96.6 % with fit for purpose accuracy. The absolute value of the difference between measured results for each

measurement pair is smaller than twice the standard measurement uncertainty of that difference, and confirms the compatibility of the methods.

ICP-OES method could be recommended for wider use.

Acknowledgements: *The current study was supported by the Fund for Scientific Research of the University of Plovdiv project NI 15-HF 001.*

REFERENCES

1. G. Crnogorac and W. Schwack, *TrAC Trends in Analytical Chemistry*, **28**(1) 40-50, (2009).
2. A. Karsaz, A. Afshar, *J. Mater. Environ.*, **7**(4) 1436-1444, (2016).
3. Regulation (EU) n0528/2012, Zineb Product-Type 21 (Anti-fouling products), S.C.o.B. Products, Editor. (2013).
4. W. Dobrat, A. Martijn, *CIPAC. Vol. Handbook E*, (1993).
5. D. Clarke, et al., *Analytical Chemistry*, **23**(12) 1842-1846, (1951).
6. J. Kragten, *Analyst*, **119**(10) 2161-2165, (1994).
7. Eurachem/CITAC QUAM Guide CG 4 (Third Edition), (2012).
8. T. Linsinger, *European Reference Materials, Application note one*, (2010).
9. J. Miller, J. Miller, *Statistics and Chemometrics for Analytical Chemistry, Fifth edition*, p. 126, (2005).
10. V. Barwick, E. Pichard, *Eurachem Guide: TAM-Introduction to VIM 3*, (2011).

СЪВМЕСТИМОСТ НА РЕЗУЛТАТИТЕ ОТ АНАЛИЗ НА АКТИВНАТА СУБСТАНЦИЯ ЦИНЕБ, ОПРЕДЕЛЕНА ЧРЕЗ СІРАС И ІСР-ОЕС МЕТОДИ

Д. К Чакърова-Димитрова, В. Й. Кметов

*Пловдивски университет "Паусий Хилендарски", Катедра Аналитична химия и компютърна химия,
ул. Цар Асен № 24, Пловдив, България*

e-mail: dilldimitrova@yahoo.com

Постъпила на 11 ноември 2016 г.; приета на 1 декември 2016 г.

(Резюме)

Представената работа оценява метрологичната съвместимост на резултатите от определянето на активната субстанция в пет партии Цинеб произведен в Агрив АД, измерени чрез класически СІРАС 25: 1993 метод в акредитираната лаборатория към Агрив АД, с тези, измерени чрез новосъздаден ІСР-ОЕС метод. Абсолютната стойност на разликата между измерените резултати за всяка двойка е по-малка от два пъти стандартната неопределеност при измерване на тази разлика, което потвърждава съвместимостта на СІРАС 25 и ІСР-ОЕС методите.

Новосъздаденият ІСР-ОЕС инструментален метод е по-бърза и по-„зелена“ алтернатива на класическия СІРАС 25 метод за определяне на активната субстанция Цинеб в биоцидни продукти.

Ключови думи: *Цинеб, СІРАС, ІСР-ОЕС, метрологична съвместимост*

Optimizing the determination of mercury in human urine by ICP-MS with a collision cell mode

M. Panova^{1*}, V. Kmetov², D. Davcheva^{1,3}, T. Tomova^{1,4}, D. Tomov¹

¹Technological Center for Emergency Medicine - Plovdiv,

²Department of Analytical Chemistry and Computer Chemistry,
University of Plovdiv "Paisii Hilendarski"

³Department of Clinical Laboratory, Medical University of Plovdiv

⁴Department of Chemical Sciences, Medical University of Plovdiv

Received November 13, 2016; Revised December 15, 2016

The applicability of ICP-MS (Thermo Scientific iCAP Qc) and possible interferences from Tungsten oxide were evaluated for mercury quantification in human urine. The mass spectrometer is equipped with a collision cell with helium gas, working with Kinetic Energy Discrimination (KED) mode. This mode is widely used to suppress polyatomic interferences, which are inherent to the ICP-MS. A demerit of the KED mode is the worsening of the sensitivity and lowering of the signal to noise ratio, especially for the lower mass region. Therefore instead of KED, STD mode (not pressurized cell) is preferable, where low limit of detections are desirable.

The present work shows that after optimizing, the mercury determinations by He KED mode, more than double improved signal to noise ratio could be obtained, compared to STD mode. Instead of decreased sensitivity, the signals for all Hg isotopes were higher and precise, when working in KED. The ratios of recorded signals were compared with the natural abundance of Hg isotopes and a very good match was estimated. This is an evidence of the absence of spectral interferences. By the optimized method instrumental detection limits of 2 ng/L (²⁰²Hg) were achieved. A certified reference material - human urine was analyzed with an excellent recovery of Hg, in the range of 99 and 101 %. A very good recovery (90-110%) was found also in human urine samples, spiked with 5 ppb Hg and diluted with DF=20.

Key words: ICP-MS, mercury determination, Hg, collision cell, human urine

INTRODUCTION

Mercury (Hg) is considered as one of the most toxic and dangerous to the human organism heavy metals [1]. At levels above the permissible concentrations Hg has toxic and carcinogenic effects on the kidneys, immune and reproductive systems, the myocardium and nervous system [2, 3, 4]. It is easily concentrated in inner organs, due to its affinity for S-H groups [3]. Hg is mainly absorbed through the respiratory system, the gastrointestinal tract and the skin. It is excreted

from the organism through urine and feces, with about two months' half-life [5].

Quantification of mercury in urine is a noninvasive method widely used for assessment of the risk of human exposure.

The substances suitable for use as biomarkers are defined through experimental and epidemiological toxicological studies among workers [6]. Mercury is also used as a biomarker in the international occupational medicine practice. Table 1 presents data on the permissible concentrations of mercury in urine [8].

Table 1. Reference levels for monitoring of the exposure to Hg (Reymond Meister, 2004)

Biological material	Without professional exposition	NOAEL*	Manifestation of clinical effect	Half-life period	Comment
Urine (µg/L)	< 5	35-50	100	60 days	Reflects the exposition of the past 2-4 months

*NOAEL - No-observed-adverse-effect level

* To whom all correspondence should be sent.

E-mail: panova22@abv.bg

In Bulgarian legislation mercury is listed along with 14 substances, which are monitored for protection of employees from the risks related to occupational exposure to chemicals. Biological environment, appropriate biomarker, biological limit and time for sampling are specified [7]. According to WHO a biological limit up to 100 µg/L is given for mercury in urine (2003) [9]. Patients, who do not consume contaminated with Hg foods, have a level of Hg in urine ≤ 0.5 µg/L [1].

Quantification of Mercury is a complicated analytical task, especially in biological materials, where the maximum permissible concentration is very low. ICP-MS is a powerful tool for trace elements determinations. Aim of this study is to optimize an ICP-MS method for determination of Hg in human urine, capable to achieve limits of quantification < 1 µg/L.

MATERIALS AND METHODS

The analysis was performed on a Thermo Scientific ICAP Qc ICP-MS (Thermo Scientific, Germany), equipped with a collision cell with helium (He) and kit for online introduction of internal standard. Running conditions for ICP-MS are summarized in Table 2.

Stock solutions of mercury (Hg) with a concentration of 1000 mg/L (Honeywell Fluka™) was used. Rhenium (CPAchem Ltd) was used as internal standard with a final working concentration of 15 µg/L. The isotope ¹⁸⁵Re was preferred because it is free of isobaric interferences. For the preparation of all solutions and reagents, ultra-pure water (18.2 M Ω.cm) from VWR Purity TU and nitric acid (HNO₃, 2 v/v) from Fisher Chemical were used. Reference material was purchased from Seronorm (Trace Elements urine, Seronorm, Nycomed AS, Oslo, Norway).

Urine samples were collected in plastic bottles. Total volume excreted was measured and recorded for each 24-h urine specimen. Specimens were stored at 4°C, and analysis was performed within 7 days. The samples were thoroughly mixed before dilution with 2% HNO₃. Two dilution factors were used (DF = 20 and DF = 100).

The certified reference material Seronorm was prepared according to the supplier instruction and diluted with 2% HNO₃ (DF = 200) before measuring.

Aqueous standards for Hg external calibration were prepared in 2% HNO₃ at concentrations of 25, 50, 100, 250 and 500 ng/L from a stock solution of 1000 mg/L Hg.

The laboratory analysis was performed by external calibration, with online introduction of internal standard rhenium.

Table 2. Optimized operating conditions of the ICP-MS ICAP Qc

Plasma conditions	
RF-power	1550 W
Nebulizer Gas Flow	0.96 L min ⁻¹
Auxilliary Gas Flow	0.80 L min ⁻¹
Plasma Gas Flow	14.00 L min ⁻¹
He gas flow	3.2 mL min ⁻¹
Mass Spectrometer Settings	
Dwell time	0.3 sec
Sweeps	15
Replicates	4
Survey run	180-220 amu

RESULTS AND DISCUSSION

Determination of mercury by ICP-MS may be performed by registration of the mercury isotopes' signals, shown in Table 3. In the same table are given the potential polyatomic interferences of Tungsten oxides. The signals of five from seven isotopes of mercury were measured - ¹⁹⁸Hg, ¹⁹⁹Hg, ²⁰⁰Hg, ²⁰¹Hg and ²⁰²Hg. Two isotopes - ¹⁹⁶Hg and ²⁰⁴Hg were excluded from data processing, due to their low natural abundance percentage. Moreover the latest is overlapped by ²⁰⁴Pb and if Lead is present in the urine samples, it could cause isobaric interference. Rhenium (¹⁸⁵Re) was used as internal standard for nonspectral interferences and sensitivity drift correction. There are five isotopes of tungsten - ¹⁸⁰W, ¹⁸²W, ¹⁸³W, ¹⁸⁴W and ¹⁸⁶W, which are able to generate oxide radicals with mass range from 196 to 202 amu. Table 3 presents the isotopes and possible interferences.

Optimization of the experimental determination was performed to achieve the best signal to noise ratio. The mass spectrometer is equipped with a collision cell with helium gas, working in Kinetic Energy Discrimination (KED) mode. This mode is widely used to suppress polyatomic interferences in ICP-MS. A demerit of the KED mode is the worsening of the sensitivity and lowering the signal to noise ratio, especially for the lower mass region. Therefore, a standard mode (not pressurized cell - STD) is preferable instead of KED, where the desirable limits of detections are low. Both KED and STD modes were tested for mercury measurements of the lowest calibrator – 25 ng/l Hg. Higher sensitivity and precision were expected for

the signals measured in STD mode. The results of the experiment, however, show that when working with a collision cell with helium gas in KED mode, RSD for all isotopes of Hg observed are almost 2 times lower than in STD mode (Figure 1).

Table 3. Mercury and tungsten isotopes with natural abundance (NA) and possible mass spectra overlaps from WO interferences

Isotop	NA %	Isotop	NA %	Interference
¹⁹⁶ Hg	0.146	¹⁸⁰ W	0.126	¹⁸⁰ W ¹⁶ O
¹⁹⁸ Hg	10.02	¹⁸² W	26.31	¹⁸² W ¹⁶ O
¹⁹⁹ Hg,	16.84	¹⁸³ W	14.28	¹⁸³ W ¹⁶ O
²⁰⁰ Hg	23.13	¹⁸⁴ W	30.64	¹⁸⁴ W ¹⁶ O
²⁰¹ Hg	13.23	¹⁸⁶ W	28.64	¹⁸⁴ W ¹⁶ OH
²⁰² Hg	29.8			¹⁸⁶ W ¹⁶ OH
²⁰⁴ Hg	6.85			²⁰⁴ Pb

This effect could be explained with better focusing of the ion beam, when the cell is working in KED mode. Probably this tolerates the passage of Hg⁺ ions, with negligible effect of their kinetic discrimination. Because the mercury isotopes are heavy enough, they are barely discriminated, when hit with Helium. Another test was performed, measuring the signals in KED with variable Helium collision gas flow. It was observed that the maximum signal to noise ratio (S/N) for all Hg isotopes measured could be recorded at 3.2 ml/min He gas flow. When a lower He flow is used the S/N ratio is dropping with up to 40%. Human urine samples were measured in KED mode at 3.2 ml/min He. In this case spectral interferences were found, due to the variable concentrations of tungsten (see Table 4). Therefore, after tune optimization, 4.925 ml/min was chosen as optimal collision gas flow. The efficiency of the interference correction was checked by scans in a mass range of 180-210 amu (atomic mass unit). The experimentally recorded signals of the five selected mercury isotopes were compared and normalized to ²⁰⁰Hg (Figure2).

A very good match with the natural abundance of the results, obtained from the analysis of 25 ng/l Hg standard and the Seronorm reference material

(DF=200), was observed. This is an evidence of the analytical selectivity of the proposed method.

The five human urine samples were measured after dilution as follows: (i) dilution factor DF=100 and (ii) dilution factor DF=20. The estimation of the matrix effect was monitored by the Internal standard shift. The drop of the signals of ¹⁸⁵Re, used as Internal standard, was insignificant for both dilution factors. Hence working with less diluted urine samples (DF=20) is preferable, related to lower methodological limit of quantification (LoQ). The use of internal standard is necessary for correction of the typical for ICP-MS sensitivity drift (see Table 4).

For better precision relatively long dwell times were selected 0.3 s per mass. A forced to Blank calibration was preferred. The calculated instrumental detection limits are as follows: 12 ng/L for ¹⁹⁸Hg; 4 ng/L for ¹⁹⁹Hg; 4 ng/L for ²⁰⁰Hg; 15 ng/L for ²⁰¹Hg; 2 ng/L for ²⁰²Hg. A very high value for BEC (background equivalent concentration) was recorded for ²⁰¹Hg (BEC=79 ng/L). For this reason only three of the isotopes (¹⁹⁹Hg ²⁰⁰Hg ²⁰²Hg) were chosen for quantitative measurements of Hg in urine. The concentrations of Hg measured in the five samples human urine are given in Table 4. The difference between the results from the three Hg isotopes is acceptable. Taking into consideration the used dilution factor DF=20, mercury could be measured in urine samples with limit of quantification 0.26 µg/L for ¹⁹⁹Hg ²⁰⁰Hg and 0.15 µg/L for ²⁰²Hg (LoQ was calculated using 10σ criteria). All patient samples tested showed lower than 5 µg/L content of Hg, from 1 to 2.7 µg/L with acceptable precision. Regardless of the variable content of Tungsten in the urine (see the signals for ¹⁸²W given in Table 4) no spectral interferences were registered.

In order to validate the method all patient urine samples were spiked with 5 µg/L Hg before dilution. The recovery of the spikes was found to be in the range from 90% to 108%, which refers the method as “fit for purpose” for quantification of mercury in human urine

A certified reference material - human urine (Seronorm Trace Elements Urine, Nycomed AS, Oslo, Norway) was analyzed with an excellent recovery of the referent concentration of Hg. The results are shown in Table 4.

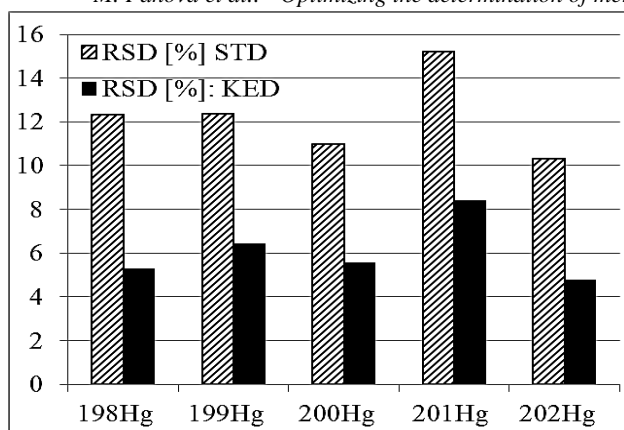


Fig. 1. RSD % obtained by STD and KED mode for 25 ng/L Hg (n=4).

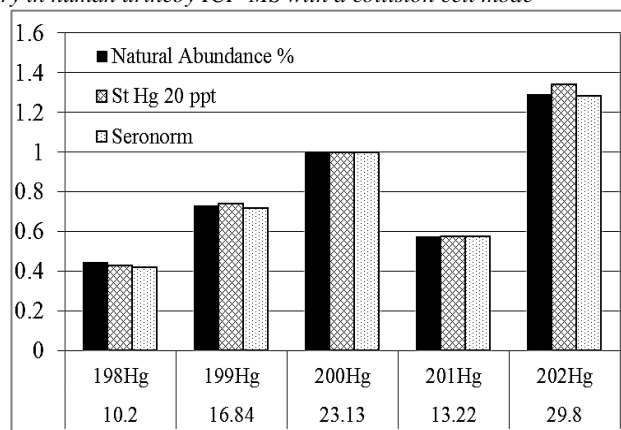


Fig. 2. Hg isotope ratio normalized to ^{200}Hg . The numbers on the bottom are natural abundance in %

Table 4. Results of ICP-MS determination of Hg ($\mu\text{g/L}$) in human urine, urine spiked with 5 $\mu\text{g/L}$ Hg and CRM – Seronorm, obtained from different isotopes. An interval is given as \pm SD, n=4. Recovery is given in brackets (R %).

	IS drift ⁽¹⁾	^{182}W (cps) ⁽²⁾	^{199}Hg	^{200}Hg	^{202}Hg
Urine 1	97.3%	16,454	1.28 \pm 0.08	1.31 \pm 0.05	1.19 \pm 0.06
Urine 2	98.5%	7,472	1.85 \pm 0.05	1.85 \pm 0.07	1.97 \pm 0.15
Urine 3	99.4%	1,415	2.49 \pm 0.12	2.69 \pm 0.13	2.63 \pm 0.013
Urine 4	98.8%	36,612	1.1 \pm 0.16	1.37 \pm 0.18	1.17 \pm 0.17
Urine 5	99.8%	35,844	0.82 \pm 0.003	0.93 \pm 0.05	0.76 \pm 0.04
Urine 1 + Hg	95.3%	16,986	5.2 (105 %)	5.2 (105 %)	5.2 (104 %)
Urine 2 + Hg	95.5%	7,320	4.5 (90 %)	4.5 (91 %)	4.5 (90 %)
Urine 3 + Hg	96.2%	1,441	5.4 (108 %)	5.4 (107 %)	5.3 (106 %)
Urine 4 + Hg	95.8%	34,646	4.7 (93 %)	4.6 (92 %)	4.6 (92 %)
Urine 5 + Hg	95.6%	33,301	4.6 (91 %)	4.4 (92 %)	4.5 (90 %)
Seronorm 40.7 (36.1 – 45.3) ⁽³⁾	95.9%	3,433	41.2 (101.2 %)	40.5 (99.5 %)	40.4 (99.3 %)

Human urine was diluted with DF=20, Seronorm was diluted with DF=200. Urine was spiked (+ Hg) with Hg 5 $\mu\text{g/L}$ before dilution. ⁽¹⁾ ^{185}Re Internal Standard drift in %; ⁽²⁾ Signals in counts per second measured for ^{182}W ; ⁽³⁾ Hg acceptable range from the Seronorm certificate

CONCLUSION

Even if Tungsten is not present in the urine of patients and the risk for a potential spectral interference for ICP-MS mercury determination is low, we recommend the collision cell with KED mode to be used. The KED mode improves the signal to noise ratio and allows reaching lower instrumental limits of quantification more than twice comparing with the STD mode. Maximum signal to noise ratio was obtained with 3.2 mL/min He collision gas flow, but to guaranty the effective interference suppression from the variety of the urine constituents it is preferable to work with 4.925 mL/min He flow. A simple dilution of collected urine with dilution factors DF=20 and use

of Re as Internal standard is enough to avoid the multiplicative matrix effects. The optimized ICP-MS method is valid for determination of mercury in human urine for concentrations higher than 0.15 $\mu\text{g/L}$ with 90-110% recovery. It is applicable for medical studies in cardiovascular toxicity, reproductive toxicity, neurotoxicity, nephrotoxicity, immunotoxicity and carcinogenicity, where ultra-trace amounts of Hg in human urine have to be measured.

REFERENCES

1. A. Riaz, S. Khan, M. T. Shah, G. Li, N. Gul, I., *Environ. Technol. Innov.*, **5**, 22 (2016).
2. B. M. W. Fong, T. S. Siu, J. S. K. Lee, S. Tam, *J. Anal. Toxicol.*, **31**, 281 (2007).

Panova et al.: – “Optimizing the determination of mercury in human urine by ICP-MS with a collision cell mode”

3. L. Perring, D. Andrey, *Analysis, At. Spectr.*, **22(5)**, 371 (2001).
4. Y. F. Li, C. Chen, B. Li, Q. Wang, J. Wang, Y. Gao, Y. Zhao, Z. Chai, *J. Anal. At. Spectrom.*, **22**, 925 (2007).
5. B. J. Ye, B. G. Kim, M. J. Jeon, S. Y. Kim, H. C. Kim, T. W. Jang, H. J. Chae, W. J. Cho, M. N. Ha, Y. S. Hong, *Ann. Occup. Env. Med.*,; **28**, 5 (2016).
6. K. H. Schaller, J. Angerer, D. Welter, H. Drexler, *Rev. Environ. Health*, **16**, 223 (2001).
7. <http://www.ciela.net/svobodna-zona-darjaven-vestnik/issue/5118/changed-repealed>.
8. R. Meister, Biological monitoring, in: Current occupational and environmental medicine. *Lange Medical books*, 655 (2004).
9. WHO, 2003, Elemental mercury and inorganic mercury compound: human health aspects, in: CICAD, vol 50. *World Health Organization, WHO, Geneva* (2003)

ОПТИМИЗИРАНЕ ОПРЕДЕЛЯНЕТО НА ЖИВАК В ЧОВЕШКА УРИНА ЧРЕЗ ICP-MS В РЕЖИМ С КОЛИЗИОННА КЛЕТКА

М. Панова¹, В. Кметов², Д. Давчева^{1,3}, Т. Томова^{1,4}, Д. Томов¹

¹Технологичен център за спешна медицина – Пловдив, e-mail: panova22@abv.bg

²Катедра аналитична химия и компютърна химия,
Пловдивски университет "Паусий Хилендарски"

³Катедра по клинична лаборатория, Медицински университет, Пловдив

⁴Катедра химически науки, Медицински университет, Пловдив

Постъпила на 13 ноември 2016 г.; приета на 15 декември 2016 г.

(Резюме)

Оценена е приложимостта на ICP-MS (Thermo Scientific ICAP Qc) и възможните интерференции от волфрамов оксид при количествено определяне на Hg в човешка урина. Масспектрометърът е оборудван с колизионна клетка с газ хелий, работеща в режим KED (Kinetic Energy Discrimination). Този режим се използва широко за подтискане на полиатомни пречения, които са присъщи на ICP-MS. Недостатък на режима KED е влошаването на чувствителността и намаляването на съотношението сигнал/шум, особено за по-ниския масов диапазон. По тази причина в случаите, изискващи ниски граници на откриване, за предпочитане е режим STD (клетката не е под налягане), вместо KED.

Настоящата работа показва, че след оптимизиране на условията за определяне на Hg в режим KED, отношението сигнал/ шум може да се подобри до два пъти, в сравнение с режим STD. Вместо намаляване на чувствителността, сигналите за всички измерени изотопи на Hg, са по-високи и с по-добра повторемост използване на KED режим. Отношенията на регистрираните сигнали на изотопите на Hg бяха сравнени с табличните стойности на тяхното природно разпространение, при което се установи много добро съвпадение, което е доказателство за липсата на спектрални пречения върху сигналите на Hg. Чрез оптимизирания метод са постигнати инструментални граници на откриване от 2 ng/L (за ²⁰²Hg). Отличен аналитичен добив (в границите от 99 до 101 %) е постигнат спрямо сертифицираната стойност на референтен материал урина. ICP-MS анализът на дотирани с 5 µg/L Hg и разредени с фактор 20 проби урина показва аналитичен добив в интервала от 90 – 110 %.

Ключови думи: ICP-MS, определяне на живак, Hg, колизионна клетка, урина

Antioxidant activity and nontoxicity of extracts from *Valeriana officinalis*,
Melissa officinalis, *Crataegus monogyna*, *Hypericum perforatum*,
Serratula coronata and combinations Antistress 1 and Antistress 2

M. Katsarova^{1*}, S. Dimitrova¹, L. Lukanov¹, F. Sadakov², P. Denev³, E. Plotnikov⁴, I. Kandilarov⁵,
I. Kostadinova⁵

¹Department of Chemistry and Biochemistry, Faculty of Pharmacy,
Medical University, 15A V. Aprilov Blvd, Plovdiv, Bulgaria

² Avicena Herb-Ltd, Plovdiv, Bulgaria

³Laboratory of Biologically Active Substances, Institute of Organic Chemistry with Centre of Phytochemistry,
Bulgarian Academy of Sciences, 139 Ruski Blvd., 4000 Plovdiv, Bulgaria

⁴Tomsk Polytechnic University, Lenin 30, Tomsk, Russia

⁵Department of Pharmacology and Clinical Pharmacology, Faculty of Medicine,
Medical University, 15A V. Aprilov Blvd, Plovdiv, Bulgaria

Received November 3, 2016; Revised December 21, 2016

In recent years, large number of preclinical and clinical studies support the hypothesis of a link between oxidative stress, anxiety and depression. In search of novel sources of antioxidants in the last years, medicinal plants traditionally used in folk medicine have been extensively studied for their antioxidant activity (AOA). The purpose of this study was to determine the antioxidant activity of the extracts of medicinal plants *Valeriana officinalis*, *Melissa officinalis*, *Crataegus monogyna*, *Hypericum perforatum*, *Serratula coronata* and their combinations Antistress 1 and Antistress 2, which used as food supplements are recommended for chronic fatigue, anxiety and stress. This was done through measuring the Oxygen Radical Absorbance Capacity (ORAC), Hydroxyl Radical Averting Capacity (HORAC) and via electrochemical method (EM). The most pronounced is AOA of the extracts from *M. officinalis* (ORAC, 6751.0±214.3 µmol TE/g, HORAC, 1887.8±51.0 µmol GAE/g and EM, 24.901±1.445 µmol/l.min) and *H. perforatum* (ORAC, 5950.5±328.4 µmol TE/g, HORAC, 2128.3±200.1 µmol GAE/g and EM, 23.605±1.334 µmol/l.min), which could be a result of the high concentration of rosemary acid in the first extract and of flavonoids in the second. They contribute to the greatest extent of the activity of Antistress 1 and Antistress 2. The conducted study for acute toxicity *in vivo* reported 100 percent survival of experimental animals, indicating that both individual and combined extracts are non toxic to the tested animals.

Key words: herb extracts, toxicity, antioxidant activity, ORAC, HORAC, voltammetry

INTRODUCTION

Oxidative stress represents a violation of pro- and antioxidant balance of the body, which is a result of either increased formation of reactive oxygen species (ROS) in the cell, which may damage lipids, proteins and DNA; or of a reduced activity of natural antioxidant system. There is plenty of evidence about the involvement of pro-oxidant agents such as peroxide radicals (ROO•), hydroxide radical (HO•), superoxide anion (O₂⁻) and singlet oxygen (¹O₂•) in the pathophysiology of aging, mutagenesis and many chronic degenerative diseases such as cancer, cardiovascular disease, Alzheimer's disease, Parkinson's disease and others [1]. The definition, which is given to antioxidant is generally "a compound which is opposed to oxidation or inhibits reactions caused by oxygen and peroxides" [2]. In biochemistry and

medicine antioxidants are enzymes or nonenzymatic substances that have the ability to dispose of ROS, or prevent their formation [3]. Phenolic compounds are a group of secondary metabolites, which include flavonoids (anthocyanins, flavones, catechins, etc), phenolic acids, stilbenes, tannins and others with antioxidant and chelating properties, and could act as reducing agents, hydrogen donors or singlet oxygen scavengers [4]. Epidemiological studies have shown that long-term intake of foods and herbal medicines rich in plant polyphenols, provides certain protection against neurological, cardiovascular disease, diabetes, osteoporosis, neurodegenerative diseases [5, 6, 7]. In the recent years, the depression is largely considered to be associated with the oxidative stress in the organism [8], which in turn leads to a demand for natural antioxidants to combat it. It is well known that the

* To whom all correspondence should be sent.
E-mail: kacarovam@abv.bg

extracts from *Valeriana officinalis*, *Melissa officinalis* and *Crataegus monogyna*, *Hypericum perforatum* have anxiolytic and sedative properties [9], *Serratula coronata* has anabolic and neuroprotective effects [10] and are successfully used in the traditional medicine for centuries. A better effect is sought by preparing combinations of these elements. One of the most famous figures of herbalism in Bulgaria in the last century is Peter Dimkov who has published three volumes of traditional herbal medicine he has collected over decades [11]. The dietary supplements Antistress 1 and Antistress 2 which are the objects of our research are based on one of these recipes. Therefore the purpose of this study is to determine the antioxidant activity of the extracts of medicinal plants *Valeriana officinalis*, *Melissa officinalis*, *Crataegus monogyna*, *Hypericum perforatum*, *Serratula coronata* and the combinations from them Antistress 1 and Antistress 2, as well as establishing their nontoxicity on experimental animals.

MATERIALS AND METHODS

Plant materials.

Individual herbs (*V. officinalis*, *M. officinalis*, *C. monogyna*, *H. perforatum* and *S. coronata*) were collected in the Rhodope Mountains, Bulgaria in July 2014. Dry extracts were prepared with extraction of individual herbs with 40% ethanol (v:v) according to the industrial technology of "Extractpharma" Ltd. Sofia, Bulgaria. Antistress1 is a combination of *V. officinalis*, *M. officinalis*, *C. monogyna* and *S. coronata* in proportion 4:3:3:1, and Antistress2 is compound of *V. officinalis*, *H. perforatum* and *S. coronata* in proportion 4.5:4.5:1. These combinations are registered as food supplements by the company "Avicena Herb" Ltd. Plovdiv, Bulgaria.

Animals.

In acute toxicity tests 90 male Wistar rats weighing 180-200 grams were used. The animals was housed under standard laboratory conditions: 12:12 dark-light cycle, 45% relative humidity, temperature $26.5 \pm 1^\circ\text{C}$ and free access to food and water. The experiments were approved by the Committee on Animal Ethics of the Bulgarian Agency for Food Safety permit №127 and decision of the ethical committee at MU Plovdiv protocol №3/21.04.2016.

Determination of Total Polyphenols.

The determination is performed by the method of Singleton and Rossi [12]. Determinations are performed on spectrophotometer Spekol 10 (Carl Zeiss, Germany).

Determination of Antioxidant Activity.

Oxygen Radical Absorbance Capacity (ORAC) method - The method developed by Ou et al., was used with some modifications [13]. This method measures the ability of an antioxidant to neutralize peroxid radicals. The method is based on the inhibition of the decline of fluorescence of fluorescein during its oxidation in the presence of an antioxidant. The thermal decomposition of 2,2'-azobis(2-amidinopropane) dihydrochloride (AAPH) is used as a peroxid radical generator. The results are expressed in μmol Trolox equivalents per gram of extract. Measurements are performed on FLUOstar OPTIMA fluorometer (BMG LABTECH, Offenburg, Germany). The excitation wavelength of 485 nm and emission wavelength of 520 nm were used.

Hydroxyl Radical Averting Capacity (HORAC) method - The method was developed by Ou et al. [14], and measures the ability of an antioxidant to form complexes in conditions of Fenton reaction, caused by the interaction between Co (II) and H_2O_2 . The results are expressed in μmol gallic acid equivalents per gram of extract. Measurements are performed on FLUOstar OPTIMA fluorometer (BMG LABTECH, Offenburg, Germany). The excitation wavelength of 485 nm and emission wavelength of 520 nm were used.

Electrochemical Method for Determination of Antioxidant Activity. The electrochemical method was used to determine the antioxidant activity [15]. The experiment's methodology consists in taking voltamperogram of cathodic electroreduction of oxygen using the "Analyst AOA" (RU.C.31.113.A N28715), connected to a PC. The antioxidant activity of the tested samples was calculated according to kinetic criterion K (in micromoles per litre·minute) indicating the quantity of the reactive oxygen species in time.

Design of Experiments to Study the Acute Toxicity of Plant Extracts. The experimental animals (90 in total) were divided into 15 groups of 6 animals. The animals were treated orally with the extracts once with a dose of 10g / kg b. w. by using a probe. The survival of the animals 24 hours after administration of the extracts is recorded.

RESULTS AND DISCUSSION

The results of the AOA of the medicinal plants we tested, determined by ORAC method are specified in Table 1 (column 2).

According to this method, the most pronounced is AOA of the extracts from *M. officinalis* and *H. perforatum*, which could be attributed to the high content of rosemary acid (55.6 ± 0.30 mg/g) in the

first extract and flavonoids respectively (62.36 ± 0.71 mg/g) in the second [16]. They contribute to the fullest extent to the activity of Antistress 1 and Antistress 2 given their share in them. The explanation for the low activity of extracts from *V. officinalis* and *S. coronata* is probably the lesser content of polyphenolic compounds on account of their characteristic terpenes and ecdysteroids.

The ORAC method is widely used by a number of teams to analyze the AOA in dry plants [17] or foods and spices [18]. Wojcikowski et al. used the ORAC method to investigate the antioxidant activity of 55 medicinal plants after sequential extraction with three solvent as a result of which they reported higher activity of the herbal extracts [19]. Kratchanova et al. performed a similar study of 25 medicinal plants as compared AOA of water and acetone extract of the dry plants [20]. They recorded higher activity of acetone extracts of *C. monogyna*, *M. officinalis* and *H. perforatum* (2163 , 1121 and 1141 $\mu\text{mol TE/g}$) compared to water extracts (364 , 996 and 629 $\mu\text{mol TE/g}$). The activities we recorded for the same plants are much higher, as they are calculated per gram of dry extract.

The flavonoids' ability to form complexes, which allows them to manifest themselves as AO was demonstrated by HORAC method, but in the scientific literature there is scarcely any information on its use. Only in recent years it was established as a criterion for determining the AOA together with ORAC method. Denev et al. used it for analysis of AOA of six herbal extracts [21] and Wasek et al. used it for twenty-seven food supplements [22]. The teams used both methods to more fully characterize the antioxidant properties of

the respective objects while determine the polyphenol content. Like them, our team used HORAC method of determining the AOA of extracts from *V.officinalis*, *C. Monogyna*, *S. Coronata*, *M. Officinalis*, *H. perforatum* and the combinations Antistress 1 and Antistress 2. The results are presented in table 1 (column 3).

The most pronounced AOA is the one of the extract of *H. Perforatum*, which is largely due to four major flavonoid - rutin, hyperozide, quercetin and apigenin with a total amount of 62.36 ± 0.71 mg/g [16]. The high activity of the Antistress 2 respectively is due to the fact that *H. Perforatum* is 4.5/10 thereof. *M. officinalis* extract also has high activity, though flavonoids were 0.9 mg/g, but dominated phenolic acids (57.1 mg/g), represented primarily by rosemary acid, then by caffeic, ferulic and p-coumaric ones [16].

In the literature there is data about the relationship between AOA and content of polyphenol compounds in herbs. Some authors report good linear relationship between these two parameters [20, 23] while others do not observe such [24]. In our experiments, good correlations were found between the total amount of polyphenols in the extracts (table1, column 4) and their ORAC ($r^2 = 0.9042$) and HORAC ($r^2 = 0.9293$) values, represented on Figure 1.

Our research is the first to make comparative assessment of ORAC and HORAC AOA of the abovementioned plants, and combined extracts Antistress 1 and Antistress 2. Determination of the antioxidant activity of each of the extracts gives better idea about their ability to act independently as antioxidants, as well as their contribution to the activity of the combined extracts.

Table 1. ORAC and HORAC antioxidant activity and polyphenol content of extracts from *V.officinalis*, *C. Monogyna*, *S. Coronata*, *M. Officinalis*, *H. perforatum* and their combinations Antistress 1 and Antistress 2

Extracts	ORAC, $\mu\text{mol TE/g}$	HORAC, $\mu\text{mol GAE/g}$	Polyphenols, mg/g
<i>M. officinalis</i>	6751.0 ± 214.3	1887.8 ± 51.0	238.96 ± 4.8
<i>H. perforatum</i>	5950.5 ± 328.4	2128.3 ± 200.1	222.29 ± 6.4
<i>C. monogyna</i>	3917.3 ± 227.8	1052.1 ± 32.5	113.04 ± 1.9
Antistress 2	3774.7 ± 99.3	1132.4 ± 44.8	132.36 ± 2.4
Antistress 1	3746.2 ± 180.1	861.7 ± 25.2	128.57 ± 2.4
<i>S. coronata</i>	1142.7 ± 25.5	575.2 ± 18.8	95.24 ± 0.3
<i>V. officinalis</i>	820.5 ± 21.9	381.6 ± 14.0	43.36 ± 1.3

Results are presented as mean \pm S.D.

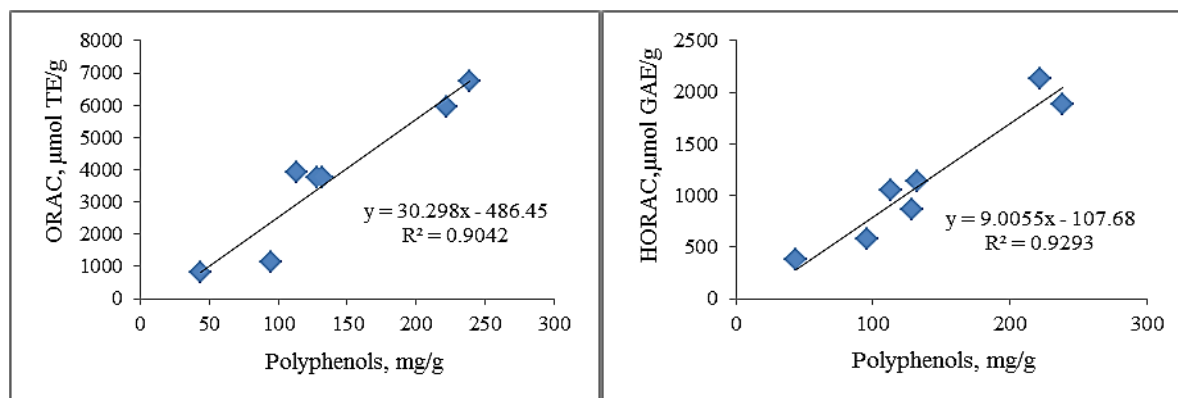


Figure 1. Correlation between the amount of polyphenols and AOA of the surveyed extracts determined by ORAC and HORAC methods

Table 2. Antioxidant activity of the extract from *V.officinalis*, *C. Monogyna*, *S. Coronata*, *M. Officinalis*, *H. perforatum* and the combinations Antistress 1 and Antistress 2, as measured by electrochemical method

Extracts	K, µmol/l.min±SD	AOA
Antistress 2	28.795±1.125	3.551
Antistress 1	27.136±1.874	3.346
<i>M. officinalis</i>	24.901±1.445	3.071
<i>H. perforatum</i>	23.605±1.334	2.911
<i>V. officinalis</i>	20.751±1.521	2.559
<i>C.monogyna</i>	17.878±0.832	2.204
<i>S. coronata</i>	15.643±0.761	1.929
Trolox	8.109±0.010	1.000

To more complete characterization of the tested extracts' AOA, an electrochemical method was used as well. The kinetic criterion values for each of the samples and the AOA calculated relative to that of Trolox are given in Table 2.

While AOA determined by ORAC and HORAC correlates directly proportional to the content of polyphenols, the activity determined by electrochemical method does not follow this correlation. From the literature it is known that the AO may act by three mechanisms: by attachment of the radical to a conjugated system of double bonds, giving hydrogen and participating in reactions with a transmission electron [25]. The used electrochemical method is applicable to AO which exhibit antioxidant activity by any of the three mechanisms. Therefore AOA of not only phenol type compounds is measured by this method. The combined extracts Antistress 1 and Antistress 2 show the most prominent AOA. This is probably due to the synergistic effect among their components - compounds of phenolic type, terpene derivatives (valerenic acid, bornyl acetate), phytosteroids such as 20-hydroxyecdysone, anthracene derivatives (hypericin) [16].

The extract from *V. officinalis* has the lowest activity based ORAC and HORAC methods but according electrochemical method it ranked fifth. This method determines the overall antioxidant potential of all types compounds in the sample. Yashin *et al.* create a database of AOA for different groups of foods and beverages using the described method [26]. According to the results obtained by Tewari *et al.*, mixed extracts combine in optimal proportion the components of different herbs, which voids the possibility of overdose in their individual administration [27].

Halliwell's longtime studies on free radicals, antioxidants and their role in the body lead to the conclusion that the *in vitro* and *in vivo* experiments in this area should go hand in hand [1]. According to these studies, even if some AO exhibit very high AOA in *in vitro* models it is not certain that *in vivo* they will prove to be prooxidants. The review article by Tirzitis and Bartosz also treat this problem [28]. In line with this, our team conducted also an experiment for determining acute toxicity of the individual extracts and combinations thereof, which is the first of a series of pharmacological tests. 24 hours after oral administration of Antistress 1, Antistress 2 and the extracts included in their composition at a dose of 10 g/kg b.w. we observed 100 percent survival of experimental animals. In the open literature the doses in which the combinations and the extracts included in their composition are used are typically in the range of 100 mg/kg b.w. to 500 mg/kg b.w. [29]. Using such big dose in our experiment gives us reason to believe that the tested products are practically nontoxic.

CONCLUSIONS

High antioxidant activity of the extracts *in vitro* is quantifies by three methods – ORAC (820 - 6751 µmol TE/g), HORAC (381-2128 µmol GAE/g) and electrochemical (15.6 - 28.7 µmol/l.min). Good correlation was observed

between the total amount of polyphenols in plant extracts combinations Antistress 1 and Antistress 2 and their antioxidant activity determined by ORAC and HORAC methods. It was confirmed that by the electrochemical method antioxidant activity of the compounds not only of phenolic type is determined but also of fitosteroids, terpene and anthracene derivatives. The extracts of *Valeriana officinalis*, *Melissa officinalis*, *Crataegus monogyna*, *Hypericum perforatum* and *Serratula coronata* and combinations Antistress 1 and Antistress 2 are nontoxic, which has been shown in *in vivo* testing for acute toxicity. This is a prerequisite for the continuation of experiments to prove the anxiolytic activity of combinations Antistress 1 and Antistress 2.

Acknowledgements: This work was supported by Research Project HO-10/2015, funded by Medical University of Plovdiv, Bulgaria.

REFERENCES

1. B. Halliwell, *Nutrition Reviews* **70**, 257-265 (2012).
2. <http://unabridged.merriam-webster.com> (2004).
3. <http://cancerweb.ncl.ac.uk/cgi-bin/omd?query=antioxidants>
4. K. B. Pandey and S. I. Rizvi, *Oxid. Med. Cell. Longev.*, **2**, 270 (2009)
5. I.C. Arts and P.C. Hollman, *Am. J. Clin. Nutr.*, **81**, 317 (2005).
6. A. García-Lafuente, E. Guillamón, A. Villares, M. Rostagno and J. Martínez, *Inflamm. Res.*, **58**, 537 (2009).
7. J. Kim, Y. Tan, L. Xiao, Y. Sun and X. Qu, *Biomed.Res. Int.*, ID 920128 (2013).
8. T. Michel, D. Pülschen, *J. Thome, Curr. Pharm. Des.*, **18**, 5890 (2012).
9. A. Sharma, A. Cardoso-Taketa, G. García, M. Villarreal, *Botanics: Targets and Therapy*, **2**, 21 (2012).
10. The Rules of Good Laboratory 9, Moscow, 2010.
11. P. Dimkov, *Handbook on Natural Healing and Living*, Fakel Publishing House, Sofia, 1939.
12. V. Singleton, J. Rossi, *Am. J. Enol. Vitic.*, **16**, 144 (1965).
13. B. Ou, M. Hampsh-Woodill, R. Prior, *J. Agric. Food Chem.*, **49**, 4619 (2001).
14. B. Ou, M. Hampsh-Woodill, J. Flanagan, E. Deemer, R. Prior, D. Huang, *J. Agric. Food Chem.*, **50**, 2772 (2002).
15. E. Korotkova, Y. Karbainov and A. Shevchuk, *J. Electroanal. Chem.*, **518**, 56. (2002).
16. M. Katsarova, S. Dimitrova, L. Lukanov, F. Sadakov, *C. R. Acad. Bulg. Sci.*, in press.
17. W. Zheng, Y. Wang, *Food Chem.*, **49**, 5165 (2001).
18. P. Ninfali, G. Mea, S. Giorgini, M. Rocchi, M. Bacchiocca, *Br. J. Nutr.*, **93**, 257 (2005).
19. K. Wojcikowski, L. Stevenson, D. Leach, H. Wohlmuth, G. Gobe, *J. Alt. Compl. Med.*, **13**, 103 (2007).
20. M. Kratchanova, P. Denev, M. Ciz, A. Lojek and A. Mihailov. *Acta Biochim. Pol.*, **57**, 229 (2010).
21. P. Denev, M. Kratchanova, M. Ciz, A. Lojek, O. Vasicek, D. Blazheva, P. Nedelcheva, L. Vojtek, P. Hyrs, *Acta Biochim. Pol.*, **61**, 3597 (2014).
22. M. Wasek, J. Giebułtowicz, M. Sochacka, K. Zawada, W. Modzelewska, L. Krześniak, P. Wroczyński, *Acta Pol. Pharm. - Drug Research*, **72**, 877 (2015).
23. V. Katalinic, M. Milos, T. Kulisic, M. Jukic, *Food Chem.*, **94**, 550 (2006).
24. P. Maisuthisakul, M. Suttajit, R. Pongsawatmanit, *Food Chem.*, **100**, 1409 (2007).
25. N. Polyakov, A. Kruppa, T. Leshina, T. Konovalova and L. Kispert, *Biol. Med.*, **31**, 43 (2001).
26. Y. Yashin, B. Nemzer, V. Ryzhnev, A. Yashin, N. Chernousova and P. Fedina, *Molecules*, **15**, 7450 (2010).
27. I. Tewari, L. Sharma, G. Girdhari Lal, *IAJPR*, **4**, (2014).
28. G. Tirzitis and G. Bartosz, *Acta Biochim. Pol.*, Review, **57**, 139 (2010).
29. M. Tortarolo, R. Braun, G. Hübner, H. Maurer, *Archives of Toxicology*, **51**, 37 (1982).

АНТИОКСИДАНТНА АКТИВНОСТ И НЕТОКСИЧНОСТ НА ЕКСТРАКТИ ОТ *Valeriana officinalis*, *Melissa officinalis*, *Crataegus monogyna*, *Hypericum perforatum*, *Serratula coronata* И КОМБИНАЦИИ АНТИСТРЕС 1 И АНТИСТРЕС 2

М. Кацарова^{1*}, С. Димитрова¹, Л. Луканов¹, Ф. Садъков², П. Денев³,
Е. Плотников⁴, И. Кандиларов⁵, И. Костадинова⁵

¹ Медицински университет-Пловдив, Фармацевтичен факултет,
катедра „Химия и биохимия“, бул. „В. Априлов“ 15А, Пловдив, e-mail: katarovam@abv.bg

² „Авицена Херб“ ООД, Пловдив

³ Българска академия на науките, Институт по органична химия с център по фитохимия,
бул. „Руски“ 139, Пловдив

⁴ Томски политехнически институт, бул. „Ленин“ 30, Томск, Русия

⁵ Медицински университет-Пловдив, Медицински факултет,
Катедра „Фармакология и клинична фармакология“, бул. „В. Априлов“ 15А, Пловдив

Постъпила на 3 ноември 2016 г.; приета на 21 декември 2016 г.

(РЕЗЮМЕ)

В последните години големият брой предклинични и клинични изследвания подкрепят хипотезата за връзката между оксидативния стрес, тревожността и депресивните състояния. В търсене на нови източници на антиоксиданти напоследък все повече се изследват лечебните растения, които от векове се използват в народната медицина. Целта на настоящото проучване е да се определи антиоксидантната активност на екстракти от лечебните растения *Valeriana officinalis*, *Melissa officinalis*, *Crataegus monogyna*, *Hypericum perforatum*, *Serratula coronata* и комбинациите от тях Антистрес 1 и Антистрес 2, които са хранителни добавки, препоръчвани при хронична умора, тревожност и стрес. Това е направено чрез измерване на Oxygen Radical Absorbance Capacity (ORAC), Hydroxyl Radical Averting Capacity (HORAC) и по електрохимичен метод. Най-изразена е антиоксидантната активност на екстрактите от *M. officinalis* (ORAC, 6751.0±214.3 μmol TE/g, HORAC, 1887.8±51.0 μmol GAE/g и 24.901±1.445 μmol/l.min) и *H. perforatum* (ORAC, 5950.5±328.4 μmol TE/g, HORAC, 2128.3±200.1 μmol GAE/g и 23.605±1.334 μmol/l.min), която вероятно е следствие от високата концентрация на розмаринова киселина в първия екстракт и съответно на флавоноиди във втория. Те допринасят в най-голяма степен за активността на Антистрес 1 и Антистрес 2. Проведено е *in vivo* изследване за остра токсичност като е отчетена 100% преживяемост на опитните животни, което доказва, че самостоятелните и комбиниранияте екстракти са нетоксични.

Ключови думи: растителни екстракти, токсичност, антиоксидантна активност, ORAC, HORAC, волтамперометрия

Co-Mn mixed oxide catalysts for purification of waste gases from *n*-hexane

I. D. Yordanova*, S. Zh. Todorova, H. G. Kolev, Z. P. Cherkezova-Zheleva

Institute of Catalysis, Bulgarian Academy of Sciences, Acad. G. Bonchev St., Bldg. 11, Sofia 1113, Bulgaria

Received November 11, 2016; Revised January 30, 2017

Single-component Co and Mn and bi-component Co-Mn oxide samples have been prepared by precipitation, characterized by different methods (XRD, TPR and XPS) and tested in the reaction of complete *n*-hexane oxidation. The highest activity demonstrated the catalyst, with Co/Mn=1 molar ratio (CoMn1). The coexisting of pairs Co²⁺-Co³⁺ and Mn³⁺-Mn⁴⁺ with the predominance of Co³⁺ and Mn⁴⁺ species, high specific surface area and low degree of crystallinity are responsible for highest catalytic activity of the CoMn1 sample.

Keywords: mixed oxide, cobalt, manganese, total oxidation, *n*-hexane

INTRODUCTION

Air pollution has been one of the European Union's main environmental policy concerns since the late 1970s [1]. In 2013, the EU proposed a Clean Air Policy Package to reduce future emissions of air pollutants until 2030. The main air pollutants are particulate matter (PM), SO₂, NH₃, NO_x, volatile organic compounds (VOCs), CH₄. Abatement of volatile organic compounds (VOCs) and carbon monoxide (CO) in the waste gases is an important task in regard to environmental protection and odour control. Such gaseous emissions are discharged by many branches of industry, such as chemistry and petrochemistry, oil and natural gas processing, energy production, machinery, polygraphy, food processing and many others. VOCs are involved in the formation of ground level ozone, ozone depletion and some of them can act as greenhouse gases [2, 3]. There are many techniques for VOCs removal, such as adsorption, absorption, biofiltration, thermal, and catalytic combustion [4, 5]. The choice of the technique to be used depends on the VOC nature, its concentration and waste gas flow rate. The catalytic combustion is a promising abatement technique for VOCs removal especially in cases when the organics cannot be recycled or it is present in low concentrations [6]. Since the catalytic combustion takes place at temperatures much lower than those required for thermal incineration, it results in lower costs and low NO_x formation. Moreover, the efficiency of VOCs catalytic combustion is higher than that of thermal incineration. There are a great number of successful commercial catalysts developed for CO and VOC total oxidation. It is well known that the catalysts for CO oxidation and VOC combustion can be classified into three categories: supported noble metals, metal oxides or supported metal oxides, mixtures of noble metal and metal

oxides. The major part of the commercial catalysts for these processes belongs to the first category, because the reaction can start at temperature as low as the room temperature. Nevertheless, there still exists a demand for development of new optimized catalysts with increased efficiency for mass and heat transfer [7, 8] and which do not contain any noble metals. The high cost of precious metals, their limited availability and sensitivity to higher temperatures and poisons has motivated the search for substitute catalysts. Among all the studied metal oxides the most active single metal oxides are those of Cu, Co, Mn and Ni [9]. Manganese and cobalt containing catalysts are less expensive and they demonstrate high activity in CO and VOCs oxidation [10, 11]. Despite the large number of studies on single component manganese oxides [12, 13] and cobalt oxide [14-17] based catalysts, there are only a few works focused on the catalytic properties of combinations of these two oxides in the combustion reaction of VOCs [18]. According to literature data the addition of manganese to the cobalt catalysts results in decrease of the Co₃O₄ particles size [19] and it also facilitates their reduction. In our previous studies [20, 21] we established that the combination between cobalt and manganese oxides changed significantly the activity in the *n*-hexane and methane oxidation and this depended on the sequence of cobalt/ manganese introduction.

The current work is orientated towards investigation of structural and catalytic properties of a series of cobalt-manganese mixed oxides. The test reaction is *n*-hexane combustion. *n*-Hexane is one of the major air pollutants being component of many emissions and effluents related to industry.

* To whom all correspondence should be sent.
E-mail: ani4ka_pk87@abv.bg

EXPERIMENTAL

Catalyst preparation

The catalyst samples were prepared using a co-precipitation procedure. Aqueous solutions of $\text{Co}(\text{NO}_3)_2 \cdot 6\text{H}_2\text{O}$ and $\text{Mn}(\text{NO}_3)_2 \cdot 4\text{H}_2\text{O}$ with different molar ratios were premixed. The single component cobalt and manganese samples were also prepared. Aqueous solution of Na_2CO_3 (1 mol/l) was added slowly to the mixed nitrate solution at continuous stirring and maintaining the temperature of 70 °C. The final pH value was 11. The precipitate was filtered and then washed several times with distilled water until reaching pH = 7. The product was then dried at 60 °C and subsequently calcined at 500 °C for 3 hours. The samples were denoted as Co, Mn, CoMn1.5, CoMn1, and CoMn3 where the number represents the Mn/Co bulk ratio.

Catalysis characterization

The specific surface area of the catalyst samples was determined by low temperature adsorption of nitrogen according to the BET method using a Nova 1200 (Quantachrome) apparatus. Prior to each measurement, the samples were degassed for 3 hours at 300 °C.

X-ray diffraction (XRD) patterns were recorded on TUR M62 apparatus, HZG-4 goniometer with Bragg-Brentano geometry, $\text{CoK}\alpha$ radiation and Fe filter. XRD data processing was performed by using the X'Pert HighScore program.

Temperature programmed reduction (TPR) was carried out feeding a flow mixture of 10 % H_2 in Ar at 10 ml/min flow rate, temperature rate of 10 °C/min up to 700 °C.

The cobalt and manganese concentrations in the catalysts were determined by Atomic absorption spectroscopy (AAS) using Perkin Elmer 5000 spectrophotometer and Inductively coupled plasma - Atomic emission spectroscopy (ICP-AES) performed by High Dispersion ICP-OES Prodigy spectrometer. The results are an average value of three parallel measurements. The measurement accuracy is 0.02% (relative standard deviation).

X-ray photoelectron spectroscopy (XPS) measurements were carried out on the ESCALAB MkII (VG Scientific) electron spectrometer at a base pressure in the analysis chamber of 5×10^{-10} mbar using twin anode $\text{MgK}\alpha/\text{AlK}\alpha$ X-ray source with excitation energies of 1253.6 and 1486.6 eV, respectively. The spectra were recorded at the total instrumental resolution (as it was measured at the FWHM of $\text{Ag}3d_{5/2}$ photoelectron line) of 1.06 and 1.18 eV for $\text{MgK}\alpha$ and $\text{AlK}\alpha$ excitation sources, respectively. The energy scale has been calibrated by normalizing the C1s line of adsorbed adventitious hydrocarbons to 285.0 eV. The processing of the

measured spectra includes a subtraction of X-ray satellites and Shirley's type of background [22]. The peak positions and areas are evaluated by a symmetrical Gaussian-Lorentzian curve fitting. The relative concentrations of the different chemical species are determined based on normalization of the peak areas to their photoionization cross-sections, calculated by Scofield [23].

Catalytic measurements

n-Hexane oxidation was carried out in a continuous flow type of glass reactor at atmospheric pressure with catalyst bed volume of about 1 cm³ (fraction 0.31–0.63 mm). External mass transfer limitations have been minimized by working at high gaseous hourly space velocity GHSV (14400 h⁻¹). The reaction temperature was measured by internal thermocouple. The concentration of *n*-hexane in air at the reactor inlet was fixed at 830 ppm. The reaction products were analysed by a HP5890 gas chromatograph equipped with thermal conductivity detector and flame ionization detector. "Aalborg" mass flow controllers were used to maintain stable gas flow rates. The gas chromatograph was calibrated based on known concentrations of *n*-hexane and the decrease in the respective peak areas was used as a measure of the conversion degree. The conversion degree was calculated as the ratio of converted to inlet quantity of hexane.

RESULTS AND DISCUSSION

The X-ray diffraction patterns of the calcined single- and bi- component samples are shown in Figure 1. The main phase in the single component Co catalyst is Co_3O_4 determined by the peaks at ($2\theta = 21.90, 36.77, 43.19, 44.95, 52.58, 65.69, 70.28, 77.49, \text{ and } 92.98$) (PDF 01-074-1657). The manganese sample (Mn) exhibited diffraction lines corresponding to Mn_2O_3 ($2\theta = 27.87, 38.34, 44.62, 65.66, 73.9$) (PDF = 01-078-0390), Mn_3O_4 ($2\theta = 21.01, 37.10, 44.67, 56.07$) (PDF = 00-016-0350) and MnO_2 ($2\theta = 33.20, 65.17$) (PDF 00-004-0591). The diffraction reflections appear at slightly smaller 2θ values in the Co-Mn mixed samples. This is direct proof for the incorporation of manganese in the lattice of Co_3O_4 . As it is known Co and Mn cations have similar ionic radii and can form stable mixed oxides members of solid-solution series [20]. The XRD reflections for CoMnO_3 ($2\theta = 28.4, 38.5, 63.8$) (PDF-00-012-0476) are visible in the spectrum of CoMn3 sample. The diffraction peaks for all bi-component samples are weak and relatively broad making difficult the phase identification. On the other hand this is an evidence for high dispersity of prepared mixed oxide materials.

Table 1 presents the results of samples characterization by N₂ adsorption, elemental analysis, and XPS.

Pure cobalt and manganese oxides have comparable surface areas while that of the bicomponent is higher. One of possible explanation is that the nano-size oxide formation is responsible for increasing in surface area. It can be seen from the table that by increasing the amount of manganese, the surface area gradually decreases.

The oxidation state of cobalt and manganese on the surface is determined by XPS analysis. Figure 2 shows the spectra in the regions of Co2p_{1/2} and Mn2p. The presence of Co²⁺ ions in the cobalt-containing samples is confirmed by the presence of a peak with binding energy 796.9 eV, together with the relatively intensive 3d→4s "shake-up" satellite with binding energy 803-804 eV (Figure 2A). The presence of Co²⁺ and Co³⁺ ions is observed in all Co-contained samples (see Table 1).

Figure 2B shows the XP spectra of manganese-containing samples in Mn2p region. Registered

binding energies in the intervals 641.5 - 642.5 eV and 642.5 - 643.5 eV are characteristic of Mn³⁺ and Mn⁴⁺ ions, respectively.

From the spectra (Figure 2B) it is determined that the concentration of Mn⁴⁺-containing species is higher than that of Mn³⁺ species.

As it can be seen from Table 1, the Co/Mn ratio in the bulk is higher than that on the surface demonstrating enrichment in manganese on the surface in the mixed samples with increasing its concentration in the sample. From the analysis of XPS data we found, also, that with increasing of the amount of manganese the relative abundance of Co³⁺ ions sharply decreases. According the authors in [9], the doping of manganese into the spinel structure of cobalt oxide increased crystal defects, which probably caused the increase of the amount of octahedrally coordinated divalent cobalt cations that are responsible for catalytic activity. As can be seen from the Table 1, Mn³⁺ and Mn⁴⁺ present simultaneously on the surface.

Table 1. Sample characterization

Sample	S _{BET} , [m ² /g]	Atomic ratio					
		Co/Mn in the bulk (elemental analysis)	Co/Mn at the surface (XPS)	Co ²⁺ [at.%]	Co ³⁺ [at.%]	Mn ³⁺ [at.%]	Mn ⁴⁺ [at.%]
Co	26	-	-	4	27	-	-
Mn	25	-	-	-	-	12	21
CoMn1	67	1.25	0.94	6	10	4	13
CoMn1.5	51	0.6	0.50	6	5	5	19
CoMn3	36	0.3	0.10	0.9	1.1	7	18

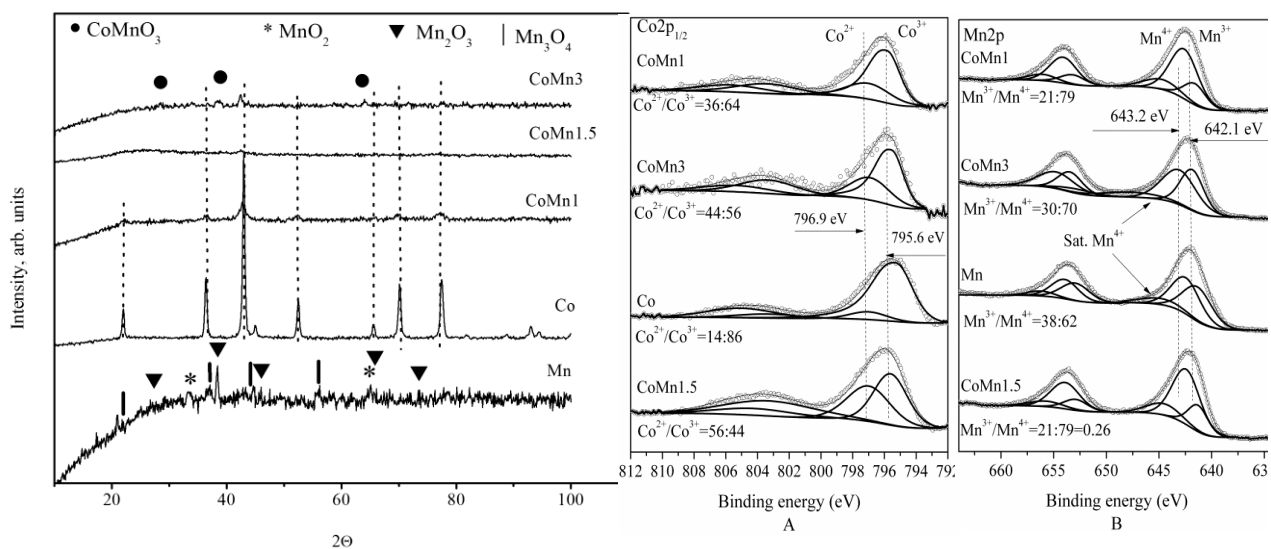


Fig. 1. XRD pattern of all studied samples

Fig. 2. XP spectra of studied samples: A) Co2p_{1/2} region; B) Mn2p region.

TPR profiles of all samples are shown in Figure 3. The monometallic Co sample exhibits two reduction peaks at around 314 °C and 382 °C. These two peaks fit well in the reduction interval of bulk Co_3O_4 powder or supported relatively large Co_3O_4 particles [24]. The peak at 314 °C is attributed to the reduction of Co_3O_4 into CoO and that at 382 °C originates from the further reduction of CoO into Co^0 . Hydrogen consumption at 302 and 433 °C is registered with the single-component manganese sample. These two reduction peaks are ascribed to the subsequent reduction of Mn_2O_3 into Mn_3O_4 and further into MnO [25].

Several overlapping peaks are appeared in the region 220–420 °C of bi-component samples. As is visible from TPR data of mono-component samples, cobalt and manganese oxide are reduced within the same temperature interval and it is difficult to make a correct assignment of the reduction peaks to the respective oxide phases. According to the authors of ref. [26] and [27] hydrogen consumption at 280 and 360 °C is due to the reduction of highly dispersed manganese oxide phase, probably in the form of 2D epitaxial layers. As it is seen from XRD (Fig. 1) the reflection patterns for Co-Mn catalyst are very broad and low intensive indicating finely dispersed particles. The low reduction temperatures for bi-component samples are with accordance with particle size effect — the smaller the particle size, the lower is the registered reduction temperature. We suggest that the reduction peaks in the temperature interval 220–420 °C come from the reduction of finely divided MnO_x and Co_3O_4 particles. The appearance of a broad peak of hydrogen consumption above 450 °C for Co-Mn oxide

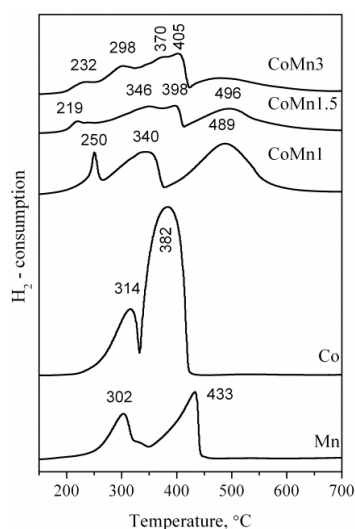


Fig. 3. TPR profiles of single- (Co, Mn) and bi-component (Co-Mn) oxides.

catalysts prepared by co-precipitation was already mentioned in [20]. It could be associated with reduction of a Co-Mn mixed oxide. Das *et al.* [28] reported the reduction of pure $(\text{Co}_{1-x}\text{Mn}_x)_3\text{O}_4$ phase at a temperature slightly above 600 °C. Due to the presence of many different phases, which are being reduced within the same temperature interval, the quantitative analysis of the TPR profiles of bi-component catalysts cannot be accurate.

The temperature dependences of the complete *n*-hexane oxidation over the mono- and bi-component catalysts are shown in Figure 4. H_2O and CO_2 were the only detectable reaction products of *n*-hexane oxidation on all investigated samples. The order of activities is as follow: $\text{CoMn1} > \text{Co} > \text{CoMn3} > \text{Mn} > \text{CoMn1.5}$.

It is well known that oxide catalysts operate in the oxidation reactions through a Mars-van Krevelen mechanism [14, 20]. According to this mechanism the VOCs are oxidized by the solid. The oxygen species introduced in the organic molecule come from the lattice. In this way the catalytic behaviour can be correlated to the lattice oxygen mobility. The lattice oxygen mobility is associated with the catalyst reducibility [29]. According to the TPR data, the reduction behavior of all bi-component samples is similar. Therefore in order to explain the difference in the catalytic activity it is necessary to search for another reason. One possible explanation is a very low crystallinity of the cobalt and manganese oxides, as it is visible from XRD data and as a consequence an increase in the concentration of the accessible active sites in these samples. The additional factor could be the simultaneous presence of Mn^{4+} – Mn^{3+} couple.

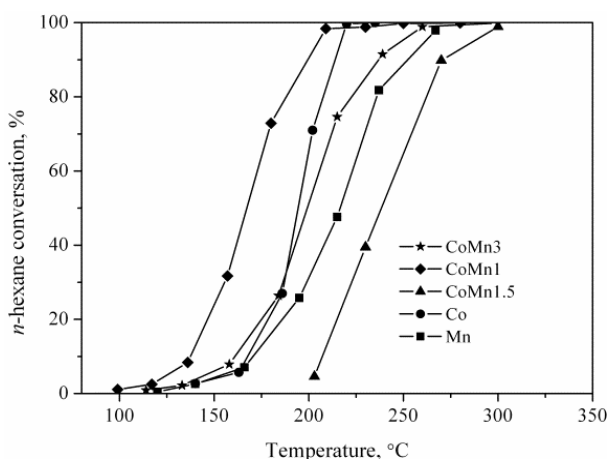


Fig. 4. Catalytic activity testing of investigated materials

It was established that catalytic activity increases when the pair Mn^{4+} - Mn^{3+} exists in the structure of the manganese oxide [20]. The other reasons for a considerable improvement in activity of CoMn1 sample could be the highest specific surface area and the simultaneous presence of Co^{2+} and Co^{3+} ions on the surface. It is well accepted that Co^{3+} is the catalytic active species in the oxidation reactions, but the presence of Co^{2+} can additionally impact on the activity, because Co^{2+} located at a relatively opened coordination position can be a centre for oxygen adsorption and formation of active oxygen species, which are a prerequisite for catalytic oxidation [6]. Obviously there are optimal ratios of Co^{2+}/Co^{3+} and Mn^{3+}/Mn^{4+} in the bi-component catalysts, which control the catalytic activity. Although the sample CoMn3 has a lowest surface area in comparison with the other bi-component oxides and manganese is the predominant component of the surface (see XPS data), it demonstrates relatively high catalytic activity. One possible explanation is the phase composition. From XRD data (Fig. 1) ilmenite $CoMnO_3$ structure was identified in this sample. It has been shown that the ilmenite-type catalysts were significantly more active for the complete catalytic oxidation of hydrocarbons [30].

CONCLUSION

The co-precipitation method used for the synthesis of bulk Co-Mn mixed oxide is suitable for obtaining catalysts with good catalytic performance in n-hexane oxidation reaction. All studied bi-component samples consisted of finely dispersed and easily reducible oxides. A significant improvement of the activity was observed over CoMn1 catalysts with a Co/Mn molar ratio of 1:1. The doping of manganese into the spinel structure of cobalt oxide decreases the crystallinity of the cobalt oxide thus increasing crystal defects, which probably causes an increase of the amount of divalent cobalt cations in a relatively opened coordination position. The coexisting of pairs Co^{2+} - Co^{3+} and Mn^{3+} - Mn^{4+} with the predominance of Co^{3+} and Mn^{4+} species and the highest specific surface area are responsible for the highest catalytic activity of the CoMn1 sample.

Acknowledgements: Program for career development of young scientists, BAS. The financial support for this work under contract DFNP-187 A-1 of Bulgarian Academy of Sciences is gratefully acknowledged. We are very thankful to Assoc. Prof. G. Kadinov for discussions.

REFERENCES

1. http://ec.europa.eu/environment/index_en.htm.

2. B. Solsona, T. Davies, T. Garcia, I. Vázquez, A. Dejoz, S. Taylor, *Appl. Catal. B.*, **84**, 176 (2008).
3. K. Everaert, J. Baeyens, *J. Hazard. Mater.*, **109**, 113 (2004).
4. J.J. Spivey, *Catal. Today*, **100**, 171 (2005).
5. S. Santos, K. Jones, R. Abdul, J. Boswell, J. Paca, *Biochem. Eng. J.*, **37**, 261 (2007).
6. A. Kołodziej, J. Łojewska, *Catal. Today*, **105**, 378 (2005).
7. A. Cybulski, J. A. Moulijn, *Catal. Rev. - Sci. Eng.*, **36**, 179 (1994).
8. S. Roy, T. Bauer, M. Al-Dahhan, P. Lehner, T. Turek, *AIChE J.*, **50**, 2918 (2004).
9. J. Li, Xi Liang, S. Xu, J. Hao, *Appl. Catal. B: Environ.*, **90**, 307, (2009).
10. M. Baldi, E. Finocchio, F. Milella, G. Busca, *Appl. Catal. B: Environ.*, **16**, 43 (1998).
11. P.-O. Larsson, A. Andersson, L.R. Wallenberg, B. Svensson, *J. Catal.*, **163**, 279 (1996).
12. A. Gil, L.M. Gandi, S.A. Korili, *Appl. Catal. A: Gen.*, **274**, 229 (2004).
13. M. Baldi, E. Finocchio, F. Milella, G. Busca, *Appl. Catal. B: Environ.*, **16**, 43 (1998).
14. Y. Kalvachev, V. Kostov-Kytin, S. Todorova, K. Tenchev, G. Kadinov, *Appl. Catal. B: Environ.*, **66**, 192 (2006).
15. P. Papaefthimiou, T. Ioannides, X. Verykios, *Appl. Catal. B: Environ.*, **13**, 175 (1997).
16. J.C. Wu, Z. Lin, F. Tsai, J. Pan, *Catal. Today*, **63**, 419 (2000).
17. J.C.-S. Wu, Z. Lin, J. Pan, M. Rei, *Appl. Catal. A: Gen.*, **219**, 117 (2000).
18. F. Kovanda, T. Rojka, J. Dobesová, V. Machovic, P. Bezdecka, L. Obalová, K. Jiráťová, T. Grygar, *J. Solid State Chem.*, **179**, 812 (2006).
19. H.G. El-Shobaky, M.A. Shouman, A.A. Attia, *Colloid Surf. A.*, **274**, 62 (2006).
20. S. Todorova, H. Kolev, J.P. Holgado, G. Kadinov, Ch. Bonev, R. Pereñíguez, A. Caballero, *Appl. Catal. B: Environ.*, **94**, 46 (2010).
21. S. Todorova, I. Yordanova, A. Naydenov, H. Kolev, Z. Cherkhezova-Zhelev, K. Tenchev, B. Kunev, *Rev. Roum. Chim.*, **59** (3-4) 259 (2014).
22. D. Shirley, *Phys. Rev. B.*, **5**, 4709 (1972).
23. J. H. Scofield, *J. Electron Spectrosc. Relat. Phenom.*, **8**, 129 (1976).
24. D. Shanke, S. Vada, E. A. Hilmen, A. Hoff, *J. Catal.*, **156**, 85 (1995).
25. F. Kapteijn, L. Singoredjo, A. Andreini, J.A. Moulijn, *Appl. Catal. B.*, **3**, 173 (1994).
26. F. Arena, T. Torre, C. Raimondo, A. Parmaliana, *Phys Chem Chem Phys.*, **3**, 1911 (2001).
27. J. Trawczyński, B. Bielak, Wł. Miśta, *Appl. Catal. B: Environ.*, **55**, 277 (2005).
28. D. Das, G. Ravichandran, D.K. Chakrabarty, *Appl. Catal. A: Gen.*, **131**, 335 (1995).
29. J.J. Li, X.Y. Xu, Z. P. Hao, W. Zhao, *J. Porous Mater* **15** 163 (2008).
30. D. Mehandjiev, E. Zhecheva, G. Ivanov, R. Ioncheva, *Appl. Catal. A: Gen.*, **167** 277 (1998).

СО-Мn СМЕСЕНИ ОКСИДНИ КАТАЛИЗАТОРИ ЗА ПРЕЧИСТВАНЕ
НА ОТПАДЪЧНИ ГАЗОВЕ ОТ *n*-HEКСАН

И. Д. Йорданова*, С. Ж. Тодорова, Х. Г. Колев, З. П. Черкезова-Желева

*Институт по катализ, Българска академия на науките, ул. Акад. Г. Бончев, бл. 11,
1113 София, България*

Постъпила на 11 ноември 2016 г.; приета на 30 януари 2017 г.

(Резюме)

Чрез методът на съутаяване са получени едно- и двукомпонентни Со-Мn оксиди. Те са изследвани с различни физикохимични методи (XRD, TPR and XPS) и изпитани в реакцията на пълно окисление на *n*-хексан. Най-високата каталитична активност проявява катализатор с молно съотношение Со/Мn=1. Едновременното присъствие на двойките Со²⁺ - Со³⁺ и Мn³⁺ - Мn⁴⁺ с преобладаващи концентрации на Со³⁺ и Мn⁴⁺ йони, високата специфична повърхност, както и ниската степен на кристалност допринасят за най-висока каталитична активност на образец СоМn1.

Ключови думи: *пълно окисление на хексан, кобалт-манганови катализатори, рентгенов фазов анализ, рентгенова фотоелектронна спектроскопия.*

Application of aziridines for the synthesis of isoquinoline derivatives

M. Penkova*, S. Nikolova

Plovdiv University, Faculty of Chemistry, Department of Organic Chemistry,
24 Tzar Assen str., 4000 Plovdiv, Bulgaria

Received November 11, 2016; Revised December 13, 2016

Aziridines are attractive and versatile building blocks in organic synthesis and medicinal chemistry because they allow convenient access to useful nitrogen-containing biologically active compounds. Many aziridine-containing compounds demonstrate very useful pharmacological activity including anticancer, antibacterial, antimicrobial activity, etc. strongly indicating that the presence of the aziridine ring in natural as well as synthetic compounds is essential for such activities. Chiral aziridines have found widespread use in organic synthesis. This manuscript shows variety of methods for the synthesis and ring-opening of three-membered aziridines and their application for the synthesis of six-membered isoquinolines.

Keywords: aziridines, synthesis, biological activity, isoquinolines

BIOLOGICAL IMPORTANCE OF AZIRIDINES RING-SYSTEM

Small heterocyclic ring systems are of central importance in theoretical, synthetic organic, bioorganic, and medicinal chemistry, and in particular aziridines are very useful and interesting systems as they occur in a number of natural and biologically active substances [1-7]. Aziridines are highly valuable heterocyclic compounds and are widely used during the synthesis of numerous drugs and biologically active natural products (and their derivatives) [8–13]. Over 100 biologically active aziridine-containing compounds demonstrate confirmed pharmacological activity including

antitumor, antimicrobial, and antibacterial effects [14].

While the aziridine group is known as a useful reaction intermediate [15, 16], it is also an interesting structural fragment in bioactive compounds. The aziridine's proton accepting properties, its rigidity and its potential reactivity can all contribute to specific molecular interactions with proteins, and indeed several important natural products such as mitomycin C [17], porfiromycin [18], and carzinophilin A [19] contain the aziridine functionality. A number of saccharide derivatives containing the aziridine group have been made, mostly as intermediates [20], but also as glycosidase inhibitors [21].

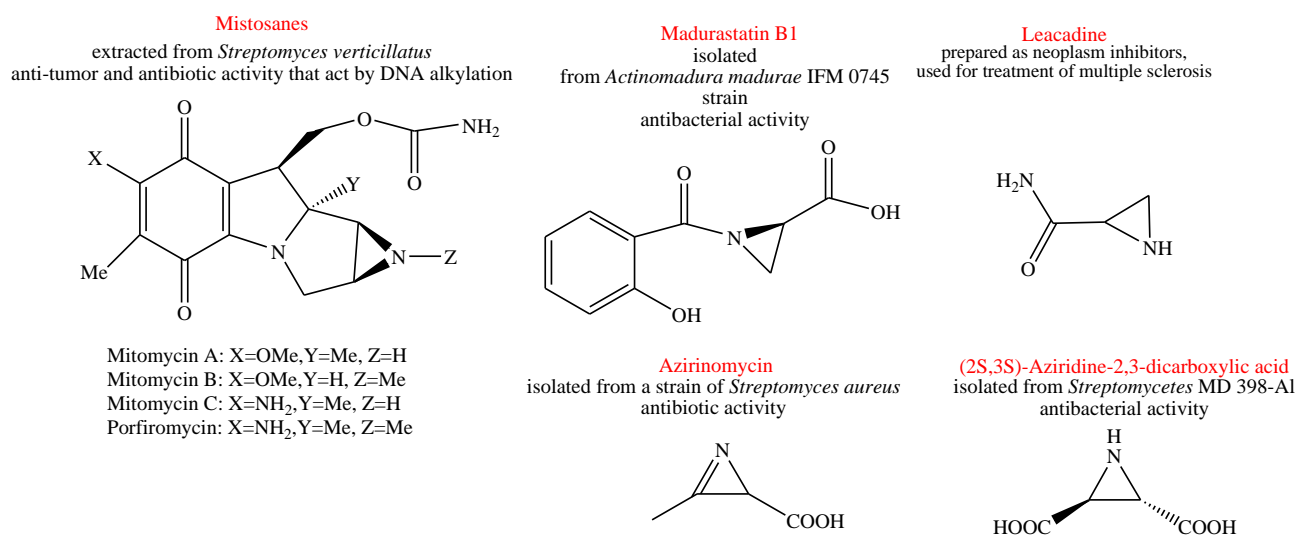


Fig. 1. Natural products containing an aziridine ring fragment.

* To whom all correspondence should be sent.
E-mail: mariya.p.penkova@gmail.com

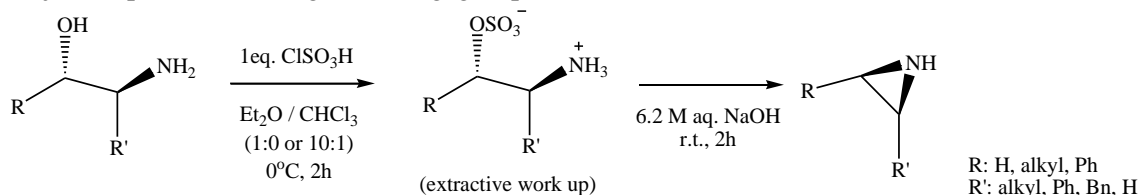
The toxicity of aziridine derivatives will depend on its own structure and activity whilst sharing the general characteristics of the aziridine group. As powerful alkylating agents, aziridines have an inherent *in vivo* potency [22, 23]. Mitomycins and porfiromycin, generally nonreactive in the natural oxidized state, behave as bifunctional ‘alkylating’ agents upon chemical or enzymatic reduction [24]. As an electrophile, substituted aziridines are subject to attack and ring-opening by endogenous nucleophiles such as nitrogenous bases in DNA base pairs, resulting in potential mutagenicity [22, 23]. Aziridine alkaloids also belong to a rare and somewhat neglected group of natural products which are known to play a seminal role in the secondary metabolism of some micro-organisms, plants and various marine organisms [25]. The aziridine-containing compounds have been of interest as both immuno-modulatory and anticancer agents since the late 1950s [26]. Polymerization products of ethylenimine, their polymerizable homologs, as well as substitution products were considered useful for disinfecting [27–29]. Aziridines are inherently strained making them attractive for study because they allow for convenient access to amines, amino alcohols, diamines, and other useful nitrogen-containing molecules. Chiral aziridines have found widespread use in organic synthesis. [30–33] The development of efficient and stereoselective methods for synthesis of aziridines is an inviting challenge in organic synthesis. General approaches to the asymmetric synthesis of aziridines through cyclization methods can be divided into two main categories: (A) nitrogen nucleophilic cyclization on the adjacent position bearing a leaving group and

(B) ring closure to three-membered ring via attack of a stabilized carbanion on the electrophilic nitrogen bearing a leaving group [34].

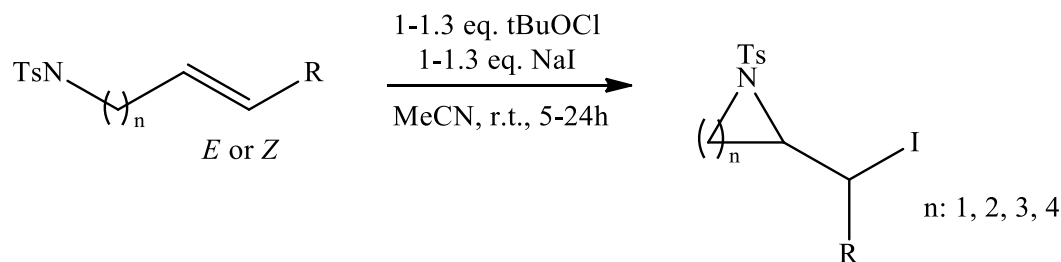
METHODS FOR AZIRIDINE SYNTHESIS

The synthesis of an aziridine derivative is most frequently accomplished in a two-step synthesis from a suitably substituted β -amino alcohol. Instead of classical and well-known Gabriel and Wenker reactions, a lot of reactions have been recently discovered. The De Kimpe Aziridine Synthesis allows the generation of various aziridines by the reaction of α -chloroimines with nucleophiles such as hydride, cyanide, or Grignard reagents. Denolf *et al.* [35] reported the Asymmetric Synthesis of Aziridines by Reduction of *N*-tert-Butanesulfinyl α -Chloro Imines. Amino alcohols were converted into their hydrogen sulfates with chlorosulfonic acid. Li *et al.* used improved, mild variation of the typical Wenker synthesis for the synthesis of aziridines [36] (.Scheme 1.)

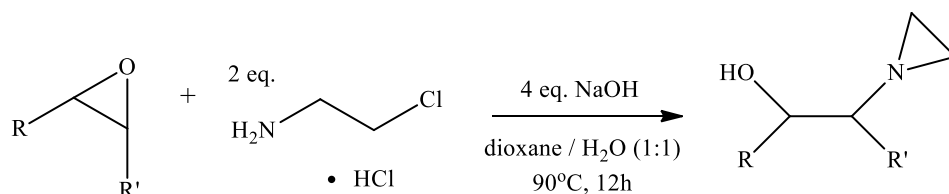
Bieber presented two alternative and complementary one-pot procedures for the direct transformation of 2-amino alcohols to *N*-tosyl aziridines [37]. The authors found that less hindered aziridines can be obtained in high yields by tosylation and *in situ* cyclization affected by potassium hydroxide in water/dichloromethane. Minakata *et al.* [38] used *tert*-butyl hypoiodite as a mild and powerful reagent for the cyclization of *N*-alkenylamides leading to various *N*-heterocycles. *N*-alkenylsulfonamides gave three- to six-membered saturated *N*-heterocycles in good yields, whereas alkenylbenzamide derivatives afforded *N*-, *O*- or *N*-, *S*-heterocycles (.Scheme 2.).



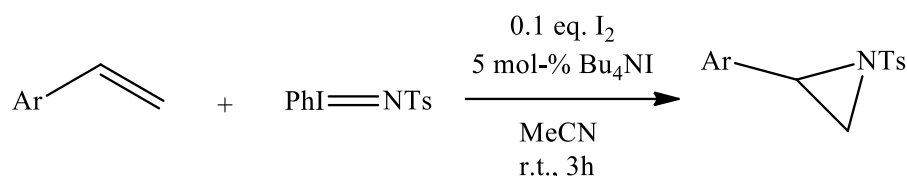
Scheme 1



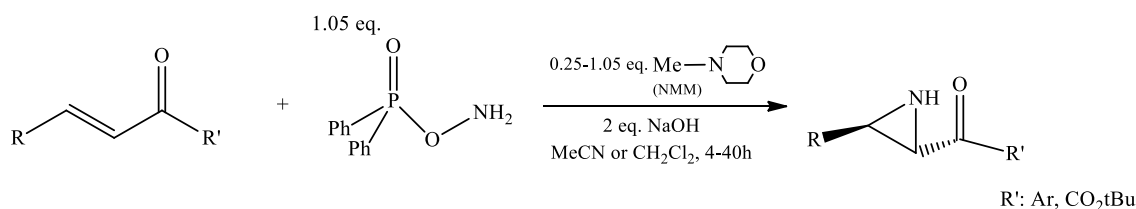
Scheme 2



Scheme 3



Scheme 4



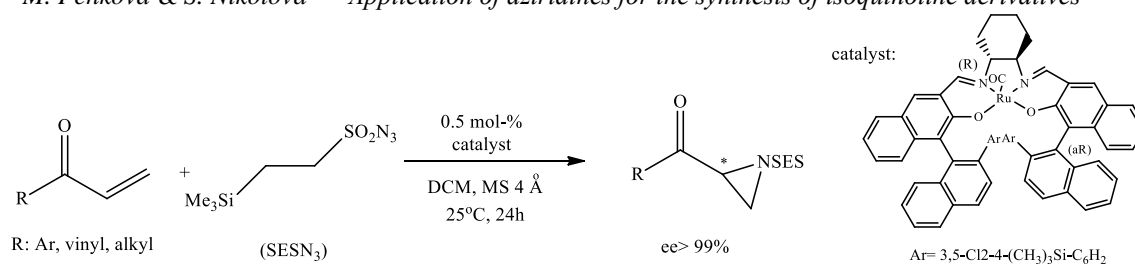
Scheme 5

Biologically important *N*- β -hydroxyethylaziridine intermediates were conveniently prepared by regioselective ring-opening reactions of various epoxides with *in situ*-generated ethyleneimine from β -chloroethylamine under basic conditions in an aqueous environment [39] (Scheme 3).

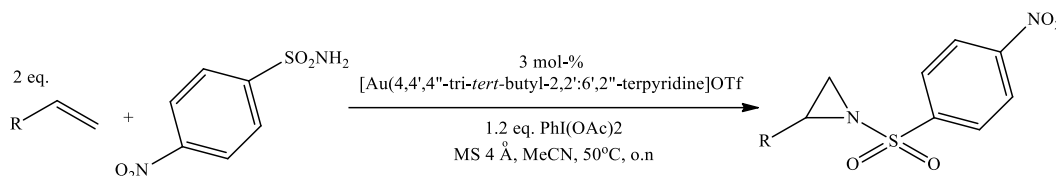
Vinylaziridines are useful and versatile synthetic intermediates, as the relief of ring-strain provides a driving force for efficient ring-opening or ring-expansion reactions. Furthermore, the vinyl group can be derivatized into interesting functionalities. The ring-closure of vicinal amino alcohols constitutes a straightforward route to aziridines. Several methods exist for this transformation, although many cannot be applied to vinylaziridines due to their acid lability. This comparative study describes the most effective sequences for the formation of N-H vinylaziridines [40]. Hodgson *et al.* recently used reaction of *N*-(2-chloroethylidene)-*tert*-butylsulfonamide with Grignard reagents or organoceriums gives terminal *N*-*tert*-butylsulfinyl aziridines in good yields and with organoceriums good diastereomeric ratios [41]. The authors also found that oxidation of terminal *N*-*tert*-butylsulfinyl aziridines provides synthetically useful terminal *N*-Bus (Bus = *tert*-butylsulfonyl) aziridines. Azzena used BH_3

complexation of *N*-alkyl-2-phenylaziridines to promote a regioselective β -lithiation. The lithiated intermediates were configurationally stable, allowing an enantioselective preparation of *cis*-2,3-disubstituted aziridines. The structure and stereochemistry of the synthesized BH_3 complexes have been proved with DFT calculations and NMR experiments [42]. A mild, efficient, and selective aziridination of olefins with *p*-toluenesulfonamide catalyzed by dirhodium(II) caprolactamate is described. Aziridine formation occurs through aminobromination and subsequent base-induced ring closure [43]. A metal-free catalytic aziridination of styrene derivatives with *N*-tosyliminophenyliodinane (PhI=NTs) is promoted by a combination of I_2 and tetrabutylammonium iodide (TBAI). TBAI₃ as highly efficient catalyst as well as *N,N*-diiodotosylamide as actual aziridination reagent are generated *in situ* [44] (Scheme 4).

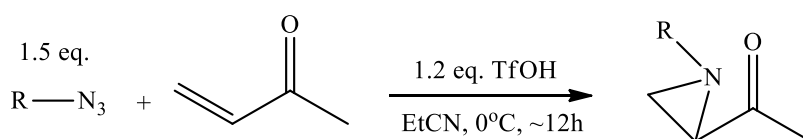
N-N ylides for the aziridination of a range of enone systems can be prepared by *in situ* amination of a tertiary amine. The amine may be used substoichiometrically, and promising levels of enantioselectivity are observed with quinine as promoter [45] (Scheme 5).



Scheme 6



Scheme 7



Scheme 8

Recently, Fukunaga reported that aziridination of vinyl ketones using SESN₃ in the presence of a Ru(CO)-salen complex provides synthetically useful enantiopure aziridinyl ketones. A formal asymmetric synthesis of (+)-PD 128907 was achieved in an eight-step sequence via aziridination [46] (Scheme 6).

Chen reported an efficient and practical aminohalogenation and *in situ* intramolecular S_N2 substitution of α,β-unsaturated esters and ketones gave *N*-*p*-tosyl-aziridine-2-ketones and carboxylates in moderate to good yields and excellent *anti* stereoselectivity [47]. Triethylamine was found to be an effective base for the *in situ* cyclization for most substrates. Li *et al.* used a gold(I) compound, supported by 4,4',4''-tri-tert-butyl-2,2':6',2''-terpyridine (*t*Bu₃tpy) as the ligand for efficient catalysis of olefin aziridination [48] (Scheme 7).

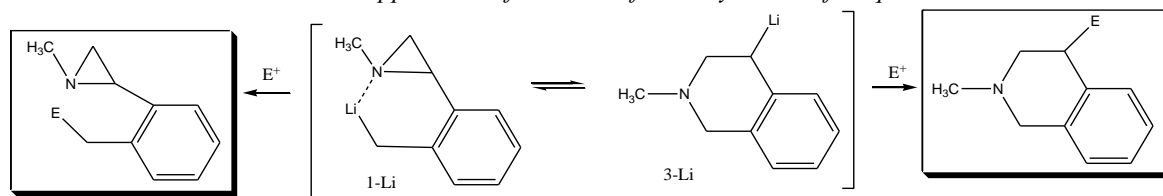
Complementary to existing routes, the Lewis acid catalyzed reactions of phenyldiazomethane with α-imino esters selectively produce *cis*-aziridine-2-carboxylates without competitive formation of enamino ester or carbene dimer byproducts [49]. An electrochemical aziridination process is described that delivers a nitrene functionality to olefins from *N*-aminophthalimide. Remarkably, both electron-rich and electron-poor olefins are converted to aziridines with high efficiency [50]. A straightforward synthesis of

aziridines is reported from electron-rich azides, electron-deficient olefins, and triflic acid in cold acetonitrile [51]. Ester substrates bearing a nucleophilic carbonyl give products of an olefin aminohydroxylation (Scheme 8).

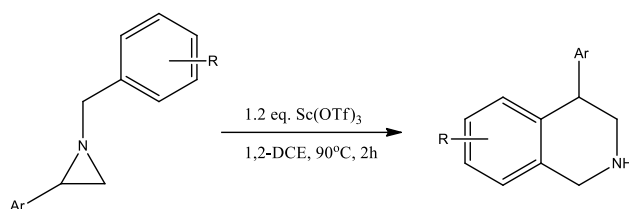
Baumann and Baxendale reported preparation of azirines from oxime precursors via mesylation and base-promoted cyclisation [52].

AZIRIDINES RING-OPENING

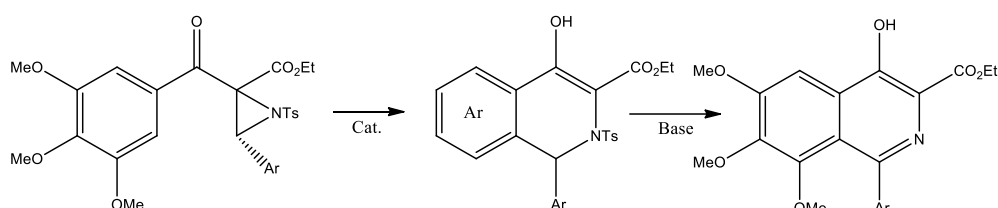
The recent studies on the chemistry of three-membered nitrogenous heterocycles [62] demonstrated the importance of this methodology to the preparation of other nitrogen-containing heterocycles. Nitrogen-containing heterocycles are ubiquitous in natural products, as well as in drugs and drug candidates.[53-55] Among nitrogenous heterocycles, the tetrahydroisoquinoline core represents a relevant structural motif frequently found in natural products and biologically active compounds.[56-59] Of the various synthetic approaches to nitrogenous heterocycles, the use of organometallic compounds has recently emerged as a particularly robust methodology [60, 61]. Recently, Giovine *et al.* reported synthesis of 1,2,3,4-Tetrahydroisoquinolines by microreactor-mediated thermal isomerization of laterally lithiated arylaziridines [63] (Scheme 9).



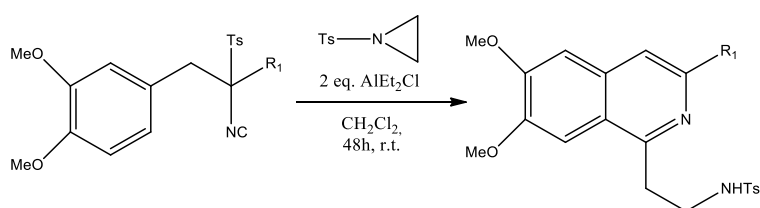
Scheme 9.



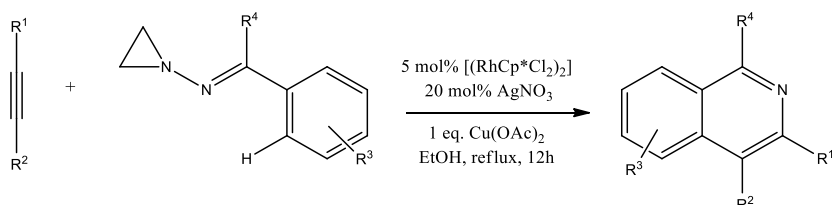
Scheme 10



Scheme 11



Scheme 12



Scheme 13

Scandium(III) triflate mediated intramolecular ring expansion of aziridines was used also as a direct access to 4-aryltetrahydroisoquinolines [64] (Scheme 10).

Wei and Zang reported a cascade ring opening/cyclization of aziridines with catalyst Yb(OTf)₃ [65] (Scheme 11).

Gutierrez *et al.* successfully used the addition to the α -benzyl TosMIC derivative with N-tosylaziridine and AlEt₂Cl to yield isoquinoline in 68% yield. Similar results were obtained in the reaction of N-tosyl aziridine and the α -benzyl TosMIC derivatives [66] (Scheme 12).

Huang *et al.* used rhodium-catalyzed synthesis of isoquinolines through selective cleavage of the N–N bond or the C=N bond followed by sequential

C–H activation and cyclization with internal alkynes [67] (Scheme 13).

CONCLUSIONS

Natural and/or synthesized aziridine-containing compounds have shown to be promising candidates for the development of new drugs toward several diseases, especially neoplasms. No doubt incorporation of an aziridine warhead will allow development of interesting new synthetic and semi-synthetic compounds with clinical utility.

Acknowledgements: The current study was accomplished in the frames of the Fund for Scientific Research of the Plovdiv University III 15-XΦ 001.

REFERENCES

1. A. K. Yudin, (ed) *Aziridines and Epoxides in Organic Synthesis*, (2006)
2. H.M.I Osborn, J. Sweeney, *Tetrahedron: Asymmetry*, **8**, 1693 (1997)
3. D. Tanner, *Angew. Chem. Int. Ed. Engl.*, **33**, 599 (1994)
4. R. S. Atkinson, *Tetrahedron*, **55**, 1519 (1999)
5. J. G. Kemp, *Comprehensive Organic Synthesis* (eds B. M. Trost and I. Fleming), **7** (1991)
6. I. D. G. Watson, L. Yu, A.K. Yudin, *Acc. Chem. Res.*, **39**, 194 (2006)
7. G. S. Singh, M. D'hooghe, N. De Kimpe, *Chem. Rev.*, **107**, 2080 (2007)
8. M.V. Gil, M.J. Arevalo, O. Lopez, *Synthesis*, **11**, 1589 (2007)
9. V.V. Fokin, P. Wu, *Organic Synthesis*, **12**, 443 (2006)
10. J.B. Sweeney, A.K. Yudin, *Aziridines and Epoxides in Organic Synthesis*, **4**, 117 (2006)
11. S.S. Murphree, A. Padwa, *Prog. Heterocycl. Chem.*, **13**, 52 (2001)
12. W. McCoull, F.A. Davis, *Synthesis*, **10**, 1347 (2000)
13. L.X. Dai, X.L. Hou, Y.G. Zhou, *Pure Appl. Chem.*, **71**, 369 (1999)
14. V. M. Dembitsky, A. O. Terent'ev, D. O. Levitsky, *Aziridine Alkaloids: Origin, Chemistry and Activity, Natural Products*, 977-1006 (2013)
15. J.B. Sweeney, *Chem. Soc. Rev.*, **31**, 247–258 (2002)
16. X.E. Hu, *Tetrahedron*, **60**, 2701 (2004)
17. S. Wakaki, H. Marumo, K. Tomioka, G. Shimizu, E. Kato, H. Kamada, S. Kudo, Y. Fujimoto, *Antibiot. Chemother.*, **8**, 228 (1958)
18. R.R. Herr, M.E. Bergy, T.E. Eble, H.K. Jahnke, *Antimicrob. Agents Ann.*, **8**, 23 (1960)
19. H. Zang, K.S. Gates, *Biochemistry*, **39**, 14968 (2000)
20. E.A. Acar, F. Glarner, U. Burger, *Helv. Chim. Acta*, **81**, 1095 (1998)
21. M.K. Tong, B. Ganem, *J. Am. Chem. Soc.*, **110**, 312 (1988)
22. J.B. Sweeney, *Chem. Soc. Rev.*, **31**, 247 (2002)
23. M. Karim, R.L. Sarma, C. Medhi, *Indian J. Chem.* **6B**, 892 (2008)
24. V.N. Iyer, W. Szybalski, *Science (N.Y.)*, **145**, 55 (1964)
25. P.A.S. Lowden, *Aziridines and Epoxides in Organic Synthesis*, **11**, 399 (2006)
26. H. Oettel, G. Wilhelm, *Arzneimit. Forsch.*, **4**, 691 (1954)
27. C. Scholler, German Patent: DE 802346 19510208 (1951)
28. Y. Hata, M. Watanabe, *Drug Metab Rev*, **26**, 575 (1994)
29. H. Jackson, RMV James, *Br J Pharm Chemother*, **25**, 223 (1965)
30. D. Tanner, *Pure & Appl. Chem.*, **65**, 1319 (1993)
31. D. Tanner, *Angew. Chem. Int. Ed. Engl.* **33**, 599 (1994)
32. W. H. Pearson, B. W. Lian, S. C. Bergmeier, *Comprehensive Heterocyclic Chemistry II*, **1** (1996)
33. K.M.L. Rai, A. Hassner, *Comprehensive Heterocyclic Chemistry II*, **61** (1996)
34. G. Cardillo, L. Gentilucci, A. Tolomelli, *Asymmetric Synthesis of Nitrogen Heterocycles*, **1**, 1 (2009)
35. B. Denolf, E. Leemans, N. De Kimpe, *J. Org. Chem.*, **72**, 3211 (2007)
36. X. Li, N. Chen, J. Xu, *Synthesis*, **20**, 3423 (2010)
37. L. W. Bieber, M. C. F. de Araujo, *Molecules*, **7**, 902 (2002)
38. S. Minakata, Y. Morino, Y. Oderaotshi, M. Komatsu, *Org. Lett.*, **8**, 3335 (2006)
39. H. Y. Kim, A. Talukdar, M. Cushman, *Org. Lett.*, **8**, 1085 (2006)
40. B. Olofsson, R. Wijtmans, P. Somfai, *Tetrahedron*, **58**, 5979 (2002)
41. D. M. Hodgson, J. Kloesges, B. Evans, *Synthesis*, **11**, 1923 (2009)
42. U. Azzena, G. Dettori, L. Pisano, B. Musio, R. Luisi, *J. Org. Chem.*, **76**, 2291 (2011)
43. A. J. Catino, J. M. Nichols, R. E. Forslund, M. P. Doyle, *Org. Lett.*, **7**, 2787 (2005)
44. K. Kiyokawa, T. Kosaka, S. Minataka, *Org. Lett.*, **15**, 4858 (2013)
45. A. Armstrong, C. A. Baxter, S. G. Lamont, A. R. Pape, R. Wincewicz, *Org. Lett.*, **9**, 351 (2007)
46. Y. Fukunaga, T. Uchida, Y. Ito, K. Matsumoto, T. Katsuki, *Org. Lett.*, **14**, 4658 (2012)
47. D. Chen, C. Timmons, L. Guo, X. Xu, G. Li, *Synthesis*, **15**, 2479 (2004)
48. Z. Li, X. Ding, C. He, *J. Org. Chem.*, **71**, 5876 (2006)
49. A. Mazumdar, Z. Xue, M. F. Mayer, *Synlett*, **13**, 2025 (2007)
50. T. Siu, A. K. Yudin, *J. Am. Chem. Soc.*, **124**, 530 (2002)
51. J. M. Mahoney, C. R. Smith, J. N. Johnston, *J. Am. Chem. Soc.*, **127**, 1354 (2005)
52. M. Baumann, I. R. Baxendale, *Synlett*, **27**, 159 (2016)
53. T. Wakimoto, T. Asakawa, S. Akahoshi, T. Suzuki, K. Nagai, H. Kawagishi, T. Kan, *Angew. Chem.*, **123**, 1200 (2011); *Angew. Chem. Int. Ed.*, **50**, 1168 (2011)
54. R. Benigni, C. Bossa, *Chem. Rev.*, **111**, 2507 (2011)
55. S. D. Roughley, A. M. Jordan, *J. Med. Chem.*, **54**, 3451 (2011)
56. J. D. Phillipson, M. F. Roberts, M. H. Zenk, *The Chemistry and Biology of Isoquinoline Alkaloids* (1985)
57. D. Jack, R. Williams, *Chem. Rev.*, **102**, 1669 (2002)
58. Y. Zhang, J. Feng, Y. Jia, X. Wang, L. Zhang, C. Liu, H. Fang, W. Xu, *J. Med. Chem.*, **54**, 2823 (2011)
59. M. Shamma, *The Isoquinoline Alkaloids: Chemistry and Pharmacology*, **25** (1972)
60. S. G. Newman, M. Lautens, *J. Am. Chem. Soc.*, **133**, 1778 (2011)
61. J. A. Bull, J. J. Mousseau, G. Pelletier, A. B. Charette, *Chem. Rev.* **112**, 2642 (2012)
62. S. Florio, R. Luisi, *Chem. Rev.*, **110**, 5128 (2010)
63. A. Giovine, B. Musio, L. Degennaro, A. Falcicchio, A. Nagaki, J. Yoshida, R. Luisi, *Chemistry*, **19**, 1872 (2013)

64. S. Tummanapalli, P. Muthuraman, Dh. N. Vangapandu, S. Majumder, *Tetrahedron Lett.*, **55**, 6787 (2014)
65. L. Wei, J. Zhang, *Chem. Commun.*, **48**, 2636 (2012)
66. S. Gutierrez, A. Coppola, D. Sucunza, C. Burgos, and J. J. Vaquero, *Org. Lett.*, **18**, 3378 (2016)
67. Xiao-Cheng Huang, Xu-Heng Yang, Ren-Jie Song, Jin-Heng Li, *J. Org. Chem.*, **79**, 1025 (2014)

ПРИЛОЖЕНИЕ НА АЗИРИДИНИ ЗА СИНТЕЗ НА ИЗОХИНОЛИНОВИ ПРОИЗВОДНИ

М. Пенкова*, С. Николова

*Пловдивски университет „Паисий Хилендарски“, Химически факултет, Катедра Органична химия,
ул. "Цар Асен" 24, Пловдив 4000
e-mail: mariya.p.penkova@gmail.com*

Постъпила на 11 ноември 2016 г.; приета на 13 декември 2016 г.

(Резюме)

Азиридините са разнообразни структурни елементи, използвани в органичния синтез и медицинската химия, тъй като позволяват удобен достъп до полезни азот-съдържащи и биологично-активни вещества. Много азиридин-съдържащи съединения проявяват фармакологична активност, в това число противоракова, антибактериална, антимицробна и др., доказващи че азиридиновият пръстен е отговорен за проявената активност. Хиралните азиридинови са често употребявани в органичния синтез. Статията описва синтезът и отварянето на тричленният пръстен на азиридините и употребата им за синтез на шестчленни изохинолини.

Ключови думи: *азиридинови, синтез, биологична активност, изохинолини*

Simultaneous HPLC determination of fat soluble vitamins, carotenoids and cholesterol in seaweed and mussel tissue

D.A. Dobрева*, V.Z. Panayotova, R.S. Stancheva, M. Stancheva

Medical University of Varna, Faculty of Pharmacy, 55 Marin Drinov St., 9000 Varna

Received November 11, 2016; Revised December 21, 2016

The aim of the present study was to develop simple method for simultaneous determination of fat soluble vitamins (all-trans retinol, cholecalciferol, ergocalciferol and α -tocopherol), carotenoids (β -carotene and astaxanthin) and cholesterol in seaweeds and mussel tissue. Reversed-phase high performance liquid chromatography system combine with UV and fluorescent detection was the method characterized with rapid, sensitive and accurate detection of all components. Extraction procedure requires small amounts of sample. The sample preparation included saponification and liquid-liquid extraction of the analytes. The method precision (relative standard deviation) was below 10% for all analytes. The method shows good linearity of all investigated components and analysis time – 32 min. The method was applied on real seaweed and mussel tissue samples and the results for the tested fat soluble analyte contents were in a good agreement with the data given by other authors.

Key words: all-trans retinol, calciferol, α -tocopherol, astaxanthin, cholesterol

INTRODUCTION

Many studies suggest that marine mollusks and edible seaweeds are valuable healthy food, low in calories and fats, and high in proteins and bioactive compounds [1, 2]. Seaweeds also have been used as permanent source of the raw materials used in pharmaceutical, food industries, medicine and cosmetics, as fodder and fertilizer [3]. Mollusks and different seaweeds are amongst the most important dietary sources of fat soluble vitamins – A, D₃ and E. They are also rich in carotenoids, which act as antioxidants [4, 5]. Overall mollusk production in Bulgaria relies on two sources – commercial fishing (for mussel and sea snail *Rapana*) and marine aquaculture (consists of mussel only) [6].

Lipid content of different marine algae is only 1-5% of dry matter and exhibits an interesting polyunsaturated fatty acid composition (particularly ω -3 and ω -6) [7]. Seaweed and mollusks tissue is a good source of some water- (B₁, B₂, B₁₂ and C) and fat soluble (β -carotene with vitamin A activity, ergocalciferol and cholecalciferol and α -tocopherol) vitamins. Vitamins derived from algae are very important due to their antioxidant activity, biochemical functions and other health benefits - prevention of cardiovascular diseases (β -carotene), decreasing blood pressure (vitamin C), reducing the risk of developing cancer (vitamins E and carotenoids) [8].

Information available about the fat soluble

vitamins, carotenoids and cholesterol content of Black mussel and different algae from Black Sea is scarce. The aim of the present work was to develop a simple and accurate method for simultaneous determination of seven fat soluble biologically active components: all-trans-retinol (vitamin A), cholecalciferol (vitamin D₃), ergocalciferol (vitamin D₂), α -tocopherol (vitamin E), β -carotene, astaxanthin and cholesterol in matrices from animal and plant origin.

EXPERIMENTAL

Instrumentation and chemicals

The chromatographic analysis was performed on HPLC system (Thermo Scientific Spectra SYSTEM) equipped with UV2000 and FL3000 detectors. All solvents were of HPLC grade specification, obtained by Sigma-AldrichTM, USA. Substances of all-trans-retinol, ergocalciferol, cholecalciferol, α -tocopherol, β -carotene, astaxanthin, cholesterol and L-ascorbic acid were all with analytical standard specifications and were supplied by Supelco (Sigma-AldrichTM, USA).

Sample preparation

Two mussel and four seaweed samples were used for evaluation the all-trans-retinol, ergocalciferol, cholecalciferol, α -tocopherol, β -carotene, astaxanthin and cholesterol contents. Sample preparation procedure was performed following the method of Dobрева *et al.* (2011) with some modifications [9]. Edible mussel and shredded algal tissue was homogenized using

* To whom all correspondence should be sent.
E-mail: diana@mu-varna.bg

kitchen homogenizer for 3 min. An aliquot of the homogenized sample (1.000 ± 0.005 g) was weighed into a glass tube with a screw cap and 1% of methanolic L-ascorbic acid and 0.5M methanolic potassium hydroxide were added. Six parallel tests of each mussel and algae samples were prepared and subjected to saponification at 50°C for 30 min. After cooling the analytes were extracted twice with *n*-hexane: dichloromethane = 2:1 (v/v) solution. Combined extracts was evaporated under nitrogen flow and dry residue was dissolved in methanol: dichloromethane solution, filtered (0.45 μ m syringe filter) and injected (20 μ l) into the HPLC system.

Chromatographic conditions

All-trans-retinol, ergocalciferol, cholecalciferol, α -tocopherol, astaxanthin, β -carotene and total cholesterol were determined simultaneously using HPLC/UV/FL system equipped with RP analytical column. Chromatographic separation was performed by a Synergi 4 μ Hydro-RP 80A pore 250x4.6 mm reversed-phase column, through a gradient at 1.1 mL/min. Solvent A consisted of methanol : water (93:7), solvent B was acetonitrile and solvent C – 2-propanol. The gradient changed as follows: 0-16.0 min, 100 % solvent A; 20.0-30.0 min, 60% solvent B and 40 % solvent C; 30.0-40.0 min, 50 % of solvent B and 50% solvent C. The gradient was then returned to 100 % of solvent A.

Detection of ergocalciferol ($\lambda = 265$ nm), cholecalciferol ($\lambda = 265$ nm), astaxanthin ($\lambda = 474$ nm), β -carotene ($\lambda = 450$ nm) and cholesterol ($\lambda = 208$ nm) was performed by UV detector. Concentrations of all-trans-retinol (at $\lambda_{ex} = 334$ nm and $\lambda_{em} = 460$ nm) and α -tocopherol (at $\lambda_{ex} = 288$ nm and $\lambda_{em} = 332$ nm) were measured by fluorescence detection.

Standards and quantification

Stock standard solutions of each analyte (1.0 mg/ml) were prepared as follows: retinol, ergocalciferol, cholecalciferol, α -tocopherol and cholesterol in 100% methanol; astaxanthin and β -carotene in 100% dichloromethane. The solutions were stored at -20°C away from light. Working solutions were prepared prior to analysis by dilution proportionally with methanol/dichloromethane. In all cases, the stock solution was analyzed together with the samples. Analyte concentrations in samples were estimated on the basis of peak areas. All samples were analyzed in triplicate. Contents of each analytes were presented as means \pm standard deviation.

RESULTS AND DISCUSSION

Chromatography

Chromatograms of combined standard solution are presented on figure 1. The quantitation was performed by the method of the external calibration, comparing the chromatographic peak areas of the samples with those of the corresponding standards.

Selected chromatographic conditions provided good separation of the analytes, in less than 40 min. Retention times (t_R) were as follows: astaxanthin $t_R = 4.5$ min, retinol $t_R = 4.9$ min, ergocalciferol $t_R = 11.1$ min, cholecalciferol $t_R = 11.7$ min, cholesterol $t_R = 19.6$ min, α -tocopherol $t_R = 12.5$ min and β -carotene $t_R = 40.3$ min. Resolution factors were greater than 1, indicating a sufficient separation.

Linearity

Each calibration curve was constructed by measuring five diluted standards from the corresponding standard solutions and by plotting peak area response against concentration of the standards. The least square linear regression analysis was applied to estimate equation of the line.

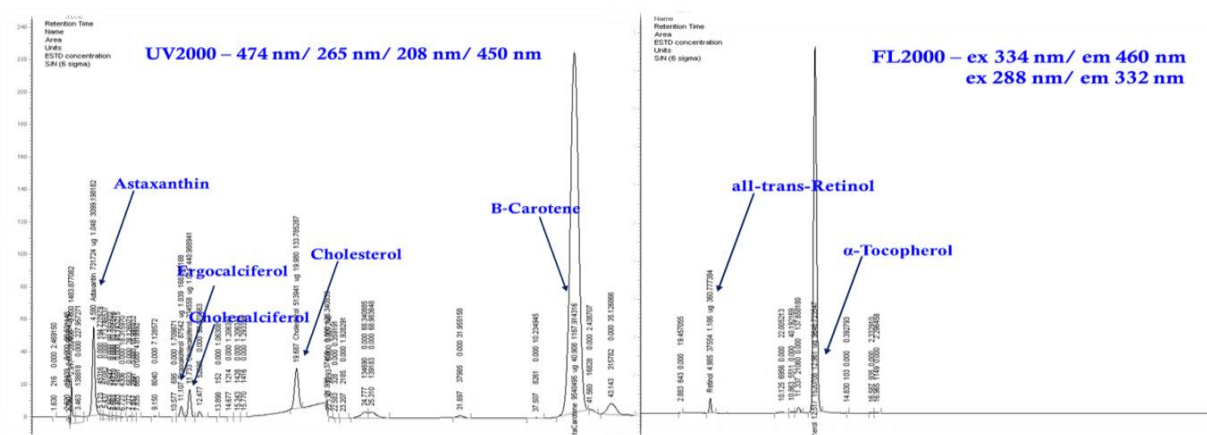


Fig. 1. HPLC chromatograms of standard solution

The received equations were: $y = 2.74 \cdot 10^5 \mu\text{g}$ for retinol; $y = 1.01 \cdot 10^5 \mu\text{g}$ for ergocalciferol; $y = 3.67 \cdot 10^6 \mu\text{g}$ for cholecalciferol, $y = 3.29 \cdot 10^5 \mu\text{g}$ for cholesterol, $y = 4.27 \cdot 10^6 \mu\text{g}$ for β -carotene, $y = 1.20 \cdot 10^6 \mu\text{g}$ for astaxanthin, and $y = 7.73 \cdot 10^6 \mu\text{g}$ for α -tocopherol. Correlation coefficients ranged from 0.9804 to 0.9983 ($n = 3$).

Precision

Six replicate determinations of each algae and mussel tissue sample were performed under optimum conditions to determine repeatability. The relative standard deviations (RSDs) were $\leq 10\%$. Recovery rates were determined by comparing the observed concentration with a spiked concentration. After hydrolysis, consequent extraction and chromatographic separation, analytical recovery exceeded 70% for astaxanthin and all-trans retinol, 80 % for β -carotene and cholecalciferol, 90% for ergocalciferol and α -tocopherol, and 102% for cholesterol.

Verification

Five seaweed and two mussel samples were analyzed to assess practical applicability of the

method (figure 2, 3). Chromatograms from UV and FL detectors of the green algae (*Ulva rigida*) sample are presented on figure 2. Peaks of cholecalciferol and all-trans-retinol are missing.

Figure 3 shows the UV and FL chromatograms of a wild mussel extract. In contrast to figure 2, peaks for all analytes are present. This is due to sample composition – edible tissue included meat and stomach content (algae).

There are many studies about optimum saponification conditions for the extraction of lipid-soluble biologically active components from different matrices [10, 11, 12, 13]. The large scale extraction methods are expensive in terms of apparatuses required, cost of solvents, and time.

Therefore, we decided to develop a few steps simple and rapid method for simultaneous determination of fat soluble vitamins (all-trans retinol, cholecalciferol, ergocalciferol and α -tocopherol), carotenoids (β -carotene and astaxanthin) and cholesterol in seaweeds and mussel tissue.

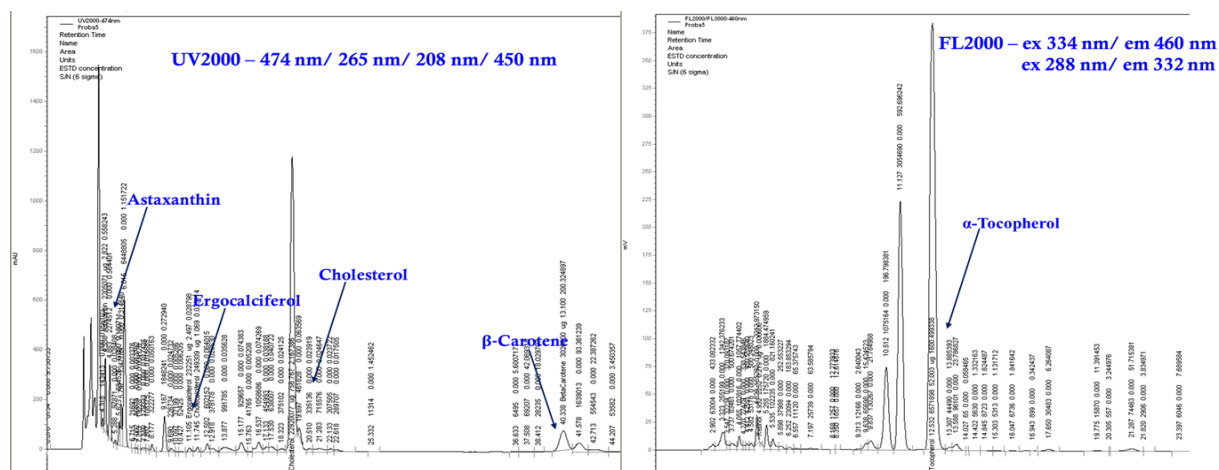


Fig. 2. HPLC chromatograms of *Ulva rigida* sample

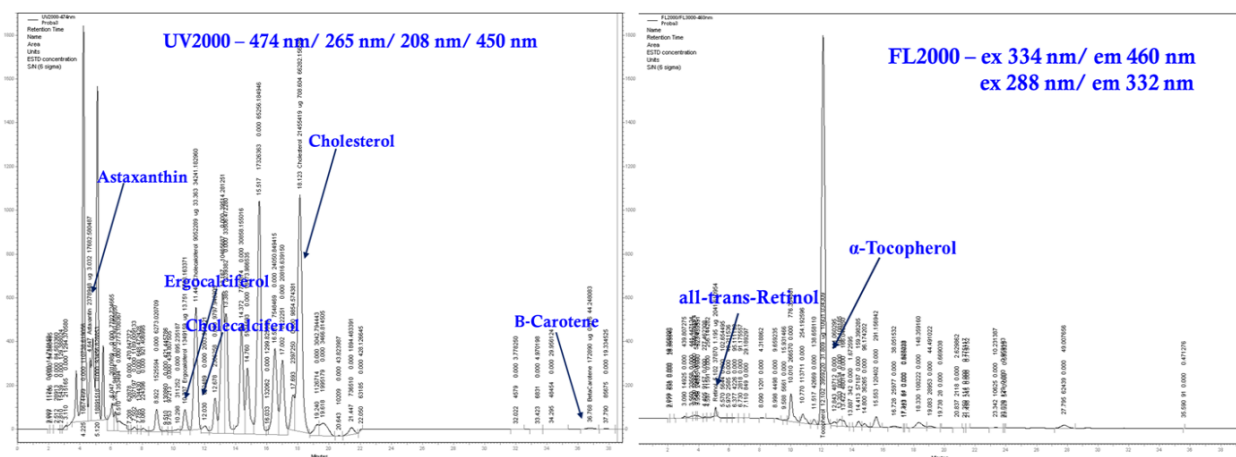


Fig. 3. HPLC chromatograms of wild mussel sample

The method was similar to those described by Dobreva *et al.*, 2011 [9]. Generally smaller amounts of sample (1.0 g) and optimal hydrolysis conditions (0.5 M KOH/CH₃OH) were used. Preservation of the analytes from oxidation was assured by adding 1% methanolic ascorbic acid.

To achieve better resolution of the fat soluble components, several compositions of the mobile phases were tested: 100% methanol; 40/60 acetonitrile/methanol (v/v); 97/3 methanol/water (v/v) and 75:20:5 = ACN:MeOH:iPrOH (v/v/v). Best resolution between vitamins D₂ and D₃, and between β -carotene and α -carotene (which are very similar structurally) was achieved when using the mobile phase ACN:MeOH:iPrOH in gradient. The standard curves in mentioned concentration ranges (in accordance with the published data) were linear with coefficients of variation greater than 0.9907 with the exception of β -carotene. The precision of the method was evaluated – it comprised of repeatability and recovery rates. Six replicate determinations of each sample were performed under the described conditions to determine repeatability. RSDs of the repeatability and the estimated recovery indicated that the method can be used for quantitative determination of the above mentioned lipid soluble analytes in seaweed and mussel tissue matrices. The amounts of the seven analyzed compounds are presented in table 1 as milligram per 100 grams wet weight (mg.100g⁻¹ww). The results are expressed as average and standard deviation (mean \pm SD). They are corrected against the calculated yield of each analyte.

Fat soluble analytes' quantity in edible tissue of wild and aquaculture mussel are closed. Present results are comparable to data published by other authors [1, 2, 4, 5, 6, 8]. Astaxanthin, vitamin D₂ and cholesterol contents in the wild sample were found slightly higher than in farmed one. On the other hand aquaculture species exhibited higher

amounts of vitamin A, vitamin E and β -carotene, but results were similar too. These results are in good agreement with those presented by other scientific groups. In comparison to our data the MacDonald (2010) reported lower amounts – 0.039 mg.100g⁻¹ww for vitamin A, 0.740 mg.100g⁻¹ww for vitamin E and 29 mg.100g⁻¹ww cholesterol in raw edible tissue of green shell mussel [14]. Other results confirming data in table 1 are presented by Danish Food Composition Databank (2009) and Öhrvik *et al.* (2012) – 0.08 mg.100g⁻¹ww and 0.067 mg.100g⁻¹ww for vitamin A, and 3.5 mg.100g⁻¹ww and 3.07 mg.100g⁻¹ww for vitamin E, respectively [15, 16]. Pospelova and Nehoroshev analyzed β -carotene content of wild Black mussel harvested in the Black Sea near Sevastopol, Ukraine [17,18] and found about 0.5 mg.100g⁻¹ww, which is in the same range as our results.

The results for the seaweed samples varied from species to species (table 1). The green and red algae present lower amount of vitamin D₂ and astaxanthin, compared to brown seaweed species. On the other hand, both brown seaweeds are characterized by high vitamin E concentrations. Algae samples, especially red species, contain very high levels of β -carotene and cholesterol. β -carotene amounts exceeded those found in fresh carrot (0.088 mg/g), which is known as excellent source of this nutrient [19]. Astaxanthin was also detected in high contents (1.39 mg.100g⁻¹ ww) in *Cystoseira barbata* – brown algal sample. This seaweed sample is also rich in α -tocopherol – 12.36 mg.100g⁻¹ ww. The high concentration of this form of vitamin E is in accordance with other published results [20], where brown algae *Cystoseira* spp. are characterized by higher amount compared to other samples. Comparing the results in table 1 with literature data, is obvious their good accordance.

Table 1. Analyte's contents in raw mussel and seaweed tissue (mg.100g⁻¹ ww)

Analyte	Mussel		Seaweed				
	Aquaculture	Wild	<i>Ulva rigida</i> (green)	<i>Chaetomorpha linum</i> (green)	<i>Gelidium crinale</i> (red)	<i>Cystoseira barbata</i> (brown)	<i>Cystoseira crinita</i> (brown)
Vitamin A	0.309 \pm 0.018	0.167 \pm 0.017	-	-	-	-	-
Vitamin D ₂	0.035 \pm 0.002	0.071 \pm 0.009	0.031 \pm 0.01	0.025 \pm 0.007	0.006 \pm 0.002	0.12 \pm 0.03	0.16 \pm 0.05
Vitamin D ₃	0.024 \pm 0.002	0.031 \pm 0.001	-	-	-	-	-
Vitamin E	4.70 \pm 0.16	2.69 \pm 0.19	1.223 \pm 0.03	1.14 \pm 0.7	1.53 \pm 0.09	3.13 \pm 0.15	12.36 \pm 0.22
Astaxanthin	0.211 \pm 0.036	0.62 \pm 0.03	0.110 \pm 0.01	0.015 \pm 0.001	0.20 \pm 0.01	0.30 \pm 0.03	1.39 \pm 0.12
β -carotene	0.232 \pm 0.017	0.066 \pm 0.009	1.702 \pm 0.04	0.017 \pm 0.003	3.38 \pm 0.09	5.57 \pm 0.20	1.88 \pm 1.31
Cholesterol	60.050 \pm 0.918	70.81 \pm 0.811	3.911 \pm 0.25	6.08 \pm 0.30	52.6 \pm 1.07	0.89 \pm 0.06	1.52 \pm 0.13

CONCLUSIONS

The method presented in this study has analytical characteristics that allow its use for quantitative simultaneous analyses of retinol, α -tocopherol, cholecalciferol, ergocalciferol, cholesterol, astaxanthin and β -carotene in mussel and seaweed matrices. The sample preparation, including extraction in a single reaction tube, characterizes the method with minimum manipulation. The method shows RSD below 10% for all analytes, good linearity for all components and short analysis time – less than 32 min.

The high concentrations of most investigated biologically active compounds (including antioxidants astaxanthin and β -carotene) indicate the possible application of Black Sea Black mussel and especially seaweeds as supplements in food and pharmaceutical industries.

REFERENCES

1. A.V Borodina, A.A. Soldatov, *Hydrobiological Journal*, **3**, 25 (2010)
2. A. A. Soldatov, T.I. Andreenko, I. V. Golovina, A. Y. Stolbov, *Journal of Evolutionary Biochemistry and Physiology*, **46**, 341 (2010)
3. N. Desnica, S. Jensen, G.G. Pórarinsdóttir, J.Ó. Jónsson, H.G. Kristinsson and H. Gunnlaugsdóttir, Icelandic Food and Biotech, Report Summary, (2011). Available online: <http://www.matis.is/media/matis/utgafa/44-11-Gaedakraekingur.pdf>
4. K. Manivannan, G. Thirumaran, Devi G. Karthikai, A. Hemalatha, P. Anantharaman, *American-Eurasian Journal of Botany* **1**, 32 (2008)
5. E. Orban, G. Di Lena, T. Nevigato, I. Casini, A. Marzetti, R. Caproni, *Food Chemistry*, **7**: 57-65, (2002)
6. T. Lorenz, (2010) <http://www.brineshrimpdirect.com/c90/Astaxanthin-in-shrimp-culturing-c85.html>.
7. National strategic plan for fisheries and aquaculture, 2007 – 2013. Ministry of agriculture and forestry, NAFA, Bulgaria. http://ec.europa.eu/fisheries/cfp/eff/national_plans/list_of_national_strategic_plans/bulgaria_en.pdf
8. K. Banerjee, R. Ghosh, S. Homechaudhuri, A. Mitra, *African Journal of Basic & Applied Sciences* **1**, 96, (2009)
9. S. Skrovankova, Seaweed Vitamins as Nutraceuticals, In: Se-Kwon Kim, (Ed), *Advances in Food and Nutrition Research*, **64**, 357, (2011)
10. D. Dobрева, B. Galunska, M. Stancheva, *Scripta Scientifica Medica*, **43**, 276 (2011)
11. A. Ahmadnia, M.A. Sahari, M. Barzegar, S.J. Seyfabad and M. Abdollahi, *American-Eurasian Journal of Sustainable Agriculture*, **2**, 285 (2008)
12. U. Ostermeyer, T. Schmidt, *European Food Research and Technology*, (2005)
13. J. Lopez-Cervantes, D.I. Sanchez-Machado, N.J. Rios-Vazquez, *Journal of Chromatography A*, **1105**, 135, (2006)
14. P. Salo-Väänänen, V. Ollilainen, P. Mattila, K. Lehtikoinen, E. Salmela-Mölsä, V. Piironen, *Food Chemistry*, **71**, 535, (2000)
15. G. MacDonald, Identification of Health and Nutritional Benefits of New Zealand Aquaculture Seafood's. Report., MacDonald and Associates Ltd, Nelson, (2010)
16. Danish Food Composition Databank, Department of Nutrition, National Food Institute, (2009)
17. V. Öhrvik, A. Malmberg, I. Mattisson, S. Wretling, C. Astrand, Fish, shellfish and fish products - analysis of nutrients. Livsmedelsverket, National food agency, Sweden, (2012)
18. N. V. Pospelova, M. V. Nekhoroshev, *Ekologiya Morya*, **124**, 62, (2003)
19. N.V. Pospelova, *Marine Ecological Journal*, **4**, 55, (2007)
20. G. Gayathri, K. Platel, J. Prakash, K. Srinivasan, *Food Chemistry*, **84**, 35 (2004)
21. Y. Durmaz, H. Duyar, S. Gokpinar, L. Taskaya, Y. Ogretmen, N. Bandarra, M. Nunes, *International Journal of Natural and Engineering Sciences*, **2**, 111 (2008)

СЪВМЕСТНО ВЕТХ ОПРЕДЕЛЯНЕ НА МАСТНОРАЗТВОРИМИ ВИТАМИНИ, КАРОТЕНОИДИ И ХОЛЕСТЕРОЛ В ТЪКАН НА ВОДОРАСЛИ И МИДИ

Д.А. Добрева*, В.З. Панайотова, Р.С. Станчева, М. Станчева

*Катедра по химия, Факултет по фармация, МУ-Варна, ул. М. Дринов 55, Варна
Постъпила на 11 ноември 2016 г.; приета на 21 декември 2016 г.*

(Резюме)

Целта на настоящото изследване бе да се разработи хроматографски метод за едновременно количествено определяне на мастноразтворими витамини (ретинол, холекалциферол, ергокалциферол и α -токоферол), каротеноиди (β -каротен и астаксантин) и холестерол в тъкан на водорасли и миди. Високоэффективната течно-хроматографска система с UV и FL детектори е метод, характеризиращ се с бързина, чувствителност и точност при откриването на всички компоненти. Екстракционната процедура се провежда с минимални количества на пробите. Пробоподготовката включва осапунване и течно-течна екстракция на анализите. Точността на метода (относително стандартно отклонение) е под 10% за всички изследвани вещества. Методът се характеризира с добра линейност при всички изследвани компоненти и време за анализ - до 32 мин. Методът бе приложен при проби от тъкани на водорасли и миди, като получените резултати за изследваните мастноразтворими анализи са близки до данни, публикувани от други автори.

Ключови думи: *ретинол, калциферол, α -токоферол, астаксантин, холестерол*

Fat soluble nutrients and fatty acids in skin and fillet of farmed rainbow trout

D.A. Dobрева*, A. Merdzhanova and L. Makedonski

Medical University of Varna, Faculty of Pharmacy, 55 Marin Drinov St., 9000 Varna

Received November 12, 2016; Revised December 21, 2016

This study compares the fat soluble components in the muscle and edible skin parts of farmed rainbow trout (*Oncorhynchus mykiss* W.) fillets, sampled at two growth stages, from fish markets from Bulgaria. Insufficient information is available about the differential fat soluble pigments, cholesterol, vitamins and fatty acid compositions of rainbow trout fillets when eating them with or without the skin left on. Vitamins A, D₃ and E, β -carotene and cholesterol were analyzed simultaneously using HPLC system with UV and FL detection (vitamins A and E). Total lipids were extracted according to Bligh and Dyer method. Analysis of fatty acid methyl esters (FAME) were performed by GC/MS. The average lipid content, the cholesterol and vitamin E amounts and the saturated fatty acids were significantly higher in the skin than in the muscle, whereas the proportion of vitamin A and D₃, eicosapentaenoic acid (C20:5 ω -3) and docosahexaenoic acid (C22:6 ω -3) were higher in the muscle.

Key words: *Oncorhynchus mykiss*, vitamins, carotenoids, cholesterol, PUFA

INTRODUCTION

It is well-known that fish consumption has nutritional and health benefits in humans. Rainbow trout (*Oncorhynchus mykiss* W.) is one of the most consumed fish species in Bulgaria and also of interest to aquaculture because of the rapid growth rate and excellent nutritional qualities of the meat [1]. Nutritional quality of fish depends especially on tissue lipid composition including fat soluble vitamins, fatty acids, cholesterol and β -carotene. In the scientific literature, chemical composition of fish is investigated from different points of view. Recently a special interest in fish lipid composition has risen because of its advantageous effects of human health which depend on its fatty acid (FA) and fat soluble vitamins content. Moreover, the optimal quantities of polyunsaturated FA/saturated FA, ω -3/ ω -6 FA ratios are considered as informative indices for nutritional quality. Comparative investigations on farmed rainbow trout lipids, FA, fat soluble vitamins content and cholesterol from Turkey were performed by Harlioglu A. (2012) [2]. Previous studies [3, 4] have reported data on the proximate and fatty acid composition of rainbow trout. Despite these facts, available information about the composition of different fat soluble pigments, cholesterol, vitamins and fatty acids of rainbow trout fillets (with or without the skin) is insufficient. It is important to investigate differences in fat soluble nutrients content in trout muscle and skin. Thus, the aim of the study was to investigate and compare β -carotene, vitamins (A, E, D₃),

cholesterol and fatty acid profile of rainbow trout filets and skin. This is the first study on β -carotene, cholesterol, vitamins and FA composition of farmed rainbow trout filets and skin in Bulgaria. The presented results will be useful when determining what differences might exist in nutrient ingestion, depending on whether a rainbow trout fillet is consumed with or without the skin.

EXPERIMENTAL

Sample collection

Samples of rainbow trout were purchased from Varna fish market during March 2015. Fish was raised in two fish farms (Plovdiv region, Hvoina village and Dospat Dam Lake) and fed on commercial feed mixtures. Analyzed specimens were divided in two groups (with three specimens in each group): group I (Rainbow trout I) – weighing 300 - 400 g; group II (Rainbow trout II) – weighing 700 - 900 g. Each specimen was filleted, muscle tissue was separated from the skin. Two medium samples were prepared.

Vitamins, pigments and cholesterol analysis

Saponification and extraction: Two skin and two muscle tissue samples were homogenized and used for evaluation of all-trans-retinol, cholecalciferol, α -tocopherol, β -carotene and cholesterol contents. Sample preparation procedure was performed following the method of Dobрева *et al.* (2011) with some modifications [5]. An aliquot of the homogenized sample (1.000 \pm 0.005 g) was weighed into a glass tube with a screw cap and 1% of methanolic L-ascorbic acid and 0.5M methanolic potassium hydroxide

* To whom all correspondence should be sent.

E-mail: diana@mu-varna.bg

were added. Six parallel tests were prepared and subjected to saponification at 50°C for 30 min. After cooling the analytes were two times extracted from samples with *n*-hexane : dichloromethane = 2:1 (v/v) solution. The combined extracts was evaporated and redissolved in methanol : dichloromethane solution, filtrated (0.45 µm syringe filter) and injected (20µl) into the HPLC system.

HPLC analysis: The chromatographic analysis was performed on HPLC system (Thermo Scientific Spectra SYSTEM) equipped with UV2000 and FL3000 detectors. All-trans-retinol, ergocalciferol, cholecalciferol, α -tocopherol, β -carotene and total cholesterol were determined simultaneously using HPLC/UV/FL system equipped with RP analytical column Synergi 4µ Hydro-RP 80A pore 250 x 4.6 mm, through a mobile phase 75:20:5 = acetonitrile : methanol : 2-propanol (ACN:MeOH:iPrOH), at 1.1 mL/min. Detection of ergocalciferol ($\lambda = 265$ nm), cholecalciferol ($\lambda = 265$ nm), β -carotene ($\lambda = 450$ nm) and cholesterol ($\lambda = 208$ nm) was performed by UV detector. Concentrations of all-trans-retinol (at $\lambda_{ex} = 334$ nm and $\lambda_{em} = 460$ nm) and α -tocopherol (at $\lambda_{ex} = 288$ nm and $\lambda_{em} = 332$ nm) were measured by fluorescence detection.

FA analysis

Lipid extraction: Portions of raw homogenate (5.000±0.001 g) were extracted according to Blich and Dyer (1959) procedure [6]. Total lipid (TL) content was determined for each sample and the results were expressed as g per 100g wet weight (g.100g⁻¹ww). The total lipid content was determined gravimetrically.

Preparation of FA methyl esters: The dry residue of the chloroform fraction was methylated by base-catalyzed transmethylation using 2M KOH in methanol and *n*-hexane [7]. After centrifugation (3500 rps), the hexane layer was separated and analyzed by GC-MS.

GS-MS analysis: The hexane layer was separated and analysed by GC-MS. Thermo Scientific FOCUS Gas Chromatograph, with Polaris Q MS detector coupled with TR-5 MS capillary column, (30 m, 0.25 mm i.d.) was used. For peaks identification mass spectra (ratio m/z) of FAME mix standard (SUPELCO 37 F.A.M.E. Mix C4 - C24) and internal Data Base (Thermo Sciences Mass Library, USA) was used. Results are expressed as a percentage of each FA with respect to the total FAs [8]. All chemicals used were of analytical and GC grade.

Statistical analysis

The results were expressed as a mean and standard deviation (mean ± SD). The obtained data was analyzed using Graph Pad Prism 6.0 software. An unpaired t-test statistical analysis was applied to estimate the differences between the analyzed samples. The comparison was made for total lipids, fat soluble vitamins, cholesterol and β -carotene and individual FA and FA groups. The differences were considered significant at $p < 0.05$.

RESULTS AND DISCUSSION

Fat soluble vitamins, β -carotene and cholesterol contents

The amounts of the analyzed compounds are presented in Table 1 as microgram per 100 grams wet weight (mg.100g⁻¹ww). The results are expressed as average and standard deviation (mean ± SD).

Results for the different analytes in skin and muscle of the two groups are close. Data for all vitamins and cholesterol, presented in Table 1 showed similar correlation. In all cases the three vitamins and cholesterol contents in Rainbow trout group II samples were higher than Rainbow trout group I. β -carotene was detected neither in the skin nor in the muscle tissue of the samples in the first group. This fact can be attributed to feed composition. García-Chavarría and Lara-Flores considered that carotenoids play a major role in commercial aquaculture [9]. They are often added in food pellets, which reflect the skin and tissue coloration.

Other fat soluble analytes found in the two groups are vitamin A and D₃. Their amounts in skin and muscle of fish in group II were several times higher ($p < 0.05$), than group I. Vitamin E ($p < 0.01$ for skin, $p > 0.05$ muscle) and cholesterol ($p < 0.05$) amounts were also higher in group II, but the results are close. Cholesterol content in both groups is low. According to Ordinance № 23/19.07.2005 consuming less than 300 mg per day of cholesterol could help maintain normal blood cholesterol levels and prevent future cardiovascular disease. This characterizes the specimens from both grow stages as very suitable for healthy diet with about three times lower cholesterol amount compared to RDA [10].

All analyzed samples are very good sources of the three fat soluble vitamins (A, D₃ and E). Vitamin A and D₃ contents in skin and muscle of Rainbow trout in group I are close to the recommendations for daily intake of those vitamins in Bulgaria [10]. While results for the corresponding vitamins in group II were several times higher than RDA.

Table 1. Fat soluble analytes contents in raw skin and muscle of rainbow trout in two growth stages (mg.100g⁻¹ ww)

	Rainbow trout I*		Rainbow trout II*	
	Skin	Muscle	Skin	Muscle
Vitamin A	0.43±0.019	0.31±0.017	1.62±0.24***	1.26±0.21***
Vitamin D₃	0.07±0.001	0.06±0.001	0.20±0.011**	0.26±0.015**
Vitamin E	7.89±0.63	28.22±1.21	16.80±1.03**	30.42±2.72
β-carotene	nd	nd	0.24±0.04	0.10±0.003
Cholesterol	66.65±7.92	46.13±4.81	75.65±6.25	47.32±4.30

* - Rainbow trout I - with weigh 300-400 g; Rainbow trout II - with weigh 700-900 g

*** p<0.001, ** p<0.01 and * p<0.05 groups I vs II

Data in Table 1 is in good agreement with those published by other authors and our previous studies [11]. Harlioğlu presented close amount of investigated compounds in rainbow trout fillet - 12.4 µg·100 g⁻¹ ww for vitamin A, 13.2 µg·100 g⁻¹ ww for vitamin D₃, 714 µg·100 g⁻¹ ww for vitamin E and 40.2 mg·100 g⁻¹ ww cholesterol [2].

Total lipid and fatty acid composition

Table 2 presents information for total lipid (TL, g.100⁻¹g wet weight) content and FA profile as well as the levels of saturated (SFA), monounsaturated (MUFA) and polyunsaturated (PUFA) fatty acids in the skin and muscle of the trout meat. PUFA/SFA and ω-6/ω-3 ratios, EPA and DHA content (g.100⁻¹g wet weight) are shown too. Both trout groups presented 70.9% higher TL (group I) and 159% (group II) in the skin compared to muscle (p<0.001). One possible reason could be the inclusion of subcutaneous adipose tissue fixed to the skin in the analyzed samples. Our findings shown that fat depot is not evenly distributed in edible parts of analyzed trout. With increasing fish weight presented results showed proportionally increase of TL content mainly in skin, whereas in muscle the inverse correlation was observed. Rebole *et al.* (2015) reported similar results for skin TL in farmed trout from Granada, Spain [3]. A common practice to lower fat intake (especially SFA) is to remove the skin, due to its higher TL content. However, in this study it was found that fish skin lipids contained higher unsaturated FA than SFA (Table 2).

Presented results showed similar FA distribution in muscle: PUFA>SFA>MUFA and in skin tissue: MUFA>SFA>PUFA, despite fish weight. Most significant differences between the muscle and skin were found for MUFA – 4.2 times (group I) and 2.2 times (group II) higher in skin compare to muscle. The content of individual FAs varied between skin and muscle samples in both analyzed groups. The major SFAs in muscle and skin were C16:0 and

C18:0 acids, but C16:0 content was significantly higher in the skin (p<0.001) than in muscle. In this study oleic (C18:1 ω-9) and linoleic acid (C18:2 ω-6) were found to be the dominant FAs in the skin in both fish groups. One possible reason for relatively higher levels of C18:2 ω-6 could be due to the necessity of fish to retain some degree of skin permeability - epidermal cell membranes should be more fluid to facilitate transport. Moreover, the predominance of C18:2 ω-6 in the farmed fish lipids has been attributed to the commercial diet where the major FA is C18:2 ω-6 [2]. These results agree with those reported by Rebole *et al.*, (2015), who observed a similar order of the major unsaturated FA in the muscle and skin of farmed rainbow trout from Spain [3]. In contrast, other researchers found that C22:6 ω-3 followed by C16:0 were the predominant FA in the skin of wild *Sardinella* species from Senegalese coast [12]. This is probably due to the use of different lipid sources in the diet; however FA composition of the farmed fish does not only depend on the feed, but on the fish metabolism as well. As a whole, the growth stage affects significantly (p > 0.05) C22:6 ω-3 (DHA) content in the fillet parts. In addition a significant interaction (p<0.001) between fillet part vs growth stage was detected. An increase in the muscle and a decrease in the skin levels of DHA with increased fish weight were observed. Rebole *et al.*, (2015) supposed that a possible reason is the greater amount of triacylglycerol-rich storage lipids deposited mainly in the skin. European Food Safety Authority (EFSA, 2012) recommends daily intake (RDI) of 0.500 g EPA + DHA [13]. The percentage values of these FAs were recalculated to g.100g⁻¹ edible tissue in order to evaluate the nutrition lipid quality based of ω-3 PUFAs content. A 100 g of edible filet portion from both analysed groups contains average 0.660-0.700 g of EPA+DHA ω-3 PUFA (Table 2) and provides 135% of EPA+DHA RDI.

Table 2. Total lipid and fatty acid composition of total lipids in the skin and muscle from farmed rainbow trout

	Rainbow trout I ⁺		Rainbow trout II ⁺	
	Skin	Muscle	Skin	Muscle
<i>Total lipid (g.100⁻¹g)</i>	5.64±0.40	3.3±0.30	6.37±0.50	2.46±0.20
<i>FA, % of total FA</i>				
6:0	0.80±0.07	0.70±0.05	0.70±0.06	0.40±0.03
8:0	1.00±0.08	0.53±0.02	0.90±0.05	0.80±0.04
10:0	1.30±0.10	0.70±0.03	0.90±0.06	0.74±0.03
12:0	1.70±0.15	0.93±0.05	1.30±0.11	1.50±0.15
14:0	2.10±0.22	1.00±0.07	1.87±0.20	1.75±0.12
16:0	22.00±1.10	20.00±1.00	23.40±1.25	17.52±0.80 ^{***}
18:0	5.55±0.40	7.50±0.60 ^{**}	7.30±0.55	3.40±0.30 ^{***}
20:0	1.00±0.07	0.25±0.01	0.60±0.03	0.50±0.01
21:0	0.15±0.01	0.10±0.01	0.20±0.01	0.10±0.01
22:0	0.60±0.02	0.20±0.01	0.70±0.03	0.30±0.02
23:0	Nd	0.15±0.01	0.10±0.01	0.34±0.02
24:0	0.55±0.02	0.30±0.02	0.45±0.02	0.22±0.01
SFA	36.65±2.50	32.38±2.20	38.50±2.40	27.57±2.00^{***}
14:1ω-5	0.45±0.02	0.60±0.03	1.05±0.08	1.00±0.06
16:1ω-7	3.95±0.25	2.95±0.20	3.00±0.32	1.60±0.13 ^{**}
18:1ω-9	31.10±2.50	3.50±0.30 ^{***}	34.00±2.40	14.54±1.05 ^{***}
22:1ω-11	1.16±0.08	1.10±0.07	0.25±0.01	0.26±0.02
24:1ω-9	1.00±0.06	0.65±0.03	0.80±0.02	0.50±0.01
MUFA	37.69±2.20	8.85±0.55^{***}	39.10±2.60	17.90±1.55^{***}
18:3ω-6	0.90±0.04	1.80±0.20	1.20±0.07	1.00±0.08
18:3ω-3	2.90±0.25	3.80±0.25 ^{**}	nd	2.72±0.10 ^{***}
18:2ω-6	12.50±1.10	20.25±1.55 ^{***}	13.73±0.30	14.45±0.55 [*]
20:5ω-3	1.00±0.04	7.95±0.50	5.20±0.25	4.70±0.20
20:4ω-6	0.70±0.02	3.90±0.28 ^{***}	Nd	4.36±0.15 ^{***}
20:3ω-6	2.00±0.07	2.50±0.20	Nd	1.45±0.05
20:3ω-3	0.50±0.01	2.00±0.15	0.20±0.01	0.22±0.01
20:2ω-6	0.40±0.01	0.70±0.06	Nd	0.75±0.02
22:6ω-3	4.00±0.30	14.87±0.95 ^{***}	1.45±0.06	24.08±2.05 ^{***}
22:2ω-6	0.80±0.02	1.00±0.08	0.60±0.02	0.80±0.05
PUFA	25.70±1.70	58.77±2.50^{***}	22.38±1.65	54.53±2.45^{***}
ω-3	8.40±0.55	28.62±2.10 ^{***}	8.65±0.60	31.72±2.60 ^{***}
ω-6	17.30±1.10	30.15±2.50 ^{***}	15.53±1.50	22.81±1.70 ^{***}
ω-6/ω-3	2.06±0.15	1.05±0.07	1.79±0.08	0.72±0.03
PUFA/SFA	0.70±0.03	1.82±0.10	0.58±0.02	1.98±0.15
EPA	0.055±0.002	0.238±0.020 ^{***}	0.320±0.022	0.110±0.005 ^{***}
DHA	0.220±0.015	0.455±0.030 ^{***}	0.090±0.004	0.550±0.050 ^{***}

⁺ - Rainbow trout I - with weigh 300-400 g; Rainbow trout II - with weigh 700-900 g

^{***} p<0.001, ^{**} p<0.01 and ^{*} p<0.05 groups I vs II

PUFA/SFA and ω -3/ ω -6 ratios are indices widely used to evaluate the nutritional quality of edible fat for human consumption. According to Department of Health (1994), PUFA/SFA ratio in human diets should be above 0.45 and ω -6/ ω -3 ratio should not exceed 4.0 [13]. In this study ω -6/ ω -3 ratio was between 2 – 2.5 times higher in the skin than in the muscle in both groups, due to a greater content of C18:2 ω -6 and smaller proportion of C22:6 ω -3 in the lipid fraction of the skin. In addition our results showed differences in the PUFA/SFA ratio. It was 2.6 – 3.4 times higher in the muscle than PUFA/SFA ratio in the skin tissue for both fish groups. In any case, ω -6/ ω -3 PUFA and PUFA/SFA ratios are within recommended levels for a healthy diet. Moreover, the information presented in this investigation confirms that the public perception that fish skin is healthier is justified.

CONCLUSIONS

In conclusion, despite its weight, rainbow trout was characterized by high contents fat soluble vitamins and low content of cholesterol in the skin and in the muscle tissue. On the other hand, muscle and skin exhibited different TL and fatty acid composition. Muscle tissue contained significantly higher levels of unsaturated ω -3 PUFA and lower levels of lipids than the skin. Based on the PUFA/SFA and ω -6/ ω -3 PUFA ratios, the nutritional quality of the muscle is better than that of the skin. A 100 g of fillet portion from both analysed groups contains average 0.660-0.700 g of EPA+DHA ω -3 PUFA and provides over than 130% of RDI. In any rate, it could be summarized that farmed rainbow trout filets, with or without the skin are rich sources of analysed fat soluble nutrients. Moreover, the assessment of the quality

and quantity of fat soluble components of commercially important trout species could lead to raising consumers' awareness and help them make better informed choices when choosing healthier food.

REFERENCES

1. L. Hadjinikolova and T. Hubenova, *Bulg.J. Agric. Sci.*, **21**, 186 (2015)
2. A. G. Harlioğlu, *Pakistan J. Zool.*, **44**, 1013 (2012)
3. A. Rebolé, S. Velasco, M.L. Rodríguez, J. Treviño, C. Alzueta, J.L. Tejedorb, L.T. Ortiza, *Food Chem.*, **174**, 614 (2015)
4. M. Oz, S. Dikel, *Food Sci. Technol.*, **3**, 56 (2015)
5. D. Dobrev, B. Galunska, M. Stancheva, *Scripta Scientifica Medica*, **43**, 276, (2011)
6. E. Bligh and W.J. Dyer, *Canad. J. Biochem. Phys.*, **37**, 913 (1959)
7. BDS EN ISO 5509:2000: Animal and vegetable fats and oils - Preparation of methyl esters of fatty acids.
8. BDS EN ISO 5508:2004: Animal and vegetable fats and oils. Analysis by gas chromatography of methyl esters of fatty acids.
9. M. García-Chavarría, M. Lara-Flores, *Research J. Fisheries & Hydrobiol.*, **8**, 38 (2013)
10. Ordinance № 23 / 19.07.2005 on the physiological feeding of population http://bg.wikipedia.org/wiki/Физиологични_норми_за_хранене#cite_note-echo-9
11. M. Stancheva, D. Dobrev, A. Merdzhanova, B. Galunska, *Scientific Papers, Plovdiv University „Paisii Hilendarski“ – Bulgaria, Chemistry*, **37**, 117 (2010)
12. J. Njinkoue, G. Barnathan, J. Miralles, E. Gaydou, A. Samb., *Comp. Biochem. Physiol., Part B*, **131**, 395 (2002)
13. EFSA. Scientific Opinion on the Tolerable Upper Intake Level of eicosapentaenoic acid (EPA), docosahexaenoic acid (DHA) and docosapentaenoic acid (DPA). *EFSA Journal*, **10**, 2815, p.48 (2012).

МАСНО-РАЗТВОРИМИ НУТРИЕНТИ И МАСНИ КИСЕЛИНИ В КОЖА И ФИЛЕ НА КУЛТИВИРАНА ДЪГОВА ПЪСТЪРВА

Д.А. Добрева, А. Мерджанова и Л. Македонски

Катедра по химия, Факултет по фармация, МУ-Варна, 9000 Варна, България

Постъпила на 11 ноември 2016 г.; приета на 21 декември 2016 г.

(Резюме)

Представеното изследване сравнява съдържанието на мастноразтворими компоненти в мускулната тъкан и кожата на дъгова пъстърва (*Oncorhynchus mykiss* W.), предмет на аквакултура. Екземплярите, пробонабирани в две групи според теглото им, са закупени от рибни търговски обекти във Варна. Установена е липсата на информация относно разликите при диетичния внос на мастноразтворими биологично активни вещества чрез консумацията на филета от пъстърва – с и без кожата. Витамини А, D₃ и Е, β-каротен и холестерол са съвместно количествено определени чрез използване на ВЕТХ система с UV и FL детектори. Общите липиди са извлечени от рибната матрица по метода на Блайт и Даер. Анализът на метиловите естери на мастните киселини беше извършен чрез използване на ГХ/МД. Данните от извършените анализи показват, че общото липидно съдържание, количеството на витамин Е и холестерол, както и това на наситените мастни киселини са значително по-високи в кожата, отколкото в мускулната тъкан. Противоположно – с по-високо в мускулната тъкан съдържание се представят витамини А и D₃, ейкозапентанова киселина (C20:5 ω-3) и докозахексанова киселина (C22:6 ω-3).

Ключови думи: *Oncorhynchus mykiss*, витамини, каротеноиди, холестерол, ПНМК

Constituent composition of *Chenopodium botrys* essential oil

D. Bojilov, S. Dagnon*, I. Ivanov

Faculty of Chemistry, Department of Organic Chemistry,
University of Plovdiv "Paisii Hilendarski", 24 Tzar Assen Str., 4000 Plovdiv, Bulgaria

Received November 11, 2016; Revised January 1, 2017

The volatile oils of *Chenopodium botrys* L. collected in six locations throughout Southern Bulgaria were obtained by hydrodistillation and analyzed by GC/FID and GC/MS. In the essential oils from the aerial parts of *C. botrys* fifty three components were identified. The chemical composition of investigated oils differed only quantitatively. Most of the constituents were oxygenated sesquiterpenes (69.08%-84.83%). The dominant components in the oils were elemol acetate (14.01%-26.32%), elemol (10.89%-18.15%), α -eudesmol (7.49%-17.84%), juniper camphor (3.58%-11.49%), α -eudesmol acetate (5.28%-6.90%), α -chenopodiol (4.04%-6.40%). For first time in the essential oils of *C. botrys* γ -costol was identified.

Key words: *Chenopodium botrys*, essential oil, elemol, elemol acetate, γ -costol

INTRODUCTION

Chenopodium botrys L. is widespread throughout Europe, West Asia and North America. The plant has been used traditionally for medicinal purposes. The essential oils isolated from aerial parts of *C. botrys* collected from Southern Serbia and Greece exhibited significant bactericidal and fungicidal activity against selected strains of microorganisms, viz. *Staphylococcus aureus*, *Bacillus subtilis*, *Escherichia coli*, *Pseudomonas aeruginosa*, *Aspergillus niger*, *Candida albicans*, *Sarcina lutea*, *Klebsiella pneumoniae*, *Salmonella enteridis* and *Shigella flexneri* [1, 2]. The *C. botrys* essential oil from Saudi Arabia possessed antimicrobial activity [3]. The alcoholic and aqueous extracts of *C. botrys* from Iran were found to have in-vitro giardicidal effect against *Giardia lamblia* cysts [4]. The oil from the aerial part of *C. botrys* collected from suburb of Kashan, Iran exhibited strong antimicrobial activity against *Staphylococcus saprophyticus* followed by *Klebsiella pneumoniae*, *Bacillus cereus*, *Staphylococcus epidermidis*, *Streptococcus mutans*, *Listeria monocytogenes* and *Salmonella typhimurium*. The oil had slight effect on *Candida albicans* and showed inhibitory effect on *Aspergillus* species and *Bacillus subtilis* [5].

The chemical composition of the essential oils of *C. botrys* varied in amount and composition according to the environmental conditions. *C. botrys* of different origins yielded 0.08-2% essential oil [6]. According to several studies, the essential oils were rich in monoterpenes [7, 8] and sesquiterpenes [2, 3, 5, 9, 10]. De Pascuale *et al*

reported the isolation of sesquiterpenes of eudesmane and guaiane type from methanol extracts of *C. botrys* [11].

The sesquiterpenes α - and β -eudesmol were found to be the major compounds in essential oil from Saudi Arabia [3]. The main components of *C. botrys* oil from North America were α - and β -chenopodiol (36%), eudesma-3,11-dien-6 α -ol (9.4%), botrydiol (9.0%), elemol (6.5%), elemol acetate (5.5%), γ -eudesmol (5.4%), and α - and β -eudesmol (3.7%); guaia-3,9-dien-11-ol (7.4%) [10]. In the oil from Greece the main components were elemol acetate (16.3%), elemol (14.1%), botrydiol (11.1%), α -chenopodiol (9.5%) and selina-3,11-dien-6 α -ol (6.1 %) [2]. Juniper camphor (16.5% and 25.7%), elemol (14.3% and 13.4%) and α -cadinol (8.2% and 11.6%), were the main compounds in the oils from two different locations in Iran [9]. *C. botrys* essential oil from Kashan, Iran contained 2,3-dehydro-4-oxo- β -ionone (22.4%), (+)-7-*epi*-amiteol (11.5%), elemol (7.4%), α -cadinol (7.0%) and *tau*-cadinol (7.0%) [5]. Major components of the essential oil of *C. botrys* collected in North of Iran were γ -terpineol (52.8%), p-cymene (19.0%) and *iso*-ascaridole (7.0%) [6]. Ascaridole (7.5% and 40%) was identified in *C. botrys* oils collected in Spain and Slovakia, respectively [8]. In Israel (Negev Desert) α -terpinene (21.4%), p-cymene (15.2%), *E*-caryophyllene (6.5%), limonene (6.1%) were identified as major components [8]. 2-(4 α .8-dimethyl-1.2.3.4.4 α .5.6.7-octahydro-naphthalen-2-yl)-prop-2-en-1-ol (27.9%) was the main compound in the essential oil of *C. botrys*, growing in Turkey [12].

In the present paper, the chemical composition

* To whom all correspondence should be sent.

E-mail: dagnon@uni-plovdiv.bg

of the oils obtained from the aerial parts of *C. botrys* harvested in six locations throughout Southern Bulgaria was examined.

EXPERIMENTAL

Plant material

The specimens of *C. botrys* were collected in six locations of Southern Bulgaria: Balkan Mountain (Shipka town), Plovdiv, Kaloyanovo, Rogosh, Ustina and Rodopa Mountain (Krichim town). The plants were collected in August, consecutively in 2012 and 2013 years, at full flowering stage. The plant material was identified by means of voucher specimens (05269 and 05271) by Assoc. Prof. Koicho Koev PhD (Faculty of Biology, Plovdiv University, Bulgaria). The voucher specimens were deposited in the herbarium of Agricultural University - Plovdiv. The aerial parts of the plants were dried at room temperature in the absence of direct sunlight. The dry material was further ground to powder and was packed into multilayer paper bags, and stored in a dark room at ambient temperature.

Isolation of essential oils

The dry powdered plant material (100 g) was subjected to hydrodistillation through a Clevenger-type apparatus for 4 h. The oil was dried on anhydrous Na₂SO₄ and kept in a cold and dark place until use.

GC-FID analysis

The Agilent 7890 GC-FID (Agilent Technologies, CA, USA) was equipped with capillary column HP-5 Agilent Technologies, CA, USA, 30 m x 0.32 mm i.d., film thickness 0.25 µm was used. The injector and detector temperatures were set at 200°C and 300°C, respectively. The column was set at 50°C for 5 min and the temperature was increased with 5°C/min to 180°C, from 180°C with 7°C/min to 230°C. The carrier gas was nitrogen at a flow rate of 1 ml/min. The split ratio was 100:1 and the injection volume was 0.2 µl.

The quantitative analysis (expressed in percent) was calculated by peak area normalization.

GC/MS analysis

GC/MS analysis was carried out using Agilent 7890 GC system combined with Agilent 5975 Inert MSD detector (quadrupole) with electron impact ionization (70 eV). A HP-5-MS column (30 m x

0.25 mm i.d., film thickness 0.25 µm) Agilent Technologies, CA, USA was used. The column was set at the same temperature program used in the GC-FID analysis. Scan time and mass range were 2 s and 50–550 m/z, respectively. The carrier gas was helium at a flow rate 1 ml/min. Samples were injected with a split ratio of 70:1 and 100:1 and the injection volume was 0.2 µl.

Identification of the compounds

Identification of the volatile constituents was established by comparison of recorded mass spectra with those of a computer library NIST 08 database (National Institute of Standardization and Technology, Gaithersburg, MD, USA) and with those of authentic compounds. Peaks identity was confirmed by referring to Kovats index data generated from a series of alkanes (relative to C₆–C₂₂ alkanes) and with the data published in the literature [13].

RESULTS AND DISCUSSION

The essential oils obtained from aerial parts of *C. botrys* were analyzed by GC/FID and GC/MS. Representative chromatographic profile of *C. botrys* essential oils is shown on Figure 1. The GC conditions led to a good separation of all components of the oils (Figure 1).

The chemical composition of investigated oils differed only quantitatively. The yield of oils of *C. botrys* from six different locations of Southern Bulgaria and two consecutive harvests ranged from 0.33% to 1.3% (v/w on dry weight basis) (Table 1).

These data point to lower yield, comparing to the yield of essential oils obtained in Greece (1.79%) [2] and Saudi Arabia (2%) [3]. In the essential oils from *C. botrys* fifty-three compounds were identified representing 86.24% to 100% of the total oil. Among these, 69.08%–84.83% belong to the class of oxygenated sesquiterpenes. The high content of oxygenated sesquiterpenes is consistent with the data on the oil composition from North America, Greece and Iran [2, 9, 10].

The main components (%) of the *C. botrys* oils from Southern Bulgaria were elemol acetate (14.01–26.32), elemol (10.89–18.15), α -eudesmol (7.49–17.84), juniper camphor (3.58–11.49), α -eudesmol acetate (5.28–6.90) and α -chenopodiol (4.04–6.40) (Table 1, Figure 2).

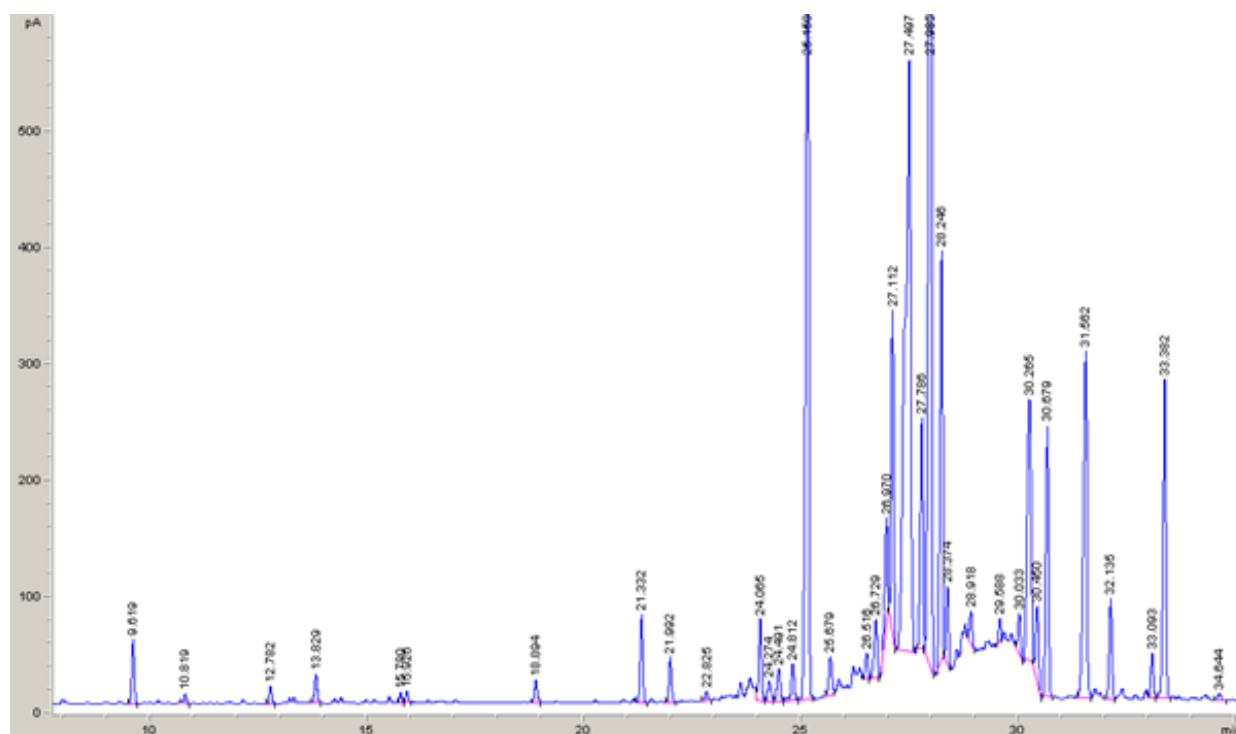


Figure 1. Representative chromatographic profile of essential oils of *C. botrys*.

Table 1. Chemical composition of essential oils of *C. botrys*. Total number of components, content obtained by normalization [%], yield [% v/w]. RI is retention index relative to C₆ – C₂₂ n-alkanes on the HP-5MS column, MS-comparison of mass spectra with those listed in the NIST 08, tr = traces (< 0.1%).

Compounds	RI	<i>C. botrys</i> from different locations of Bulgaria, %					
		Sh-12	K-12	Kr-12	Pl-13	U-13	R-13
Bornylene	893	tr	tr	tr	tr	tr	tr
α -Pinene	908	tr	tr	tr	tr	tr	tr
β -Pinene	925	tr	tr	tr	tr	tr	tr
α -Fenchene	939	tr	tr	tr	tr	tr	tr
Camphene	941	tr	tr	tr	tr	tr	0.64
2,3-Dehydro-1,8-cineole	988	tr	tr	tr	tr	tr	tr
Myrcene	990	0.83	2.51	8.49	0.14	0.52	7.89
α -Limonene	1030	0.11	0.34	tr	tr	tr	0.83
γ -Terpinene	1062	tr	tr	tr	tr	tr	tr
(Z)-Sabinene hydrate	1072	tr	tr	tr	tr	tr	tr
Fenchone	1091	0.23	0.42	tr	0.15	0.23	1.12
<i>exo</i> -Fenchol	1117	tr	tr	tr	tr	tr	tr
<i>cis</i> - β -Terpineol	1126	0.43	0.77	tr	0.47	0.60	1.72
Terpinol hydrate	1139	tr	tr	tr	tr	tr	tr
p-Menth-2-en-1-ol	1145	tr	tr	tr	tr	tr	tr
<i>trans</i> -dehydro- α -Terpineol	1148	tr	tr	tr	tr	tr	tr
Borneol	1169	tr	tr	tr	tr	tr	tr
Terpinen-4-ol	1180	0.12	0.20	tr	tr	tr	tr
3,9-Epoxy-1-p-menthene	1187	tr	tr	tr	tr	tr	tr
α -Terpineol	1193	0.14	0.21	tr	tr	0.15	tr
<i>cis</i> -Piperitol	1198	tr	tr	tr	tr	tr	tr

Table 1. *Continued.*

Compounds	RI	<i>C. botrys</i> from different locations of Bulgaria, %					
		Sh-12	K-12	Kr-12	Pl-13	U-13	R-13
p-Menth-1-en-9-ol	1311	0.33	0.43	7.11	0.15	0.19	tr
α -Copaene	1380	tr	tr	tr	tr	tr	tr
β -Elemene	1395	1.20	1.16	5.09	0.88	1.34	1.39
α -Gurjunene	1414	tr	tr	tr	tr	tr	tr
β -Caryophyllene	1425	0.63	1.37	4.70	0.78	0.98	1.27
α -Humulene	1460	0.14	0.31	tr	0.18	0.20	tr
Z-Caryophyllene	1475	tr	tr	tr	tr	tr	tr
Germacrene D	1488	tr	tr	tr	tr	tr	tr
β -Selinene	1494	0.21	0.23	tr	0.14	0.14	tr
α -Selinene	1503	0.26	0.31	tr	0.22	0.28	tr
α -Muurolene	1508	tr	tr	tr	tr	tr	tr
Germacrene A	1515	1.02	2.59	5.54	2.17	2.47	2.82
γ -Cadinene	1521	0.32	0.41	tr	0.28	0.40	tr
δ -Cadinene	1530	0.52	0.59	tr	0.61	0.77	0.74
α -Copaen-11-ol	1545	0.51	0.42	tr	0.26	0.32	tr
α -Calacorene	1551	tr	tr	tr	tr	tr	tr
Elemol	1560	13.53	10.89	18.15	12.95	14.80	15.15
Caryophyllene oxide	1583	0.60	1.00	tr	0.97	0.88	1.07
γ -Eudesmol	1644	1.76	1.30	tr	1.00	1.12	1.00
γ -Costol	1653	4.22	4.35	tr	4.76	2.94	2.56
α -Eudesmol	1671	17.56	17.84	7.49	14.92	13.10	12.95
Elemol acetate	1693	16.77	14.01	26.32	18.95	19.25	14.42
Juniper camphor	1713	6.05	3.92	11.49	3.58	5.27	4.72
Guaiol acetate	1735	0.45	0.87	tr	0.76	1.49	1.16
Hinesol acetate	1787	0.57	0.65	tr	0.70	0.68	0.60
α -Eudesmol acetate	1799	5.58	6.07	5.63	6.90	5.70	5.28
β -Chenopodiol	1830	4.07	2.65	tr	3.09	3.52	2.45
α -Chenopodiol	1876	6.34	4.04	tr	6.00	6.40	4.73
β -Chenopodiol-6-acetate	1904	1.43	1.47	tr	1.40	1.25	1.05
Acetoxyeudesman-4- α -ol-11	1957	0.61	0.60	tr	0.77	0.67	0.66
α -Chenopodiol-6-acetate	1977	4.78	4.31	tr	5.72	4.51	3.89
n-Heneicosane	2087	tr	tr	tr	tr	tr	tr
Total compounds		53	53	53	53	53	53
Yield, % (v/w)		0.6	0.6	0.33	0.68	1	1.3
Total identified, %		91.32	86.24	100.00	88.9	90.17	90.11
Monoterpenes, %		0.94	2.85	8.49	0.14	0.52	9.36
Oxygenated monoterpenes, %		1.25	2.03	7.11	0.77	1.17	2.84
Sesquiterpenes, %		4.3	6.97	15.33	5.26	6.58	6.22
Oxygenated sesquiterpenes, %		84.83	74.39	69.08	82.73	81.9	71.69

Sh-Shipka, K-Kaloyanovo, Kr-Krichim, Pl-Plovdiv, U-Ustina, R-Rogosh
12 and 13 - Harvest in two consecutive years 2012 and 2013, respectively

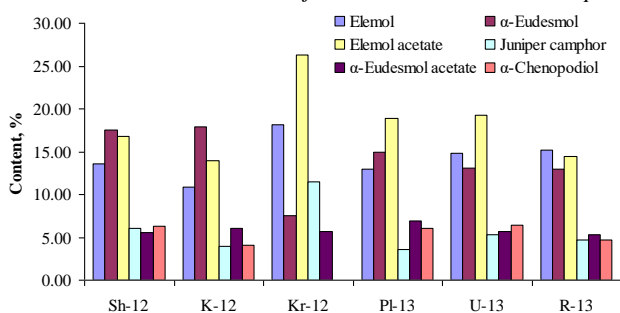


Figure 2. Content (%) of the main components in *C. botrys* essential oils

This composition of oils is close to the data reported for the essential oil from Greece [2]. Elemol acetate was not found in the essential oil from Iran [5,9]. Thus, there are significant differences in the qualitative composition of the essential oil of *C. botrys* from different geographical locations. The essential oil from Greece and North America contained botridiol [2,10], from Iran 2,3-dehydro-4-oxo- β -lonone and (+)-7-*epi*-amiteol [5]. These compounds were not found in the investigated essential oils from Southern Bulgaria. In all oils γ -costol was identified, which has not been reported by other authors. The components γ -costol, α - and β -chenopodiol, α - and β -chenopodiol-6-acetate in the oil from Krichim (Kr-12) were in trace amounts (Table 1). Nevertheless, the content of oxygenated sesquiterpenes in this oil is lower than 70%, the content of elemol acetate (26.32%) and elemol (18.15%) is the highest, comparing to others (Figure 2). Carroll *et al.* tested oil rich in elemol against mites *Ixodes scapularis* and *Amblyomma americanum* and have found that about 2-4 hours oil repel mites over 50% [14].

CONCLUSION

The chemical composition of essential oils of *C. botrys* from six different locations of Southern Bulgaria in two consecutive harvests differed only quantitatively. The oil is rich in elemol and elemol acetate. For first time in the essential oil of *C. botrys* γ -costol was identified.

Acknowledgment: The financial support from the Fund of Scientific Research of the Plovdiv University, project H115-X Φ -001 is gratefully acknowledged.

REFERENCES

- Z. D. Maksimović, S. Dordević, M. Mraović, *Fitoterapia*, **76**, 112 (2005).
- O. Tzakou, A. Pizzimenti, F. C. Pizzimenti, V. Sdrafkakis, E. M. Galati, *J Essent Oil Res*, **19**, 292 (2007).
- A. M. El-Sayed, M. A. Al-Yahya, M. M. A. Hassan, *Int. J. Crude Drug Res*, **27**, 185 (1989).
- M. Rezaeemanesh, Sh. Shirbazoo, N. Pouryaghoub, *Journal of Torbat Heydariyeh University of Medical Sciences*, **1**, 19 (2013).
- M. Mahboubi, F. G. Bidgoli, N. Farzin, *J Essent Oil-Bearing Plants*, **14**: 498-503 (2011).
- K. Morteza-Semnani, *Pharm Biomed Res*, **1(2)**, 1 (2015).
- N. Mokhtari-Karchegani, L. Amjad, M. Ranjbar, *Advances in Environmental Biology*, **8(24)**, 43 (2014).
- V. Dembitsky, I. Shkrob, L. O. Hanus, *Biomed Pap Med Fac Univ Palacky Olomouc Czech Repub*, **152**, 209 (2008).
- A. Feizbakhsh, S. Sedaghat, M. S. Tehrani, A. Rustaiyan, S. Masoudi, *J Essent Oil Res*, **15**, 193 (2003).
- A. G. Bedrossian, P. S. Beauchamp, B. Bernichi, V. Dev, K. Z. Kitaw, H. Rechtshaffen, A. T. Bottini, H. Hope, *J Essent Oil Res*, **13**, 393 (2001).
- T. J. De Pascual, I. S. Bellido, M. S. González, *Tetrahedron*, **36**, 371 (1980).
- S. Karabörklü, A. Ayvaz, S. Yilmaz, M. Akbulut, *J Econ Entomol*, **104**, 1212 (2011).
- R. P. Adams, Identification of essential oil components by gas chromatography/quadrupole mass spectroscopy, Allured: Carol Stream, IL, 2001.
- J. F. Carroll, G. Paluch, J. Coats, M. Kramer, *Experimental and Applied Acarology*, **51(4)**, 383 (2010).

СЪСТАВ НА ЕТЕРИЧНОТО МАСЛО ОТ *Chenopodium botrys*

Д. Божилов, С. Даньо*, И. Иванов

Пловдивски Университет „Паисий Хилендарски”, Катедра Органична химия,
ул. Цар Асен, 24, 4000 Пловдив

Постъпила на 11 ноември 2016 г.; приета на 1 януари 2017 г.

(Резюме)

Етеричното масло от *Chenopodium botrys* L., събирано от шест района на Южна България, беше получено чрез хидродестилация и анализирано с ГХ/ПИД и ГХ/МС. В етеричните масла от наземната част на *C. botrys* бяха идентифицирани петдесет и три съединения. Химичният състав на изследваните масла се различава само количествено. В състава на маслото преобладават сесквитерпеноиди (69.08%-84.83%). Основните компоненти на етеричното масло от *C. botrys* са елемолацетат (14.01%-26.32%), елемол (10.89%-18.15%), α -еудезмол (7.49%-17.84%), хвойнов камфор (3.58%-11.49%), α -еудезмол ацетат (5.28%-6.90%), α -хеноподиол (4.04%-6.40%). В етеричното масло от *C. botrys* за първи път беше идентифициран γ -костол.

Ключови думи: *Chenopodium botrys*, етерично масло, елемол, елемол ацетат, γ -костол

Purification of lipase from *Aspergillus carbonarius* NRRL369 by ATPS PEG/potassium phosphate

H.N. Panajotova^{1*}, H.N. Strinska¹, V. D. Gandova², V.T. Dobрева³,
B.J. Zhekova¹, G.T. Dobrev¹

¹Department of Biochemistry and Molecular Biology, University of Food Technologies,
26 Maritza Blvd., 4002 Plovdiv, Bulgaria,

²Department of Inorganic Chemistry and Physical Chemistry, University of Food Technologies,
26 Maritza Blvd., 4002 Plovdiv, Bulgaria

³Department of Engineering Ecology, University of Food Technologies,
26 Maritza Blvd., 4002 Plovdiv, Bulgaria

Received November 2, 2016; Revised December 23, 2016

In this research purification of lipase from *Aspergillus carbonarius* NRRL369 by aqueous two-phase system (ATPS) was studied. Binodal curves of PEG 400/potassium phosphate and PEG 4000/potassium phosphate were developed and appropriate concentrations of the two components were chosen for examination of the purification process. For all ATPS some thermodynamic parameters were calculated to describe the process. Purification of lipase by different ATPSs was tested. It was noticed that increasing of molecular weight of PEG leads to increasing of purification factor of lipase. The results revealed that for lipase purification an ATPS 24% PEG4000/15% potassium phosphate was the most suitable. By using this ATPS high purification factor (10.18) and lipase yield (90.68%) were achieved. Addition of NaCl affects lipase purification. Including 6% NaCl in ATPS 24% PEG4000/15% potassium phosphate increases the purification factor from 10.18 to 14.08 and final lipase yield 88.81% was achieved.

Keywords: lipase, purification, aqueous two-phase system, *Asp. carbonarius*

INTRODUCTION

Lipases (triglycerol acyl-hydrolases E.C. 3.1.1.3) are enzymes that catalyze the hydrolysis of water insoluble triglycerides to di and monoacylglycerides, free fatty acids and glycerol. Lipases catalyze also the reverse reactions of esterification and transesterification in organic solvent medium [1-3]. Because of the high number of reactions catalyzed by these enzymes, lipases have widespread application in many industries including organic synthesis, paper manufacturing, oleochemistry, dairy, cosmetics, biosensors, and detergents [4].

The main procedure for lipase production is fermentative process of microbial producers. Fungus are preferred sources for lipase production because the enzyme is extracellular which facilitates the technological scheme [4, 5].

Development of specific methods for lipase purification is important because highly purified enzymes are able to be applied in medicine and analytical chemistry also that gives opportunity the mechanism of action to be studied [6]. The aqueous two-phase system (ATPS) technique is an ideal

method for protein separation and purification, because it is fast and economical. The processes are easy to implement because the clarification, concentration and partial purification of the target product can be carried out in one step [7]. This system, consisting of two liquid phases that are immiscible beyond a critical concentration, has high selectivity and recovery yield of biomolecules. That makes the ATPS possible strategy for purification of a desired protein (including enzymes as lipases) in large-scale. The ATPSs that are currently in use are usually based on, polymer/polymer system (polyethylene glycol (PEG)/dextran), or polymer/salt system (PEG/potassium phosphate). The partition of proteins in the ATPS is influenced by many factors, such as protein properties (e.g. hydrophobicity, molecular size, weight and conformation, net electrical charge), type and concentration of salts, polymer molecular mass and environmental conditions [8].

In the present study, the partitioning behavior of lipase in various PEG/potassium phosphate ATPSs and the feasibility of utilizing these systems for purification of lipase produced from *Aspergillus carbonarius* NRRL369 was investigated.

* To whom all correspondence should be sent.

E-mail: angelovatina84@yahoo.com

EXPERIMENTAL

Microorganism and lipase production

A strain of *Aspergillus carbonarius* NRRL369 from ARS Culture Collection was used for lipase biosynthesis. Storage of the strain and inoculum preparation were accomplished as described by Dobrev *et al.* [9]. Submerged cultivation of the strain was performed in 500-mL Erlenmeyer flasks, containing 50 mL nutrient medium containing (g/L): rapeseed oil 20.0, meat extract 5.6, MgSO₄ 1.0, KH₂PO₄ 4.0 and Tween 80 20.0. After sterilization the medium was inoculated with 5.0 mL inoculum and the strain was grown at 27°C for 64 h with a 180 rpm rotary shaking.

Lipase activity assay

Lipase activity was determined by titrimetry using olive oil emulsion (25 mL of olive oil and 75 mL of 7% Arabic gum in a homogenizer for 2 min). The reaction mixture containing 2 mL of olive oil emulsion, 2 mL of phosphate buffer with pH 6.0, and 1 mL of enzyme was incubated at 35°C for 20 min. The reaction was immediately stopped after the incubation period by the addition of 7 mL acetone : ethanol mixture (1:1 v/v), and the released free fatty acids were titrated with 50 mM NaOH. One unit (U) of lipase activity was defined as the amount that released 1 μmol of fatty acid per min [10].

Protein assay

Protein concentration was measured by the method of Bradford [11].

Phase diagrams and APTS preparation

The binodal curves were estimated using turbidometric titration [12].

All APTS were prepared in 15 mL graduated centrifuge tubes. To study the effects of PEG molecular weight and salt concentration on the partitioning of lipase from the cell-free fermentation broth, different concentrations of PEG (400, 4000) and 40% phosphate salts (K₂HPO₄/KH₂PO₄) were mixed. The tubes were shaken on vortex for 2 min, followed by centrifugation for 20 min at 4000 rpm to assist phase separation.

After phase separation and visual estimation of the top and bottom phases, the volumes of the phases were used to estimate the volume ratio. The samples of the top and bottom phases were carefully withdrawn. Aliquots from each phase were analyzed to determine the enzyme activity and protein concentration [13].

Determination of selectivity, purification factor and yield

The protein partition coefficient (K_p) in the APTS was defined as:

$$K_p = C_{p,t}/C_{p,b} \quad (1)$$

where $C_{p,t}$ and $C_{p,b}$ are the concentrations of protein in the top and bottom phases.

The partition coefficient for lipase activity (K_e) in the APTS was calculated:

$$K_e = A_t/A_b \quad (2)$$

where A_t and A_b are the enzyme activity in the top and bottom phases.

Yield (Y, %) of lipase in the top phase was also calculated:

$$Y\% = \frac{100}{((V_r K_e)^{-1} + 1)} \quad (3)$$

where V_r is the volume ratio of the top phase to the bottom phase (V_t/V_b).

Selectivity (S) was calculated as:

$$S = \frac{K_e}{K_p} = \frac{A_t C_{p,b}}{A_b C_{p,t}} \quad (4)$$

The purification factor in the top phase (PF_{top}) was defined as:

$$PF_{top} = SA_t/SA_i \quad (5)$$

where SA_t and SA_i are the specific activities in the top phase and the crude enzyme, respectively. Also, the specific activity (SA) represents the ratio:

$$SA = \frac{A}{C_p} \quad (6)$$

where A and C_p are the enzyme activity and the total protein [13].

Thermodynamic parameters of APTS

The enthalpy change (ΔH) was calculated by van Hoff's equation (7), free energy of Gibbs change (ΔG) and the entropy change (ΔS) were calculated using classical thermodynamic equations (8, 9) [13]:

$$\ln K_e = -\frac{\Delta H}{r} \times \frac{1}{T} + \frac{\Delta S}{R} \quad (7)$$

$$\Delta G = \Delta H - T\Delta S \quad (8)$$

$$\Delta G = -RT \ln K_e \quad (9)$$

SDS-PAGE electrophoresis

SDS-PAGE was performed in a Cleaver Scientific Ltd; OmniPAGE Electrophoresis System CVS10DSYS, at 20 mA using a method described by Laemmli [14]. The acrylamide gel was prepared as a 15% resolving gel. Protein samples recovered from the top phase were concentrated and precipitated using 10% trichloroacetic acid (TCA) solution, which removed the salts that affect the electrophoresis process. The gel was stained with a

buffer solution consisting of 0.2% (v/v) Coomassie® Brilliant Blue G-250.

RESULTS AND DISCUSSION

Phase diagrams for PEG/potassium phosphate systems

PEG/potassium phosphate APTSs were formed by PEG 400 and PEG 4000 and potassium phosphate. Single phase and two-phase systems were separated by the binodal curves. Two phases

were formed above the binodal curve (Fig.1). As the compositions of ATPS below the binodal curve, the system becomes homogenous. The concentration of PEG and salt solution required for formation of ATPSs decrease, when PEG with high molecular weight (PEG 4000) was used. The concept of stability ratio was applied to select appropriate APTS.

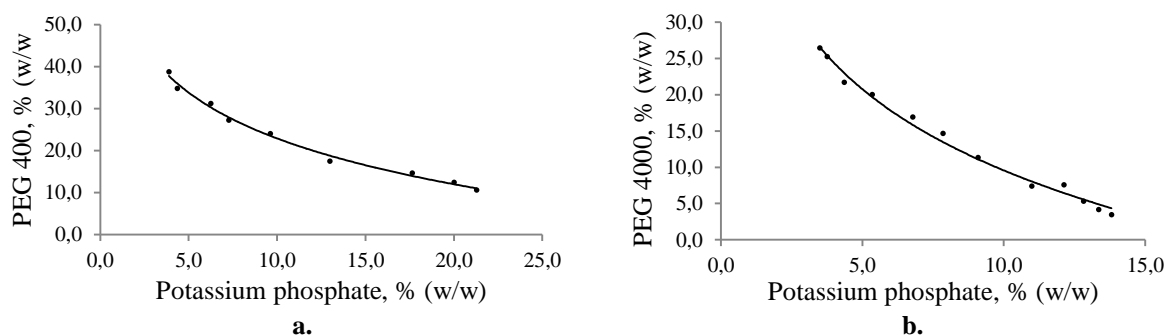


Fig. 1. Phase diagrams for PEG/potassium phosphate ATPSs: a. PEG 400, b. PEG 4000

Table 1. Characteristics of ATPSs PEG 400/potassium phosphate

PEG,%	Potassium phosphate,%	R_v	K_e	K_p	S	ΔG , kJ/mol	ΔH , kJ/mol	$T\Delta S$, kJ/mol
22	15	8.10	133.30	0.14	952.14	-12.12	-22.60	-10.48
24	15	3.58	50.00	0.07	714.29	-9.69	-21.60	-11.86
26	15	3.65	5.00	0.09	55.56	-3.98	-19.10	-15.08
28	15	4.29	4.00	0.06	66.67	-3.43	-18.80	-15.40
22	17	2.80	1.40	0.29	4.83	-0.83	-17.70	-16.87
24	17	2.33	0.37	0.18	2.06	2.33	-16.32	-18.66
26	17	2.20	0.39	0.22	1.77	2.46	-16.27	-18.73
28	17	2.82	2.40	0.19	12.63	-2.16	-18.28	-16.11
22	19	1.83	1.40	0.38	3.68	-0.83	-17.70	-16.87
24	19	1.89	0.62	0.16	3.88	1.18	-16.82	-18.01
26	19	1.93	9.00	0.18	50.00	-5.44	-19.70	-14.26

Table 2. Characteristics of ATPSs PEG 4000/potassium phosphate

PEG%	Potassium phosphate,%	R_v	K_e	K_p	S	ΔG , kJ/mol	ΔH , kJ/mol	$T\Delta S$, kJ/mol
20	15	1.94	10.00	0.10	100.00	-5.70	-19.82	-14.11
22	15	2.44	6.00	0.10	60.00	-3.99	-19.07	-15.08
24	15	1.46	6.67	0.04	166.75	-4.71	-19.38	-14.67
26	15	1.62	5.00	0.04	125.00	-3.99	-19.07	-15.08
20	17	1.37	11.00	2.53	4.35	-5.94	-19.92	-13.97
22	17	1.42	8.33	0.91	9.15	-5.25	-19.62	-14.36
24	17	1.79	26.00	0.59	44.07	-8.07	-20.84	-12.77
26	17	1.97	11.50	0.45	25.56	-6.05	-19.97	-13.91
20	19	1.18	15.00	0.06	250.00	-6.71	-20.25	-13.54
22	19	1.29	6.50	0.07	92.86	-4.64	-19.35	-14.71
24	19	1.43	3.67	0.22	16.68	-3.22	-18.69	-15.46
26	19	1.74	5.00	0.03	166.67	-3.99	-19.07	-15.08

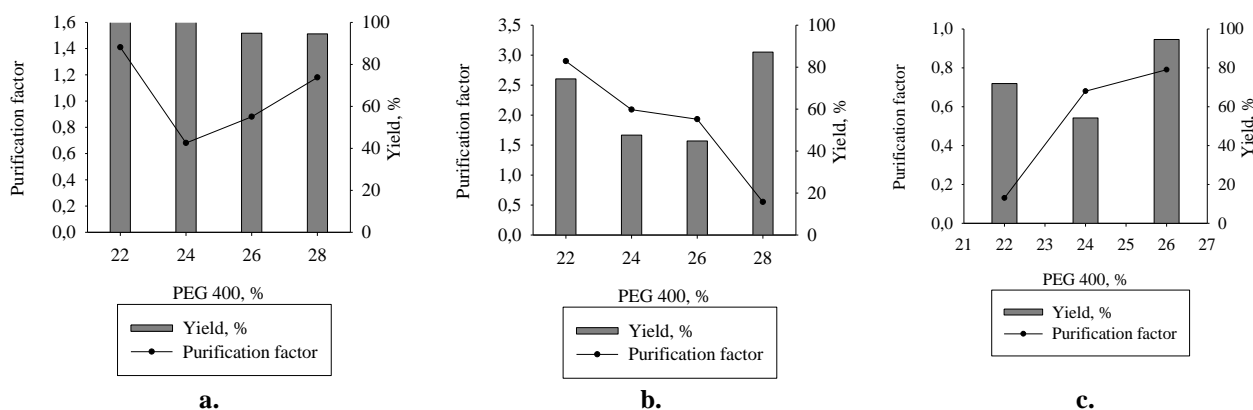


Fig. 2. Lipase purification with ATPS: a. PEG 400/15% potassium phosphate, b. PEG 400/17% potassium phosphate, c. PEG 400/19% potassium phosphate

Purification of lipase using ATPSs

PEG molecular weight can have an important role on the partition behavior of proteins. Enzymes were extracted by the polymer phase because of the polymer–protein interactions, while the accompanying proteins remained in the salt phase. Table 1 shows the main characteristics of lipase purification in PEG 400/potassium phosphate ATPS.

The partition coefficients of the enzyme (K_e) were found to be higher than 1 in most of the systems, indicating that the lipase is accumulated in the top phase. The partition coefficient of the protein (K_p) is around 1 or less than 1, which shows that the most of the protein is in the bottom phase. That is a prerequisite for a high selectivity of the ATPSs and purification of the enzyme.

The volume ratio (R_v) has values higher than 1 which indicates that the top phase has a higher volume than the bottom phase. Increase of the potassium phosphate concentration led to decrease of the R_v .

Changes of some thermodynamic parameters – enthalpy (ΔH), entropy (ΔS) and the free Gibbs energy (ΔG) of the systems were calculated which are characteristics of the stability of the systems. Free Gibbs energy (ΔG) has negative values in most of the cases which indicates that the partition of the enzyme in the top phase is a spontaneous process. Values of the change in the enthalpy (ΔH) and the entropy (ΔS) reveal that the process was exothermic.

On Fig. 2 lipase yield and purification factor in the top phases of ATPSs with different concentrations of PEG 400 and potassium

phosphate are presented. As seen from the chart the highest purification factor was achieved with ATPS 22% PEG 400/17% potassium phosphate. The purification factor was about 3.00 but the yield was lower – about 75%. Highest yield was achieved with 15% potassium phosphate but the purification factor was about 1.00.

Purification of lipase from *Aspergillus carbonarius* NRRL369 with ATPS PEG 4000/potassium phosphate was also examined. As seen from Table 2 in all of the ATPSs with PEG 4000 K_e was higher than 1 and K_p was less than 1. That resulted in high selectivity of the systems (mostly between 25 and 250).

It can also be noticed that the purification factor of the enzyme was much higher when using PEG 4000 (reached 10.18) for ATPSs than when using PEG 400 (up to 2.9). That means that PEG 4000 was more effective for lipase purification than PEG 400. Barbosa *et al.* also confirmed that the increase of the molecular mass of PEG leads to increase of the efficiency of the process [13].

In most cases R_v had values between 1 and 2.

As seen from the thermodynamic parameters lipase partition was spontaneous exothermic process. Negative values of the free Gibbs energy revealed that systems were more stable than the ATPSs with PEG 400.

On Fig. 3 protein purification and lipase yield for some ATPSs PEG 4000/potassium phosphate with different concentrations of the two components are shown. As seen from the chart when PEG 4000 was used most of the ATPSs resulted in a purification factor higher than 1.

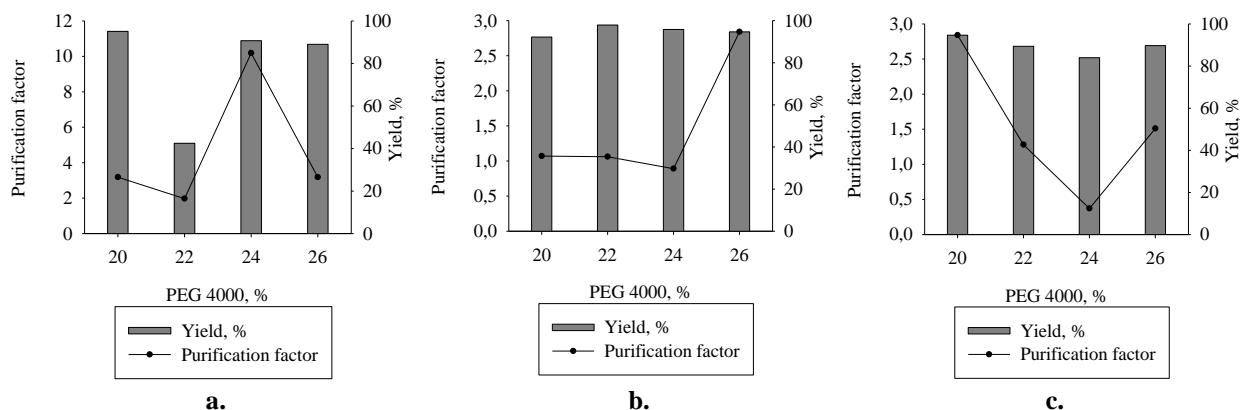


Fig. 3. Lipase purification with ATPS: a. PEG 4000/15% potassium phosphate, b. PEG 4000/17% potassium phosphate, c. PEG 4000/17% potassium phosphate

Table 3. Characteristics of ATPS 24% PEG 4000/15% potassium phosphate/NaCl

NaCl, %	R_v	K_e	K_p	S	ΔG , kJ/mol	ΔH , kJ/mol	$T\Delta S$, kJ/mol
0	1.46	6.67	0.04	166.75	-4.70	-19.82	-15.12
2	1.36	5.00	0.06	83.33	-3.99	-19.07	-15.08
4	1.22	4.00	0.10	40.00	-3.44	-19.39	-15.95
6	1.13	7.00	0.04	175.00	-4.82	-19.07	-14.25

The highest purification factor (10.18) was achieved with ATPS 24% PEG 4000/15% potassium phosphate. In this case lipase yield was also high – 90.68%. Because of that this ATPS was chosen for further experiments.

Effect of neutral salts on lipase partitioning

Addition of neutral salts to aqueous solutions provides one of the versatile means by which the selectivity and the yield of target molecules can be manipulated [15]. Changes in the salt type often produce an electrical potential difference between the two phases caused by the preference of one of the ions for one phase relative to the other. The effects of neutral salt were shown in Table 3 and Fig. 4. The ATPS with composition 24% PEG 4000/15% potassium phosphate was carried out with NaCl salt at concentration 2%, 4%, 6%, 8%.

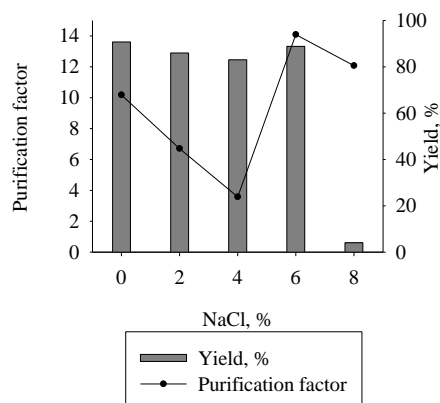


Fig. 4. Lipase purification with ATPS 24% PEG 4000/15% potassium phosphate/NaCl

The results for the influence of NaCl on ATPSs 24% PEG 4000/15% potassium phosphate shows that with the increase of the salt concentration to 6% R_v decreased to 1.13. With this concentration of the NaCl increase of the K_e was achieved while K_p had the same value. Because of that selectivity in the top phase was also increased.

As seen from the negative values of thermodynamic parameters the process was spontaneous and exothermic. Higher negative value of the free Gibbs energy when 6% NaCl was added shows that this system was more stable than the others.

When the concentration of NaCl was higher than 6% that led to crystallization of the salts and inconclusive results.

As seen from Fig. 4 with the increase of the NaCl concentration up to 4.0% the purification factor and lipase yield decreased from 10 to 4. The highest purification factor (14.08) was achieved when 6% NaCl was added to the system (ATPS 24% PEG 4000/ 15% potassium phosphate). In this case lipase yield was 88.81 which was relatively high. With increasing of NaCl concentration above 6% a decrease of the purification factor (12.07) and low lipase yield (14.73%) was achieved. A possible reason for this decrease is crystallization of the salts observed in these conditions.

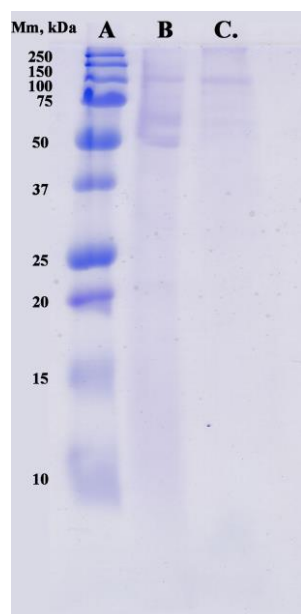


Fig. 5. SDS-PAGE electrophoresis of lipase from *A. carbonarius*: A. Protein markers, B. Cultural broth. C. Lipase from top phase of ATPS 24%PEG 4000/15%potassium phosphate/6%NaCl

As a result of this study an ATPS 24% PEG 4000/15% potassium phosphate/6% NaCl was chosen for optimal lipase purification and SDS-PAGE electrophoresis was performed (Fig. 5). As seen from the SDS-PAGE only two protein bands were isolated (Mm 100 and 250 kDa) which are possible to be multiple forms of lipase. Compared with the cultural broth (B) by using this ATPS, high purification was achieved.

CONCLUSION

ATPS is an easy, fast and effective method for purification of different biomolecules including enzymes. In this study purification of lipase from *Aspergillus carbonarius* NRRL369 was performed by using PEG/potassium phosphate ATPS. It was noticed that increasing of molecular weight of PEG leads to increasing of purification factor of lipase. As a result an ATPS 24%PEG 4000/15% potassium phosphate/6% NaCl was chosen because of the high purification factor (14.08) and lipase yield (88.81%).

Acknowledgements: We acknowledge the financial support of Bulgarian Science Fund, Ministry of Education and Science (Project Young Scientist 03/59 - 2011).

REFERENCES

1. G.S. Padilha, J.C.C. Santana, R.M. Alegre, B. Tambourgi, *Braz. Arch. Biol. Technol.*, **55**, 7 (2012).
2. P.Y. Stergiou, A.Foukis, M.Filippou, M. Koukouritaki, M. Parapouli, L.G. Theodorou, E. Hatziloukas, A.Afendra, A.Pandey, E.M. Papamichael, *Biotechnol. Adv.*, **31**, 1846 (2013).
3. A. Salihu, Z. Alam, M.I.A.Karim, H.M. Salleh, *Arab. J. Chem.*, **7**, 1159(2014).
4. C.H. Tan, P.L. Show, C.W. Ooi, E.P. Ng, J.C. Lan, T.C. Ling, *Biotechnol. J.*, **10**, 31 (2015).
5. S. Thakur, *IJSER*, **3** (2012).
6. S.M. Basheer, S. Chellappan, P.S. Beena, R.V. Sukumaran, K.K. Elyas, M. Chandrasekaran, *New Biotechnol.*, **28**, 627 (2011).
7. A.M. Goja, H.Yang, M.Cui, C.Li, *J.Bioprocess.Biotechniq.*, **4**, 140 (2013).
8. M. Amid, M.Y. Manap, M. Hussin S. Mustafa, *Molecules*, **20**, 11185 (2015).
9. G. Dobrev, B. Zhekova, V. Dobрева, H. Strinska, P. Doykina, A. Krastanov, *Biocatal. Agric.Biotechnol.*, **4**, 77 (2015).
10. J.N. Prazeres, J.A.B. Cruz, G.M. Pastore, *Braz.J.Microbiol.*, **37**, 505 (2006).
11. M.M. Bradford, *Anal Biochem*, **72**, 248 (1976).
12. H.O. Johanson, E. Feitosa, A. Pessoa, *Polymers*, **3**, 587 (2011).
13. J.M.P. Barbosa, R.L. Souza, A.T. Fricks, G.M. Zanin, C.M.F. Soares, Á.S. Lima, *J.Chromatogr. B*, **879**, 3853 (2011).
14. U.K. Laemmli, *Nature*, **227**, 680 (1970).
15. M. Anvari, *Biotechnol.Biotechnol. Equip.*, **29**, 723 (2015).

ПРЕЧИСТВАНЕ НА ЛИПАЗА ОТ *Aspergillus carbonarius* NRRL369 С ДВУФАЗНИ ВОДНИ СИСТЕМИ ПОЛИЕТИЛЕН ГЛИКОЛ/КАЛИЕВ ФОСФАТ

Х.Н. Панайотова^{1*}, Х.Н. Стринска¹, В.Д. Гандова²,
В.Ц. Добрева³, Б.Й. Жекова¹, Г.Т. Добрев¹

¹Катедра „Биохимия и молекулярна биология“, Университет по хранителни технологии,
бул. „Марица“ 26, Пловдив 4002, България, E-mail: angelovatina84@yahoo.com

²Катедра неорганична химия и физикохимия, Университет по хранителни технологии,
бул. „Марица“ 26, гр. Пловдив 4002, България

³Катедра по инженерна екология, Университет по хранителни технологии,
бул. „Марица“ 26, гр. Пловдив 4002, България

Постъпила на 2 ноември 2016 г.; приета на 23 декември 2016 г.

(Резюме)

Изследвано е пречистването на липаза от *Aspergillus carbonarius* NRRL369 с двуфазно водни системи. Построени са бинодалните криви на двуфазни водни системи ПЕГ 400/калиев фосфат и ПЕГ 4000/калиев фосфат и са избрани подходящи концентрации на двата компонента за изследване на процеса на пречистване. За всички двуфазни водни системи са изчислени термодинамичните параметри, за да се опишат процесите. Изследвано е пречистването на липаза с различни двуфазни водни системи. Установено е, че повишаването на молекулната маса на ПЕГ води до повишаване степента на пречистване на липазата. Резултатите показват, че най-подходяща за пречистването на липаза е двуфазна водна система със състав 24% ПЕГ 4000/15% калиев фосфат. Постигнат е добив на липаза 90.68% и степен на пречистване 10.18 пъти. Добавянето на 6% NaCl към двуфазна водна система със състав 24% ПЕГ 4000/15% калиев фосфат повишава степента на пречистване до 14.08 пъти, като крайния добив е 88.81%.

Ключови думи: липаза, пречистване, двуфазни системи, *Asp. Carbonarius*

Isolation and purification of lipase from *Rhizopus arrhizus* by ultrafiltration and fractional precipitation

H.N. Strinska^{1*}, D.N. Petrov², H.N. Panajotova¹, V.T. Dobрева³, B.J. Zhekova¹, G.T. Dobrev¹

¹Department of Biochemistry and Molecular Biology, University of Food Technologies, 26 Maritza Blvd., 4002 Plovdiv, Bulgaria,

²Department of Physical Chemistry, University of Plovdiv 24 "Tzar Assen" Str., Plovdiv 4000, Bulgaria

³Department of Engineering Ecology, University of Food Technologies, 26 Maritza Blvd., 4002 Plovdiv, Bulgaria

Received November 2, 2016; Revised December 23, 2016;

Isolation and purification of lipase with ultrafiltration, fractional precipitation with (NH₄)₂SO₄, organic solvents and PEG 400 of culture broth containing lipase from *Rhizopus arrhizus* was investigated. By using polyacrylonitrile membranes with different size of pores (10-100 kDa) low yields of lipase activity were achieved. A possible reason was adsorption of the protein molecules on the membranes. During fractional precipitation with 60% (NH₄)₂SO₄ purification fold 1.3 and lipase yield about 80% were reached. Fractional precipitation with ethanol, acetone and isopropanol led to inactivation of the enzyme which was the reason for the low purification factor. Probably the low yields were occurred due to the polarity of the medium because in these conditions dielectric constant remained constant – 1.83. The highest lipase yield (95%) and purification factor (3.5-fold) were accomplished by fractional precipitation with 60% PEG 400. In this case dielectric constant of the medium was 1.97.

Keywords: lipase, purification, ultrafiltration, fractional precipitation, dielectric constant

INTRODUCTION

Lipases (E.C. 3.1.1.3) are a group of enzymes that in presence of water catalyze hydrolysis of triacylglycerol to mono-, diacylglycerol, free fatty acids and glycerol and in anhydrous medium – reactions of esterification, transesterification and interesterification. Also lipases catalyze reactions of alcoholysis, acidolysis and aminolysis [1].

Ultrafiltration, fractional precipitation with (NH₄)₂SO₄ and organic solvents are classical approaches and common first step in many schemes for purification of different enzymes.

Ultrafiltration is a wide used method for concentration of enzymes and takes part in many schemes for different enzyme purification, including lipase. Ultrafiltration is an effective technique which may lead to 5-fold concentration with high yield of the target protein because it is held at room temperature and thermal inactivation is not possible. This method also leads to partial purification as proteins with lower molecular masses pass through the membrane into permeate [2-5].

The first step in many purification schemes is fractional purification, when (NH₄)₂SO₄ is the most common substance. Fractional precipitation with acetone, ethanol and organic acid is also used in

practice [6].

By using (NH₄)₂SO₄ for fractional precipitation high yields and purification folds of lipases are achieved. Gaikawari *et al.* [7] accomplished 90.67% lipase yield and more than 5 purification fold and Bose *et al.* [8] – 82.9% lipase yield and purification fold 4.48.

Another option for isolation and purification of enzymes is fractional precipitation with organic solvents. Dandavate *et al.* [9] used acetone for fractional precipitation and achieved high purification fold – 13.77 but low lipase yield - 37.0%.

Polyethylene glycol (PEG) is another option for fractional precipitation of enzymes. Degerli *et al.* [10] used 10% PEG 8000 for fractional precipitation and achieved 97.92% lipase yield and 13.42 purification fold. Romero *et al.* [11] used PEG 20000 for concentration of the enzyme solution and native electrophoresis was then applied. After these two steps purification fold 8.4 and lipase yield 47% were achieved.

The aim of this study is isolation and partial purification of lipase from *Rhizopus arrhizus* by ultrafiltration, fractional precipitation with (NH₄)₂SO₄, organic solvents and PEG 400.

* To whom all correspondence should be sent.

E-mail: hstrinska@gmail.com

EXPERIMENTAL

Microorganism and lipase production

The studied *Rhizopus arrhizus* strain used in this study was provided by Biovet® Peshtera. Growth medium, inoculum preparation and submerged cultivation conditions were described in previous article [12]. Fermentation medium was containing: corn starch 10.5; tryptone 6.6; $\text{NH}_4\text{H}_2\text{PO}_4$ 7.1; $(\text{NH}_4)_2\text{C}_2\text{O}_4$ 1.0; MgSO_4 1.5; KCl 1.9.

Ultrafiltration

Ultrafiltration of 50 cm³ cultural broth with ultrafiltration cell Amikon® was applied and 5-fold concentration was performed. Polyacrylonitrile ultrafiltration membranes 10, 20, 25, 50 and 100 kDa were used. The process was carried out at room temperature and work pressure 0.5 MPa. Lipase activity and content of protein in concentrate, permeate and ultrafiltration membrane were analyzed.

Fractional precipitation with $(\text{NH}_4)_2\text{SO}_4$

To a cultural broth with known volume $(\text{NH}_4)_2\text{SO}_4$ was added in such quantity that defined degree of saturation (10-80%) to be achieved. Solutions were let for stabilization of the precipitate at 4°C for 1 h and then were centrifuged at 4000 rpm for 40 min. The precipitates were diluted with distilled water to a defined volume and lipase activity and content of protein were analyzed.

Fractional precipitation with organic solvents

To a cultural broth with known volume acetone, ethanol and isopropanol were added in such quantity that defined concentration (10-80%) to be achieved. Solutions were let for stabilization of the precipitate at 4°C for 1 h and then were centrifuged at 4000 rpm for 40 min. The precipitates were diluted with distilled water to a defined volume and lipase activity and content of protein were analyzed.

Fractional precipitation with PEG 400

To a cultural broth with known volume PEG 400 was added in such quantity that concentration (20-70%) to be achieved. Solutions were let for stabilization of the precipitate at 4°C for 1 h and then were centrifuged at 4000 rpm for 40 min. The precipitates were diluted with distilled water to a defined volume and lipase activity and content of protein were analyzed.

Lipase assay

Lipase activity was measured by spectrophotometric method using p-nitrophenyl palmitate as substrate buffered with Tris-HCl pH 9.0 [13]. The reaction mixture, containing

2.4 cm³ of 0.8 mM substrate and 0.1 cm³ of enzyme solution, was incubated for 15 min at 35°C. The enzyme reaction was stopped by adding 1.0 cm³ saturated solution of lead (II) acetate. After centrifugation absorbance was measured at 405 nm. One unit of enzyme activity was defined as the amount of enzyme that released one μmol of p-nitrophenol per minute under the assay conditions described.

Lipase assay of ultrafiltration membrane

A part of the ultrafiltration membrane with size 1.0 cm² was cut and placed in a test tube containing 2.4 cm³ of 0.8 mM substrate and 1.0 cm³ water and the reaction mixture was incubated for 15 min at 35°C. The enzyme reaction was stopped by adding 1.0 cm³ saturated solution of lead (II) acetate after the membrane was subtracted. After centrifugation absorbance was measured at 405 nm. One unit of enzyme activity was defined as the amount of enzyme that released one μmol of p-nitrophenol per minute under the assay conditions described.

Protein assay

Protein was quantified by Lowry assay [14].

SDS-PAGE electrophoresis

The purified lipase was analyzed electrophoretically on Cleaver Scientific Ltd; OmniPAGE Electrophoresis System CVS10DSYS, at 20 mA. 15% polyacrylamide gels in the presence of SDS as described by Laemmli [15].

Dielectric constant measurement

Dielectric constant was measured refractometric using a laser microrefractometer. Laser pointer generating at wavelength of 532 nm is used as a light source. The sample was placed between a glass prism and metal diffraction grating. At angles smaller than the critical angle of total internal reflection, the laser beam passes through a glass prism, sample and diffract from the metal grating. The critical angle (φ_{cr}) was measured in the air and the refractive index of the sample (n) in calculated by the formula [16, 17]:

$$n = N \sin \left[A - \arcsin \left(\frac{\sin \varphi_{cr}}{N} \right) \right] \quad (1)$$

where $A = 64.7^\circ$ is the refraction angle of the prism,

N is the refractive index of the prism for the used wavelength (1.7480).

Dielectric permittivity of the samples can be obtained using the Maxwell relation [18]:

$$\varepsilon = n^2 \quad (2)$$

RESULTS AND DISCUSSION

Isolation and concentration of lipase from cultural broth obtained by submerged fermentation of *Rhizopus arrhizus* was performed.

Table 1 represents the results from ultrafiltration of the studied enzyme. As seen from the table, when membranes 10, 20 and 25 kDa were used very low lipase yield in the concentrates were reached while there were no lipase activity in the permeates. When ultrafiltration membranes 50 and 100 kDa were used there were enzyme activity in concentrates and in permeates as well. However, the lipase yields in concentrates and permeates were between 55 – 60%. This is low yield for this technique because during the procedure there is no increasing in the temperature which could result in a thermal inactivation of the enzyme. These results are comparable with other reports. For example Gaur *et al.* [3] achieved 60.8% lipase yield and 0.9 purification fold by ultrafiltration of lipase from *Pseudomonas aeruginosa* with ultrafiltration membrane with pore size 30 kDa.

As lipases are water soluble enzymes and the substrate – fat soluble, catalysis proceeds in the interfacial surface between water and oil phases. This is possible because of the hydrophobic domain in the lipase molecules, which allows the enzyme to adsorb on the substrate. It is possible adsorption of the lipase on the ultrafiltration membrane to be a reason for low activity yields [1, 5].

Another possible reason for inactivation of lipase is protein-protein interaction in the concentrate. During concentration protein molecules interact each other with their hydrophobic domains [19] which may inactivate the enzyme.

In order to confirm the hypothesis for adsorption of the molecules of the enzyme on the ultrafiltration membrane, lipase activity of the membranes was examined after the ultrafiltration was performed (Table 2). As seen from the results lipase activity was recorded at all of the membranes. However, these results could not be used the adsorbed lipase to be quantified because of changes in kinetics of the reactions during immobilization of the biocatalyst. As a result of this experiment the hypothesis that some of the lipase was adsorbed on the ultrafiltration membranes was confirmed.

From the obtained results we can conclude that ultrafiltration with polyacrylonitrile membranes 10-100 kDa is not suitable technique for concentration of lipase from *Rhizopus arrhizus*.

Fractional precipitation with $(\text{NH}_4)_2\text{SO}_4$ is a traditional method for isolation of enzymes.

$(\text{NH}_4)_2\text{SO}_4$ is more commonly used for fractional precipitation of lipase because it leads to high lipase yield. At 80% degree of saturation a lipase yield over 50% was accomplished. The highest purification fold – 1.17 and yield 30% was achieved (Fig. 1).

Table 1. Ultrafiltration

	V, cm ³	Total lipase activity, U	Specific activity, U/mg	Yield, %	Purification factor
Crude enzyme	50	86.23	26.75	100	1.00
Membrane 10 kDa					
Concentrate	10	16.62	11.09	19.27	0.41
Permeate	40	0.01	0.00	0.01	0.00
Membrane 20 kDa					
Concentrate	10	23.72	13.07	27.50	0.49
Permeate	40	0.09	0.16	0.10	0.01
Membrane 25 kDa					
Concentrate	10	40.67	15.18	47.16	0.57
Permeate	40	0.07	0.11	0.08	0.00
Membrane 50 kDa					
Concentrate	10	45.35	23.77	52.59	0.89
Permeate	40	13.07	19.28	15.15	0.75
Membrane 100 kDa					
Concentrate	10	45.08	20.11	52.27	0.75
Permeate	40	11.01	4.71	12.77	0.18

Table 2. Lipase activity on ultrafiltration membranes

Membrane, kDa	Area, cm ²	Total activity, U
10	16	1.42
20	16	2.23
25	16	1.02
50	16	1.57
100	16	1.04

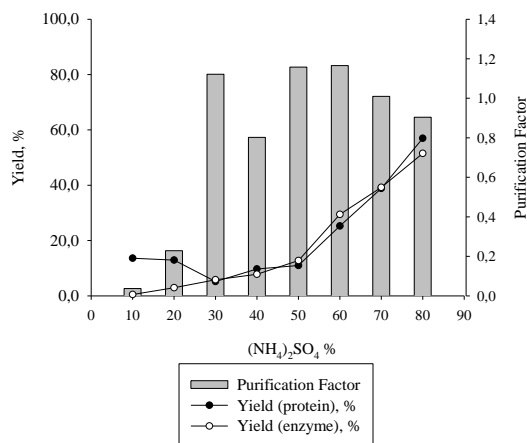


Fig. 1. Fractional precipitation with (NH₄)₂SO₄

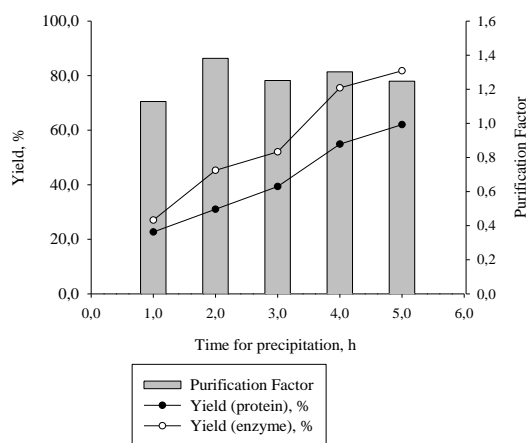


Fig. 2. Time for fractional precipitation with 60% (NH₄)₂SO₄

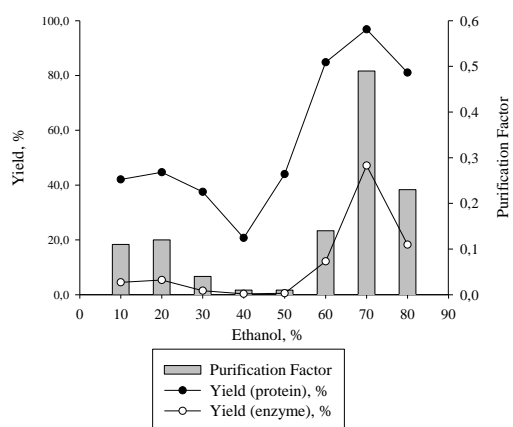


Fig. 3. Fractional precipitation with ethanol

Additional experiment was obtained in order to enhance the time for precipitate formation with 60% (NH₄)₂SO₄. Fig 2 reveals that with the enhancement of time (1-5 h) for precipitation, lipase yield also increased – from 30% to 80%. As seen from the chart lipase yield at 4th h was 75.50% and at 5th h – 81.75%. Protein yield also enhanced and the purification factor remained relatively constant – between 1.15 and 1.30 fold.

As a result of this experiment we could conclude that when fractional precipitation with (NH₄)₂SO₄ for 4 h was used lipase yield 75.50% and purification factor 1.30 was accomplished.

Traditional method for isolation of enzymes is their selective fractional precipitation with organic solvents such as ethanol, acetone and isopropanol.

Fig. 3 reveals the results for fractional precipitation with ethanol. The highest yield (almost 50%) was achieved when 70% ethanol was used. It can be noticed that at 40% and 50% ethanol the enzyme is almost completely inactivated. Because of the activity loss, the purification fold decreased.

Similar results were obtained for fractional precipitation of lipase with isopropanol and acetone (Fig. 4 and Fig. 5).

When isopropanol and acetone were used the highest lipase yield was accomplished at 80% of the organic solvent – respectively 52.98% and 74.83%. In both cases a decrease in the lipase activity was noticed between 30 and 40% of each of the solvents.

Yu *et al.* [20] explained the inactivation effect with changes of polarity of the medium and the influence of the polarity on the hydrophobic effects, which have a crucial role in formation of the tertiary structure of the proteins. Hydrophobic effects in the protein molecules are a result from the pressure of the water medium. Addition of organic solvent removed a part of the hydration shell, which results in changes in the native conformation which may lead to inactivation [20]. Respectively polarity of the medium, which impact on the hydrophobic effects of formation of the three dimensional structure of the proteins may be the factor which leads to inactivation of lipase at these conditions. In order to examine the hypothesis, dielectric constant, which is a measure for the polarity of the medium, was measured for the samples where the strongest inhibition was noticed (Table 3). As seen from the table dielectric constants at the stated conditions were with the same values – 1.83.

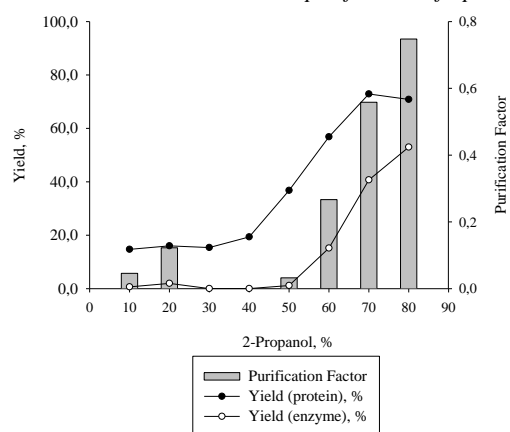


Fig. 4. Fractional precipitation with isopropanol

Table 3. Dielectric constant of water and some concentrations of organic solvents

Solution	Dielectric constant ϵ at 532 nm	Lipase activity, U.dm ⁻³
Lipase aqueous solution	1.79	1009.71
Lipase in 50 % Ethanol	1.83	4.30
Lipase in 40 % Ethanol	1.83	2.55
Lipase in 40 % 2- Propanol	1.83	0.02
Lipase in 30 % 2- Propanol	1.83	0.02
Lipase in 40 % Acetone	1.83	90.15
Lipase in 30% Acetone	1.83	96.64
Lipase in 40 % PEG 400	1.89	1351.53
Lipase in 50 % PEG 400	1.97	2165.43

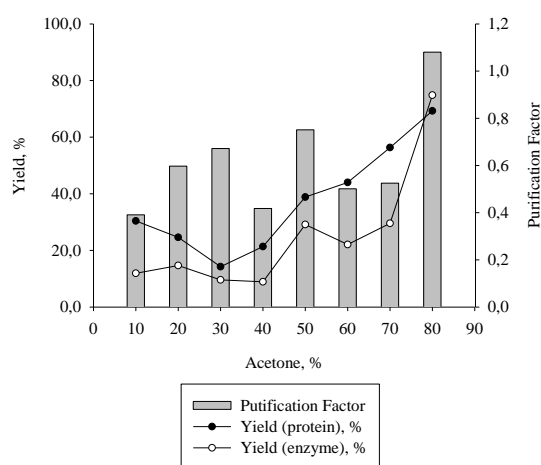


Fig. 5. Fractional precipitation with acetone

The obtained results are a partial proof of the hypothesis that the reached polarity at usage of these concentrations of organic solvents was a possible reason for lipase inactivation.

Some authors describe usage of PEG for fractional precipitation of lipase and relatively high yields are reported [10]. High yield and purification fold were achieved by fractional precipitation of lipase by PEG 400 (Fig. 6).

The highest purification factor, more than 4.0 fold, was accomplished at 30% PEG 400. Lipase yield in this case was almost 60%. Yield over 95% was obtained by using 60% and 70% PEG 400 but in

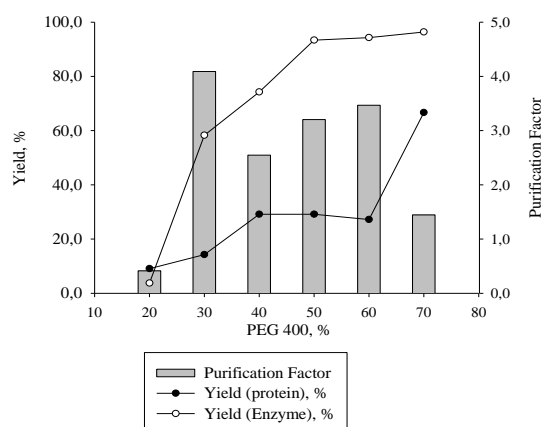


Fig. 6. Fractional precipitation with PEG 400 these cases purification factor decreased – respectively 3.5 and 1.4 fold.

Degerli *et al.* [10] also used polymer and by using 10% PEG 8000 97.92% yield and purification factor 13.42 fold was achieved.

Dielectric constants of the solutions of PEG (Table 3) differed from those of the organic solvents. Dielectric constant 1.97 was measured at lipase solution containing 50% PEG 400. In this case lipase yield 93.36% was reached and purification factor 3.20 was accomplished.

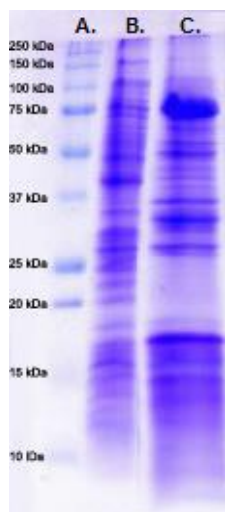


Fig. 7. SDS-PAGE electrophoresis – fractional precipitation with 60% PEG 400: A- protein markers; B -cultural broth; C - after fractional precipitation with PEG 400

In order to confirm the purification of the enzyme after fractional precipitation with 60% PEG 400 SDS-PAGE was performed (Fig. 7). As seen from the figure, many protein bands with molecule masses between 20 and 30 kDa and higher than 100 kDa were absent. That indicates that fractional precipitation with PEG 400 leads to partial purification of lipase from *Rhizopus arrhizus*.

CONCLUSION

In this study was established that ultrafiltration was not suitable for concentration of lipase from *Rhizopus arrhizus*. Lipase activity on the ultrafiltration membrane proved that a reason for low lipase yield was adsorption of the enzyme on the membranes. When fractional precipitation with ethanol, isopropanol and acetone was applied very low lipase yields were reached because of inactivation of the enzyme. The highest lipase yield – 94.29% and purification factor 3.47 were accomplished when 60% PEG 400 was used for fractional precipitation.

Acknowledgements: The authors are grateful to Biovet® Peshtera for providing us the opportunity to work with the studied strain *Rhizopus arrhizus*.

REFERENCES

1. P.Y.Stergiou, A.Foukis, M.Filippou, M.Koukouritaki, M.Parapouli, L.G.Theodorou, E.Hatziloukas, A.Afendra, A.Pandey, E.M.Papamichael, *Biotechnol. Adv.*, **31**, 1846 (2013).
2. M.F.Jesus, R.N.Branco, G.L.Sant'anna, D.M.G.Freire, J.G.Silva, *Braz. J. Chem. Eng.*, **16**, 113 (1999).
3. R.Gaur, A.Gupta, S.K.Khare, *Process Biochem.*, **43**, 1040 (2008).
4. W.Stuer, K.E.Jaeger, U.K.Winkler, *J. Bacteriol.*, **168**, 1070 (1986).
5. Y.Fang, X.J.Huang, P.C.Chen Z.K.Xu, *BMB Rep.*, **44**, 87 (2011).
6. R.K.Saxena, A.Sheoran, B.Giri, W.S.Davidson, *J. Microbiol. Methods*, **52**, 1 (2008).
7. R.P.Gaikaiwari, S.A.Wagh, B.D.Kulkarni, *Bioresour. Technol.*, **108**, 224 (2012).
8. A.Bose, H. Kehara, *Biocatal. Agric. Biotechnol.*, **2**, 255 (2013).
9. V.Dandavate, J.Jinjala, H.Kehria, D.Madamwar, *Bioresour. Technol.*, **100**, 3374 (2002).
10. N.Dagerli, M.A.Akpinar, *Turk. J. Biol.*, **26**, 133 (2002).
11. C.Romero, L.Pera, F.Loto, C.Vallejos, G.Castro, *Biocatal. Agric. Biotechnol.*, **1**, 25 (2012).
12. H.Strinska, V.Dobreva, B.Zhekova, G.Dobrev, *Int. J. Biochem. Res. Rev.*, **5**, 178 (2015).
13. R.Kaushik, S.Saran, J.Isar, R.K.Saxena, *J. Mol. Catal. B: Enzym.*, **40**, 121 (2006).
14. O.H.Lowry, N.J.Rosebrough, A.L.Farr, R.J.Randall, *J. Biol. Chem.*, **193**, 265 (1951).
15. U.K. Laemmli, *Nature*, **227**, 680 (1970).
16. S.Sainov, N.Dushkina, *Appl. Opt.*, **29**, 1406 (1990).
17. I.Vlaeva, T.Yovcheva, K.Zdravkov, G.Minchev, E.Stoykova, in: Proc. SPIE 7027 (2008).
18. W.C.Tan, K.Koughia, J.Singh, S.O.Kasap, in: Optical Properties of Condensed Matter and Applications (ed J. Singh), John Wiley & Sons, Ltd, Chichester, UK, 2006.
19. S.Jones, J.M.Thornton, Proc. Natl. Acad. Sci USA **93**, 1996.
20. G.Barth, *Yarrowia lipolytica*: Biotechnological Applications. Springer Science & Business Media, 2013.

ИЗОЛИРАНЕ И ПРЕЧИСТВАНЕ НА ЛИПАЗА ОТ *Rhizopus arrhizus* С УЛТРАФИЛТРАЦИЯ И ФРАКЦИОННО УТАЯВАНЕ

Х. Н. Стринска^{1*}, Д. Н. Петров², Х. Н. Панайотова¹, В. Ц. Добрева³,
Б. Й. Жекова¹, Г. Т. Добрев¹

¹Катедра „Биохимия и молекулярна биология“, Университет по хранителни технологии,
бул. „Марица“ 26, гр. Пловдив 4002, България, E-mail: hstrinska@gmail.com

²Катедра „Физикохимия“, Пловдивски университет „Паусий Хилендарски“,
ул. „Цар Асен“ 24, гр. Пловдив 4000, България

³Катедра по инженерна екология, Университет по хранителни технологии,
бул. „Марица“ 26, гр. Пловдив 4002, България

Постъпила на 2 ноември 2016 г.; приета на 23 декември 2016 г.

(Резюме)

Проведено е изолиране и пречистване на липаза чрез ултрафилтрация, фракционно утаяване с $(\text{NH}_4)_2\text{SO}_4$, органични разтворители и ПЕГ 400 от културална течност на *Rhizopus arrhizus*. При ултрафилтрацията с полиакрилонитрилни мембрани с различен размер на порите (10-100 kDa) е постигнат нисък добив, което вероятно се дължи на адсорбция на белтъчните молекули върху мембраните. При фракционно утаяване с 60% $(\text{NH}_4)_2\text{SO}_4$ е получена степен на пречистване 1.3 пъти и добив на липаза около 80%. Фракционното утаяване с етанол, изопропанол и ацетон води до инактивиране на ензима, в резултат на което е отчетена и ниска степен на пречистване. Вероятно това се дължи на промяна в полярността на средата, тъй като диелектричната константа при тези условия има една и съща стойност – 1.83. Най-висок добив (95%) и степен на пречистване (3.5 пъти) са получени чрез фракционно утаяване с 60 % ПЕГ 400. В този случай диелектричната константа на средата е 1.97.

Ключови думи: липаза, пречистване, ултрафилтрация, фракционно утаяване, диелектрична константа

Synthesis and characterization of Sr₂Be₂B₂O₇ by XRD and FTIR

H. Karabulut^{1*}, İ. Pekgözlü², A.S. Başak³, A. Mergen³

¹Trakya University, Science Faculty, Edirne 22030, Turkey

²Bartın University, Engineering Faculty, Bartın 74100, Turkey

³Marmara University, Art and Science Faculty, Istanbul 34722, Turkey

Received November 11, 2016; Revised January 21, 2017

In this work pure Sr₂Be₂B₂O₇ material was prepared by solid-state reaction at 950°C in air. The stoichiometric amounts of SrO, BeO and H₃BO₃ were used as starting materials. Phase analysis of the synthesized materials was carried out using powder X-ray diffraction (XRD). They were characterized by Fourier transform infrared spectroscopy (FTIR) as well.

Keywords: strontium beryllium borate, XRD, FTIR

INTRODUCTION

Pure and doped borates have been used in many areas such as germicidal drinking water purification, non-linear optics, photocopying, phototherapy, sunlamps, laundry marking, blueprinting, instrumental dial illumination, window displays, etc. [1-8].

The studies that are carried on Sr₂Be₂B₂O₇ exist rarely in the literature since it is just a new compound. Investigations are usually focused on the single crystal synthesis by using different methods and NLO applications [4-8].

In this work pure Sr₂Be₂B₂O₇ material was prepared by solid-state reaction. The phase analysis of all synthesized materials was carried out using powder X-ray diffraction (XRD). Also the synthesized materials were characterized by Fourier transform infrared spectroscopy (FTIR).

EXPERIMENTAL

Pure Sr₂Be₂B₂O₇ material was prepared by a solid-state method at 950 °C in air. Stoichiometric amounts of SrO, BeO and H₃BO₃ were used as starting materials (SrO and BeO were produced by calcinations of related metal nitrates and/or carbonates). After adding suitable amount of acetone into reaction medium, the precursors were introduced into a muffle furnace and maintained at 500 °C for 2 h. The precursor powders were thoroughly mixed and then slowly heated at 950°C for 12 h in air.

Reaction:



The XRD structural analysis of Sr₂Be₂B₂O₇ material was performed on an X-ray Phillips X'Pert Pro equipped with Cu K α (30 kV, 15 mA, $\lambda=1.54051$ Å) radiation at room temperature. Scanning was generally performed between 10° and 90° 2 θ . Measurement was made with 0.0330° step size at 25°C.

The Fourier transform infrared spectra between 500 and 4000 cm⁻¹ were measured at room temperature with a Shimadzu 8303 FTIR spectrometer. All samples were prepared as KBr pellets.

RESULTS AND DISCUSSION

The XRD pattern of Sr₂Be₂B₂O₇ is presented in Fig. 1. It is in a full agreement with the JCPDS (82-2448).

To determine the coordination environments of both B–O and Be–O in the Sr₂Be₂B₂O₇ structure, the FTIR spectra of Sr₂Be₂B₂O₇ were measured at room temperature. As seen in Fig. 2, the strong bands observed at 614.99, 697.75 and 1241.77 cm⁻¹ should be assigned to the B–O vibrations of the triangular [BO₃] groups [1, 5, 9, 10], while the band with a peak at 890.66 cm⁻¹ should be attributed to the Be–O vibration of the tetragonal [BeO₄] group [5]. FTIR spectrum data of Sr₂Be₂B₂O₇ are listed in Table 1.

Point group of Sr₂Be₂B₂O₇ (SBBO) is D_{3h}. Geometric parameters of the synthesized borate are P6̄c2, a=b=4.683 Å, c=15.311 Å, $\alpha=\beta=90^\circ$, $\gamma=120^\circ$ [4, 7, 11].

* To whom all correspondence should be sent.

E-mail: hkarabulut@marmara.edu.tr

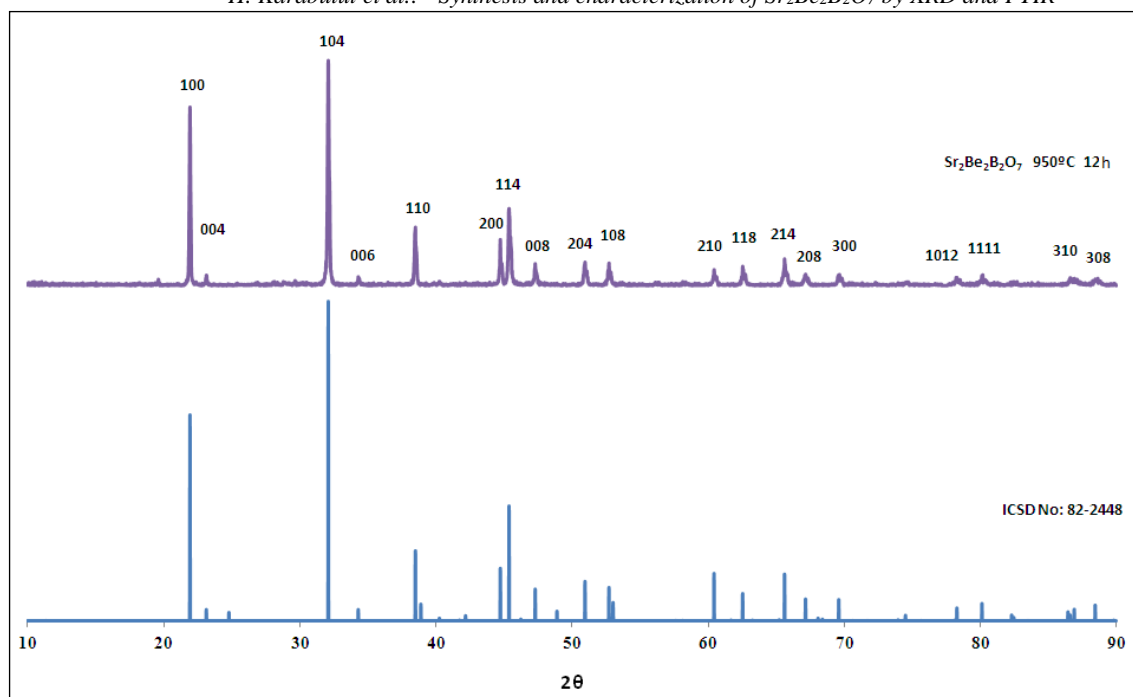


Fig. 1. XRD pattern of Sr₂Be₂B₂O₇ prepared by a solid-state synthesis

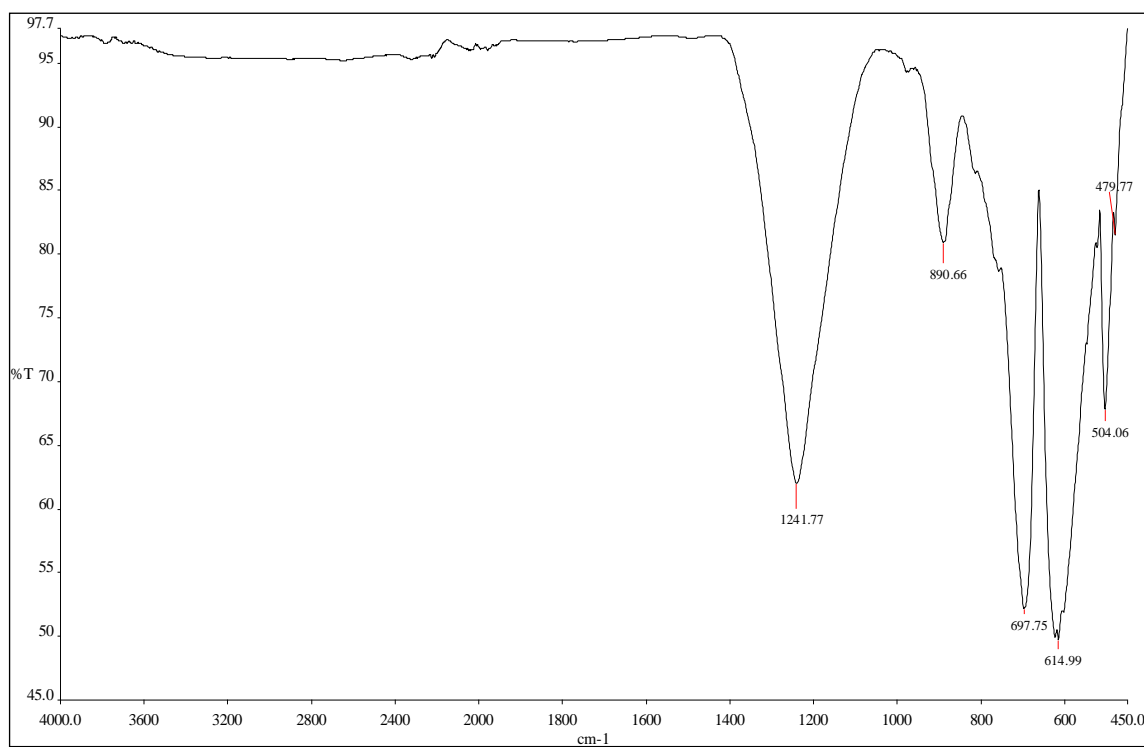


Fig. 2. Infrared spectra of Sr₂Be₂B₂O₇ prepared by a solid-state synthesis

Table 1. FTIR spectrum data of Sr₂Be₂B₂O₇

Assignments	$\nu_3(\text{BO}_3)$	$\nu_3(\text{BeO}_4)$	$\nu_2(\text{BO}_3)$	$\nu_4(\text{BO}_3)$
Frequency (cm ⁻¹)	1241.77	890.66	697.75	614.99

According to these data it can be concluded that two possible sites available for incorporating activator ions (such as Dy³⁺, Sm³⁺, Tb³⁺, Eu³⁺, Pb²⁺, etc.) in Sr₂Be₂B₂O₇ lattice are either the Sr²⁺ sites or the Be²⁺ sites. The Dy³⁺ (0.912 Å for CN = 6), Sm³⁺ (0.958 Å for CN = 6), Tb³⁺ (0.923 Å for CN = 6), and Pb²⁺ (1.19 Å for CN = 6) ions are of a much larger ionic radius, compared with that of the Be²⁺ (0.27 Å for CN = 4) ion. However, the ionic radius of Sr²⁺ (1.18 Å for CN = 6) is larger than that of the activator ions. So in the first luminescence study that was made by our research group [5], the Sr²⁺ ions in the Sr₂Be₂B₂O₇ lattice were replaced by the mentioned activator ions (Dy³⁺, Sm³⁺, Tb³⁺, Pb²⁺).

CONCLUSION

Sr₂Be₂B₂O₇ material was prepared by solid-state reaction. The phase analysis of the synthesized material was carried out using powder XRD and characterized by FTIR. The XRD pattern of the synthesized material is in agreement with the JCPDS (82-2448). Also the coordination environments of both B–O and Be–O in the Sr₂Be₂B₂O₇ structure were confirmed by FTIR measurement.

Acknowledgements: This study was financially supported by the foundation of The Scientific and Technological Research Council of Turkey (Project No. 212T250).

REFERENCES

1. İ. Pekgozlu, E. Erdoğmuş, B. Demirel, M.S. Gök, H. Karabulut, A.S. Başak. *J. Luminescence*, **131**, 2290 (2011).
2. D. S. Thakare, S. K. Omanvar, P. L. Muthal, S. M. Dhopte, V. K. Kondawar, S. V. Moharil, *Phys. Status Solidi A*, **201**, 574, (2004).
3. H. A. Klasens, A. H. Hoekstra, A. P. M. Cox, *J. Electrochem. Soc.*, **104**, 93, (1957).
4. C. Chen, Y. Wang, B. Wu, K. Wu, W. Zheng, and L. Yu, *Nature*, **373**, 322, (1995).
5. İ. Pekgozlu, H. Karabulut, A. Mergen, A. S. Başak, *J. Appl. Spectroscopy*, **83**, 504 (2016).
6. P. Becker, *Adv. Mater.*, **10**, No. 13, 979–992, (1998).
7. Z. Lin, Z. Wang, C. Chen, *J. Appl. Physics*, **93**, 9717 (2003).
8. J. W. Kolis, C. D. McMillen, H. G. Giesber, *US Patent*, US007591896B2, (2009).
9. L. Wu, X. L. Chen, H. Li, M. He, L. Dai, X. Z. Li, Y. P. Xu, *J. Solid State Chem.*, **177**, 1111 (2004).
10. A. Rulmont, M. Almou, *Spectrochim. Acta*, **45A**, 603, (1989).
11. X. Y. Meng, X. H. Wen and G. L. Liu, **52**, 1277 (2008).

СИНТЕЗ И ОХАРАКТЕРИЗИРАНЕ НА Sr₂Be₂B₂O₇ ПОСРЕДСТВОМ XRD И FTIR

Х. Карабулут^{1*}, И. Пекгюзлу², А.С. Башак³, А. Мерген³

¹Тракийски университет, Природонаучен факултет, Одрин 22030, Турция

²Бартънски университет, Инженерен факултет, Бартън 74100, Турция

³Мармарски университет, Факултет по наука и изкуство, Истанбул 34722, Турция

Постъпила на 11 ноември 2016 г.; приета на 21 януари 2017 г.

(Резюме)

В тази работа е получен чист материал от Sr₂Be₂B₂O₇ чрез твърдофазна реакция при 950°C във въздушна среда. Като изходни материали са използвани стехиометрични количества от SrO, BeO и H₃BO₃. С помощта на прахов рентгеноструктурен анализ (XRD) е извършен фазов анализ на синтезираните материали. Последните са охарактеризирани и чрез инфрачервена спектроскопия с Фурие-трансформация (FTIR).

Ключови думи: Стронциев берилиев борат, Рентгеноструктурен анализ, Инфрачервена спектроскопия с Фурие трансформация

Application of X-ray and SEM–EDS evaluation of the main digestion methods for determination of macroelements in soil

K. Ivanov^{1*}, P. Zapryanova¹, V. Angelova¹, L. Dospatliev²

¹Department of Chemistry, University of Agriculture, 4000 Plovdiv, Bulgaria

²Department of Pharmacology, Animal Physiology and Physiological Chemistry, Trakia University, Stara Zagora, Bulgaria

Received November 14, 2016; Revised December 2, 2016

Two commonly used digestion methods - acid digestion and microwave digestion in different variants (ISO 11466; EPA Method 3051; EPA Method 3052; ISO 14869-1; GB, Standing committee of analysis, ISBN 0117519081 and HNO₃ + HClO₄ acid mixture), were compared for digestion of three certified soil samples, corresponding to two main soil types in Bulgaria - Light Alluvial-deluvial Meadow Soil and Light Meadow Cinnamon Soil. Three main macroelements (K, Ca and Mg) were analyzed using AAS spectrometer Spektra AA 220, Varian, Australia. To elucidate the problems with elemental recovery X-Ray and SEM–EDS analysis of all residues after digestion were performed. The X-ray investigation showed the formation of KClO₄ when HClO₄ was used as a part of the acids mixture. The result was confirmed by Energy dispersive X-ray microanalysis. The use of HF at Ca and Mg determination led to the formation of KClO₄, CaF₂ and MgF₂.

Keywords: digestion methods, soil, K, Ca, Mg.

INTRODUCTION

Potassium, calcium and magnesium are essential macroelements in soil and important nutrients for plants [1]. A significant portion of potassium in the soil is in the minerals which belong to the group of feldspars (orthoclase, sanidine, microcline) and is hardly accessible for plants. The potassium contained in mica is less related and relatively easily accessible. The most important source of potassium for plants are secondary clay minerals such as illite. Calcium and magnesium are present in the crystal lattice of soil minerals in exchangeable form easily assimilated by plants, as well as salts (chlorides, sulfates, nitrates, carbonates and phosphates). They determine to a significant extent some of the important soil characteristics and the related fertility. Calcium improves the overall physical, physico-mechanical and aqueous properties of the soil. In the less fertile podzolic soils, which are characterized by a small amount of calcium and magnesium, the soil reaction is highly acidic. This favours the decomposition of carbonates and the destruction of soil, as well as the blocking of phosphorus in Al- and Fe-phosphates [2]. For these reasons, of essential importance is the determination not only of the mobile and easily absorbed by plants forms of K, Ca and Mg, but their total amounts, defining some of the basic soil characteristics.

The objective of the study is to assess the capabilities of the most common standardized and non-standardized methods of mineralization and to

outline their boundaries of applicability in determining the total amount of the main macroelements in soil.

MATERIALS AND METHODS

Three certified soil samples corresponding to two main soil types in Bulgaria were used in the study: Light Alluvial-deluvial Meadow Soil PS-1, SOOMET № 0001 BG, SOD № 310a98; Light Meadow Cinnamonic Soil PS-2, SOOMET № 0002 BG, SOD №311a98 and Light Alluvial-deluvial Meadow Soil PS-3, SOOMET № 0003 BG, SOD № 312a98. The content of K, Ca and Mg in the certified samples is presented in Table 1.

Table 1. Content of K, Ca and Mg (as oxides, %) in the certified samples. X_{CRM} is the certified value and U_{CRM} - the indefiniteness of the certified value.

Element	PS – 1		PS – 2		PS – 3	
	X _{CRM} %	U _{CRM} %	X _{CRM} %	U _{CRM} %	X _{CRM} %	U _{CRM} %
K ₂ O	2.26	0.13	2.75	0.12	2.38	0.13
CaO	14.73	0.36	2.88	0.09	7.34	0.18
MgO	3.07	0.15	1.65	0.12	2.28	0.12

Six most commonly used methods for sample preparation were used as follows:

- ISO 11466 [3]: 1 g air-dried soil + 21 ml HCl and 7 ml HNO₃, heating two hours at 180 – 200 °C.

* To whom all correspondence should be sent.
E-mail: kivanov1@abv.bg

- 1 g air-dried soil + 15 ml HNO₃ and 5 ml HClO₄, heating two hours at 180 - 200 °C [4].
- EPA Method 3051 [5]: 1 g air-dried + 10 ml HNO₃, digestion in microwave system Milestone 1200 MEGA.
- EPA Method 3052 [6]: 1 g air-dried soil + 9 ml HNO₃, 3 ml HF, 2 ml HCl and 2 ml H₂O₂, digestion in microwave system Milestone 1200 MEGA.
- ISO 14869-1 [7]: 0.25 g air-dried soil in a platinum melting-pot, dry ashing for 3 hours at 450 °C + 5.0 ml HF and 1 ml HClO₄ (after cooling to room temperature). Second heating until the dense steams of the HClO₄ and SiF₄ disappear. After cooling to room temperature 1.0 ml nitric acid and 5.0 ml H₂O are added.
- ISBN 01175 19081 [8]: *Part 1*: 3.0 g air-dried soil + 22.5 ml HCl and 7.5 ml HNO₃, heating to boiling for 2 hours, filtration and dilution to 100 ml with 12.5% nitric acid *Part 2*: drying of the remaining undissolved part after the first stage at 105 °C and transferring in a teflon container with a well closing lid + 5 ml HF acid and heating for 30 minutes at 140-150 °C. Finally, after cooling 50 ml saturated solution of boron acid is added.

The XRD patterns were recorded on a Philips PW 1050 diffractometer, equipped with Cu K α tube and a scintillation detector. SEM images were recorded in a JSM 6390 electron microscope (Japan) in conjunction with energy dispersive X-ray spectroscopy (EDS, Oxford INCA Energy 350) equipped with ultrahigh resolution scanning system (ASID-3D)

To determine the elements content in the solution after digestion of the samples atomic absorption spectrometer (Spectra AA-220, Varian, Australia) was used.

RESULTS AND DISCUSSION

The results from the determination of the total content of K, Ca and Mg in the three certified soil samples are presented in Table 2, where R shows the extent of extraction of the element in percents from the certified value ($R = X / X_{CRM} \cdot 100$).

Determination of potassium

The unsatisfactory results for the three certified samples in the use of methods 1 to 3 (48.5 - 61.6%) and practically the complete extraction of potassium with the use of methods 4 and 6 make an impression. It is well known that the independent use of HNO₃ leads to a partial extraction of potassium from the soil samples [9]. Its combination with HCl acid (method 1) insignificantly increases the rate of recovery. The results are consistent with the results of Kackstaetter and Heinrichs [10] according to which aqua regia provides a satisfactory extraction

of many basic elements, but limited extraction of Al and K.

Unsatisfactory results (<75%) in the study of river sediments and soils are received also by Krause *et al.* [11]. The use of HClO₄ (methods 2 and 5) leads to different results depending on the composition of the acid mixture. The result of its combination with HNO₃ (method 2) is unsatisfactory. This is probably due to the incomplete dissolution of aluminosilicate matrix and the formation of a sediment of an insoluble potassium perchlorate. To clarify this problem, we studied the insoluble sediment after decomposition of the samples by methods 2 by X-Ray and SEM-EDS analysis. The results of powder X-ray analysis presented in Fig. 1 indicates the presence of roentgenamorphous phases (the so called halo peaks) that differ low intensity and great half-width x-ray diffraction peaks of high disperse phases, among which the largest is the percentage of KClO₄ (PDF - 70-0488). This result is also confirmed by the SEM-EDS analysis of the same sediment (Fig.2 and Table 3). The results of the integral elemental analysis (Table 3) show that only part of the potassium is linked in KClO₄. The rest is obviously included in the insoluble siliceous matrix.

The inclusion of HF in the acidic mixture used in the mineralization is not sufficient for the complete extraction of potassium from the soil samples. This is confirmed by the results obtained by method 5 (HNO₃ + HClO₄ + HF). Even though to a lesser degree, in this case the formation of sediment is observed in the mineralization of all samples.

Fig. 3 presents the results of powder X-ray analysis of a soil sample, digested by method 5. The analysis of the roentgenogram shows the presence of almost roentgen-amorphous phases (the so called halo peaks) that differ low intensity and great half-width x-ray diffraction peaks of high disperse phases, among which the largest is the percentage of KClO₄ (PDF - 70-0488), MgF₂ (PDF - 38-0882), CaF₂ (PDF - 77-2094). There is a presence and a small amount of SiO₂ (PDF 88-2302), as well as aluminosilicate phase, containing magnesium and iron - probably Mg_{0.8}Fe_{0.2}Al₂Si₂O₆(OH)₄ (PDF -83-1944).

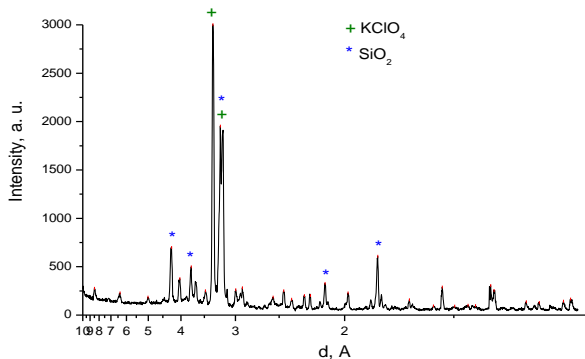


Fig. 1. X-ray pattern of the residue after digestion of the certified sample by mixture of HNO₃ and HClO₄

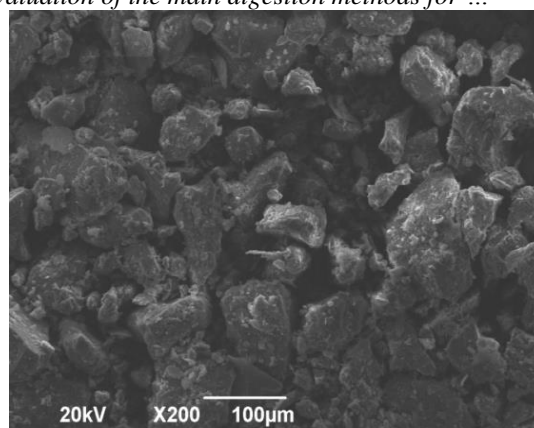


Fig. 2. SEM images of the residue after digestion of the certified sample by mixture of HNO₃ and HClO₄

Table 2. Efficacy of the digestion methods at the determination of Ca (as CaO), Mg (as MgO) and K (as K₂O). in certified soils. * - “acceptable” results

Element		K			Ca			Mg		
Soil	Method	X, %	U _x , %	R	X, %	U _x , %	R	X, %	U _x , %	R
PS-1	1	0.68	0.05	30.1	12.12	0.36	82.3	2.31	0.16	75.2
	2	0.75	0.05	33.2	13.00	0.39	88.3	2.20	0.15	71.7
	3	0.57	0.04	25.2	13.42	0.40	91.1	2.04	0.14	66.5
	4	2.15	0.15	95.1	12.50	0.38	84.9	2.50	0.18	81.4
	5	2.01	0.14	88.9	12.90	0.39	87.6	2.54	0.18	82.7
	6	2.28	0.16	100.9	14.00	0.42	97.0	2.89	0.20	98.1
PS-2	1	0.55	0.04	20.0	1.29	0.04	44.8	0.95	0.07	57.6
	2	0.60	0.04	21.8	1.38	0.04	47.9	0.98	0.07	59.4
	3	0.42	0.03	15.3	1.54	0.05	52.1	0.82	0.06	49.7
	4	2.68	0.19	97.5	2.20	0.07	76.4	1.26	0.09	76.4
	5	2.39	0.17	86.9	2.36	0.07	81.9	1.57	0.11	95.2
	6	2.80	0.20	101.8	2.50	0.08	96.8	1.60	0.11	96.9
PS-3	1	0.51	0.04	21.4	3.90	0.12	53.1	1.44	0.10	63.2
	2	0.53	0.04	22.3	3.60	0.11	49.0	1.42	0.10	62.3
	3	0.50	0.04	21.0	3.80	0.11	51.8	1.34	0.09	58.8
	4	2.15	0.15	90.3	6.10	0.18	83.1	2.10	0.15	92.1
	5	2.10	0.15	88.2	6.25	0.19	85.1	2.17	0.15	95.2
	6	2.34	0.16	98.3	7.31	0.22	99.6	2.21	0.15	96.9

The results of the XRD analysis were verified by the SEM-EDS analysis (Fig. 4). The majority of the particles contained in the sediment are larger than 20 µm and are covered with mini crystallites (<0.1 µm) in the form of a sponge. The integrated EDS analysis shows the contents of K, Ca, Mg, F and Cl, included in the composition of the less soluble fluorides of calcium, magnesium and KClO₄, as well as the presence of Al, Si, Fe and Na. The use of HF in the absence of HClO₄ (Method 6) results in the complete extraction of potassium by the three certified samples (Table 2). The results presented in Tables 2 and 3 and Figures 1-4 show that the digestion method is a dominant factor in determining the content of K in soils.

Table 3. SEM/EDS examination (integral spectrum) after digestion of the certified sample by mixture of HNO₃ + HClO₄ + HF (ISO14869-1)

Element	Weight %	Atom %
Al	6.68	4.84
Si	26.08	18.15
Cl	0.61	0.34
K	2.23	1.11
Na	1.94	1.65
Ca	1.17	0.57
Ti	0.88	0.36
Fe	0.95	0.33
O	59.47	72.65

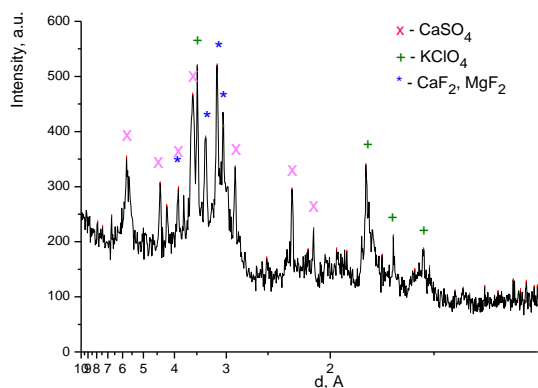


Fig. 3. X-ray pattern of the residue after digestion of the certified sample by mixture of $\text{HNO}_3 + \text{HClO}_4 + \text{HF}$ (ISO14869-1).

Determination of Ca and Mg

The results for Ca and Mg extraction (Table 2) are very different from those of potassium and are specific for each certified soil. In this case, the efficiency of extraction depends on the method of sample digestion, and on the soil type. The better extraction of Ca by PS -1 through all methods (> 80%) demonstrates the significant influence of soil type on results. In this model the basic amount of Ca is linked in an easily soluble calcium (16%) and dolomite (9%). The content of these components in the PS-3 significantly reduces as opposed to quartz and hardly soluble primary soil minerals, and PS - 2 contains only 2% calcite. This leads to a significant reduction in the rate of extraction in these samples through the first 3 methods. The relatively low level of leaching of calcium through methods 4 and 5 despite the use of acid mixtures disrupting largely silicate matrix. This leads to a significant reduction in the rate of extraction in these samples through the first 3 methods. The relatively low level of extraction of calcium through methods 4 and 5 is noteworthy despite the use of acid mixtures significantly disrupting the silicate matrix. The reason for this is the formation of insoluble fluorides which precipitate and significantly reduce the final result. This is confirmed by the results of the XRD and SEM–EDS analysis of insoluble sediment after digestion of the sample by method 5 (BSS/ISO14869-1), presented Fig. 3 and Table 3. Although crystal phases are highly dispersed, the presence of CaF_2 in the sediment is undeniable. The addition of H_3BO_3 in method 6 links the unreacted HF and prevents the formation of such fluorides, allowing the measurement of the total quantity of extracted calcium.

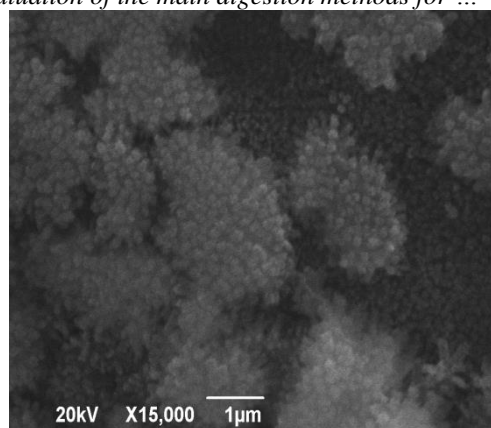


Fig. 4. SEM images of the residue after digestion of the certified sample by mixture of $\text{HNO}_3 + \text{HClO}_4 + \text{HF}$ (ISO14869-1).

Comparable with the results for Ca are the results obtained in the determination of the content of Mg. The highest degree of extraction by methods 1, 2 and 3 has been established in soil sample PS-1, containing easily soluble dolomite (9%) and magnesium (2%). In the other certified samples these components are missing, which explains the lower results. Significant increase of the results for all samples (> 80% extraction) is observed in the use of HF (methods 4, 5 and 6).

The comparative study of six of the most widely used methods of mineralization of soil samples for analysis of the content of K, Ca and Mg shows that:

1. The degree of extraction of the various elements is different and depends on the method of mineralization, as well as on the soil type. Acceptable results (over 80% extraction) for all tested elements can only be obtained by the methods of mineralization, involving the use of HF, and total extraction is only possible by method 6 (ISBN 19 081 01175)
2. The degree of extraction of K strongly increases with the increase of the aggressiveness of the acid mixture used. In this case, the method of sample preparation is dominant. In Ca, Mg the degree of extraction depends on the aggressiveness of the acid mixture used, as well as on the soil type.
3. The use of HClO_4 in the determination of K and HF in the determination of Ca and Mg leads to inaccurate results due to the formation of poorly soluble sediments from KClO_4 , CaF_2 and MgF_2 .

REFERENCES

1. A. Kabata – Pendias, *Trace elements in soil and plants*, 4th ed., Taylor and Francis group, (2011).
2. St. Ganev, *Contemporary soil chemistry*, Publishing House Science and Art, Sofia, (1990).

Ivanov et al. – “Application of X-Ray and SEM–EDS evaluation of the main digestion methods for ...”

3. ISO 11466, *Soil quality-extraction of trace elements soluble in aqua regia*, (1995).
4. C. Micó, M. Peris, J. Sánchez, L. Recatalá, *Commun Soil Sci. Plant Anal.*, **39**, 890 (2008).
5. EPA Method 3051, *Microwave assisted acid digestion of sediments, sludge, soils and oils*, (1994).
6. EPA Method 3052, *Microwave assisted acid digestion of siliceous and organically based matrices including ash, biological tissue, oil contaminated soil, sediment, sludge and soil*, (1996).
7. ISO 14869-1, *Quality of the soils. Mineralization for determining the total content of elements. Part 1: Mineralization with fluoride hydrogen and perchloric acid*, (2002).
8. GB Standing Committee of analysis. *Determination of Acid Soluble Cadmium, Chromium, Copper, Iron, Lead, Manganese, Mercury, Nickel and Zinc in Soils, Sediments and Sewage Sludge following Reflux Digestion with a Hydrochloric and Nitric Acid Mixture*, Paperback, Publisher H.M.S.O., ISBN-10: 0-11-751908-1, 36 (1987).
9. M. I. Kisser, *Digestion of solid matrices Part 1: Digestion with Aqua Regia Report of evaluation study*, HORIZONTAL – 18, internet address, (2005).
10. U. Kackstaetter, G. Heinrichs, *Water air soil poll*, **95**, 119 (1997).
11. P. Krause, B. Erbsloh, R. Pepelink, A. Prang, *Fres. J. Anal. Chem.*, **59**, 938 (1987).

ПРИЛОЖЕНИЕ НА РЕНТГЕНОСТРУКТУРНИЯ АНАЛИЗ И ЕЛЕКТРОННАТА МИКРОСКОПИЯ ПРИ ОЦЕНКАТА НА ОСНОВНИТЕ МЕТОДИ ЗА ПОДГОТОВКА НА ПОЧВЕНИ ПРОБИ ЗА АНАЛИЗ НА МАКРОЕЛЕМЕНТИ

К. И. Иванов¹, П. А. Запрянова¹, В. Р. Ангелова¹, Л. К. Доспатлиев²,

¹Катедра „Обща химия“, Аграрен университет, 4000 Пловдив, България

²Катедра „Фармакология, физиология на животните и физиологична химия“, Тракийски университет, Стара Загора, България

Постъпила на 14 ноември 2016 г.; приета на 2 декември 2016 г.

(Резюме)

Сравнени са два от най-често използваните методи за разлагане на почвени проби при анализ на микро- и макроелементи - киселинно разлагане и микровълнова минерализация, в различни варианти (ISO 11466; EPA Method 3051; EPA Method 3052; ISO 14869-1; GB, Standing committee of analysis, ISBN 0117519081 и смес от HNO₃ и HClO₄ киселина). Използвани са 3 сертифицирани почвени образци, отговарящи на 2 типа почви, широко разпространени в България: Светла алувиално-делувиална ливадна почва и Светла ливадно канелена почва. Определено е съдържанието на три основни макроелементи (K, Ca и Mg), като количествените измервания са извършени на атомно абсорбционен спектрометър Spekra AA 220, Varian, Australia. За да се изясни проблема със степента на извличане на елементите и факторите, които влияят върху нея, неразтворимите утайки след разлагане на пробите са изследвани с рентгеноструктурен анализ и сканираща електронна микроскопия. Установено е, че използването на HClO₄ при определяне съдържанието на K и на HF при определяне съдържанието на Ca и Mg води до формирането на неразтворими утайки от KClO₄, CaF₂ и MgF₂.

Ключови думи: пробоподготовка, почва, K, Ca, Mg.

Optimization of the operating conditions in inductively coupled plasma optical emission spectrometry

N.S. Velitchkova^{1*}, S.V. Velichkov², M. G. Karadjov¹, N. N. Daskalova²

¹Geological Institute, Bulgarian Academy of Sciences,
Acad. G. Bontchev Str., bl. 24, 1113 Sofia, Bulgaria

²Institute of General and Inorganic Chemistry, Bulgarian Academy of Sciences,
Acad. G. Bontchev Str., bl. 11, 1113 Sofia, Bulgaria

Received November 8, 2016; Revised December 22, 2016

Optimization of the plasma operating conditions was carried out in aspect to achieve the lowest possible detection limits by using radial viewing 40.68 MHz inductively coupled plasma optical emission spectrometry (ICP-OES). Mg II 280.270 nm / Mg I 285.213 nm line intensity ratios (Mg II / Mg I) was measured to evaluate the robustness of the plasma operating conditions. The operating conditions were affected by varying: incident power, carrier and sheathing gas flow rates. The relationship between the magnitude of Mg II / Mg I ratios and excitation temperature in ICP was obtained. The results show that the excitation conditions in ICP have to be modified only by varying the incident power and the sheathing gas flow rates at an optimal value of the carrier gas flow rate. In this case the aerosol formation and transport processes are the same under different excitation conditions in ICP. The excitation conditions from non robust to robust were varied for minimization of the detection limits in the determination of elements by using the selected prominent lines with different spectral characteristics in the presence of “pure” and complex matrices.

Keywords: ICP-OES, Optimization of operating condition, Traces of elements, Detection limits

INTRODUCTION

The optimization of the operating conditions was carried out in aspect to lower the detection limits by radial viewing inductively coupled plasma optical emission spectrometry (ICP-OES). The optimization procedure includes the following steps: line selection according to the absence or the lowest possible level of spectral interference; influence of the operating parameters (incident power, carrier and sheathing gas flow rates) on the net line and background intensities [1].

The sensitivities of different line intensity ratios were used to control the excitation conditions in ICP-OES. The Mg II 280.270 nm/Mg I 285.213 nm line intensity ratios (Mg II/Mg I) was found to remain a good compromise to follow the change in the plasma conditions. An advantage of this ratio is to be independent of the detector. Therefore, the absolute value of the ratio Mg II / Mg I can be used also for comparison of different ICP systems and operating conditions. This ratio has been widely used and is an appropriate test [2].

Some authors pay attention on the calculation of correction factor for the magnesium atom to ion line intensity signals when a blank solution is contaminated by magnesium [3]. There should be noted, that depending on the optical system, the two

magnesium lines may be located in adjacent orders, or at different locations within the same order, it may be necessary to compensate for a different wavelength response. A simple way to establish a correction factor is to assume that the continuum has a constant value in the range from 280 to 285 nm. It is then sufficient to measure the background emission at 280.2 nm and 285.2 nm [2]. Therefore, the background must be measured in the spectral windows around the corresponding magnesium spectral lines. In addition, when a blank solution is contaminated by magnesium, the background signals should be measured in λ_a of corresponding magnesium lines in order to obtain correct net line signals for the both magnesium lines.

Analytical performance in the optimization of an ICP-OES in order to minimize both the spectral interference level and the detection limits in the presence of line rich emission matrices requires the optimum line selection. The optimum line selection for trace analysis requires the choice of prominent lines free or negligibly influenced by line interference. This is the first essential optimization step [4, 5].

A large number of research groups have investigated the non-spectral matrix effects in order to suppress or eliminate this type of interference. The robust plasma conditions are more appropriate when compared to the non-robust plasma conditions. The

* To whom all correspondence should be sent.
E-mail: niaveli@geology.bas.bg

general conclusion from the investigations was that the total elimination of error from non-spectral interferences cannot be achieved under robust operating conditions, but only by precise matching of the acid and matrix contents in both the reference and the sample solutions [6-9].

Studies on the impact of operating conditions on the detection limits require the signal - to background ratios to be maximized and the relative standard deviation of the background signal to be minimized [1, 10, 11].

The purpose of the present paper is to investigate the possibilities of radial viewing 40.68 MHz ICP-OES to achieve the lowest possible detection limits by optimizing of the operating conditions. For this purpose the following data have been compiled by varying the carrier gas flow rate, incident power and sheathing gas flow rate:

(i) Different Mg II /Mg I line intensity ratios for control of the robustness of the plasma excitation conditions;

(ii) Relationship of the Mg II / Mg I and the excitation temperature (T_{exc});

(iii) Application of the methodology for optimization of the operating conditions in order to obtain the lowest possible detection limits in pure solvent and the true detection limits in the presence of "pure" and complex matrices.

EXPERIMENTAL

Instrumentation

The experiments were performed with a radial viewing ICP-OES system ULTIMA 2, Horiba group, Jobin Yvon, (Longjumeau, France), Meinhard nebulizer type P/N ER 2050 – 0710N and high dynamic detector based on photomultiplier tubes. The operating conditions were affected by different constant and variable parameters.

Reagents and test solutions

The concentration of magnesium in test solution for the plasma robustness measurement was $10 \mu\text{g ml}^{-1}$ and the concentration of titanium in solution for the temperature measurement was $8 \mu\text{g ml}^{-1}$.

In the determination of Sc, Y, La, Ce, Nd, Sm, Eu, Gd, Tb, Dy, Ho, Er, Tm and Yb the pure solvent contains 22 mg ml^{-1} solution of hydrochloric acid in double – distilled water. In the determination of rare earth elements (REE's) in lutetium oxide, the solutions contain all analytes and 8.79 mg ml^{-1} lutetium.

In the determination of Ce, Nd, Eu, Yb, Tm, Ga, Cr, Nb, Ni, Mn, Ge and Zr as dopants in single

crystals of potassium titanylphosphate (KTP) the pure solvent contains $142 \text{ mg ml}^{-1} \text{ H}_2\text{SO}_4$ and approximately $0.02 \text{ mg ml}^{-1} \text{ H}_2\text{O}_2$. The final concentration of KTP matrix was 8 mg ml^{-1} , $142 \text{ mg ml}^{-1} \text{ H}_2\text{SO}_4$ and approximately $0.02 \text{ mg ml}^{-1} \text{ H}_2\text{O}_2$. Plastic or polytetrafluoroethylene ware was used throughout.

RESULTS AND DISCUSSION

Evaluation of the robustness of the operating conditions by Mg II / Mg I in ICP

The operating conditions were affected by varying:

(i) Carrier gas flow rate and sheathing gas flow rate at a constant value of incident power;

(ii) Incident power and the sheathing gas flow rate, whereas the carrier gas flow rate remained a constant value (0.4 l min^{-1}). This is an optimal value for carrier gas flow rate, in accordance with the recommendations for the Meinhard nebulizer.

Influence of carrier gas flow rate and sheathing gas flow rate at a constant value of the incident power

The effect of carrier and sheathing gas flow rates as variable parameters at a constant value of incident power of 1000 W on the Mg II / Mg I in pure solvent is presented in Figure 1.

Three different shape curves were obtained:

(i) The bell-shaped curves were derived by varying:

- By varying the carrier gas flow rates from 0.2 l min^{-1} to 0.7 l min^{-1} (without sheath gas flow) (Fig. 1, curve 1). The highest of Mg II / Mg I ratios were obtained at carrier gas flow rates from 0.4 to 0.6 l min^{-1} i.e., at optimal carrier gas flow rates for this type of nebulizer, which ensures the highest efficiency. This value is noted from the manufacturer for each type of nebulizer separately;

- By varying sheath gas flow rates from 0 to 1.0 l min^{-1} at a constant value of the carrier gas flow rates 0.2 l min^{-1} (Fig. 1 curve 2). The carrier gas flow rate of 0.2 l min^{-1} (without sheath gas) is lower than the optimal rate. This value is not enough for an effective transfer of the aerosols to the inductively coupled plasma. The net line signals of Mg II 280.270 nm and Mg I 285.213 nm as well as the corresponding Mg II / Mg I ratios are very low. By adding 0.2 l min^{-1} sheath gas, the Mg II / Mg I ratios increase significantly, because here the sheath gas flow rate ensures more effective transport of the aerosols to the plasma and more effective exchange of the energy between the high frequency field and the central channel.

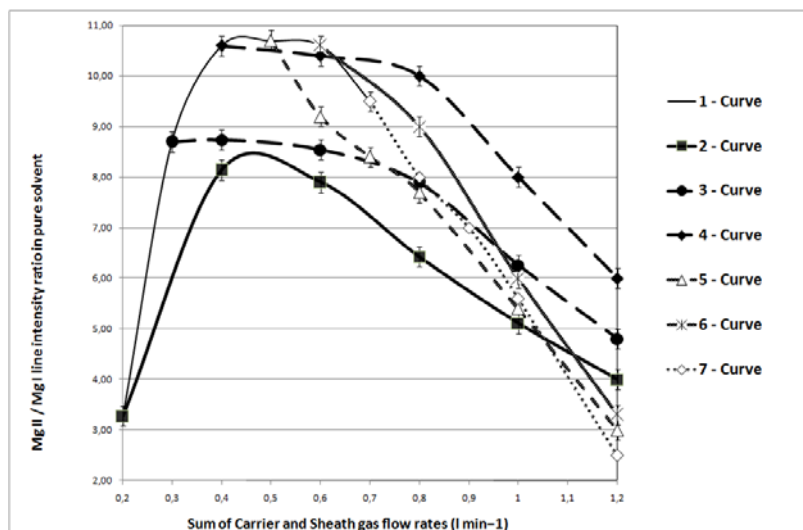


Fig. 1. Effect of carrier and sheathing gas flow rates as variable parameters at a constant value of incident power (1 000 W) on the Mg II / Mg I in pure solvent: **Curve 1** - variable carrier gas flow rates without sheathing gas; **Curve 2** - constant carrier gas flow = 0.2 l min⁻¹ + variable sheathing gas; **Curve 3** - constant carrier gas flow = 0.3 l min⁻¹ + variable sheathing gas; **Curve 4** - constant carrier gas flow = 0.4 l min⁻¹ + variable sheathing gas; **Curve 5** - constant carrier gas flow = 0.5 l min⁻¹ + variable sheathing gas; **Curve 6** - constant carrier gas flow = 0.6 l min⁻¹ + variable sheathing gas and **Curve 7** - constant carrier gas flow = 0.7 l min⁻¹ + variable sheathing gas.

The exchange of energy between the high frequency field and the central channel is critical [12].

Therefore, the bell-shaped curves can be obtained when the investigation of the relation between Mg II / Mg I ratios and the carrier gas flow rates begins with a value of carrier gas lower than the corresponding optimal value for a given nebulizer.

(ii) The second types of curves are with plateau (Fig. 1, curves 3 and 4). The constant value of the magnitude of the Mg II / Mg I ratios were derived in both cases:

- Carrier gas flow rate 0.3 l min⁻¹ and sum of carrier and sheath gas flow rates 0.4 l min⁻¹ + 0.2 l min⁻¹ (Fig. 1, curves 3);

- Carrier gas flow rate 0.4 l min⁻¹ and sum of carrier and sheath gas flow rates 0.4 l min⁻¹ + 0.2 l min⁻¹ (Fig. 1 curves 4).

The influence of energy transfer between the plasma and the injected species was found to be insignificant by adding 0.1 or 0.2 l min⁻¹ sheath gas flows to the 0.3 or 0.4 l min⁻¹ to the carrier gas flow [12]. Here the Mg II / Mg I ratio remains constant. Further, by increasing of the sheath gas at the above mentioned constant carrier gas flow rates, the Mg II / Mg I ratio decrease slightly (Table 1, Fig. 1, curves 3 and 4).

(iii) The third type of curves show, that with the increase of the sheath gas flow rates at constant carrier gas flow rates 0.5, 0.6 or 0.7 l min⁻¹, the magnitude of the Mg II / Mg I ratio decrease (Fig. 1, curves 5, 6 and 7). Under these experimental

conditions the sheath gas flow rates influence significantly the energy transfer between the plasma and the injected species and the magnitude of the Mg II / Mg I ratio decrease. The laminar sheath gas and the carrier gas enter into the plasma separately (without mixing) and influence in a different way the processes in the inductively coupled plasma [12].

There should be underlined that in the literature different curve shapes are published for inductively coupled plasmas (radial and axial viewing), by using different type of nebulizers and spray chambers [13 - 21]. In the present paper all types of curves were obtained by using a radial viewing 40.68 MHz ICP and Meinhard nebulizer, type P/N ER 2050 – 0710N. The relative standard deviation in the determination of the Mg II/Mg I ratios is 5%.

Influence of incident power and sheathing gas flow rate on the Mg II / Mg I ratio in pure solvent at a constant value of carrier gas flow rate

The corresponding results for different values of incident power and sum of carrier and sheathing gas flow rates are shown on the Fig. 2, A and B. The following conclusions can be drawn:

(i) The magnitude of the Mg II / Mg I ratios do not change for a sum of carrier and sheathing gas flow rates between 0.4 and 0.6 l min⁻¹ for different values of incident power in pure solvent (Fig. 2 A and B). Probably for a sheathing gas flow rate of 0.2 l min⁻¹, the energy transfer between the plasma and the injected species is not influenced [12], regardless of the magnitude of incident power. Further, with increasing of the sheathing gas flow rate, the Mg II /

Mg I decreases. The shape of the curves (Fig. 2A) follow the same pattern as the curves 3 and 4 (Fig. 1). By increasing the sum of carrier and sheathing gas flow rates higher than 0.6 l min⁻¹ the Mg II / Mg I ratios decrease and follow the shape of the curves, shown on Fig.1 (curves 5, 6 and 7).

(ii) Higher Mg II / Mg I ratios are obtained with a lower sum of carrier and sheathing gas flow rates for a given incident power. The Mg II / Mg I ratios increase with the increasing of the incident power for all sums of carrier and sheathing gas flow rates (Fig.2, A).

(iii) Equal Mg II/Mg I ratios can be obtained for different combinations of sums of carrier and sheathing gas flow rates and incident powers.

Relationship between the Mg II / Mg I ratio and the plasma excitation temperature (T_{exc})

The relationship between the magnitude of Mg II /Mg I and T_{exc} in a pure solvent was derived. The T_{exc} was measured by the Boltzmann plot method with titanium lines for nine combinations between incident power and sheathing gas flow rates [22].

Five values for the T_{exc} were obtained with each of the eight combinations (Table 1, column 3). In all

cases T_{exc} ± 200 K was obtained. The results show that higher Mg II / Mg I ratios correspond to higher values of T_{exc}.

It could be concluded that the excitation conditions in ICP have to be modified by varying the incident power and the sheathing gas flow rates at an optimal value for the carrier gas flow rate, in accordance with the recommendations for the Meinhard nebulizer. The equipment with sheathing gas device gives possibility to change the ionization and excitation conditions of the plasma by varying the sheathing gas flow and the incident power at a constant optimal value of the carrier gas. The carrier flow is not only a very critical parameter of the ICP but also a nebulizer parameter that governs the amount of aerosol carried to the plasma [1]. At constant optimal value of carrier gas flow rate the aerosol formation and transport processes do not change under different excitation conditions in ICP.

There should be noted that by using ICP-OES equipments without sheathing gas device, the change of the operating conditions can be achieved by varying the incident power at an optimal carrier gas flow rate.

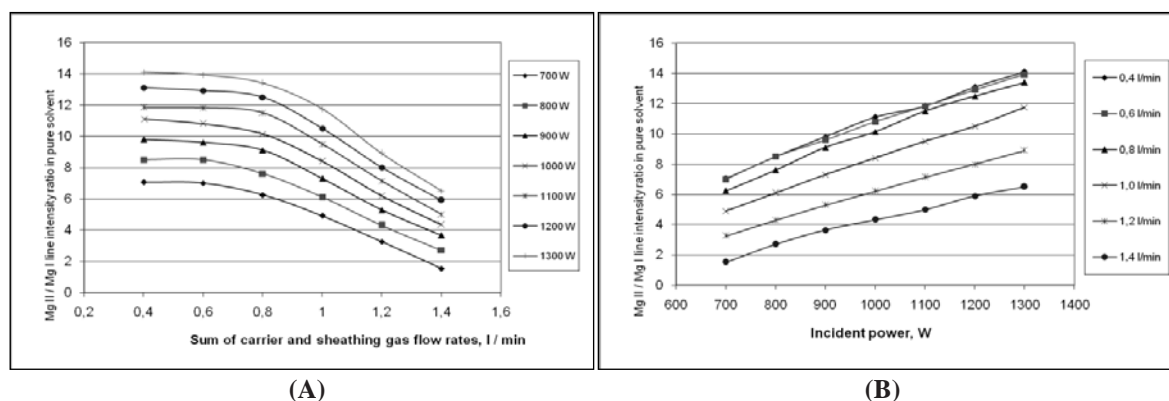


Fig.2. Effect of incident power (A) and sheathing gas flow rate (B) on the Mg II / Mg I ratio in pure solvent at a constant value of carrier gas flow rate

Table 1. Type of operating conditions obtained at a constant optimal value of the carrier gas flow rate of 0.4 l min⁻¹, variable sheathing gas flow rate and incident power

Type of operating conditions	Mg II / Mg I	T _{exc} , K	Incident power, W	Sum of carrier and sheathing gas flow rates, l min ⁻¹
Non-robust	1.8	5200 ± 200	700	1.4 = 0.4 + 1.0
	3.6	6000 ± 200	700	1.2 = 0.4 + 0.8
Semi-robust	6.0	6580 ± 200	800	1.0 = 0.4 + 0.6
	6.0	6580 ± 200	1 000	1.2 = 0.4 + 0.8;
Robust	11	7200 ± 200	1 000	0.4 = 0.4 + 0
	11	7200 ± 200	1 100	0.8 = 0.4 + 0.4
	12	7500 ± 200	1 100	0.6 = 0.4 + 0.2
	12	7500 ± 200	1 200	0.8 = 0.4 + 0.4

Table 1 summarizes the type of excitation conditions, which were obtained by radial viewing

40.68 MHz ICP. Hence, by varying the excitation conditions from non-robust to robust (Table 1) the

lowest possible detection limits in pure solvent and in the presence of different matrices can be achieved. The above mentioned methodology was applied for optimization of the operating conditions in order to minimize the detection limits in the determination of trace of elements in the presence of different matrix constituents.

Minimization of the true detection limits in the determination of Sc, Y, La, Ce, Pr, Nd, Sm, Eu, Gd, Tb, Dy, Ho, Er, Tm and Yb in pure solvent and in the presence of 10 mg ml⁻¹ lutetium oxide (8.79 mg ml⁻¹ lutetium) as matrix

Lutetium is a typical rare earth element characterized by a full f-level. This element emits a relatively smaller number of spectral lines in comparison to the REEs from cerium to erbium. Besides, in the presence of matrix lutetium, the strong LuO bands have been registered at $T_{exc} \approx 6200$ K around the prominent lines of La, Ce, Pr, Nd, Sm and Eu. The intensities of the molecular bands considerably decrease or disappear altogether at $T_{exc} \approx 7200$ K. Optimal line selection for trace analysis require the choice of the prominent lines free or negligibly influenced by line interference [4].

The detection limits in pure solvent were calculated in accordance to Eq. (1) [1]:

$$C_L = 2\sqrt{2} \times 0.01 \times RSDB \times BEC \quad (1)$$

The true detection limit ($C_{L\ true}$) in the presence of "pure" rare earth matrices was expressed by Q - values for line interference [$Q_I(\lambda_a)$] and wing background interference [$Q_W(\Delta\lambda_a)$] levels, respectively in accordance with (Eq. (2)) [4].

$$C_{L\ true} = 2/5 Q_I(\lambda_a) \times C_1 + 2\sqrt{2} \times 0.01 \times RSDBL \times [BEC + Q_I(\lambda_a) \times C_1 + Q_W(\Delta\lambda_a) \times C_1] \quad (2)$$

The magnitude of [$Q_I(\lambda_a)$] values is of primary importance for the magnitude of the true detection limits. The influence of the wing background interference levels [$Q_W(\Delta\lambda_a)$] is negligible (Eq. 2).

The effect of the operating conditions (varying from non-robust to robust) on the magnitude of background equivalent concentration in pure solvent (BEC), [$Q_I(\lambda_a)$] values for line interferences and

[$Q_W(\Delta\lambda_a)$] values for wing interferences in the presence of 8.79 mg ml⁻¹ lutetium for the selected analysis lines of Sc, Y, La, Ce, Pr, Nd, Sm, Eu, Gd, Tb, Dy, Ho, Er, Tm and Yb were studied. The lowest values of BEC, [$Q_I(\lambda_a)$] and [$Q_W(\Delta\lambda_a)$] values were measured at Mg II / Mg I ratio of about 3.6 which corresponds to ($T_{exc} \approx 6000$ K).

By using BEC, [$Q_I(\lambda_a)$] and [$Q_W(\Delta\lambda_a)$] values in the presence of 8.79 mg ml⁻¹ lutetium as matrix, which were measured under different excitation conditions (non-robust, semi robust and robust) (Table 1), the detection limits in pure solvent by (Eq. 1) and the true detection limits by Eq.(2) were obtained.

Figure 3 A and B shows the relationships between the Mg II / Mg I ratios and the detection limits in pure solvent (A) and the true detection limits in the presence of 8.79 mg ml⁻¹ lutetium in solution (B).

In conclusion, the non-robust conditions at $T_{exc} \approx 6000$ K (Mg II / Mg I = 3.6) proved to be more appropriate for the determination of traces of REE's in a pure solvent and in the presence of 8.79 mg ml⁻¹ lutetium as a matrix as compared to the robust conditions. The detection limits under non-robust excitation conditions at $T_{exc} \approx 6000$ K (Mg II / Mg I = 3.6) are between 3 and 6 times lower than under robust excitation conditions at $T_{exc} \approx 7200$ K (Mg II / Mg I = 10) in pure solvent as well as in the presence of lutetium oxide as a matrix for the analytes Sc, Y, La, Pr, Sm, Eu, Gd, Tb, Dy, Ho, Er, Tm and Yb.

Q-values due to LuO molecular bands for the analysis lines of cerium (Ce II 413.765 nm) and neodymium (Nd II 401.225 nm) decrease with the increase of the Mg II / Mg I ratio in the presence of a lutetium matrix. Q-values for line interference [$Q_I(\lambda_a)$] are equal to zero for Mg II / Mg I from 9 or 11 in the case of Nd II 401.225 nm or Ce II 413.380 nm, respectively, i.e. at an $T_{exc} \approx 7200$ K [4]. In addition the sums of the ionization and excitation potentials for the ionic prominent lines of REE's vary from 8.9 to 10.0 V [23, 24]. This conclusion is in accordance with [25].

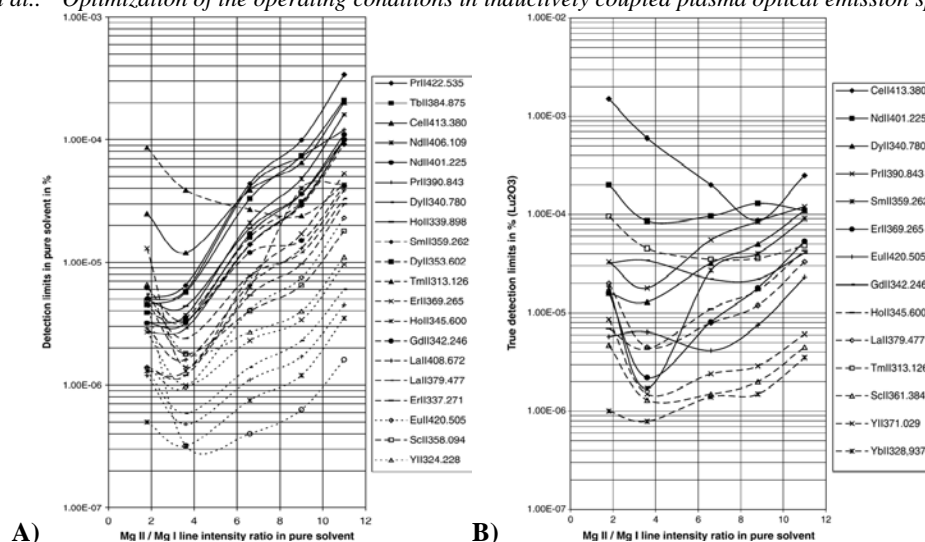


Fig. 3. Relationship between Mg II 280.270 nm / Mg I 285.213 nm line intensity ratios and the detection limits in pure solvent (A) and the true detection limits in the presence of 8.79 mg ml⁻¹ lutetium in solution (B)

By using the selected prominent lines (in nm) the following detection limits (in %) were reached:

(i) Detection limits in pure solvent (C_L) (in %): Sc II 358.094 - 1.9×10^{-6} , Y II 324.228 - 1.8×10^{-6} , Y II 360.073 - 1.0×10^{-6} , Y II 360.073 - 1.0×10^{-6} , La II 408.672 - 1.0×10^{-6} , Ce II 413.380 - 1.1×10^{-5} , Pr II 422.293 - 6.5×10^{-6} , Nd II 406.109 - 3.3×10^{-6} , Sm II 359.260 - 4.3×10^{-6} , Eu II 420.505 - 1.0×10^{-6} , Gd II 342.247 - 3.4×10^{-6} , Tb II 356.852 - 5.7×10^{-6} , Dy II 353.602 - 4.0×10^{-6} , Ho II 339.898 - 4.4×10^{-6} , Er II 337.271 - 1.3×10^{-6} , Tm II 313.126 - 3.9×10^{-5} , Yb II 328.937 - 3.0×10^{-7} and Lu II 261.542 - 3.0×10^{-7} .

(ii) True detection limits ($C_{L \text{ true}}$) in the presence of 8.79 mg ml⁻¹ lutetium as matrix (in %): Sc II 361.384 - 1.3×10^{-6} , Y II 371.030 - 1.5×10^{-6} , La II 379.478 - 4.5×10^{-6} , Ce II 413.765 - 8.7×10^{-5} , Pr II 390.844 - 1.8×10^{-5} , Nd II 401.225 - 1.1×10^{-4} , Sm II 359.260 - 1.2×10^{-5} , Eu II 420.505 - 6.4×10^{-6} , Gd II 342.247 - 3.4×10^{-5} , Tb II 384.873 - 1.4×10^{-5} , Dy II 340.780 - 1.3×10^{-5} , Ho II 345.600 - 4.3×10^{-6} , Er II 369.265 - 2.2×10^{-6} , Tm II 313.126 - 4.5×10^{-5} , Yb II 328.937 - 7.9×10^{-7} .

There would be noted that in the case of a lutetium matrix, for Ce and Nd the lowest detection limits were obtained under robust excitation conditions. The LuO bands registered around Ce II 413.380 nm and Nd II 401.225 nm disappeared at higher excitation temperatures [4]. In the presence of a lutetium matrix, the line interference level is lower in comparison with the rare earth matrices from cerium to erbium and the worsening of the true detection limit is negligible in comparison with the detection limits in pure solvent.

Minimization of the true detection limits in presence of 8 mg ml⁻¹ KTP

Single crystals of potassium titanylphosphate (KTP) doped with Ce, Nd, Eu, Yb, Tm, Ga, Cr, Nb, Ni, Mn, Ge and Zr are excellent materials for electrooptical applications and laser technique. The methodology for optimization was applied by using the selected analysis lines [5]. Tables 2 and 3 present the selected prominent lines (columns 1) with different sums of ionization and excitation potentials (columns 2) and true detection limits (in %) with respect to the dissolved solid (8 mg ml⁻¹ KTP in solution) (columns 3).

The results from Tables 2 and 3 demonstrate that by varying T_{exc} , the plasma emits spectral lines with different net line signals depending on the sums of the ionization and excitation potentials of the selected ionic analysis lines.

Table 2. True detection limits ($C_{L \text{ true}}$) for Ce, Nd, Eu, Yb, Tm and Ga with respect to the dissolved solid in solution for solid concentration of 8 mg ml⁻¹ KTP (in %)

Selected analysis lines, λ , nm	Optimal excitation temperature $T_{\text{exc}} \approx 6000$ K (Mg II / Mg I = 3.6)	
	Sum = ionization + excitation potentials, (V) [23, 24]	$C_{L \text{ true}}$ (%)
Ce II 413.380	9.33	2.6×10^{-4}
Nd II 406.109	9.01	6.6×10^{-4}
Eu II 381.967	8.91	1.0×10^{-5}
Yb II 328.937	10.02	3.3×10^{-5}
Tm II 317.283	10.02	4.0×10^{-5}
Ga I 294.364	10.31	1.3×10^{-4}

Table 3. True detection limits ($C_{L \text{ true}}$) for Nb, Ni, Mn, Ge and Zr with respect to the dissolved solid in solution for solid concentration of 8 mg ml⁻¹ KTP (in %)

Optimal excitation temperature $T_{\text{exc}} \approx 7200$ K (Mg II / Mg I = 10)		
Selected analysis lines, λ , nm	Sum = ionization + excitation potentials, (V) [23, 24]	$C_{L \text{ true}}$ (%)
Nb II 269.706	11.63	2.0×10^{-4}
Ni II 221.647	14.26	1.6×10^{-4}
Mn II 257.610	12.14	2.5×10^{-5}
Ge II 265.158	12.57	1.6×10^{-2}
Zr II 343.823	12.53	4.6×10^{-5}

The lowest true detection limits for the elements Ce, Nd, Eu, Yb, Tm, Ga were obtained at optimal excitation temperature $T_{\text{exc}} \approx 6000$ K (Mg II / Mg I = 3.6). The sum of the ionization and excitation potentials for the ionic prominent lines of rare earth elements varies from 8.9 V to 10.3V (Table 2, column 2) [23, 24]. For Cr, Nb, Ni, Mn, Ge and Zr the lowest true detection limit were obtained at optimal excitation temperature $T_{\text{exc}} \approx 7200$ K (Mg II / Mg I = 10) in pure solvent and in the presence of a KTP matrix. The sum of the ionization and excitation potentials for the ionic prominent lines of these elements varies from 11.6 V to 14.26 V (Table 3, column 2) [23, 24].

CONCLUSIONS

Improvement of the detection limits from three to six times in pure solvent and the true detection limits in the presence of different matrix was achieved by optimisation of the plasma operating conditions. The lowest possible detection limits were obtained under different excitation conditions depending on the spectral characteristics of the selected prominent lines and the interfering matrix lines. There should be noted that the type of background as molecular bands must be taken into account in the optimization of the operating conditions in the determination of REE's in the presence of lutetium as matrix.

REFERENCES

1. P.W.J.M. Boumans, Basic concepts and characteristics of ICP-AES, in: Boumans (Ed.), Inductively Coupled Plasma Emission Spectroscopy, Part 1, Methodology, Instrumentation, and Performance, Wiley, New York, 1987, p. 100, Chapter 4.
2. J. Dennaud, A. Howes, E. Poussel, J.M. Mermet, *Spectrochim. Acta Part B* **56**, 101 (2001).
3. E. Abad-Peña, M.T. Larrea-Marin, M. Villanueva-Tagle, M. Simeón Pomares-Alfonso, *Spectroscopy Letters* **49**, 19 (2016).
4. S. Velichkov, E. Kostadinova, N. Daskalova, *Spectrochim. Acta Part B* **53** 1863 (1998).
5. N. Daskalova, S. Velichkov, P. Slavova, E. Ivanova, L. Aleksieva, *Spectrochim. Acta Part B* **52**, 257 (1997).
6. M. Stepan, P. Musil, E. Poussel, J.M. Mermet, *Spectrochim. Acta Part B* **56**, 443 (2001).
7. J.M. Mermet, *Anal. Chim. Acta* **250**, 85 (1991).
8. G.C.-Y. Chan, W.T. Chan, X. Mao, R.E. Russo, *Spectrochim. Acta Part B* **56**, 77 (2001).
9. C.Y. Chan, G.M. Hieftje, *Spectrochim. Acta Part B* **61**, 642 (2006).
10. M.W. Blades, G. Horlick, *Spectrochim. Acta Part B* **36**, 871 (1981).
11. H. Kawaguchi, T. Ito, A. Mizuike, *Spectrochim. Acta Part B* **36**, 615 (1981).
12. M. Murillo, J.M. Mermet, *Spectrochim. Acta Part B* **42**, 1151 (1987).
13. M. Carré, K. Lebas, M. Marichy, M. Mermet, E. Poussel, J.M. Mermet, *Spectrochim. Acta Part B* **50**, 271 (1995).
14. I. Novotny, I.C. Farinas, Wan-Jia-Iiang, E. Poussel, J.-M. Mermet, *Spectrochim. Acta Part B* **51**, 1517 (1996).
15. M. Grotti, E. Magi, R. Frache, *J. Anal. At. Spectrom.* **15**, 89 (2000).
16. P. Masson, A. Vives, D. Orignac, T. Prunet, *J. Anal. At. Spectrom.* **15**, 543 (2000).
17. J. Dennaud, A. Howes, E. Poussel, J.M. Mermet, *Spectrochim. Acta Part B* **56**, 101 (2001).
18. M. Iglésias, T. Vaculovic, J. Studynkova, E. Poussel, J.M. Mermet, *Spectrochim. Acta Part B* **59**, 1841 (2004).
19. A. Chazi, S. Qamar, *J. Chem. Sic. Pak.* **29**, 307 (2007).
20. A. Guimarães-Silva, J. de Lena, R. Froes, L. Costa, C. Nascentes, *J. Braz. Chem. Soc.* **23**, 753 (2012).
21. A. Oliveira, N. Baccan, S. Cadore, *J. Braz. Chem. Soc.* **23**, 838 (2012).
22. J.M. Mermet, Spectroscopic diagnostics: basic concepts, in: P.W.J.M. Boumans (Ed.), Inductively Coupled Plasma Emission Spectroscopy, Part 1, Methodology, Instrumentation and Performance, Wiley, New York, 1987, p. 353, Chapter 10.
23. A. Zaidel, V. Prokofev, S. Raiskii, V. Slavnyi, E. Ya Shreider, Tables of spectral lines, IFI / Plenum, New York, 1970.
24. J. Wysocka-Lisec, Spectrum Lines of Rare Earths Arranged by Wavelengths, Lubelskie Towarzystwo Naukowe, Lodz, 1970.
25. C. Dubuisson, E. Poussel, J. L. Todoli, Mermet, *Spectrochim. Acta B* **53**, 593 (1998).

ОПТИМИЗИРАНЕ НА РАБОТНИТЕ УСЛОВИЯ ПРИ ОПТИЧНАТА ЕМИСИОННА СПЕКТРОМЕТРИЯ С ИНДУКТИВНО СВЪРЗАНА ПЛАЗМА

Н. С. Величкова^{1*}, С. В. Величков², М. Г. Караджов¹, Н. Н. Даскалова²

¹ *Геологически институт, Българска Академия на Науките, ул. „Акад. Г. Бончев” бл. 24, 1113 София, България, e-mail: niaveli@geology.bas.bg*

² *Институт по обща и неорганична химия, Българска Академия на Науките, ул. „Акад. Г. Бончев” бл. 11, 1113 София, България, e-mail: nonidas@hotmail.com*

Постъпила на 8 ноември 2016 г.; приета на 22 декември 2016 г.

(Резюме)

Оптимизирането на работните условия беше изследвано с цел понижаване на границите на откриване при оптичната емисионна спектрометрия с 40.68 MHz индуктивно свързана плазма с радиално наблюдение (ИСП-ОЕС). Mg II 280.270 nm / Mg I 285.213 nm (Mg II / Mg I) интензитетно отношение беше използвано за оценка на твърдостта на работните условия в плазмата. Работните условия бяха променяни чрез вариране на входящата мощност, аерозол носещия и обгръщащия газови потоци. Получена е експерименталната зависимост между големината на Mg II / Mg I и температурата за възбуждане в ИСП. Резултатите показват, че условията за възбуждане в ИСП трябва да се променят от меки към твърди чрез вариране на входящата мощност и обгръщащия газов поток при оптималната стойност на аерозол-носещия поток. В този случай процесите на формирането и транспортирането на аерозолите остават едни същи при различните условия за възбуждане. Чрез промяна на работните условия в плазмата от меки до твърди бяха постигнати най-ниски граници на откриване при определяне на елементи в еднокомпонентни и многокомпонентни матрици, използвайки избраните аналитични линии с различни спектрални характеристики.

Ключови думи: *ИСП-ОЕС, Оптимизиране на работните условия, Следи от елементи, Граници на откриване*

Synthesis and characterization of lanthanoid complexes with 3, 3'- [(4-bromophenyl)methylene]bis (4-hydroxy-2h-1-benzopyrane-2-one)

V. I. Kircheva^{1*}, J. Ts. Zaharieva¹, I. Manolov², M. M. Milanova¹

¹*Sofia University, Faculty of Chemistry and Pharmacy, Department of Inorganic Chemistry,
1, Bourchier, 1164 Sofia, Bulgaria*

²*Medical University, Faculty of Pharmacy, Department of Organic Chemistry,
2, Dunav Str., 1000 Sofia, Bulgaria*

Received November 11, 2016; Revised January 21, 2017

Complexes of coumarin derivate 3, 3'-[(4-bromophenyl)methylene]bis-(4-hydroxy-2H-1-benzopyrane-2-one), with some lanthanoid ions Ln(III) = La(III), Nd(III), Eu(III), Gd(III), and Tb(III) were synthesized. The complexes obtained were characterized by means of elemental analysis, IR spectroscopy, UV-Vis spectroscopy, fluorescence spectroscopy and microscopy. The spectral data of the synthesized complexes were interpreted on the basis of comparison with the spectra of the free ligand in order to determine the mode of coordination in the complexes. Results from the IR spectra suggested that the coordination is through the carbonyl oxygen atom as well as through the deprotonated hydroxyl group. The complexes possess optical properties shown by their absorption in the UV/Vis region. The excitation and emission spectra of Tb(III) complex were taken in solid state. The lifetime of the excited state was measured.

Key words: Lanthanoids, Complexes, Biscoumarins, IR spectroscopy, Optical properties.

INTRODUCTION

The coumarin (also known as 1,2-benzopyrone) and its derivatives are a large class of chemical compounds with arising interest during the last few years. Most of them are naturally occurring and can be found in plants, bacteria and fungi [1, 2]. Coumarin compounds can be synthesized using different chemical methods such as Pechman reaction [3, 4], Knoevenagel condensation [5, 6], and etc. Different types of substitution of the parent ring suppose that coumarins are extremely variable in structure resulting in large variety in their properties. Some of them are used as drugs in medicine [7, 8], as well as pharmacological agents [9-11]. Coumarins can be used as optic agents, since fluorescent coumarin derivatives have been widely used in many applications from cell biology, medicinal analysis, lasers, and sensors to the advanced photochemical systems [12-15], because of their extended spectral range, high emission quantum yields, photostability, and good solubility in the safest solvents.

Recently coumarin compounds have been investigated for their coordination ability. In literature there is a lot of data concerning coordination properties of coumarins towards different metal ions [16-19]. It is important to understand the relationship between structure of the synthesized metal complexes and their properties.

Some authors have observed the influence of the complexation on biological properties; they pointed out that the metal ion can improve the biological activity of the investigated compounds [20-22]. Other articles have described the influence of the metal ion on their spectroscopic properties [22-24].

During last few years compounds of 3,3'-benzylidene-bis[4-hydroxycoumarin] with different substitution in the benzylidene ring have been synthesized and investigated [25-27]. Synthesis of their lanthanoid complexes is another area of scientific interest. The synthesized complexes were investigated by different physicochemical methods and molecular modeling methods [27, 28]. Their pharmacological properties were also tested [29]. Complexes showed good optical properties, which can be well-preserved after their immobilization in different matrices [23, 30].

In the current research we used the coumarin compound 3,3'-[(4-bromophenyl)methylene]bis-(4-hydroxy-2H-1-benzopyrane-2-one), C₂₅H₁₅O₆Br. It belongs to the group of 3,3'-benzylidene-bis(4-hydroxy-2H-1-benzopyrane-2-one) derivatives, with different substitutes like –OH, –NO₂, –OCH₃, –Cl, etc. This compound (named for short L15-Br) possess –Br substitute on *para* position in the benzylidene ring (Fig. 1).

* To whom all correspondence should be sent.

E-mail: vesi_ch@abv.bg

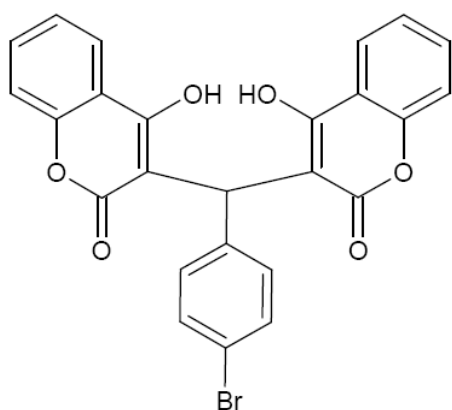


Fig. 1. Chemical formula of 3,3'-[(4-bromophenyl)-methylene]bis-(4-hydroxy-2H-1-benzopyrane-2-one), (L15-Br)

We synthesized complexes of L15-Br with some lanthanoid ions – La(III), Nd(III), Eu(III), Gd(III), and Tb(III) – and studied their structures and properties by physicochemical methods.

EXPERIMENTAL

Chemicals used for the experiments were of analytical grade. A coumarin compound 3, 3'-[(4-bromophenyl)methylene]bis-(4-hydroxy-2H-1-benzopyrane-2-one), $C_{25}H_{15}O_6Br$, synthesized by Knoevenagel condensation [31], was used as a ligand.

Metal salts used were lanthanoid nitrates hydrates, among them $Nd(NO_3)_3 \cdot 6H_2O$ was purchased from Fluka, $La(NO_3)_3 \cdot 6H_2O$ was purchased from Merck, both were of p.a. grade. The others like $Tb(NO_3)_3 \cdot 7H_2O$, $Eu(NO_3)_3 \cdot 8H_2O$, $Gd(NO_3)_3 \cdot 9H_2O$ were prepared by dissolving the lanthanoid oxides in diluted nitric acid, followed by crystallization and recrystallization. The hydrated water was determined by complexometric titration. Ethyl alcohol, dimethyl sulfoxide and acetone were used as solvents.

Complexes were synthesized in two steps. As a first step the ligand was dissolved in water/ethanol solution under magnetic stirring and 1M NaOH (aqueous solution) was added dropwise in order to deprotonate a hydroxyl group of the ligand. The stirring continued until complete dissolution of the ligand. To the solution formed, as a second step, the ethanol solution of the lanthanoid nitrate was added dropwise. The suspension obtained was kept stirred for 3 hours, and then filtered and washed several times with water. The drying in a desiccator to constant mass resulted in a powder probe. All the samples were recrystallized by acetone, except Eu(III) complex, which was recrystallized by ethanol.

The complexes synthesized were characterized by automatic analyzer EuroEA 3000, which allows

simultaneous determination of the content of carbon, hydrogen and nitrogen in samples of organic compounds and materials. The content of the metal ion was determined by complexometric titration in ethanol media.

The IR spectra of the ligand and the complexes were registered in KBr pellets with a diameter of 13 mm. The spectra were recorded on a Thermo Scientific Nicolet iS5 Fourier-Transform IR spectrometer (DTGS detector) at a spectral resolution of 2 cm^{-1} and accumulation of 64 scans. The spectra were scanned in the $4000 - 400\text{ cm}^{-1}$ range.

Optical properties were investigated with an Evolution 300 UV-Vis spectrometer (Thermo Scientific) and a Cary Eclipse spectrometer with a xenon lamp as the excitation source as well as on an N-400M fluorescence microscopy.

RESULTS AND DISCUSSION

Elemental analysis

The elemental analysis data obtained served as a basis for determination of empirical formulae of the compounds. It turned out that there is a good agreement between the calculated values and the found. On that base we suggested that every lanthanoid ion binds with three molecules of the ligand and different number of water molecules, in agreement with preferred high coordination number of the metal ion. The so synthesized complexes are proposed to be with $Ln(HL)_3 \cdot nH_2O$ stoichiometry for La(III), Nd(III), Eu(III), Gd(III), Tb(III), where $HL = (C_{25}H_{14}O_6Br)^-$ is the mono-deprotonated form of the ligand, since sodium hydroxide was used in synthetic procedure. The complexes were found to be soluble in dimethyl sulfoxide, dichloromethane, and dimethylformamide, slightly soluble in ethanol but insoluble in water. The elemental composition (in %), the formulae with the coordination water included as well as the respective symbols used for the complexes, are presented below:

LaL15-Br, $La(HL)_3 \cdot H_2O$; %C (55.34/55.52), %H (2.72/3.32), %La (8.53/7.98),

NdL15-Br, $Nd(HL)_3 \cdot 3H_2O$; %C (53.96/53.08), %H (2.89/3.34), %Nd (8.64/8.73),

EuL15-Br, $Eu(HL)_3 \cdot H_2O$; %C (55.41/54.88), %H (2.89/2.68), %Eu (9.10/9.27);

GdL15-Br, $Gd(HL)_3 \cdot 2H_2O$; %C (54.13/54.15), %H (2.78/3.05), %Gd (9.44/9.99),

TbL15-Br, $Tb(HL)_3 \cdot 2H_2O$; %C (54.07/53.87), %H (2.78/3.03), %Tb (9.54/9.24).

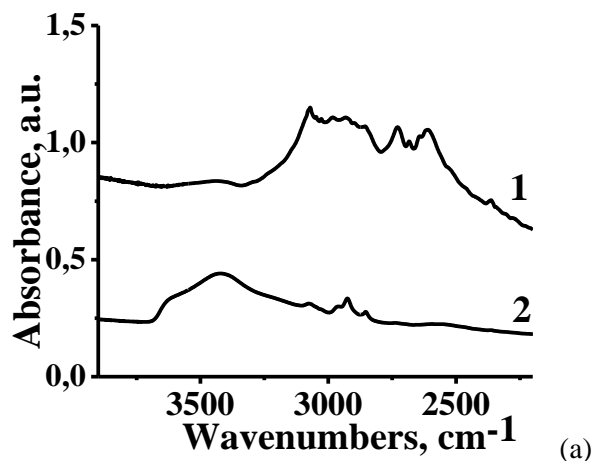
Infrared spectroscopy of the free ligand and NdL15-Br

Our efforts for single crystals preparation of the complexes turned out to be unsuccessful. That is

why a vibrational analysis was used as an opportunity to reveal the possible mode of coordination. The infrared spectra of the complexes were interpreted on the basis of the comparison with the spectrum of the free ligand.

The IR spectra of the ligand L15-Br (1) and NdL15-Br (2) in the range 3900-1800 cm^{-1} (a) and in the range 1700-1200 cm^{-1} (b) were recorded (Figure 2). In the spectrum of the free ligand intensive bands at 1669 cm^{-1} and 1617 cm^{-1} were observed, which can be assigned for the carbonyl oxygen atom (C=O) [27, 32]. The bands observed are lower than the shift for the free carbonyl group [27, 32]. That fact can be attributed to the participation of the carbonyl group in stable C=O \cdots H bridges. In the spectra of the complexes these bands were shifted to lower wavenumbers. The band observed at 1598 cm^{-1} in the spectrum of NdL15-Br can be attributed to the ν_{sym} (C=O) [33]. That band is the most informative about the participation of the oxygen atom from the carbonyl group in coordination with Ln(III) ion. The shoulder observed at 1620 cm^{-1} can be assigned to the asymmetric vibration of the carbonyl group [27, 32]. Bands appearing at 1605, 1562, 1486 and 1455 cm^{-1} in the spectrum of the ligand corresponded to the vibration of the phenolic ring. In the spectrum of the complex they were shifted to lower wavenumbers.

In the IR spectrum of the ligand the weak band at 3073 cm^{-1} can be assigned to the $\nu(\text{OH})$ vibrations [27, 32]. This band was not observed in the spectrum of the complex, indicating that the deprotonated form was involved in complexation. The broad band in the range 3750 – 3100 cm^{-1} , observed in the spectrum of NdL15-Br (Figure 2, a 2), was assigned to the $\nu(\text{O-H})$ vibrations of coordinated water [27, 32] and did not appear in the spectrum of the ligand.



The spectral behavior of the complexes synthesized is similar. So based on that reason we can conclude that the coordination of the lanthanoid ion is identical in the formed complexes, i.e. they are isostructural. The coordinated water registered by IR spectra supports the elemental analysis data and the proposed empirical formulae of the complexes. The coordinated water molecules along with the three molecules of the mono-deprotonated ligand in Ln(HL)₃ reassure a coordination number higher than six for the lanthanoid ion. This is in a good agreement with the high coordination numbers known for the lanthanide ions [34].

Electronic spectra

The absorption spectra of the free ligand and its Ln(III) complexes were recorded (Figure 3). Compared to the UV-Vis spectrum of the ligand, changes are observed in the spectra of the complexes. In the spectrum of the free ligand an intense broad band from 260 to 337 nm, indicating a π - π^* transition is observed. The complexes absorb throughout the interval 200-900 nm with local maxima in the UV region up to 350 nm and in the visible region (for NdL15-Br).

In the absorption spectrum of NdL15-Br (Figure 3) a broad band around 300 nm with intensity lower than the one observed in the ligand. That band can be assigned to the transition in the ligand. Bands with lower intensity due to f-f transitions appeared at region 430-900 nm. The absorption bands of Nd(III) in the visible and NIR region appear due to transitions from the ground levels of $^4I_{9/2}$ to the excited J- levels of the 4f configurations [35].

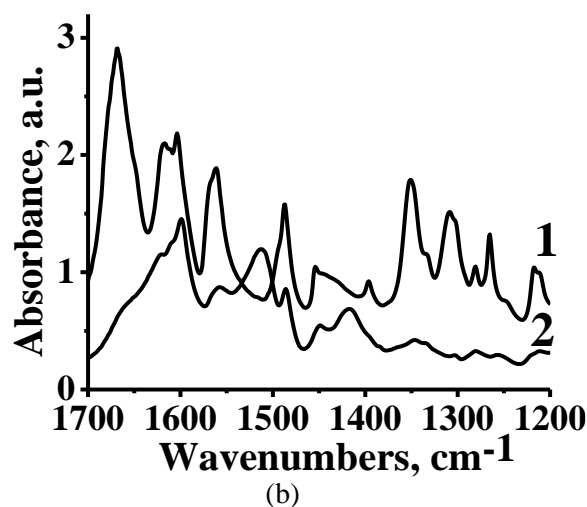


Fig. 2. IR spectra of the ligand (1) and NdL15-Br (2) in the range 3900-1800 cm^{-1} (a) and in the range 1700-1200 cm^{-1} (b)

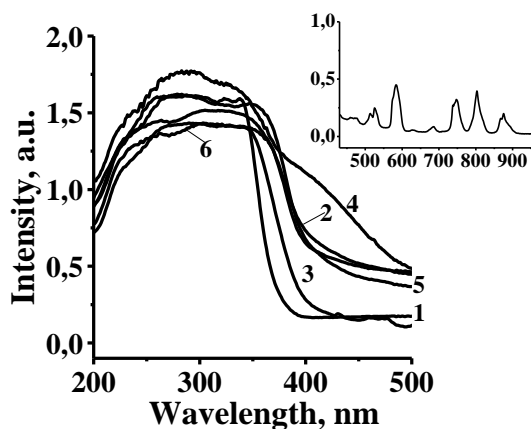


Fig. 3. UV - Vis spectra of the free ligand (1) and the complexes LaL15-Br (2), NdL15-Br (3), EuL15-Br (4), GdL15-Br (5), TbL15-Br (6), inset f-f transitions for NdL15-Br

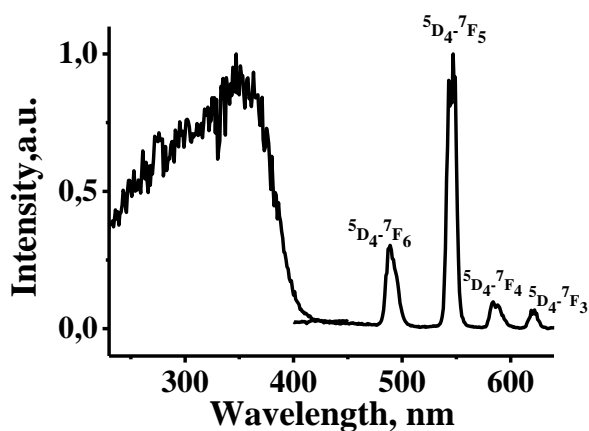


Fig. 4. Excitation and emission spectra of powdered terbium complex

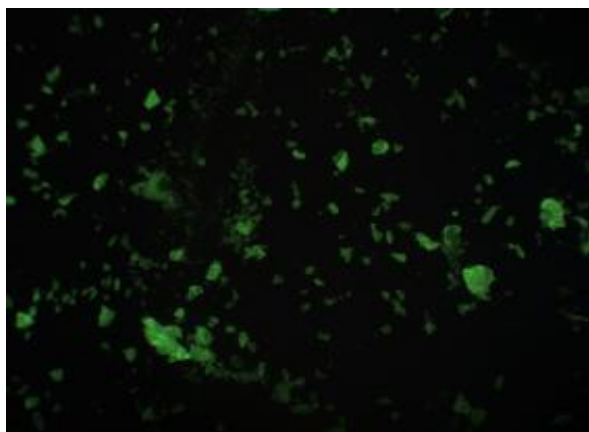


Fig. 5. Fluorescent microscope image for the sample of TbL15-Br

Excitation and emission spectra

The luminescence nature of Ln(III) ions is well known, but still an interesting area in the science investigations [36]. Complexes of Ln(III) with optical properties usually consist of organic molecules, capable of transferring energy to the metal ion and overcoming their low extinction coefficient [34]. In case of ion with luminescence in

visible region, such as Tb(III) ion, the organic component should be excited in the UV area, allowing effective charge transfer from the ligand to the metal ion.

The luminescence properties of the powdered probe of TbL15-Br complex were investigated under ultraviolet excitation.

The excitation spectrum was recorded with excitation maximum around 350 nm (Figure 4). The emission spectrum (Figure 4) showed characteristic emission bands of the Tb(III) ion at about 489 nm ($^5D_4-^7F_6$), 583, 588 nm ($^5D_4-^7F_4$) and 621 nm, corresponding to $^5D_4-^7F_3$ transitions. The transition $^5D_4-^7F_5$ is presented with an intensive emission band splitted at 543, 547 and 548 nm. Transitions are from the lowest excited state 5D_4 of Tb(III) ion to the highest ground state 7F_0 and next 7F_1 ($J= 0-6$) [23]. Green emission of Tb(III) was observed with fluorescence microscopy, and it is concerned as reliable proof for presence of the ion (Figure 5). The lifetime of the excited state of powdered probe of TbL15-Br was found to be 465 μ s.

Obviously the content of water in the inner sphere of Tb(III) complex did not interfere its fluorescence. That was not the case with the other complexes. For example complex of Eu(III) did not show any luminescence under UV light irradiation, probably because of the water content. It is well known that the photophysical properties of Eu(III) ion and Tb(III) ion markedly depend on their environment, i.e. the luminescence is strongly decreased by the presence of water molecules in the coordination sphere [37]. Besides, excitation and absorption spectra matched for Tb(III) complex only, suggesting that the charge transfer from the ligand to Eu(III) was not enough to sensitized the metal ion.

CONCLUSION

Complexes of coumarin derivate 3,3'-[(4-bromophenyl)methylene]bis-(4-hydroxy-2H-1-benzopyrane-2-one) with some lanthanoid ions such as La(III), Nd(III), Eu(III), Gd(III), and Tb(III) were successfully synthesized. The IR-spectra elucidated the possibilities for coordination of the metal ion to the OH deprotonated and the C=O oxygen atom. The Tb(III) complex of 3,3'-[(4-bromophenyl)methylene]bis-(4-hydroxy-2H-1-benzopyran-2-one) showed luminescent properties.

Acknowledgement: The current study was accomplished in the frames of the Project DO 02 129/08 financed by Bulgarian Fund for Scientific Investigations.

REFERENCES

1. M.W-Hajnos, J. Sherma, *Liq. Chrom. Photochem Analysis*, **102**, 513 (2011).

2. F. Borges, F. Roleira; N. Mihalzes, L. Santana, E. Uriarte, *Curr. Med. Chem.*, **12**, 887 (2005).
3. M. K. Potdar, S. Mohile, M. M. Salunkhe, *Tetrahedron Letters*, **42**, 9285 (2001).
4. K. K. Upadhyay, R. K. Mishra, A. Kumar, *Catal. Lett.*, **121**, 118 (2008).
5. A. Song, X. Wang, K. S. Lam, *Tetrahedron Letters*, **44**, 1755 (2003).
6. F. Bigi, L. Chesini, R. Maggi, G. Sartori, *J. Org. Chem.*, **64**, 1033 (1999).
7. H. Chen, Ch. T. Walsch, *Chemistry and Biology*, **8**, 301 (2001).
8. A. M. Holbrook, J. A. Pereira, R. Labiris, H. McDonald, J. D. Douketis, M. Crowther, Ph. S. Wells, *Arch. Intern. Med.*, **165**, 1095 (2005).
9. I. Kostova, S. Raleva, P. Genova, R. Argirova, *Bioinorg. Chem. Appl.*, **2006**, 1 (2005).
10. S. Y. Kang, K. Y. Lee, S. H. Sung, M. J. Park, *J. Nat. Prod.*, **64**, 683 (2001).
11. R. S. Keri, K. M. Hosamani, R. V. Shingalapur, M. H. Hugar, *Eur. J. Med. Chem.*, **45**, 2597 (2010).
12. M.-T. Alonso, E. Brunet, O. Juanes, J.-C. Rodriguez-Ubis, *J. Photochem. Photobiol. A: Chemistry*, **147**, 113 (2002).
13. S. Jie, *Chem. Res. Chin. Univ.*, **27**(5) 769 (2011).
14. I. Kosiova, P. Kois, In General Organic Synthesis (Proc. 10th Int. Electronic Conf. Synth. Org. Chem., 1-30 November, Sciforum Electronic Conference Series, **10** 2006).
15. S.-T. Huang, J.-L. Jian, A.-Z. Peng, K.-L. Wang, C.-M. Lin, C.-H. Huang, T. C.-K. Yang, *Dyes and Pigments*, **86**, 6 (2010).
16. B. S. Creaven, M. Devereux, D. Karcz, A. Kellett, M. McCann, A. Noble, M. Walsch, *J. Inorg. Chem.*, **103**, 1196 (2009).
17. G. R. Jani, K. B. Vyas, K. S. Nimavat, J. Franko, *Der Pharma Chemica*, **1**, 304 (2009).
18. I. Kostova, G. Momekov, *Eur. J. Med. Chem.*, **43**, 178 (2008).
19. C. Feau, E. Klein, P. Kerth, L. Lebeau, *Bioorg. Med. Chem. Letters*, **17**, 1449 (2009).
20. I. Kostova, I. Manolov, I. Nikolova, S. Konstantinov, M. Karaivanova, *Eur. J. Med. Chem.*, **36**, 339 (2001).
21. I. Kostova, Ts. Stefanova, *J. Trace elem. Med. and Biol.*, **24**, 7 (2010).
22. I. Georgieva, Tz. Mihaylov, N. Trendafilova, *J. Inorg. Biochem.*, **135**, 100 (2014).
23. D. K. Elenkova, M. M. Getsova, J. Ts. Zaharieva, I. Manolov, M. M. Milanova, *Centr. Eur. J. Chem.*, **11**, 1032 (2013).
24. S.-G. Roh, N. S. Baek, K.-S. Hong, H. K. Kim, *Bull. Korean Chem. Soc.*, **25**, 343 (2004).
25. D. Završnik, S. Muratovic, D. Makuc, J. Plavec, M. Cetina, A. Nagl, E. De. Clercq, J. Balzarini, M. Mintas, *Molecules*, **16**, 6023 (2011).
26. H. Mehrabi, H. Abusaidi, *J. Iran. Chem. Soc.*, **7**, 890 (2010).
27. I. Kostova, N. Trendafilova, G. Momekov, *J. Inorg. Biochem.*, **99**, 477 (2005).
28. I. Kostova, R. Kostova, G. Momekov, N. Trendafilova, M. Karaivanova, *J. Trace Elem. Med. Biol.*, **18**, 219 (2005).
29. I. Kostova, I. Manolov, G. Momekov, Tz. Tzanova, S. Konstantinov, M. Karaivanova, *Eur. J. Med. Chem.*, **40**, 1246 (2005).
30. D. Elenkova, J. Zaharieva, M. Getsova, I. Manolov, M. Milanova, S. Stach, Ş. Ţâlu, *Int. J. Polym. Anal. Charact.*, **20**, 42 (2015).
31. I. Manolov, C. M. Mössmer. *Anal. Sci.*, **23**, 63 (2007).
32. K. Nakamoto, *IR Spectra of Inorganic and Coordination Compounds*, John Wiley & Sons, (1978).
33. M. Getsova, V. Kircheva, J. Zaharieva, I. Manolov, H. Naruke, M. Milanova, *JOAM*, **14**, 685 (2012).
34. S. A. Cotton, *Lanthanide and Actinide Chemistry*, John Wiley and Sons Ltd, Chichester, 2006.
35. H. A. Hussain, K. Iftikhar, *Spec. Chim. Acta*, Part A, **59**, 1061 (2003).
36. K. Binnemans, *Chem. Rev.* **109**, 4283 (2009).
37. Y. Haas, G. Stein, *J. Chem Phys.*, **75**, 3668 (1971).

СИНТЕЗ И ОХАРАКТЕРИЗИРАНЕ НА ЛАНТАНОИДНИ КОМПЛЕКСИ С 3,3'- (4-БРОМОФЕНИЛМЕТИЛЕН)БИС(4-ХИДРОКСИ-2*H*-1-БЕНЗОПИРАН-2-ОН)

В. И. Кирчева¹, Й. Цв. Захариева¹, И. Манолов², М. М. Миланова¹

¹Софийски Университет „Св. Кл. Охридски“, Факултет по химия и фармация, Катедра „Неорганична химия“, бул. Дж. Баучер № 1, София 1164, България

²Медицински Университет, Фармацевтичен факултет, Катедра Органична химия, ул. Дунав № 2, София 1000, България

Постъпила на 11 ноември 2016 г.; приета на 21 януари 2017 г.

(Резюме)

Синтезирани са комплекси на 3,3'-(4-бромобензилметилена)бис(4-хидрокси-2*H*-1-бензопиран-2-он) с някои лантаноидни йони Ln(III) = [La(III), Nd(III), Eu(III), Gd(III), Tb(III)]. Получените комплекси са охарактеризирани с помощта на елементарен анализ, ИЧ спектроскопия, UV-Vis спектроскопия, флуоресцентна спектроскопия и микроскопия. Спектрите на комплексите са сравнени с тези на свободния лиганд, за да може да бъде направено предположение за начина на координиране на металния йон към лиганда. Данните от ИЧ-спектъра на комплексите ни дават основание да предположим, че металният йон координира с карбонилния кислороден атом, както и с депротонираната хидроксилна група на лиганда. Оптичните свойства на комплексите са показани чрез абсорбция в UV- Vis областта. Регистрирани са спектрите на възбуждане и емисия на прахова проба на Tb(III) комплекс. Измерено е времето на живот във възбудено състояние за праховата проба.

Ключови думи: Лантаноиди, Комплекси, Бискумарини, ИЧ спектроскопия, Оптични свойства

Molecular design of electron-donor materials for fullerene-based organic solar cells

M. Spassova^{1*}, S. Angelova¹, M. Kandinska², A. Vasilev², S. Kitova³, J. Dikova³

¹ Institute of Organic Chemistry with Centre of Phytochemistry,
Bulgarian Academy of Sciences, Sofia, 1113 Bulgaria

² Faculty of Chemistry and Pharmacy, Sofia University "St. Kliment Ohridski", 1164 Sofia, Bulgaria

³ Institute for Optical Materials and Technologies "Acad. J. Malinowski",
Bulgarian Academy of Sciences, 1113 Sofia, Bulgaria

Received November 11, 2016; Revised December 14, 2016

A set of model symmetrical and unsymmetrically substituted squaraine and croconine dyes is designed as potential electron donor component in organic photovoltaic bulk heterojunction solar cell (BHJ) where [60]PCBM fullerene is set as acceptor. Ground-state geometries and electronic structures were investigated using density functional theory (DFT) and time-dependent (TD-DFT) density functional theory at the B3LYP/6-31+G(d,p) level. The effects of the electron-rich heterocycles on these squarilium/croconium based organic dyes are studied with respect to the electronic and transport properties of the systems. The estimated HOMO-LUMO gaps of all model dyes fall in the range of the typical organic semiconductors' gap of about 2 eV. The HOMO and LUMO energy levels of the dyes are compared with respect to the acceptor's and the rigorous conditions for an effective charge transfer is discussed. The calculated high values of the oscillator strengths for all proposed dyes are indicative for large absorption coefficient. Based on the optimized molecular geometries, relative positions of the frontier orbitals, absorption maxima and transport properties we propose some of these dyes as suitable components for optoelectronic devices.

Keywords: *squaraines, croconines, fullerene, DFT, transport properties*

INTRODUCTION

Organic Photovoltaics (OPVs) have recently attracted considerable attention as potentially cheap, lightweight, and flexible sources for renewable energy and are promising materials for harvesting solar energy. The ease of their processing and less environmental aggressiveness compared to inorganic solar cells make them objects of extensive elaboration. Exploring new organic materials by revealing relationship between molecular structure and optoelectronic properties is one of the paramount approaches to achieve high-performance OPVs. The performance of the OPVs crucially depends on the donor constituents which should satisfy requirements for large absorption coefficient, low bandgap, high charge mobility, environmental stability, suitable HOMO/LUMO level and solubility [1].

Although non-fullerene-based acceptors are recently in the focus of the search of new promising acceptor materials for bulk heterojunction (BHJ) solar cells (BHJ cells consist of a n-type highly conjugated electron acceptor with high electron affinity and a p-type electron donating part [2]),

fullerene derivatives like [60] PCBM and [70] PCBM are, so far, the most widely used electron acceptors in organic photovoltaic cells [3]. Their unique spherical shape, molecular rigidity and large π -delocalization over the three-dimensional (3D) framework determine their low reorganization energy for electron transport [4] and the ultrafast charge transfer [2b]. BHJ solar cell where conjugated polymers or small organic molecules are blended with fullerenes represents an efficient way for rapid exciton dissociation [5].

Squarylium dyes (squaraines) are derivatives of squaric acid (3,4-dihydroxy-3-cyclobutene-1,2-dione, quadratic acid), a condensation product of squaric acid and electron-rich aromatics or heterocycles. They are well-known as highly efficient absorbers for organic photovoltaics (OPV) applications [6, 7]. Squaraine dyes feature sharp and intense absorption, typically in the red to the near infrared (NIR) region. Squaraine film absorption is quite broad with large absorption coefficient, which is highly beneficial for sunlight absorption of the photoactive layer [8]. Many studies are addressed to the structural optimization of squaraine dyes for dye-sensitized solar cells. In order to improve their performance strategies like introduction of donors, acceptors, conjugated linkers, etc. aiming at tuning

* To whom all correspondence should be sent.
E-mail: mspasova@orgchm.bas.bg

their HOMO, LUMO, HOMO-LUMO gap (HLG) and absorption were adopted [9-12]. Croconium dyes (croconines) are Knoevenagel condensation products of croconic acid (4,5-dihydroxycyclopent-4-ene-1,2,3-trione) and heterocyclic CH-acids and they have properties similar to those of the squaraines [13] with strong and broad absorption in infrared region and are also foreseen for application as electron donor in solution processed BHJ solar cells [14].

In this work, motivated by the promising results from the optical modelling of a symmetrical squaraine SQ1 (2-(5-(((2,2-diphenylhydrazono)methyl)-1-hexyl-1H-pyrrol-2-yl)-4-(5-(2,2-diphenylhydrazono)-ylidenemethyl)-1-hexyl-2H-pyrrol-1-ium)-3-oxocyclo-but-1-enolate) [7] we performed DFT and TDDFT calculations on the geometries, electronic structures and absorption spectra of a model set of three squaraine and croconine dyes. Quantum chemistry is an extremely powerful and low-cost tool for beforehand molecular designs of new efficient dyes. The computational methodologies based on density functional theory (DFT) and time-dependent DFT (TDDFT) provide reliable geometrical, electronic and spectroscopic properties for various dyes [15, 16]. The calculations of hole and electron reorganization energies, as well as exciton binding energies, aim at assessment of transport properties of the proposed dyes. The analysis of these quantities allows for rational design of more efficient electron-donor components which in conjunction with PCBM would satisfy the different criteria for OPV materials.

COMPUTATIONAL DETAILS

The reorganization energy (λ) is used to access crudely the electron-, and hole mobility of the proposed organic chromophores. The internal reorganization energies (for isolated molecules the external part is often neglected) for hole transport (λ^+) and electron transport (λ^-) are calculated following the so called "4-point model" [17] as:

$$\lambda^\pm = \lambda_1^\pm + \lambda_2^\pm$$

$$\lambda_1^\pm = E_\pm(Q_n) - E_\pm(Q_\pm)$$

$$\lambda_2^\pm = E_n(Q_\pm) - E_n(Q_n)$$

where $E_\pm(Q_n)$, $E_\pm(Q_\pm)$, $E_n(Q_\pm)$ and $E_n(Q_n)$ are the total energies of the: charged state in the neutral geometry, charged state in the charged state geometry, neutral state in the charged state

geometry, and neutral state in the neutral geometry, respectively.

Another indicator of optoelectronic performance is the exciton binding energy - the Coulomb interaction energy that stabilizes the exciton (bounded electron-hole pair) with respect to free electron and hole. Exciton binding energy is defined as difference between fundamental gap (E_g) and optical gap (E_{opt}) of a molecule $E_{bind}=E_g-E_{opt}$ where E_g is defined as the difference between the vertical ionization potential IP and vertical electron affinity EA $E_g=IP-EA$.

All calculations were carried out with Becke's three-parameter hybrid exchange-correlation functional B3LYP [18] with double- ζ polarized basis set, 6-31+G(d,p). It has been shown that this functional performs well in predicting molecular geometries and optical gaps [19] and gives results in good agreement with experiment for exciton binding energy of acene [15]. For the sake of the consistency the same functional (B3LYP) was used in molecular frontier orbital energy calculations although it is known that systematically underestimates the HLG by 0.2-0.3 eV [19, 22]. The Gaussian 09 program [20] is used for quantum chemical calculations and PyMOL molecular graphics software for generating the molecular graphics images [21].

RESULTS AND DISCUSSION

A set of 3 squaraines and 3 croconines with different substituents has been designed to screen dyes with desired properties (Figure 1). The DFT calculated frontier orbital energies, HOMO-LUMO gaps, as well as TDDFT obtained excitation energies and oscillator strengths of the model donor dyes and the acceptor [60]PCBM are listed in Table 1. The absolute position of HOMO and LUMO levels enables ranking of the substituents employed. The HOMO energy levels of both series (SQs and CRs) do not differ significantly. However, the LUMO levels of CR's are considerably lower (about 0.5 eV) which leads to a smaller HOMO-LUMO gap for CR's. Generally, the estimated HLG's of all model dyes are low enough, which is one of the inevitable requirement for a good donor constituents. They are in the ranges 1.8-2.02 eV and 1.37-1.53 eV for SQ's and CR's, respectively, and even accounting for the HLG's underestimation by B3LYP the most of the proposed structures HLG's are close to the typical organic semiconductors' gap of about 2 eV.

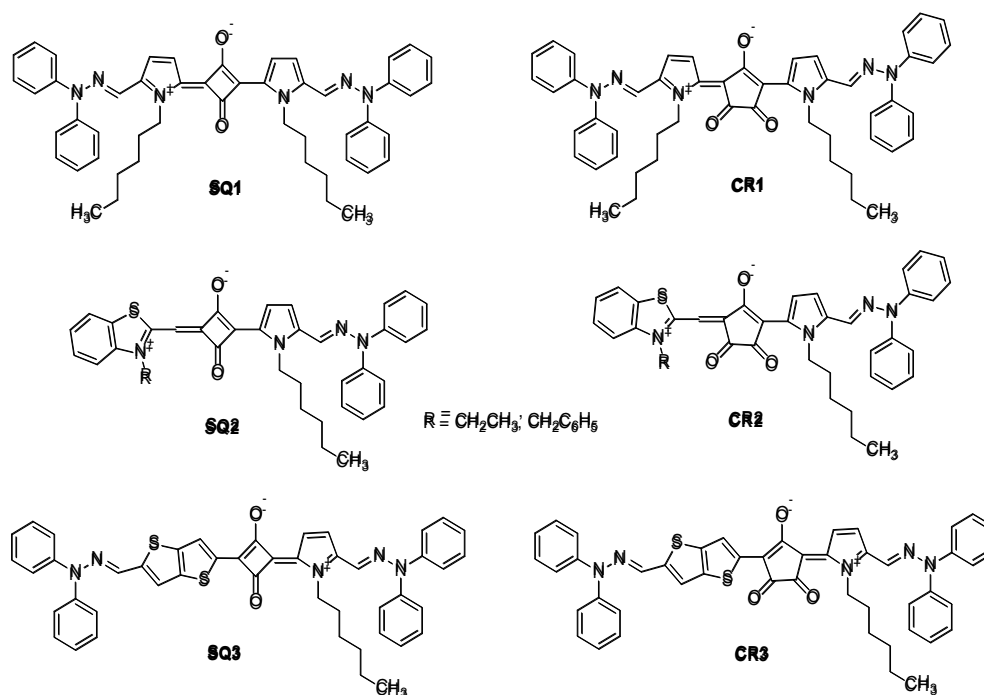


Figure 1. Structures of the proposed squaraines and croconines.

Table 1. B3LYP/6-31+G(d,p) calculated HOMO and LUMO energies, HOMO-LUMO gap (HLG), and excitation energies E_{exc} in eV, wavelengths λ_{max} in nm and oscillator strength f .

Compound	HOMO	LUMO	HLG	E_{exc}	λ_{max}	f
SQ1	-5.12	-3.19	1.93	1.877	660.7	1.63
SQ2_Et	-4.87	-2.85	2.02	1.970	629.3	1.25
SQ2_Bz	-4.87	-2.85	2.02	1.957	633.6	1.26
SQ3	-5.09	-3.29	1.80	1.794	691.0	2.23
CR1	-5.17	-3.74	1.43	1.522	814.9	1.24
CR2_Et	-4.94	-3.41	1.53	1.618	766.5	1.06
CR2_Bz	-4.93	-3.40	1.53	1.611	769.5	1.06
CR3	-5.14	-3.77	1.37	1.497	828.2	1.82
[60]PCBM	-6.06	-3.53	2.53	1.899	652.8	0.00

In fact, SQ's and CR's are inherent donor-acceptor-donor systems [23] and for such molecular architectures the growing interest is dictated by their efficient low bandgaps and wide spectral coverage [24]. The visualization of the spatial distribution of the frontier orbitals (Figure 2) allows for distinguishing the donor and acceptor units. The HOMO orbitals of all studied structures are spread over the whole conjugated chain lengths (which is one of the prerequisites for achieving high power conversion efficiency), whereas LUMO's are localized predominantly on the central four- and five membered rings (squaric and croconic cores). Neither HOMO nor LUMO are located at the ethyl and benzyl side-chain groups attached to the benzothiazole rings of SQ2 and CR2 because of the lack of conjugation with the backbone. Consequently, their presence does not affect the energy level positions. These solubilizing groups are

proposed solely for achievement of good blend morphology.

In the view of an efficient OPV application frontier orbital energies of the donor (dyes) should satisfy many criteria. Along the requirements for absolute energies of HOMO and LUMO of the donor against the vacuum level [1] the rigorous condition for an effective charge transfer requires that the frontier orbitals of the donor must be 0.2-0.3 eV higher than the corresponding acceptor's orbitals.

The LUMO levels of CR1 and CR3 fall below the LUMO level of the fullerene [60]PCBM (Table 1). This means that these croconines cannot serve as donor in this blend. The LUMO levels of the unsymmetrical CR2's (with ethyl or benzyl group) are also very close to the LUMO of the acceptor system situated just 0.12 eV above. This small difference means that no efficient charge separation is expected. Contrary, SQ2's LUMO's are too high

versus PCBM's which suggests that greater energy loss would be occurred in the BHJ. The LUMO levels of the SQs are properly positioned with respect to the acceptor's. However, the requirement for LUMO (donor) – LUMO (acceptor) > 0.2–0.3 eV is fulfilled only for SQ1 and SQ3. Nevertheless, in this respect, these dyes perform better than some newly proposed merocyanine dyes [25].

Absorption

DDFT/B3LYP/6-31+G(d,p) calculations of the excitation energies E_{exc} and corresponding wavelengths λ_{max} (Table 1) predict strong absorption in the red and NIR region of the spectrum. These results are in good agreement with the experimental findings for similar squarilium and croconium dyes [13]. The croconium dyes absorb at significantly longer wavelengths than the squarilium (Figure 3) as the difference for CR3 and SQ3 is about 0.30 eV and up to 0.35 eV for the rest of the molecules. Within the series SQ3 and CR3 are red-shifted with respect to SQ2 and CR2 by about 0.20 – 0.17 eV, respectively, and, in a lesser extend to SQ1 and CR1.

On the basis of the calculated high values of the oscillator strengths all proposed dyes fulfill the requirement for large absorption coefficient (especially for SQ3 and CR3) as SQ's absorb more intensively than CR's.

Transport properties

The assessment of the transport properties of the studied dyes is made by considering the internal reorganization energy λ and exciton binding energy E_{bind} . The small λ is precondition for high charge mobility; small E_{bind} is prerequisite for high charge separation efficiency which is needed for photovoltaic applications whereas high exciton binding energy is necessary for light-emitting devices.

According to the theoretical estimations the proposed systems are better hole than electron transport materials since the reorganization energy for hole transport λ^+ is smaller than for electron λ^- transport (Figure 6a). The ratio between these two energies λ^+/λ^- is lower than 1.0 for all chromophores, which evidences their p-type character. The smallest values of this ratio are found for the symmetrical SQ1 and CR1 dyes (0.58 and 0.61, respectively) which suggest that these chromophores should exhibit most clearly pronounced donor character. On the other hand their absolute values of λ^+ is the largest amongst the studied structures. SQ3 and CR3 have the smallest reorganization energies λ^+ and λ^- among the studied and they are the expected to have better hole transport properties. SQ2 and CR2 have larger values of the ratio (0.79 and 0.76,

respectively) and closer to 1.0 which suggests enhanced ambipolar character.

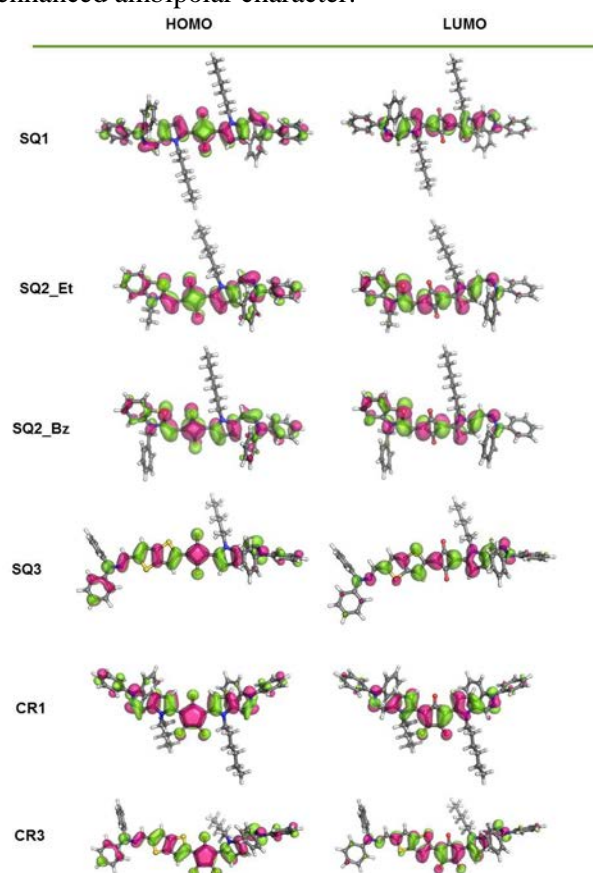


Figure 2. Frontier MO orbitals.

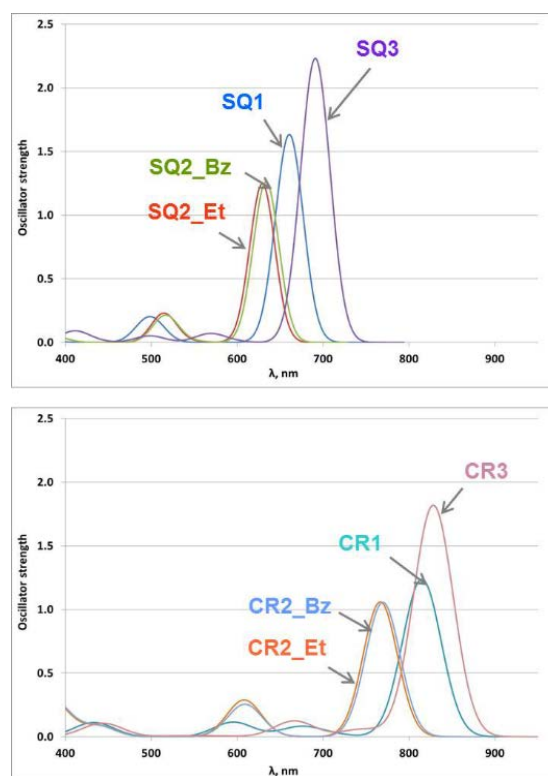


Figure 3. Simulated absorption spectra of: a) SQ's, b) CR's.

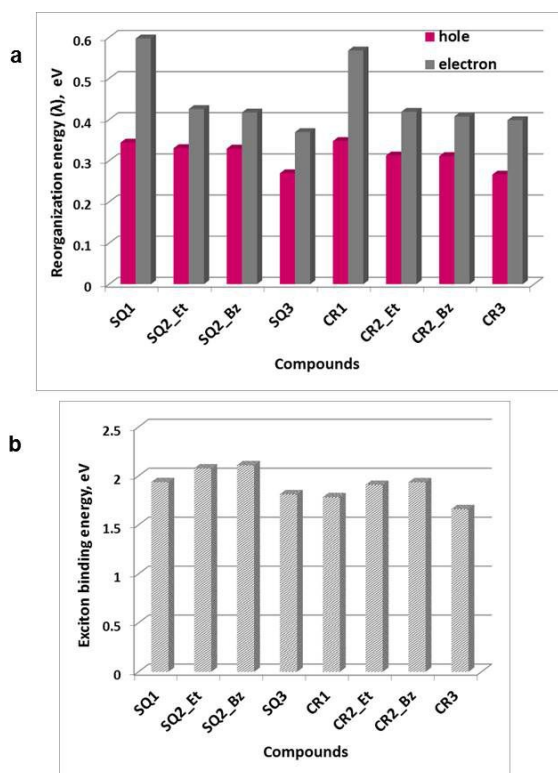


Figure 4. B3LYP/6-31+G(d,p) calculated: a) internal reorganization energies for hole and electron in eV, and, b) exciton binding energies for SQ' and CR's in eV.

Generally, the different substituents do not affect substantially the reorganization energies for electron and hole. The calculated values for λ are high in comparison of many other organic semiconductors [26] but comparable with values for some organic amines proposed for efficient organic electroluminescence (OLED) devices [27]. Also, there is no big difference between the corresponding dyes of the two series, i.e. the central acceptor fragments SQ or CR do not influence the reorganization energy. It might be helpful to propose new molecular architecture, ex. by increasing the extent of the electron delocalization which could lead to smaller reorganization energy.

The calculated exciton binding energies for the proposed dyes vary from 1.66 eV for CR3 to 2.11 eV for SQ2_Bz. These values are much higher than the reported for most of the organic semiconductors, ranging from 0 to 1.5 eV [28]. SQ2 and CR2 have largest exciton binding energies and are about 0.3 eV and 0.27 eV larger than E_{bind} for SQ3 and CR3, respectively.

CONCLUSIONS

Most of the proposed croconium and squarylium dyes satisfy the different criteria for efficient donor components for BHJ solar cell applications. The theoretical results predict low HLG's and intense red and NIR absorption. The estimated HLG's of all

model dyes fall in the range of the typical organic semiconductors' gap of about 2 eV. The type of the central core fragment mainly affects the LUMO orbital energies. The replacement of central squaric fragment by croconic cores leads to a lower HLG and red shift in the absorption while the calculated oscillator strengths are lowered. Only SQ1's and SQ3's frontier orbitals satisfy all requirements for proper position with respect to HOMO and LUMO of the acceptor [60]PCBM. Due to the estimated smaller reorganization energy for hole than for electron these dyes are referred as p-type semiconductors which confirms their donor abilities. Considering the calculated reorganization energies λ and exciton binding energies E_{bind} the favorite structures are SQ3 and CR3.

Nevertheless, all dyes show comparatively high values of λ and E_{bind} which suggests moderate charge transport properties. These dyes can further be modified by adopting proper strategies toward reducing the reorganization energies and exciton binding energies in order to achieve more efficient charge mobility and charge separation.

Acknowledgements: We acknowledge the financial support of the Bulgarian Fund for Scientific Research under Grant DFNI E 02/11 (19.12.2014) «SunStore». The calculations were performed on the computer system installed at IOCCP-BAS with the financial support of the Bulgarian Scientific Fund under Project "MADARA" (RNF01/0110, contract no. DO02-52/2008).

REFERENCES

1. Q. Ye, C. Chi, Conjugated Polymers for Organic Solar Cells (Chapter 21), in: Solar Cells - New Aspects and Solutions, L. A. Kosyachenko (ed), ISBN 978-953-307-761-1, InTech, 2011.
2. (a) C. Zhan, J. Yao, *Chem. Mater.*, **28**, 1948 (2016); (b) W. Senevirathna, C. M. Daddario, G. Sauv e, *J. Phys. Chem. Lett.*, **5**, 935 (2014); (c) X. Liu, P. Cai, D. C. Chen, J. W. Chen, S. J. Su, Y. Cao, *Science China Chemistry*, **57**, 973 (2014); (d) Y. Zhou, J. Pei, Q. Dong, X. Sun, Y. Liu, W. Tian, *J. Phys. Chem. C.*, **113**, 7882 (2009).
3. J. Hou, X. Guo, Active Layer Materials for Organic Solar Cells (Chapter 2), in: Organic Solar Cells, Green Energy and Technology, H. Choy (ed.), Springer-Verlag London, 2013.
4. P. Hudhomme, An overview of molecular acceptors for organic solar cells. *EPJ Photovoltaics*, **4**, 40401 (2013).
5. M. C. Scharber, D. M uhlbacher, M. Koppe, P. Denk, C. Waldauf, A. J. Heeger, C. J. Brabec, *Adv. Mater.*, **18**, 789 (2006).
6. (a) G. Chen, H. Sasabe, T. Igrashi, Z. Hong, J. Kido, *J. Mater. Chem. A*, **3**, 14517 (2015); (b) F. Silvestri, M. D. Irwin, L. Beverina, A. Facchetti, G. A. Pagani,

- T. J. Marks, *J. Am. Chem. Soc.*, **130**, 17640 (2008);
(c) U. Mayerhoffer, K. Deing, K. Grub, H. Braunschweig, K. Meerholz, F. Wurthner, *Angew. Chem. Int. Ed.*, **48**, 8776 (2009).
7. S. Kitova, D. Stoyanova, J. Dikova, M. Kandinska, A. Vasilev, S. Angelova, *Journal of Physics: Conference Series*, **558**, 012052 (2014).
8. (a) G. W. Scott, K. Tran, *J. Phys. Chem.*, **98**, 11563 (1994); (b) N. J. Hestand, C. Zheng, A. R. Penmetcha, B. Cona, J. A. Cody, F. C. Spano, C. J. Collison, *J. Phys. Chem. C*, **119**, 18964 (2015).
9. S. Soman, M. A. Rahim, S. Lingamoorthy, C. H. Suresh, S. Das, *Phys. Chem. Chem. Phys.* **17**, 23095 (2015).
10. S. So, H. Choi, H. Ko, C. Kim, S. Paek, N. Cho, K. Song, J. Lee, J. Ko, *Sol. Energy Mater. & Sol. Cells*, **98**, 224 (2012).
11. S. Soman, M. A. Rahim, S. Lingamoorthy, C. H. Suresh, S. Das, *Phys. Chem. Chem. Phys.*, **17**, 23095 (2015).
12. S. L. Lam, X. Liu, F. Zhao, C.-L. K. Lee, W. L. Kwan, *Chem. Commun.*, **49**, 4543 (2013).
13. S. Yasui, M. Matsuoka, T. Kitao, *Dyes and Pigments*, **10**, 13 (1988).
14. S. Kitova, D. Stoyanova, J. Dikova, A. Vassilev, M. Kandinska, S. Angelova, *Nanoscience & Nanotechnology*, **14**, 70 (2014).
15. G. Cappellini, G. Mallocci, G. Mulas, *Superlattices and Microstructures*, **46**, 14 (2009).
16. G. García, M. Moral, A. Garzón, J. M. Granadino-Roldán, A. Navarro, M. Fernández-Gómez, *Organic Electronics*, **13**, 3244 (2012).
17. S. F. Nelsen, S. C. Blackstock, Y. Kim, *J. Am. Chem. Soc.*, **109**, 677 (1987).
18. A. Becke, *Chem. Phys.*, **98**, 5648 (1993).
19. S. Refaely-Abramson, R. Baer, L. Kronik, *Phys. Rev. B*, **84**, 075144 (2011).
20. M. J. Frisch et al., Gaussian 09, Gaussian Inc., W. C., 2013.
21. The PyMOL Molecular Graphics System, Version 1.7.6.6, Schrödinger, LLC.
22. (a) A. J. Garza, G. E. Scuseria, *J. Phys. Chem. Lett.*, **7**, 4165 (2016); (b) H. Xiao, J. Tahir-Kheli, W. A. Goddard III, *J. Phys. Chem. Lett.*, **2**, 212 (2011).
23. S.-Y. Park, K. Jun, S.-W. Oh, *Bull. Korean Chem. Soc.*, **26**, 428 (2005).
24. P. S. V. Kumar, E. Varathan, D. Vijay, V. Subramanian, *Proc. Natl. Acad. Sci., India, Sect. A Phys. Sci.*, **86**, 297 (2016).
25. J. Dikova, S. Kitova, D. Stoyanova, A. Vasilev, T. Deligeorgiev, S. Angelova, *Bulg. Chem. Commun.*, **45B**, 175 (2013).
26. L. Wang, G. Nan, X. Yang, Q. Peng, Q. Lia, Z. Shuai, *Chem. Soc. Rev.*, **39**, 423 (2010).
27. B. C. Lin, C. P. Cheng, Z. P. M. Lao, *J. Phys. Chem. A*, **107**, 5241 (2003).
28. M. Knupfer, *Appl. Phys. A*, **77**, 623 (2003).

МОЛЕКУЛЕН ДИЗАЙН НА ЕЛЕКТРОН-ДОНОРНИ МАТЕРИАЛИ ЗА ФУЛЕРЕН-БАЗИРАНИ СЛЪНЧЕВИ КЛЕТКИ

М. Спасова¹, С. Ангелова¹, М. Къндинска², А. Василев², С. Китова³, Ю. Дикова³

¹ *Институт по органична химия с Център по фитохимия,
Българска академия на науките, София, 1113, България*

² *Факултет по химия и фармация, Софийски университет „Св. Климент Охридски“,
1164 София, България*

³ *Институт по оптически материали и технологии „Акад. Йордан Малиновски“,
Българска академия на науките, София, 1113, България*

Постъпила на 11 ноември 2016 г.; приета на 14 декември 2016 г.

(Резюме)

Моделни симетрично и несиметрично заместени скуарилиеви и крокониеви багрила са предложени като потенциални донори на електрони в органични фотоволтаични слънчеви клетки с акцепторен компонент [60]PCBM фулерен. Геометриите и електронните структури в основно състояние са изследвани с помощта на теория на функционала на плътността (DFT) и зависещата от времето теория на функционала на плътността (TD-DFT) на ниво B3LYP/6-31+G(d,p). Ефектите на богатите на електрони хетероцикли върху скуарилиевите/крокониеви органични багрила са изследвани по отношение на електронните и транспортни свойства на системите. Очакваните забранени зони на всички моделни съединения са от порядъка на типичните за органичните полупроводници зони - около 2 eV. Енергиите на HOMO и LUMO орбиталите на багрилата са сравнени с тези на акцептора и са дискутирани стриктните условия за ефективен пренос на заряд. Изчислените високи стойности за силата на осцилатора за всички предложени съединения са показателни за голям коефициент на поглъщане. Въз основа на оптимизираните молекулни геометрии, относителните позиции на орбиталите, абсорбционните максимуми и транспортните свойства може да се заключи, че някои от багрилата, които предлагаме, са подходящи компоненти за оптоелектронни устройства.

Ключови думи: скуарилиеви багрила, крокониеви багрила, фулерен, теория на функционала на плътността, транспортни свойства

Investigation of photocatalytic properties of pure and Ln (La³⁺, Eu³⁺, Ce³⁺) – modified ZnO powders synthesized by thermal method

N. V. Kaneva^{1*}, A. S. Bojinova¹, K. I. Papazova¹, D. Tz. Dimitrov¹, A. E. Eliyas²

¹ *Laboratory of Nanoparticle Science and Technology, Department of General and Inorganic Chemistry, Faculty of Chemistry and Pharmacy, University of Sofia, 1 James Bourchier, 1164 Sofia, Bulgaria*

² *Institute of Catalysis, Bulgarian Academy of Sciences, Acad. G. Bonchev St., Bldg. 11, Sofia 1113, Bulgaria*

Received November 7, 2016; Revised January 4, 2017

Simple and fast thermal method is used to synthesize ZnO and Ln–modified (La³⁺, Eu³⁺, Ce³⁺) ZnO powders. Nanocrystalline photocatalysts with 2.0 mol% concentration are annealed at 100°C for 1h. The pure and doped powders are characterized by a variety of characterization techniques such as X-ray diffraction (XRD), scanning electron microscopy (SEM).

The photocatalytic action of the mixtures is tested in photocatalytic oxidation of ethylene as model air pollutant (5000 ppm feed concentration) in gas-phase flat-plate continuous flow photocatalytic reactor at maximum ethylene contact time of 4 min and optimal relative humidity 30%. The powder-form samples are suspended in water and after sonication (24 kHz) to disintegrate agglomerates the slurry was deposited by the capillary method on TLC sheets (Merck) to obtain 1 mg/cm² loading. The photoactivity testing was carried out using UV-A and UV-C illumination (0.014 W/cm²). Sample 3 (Ce³⁺-doped)/ZnO was superior to pure ZnO. It gave the highest conversion degrees both under UV-A and UV-C illumination, whereupon the latter yielded superior performance. There was no activity under visible light illumination due to the wide band gap.

Key words: ZnO, rare earths, powders, photocatalysis

INTRODUCTION

As a new-generation multifunctional II-VI semiconductor material, ZnO has received extensive attention in recent years. Due to the direct wide bandgap of 3.37 eV and a large exciton binding energy of 60meV at room temperature [1], zinc oxide combine interesting properties such as non-toxicity, good photocatalytic properties, high luminous transmittance, hardness, optical and piezoelectric behavior and its low price [2]. Therefore, it is not surprising that it has been under intensive investigation.

The dependence of the properties on the size of the ZnO has led to many interesting application of particles [3] especially by tuning the band gap of the semiconductors [4].

The investigation on the preparation and properties of ZnO has attracted a great deal of attention, and a variety of methods have been employed to fabricate this material, including sol-gel, precipitation, micro-emulsion, solvothermal, hydrothermal methods [5 – 9]. However, there are not many efforts regarding low temperature chemical techniques [10]. It has been demonstrated that the hydrothermal synthesis is a feasible route for

the preparation of ZnO with controlled morphology, structure and surface area [11, 12]. For photocatalytic applications, the improvement of the photoactivity might be achieved by influencing those properties that control either the charge carrier dynamics (carrier generation, transfer and diffusion) or the surface catalytic process, which are the quality of the structure and the surface features. In this sense, it is widely reported that the hydrothermal synthesis would provide the adequate structural and surface properties for photocatalytic applications [13].

In the present study, we prepared for the first time high-quality ZnO materials using hydrothermal method. The photocatalytic activity of ZnO has been carried out in a gas-phase flat-plate continuous flow reactor using ethylene as model air contaminant under ultraviolet (UVA and UVC) and visible light. The improvement of the photocatalytic efficiency of ZnO might be achieved by modified with rare earths (La³⁺, Ce³⁺, Eu³⁺). The nanosized pure and RE powders are characterized by X-ray diffraction and Scanning Electron Microscopy. We concluded that hydrothermal treatment of pure and doped ZnO grant the finest performance in the catalyst for photocatalytic application.

* To whom all correspondence should be sent.

E-mail: nina_k@abv.bg

EXPERIMENTAL

Commercial zinc oxide powder (>99.0%), Eu₂O₃ (>99.0%), Ce(NO₃)₃·6H₂O (>99.0%), La₂O₃ (>99.0%) and absolute ethanol were obtained from Fluka.

Pure and modified ZnO powders were synthesized by green, simple and fast hydrothermal method. La/ZnO photocatalysts were prepared using zinc oxide commercial powder and La₂O₃. The substances were mixed in a glass vessel, and then ethanol was added as a mixing medium. The resultant clear solution was sonicated for additional 30 min and dried at 100°C for 1 h in order to obtain the ZnO/La powders for photocatalytic tests. In our previous work, we experimentally found that the optimal RE concentration is 2 mol% [14]. The remaining catalysts (Ce/ZnO and Eu/ZnO) were prepared at the same conditions and optimal concentration of 2 mol% of RE ions (Ce³⁺ and Eu³⁺).

The as-obtained nanosized powders (pure ZnO and RE-modified ZnO) were first imaged by Scanning Electron Microscope (SEM) JSM-5510 (JEOL), operated at 10 kV of acceleration voltage. The investigated samples were coated with gold by JFC-1200 fine coater (JEOL) before observation. The X-ray diffraction (XRD) was recorded at room temperature on a powder diffractometer (Siemens D500 with CuK_α radiation within 2θ range 30–70° at a step of 0.05° 2θ and counting time 2 s/step). The average crystallite sizes were estimated according to the Scherrer's equation [15]:

$$d_{hkl} = k\lambda / \beta \cos(2\theta) \quad (1)$$

where d_{hkl} is the average crystallite size (nm), λ is the wavelength of CuK_α radiation ($\lambda = 0.154056$ nm), θ is the Bragg's angle of diffraction, β is the full-width at half maximum intensity of the peak observed at $2\theta = 25.20^\circ$ (converted to radian) and k is a constant usually applied as ~0.9.

The photocatalytic activities of the 4 powder – form samples (pure ZnO and 3 modified samples) has been carried out in a gas-phase flat-plate continuous flow reactor using ethylene as model air contaminant. The course of the photocatalytic reaction of complete oxidation of ethylene is monitored using a gas-analyzer (LANCOM III, Land Instruments Co., England), equipped with chemisorption sensor for total hydrocarbons content in the gaseous mixture (ppm C_xH_y). The feed composition at the reactor inlet was 0.5% (5000 ppm) C₂H₄, 10% O₂, 89.5% N₂ (four-channel mass flow controller Matheson model 8249). Two of the channels were feeding nitrogen – dry N₂ flow directly into the reactor, and moisturized N₂ (after

passing first through a water vapor saturator). The use of two channels enables varying the water vapor content in the feed mixture. Our previous experiments established 30% Relative Humidity (RH), to be the optimum [16, 17]:

$$RH = [F_{N_2\text{moist}} / (F_{N_2\text{dry}} + F_{N_2\text{moist}} + F_{O_2} + F_{C_2H_4})] 100(\%) \quad (2)$$

where F_i denotes the various feed flow rates (ml/min). The feed H₂O molecules are needed to photogenerate the highly active hydroxyl radicals °OH, capable of destroying various classes of organic compounds. Feeding ethylene and oxygen by two different channels, regulated independently of each other, enables varying the C₂H₄:O₂ ratio (large stoichiometric excess of oxygen with respect to C₂H₄ in all our experimental runs). In this case we can accept that O₂ concentration is practically unchanged in our experiments, so its value can be included in the value of the efficient rate constant k_{eff} in the kinetic equation:

$$R_{C_2H_4} = k_{\text{eff}} \cdot C_{C_2H_4} / (1 + K_{O_2} \cdot C_{O_2} + K_{C_2H_4} \cdot C_{C_2H_4}) \quad (3)$$

The equation (3) includes the rate of ethylene consumption $R_{C_2H_4}$ (mol/h.g-cat), $C_{C_2H_4}$ is the outlet concentration (mol/cm³), while K_{O_2} and $K_{C_2H_4}$ are the adsorption-desorption equilibrium constants i.e. Langmuir-Hinshelwood type of mechanism with both reactants in adsorbed state on the surface. The rate limiting step is the interaction between the two adsorbed molecules. No inhibiting effect of the reaction products CO₂ and H₂O is observed. The use of k_{eff} means that the applied approach is "formal kinetics", in which the efficient rate constant k_{eff} has complex physical meaning, comprising rate constant, adsorption equilibrium constant and reactant concentration. The ethylene contact time τ_c was 4 min i.e. the maximal possible contact time at the lowest inlet flow rate of ethylene that the ethylene channel can allow. At this maximal τ_c we achieved the maximal conversion degree of ethylene photocatalytic oxidation.

The dimensions of the flat plate quartz window were 5 cm width x 15 cm length, allowing simultaneous accommodation of 2 lamps Philips TL4W/08 F4T5/BLB of total light power 8 Watts, placed on top of the window (distance of illumination 0 cm) supplying light intensity of 0.014 W/cm² polychromatic illumination of wave length range 320–400 nm ($\lambda_{\text{max}} = 365$ nm).

Two lamps Philips TUV 4W/G4 T5 (monochromatic illumination $\lambda = 254$ nm) (total light power 8 Watts), at 0 cm distance, the same illumination intensity of 0.014 W/cm², but much higher energy of the photons. The visible light irradiation was accomplished by linear halogen lamp

Tungsramp 500 Watts K1R7s supplying illumination intensity 8.9 mW/cm² (9700 Lm) at 50 cm distance of illumination to avoid overheating of the explosive C₂H₄-O₂ mixture [16, 17].

Thin layer chromatography (TLC) sheet (Merck Art.5554 Kieselgel 60 F254) pre-coated with SiO₂ was used to deposit the ZnO slurry by capillary method. The sheet had dimensions 4.2 cm x 13.4 cm of total geometric surface area 56 cm². To obtain 1mg/cm² coating 56 mg of the powder-form sample were weighed, suspended and then sonicated (Hielscher UP 200S, 24 kHz). Then the so obtained suspension was deposited drop-by-drop by capillary using directing air stream to obtain a uniform thin film on the SiO₂ coating.

RESULTS AND DISCUSSION

The SEM images of the as-prepared ZnO and RE-modified (La³⁺, Eu³⁺ or Ce³⁺) ZnO powders are shown in Fig. 1. As seen, the morphology of all samples is well ordered. ZnO/Ln powders are flowerlike in shape with average diameter size of about 0.4–0.45 μm (determined from the SEM images). An average particle size of 0.25 μm for ZnO nanocomposite. The surface of the pure and RE-modified ZnO samples does not show any changes. So, the type of rare earths does not influence the morphology. The SEM images of the four powders are similar.

X-ray diffractogram of the powders is analyzed to obtain information about various crystalline aspects. Fig. 2 shows that XRD patterns of synthesized pure ZnO. The sharp and intense peaks indicate that ZnO have high crystallinity and polycrystalline structure. The XRD peaks for (100), (002) and (101) planes of pure ZnO correspond to hexagonal wurtzite crystalline phase. The high intensity of (101) peak suggests that the growth of nanoparticles has taken place along this direction of crystallization of ZnO. No characteristic peaks of impurity phases such as Zn or Zn(OH)₂ are observed for all samples. The XRD spectras of the RE-modified ZnO powders are almost similar to that of ZnO [18], which can be due to their low concentration (2 mol%) in the ZnO nanocomposite. There is no change in the crystal structure. This also indicates that Ln³⁺ is uniformly dispersed between ZnO nanoparticles in the form of small Ln₂O₃ clusters. The crystallite average size of pure ZnO is found to be 36.68 nm, calculated by Sherrer's formula (Eq. 1).

In order to determine the photocatalytic activity of ZnO and RE-modified ZnO powders, a series of experiments are carried out with ethylene as model

air pollutant in gas-phase flat-plate continuous flow photocatalytic reactor.

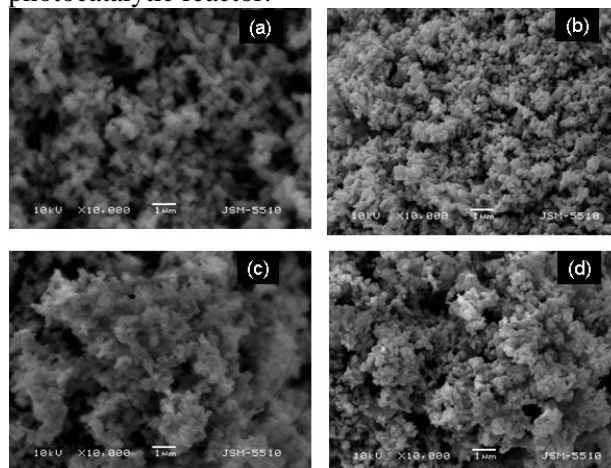


Fig. 1. SEM images of pure (a) and Eu³⁺ (b), La³⁺ (c), Ce³⁺ (d) – modified ZnO powders.

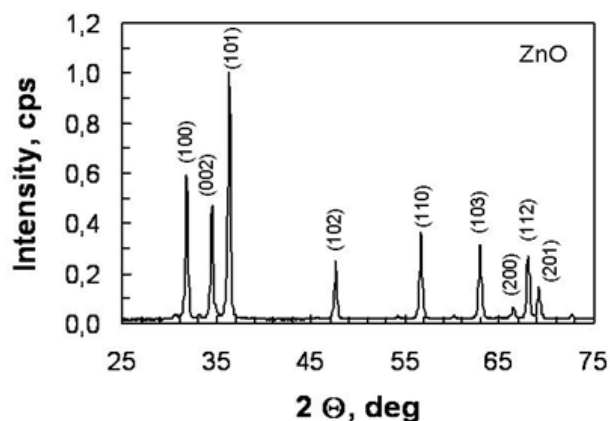


Fig. 2. XRD spectra of pure ZnO powder

The experiments carried out with UV-C illumination show higher degrees of photooxidation of ethylene in comparison with the experiments with UV-A light illumination (Fig. 3). The photocatalytic tests under visible light (intensity – 0.89 W/cm²) did not show reduced conversion of ethylene for the same reaction time.

As seen from Fig. 3, the photocatalytic efficiency is highest for the modified ZnO powders with Eu³⁺ (C₂H₄ conversion (%) – 5.1 and 8.2, under UV-A and UV-C irradiation). The modified samples with lanthanum oxide have a higher activity and faster degrade the pollutant (C₂H₄ conversion (%) – 4.6 and 7.8, under UV-A and UV-C irradiation) in comparison with the pure ZnO nanocomposite (C₂H₄ conversion (%) – 3.9 and 7.4, under UV-A and UV-C irradiation). The lowest photocatalytic properties have Ce – modified ZnO powders.

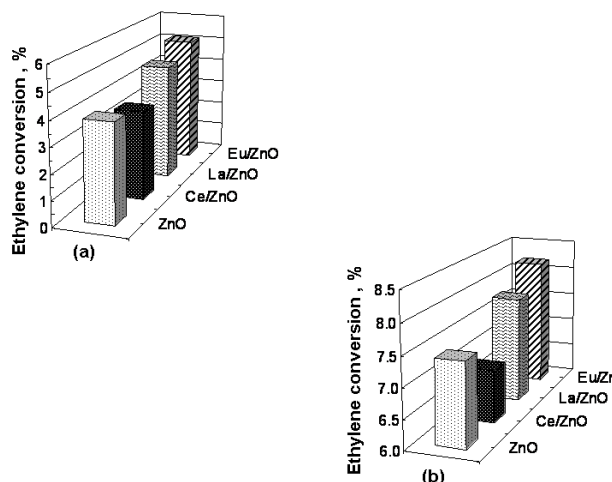


Fig. 3. Degrees of photooxidation of C₂H₄ under (a) UV-A and (b) UV-C irradiation with intensity 0.014 W/cm², τ_c = 4 min, 30% RH and O₂ excess over 4 ZnO photocatalysts (1 mg/cm²)

CONCLUSIONS

We are prepared pure and rare earth modified ZnO samples by hydrothermal method. The nanosized powders are characterized by Scanning Electron Microscopy and X-ray diffraction. The powders (pure and modified) are spherical in shape belonging to hexagonal wurtzite structures, which demonstrates that the RE³⁺ ions have no effect on the crystal structure. There is no photocatalytic activity under visible light due to the wide band gap of ZnO. UV-C light gives higher conversion degree owing to the higher photon energy than UV-A light. The experimental result shows that the nanosized Eu-modified powders have highest activity and fastest photocatalytic degradation the ethylene as model air pollutant. The photocatalytic efficiency of pure ZnO particles is lower than the activity achieved by La modified sample under UV-light irradiation. All these observations prove that RE-modified ZnO is a potential candidate for the practical application in photocatalytic degradation of organic contaminants.

Acknowledgements: This research is financially supported by the Russian Ministry of Education as part of the base portion of the state task № 2014/151 (Project Code 117), DFNI-T02/16 (№2742) and FP7 Horizon 2020.

REFERENCES

1. Y.F. Chen, D.M. Bagnall, H. Koh, K. Park, K. Hiraga, Z. Zhu, T. Yao, *Journal of Applied Physics*, **84**, 3912 (1998).
2. H. Lu, Y. Wang, X. Lin, *Material Letters*, **63**, 2321 (2009).
3. R.P. Andres, R. S. Averbach, W. L. Brown, L. E. Brusa, W. A. Goddard, A. Kaldora, S. G. Louiea, M. Moscovitsa, P. S. Peercya, S. J. Rileya, R. W. Siegela, F. Spaepen, Y. Wang, *Journal of Materials Research*, **4**, 704 (1989).
4. Y. Wang, N. Herron, *Physic Revue B*, **42**, 7253 (1990).
5. R. M. Alwan, Q. A. Kadhim, K. M. Sahan, R. A. Ali, R. J. Mahdi, N. A. Kassim, A. N. Jassim, *Nanoscience and Nanotechnology*, **5**, 1 (2015).
6. Y. Wang, Ch. Zhang, S. Bi, G. Luo, *Powder Technology*, **202**, 130 (2010).
7. Ö. A. Yildırım, C. Durucan, *Journal of Alloys and Compounds*, **506**, 944 (2010).
8. J. Wua, X. Shena, L. Jianga, K. Wanga, K. Chen, *Applied Surface Science*, **256**, 2826 (2010).
9. A.A. Ismail, A. El-Midany, E.A. Abdel-Aal, H. El-Shall, *Materials Letters*, **59**, 1924 (2005).
10. H. Van den Rul, D. Mondelaers, M.K. Van Bael, J. Mullens, *Journal of Sol–Gel Science Techology*, **39**, 41 (2006).
11. U. Pal, P. Santiago, *Journal of Physical Chemistry B*, **109**, 15317 (2005).
12. F. Xu, Z.-Y. Yuan, G.-H. Du, M. Halasa, B.-L. Su, *Applied Physics A*, **86**, 181 (2007).
13. J. Xie, H. Wanga, M. Duana, L. Zhang, *Applied Surface Science*, **257**, 6358 (2011).
14. N. Kaneva, A. Bojinova, K. Papazova, D. Dimitrov, *Catalysis Today*, **252**, 113 (2015).
15. B.D. Cullity, S.R. Stock, *Elements of X-ray Diffraction*, 3rd ed., Prentice-Hall, Inc., New Jersey, 388 (2001).
16. A. Eliyas, L. Dimitrov, D. Paneva, E. Stoyanova, I. Mitov, "Science Series "Nanoscience & Nanotechnology" Eds. E. Balabanova, I. Dragieva , **9**, 58 (2009).
17. A. Eliyas, K. Kumbilieva, L. Petrov, "Science Series "Nanoscience & Nanotechnology", Eds. E. Balabanova, I. Dragieva , **9**, 50 (2009).
18. M. Lucas, J. Peres, *Dyes & Pigments*, **71**, 236 (2006).

ИЗСЛЕДВАНЕ ФОТОКАТАЛИТИЧНИТЕ СВОЙСТВА НА ЧИСТИ И Ln (La^{3+} , Eu^{3+} , Ce^{3+}) – МОДИФИЦИРАНИ ZnO ПРАХОВЕ, СИНТЕЗИРАНИ ЧРЕЗ ТЕРМАЛЕН МЕТОД

Н.В. Кънева^{1*}, А.С. Божинова¹, К.И. Папазова¹, Д.Ц. Димитров¹, А.Е. Елиас²

¹Лаборатория по наука и технология на наночастиците, Катедра по обща и неорганична химия, Факултет по химия и фармация, Софийски университет, бул. “Джеймс Баучер” 1, 1164, София, България

²Институт по Катализа, Българска Академия на Науките, ул. Акад. Г. Бончев 11, София 1113, България

Постъпила на 7 ноември 2016 г.; приета на 4 януари 2017 г.

(Резюме)

Прост и бърз термален метод е използван за синтезирането на ZnO и Ln-модифицирани (La^{3+} , Eu^{3+} , Ce^{3+}) ZnO прахове. Нанокристалните фотокатализатори с концентрация 2.0 мол% са накалиени при 100°C за 1 час. Чистите и модифицираните прахове са характеризирани с различни техники, такива като Рентгенова дифракция, Сканиращ електронен микроскоп.

Фотокаталитичното действие на смесите е тествано за фотокаталитично окисление на етилен (замърсител на въздух) в газова фаза, използвайки фотокаталитичен реактор – скорост 5000 rpm, максимално контактно време на етилен 4 мин и оптимална относителна влажност 30%. Пробите от прах се суспендират във вода и се подлагат на ултразвук (24 kHz) с цел раздробяване на големите агломерати в разтвора. За експериментите се използва TLC капиларен метод. Фотокаталитичните тестове са проведени в присъствие на UV-A и UV-C светлина (0.014 W/cm²). Проба 3 (Ce^{3+} -модифициран)/ZnO притежава най-висока ефективност при облъчване с UV-A и UV-C светлина, превъзхождайки чистият ZnO. Модифицираният фотокатализатор не е активен в присъствие на видима светлина, което се дължи на ширината на забранената му зона.

Ключови думи: ZnO, редкоземни елементи, прахове, фотокатализа

Electrochemically modified with osmium graphite: catalytic activity and application to the amperometric detection of hydrogen peroxide

T. M. Dodevska^{1*}, N. D. Dimcheva², E. G. Horozova², Y. L. Lazarova¹

¹University of Food Technologies, Department of Inorganic Chemistry and Physical Chemistry,
26 Maritsa Blvd., Plovdiv 4002, Bulgaria

²University of Plovdiv "Paisii Hilendarski", Department of Physical Chemistry,
24 Tsar Assen Str., Plovdiv 4000, Bulgaria

Received November 7, 2016; Revised January 23, 2017

A new electrochemical method for deposition of Os on carbon carrier is reported. The metal phase was electrodeposited onto graphite under potentiodynamic conditions, using cyclic voltammetry over the potential range from -0.8 to 0 V (vs. Ag/AgCl, 3 M KCl). In order to obtain modified electrode with high catalytic activity in the reduction of hydrogen peroxide, the number of cycles and the scan rate of the electrodeposition process were optimized. It was found that the graphite modified with Os for 10 cycles with a scan rate of 0.01 V s⁻¹ possesses the highest catalytic activity in respect to the target reaction. The electrochemical behavior of the so produced electrode-catalyst was examined at different pHs at potentials of 0 V and -0.05 V. The modified electrode shows good analytical performance at hydrogen peroxide determination in neutral medium: a wide dynamic range (up to 5 mM) and a sensitivity of 426 $\mu\text{A mM}^{-1} \text{cm}^{-2}$ at an applied potential of -0.05 V (sensitivity of 364 $\mu\text{A mM}^{-1} \text{cm}^{-2}$ at potential of 0 V, respectively), which makes it a promising transducing material for the development of electrochemical peroxide sensors and, eventually, biosensors.

Key words: osmium, modified electrodes, electrodeposition, electrocatalyst, hydrogen peroxide reduction

INTRODUCTION

In the recent years, the electrochemical properties of osmium (Os) have been intensively studied mainly for the development of fuel cells. The interest to this transition metal is connected not only with the significant electrocatalytic activity in numerous processes, but also with the substantial advantage in the price – osmium being four times cheaper than platinum, traditionally used in developing catalysts.

It is well known that the electrocatalytic activity of metal deposits depends on their sizes, shapes, structural features and population on the surface of the carrier. Such parameters depend on both nature and pre-treatment of the carrier, and the procedure for deposition of the metal phase. Numerous different physical, chemical and electrochemical methods for obtaining osmium catalysts have been applied: vapor deposition at high temperature [1, 2], microwave synthesis [3], chemical (sol-gel) deposition [4], electrochemical deposition under either constant current [5,6] or potential [7,8], as the most commonly used precursor for the deposition of Os is hexachloroosmiate (IV) anion $[\text{OsCl}_6]^{2-}$.

Kua and Goddard suggested that pure metallic Os should be examined as Direct Methanol Fuel Cell (DMFC) catalyst because this metal is capable of catalyzing both dehydrogenation of methanol and water dehydrogenation without a co-catalyst [9]. The electrocatalytic properties of osmium

electrodeposits on Pt in acidic solutions of methanol, ethanol, propanol, formaldehyde and acetaldehyde have been studied [10]. The results showed that at low overpotentials the electrocatalytic activity of Os exceeded that of Pt during electrooxidation of methanol, ethanol and acetaldehyde. The adsorption and electrooxidation of CO, methanol, ethanol, and formic acid on glassy carbon modified with Os were examined in details by Orozco and coworkers by means of cyclic voltamperometry (CV) and infrared spectrometry with Fourier transformation (FTIRS) [11]. In order to develop a new anode material for Direct Borohydride Fuel Cell (DBFC), Os-film with thickness up to 140 nm on Pt/quartz was obtained [12]. The film was electrodeposited from a solution of $(\text{NH}_4)_2\text{OsCl}_6$ in HClO_4 by applying a differential pulse voltammetry (DPV). The analysis of the film carried out by X-ray photoelectron spectroscopy (XPS) indicated the presence of both Os and oxide (OsO_2). The authors compared the electrocatalytic activity of several electrodes modified with Os-films with varying thickness, in the reaction of electrooxidation of BH_4^- in 2 M NaOH.

To the best of our knowledge, there are no results concerning the application of osmium as a catalytically active component in electrocatalysts for reduction of hydrogen peroxide (H_2O_2). The development of effective and accessible materials

* To whom all correspondence should be sent.
E-mail: dodevska@mail.bg

with pre-defined operational characteristics for quantitative determination of H_2O_2 at low potentials is relevant not only for the establishment of amperometric analysis of H_2O_2 , but also for developing selective first generation biosensors. Hydrogen peroxide has wide and diverse applications in many fields – food processing, textile industry, paper bleaching, disinfecting and cleaning products, pharmaceutical, clinical and environmental analyses. H_2O_2 is also a catalytic by-product from enzyme-catalysed oxidation of metabolites such as glucose, lactate, ethanol, cholesterol, xanthine, etc. Therefore, the development of highly sensitive, interference-free and simple methods for reliable, fast and low-cost quantitative analysis of H_2O_2 over the micro- and nanomolar concentration ranges applicable in the control of numerous technological processes, as well as environmental and biochemical monitoring, is practically important and widely investigated.

In this connection, the present work deals with the studies on the electrochemical behavior of graphite modified with osmium and the characterization of the produced electrode-catalyst with respect to quantitative amperometric determination of H_2O_2 at low applied potentials. A new electrochemical method for deposition of osmium on carbon carrier was reported – the metal phase was electrodeposited onto graphite under potentiodynamic conditions, using cyclic voltammetry over the working potential range from -0.8 to 0 V (vs. Ag/AgCl, 3 M KCl). In order to obtain modified electrode with high catalytic activity in the reduction of H_2O_2 , the number of cycles and the scan rate of the electrodepositing process were optimized.

MATERIALS AND METHODS

Materials

The working electrode was disc from spectroscopic graphite with diameter of the working surface $d=5.6$ mm and visible surface area *ca.* 25 mm² (RWO, Ringsdorf, Germany).

$(\text{NH}_4)_2\text{OsCl}_6$ (Fluka); NaClO_4 (Fluka); H_2O_2 (Fluka); Na_2HPO_4 and NaH_2PO_4 (Sigma-Aldrich) were of analytical grade and used as received. 0.1 M buffer solutions were prepared with monobasic and dibasic sodium phosphates dissolved in double distilled water with various pHs, adjusted with a pH meter MS 2006 (Microsyst, Bulgaria).

Apparatus and measurements

The electrochemical measurements were performed using computer controlled electrochemical workstation EmStat2 (PalmSens BV, The Nederland), equipped with PSTrace 2.5.2

software, in a conventional three-electrode cell, including a working electrode (modified with osmium graphite or a bare graphite electrode), a Ag/AgCl (3 M KCl) reference electrode, and a platinum auxiliary electrode. All the electrochemical measurements were carried out in 0.1 M phosphate buffer solutions (PBS) at temperature of 25 °C.

Preparation of the modified electrodes

Before modification the bare graphite electrode was carefully polished to mirror-like finish with emery paper with decreasing particle size (P800, P1200 and P2000), rinsed with double distilled water and sonicated in water for 3 min. The working surface of the cleaned and polished electrode was modified through direct electrodeposition of osmium by means of CV over the potential range from 0 to -0.8 V (vs. Ag/AgCl, 3 M KCl) from electrolyte containing 5 mM $(\text{NH}_4)_2\text{OsCl}_6$ and 0.1 M NaClO_4 . The scan rate and the number of cycles are varied to obtain modified electrode with optimized electrocatalytic properties in the target reaction (electroreduction of H_2O_2). To indicate the type of the modified with osmium graphite electrode we take the following notations: Os_number of cycles_scan rate/Gr (for example: graphite modified by applying 10 cycles at a rate of 5 mV s⁻¹ will be denoted in the text as Os_10c_v5/Gr).

RESULTS AND DISCUSSION

Fig. 1 displays the CVs of electrodeposition process of osmium particles onto graphite electrode which begins at potential of 0 V and ends at the negative potential of -0.8 V. It can be seen that the reduction peak of Os particles occurs at the potential of -0.45 V and remains unchanged with increasing the number of cycles. At the same time the oxidation process takes place at -0.25 V (for the first cycle) and this peak is shifted to more positive potentials by increasing the number of cycles (-0.19 V for the 20th cycle). For the continuous cycles, the reduction and the oxidation peaks of the Os particles were clearly increasing. The observed features confirm that the electrodeposition of osmium takes place at the graphite surface.

Following the development of effective electrocatalyst of H_2O_2 reduction, we focused on the optimization of the number of cycles and the scan rate of the electrodepositing process. The effect of the number of cycles on the electrocatalytic activity of the electrodes was first investigated. Four different types of electrodes were fabricated by cycling at scan rate of 10 mV s⁻¹ for 5, 8, 10 and 20 cycles, respectively. In order to obtain a prior information about the catalytic activity in reduction of hydrogen peroxide for each of the so-produced

electrodes an amperometric response was recorded in the presence of 0.5 mM H₂O₂ at a constant potential of 0 V in 0.1 M PBS (pH 7.0). Cathode currents in presence of H₂O₂ resulting from its electrochemical reduction were observed for all four modified electrodes; the background subtracted steady-state responses of the electrodes are shown in Fig. 2. The current response increased remarkably as the number of cycles increased and reached a maximal value (52 μA) at an electrode modified with 10 cycles. As shown, the amperometric response does not change with further increase of the number of cycles and the catalytic ability of the electrodes type Os_{10c_v10}/Gr and type Os_{20c_v10}/Gr toward reduction of H₂O₂ is identical. Therefore electrode type Os_{20c_v10}/Gr was not used in further investigations.

In the next step, the other three types modified electrodes were tested for amperometric detection of H₂O₂ at low working potentials. The concentration dependence of the amperometric response of the electrodes was investigated by means of constant potential amperometry at potentials of -0.05 and 0 V in 0.1 M PBS at pH 7.0 and the basic operational parameters of each modified electrode were deduced (Table 1). The chronoamperometric records indicate that for all types of modified electrodes the reductive current increased stepwise upon introducing in the buffer aliquots of the H₂O₂ stock solution. The electrode sensitivity was determined as the slope of the linear portion of the calibration graph (divided by geometric electrode area), build on the basis of the chronoamperometric measurements. From the data presented in Table 1 it is evident that for all modified electrodes at pH 7.0 as the polarization potential become more negative, the sensitivity increases and the range of the strict linear dependence of the signal shortens.

In order to establish the effect of electrodeposition scan rate on the activity of the catalysts in the target reaction, graphite electrodes were modified for 10 cycles at scan rates of 5, 10, 25 and 50 mV s⁻¹, respectively. With all four types of modified electrodes, the current signal in the presence of 0.5 mM H₂O₂ at a constant potential of 0 V (pH 7.0) was examined.

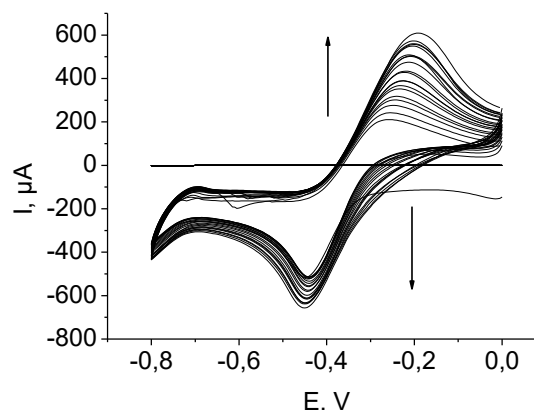


Fig. 1. Potentiodynamic electrodeposition of Os particles on graphite electrode from 5 mM (NH₄)₂OsCl₆ containing 0.1 M NaClO₄; potential scan between 0 to -0.8 V for 20 cycles; scan rate of 10 mV s⁻¹.

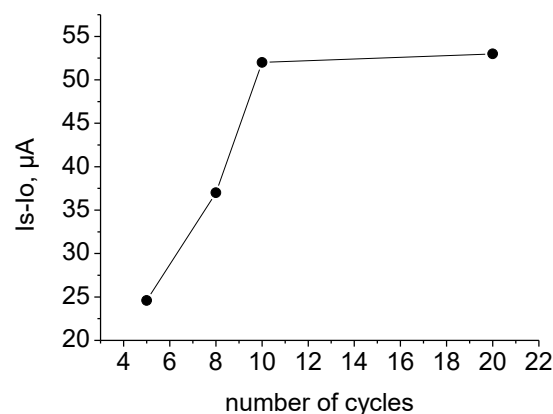


Fig. 2. Effect of the number of electrodeposition cycles (scan rate of 10 mV s⁻¹) on the amperometric responses of the modified electrodes toward the reduction of H₂O₂. Supporting electrolyte: 0.1 M PBS (pH 7.0) containing 0.5 mM H₂O₂; applied potential: 0 V.

Table 1. Operational parameters of graphite electrodes modified with osmium by means of CV (from 0 to -0.8 V) with 5, 8 and 10 cycles at scan rate of 10 mV s⁻¹; reference electrode Ag/AgCl, 3 M KCl; background electrolyte 0.1 M PBS.

E, V	Electrode sensitivity, μA mM ⁻¹ cm ⁻²		
	Linearity, mM		
	Os _{5c_v10} /Gr	Os _{8c_v10} /Gr	Os _{10c_v10} /Gr
-0.05	188 7 mM (r ² =0.98 ₉)	264 5.6 mM (r ² =0.99 ₄)	426 5 mM (r ² =0.99 ₇)
0	144 7.5 mM (r ² =0.98 ₈)	232 6.3 mM (r ² =0.99 ₃)	364 5.6 mM (r ² =0.99 ₅)

Table 2. Operational parameters of modified electrode type Os_10c_v10/Gr at various pH values; reference electrode Ag/AgCl, 3 M KCl; background electrolyte 0.1 M PBS.

E, V	Electrode sensitivity, $\mu\text{A mM}^{-1} \text{cm}^{-2}$				
	Linearity, mM				
	pH 5.0	pH 6.0	pH 7.0	pH 8.0	pH 9.0
-0.05	308	430	426	288	188
	0.7 mM ($r^2=0.99_4$)	2.7 mM ($r^2=0.99_3$)	5 mM ($r^2=0.99_7$)	3.5 mM ($r^2=0.98_9$)	1.7 mM ($r^2=0.96_6$)
0	176	390	364	256	
	1.2 mM ($r^2=0.99_8$)	4.7 mM ($r^2=0.99_8$)	5.6 mM ($r^2=0.99_5$)	5.3 mM ($r^2=0.98_1$)	

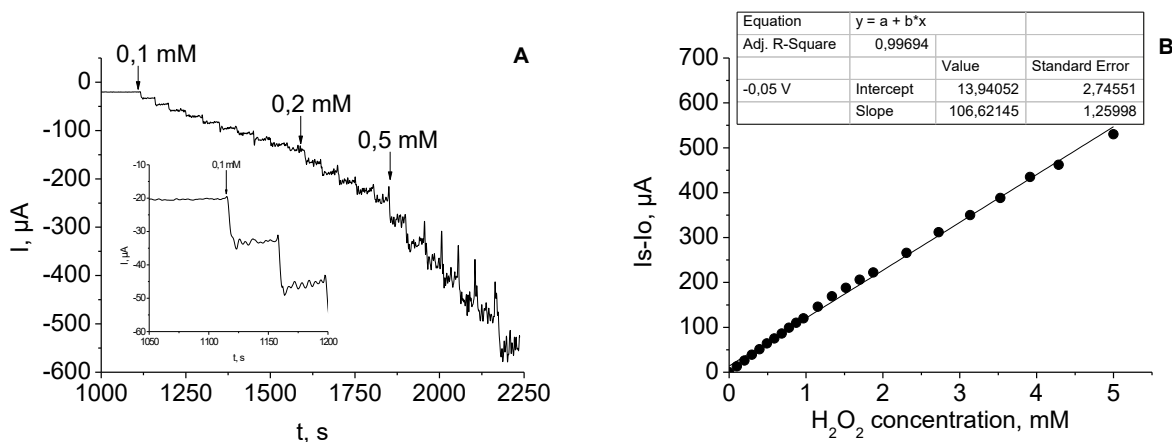


Fig. 3. A) Amperometric response of the modified electrode type Os_10c_v10/Gr to successive addition of H_2O_2 into stirred 0.1 M PBS (pH 7.0) at an applied potential of -0.05 V; inset shows the initial section of the response upon addition of the first portions of 0.1 mM H_2O_2 . B) The corresponding calibration line (the dependence of the electrode response on the concentration of H_2O_2).

The electrode response was found to decrease linearly with increasing the scan rate from 10 to 50 mV s^{-1} ($y = -0.3776x + 56.031$, $r^2 = 0.99_8$). These experimental data suggest that the increase of the scan rate during electrodeposition results in smaller amount of catalytically active metal phase formed onto graphite surface. At the same time the catalytic current (48 μA) of the modified electrode type Os_10c_v5/Gr is lower compared with that of the electrode type Os_10c_v10/Gr, i.e. the application of scan rate lower than 10 mV s^{-1} does not result in obtaining more active metal deposition. Based on these results, 10 cycles at scan rate of 10 mV s^{-1} were selected as optimal conditions for electrodeposition.

The effect of pH of the PBS on the catalytic activity towards the reduction of H_2O_2 was also investigated. The basic operational characteristics of the electrode type Os_10c_v10/Gr, determined in 0.1 M PBS over pH range 5.0 – 9.0 at potentials of -0.05 and 0 V, are provided in Table 2. The modified electrode showed higher electrocatalytic activity at an applied potential of -0.05 V in PBS with pHs 6.0 and 7.0. The linear dynamic range of the electrode response also differs depending on the applied potential and the pH value of the buffer solution. The linearity range of the signal shortens gradually with

increasing the acidity of the background electrolyte. The same effect was observed when increasing pH value over 7.0. Thus the pH value 7.0 was selected as optimal for the determination of H_2O_2 with the here presented modified electrode.

Fig. 3A shows the typical current-time (I-t) plot upon the successive injection of H_2O_2 at an applied potential of -0.05 V. A well-defined response was observed during the successive additions of 0.1 mM, 0.2 mM and 0.5 mM H_2O_2 , respectively. These results evidence a stable and efficient catalytic property of osmium. It can also be observed that the modified electrode type Os_10c_v10/Gr responds rapidly to the changes of H_2O_2 concentration, producing steady-state signal within 10 s. The corresponding calibration curve is presented in Fig. 3B. The linear response was proportional to the H_2O_2 concentration up to 5.0 mM (correlation coefficient of 0.997) with a sensitivity of 106.62 $\mu\text{A mM}^{-1}$ (or 426 $\mu\text{A mM}^{-1} \text{cm}^{-2}$) and a detection limit of 10 μM (at a signal-to-noise ratio of 3). The reproducibility of the current signal for the same electrode to 1 mM H_2O_2 was examined. The relative standard deviation (RSD) was calculated to be 3 % for 4 successive measurements.

Table 3. Comparison of the analytical characteristics of amperometric sensors for H₂O₂ detection reported in the literature with the achieved in the present work.

Electrode modifier/(Electrode)	E, V (vs. Ag/AgCl)	Electrolyte	Sensitivity, $\mu\text{A mM}^{-1} \text{cm}^{-2}$	Detection limit, μM	Ref.
Fe ₃ O ₄ /chitosan/(GC rotating electrode)	-0.2	pH 7.0	9.6 $\mu\text{A mM}^{-1}$	7.4	[13]
PtNW-CNT-CHIT/(GC)	-0.1 (vs. SCE)	1/15M PB pH 6.98	260	-	[14]
Co ₃ O ₄ nanowalls/(GC)	-0.2	0.01 M PBS pH 7.4	80.74 * (4.84 $\mu\text{A mM}^{-1}$)	10	[15]
PdNPs-PAA/(Au)	-0.1 (vs. SCE)	PBS pH 7.0	232	5	[16]
Ag/(GC)	-0.2	0.1 M PBS pH 7.6	104.53 * (7.39 $\mu\text{A mM}^{-1}$)	0.5	[17]
PVA-MWCNTs-PtNPs/(GC)	0	0.1 M PBS pH 7.0	122.63	0.7	[18]
Ag microparticles/(SPC)	-0.4	0.01 M PBS pH 7.4	138.4	50	[19]
Pd/PEDOT nanospheres/(GC)	-0.2 (vs. SCE)	0.1 M PBS pH 7.0	215.3	2.84	[20]
Graphene-AgNPLs/(GC)	-0.5	0.2 M PBS pH 7.0	183.5	3	[21]
MWCNT/Pt nanohybrids/(Pt)	0	PBS pH 7.0	205.8	0.3	[22]
Os/(Gr)	-0.05 0	0.1 M PBS pH 7.0	426 364	10	This work

*Calculated from the data in paper

A large number of H₂O₂ sensors have been reported in literature. The performance of the sensors is greatly dependent on the supporting electrolyte, applied potential, electrode material and surface area, therefore it is difficult to compare one sensor to others. Various H₂O₂ sensors, based on transition and noble metal particles-modified electrodes, have been listed in Table 3 with respect to the operational conditions, sensitivity and detection limit. It can be seen that the proposed Os-modified graphite electrode possess the sufficient capability for amperometric detection of H₂O₂. Compared with other modified electrodes employed as H₂O₂ sensors in neutral medium, it showed much higher sensitivity. In contrast to other H₂O₂ amperometric sensors of previous literature reports [13-17, 19, 20], the applied potential for the modified electrode Os_{10c_v10}/Gr is much lower. At such a low potentials (0 V and -0.05 V), the background current decreases and the response of other electroactive species can be minimized or totally eliminated, which is crucial for the selectivity of the analytical system.

CONCLUSION

The current work provides a new facile strategy to construct hydrogen peroxide sensor based on

osmium, electrodeposited on graphite electrode. The number of cycles and the scan rate of the electrodeposition process (cyclic voltammetry) were purposefully altered and the catalytic activity in the reduction of H₂O₂ for each of the produced electrodes was examined. The electrode modified with 10 cycles at scan rate of 0.01 V s⁻¹ exhibits the best analytical performance for the amperometric H₂O₂ detection. The optimal working pH value (7.0), the high sensitivity (426 $\mu\text{A mM}^{-1} \text{cm}^{-2}$) and the extended dynamic range of the response (up to 5 mM) at an applied potential as low as -0.05 V, makes it an attractive novel material for electrochemical H₂O₂ sensing and promising candidate for designing biosensing systems.

Acknowledgment: Authors gratefully acknowledge the financial support from the University of Plovdiv Research Fund (grant HII 15 – XΦ 001).

REFERENCES

1. C. Li, W. K. Leong, K. P. Loh, *Appl. Organomet. Chem.*, **33**, 196 (2009).
2. Y. Chi, H-L Yu, W-L Ching, C-S Liu, Y-L Chen, T-Y Chou, S-M Peng, G-H Lee, *J. Mat. Chem.*, **12**, 1363 (2002).
3. E. Borja-Arco, O. Jimenez-Sandoval, J. Escalante-Garcia, L. Magallon-Cacho, P. J. Sebastian, *Int. J. Electrochem.*, Article ID 830541, 8 pages, (2011).

4. M. Atwan, D. Northwood, E. Gyenge, *Int. J. Hydrog. Energy*, **30**, 1323 (2005).
5. V. Lam, D. Kannangara, A. Alfantazi, E. Gyenge, *J. Power Sources*, **212**, 57 (2012).
6. V. Lam, E. Gyenge, *J. Electrochem. Soc.*, **155**, 1155 (2008).
7. V. Pacheco Santos, V. Del Colle, R. M. Bezerra, G. Tremiliosi-Filho, *Electrochim. Acta*, **49**, 1221 (2004).
8. U. Koponen, M. Bergelin, M. Wasberg, *J. Electroanal. Chem.*, **531**, 87 (2002).
9. J. Kua, W. A. Goddard, *J. Am. Chem. Soc.*, **121**, 10928 (1999).
10. O. A. Petrii, V. D. Kalinin, *Russ. J. Electrochem.*, **35**, 627 (1999).
11. G. Orozco, C. Gutierrez, *J. Electroanal. Chem.*, **484**, 64 (2000).
12. A. Ignaszak, E. Gyenge, *Electrochim. Acta*, **95**, 268 (2013).
13. M. Lin, H. Leu, *Electroanalysis*, **17**, 2068 (2005).
14. F. Qu, M. Yang, G. Shen, R. Yu, *Biosens. Bioelectron.*, **22**, 1749 (2007).
15. W. Jia, M. Guo, Z. Zheng, T. Yu, E. Rodriguez, Y. Wang, Y. Lei, *J. Electroanal. Chem.*, **625**, 27 (2009).
16. Y. Tang, Y. Cao, S. Wang, G. Shen, R. Yu, *Sens. Actuat. B*, **137**, 736 (2009).
17. X. Qin, H. Wang, X. Wang, Z. Miao, Y. Fang, Q. Chen, X. Shao, *Electrochim. Acta*, **56**, 3170 (2011).
18. Y. Fang, D. Zhang, X. Qin, Z. Miao, S. Takahashi, J. Anzai, Q. Chen, *Electrochim. Acta*, **70**, 266 (2012).
19. W-H Hsiao, H-Y Chen, T-M Cheng, T-K Huang, Y-L Chen, C-Y Lee, H-T Chi, *J. Chin. Chem. Soc.*, **59**, 500 (2012).
20. F. Jiang, R. Yue, Y. Du, J. Xu, P. Yang, *Biosens. Bioelectron.*, **44**, 127 (2013).
21. L. Zhong, S. Gan, X. Fu, F. Li, D. Han, L. Guo, L. Niu, *Electrochim. Acta*, **89**, 222 (2013).
22. Z. Miao, D. Zhang, Q. Chen, *Materials*, **7**, 2945 (2014).

ЕЛЕКТРОХИМИЧНО МОДИФИЦИРАН С ОСМИЙ ГРАФИТ: КАТАЛИТИЧНА АКТИВНОСТ И ПРИЛОЖЕНИЕ ЗА АМПЕРОМЕТРИЧНА ДЕТЕКЦИЯ НА ВОДОРОДЕН ПЕРОКСИД

T. M. Додевска^{1*}, Н. Д. Димчева², Е. Г. Хорозова², Я. Л. Лазарова¹

¹Университет по хранителни технологии, кат. "Неорганична химия и физикохимия", бул. „Марица“ 26, Пловдив 4002, България

²Пловдивски университет „Паисий Хилендарски“, кат. "Физикохимия", ул. „Цар Асен“ 24, Пловдив 4000, България

Постъпила на 7 ноември 2016 г.; приета на 23 януари 2017 г.

(Резюме)

Представен е нов електрохимичен метод за отлагане на осмий върху въглероден носител. Металната фаза е отложена върху графит в потенциодинамични условия, използвайки циклична волтамперометрия в диапазон от потенциали от -0.8 до 0 V (vs. Ag/AgCl, 3 M KCl). С цел получаване на модифициран електрод с висока каталитична активност при редукция на водороден пероксид, са оптимизирани броят цикли и скоростта на изменение на потенциала при процеса на електроотлагане. Установено е, че графитът, модифициран с осмий чрез 10 цикъла при скорост 0.01 V s⁻¹, проявява най-висока каталитична активност в целевата реакция. Електрохимичното поведение на така разработения електрокатализатор е изучено при различни стойности на рН при работни потенциали 0 V и -0.05 V. Модифицираният електрод има много добри аналитични характеристики при определяне на водороден пероксид в неутрална среда: широка област на линейна концентрационна зависимост на сигнала (до 5 mM) и чувствителност 426 μA mM⁻¹ cm⁻² при потенциал -0.05 V (чувствителност 364 μA mM⁻¹ cm⁻² при потенциал 0 V, съответно), които го характеризират като подходящ базов трансдюсер (преобразувател на сигнала) за разработването на електрохимични сензори за пероксида и, евентуално - биосензори.

Ключови думи: осмий, модифицирани електроди, електроотлагане, електрокатализатор, редукция на водороден пероксид

Ni(II) complexes of 4- and 5- nitro-substituted heteroaryl cinnamoyl derivatives

P.E. Marinova^{1*}, I.D. Nikolova², M.N. Marinov³, S.H. Tsoneva¹, A.N. Dimitrov¹, N.M. Stoyanov²

¹University of Plovdiv, Faculty of Chemistry, 24 Tzar Assen St., 4000 Plovdiv, Bulgaria

²University of Ruse – Razgrad Branch, Department of Chemistry and Chemical Technology, 47 Aprilsko Vastanie St, 7200 Razgrad, Bulgaria

³Agricultural University – Plovdiv, Faculty of Plant Protection and Agroecology, Department of General Chemistry, 12 Mendeleev Blvd, 4000 Plovdiv, Bulgaria

Received November 4, 2016; Revised January 21, 2017

A series of Ni(II) complexes with 4- and 5- nitro-substituted heteroaryl cinnamoyl derivatives were synthesized. All complexes were obtained with the metal to ligand ratio 1:2. The present study is focused on Ni(II) complexes of 4- and 5- nitro-substituted heteroaryl cinnamoyl derivatives (**L1-L8**), synthesized from Ni(CH₃COO)₂·4H₂O. The structures of the complexes were investigated by elemental analysis and spectroscopic UV-Vis and IR methods and one of them with Raman spectroscopy. The presence of two water molecules in the inner coordination sphere of all Ni(II) complexes was suggested.

Key words: Nitro-Substituted Heteroaryl Cinnamoyl Derivatives, Metal Complexes, IR

INTRODUCTION

2-Acetyl-1,3-indandione and its derivatives possess a wide array of important physiological activities. Some of them have antimicrobial activity [1], antiparasitical [2] and anticonvulsant effect [3]. Extensive publications and reviews, mainly from Alfimov *et al.* [4] and Chetkina *et al.* [5], focus on the study of the molecular receptors based on photochromic crown ethers and complex formation and the X-ray structure of single crystals of the 1,3-indandione and 1,3-dicyanomethyleneindan derivatives.

Recently, we reported the synthesis and structure of 2-(1-hydroxy-3-phenyl-allylidene)-2*H*-inden-1,3-dione, 2-(3-thiophene-2-yl-1-hydroxy-allylidene)-2*H*-inden-1,3-dione, 2-(3-thiophene-3-yl-1-hydroxy-allylidene)-2*H*-inden-1,3-dione, 2-(3-furane-2-yl-1-hydroxy-allylidene)-2*H*-inden-1,3-dione and their Cu(II), Cd(II), Zn(II), Co(II) and Ni(II) complexes [6] and 2-[1-hydroxy-3-phenyl-allylidene]-indan-1,3-dione, 2-[1-hydroxy-3-(4-fluoro-phenyl)-allylidene]-indan-1,3-dione, 2-[1-hydroxy-3-(4-chloro-phenyl)-allylidene]-indan-1,3-dione, 2-[1-hydroxy-3-(4-methyl-phenyl)-allylidene]-indan-1,3-dione, 2-[1-hydroxy-3-(4-cyano-phenyl)-allylidene]-indan-1,3-dione, 2-[1-hydroxy-3-(4-methoxy-phenyl)-allylidene]-indan-1,3-dione, 2-[1-hydroxy-3-(4-dimethylamino-phenyl)-allylidene]-indan-1,3-dione with Cu(II), Cd(II), Zn(II), Co(II) and Ni(II) complexes [7] and 2-(1-hydroxy-3-(4-fluoro-phenyl)-allylidene)-2*H*-

indene-1,3-dione and its Cu(II), Zn(II) and Cd(II) complexes [8].

There is no X-ray data of metal complexes with 4- and 5- nitro-substituted heteroaryl cinnamoyl derivatives in the Cambridge Structural Data Base. For this reason, the goal of current paper is to study the composition and structure of a series of metal complexes with 4- and 5- nitro-substituted heteroaryl cinnamoyl derivatives.

In the present work we describe the synthesis and reaction conditions to obtain new Ni(II) complexes of 2-[1-hydroxy-3-(thiophen-2-yl)prop-2-en-1-ylidene]-4-nitro-1*H*-indene-1,3(2*H*)-dione (**L1**), 2-[1-hydroxy-3-(thiophen-3-yl)prop-2-en-1-ylidene]-4-nitro-1*H*-indene-1,3(2*H*)-dione (**L2**), 2-[3-(furan-2-yl)-1-hydroxyprop-2-en-1-ylidene]-4-nitro-1*H*-indene-1,3(2*H*)-dione (**L3**), 2-[1-hydroxy-3-(1*H*-pyrrol-2-yl)prop-2-en-1-ylidene]-4-nitro-1*H*-indene-1,3(2*H*)-dione (**L4**), 2-[1-hydroxy-3-(thiophen-2-yl)prop-2-en-1-ylidene]-5-nitro-1*H*-indene-1,3(2*H*)-dione (**L5**), 2-[1-hydroxy-3-(thiophen-3-yl)prop-2-en-1-ylidene]-5-nitro-1*H*-indene-1,3(2*H*)-dione (**L6**), 2-[3-(furan-2-yl)-1-hydroxyprop-2-en-1-ylidene]-5-nitro-1*H*-indene-1,3(2*H*)-dione (**L7**) and 2-[1-hydroxy-3-(1*H*-pyrrol-2-yl)prop-2-en-1-ylidene]-5-nitro-1*H*-indene-1,3(2*H*)-dione (**L8**) with general formula given in Figure 1. We characterize the obtained complexes as well.

* To whom all correspondence should be sent.
E-mail: petia_marinova@abv.bg

EXPERIMENTAL

Metal salt $\text{Ni}(\text{CH}_3\text{COO})_2 \cdot 4\text{H}_2\text{O}$ - Fluka) and solvents used for the synthesis of the complexes were with a p.a. qualification. UV/Vis spectra of **L1-L8** and its metal complexes were measured on a Lambda 9 Perkin-Elmer UV/Vis/NIR Spectrophotometer from 200 nm to 1000 nm. The IR spectra of **L1-L8** were registered in KBr pellet on a Bruker FT-IR VERTEX 70 Spectrometer from 4000 cm^{-1} to 400 cm^{-1} at resolution 2 cm^{-1} with 25 scans. The IR spectra of the Ni(II) complexes of **L1-L8** were registered in KBr pellet on a 1750 FTIR-Perkin-Elmer Spectrophotometer.

Synthesis of Ni(II) complexes with 4- nitro-substituted heteroaryl cinnamoyl derivatives (**L1-L4**) and 5- nitro-substituted heteroaryl cinnamoyl derivatives (**L5-L8**)

0.001 mol (g) of L1-L8 in 7 cm^3 dioxane

0.0005 mol (g) of $\text{Ni}(\text{CH}_3\text{COO})_2 \cdot 4\text{H}_2\text{O}$ in 10 cm^3 CH_3OH

All metal complexes were obtained after mixing methanol solutions of the $\text{Ni}(\text{CH}_3\text{COO})_2 \cdot 4\text{H}_2\text{O}$ and the corresponding ligands (**L1-L8**), dissolved in dioxane, in metal-to-ligand ratio 1:2. Non-charged complexes were formed as precipitates, which were further filtrated, repeatedly washed with H_2O , and dried over CaCl_2 for 2 weeks. It was found out that the complexes were soluble in THF and DMSO. Selected IR frequencies and elemental analyses data are presented in Tables 1, 2 and 3, respectively.

The spectral data of the compounds obtained were as follows:

4- NO_2 -substituted heteroaryl cinnamoyl derivatives and their Ni(II) complexes (**L1-L4**)

UV-Vis (DMSO) L1 $\lambda_{\text{max}} = 325 \text{ nm}, 382 \text{ nm}$

UV-Vis (DMSO) Ni(II)L1 $\lambda_{\text{max}} = 254 \text{ nm}, 395 \text{ nm}$

Raman ($\nu_{\text{max}}, \text{cm}^{-1}$) L1: 1601, 1500, 1413, 1368, 1274, 1204, 345

UV-Vis (DMSO) L2 $\lambda_{\text{max}} = 300 \text{ nm}, 377 \text{ nm}$

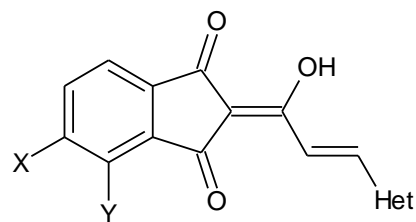
UV-Vis (DMSO) Ni(II)L2 $\lambda_{\text{max}} = 254 \text{ nm}, 313 \text{ nm}, 384 \text{ nm}$

UV-Vis (DMSO) L3 $\lambda_{\text{max}} = 325 \text{ nm}, 384 \text{ nm}$

UV-Vis (DMSO) Ni(II)L3 $\lambda_{\text{max}} = 254 \text{ nm}, 401 \text{ nm}$

Raman ($\nu_{\text{max}}, \text{cm}^{-1}$) L3: 1611, 1578, 1457, 1392, 1351, 1276, 1267, 1205, 1148, 1112, 1072, 1023, 886, 624, 400

UV-Vis (DMSO) L4 $\lambda_{\text{max}} = 285 \text{ nm}, 333 \text{ nm}, 455 \text{ nm}, 488 \text{ nm}$



X = H, Y = NO_2 (**L1-L4**); X = NO_2 , Y = H (**L5-L8**)

L1-L4: 4-nitro-substituted heteroaryl cinnamoyl derivatives

L5-L8: 5-nitro-substituted heteroaryl cinnamoyl derivatives

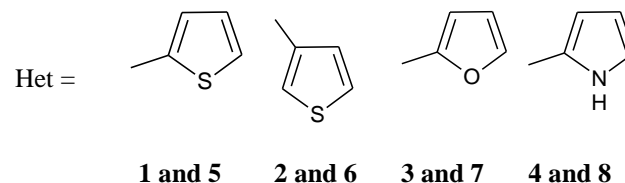


Figure 1. General formula of **L1-L8**

5- NO_2 -substituted heteroaryl cinnamoyl derivatives and their Ni(II) complexes (**L5-L8**)

UV-Vis (DMSO) L5 $\lambda_{\text{max}} = 278 \text{ nm}, 387 \text{ nm}, 394 \text{ nm}$
UV-Vis (DMSO) Ni(II) L5 $\lambda_{\text{max}} = 255 \text{ nm}, 323 \text{ nm}, 387 \text{ nm}$

Raman ($\nu_{\text{max}}, \text{cm}^{-1}$) Ni(II)L5: 1686, 1645, 1610, 1588, 1484, 1412, 1362, 1345, 1275, 1215, 1062, 1046

UV-Vis (DMSO) L6 $\lambda_{\text{max}} = 282 \text{ nm}, 360 \text{ nm}, 427 \text{ nm}$

UV-Vis (DMSO) Ni(II)L6 $\lambda_{\text{max}} = 255 \text{ nm}, 307 \text{ nm}, 385 \text{ nm}$

UV-Vis (DMSO) L7 $\lambda_{\text{max}} = 320 \text{ nm}, 378 \text{ nm}, 452 \text{ nm}$

UV-Vis (DMSO) Ni(II)L7 $\lambda_{\text{max}} = 254 \text{ nm}, 322 \text{ nm}, 390 \text{ nm}$

UV-Vis (DMSO) L8 $\lambda_{\text{max}} = 286 \text{ nm}, 338 \text{ nm}, 460 \text{ nm}$

The resulting complexes are light brown to dark brown crystalline substances with melting points above 370°C. The yields were as follows: NiL1 – 45 %; NiL2 - 40 % NiL3 - 53 %; NiL4 - 33 %; NiL5 - 61 %; NiL6 - 52 %; NiL7 - 67 %; NiL8 - 42%.

RESULTS AND DISCUSSION

Complexation with Ni(II) were conducted using metal salt, namely $\text{Ni}(\text{CH}_3\text{COO})_2 \cdot 4\text{H}_2\text{O}$ at molar ratio M:L = 1:2. Neutral complexes were synthesized and isolated as brown or black precipitates, respectively. All complexes were investigated by means of elemental analysis, UV-Vis and IR spectroscopy. The elemental analysis data show metal-to-ligand ratio 1:2 and presence of two water molecules for all Ni(II) complexes. The data from the absorption spectra of the free ligands **L1-L8** and their Ni(II) complexes in DMSO are listed in the experimental part. In the UV/Vis spectra of the all metal complexes, one new maximum appeared at 254 nm. Selected IR frequencies and elemental

analyses data are listed in Tables 2, 3 and 1, respectively.

Table 1. Elemental analysis data of the Ni(II) complexes with 4- and 5- nitro-substituted heteroaryl cinnamoyl derivatives

Compound	C %		H %		N %		S %		Ni %	
	calc.	found	calc.	found	calc.	found	calc.	found	calc.	found
NiL1	51.43	51.06	2.70	2.78	3.75	3.66	8.58	8.43	7.85	7.59
NiL2	51.43	51.17	2.70	2.81	3.75	3.58	8.58	8.41	7.85	7.66
NiL3	53.54	53.43	3.07	2.89	3.90	3.74	-	-	8.18	7.97
NiL4	53.89	53.77	3.11	3.00	7.86	7.79	-	-	8.23	8.09
NiL5	51.43	51.11	2.70	2.84	3.75	3.63	8.58	8.37	7.85	7.61
NiL6	51.43	51.01	2.70	2.67	3.75	3.58	8.548	8.44	7.85	7.57
NiL7	53.54	53.33	3.07	2.91	3.90	3.78	-	-	8.18	8.00
NiL8	53.89	53.62	3.11	3.02	7.86	7.67	-	-	8.23	8.11

Table 2. Selected IR frequencies for Ni(II) complexes with 4-NO₂-substituted heteroaryl cinnamoyl derivatives.

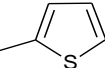
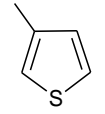
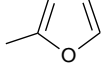
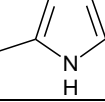
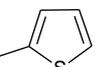
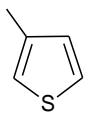
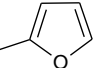
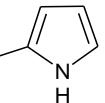
No	VOH	VNH	V _{ar}	VC=O	VC=O'	VC=C	VC=C(Het)	V _{as} NO ₂	V _s NO ₂	δ _{OH}	V=CH	V ₂ -Thiophen	V ₃ -Thiophen
NiL1 	3251		3065	1674	1631	1613	1577	1532	1352	1275	961	824	-
NiL2 	3270		3058	1667	1619	1582	1571	1533	1349	1248	961	-	785
NiL3 	3363		3057	1674	1635	1619	1582	1538	1351	1264	961	-	-
NiL4 	3276	3221	3058	1674	1630	1614	1588	1532	1343	1256	961	-	-

Table 3. Selected IR frequencies for Ni(II) complexes with 5-NO₂-substituted heteroaryl cinnamoyl derivatives.

No	VOH	VNH	V _{ar}	VC=O	VC=O'	VC=C	VC=C(Het)	V _{as} NO ₂	V _s NO ₂	δ _{OH}	V=CH	V ₂ -Thiophen	V ₃ -Thiophen
NiL5 	3272		3085	1692	1627	1613	1570	1528	1342	1255	977	839	-
NiL6 	3098		3064	1713	1625	1612	1578	1544	1338	1240	985	-	799
NiL7 	3325		3061	1693	1635	1614	1577	1528	1342	1257	982	-	-
NiL8 	3275	3225	3060	1694	1630	1613	1589	1528	1343	1255	988	-	-

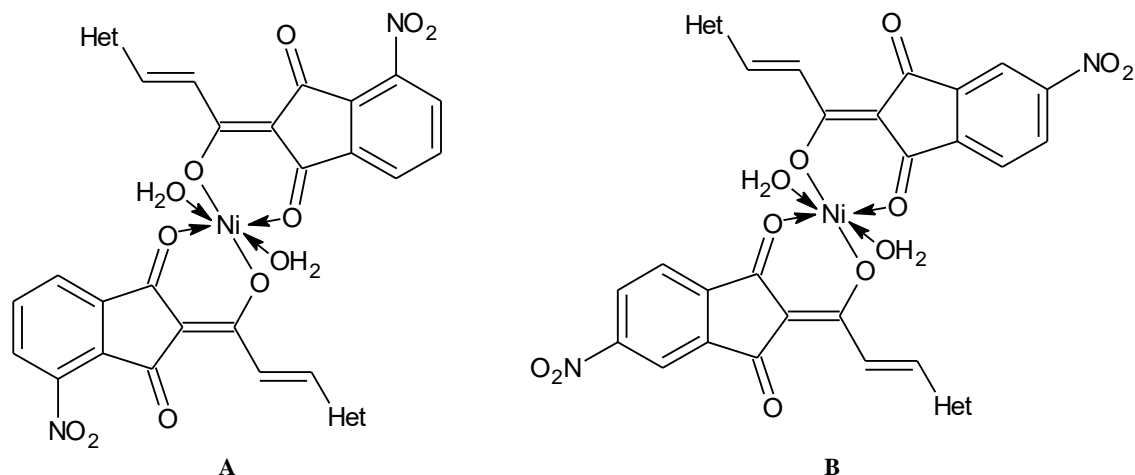


Figure 2. Suggested structures of the Ni(II)L1- Ni(II)L4 (A) and Ni(II)L5 – Ni(II)L8 (B) complexes

In order to evaluate the mode of coordination of the ligand to the metal ions, the IR spectra of the ligands **L1-L8**, as well as of their Ni(II) complexes were recorded. In the IR-spectrum of the pure ligands **L1-L8** a band of -OH group was observed between 3502-3438 cm^{-1} . The vibrational frequencies for the OH group are absent in the spectra of the complexes. Thereby, the free ligands coordinate as bidentate monoanion forming 6-membered chelate ring with the metal ion. Based on the obtained results it is suggested that the composition of the complexes is $[\text{M}(\text{L})_2 \cdot 2\text{H}_2\text{O}]$. Based on the experimental data, the most probable structure for the Ni(II) complexes was suggested with deprotonated OH group of 4- and 5-nitro-cinnamoyl derivatives. Based on previous studies on the structure of metal complexes of 2-acetyl-1,3-indandione [9-11], it is supposed that the Ni(II) complexes contain at least two water molecules, axially coordinated to the metal center. It is seen that nitro complexes exhibit $\nu_a(\text{NO}_2)$ and $\nu_s(\text{NO}_2)$ in the 1470–1370 and 1340–1320 cm^{-1} regions, respectively. Thus $\nu_a(\text{NO}_2)$ shifts markedly to a higher frequency, whereas $\nu_s(\text{NO}_2)$ changes very little on coordination [12]. The most probable structures of the all complexes was suggested and depicted in Figure 2.

It was not possible to measure Raman spectra of the free ligands **L2**, **L5**, **L6**, **L7** and **L8** and their metal complexes - the sample burned even at 1 mW laser power. Only the Raman spectra of the free ligands **L1**, **L3** and Ni(II)L5 complex were measured. In the Raman spectrum of **L1** and **L3** the band at 1601 cm^{-1} and 1611 cm^{-1} can be attributed to stretching vibrations of C=C. In the Raman spectrum of Ni(II)L5 complex the band of the carbonyl group appears at 1686 cm^{-1} . In the same spectrum the band of the NO_2 group appears at 1345 cm^{-1} . In the IR spectrum of Ni(II)L5 complex the

same band was observed at 1342 cm^{-1} . The band in the Raman spectrum of **L1** and **L3** at 1368 cm^{-1} and 1351 cm^{-1} was observed at 1357 and 1355 cm^{-1} in the IR spectrum were for stretching vibrations of NO_2 group, respectively.

The ligands coordinate in a bidentate way as monoanions after deprotonation of the enolic OH group. This is confirmed by the IR data of the metal complexes, which are compared with those of the free ligands and presented in Table 2 and 3. The IR data of the 4- and 5-nitro-substituted heteroaryl cinnamoyl derivatives are presented in a previous work of ours [13].

CONCLUSIONS

The synthesis of eight new Ni(II) complexes with 4- and 5- nitro-substituted heteroaryl cinnamoyl derivatives have been described. A series of non-charged complexes with Ni(II) was isolated and analyzed by elemental analyses, UV-Vis and IR spectroscopy. For the Ni(II) complexes a octahedral structure was proposed.

REFERENCES

1. C. H. Hassall, *Experientia*, **6**, 462 (1950).
2. L. W. Hazleton, W. H. Dolben, *Pat. USA* 2 884 357 (1959).
3. J. T. Correll, L. L. Coleman, *Proc. Soc. Biol. Med.*, **80**, 139 (1952).
4. M. V. Alfimov, O. A. Fedorova, S. P. Gromov, *J. Photochem. Photobiol., A*, **158**, 183 (2003).
5. L. A. Chetkina and V. K. Belsky, *Crystallography Reports*, **53**(4), 579 (2008).
6. A. Ahmedova, V. Atanasov, P. Marinova, N. Stoyanov, M. Mitewa, *Cent. Eur. J. Chem.*, **7**, 429 (2009).
7. A. Ahmedova, P. Marinova, G. Pavlović, M. Guncheva, N. Stoyanov, M. Mitewa, *J. Iran. Chem. Soc.*, **9**, 297 (2012).

8. A. Ahmedova, P. Marinova, S. Ciattini, N. Stoyanov, M. Springborg, M. Mitewa, *Struct. Chem.*, **20**, 101 (2009).
9. A. Ahmedova, O. Cador, L. Sorace, S. Ciattini, D. Gatteschi, M. Mitewa, *J. Coord. Chem.* **61**, 3879 (2008).
10. A. Ahmedova, V. Rusanov, A. Hazell, J. Wolny, G. Gochev, A.X. Trautwein, M. Mitewa, *Inorg. Chim. Acta* **359**, 3123 (2006).
11. V. Enchev, A. Ahmedova, G. Ivanova, I. Wawer, N. Stoyanov, M. Mitewa, *J. Mol. Str.* **595**, 67 (2001).
12. K. Nakamoto, *Infrared and Raman Spectra of Inorganic and Coordination Compounds, Part B: Applications in Coordination, Organometallic and Bioinorganic Chemistry, Sixth Edition*, Published by John Wiley & Sons, Inc., Hoboken, New Jersey, p.52, 2009.
13. M. Marinov, I. Nikolova, P. Marinova, N. Stoyanov, P. Penchev, K. Ivanov, *University of Ruse “Angel Kanchev” Proceedings*, **54**(10.2), 62 (2015).

КОМПЛЕКСИ НА Ni(II) С 4- И 5- НИТРО-ЗАМЕСТЕНИ ХЕТЕРОАРИЛ ЦИНАМОИЛНИ ПРОИЗВОДНИ

П.Е. Маринова^{1*}, И.Д. Николова², М.Н. Маринов³, С.Х. Цонева¹, А.Н. Димитров¹, Н.М. Стоянов²

¹ ПУ „П. Хилендарски”, Химически факултет, Пловдив, 4000, ул. „Цар Асен” № 24

² Русенски университет-Филиал Разград, Катедра „Химия и химични технологии”, Разград, 7200, ул. „Априлско въстание” № 47

³ Аграрен университет-Пловдив, Факултет по растителна защита и агроекология, Катедра „Обща химия”, Пловдив, 4000, бул. „Менделеев” № 12

Постъпила на 4 ноември 2016 г.; приета на 21 януари 2017 г.

(Резюме)

Целта на настоящата разработка е получаването на нови комплекси на Ni(II) с 4- и 5- нитро-заместени хетероарил цинамоилни производни с потенциално биологично действие. Структурата на получените осем метални комплекси е изследвана с елементарен анализ и UV-Vis, ИЧ-спектроскопски методи (за един от тях и с Раманова спектроскопия). Въз основа на получените експериментални резултати считаме, че най-вероятно лигандите са координирани бидентатно, като моноанион след депротониране на енолната -ОН група. Предполага се октаедрична геометрия на металния център с 2 органични лигандни молекули и 2 молекули вода координирани към Ni(II).

Ключови думи: 4- и 5- нитро-заместени хетероарилни цинамоилни производни, метални комплекси, ИЧ

Catalytic oxidation of formaldehyde in aqueous solutions over NiO_x/CeO₂

M. K. Stoyanova*, St. G. Christoskova, D. N. Petrov, V. V. Ivanova

Department of Physical Chemistry, University of Plovdiv,
24 Tzar Asen Str., 4000 Plovdiv, Bulgaria

Received November 12, 2016; Revised December 7, 2016

The catalytic performance of NiO_x supported on CeO₂ prepared by modified precipitation-oxidation method for the complete oxidation of formaldehyde (HCHO) with NaOCl in aqueous solutions was explored. The as-prepared catalyst was characterized by XRD, HRTEM, FTIR and chemical analyses. It has been found that under the applied synthesis conditions nanosized and well dispersed on the surface of CeO₂ non-stoichiometric Ni₁₅O₁₆ oxide was obtained. The catalytic activity of the NiO_x/CeO₂ was found better than both the unsupported bulk analogue and physical mixture of NiO_x and CeO₂, suggesting a synergistic effect of active oxide phase and support. The effect of main operational parameters influencing HCHO degradation efficiency such as catalyst loading, temperature, and oxidant concentration were studied. Factorial experimental design approach was applied to assess the effects of these parameters on the effectiveness of the oxidation process. Results obtained revealed that the optimal conditions for achieving fast and complete degradation of HCHO are temperature 30°C, catalyst loading 1.5 g dm⁻³, and NaOCl concentration 15 ml dm⁻³. Therefore, NiO_x/CeO₂ catalyst can be successfully used for the treatment of wastewaters with high concentration of formaldehyde.

Key words: formaldehyde, catalytic oxidation, NiO_x/CeO₂ catalyst, NaOCl.

INTRODUCTION

Formaldehyde (HCHO) is a key compound in organic synthesis, widely used in many industrial activities such as synthesis of resins, medicinal products, drugs and others, too numerous to be mentioned. Therefore, wastewaters arising from these industrial manufactures may contain significant amounts of formaldehyde, which is considered as highly toxic and carcinogenic compound even at low concentrations. Thus, frequently release of HCHO in water systems may cause serious environmental pollution and risk for the surrounding biological populations.

Effluents containing high concentration of formaldehyde, 2000 – 4000 ppm, are traditionally treated by biological methods because of their low cost and simplicity [1, 2]. However, it has been found that these concentrations are toxic for the bacterial cultures used, and thus the biological treatment could be easily inhibited by damaging the DNA of the microorganisms [3]. Wet oxidation processes (WO) have been used in the treatment of HCHO containing wastewaters. In this method, the oxidation reaction takes place in aqueous phase where the formaldehyde molecules are oxidized with pure oxygen or air at high temperatures (180 – 315°C) and pressures (up to 150 bar). However, in this case many intermediate products have been

detected, such as carboxylic acids, which is therefore necessary of a post-treatment stage [4]. Catalytic wet oxidation (CWO) is an interesting and advanced alternative to WO, since the harmful molecule can be completely oxidized into CO₂ and water in the presence of solid catalyst at milder reaction conditions.

Silva *et al.* have used several heterogeneous composite metal catalysts for oxidation of high formaldehyde containing industrial effluents (800 – 1500 ppm). The reaction has been carried out in a high-pressure reactor at 190 – 220 °C and 15 - 35 bar of pressure. It has been found that the Mn/Ce catalyst is the most active among the Mn/Ce, Co/Ce and Ag/Ce catalysts, leading to 99.4 % TOC conversion. Moreover, the application of the Mn/Ce catalyst for treatment of wastewaters from formaldehyde industry has been also discussed [5].

Pt/Al₂O₃ catalyst has been tested in CWO reaction for formaldehyde oxidation at 80 °C. It is shown that 80 % elimination of HCHO with initial concentration of 200 ppm, has been achieved for 4 hours. However, byproducts such as acetic and oxalic acids have been also determined [6].

A combination of catalytic advanced oxidation process of O₃/MgO/H₂O₂ with biological treatment has been used for complete mineralization of concentrated formaldehyde wastewaters. It has been shown that 98 % of COD removal has been achieved after 24 hours of reaction under optimum conditions

* To whom all correspondence should be sent.

E-mail: marianas@uni-plovdiv.bg

– 5 g/L MgO powder, pH = 8, and 0.09 mol/L H₂O₂. Radical oxidation mechanism has been also proven [7].

It should be noted that the literature data concerning the catalytic oxidation of formaldehyde in liquid phase is very scarce. Therefore, it is important to develop an efficient, cheap and stable catalyst for complete oxidation of HCHO in aqueous phase. The aim of the present study is to synthesize and characterize the supported NiO_x/CeO₂ catalyst and to explore its catalytic activity for low-temperature complete oxidation of HCHO in aqueous solutions using NaOCl as oxidant.

EXPERIMENTAL

The NiO_x/CeO₂ catalyst was prepared by deposition-precipitation technique with reverse order of precipitation. Solid CeO₂ (Aldrich) was suspended in a fixed volume of 0.1 M aqueous solution of Ni(NO₃)₂·6H₂O, in an amount necessary to achieve an atomic ratio of Ni:Ce = 1:1, followed by dropwise addition of a mixture of 4 M NaOH and NaOCl at constant stirring by the ultrasonic homogenizer to yield a black precipitate. The latter was allowed to age in the mother solution for 24 hours, followed by filtration, washing with distilled water to a negative reaction towards Cl⁻ ions and neutral pH. The precipitate was dried at 105 °C to constant mass. For comparison, bulk NiO_x was prepared according to the same procedure but in the absence of CeO₂.

X-ray diffraction measurement (XRD) was performed using TUR-MA 62 (Germany) diffractometer with filtered Cu K α radiation ($\lambda = 1.5406$ Å) at U = 37 kV, and I = 20 mA, equipped with a computerized HZG-4 goniometer. The phase identification was carried out using JCPDS database. The FTIR spectra were taken on a Vertex 70 spectrophotometer (Bruker), with 2 cm⁻¹ resolution, in KBr pellets (1 mg of the corresponding sample in 100 mg KBr). The surface morphology of the samples was characterized on high-resolution transmission electron microscope JEOL JEM 2100 operating at an accelerating voltage of 200 kV. The total (O*) and the surface (O_s*) active oxygen content of the as-prepared samples was determined iodometrically [20, 21]. The amount of nickel in the prepared samples was measured by atomic absorption spectroscopy (AAS, Perkin-Elmer).

The process of low temperature (20 – 30°C) catalytic oxidation of HCHO was carried out in a thermostated 400 cm³ glass reactor under constant stirring. In a typical run, 200 ml 50 mg dm⁻³ HCHO

aqueous solution was saturated with oxygen by bubbling air under atmospheric pressure for 30 minutes. Then a predefined volume of 10% aqueous solution of NaOCl was added into the solution. The experiment was initiated by the addition of a fixed amount of catalyst. At specific time intervals, samples of 5 cm³ were withdrawn from the suspension and were centrifuged at 4000 rpm for 1 min to remove the catalyst. The concentration of HCHO in the filtrate was monitored spectrophotometrically ($\lambda_{\max}=565$ nm) using Spectroquant® Formaldehyde test (Merck), compatible with the spectrophotometer NOVA 400 (Merck). The UV–Vis spectra were recorded by two-beam scanning UV-Vis spectrophotometer (Cintra 101). All experiments were conducted in triplicate to ensure the reproducibility of experimental results.

RESULTS AND DISCUSSION

The experimental XRD patterns in Fig. 1 reveal that the as-prepared NiO_x/CeO₂ sample and the support CeO₂ represent a cubic fluorite crystallographic phase of ceria with space group Fm3m (225) (JCPDS 81-0792). There were no additional diffraction peaks in the XRD spectrum of NiO_x/CeO₂ although the Ni content in the supported catalyst was close to preparation settings as reveal from the AAS analysis. The absence of distinct reflections of Ni-containing oxide phase could be due to its amorphous character (as found for bulk NiO_x), as well as to the formation of highly-dispersed oxide layer on the CeO₂ surface. Moreover, the reflexes of NiO_x/CeO₂ were apparently broader and less intense, indicating smaller particle size compared with bare support. It was found that the bulk is amorphous.

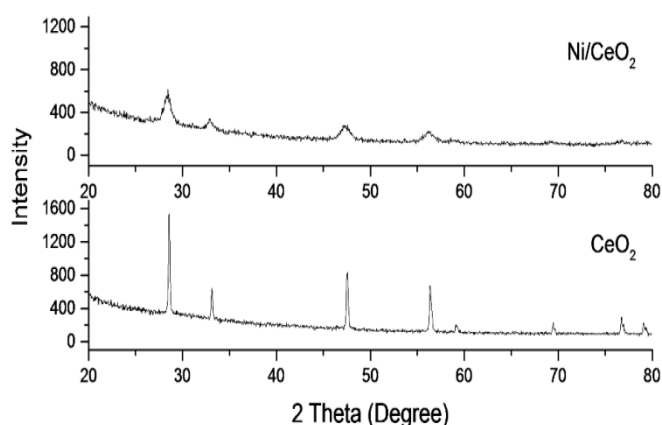


Figure 1. XRD patterns of bulk and CeO₂ supported NiO_x

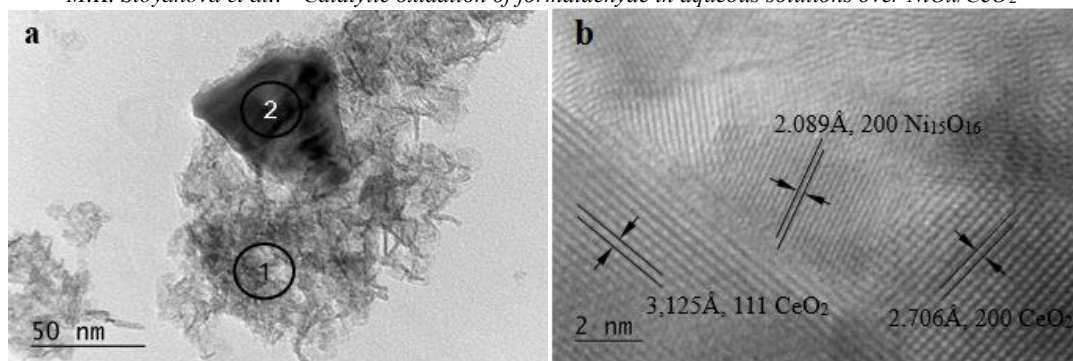


Figure 2. (a) Bright field TEM and (b) HRTEM images of the NiOx/CeO₂ catalyst

The presence of NiOx nanoparticles in NiOx/CeO₂ was confirmed by TEM and HRTEM (Fig. 2). As observed in Fig. 2a, the NiOx/CeO₂ was composed of two types of morphologically-different particles. The first type of particles (No 1 in the image) are elongated, smaller in size and form large aggregates numbering hundreds of particles clustered around the large ones. Indexations of the SAED patterns (not shown) reveal that they correspond to the non-stoichiometric nickel oxide (Ni₁₅O₁₆, JCPDS 72-1464). Other particles (No 2), with sizes of about 50 nm are electronically-dense and apparently well faceted. The analysis of the diffraction pattern showed that they consist of CeO₂. Well-defined lattice fringes in the HRTEM image of the NiOx/CeO₂ sample (Fig. 2b), corresponding to the two types of structures, revealed the existence of a well-crystallized nanoparticles.

The FTIR spectra of bulk and CeO₂ supported NiOx catalysts are shown in Fig. 3. A characteristic feature of the both spectra is the presence of a broad and intense band at ca. 573 cm⁻¹, which is due to the stretching vibrations of the surface Ni - O bond and accounts for the presence of active oxygen in the samples. The lower intensity of the band in the IR spectrum of the NiOx/CeO₂ indicates the lower content of active oxygen (5.3%) compared with bulk NiOx (8.1%) as confirmed by the chemical analysis. It should be noted that the O_s* of both samples constitutes about 75 % of the total active oxygen. This loosely bonded surface oxygen is a key factor determining high activity of the catalyst in oxidation reactions.

In order to assess the catalytic performance of NiOx/CeO₂, series of HCHO oxidation experiment were carried out for comparison. The results of the comparative study of the kinetics of HCHO oxidation in various systems are displayed in Fig. 4. The temporal spectral changes of HCHO in solution during oxidative degradation on NiOx/CeO₂ sample are depicted in Fig. 5.

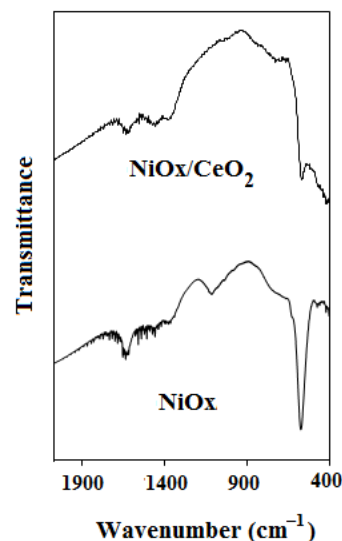


Figure 3. FTIR spectra of bulk NiOx and supported NiOx/CeO₂

As can be seen from the presented data, in the absence of catalyst the oxidation of formaldehyde proceeded with low rate – nearly 19% of HCHO is oxidized within 30 min. Evidently, NaOCl itself has limited ability to oxidize organics although it is a strong oxidizing agent. In the presence of unsupported NiO_x but without addition of oxidant (depletive oxidation), the concentration of HCHO decreased only around 37% in the first twenty minutes and was kept unchanged afterwards. Experiments carried out using NiOx/CeO₂ alone showed a similar trend with only 7% decrease in final degradation efficiency compared to bulk oxide. Since around 8-fold decrease in the active oxygen content of the catalysts after depletive oxidation was found (confirmed by chemical analysis), it may be speculated that under these conditions HCHO has been oxidized by the O* and, at its depletion, the oxidation process has been stopped. HCHO oxidation over bare CeO₂ slightly differs from PMS self-oxidation, implying that pure support did not exhibit catalytic activity in the studied reaction.

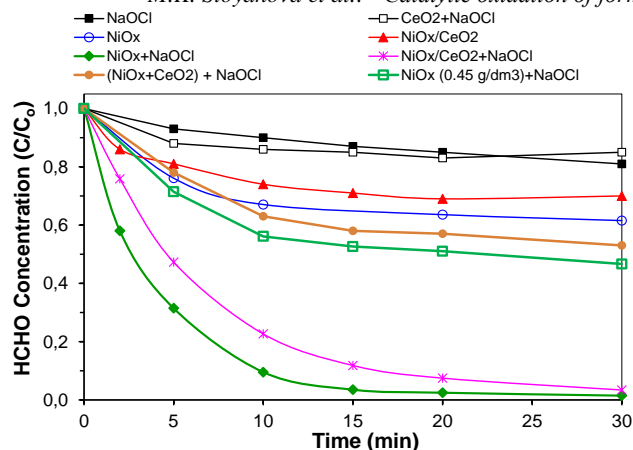


Figure 4. HCHO degradation with time in different systems. Reaction conditions: 50 mg dm⁻³ HCHO, 1.5 g dm⁻³ catalyst loading, 5 ml dm⁻³ NaOCl, 20°C.

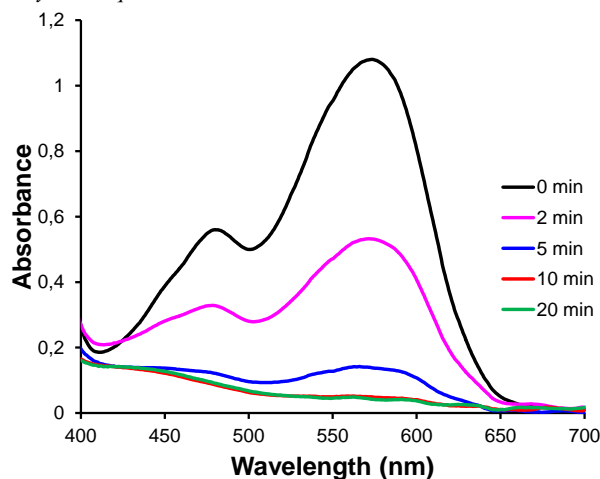


Figure 5. UV-vis spectral changes of HCHO during heterogeneous catalytic oxidation over NiOx/CeO₂. Reaction conditions: 50 mg dm⁻³ HCHO, 1.5 g dm⁻³ catalyst loading, 15 ml dm⁻³ NaOCl, 30°C.

As can be seen from the presented data, in the absence of catalyst the oxidation of formaldehyde proceeded with low rate – nearly 19% of HCHO is oxidized within 30 min. Evidently, NaOCl itself has limited ability to oxidize organics although it is a strong oxidizing agent. In the presence of unsupported NiOx but without addition of oxidant (depletive oxidation), the concentration of HCHO decreased only around 37% in the first twenty minutes and was kept unchanged afterwards. Experiments carried out using NiOx/CeO₂ alone showed a similar trend with only 7% decrease in final degradation efficiency compared to bulk oxide. Since around 8-fold decrease in the active oxygen content of the catalysts after depletive oxidation was found (confirmed by chemical analysis), it may be speculated that under these conditions HCHO has been oxidized by the O* and, at its depletion, the oxidation process has been stopped. HCHO oxidation over bare CeO₂ slightly differs from PMS self-oxidation, implying that pure support did not exhibit catalytic activity in the studied reaction.

However, the simultaneous presence of catalyst and oxidant significantly improved the removal rate of HCHO under the similar conditions. More than 96% of HCHO was oxidized within 30 min using NiOx/CeO₂. The performance of the supported catalyst was found slightly inferior than that of bulk NiOx although the lower content of the catalytically active phase in the NiOx/CeO₂ (30 wt.%). However, when the oxidation was carried out with concentration of NiOx corresponding to its loading on CeO₂, there is still 47% of HCHO remaining in

the first 30 min. Based on these results it might be concluded that deposition of NiOx on the CeO₂ support results in a synergistic effect in catalytic activity. Due to high dispersion of NiOx on CeO₂, more amounts of active sites (NiOx) were produced on the NiOx/CeO₂ surface than bulk nickel oxide. The synergistic coupling between NiOx and CeO₂ in supported sample was also confirmed by the considerably lower catalytic activity of simple physical mixture of NiOx and CeO₂.

Under all tested conditions, the HCHO oxidative degradation followed a pseudo first order kinetics confirmed by the linear plots of ln(C₀/C) versus time (Fig. 6). The reaction rate constants (k) and regression coefficients (R²) of the model fitting are given in Table 1.

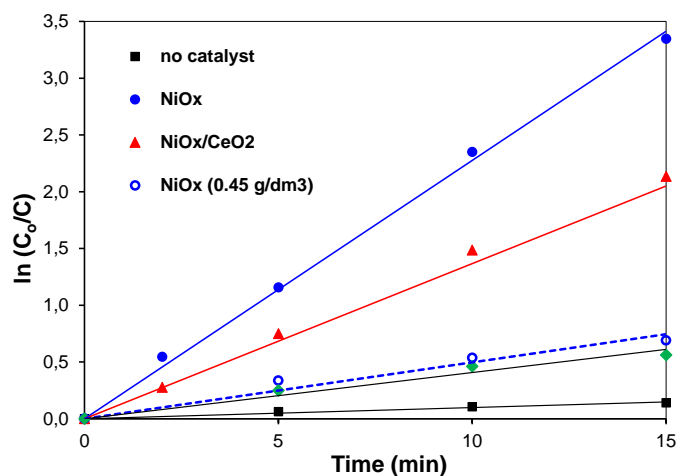


Figure 6. Linear dependences lnC₀/C = f (t) (reaction conditions were the same as those indicated in Fig. 4).

Table 1. Pseudo-first order rate constants of the HCHO oxidation process in different systems (1.5 g dm⁻³ catalyst loading, 5 ml dm⁻³ NaOCl, 20°C)

Catalyst	k (min ⁻¹)	R ²
No catalyst	0.011	0.982
NiOx	0.227	0.997
NiOx (0.45 g dm ⁻³)	0.049	0.982
NiOx/CeO ₂	0.137	0.991
NiOx+CeO ₂	0.041	0.986

The optimization of the variables affecting the catalytic oxidation of HCHO in aqueous solutions over NiOx/CeO₂ catalyst was carried out following the factorial design of experiments. The variable factors chosen were concentration of catalyst (X₁), concentration of oxidant (X₂), and temperature (X₃). The response measured (Y), through which the effectiveness of the applied method has been assessed, was the degree HCHO degradation in the 10 min from the start of the process (α₁₀, %). Table 2 shows the experimental matrix for the 2ⁿ factorial

design (n factors, each run at two levels). It has been worked with double trials in order to make it possible to check for the homogeneity of the dispersions throughout the entire factor space.

Based on the experimental results the following first-order polynomial response equation was obtained, showing the effect of individual variables and interaction effects for HCHO oxidative degradation:

$$Y = 79.91 + 9.44X_1 + 8.22X_2 + 7.27X_3 + 2.96X_1X_2 - 0.11X_1X_3 - 2.10X_2X_3 - 1.46X_1X_2X_3$$

According to this equation, the studied factors have positive effect on the effectiveness of the catalytic process with the strongest influence being on the amount of the catalyst (Fig.7). The rate constant increased ca. 2 times with increasing NiOx/CeO₂ concentration from 0.5 g dm⁻³ to 1.5 g dm⁻³ with identical other factors due to the availability of more active sites on the catalyst surface for activation of oxidant. Maximum purification effect for shortest time (ca. 10 min) was achieved at upper level of the three factors.

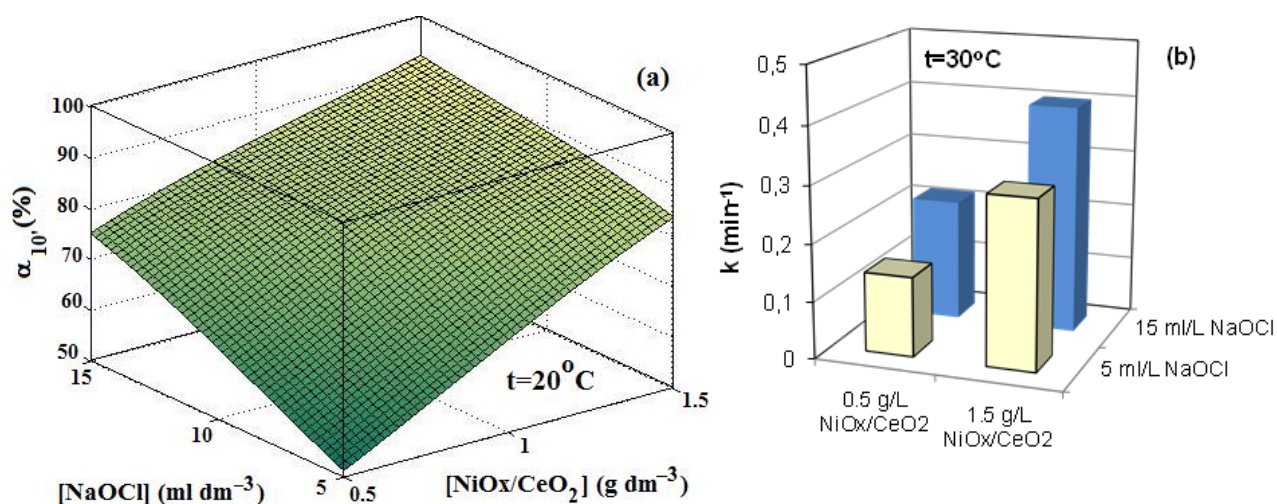


Figure 7. Interaction effect of the studied variable factors on (a) the degree of HCHO catalytic degradation over NiOx/CeO₂ and (b) the rate constant.

Table 2. Experimental matrix and results of the factorial design for HCHO catalytic oxidation over NiOx/CeO₂

Run	Variable factors						Response
	Experimental values			Codified values			Y (%)
	[NiOx/CeO ₂] (g dm ⁻³)	[NaOCl] (ml dm ⁻³)	T (°C)	X ₁	X ₂	X ₃	
1	0.5	5.0	20	-1	-1	-1	51.3
2	1.5	5.0	20	1	-1	-1	73.4
3	0.5	15.0	20	-1	1	-1	74.9
4	1.5	15.0	20	1	1	-1	91.0
5	0.5	5.0	30	-1	-1	1	67.3
6	1.5	5.0	30	1	-1	1	94.8
7	0.5	15.0	30	-1	1	1	88.4
8	1.5	15.0	30	1	1	1	98.2

CONCLUSIONS

In this study, nanosized NiO_x supported on CeO₂ was prepared and its catalytic performance was thoroughly evaluated for oxidative degradation of HCHO in aqueous solutions using NaOCl as oxidant. Characterization data showed that the synthesis procedure led to formation of nanosized non-stoichiometric nickel oxide Ni₁₅O₁₆ with high dispersion on the surface of ceria. The as-prepared NiO_x/CeO₂ presented higher efficiency for HCHO degradation than bulk NiO_x and mechanical mixture of active phase and support. It might be suggested that a synergistic effect is produced at loading a catalytically active NiO_x phase onto CeO₂. Using 1.5 g dm⁻³ NiO_x/CeO₂, conversion rate of more than 98 % has been achieved for 10 minutes at 30°C. Process optimization performed by applying the factorial design showed that the HCHO degradation efficiency and rate are positively influenced on the studied operational parameters, with the strongest effect being of the catalyst amount. The synthesized catalytic system could be regarded as promising heterogeneous catalyst for the degradation of organic pollutants in water.

Acknowledgements: Authors gratefully acknowledge financial support by the National Science Fund (Project DFNI-T02/4) and by the University of Plovdiv Research Fund (Project NI HF-2015).

REFERENCES

1. Z. Lu, W. Hegemann, *Water Res.*, **32**, 209 (1998).
2. G. Vidal, Z. P. Jiang, F. Omil, F. Thalasso, R. Me'ndez, J. M. Lema, *Bioresour. Technol.*, **70**, 283 (1999).
3. M. E. Andersen, J. E. Dennison, *The Science of the Total Environment*, **274**, 3 (2001).
4. A. M. T. Silva, R. M. Quinta-Ferreira, J. Levec, *Ind. Eng. Chem. Res.*, **42**, 5099 (2003).
5. A. M. T. Silva, I. M. Castelo-Branco, R. M. Quinta-Ferreira, J. Levec, *Chem. Eng. Sci.*, **58**, 963 (2003).
6. M. Gutierrez-Arzaluz, M. Torres-Rodriguez, V. Mugica-Alvarez, J. Aguilar-Pliego, M. A. Romero-Romo, *Int. J. Environ. Sci. Develop.*, **7**, 166 (2016).
7. G. Moussavi, A. Yazdanbakhsh, M. Heidarizad, *J. Hazard. Matt.*, **171**, 907 (2009).

КАТАЛИТИЧНО ОКИСЛЕНИЕ НА ФОРМАЛДЕХИД ВЪВ ВОДНИ РАЗТВОРИ ВЪРХУ NiO_x/CeO₂

М. Стоянова*, Ст. Г. Христоскова, Д. Н. Петров, В. В. Иванова

Кат. „Физикохимия”, Пловдивски университет „Паисий Хилендарски”, ул. „Цар Асен” 24, 4000 Пловдив, България

Постъпила на 12 ноември 2016 г.; приета на 7 декември 2016 г.

(Резюме)

Изследвано е каталитичното поведение на NiO_x нанесен върху CeO₂, получен по модифициран утаечно-окислителен метод, в реакция на пълно окисление на формалдехид (HCHO) във водни разтвори. Синтезираният катализатор е охарактеризиран чрез XRD, HRTEM, FTIR и химически анализ. Установено е, че условията на синтеза благоприятстват получаването на наноразмерен нестехиометричен Ni₁₅O₁₆, добре диспергиран върху повърхността на CeO₂. NiO_x/CeO₂ демонстрира по-висока каталитична активност в сравнение с ненанесения масивен аналог и физична смес от NiO_x и CeO₂, което предполага синергичен ефект между активната фаза и носителя. Изследвано е влиянието на основни реакционни параметри като количество на катализатора, температура и концентрация на окислителя върху ефективността на процеса на каталитично окисление на HCHO. Проведен е многофакторен експеримент за оценка влиянието на тези параметри върху ефективността на окислителния процес. Резултатите показват, че оптималните условия за бързо и пълно окисление на HCHO са температура 30°C, количество на катализатора 1.5 g dm⁻³ и концентрация на NaOCl 15 ml dm⁻³. Синтезираният NiO_x/CeO₂ катализатор може успешно да се използва за пречистването на отпадни води, съдържащи формалдехид във високи концентрации.

Ключови думи: формалдехид, каталитично окисление, NiO_x/CeO₂; NaOCl

Recent applications of polymer materials in biomedical sciences

L. H. Yoanidu^{1*}, Y. I. Uzunova¹, I. D. Stefanova²

Medical University-Plovdiv, Bulgaria, Faculty of Pharmacy

¹Department of Chemistry and Biochemistry,

²Department of Medical Physics and Biophysics,

15A V. Aprilov Blvd., 4002 Plovdiv, Bulgaria

Received November 11, 2016; Revised December 21, 2016

There has been a rapid development of novel polymer materials in the last decade, due to their versatile nature and the vast array of fields where these materials are utilized. Stimuli-responsive polymers have found their application in the construction of novel drug delivery systems. Self-healing polymers are useful in the creation of implant materials. Combinations of natural and conductive polymers could be beneficial in tissue regeneration. The objective of this mini review is to outline the achievements in the last decade, regarding polymer materials used in innovative pharmaceuticals, as well as in tissue engineering.

Key words: polymers, nanocarriers, hydrogels, scaffolds, implants

INTRODUCTION

Polymer materials have been an object of interest in the biomedical field, since they allow the construction and modernization of many devices ranging from novel drug delivery systems to various implants. There is a wide variety of polymers, which allows for choosing optimal properties for the purpose of use. Natural and synthetic polymers have found their application in biomedicine, either used separately, or in combination as co-block polymers or hybrid polymers. Biopolymers presently used in different areas of biomedicine are primarily polysaccharides-chitosan and its derivatives, dextran, cellulose, hyaluronic acid (HA), pullulan, alginates due to their biocompatibility, low cytotoxicity and diverse chemical properties have become the basis for development of novel drug delivery systems (DDS) as well as biomaterials in tissue engineering and wound healing [1]. Polypeptides [2] and proteins-collagen [3, 4] and gelatin [5] are also applicable materials. Synthetic polymers and copolymers have found their application in the production of extracorporeal devices, joint implants, as well as a variety of pharmaceutical formulations. Frequently used polymers are poly(ethylene glycol) (PEG), poly(lactic acid) (PLA), poly(ϵ -caprolactone) (PCL), poly(N-isopropylacryl amide) (PNIPAAm), derivatives of methacrylic acid, poly(vinylalcohol) (PVA), poly(N-vinylpyrrolidone) (PVP),

poly(glycolic acid) (PGA), poly(lactic-co-glycolide) (PLGA) copolymers, poly(glycerol sebacate), polyhydroxyalkanoate [6]. The tendency in the development of novel polymeric materials is to incorporate both types in the construction of the material as well as to conjugate synthetic polymers with growth factors or adhesion molecules in order to ensure better biocompatibility [7]. This article aims to present some of the recent applications of polymer materials, focusing on the opportunities these materials provide for creating innovative pharmaceutical formulations for cancer treatment, tissue regeneration and implant materials.

PHARMACEUTICAL APPLICATIONS

The need for constant introduction of novel drug delivery systems stems from the challenges current therapies pose as well as the development of modern therapies for a number of diseases, among which cancer being one of the leading causes of death.

Polymeric nanoparticles, micelles and hydrogels are presently created to meet the needs of oncology treatment. Various stimuli are used as triggers, which could lead to targeted and controlled drug release. pH-sensitive drug delivery systems have been fashioned by using different types of polymers that could initially possess functional moieties which make them react to changes in the pH or suitable acid-sensitive linkers are employed in their preparation [8]. A recent study reports the preparation a chitosan based DDS, which incorporates an appropriate pH-sensitive

* To whom all correspondence should be sent.

E-mail: lubka84@abv.bg

adjuvant [9]. Due to that the doxorubicin (DOX) loaded chitosan-tripolyphosphate nanoparticles (NPs), undergo membranolytic changes in the acidic medium, typical for endosomes and lysosomes. In another study poly(aspartamide) grafted with L-Lysine and hydrazine was used as a biocompatible polymer matrix. DOX was incorporated via formation of hydrazone bonds that allow for an acid-triggered drug release, but would be stable under physiological pH [2]. In a similar fashion Zang *et al.* [10] used a chemical reaction which led to the formation of a Schiff base between DOX and the methoxy-poly(ethylene glycol)-aldehyde (mPEG) chain. Hydrophobic agent curcumin could be encapsulated in formed NPs. After successful internalization of the NPs, Schiff base would disintegrate and simultaneous delivery of both substances would be obtained.

Polymer materials responsive to changes in the levels of glutathione aim at destabilization of the carrier in a reduced environment and release of the incorporated drug. This could be achieved by the introduction of disulfide bonds cleavable in the presence of reducing agents. Several studies reported the preparation of such systems. Tang *et al.* [11] proposed novel redox-responsive star-shaped micelles and utilized a PEG-PCL copolymer, with disulfide bonds as redox-sensitive linkers. This polymer presented several advantages compared to linear polymers such as enhanced stability, presence of a greater number of functional groups for further modification and better loading capacity. HA was used for the preparation of a polymer-drug conjugate, for the delivery of paclitaxel (PTX). Disulfide bond was introduced via modification of paclitaxel with 3,3'-dithiodipropionic acid. HA shows specific affinity towards CD44 bearing cells, a fact used to achieve targetability [12]. Human serum albumin (HSA) crosslinked with dithiobis(succinimidyl propionate) was utilized in NPs which served as a vehicle for photosensitizer Chlorin e6. Due to the inclusion of the thiol-cleavable bonds in the structure of the cross-linker the developed system disintegrated in the intracellular reducing environment. Redox-sensitive HSA-NPs produced optimal cytotoxicity in comparison to the free photosensitizer and to NPs that incorporated glutaraldehyde, a non-redox responsive crosslinker [13].

Natural and synthetic thermo-responsive polymers are applicable materials in targeted and controlled drug release [14]. Hu *et al.* [15] proposed a novel drug delivery system, based on a triblock copolymer consisting of a poly(L-lactide) central block and two poly(N-isopropylacrylamide-co-N,N-dimethylacrylamide) lateral blocks. The obtained

micelles displayed thermo-responsive phase transition and in temperatures higher than their lower critical solution temperature (LCST) the lateral blocks experienced dehydration. This led to a much higher drug release and improved drug accumulation in tumor mass, which displays temperatures above the LCST. Rejinold and co-workers [16] prepared thermo-responsive fibrinogen-graft-PNIPAAm nanogels. Fibrinogen could target overexpressed $\alpha_1\beta_5$ integrin receptors on the surface of breast cancer cells. Through a series of in vitro studies the authors demonstrated improved drug release in temperatures above the LCST as well as specific toxicity to MCF-7 cells.

Polymers that could react to changes in glucose levels are currently investigated for the preparation of insulin delivering systems. Yao *et al.* [17] synthesized thermo- and glucose-responsive polymeric micelles, by including PNIPAAm into the structure of monomethoxy poly(ethyleneglycol)-block-poly(phenylboronate ester) acrylate. Glucose responsiveness was achieved by incorporating phenylboronic acid (PBA) in the polymer. Micelles obtained by random polymerization displayed different insulin release in normal and pathological glucose concentrations, which was attributed to polymer architecture. A microgel based on glucosyloxyethyl acrylated chitosan (GEA-chitosan) and immobilized concanavalin-A was designed by another group. GEA-chitosan offers the possibility of increased insulin loading, while concanavalin-A provides response to changes in glucose concentration. The microgel displayed pulsatile insulin release, in response to changes in the glucose level and could be utilized as an insulin delivery system, glucose sensor or an actuator after further investigation and optimization of its properties [18].

TISSUE ENGINEERING

Polymeric materials have found extensive application in the construction of scaffolds for the purposes of tissue engineering. Polymeric scaffolds are meant to ensure cell adhesion and proliferation, and should be fashioned in a way that fulfills requirements such as biocompatibility, biodegradability, suitable mechanical properties, porosity, and supply of oxygen and nutrients to the cells [19]. Electrical stimulation could be beneficial for neural and muscle tissue regeneration. A recent review names more than twenty five conductive polymers and emphasizes on their versatility and the possibilities for utilizing these polymers in a variety of devices in the biomedical field. Polypyrrole, polythiophene derivatives, polyaniline are commonly used conductive polymers, but due to constant development and modification of these

polymers novel and improved electro conductive materials are now emerging such as polypyrrole-thiophene oligomers, poly(3,4-alkylenedioxy-pyrrole), PLA and aniline pentamer copolymer etc [20]. Conductive polymers do not possess suitable mechanical or chemical properties to be used as biomaterials by themselves. Combinations of different polymers, as well as inclusion of inorganic materials in the matrices, allow for tailoring of the properties of biomaterials in accordance with the specific tissue requirements.

In a recent study a composite scaffold was produced by incorporating bioglass nanoparticles and collagen in a chitosan hydrogel, for the purposes of bone tissue repair. To overcome the low mechanical strength of collagen it was incorporated in a thermoresponsive modified chitosan matrix. This provided optimal mechanical properties as well as suitable porosity of the material, as well as an opportunity of in situ gelation, after injecting the composite [3]. Polymeric scaffolds for bone and cartilage repair were successfully synthesized by combining HA with dextran and hydroxyethyl methacrylate [21]. Collagen type 1 is reported as a suitable polymer for obtaining scaffolds in cases of neural damage serving as a medium which could improve the proliferation and differentiation of neural stem cells, and thus offer potential treatment in spinal cord injury [4]. Collagen combined with chitosan was used as a supporting structure for bone marrow mesenchymal stem cells, and the co-transplantation was shown to be favorable in terms of cell viability and retention of cells in treated areas [22]. A polypyrrole/ poly(D,L-lactic acid) conduit exerted a positive effect on the axon regeneration and myelination compared to those in poly(D,L-lactic acid) conduits, which demonstrates the beneficial effect of including a conductive polymer [23]. PLGA-poly(3-hexylthiophene) axially aligned nanofibers displayed improved conductivity compared to random ones and had a positive influence on the adhesion and proliferation of Schwann cells, indicating the potentials as scaffold for neural tissue engineering [24]. Natural polymers are suitable materials in treating damages to cardiac tissue. Chitosan/fibrin, chitosan/alginate/collagen scaffolds were investigated as patch materials, but lacked tensile strength. Pok *et al.* prepared a scaffold of chitosan and gelatin and synthetic polymer PCL which combines the soft gel structure and biodegradability of natural polymers and the additional mechanical strength of the PCL core [25]. A polypyrrole/chitosan injectable hydrogel was studied as a material for supporting injured heart as well as providing a connection between healthy myocardium and viable cardiomyocytes. Through a

series of in vitro and in vivo experiments the authors demonstrated that this novel biomaterial may lead to enhanced myocardial recovery [26]. Gelatin and aniline pentamer hydrogels were prepared where the inclusion of the natural polymer led to reduced cytotoxicity of the conductive polymer [5].

IMPLANT MATERIALS

In recent years advancements have been made in the development of implants to replace damaged organs and tissues. However with time the implanted material usually suffers from mechanical or chemical damage which creates a necessity for novel approaches in solving this issue. A class of self-healing materials is now under investigation as an emerging new strategy for overcoming the problem of implant longevity. Mimicking naturally occurring processes like DNA or protein repair, ideally those materials would be able to sense, halt and repair damages on a microscopic level. In a thorough review by A. Brochu [27] and co-workers several generations of self-healing materials have been described based on the ability of the material to repair when damaged. Some of the materials utilize the incorporation of a microencapsulated healing agent which upon contact with cracks or damages would be released and others rely on the formation of dynamic chemical bonds and interactions. A novel dental composite was constructed based on the strategy of encapsulating a healing agent into microcapsules intended to be released in case a propagating crack occurs. Successful crack healing was observed in the model composites when silica microcapsules that contained polyacrylic acid as a healing liquid were dispersed in a polymer resin network formed by monomers 2-bis(4-(2-hydroxy-3-methacryloxypropoxy)phenyl)propane (Bis-GMA) and hydroxyethyl-methacrylate (HEMA). This healing liquid is intended to react with strontium fluoroaluminosilicate particles and form a glass ionomer cement to heal the defect. As a major advantage the authors of the study pointed the biocompatibility of all materials used and suggested further addition of active components such as antimicrobial agents and hydroxyapatite for improving the qualities of the composite [28]. This strategy was applied by Wu *et al.* [29] in the preparation of a dental composite with poly(urea-formaldehyde) microcapsule containing triethylene glycol dimethacrylate (TEGDMA) and N,N-dihydroxyethyl-p-toluidine as a healing liquid. In the composite two other components were included - dimethylaminohexadecyl methacrylate for its antibacterial properties and nanoparticles of amorphous calcium phosphate to achieve remineralization. The polymer matrix was prepared

by BisGMA and TEGDMA. The authors reported that this first of its kind dental composite offers a promising way of preventing bulk fracture and secondary caries.

Although the majority of research on self-healing materials so far has been done on cements, adhesives and composites this new strategy of obtaining novel biomaterials is now applied in the construction of hydrogels. These materials could potentially find applications in the biomedical field and lead to improved performance of the devices made out of them. As we already mentioned injectable hydrogels as biomaterials have many advantages when applied as tissue scaffold materials or drug delivery systems. Recent studies have reported the preparation of stimuli-responsive and self-healing hydrogels. Miao *et al.* [30] designed a thermo-responsive, self-healing hydrogel based on alginate grafted with β -cyclodextrin. As a thermo-sensitive polymer Pluronic® F108 (poly(ethylene glycol)-*b*-poly(propylene glycol)-*b*-poly(ethylene glycol)) was included in the hydrogel on the basis of host-guest interactions. The physically dual-crosslinked hydrogel displayed thermo-responsive and self-healing properties when tested in vitro. Another study was conducted where a number of hydrogels were prepared using PEG macromonomers obtained by conjugation with either a derivative of phenylboronic acid or with a diol [31]. Self-healing hydrogels were formed due to the reversible interactions between phenylboronic acid moieties and diol moieties. Hydrogels prepared under pH 7 were subjected to shear-thinning and self-healing tests. PEG-4-carboxyphenylboronic acid (PEG-PBA) and PEG-4-carboxy-3-fluorophenylboronic acid (PEG-FPBA) gels were observed to completely recover their viscosity after network disruption, and additionally PEG-FPBA gel reformation from two pieces was observed. Glucose-responsive behavior of prepared hydrogels and cytocompatibility were also established. The prepared hydrogels could be a useful platform for drug delivery or tissue engineering.

CONCLUSION

A large variety of polymeric materials has been created for biomedical applications. Through combining synthetic and natural polymers the properties of resulting polymeric materials are upgraded or new properties of resulting materials are obtained. Novel techniques of producing polymeric materials have also played a crucial role in the construction of modern pharmaceuticals and implant materials. Even though significant improvements have been made so far, there are still challenges posed by the physical and chemical characteristic of

polymer materials. Future endeavors should be directed at obtaining better biocompatibility, tunable mechanical and chemical properties and safe commercial use of these materials.

REFERENCES

1. D. Dheer, D. Arora, S. Jaglan, R. K. Rawal R. Shankar, *J Drug Target*, doi: 10.3109/1061186X.2016.1172589
2. N. Liu, J. Han, X. Zhang, Y. Yang, Y. Liu, Y. Wang, G. Wu, *Colloids Surf B: Biointerfaces*, **145**: 401–409 (2016)
3. C. D. F. Moreira, S. M. Carvalho, H. S. Mansur, M. M. Pereira, *Mater Sci and Eng C*, **58**: 1207–1216 (2016)
4. F. Huang, Q. Shen, J. Zhao, *Neural Regen Res*, **8** (4): 313–319. (2013);
5. Y. Liu, J. Hu, X. Zhuang, P. Zhang, Y. Wei, X. Wang, X Chen, *Macromol Biosci*, **12**: 241–250. (2011)
6. T. J. Keane, S. F. Badylak, *Semin Pediatr Surg*, **23**: 112–118 (2014)
7. M.F. Maitz, *Biosurface and Biotribology*, **1**: 161–176 (2015)
8. T. Thambi, J. H. Park and D. S. Lee, *Biomater. Sci*, **4**: 55–69 (2016)
9. D. R. Nogueira-Librelotto, L. E. Scheeren, M. P. Vinardell, M. Mitjans, C. M. B. Rolim, *Colloids Surf B: Biointerfaces*, **147**: 326–335 (2016)
10. Y. Zhang, C. Yang, W. Wang, J. Liu, Q. Liu, F. Huang, L. Chu, H. Gao, Ch. Li, D. Kong, Q. Liu, J. Liu *Scientific Reports*, 6:21225 doi: 10.1038/srep21225 1 (2016)
11. Z. Tang, L. Zhang, Y. Wanga, D. Li, Z. Zhong, S. Zhou, *Acta Biomater*, **42**: 232–246 (2016)
12. S. Yin, J. Huai, X. Chen, Y. Yang, X. Zhang, Y. Gan, G. Wangd, X. Gu, J. Li, *Acta Biomater*, **26** 274–285 (2015)
13. A. M. Molina, M. Morales-Cruz, M. Benítez, K. Berríos, C. M. Figueroa, K. Griebenow, *J Nanomed Nanotechnol*, **6** (3) (2016) doi:10.4172/2157-7439.1000294
14. M. R. Matanovic, J. Kristl, P. A. Grabnar, *Int J Pharm*, **472**: 262–275 (2014)
15. Y. Hu, V. Darcos, S. Monge, S. Li, Y. Zhou, F. Su, *Int J Pharm*, **476**: 31–40 (2014)
16. N. S. Rejinold, T. Baby, K. P. Chennazhi, R. Jayakumar, *Colloids Surf B: Biointerfaces*, **114**: 209–217 (2014)
17. Y. Yao, H. Shen, G. Zhang, J. Yang, X. Jin, *J Colloid Interface Sci*, **431**: 216–222 (2014)
18. R. Yina, K. Wangb, Sh. Duc, L. Chenc, J. Niec, W. Zhanga, *Carbohydr Polym*, **103**: 369–376 (2014)
19. B. Guo, B. Lei, P. Li, P. X. Ma, *Regenerative Biomaterials*, **2** (1): 47–57 (2015)
20. R. Balint, N. J. Cassidy, S. H. Cartmell, *Acta Biomater*, **10**: 2341–2353 (2014)
21. A. Asti, L. Gioglio, *Int J Artif Organs*, **37** (3): 187–205 (2014)
22. F. Yan, W. Yue, Y. Zhang, G. Mao, K. Gao, Z. Zuo, Y. Zhang, H. Lu, *Neural Regen Res*, **10** (9): 1421–1426 (2015)

23. H. Xu, J. M. Holzwarth, Y. Yan, P. Xu, H. Zheng, Y. Yin, Sh. Li, P. X. Mab, *Biomaterials*. **35**(1): 225-235 (2014)
24. A. Subramanian, UM Krishnan, S. Sethuraman, *J Mater Sci Mater Med*, **23**: 1797–809 (2012)
25. S. Pok, J. D. Myers, S. V. Madihally, J. G. Jacot, *Acta Biomater*, **9** (3):5630–5642 (2013)
26. A. Mihic, Zh. Cui, J. Wu, G. Vlacic, Y. Miyagi, Sh.-H. Li, S. Lu, H.-W. Sung, R. D. Weisel, R.-K. Li, *Circulation*, **132**: 772-784 (2015)
27. A. B. W. Brochu, S. L. Craig, W. M. Reiche, *J Biomed Mater Res A*, **96** (2): (2011)
28. G. Huyang, A. E. Debertin, *J. Sun, Mater Des* **94**: 295–302 (2016)
29. J. Wu, M. D. Weir, M. A. S. Melo, H. H. K. Xu, *J Dent*, **43** (3): 317–326. (2015)
30. T. Miao, S. L. Fenn, P. N. Charron, R. A. Oldinski, *Biomacromolecules*. **16** (12): 3740–3750 (2015)
31. V. Yesilyurt, M. J Webber, E. A Appel, C. Godwin, R. Langer., D. G. Anderson, *Adv Mater*, **28** (1): 86–91 (2016)

СЪВРЕМЕННИ ПРИЛОЖЕНИЯ НА ПОЛИМЕРНИТЕ МАТЕРИАЛИ В БИМЕДИЦИНСКИТЕ НАУКИ

Л. Х. Йоаниду¹, Й. И. Узунова¹, И. Д. Стефанова²

Медицински Университет-Пловдив, Фармацевтичен факултет,

¹ *Катедра „Химия и биохимия“,*

² *Катедра „Медицинска физика и биофизика“,*

бул. В. Априлов 15А, 4002, Пловдив, e-mail: lubka84@abv.bg

Постъпила на 11 ноември 2016 г.; приета на 21 декември 2016 г.

(РЕЗЮМЕ)

Разнообразието на полимери и възможностите за приложението им в различни направления на биомедицината, доведе до усилено разработване и проучване на нови полимерни системи. Полимери реагиращи на разнообразни фактори на средата се използват за създаване на иновативни лекарство-доставящи системи. Проучват се самовъзстановяващи се полимери и възможностите за включването им в нови материали за импланти. Комбинация от биополимери и синтетични проводими полимери се очертава като подходяща стратегия за постигане на тъканна регенерация. Целта на този мини обзор е да представи последните постижения в разработването и приложението на полимерни материали в медицината.

Ключови думи: полимери, полимерни наночастици, хидрогелове, полимерни подложки, импланти

ZnO/TiO₂ coupled semiconductor photocatalysts

S. Siuleiman, N. Kaneva, A. Bojinova*, D. Dimitrov, K. Papazova,

Laboratory of Nanoparticle Science and Technology, Department of General and Inorganic Chemistry,
Faculty of Chemistry and Pharmacy, University of Sofia,
1 James Bourchier Blvd., Sofia 1164, Bulgaria

Received November 11, 2016; Revised December 20, 2016

The present study is directed to clarify the influence of the ratio of TiO₂ to ZnO, containing in the nanocomposite powder samples, on their activity as photocatalysts in slurry. A series of samples corresponding to different percentages of titania are prepared from commercial brands. The phase composition and crystallinity of the samples is characterized by X-ray diffraction. The surface morphology of the samples is observed via scanning electron microscope. The photocatalytic action of the composites is tested in UV and visible light induced degradation of two model pollutants: azo dye Orange II (O II) used as cosmetic colorant CI 15510 and triarylmethane dye Brilliant Green (BG), used as food colorant E142.

Key words: ZnO/TiO₂ composite, photocatalysis, Orange II, Brilliant Green, UV, visible light

INTRODUCTION

Photocatalysis is an attractive solution for water and air purification from various pollutants in low concentrations under light illumination. Titania and zinc oxide are the most popular oxides used in heterogeneous photocatalysis due to their unique properties [1, 2].

TiO₂ has relatively large band gap (3.2 eV for anatase modification). It is most widely used photocatalyst since it is chemically stable, nontoxic and natural material [3]. ZnO has also been considered as a suitable alternative of TiO₂ because of its comparability with TiO₂ band gap energy and its relatively lower cost of production [4, 5]. ZnO is a semiconductor with a direct wide band gap energy (3.37 eV) and has a large exciton binding energy (60 meV) at room temperature [6]. The band gaps values of TiO₂ and ZnO show that near UV irradiation is needed for photo activation of both oxides.

The photoactivity of a photocatalysts depends on several key properties: crystal phase, light exposed surface area, uncoordinated surface sites, lattice defects and degree of crystallinity. The application of composite materials allows morphology control, improvement and fine tuning of most of the above properties. Additionally, composite heterostructures can create suitable mid-band-gap electronic states which can alter charge migration or produce a red shift in the absorption spectrum. Further, formation of heterojunctions between the materials can yield visible light absorption. The application of heterostructured catalysts with adjustable bandgaps, enhanced stability and photocatalytic performance, gives the possibility to realize sufficient charge

separation, an increased lifetime of the charge carriers and enhanced interfacial charge transfer to the adsorbed species favoring their photooxidation and further mineralization [7-11]. A plenty of investigations on nanostructured ZnO/TiO₂ composites with different configurations and morphologies are performed in order to obtain more efficient photocatalytic degradation [9, 12-14].

It is of interest to understand how the differences between TiO₂ and ZnO may affect the overall catalytic processes. As the first step, this investigation is focused on the influence of the ZnO and TiO₂ content in the heterostructured composite on the UV and visible light induced degradation of two model pollutants: azo dye Orange II (O II) used as cosmetic colorant CI 15510 and triarylmethane dye Brilliant Green (BG), used as food colorant E142.

EXPERIMENTAL

The oxides TiO₂ anatase from KRONOS-Germany and ZnO from Sigma Aldrich were used for the composite ZnO/TiO₂ powders preparation. The initial charge for the composite was prepared from thoroughly homogenized commercial oxide powders. Seven series of samples with composition corresponding to 10, 25, 40, 50, 60, 75 and 90% ZnO content were prepared. As mixing media a small quantity of ethanol (Institute of Pure Substances, Sofia University) was added to assure better contact between both oxides. Then the mixtures were sonicated for 10 min, after that thermally treated for 2 h at 200°C to assure complete removal of the ethanol residue and finally well stirred in a glass mortar to obtain fine powder.

* To whom all correspondence should be sent.
E-mail: a_bojinova@hotmail.com

The phase composition and crystallinity of as-prepared composites was identified by X-Ray analysis (diffractometer Siemens D 500 CuK α source of radiation at a step of 0.05 deg for 2 θ and counting time 2 s/step). The surface area of the dry composite powders, was determined by BET analyses using N₂ adsorption. The surface morphology of the samples was observed via scanning electron microscopy (JSM-5510 JEOL).

The characteristics of two model pollutants Orange II and Brilliant Green are presented in Table 1.

The as-prepared ZnO/TiO₂ samples were tested in photodegradation of O II or BG from water solution by a standard testing procedure [15]. The dye solution volume was 250 ml. The catalysts loading was 1g L⁻¹. The initial concentration was 20 ppm for O II and for BG. The sources of light

illumination were as follows: UVA lamp (Sylvania 18W BLB T8, emitting mainly in the range of 315-400 nm) placed at 10 cm above and linear Tungfram lamp (500 W K1R7s 9700 Lm, maximal emission at 700 nm) for the visible irradiation fixed at 25 cm above the treated solution. Aliquot samples from the investigated solution were taken regularly at fixed time intervals and analyzed by UV-VIS spectrophotometer (Thermo scientific, Type Evolution 300 BB) at the maximal absorption of the contaminants. After the measurement, the aliquots were returned back to the pollutants solution. The solutions were stirred constantly by electromagnetic stirrer (rotation speed of 400 rpm). All the photocatalytic tests were performed at room temperature of 23±2°C.

Table 1. Characteristic data of the organic dyes used in the photocatalytic experiments

Contaminant	O II	BG
Empirical formula:	C ₁₆ H ₁₁ N ₂ NaO ₄ S	C ₂₇ H ₃₃ N ₂ .HO ₄ S
Molar mass:	350.32 g/mol	482.64 g/mol
Absorption maximum (in water):	484 nm	
Minimum dye content:	85%	90%
Synonyms:	4-(2-Hydroxy-1-naphthylazo)benzenesulfonic acid sodium salt, Acid Orange 7, Acid Orange A, Orange II, Tropaeolin 000 No. 2	Astradiamant green GX, Basic Green 1, Diamond Green, Emerald Green, Solid green JJO, Diamond green G, Ethyl Green, Aniline green, Benzaldehyde green, Fast green J

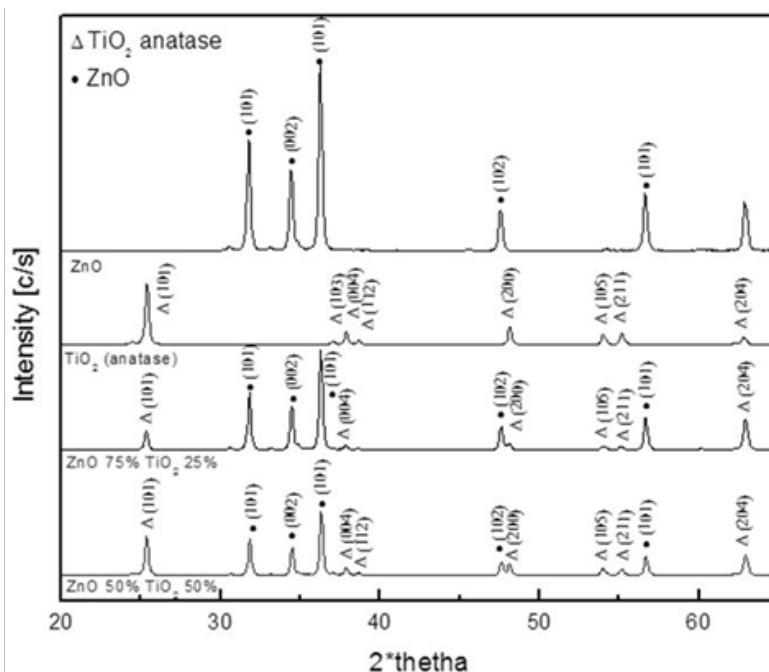


Fig. 1. Comparative XRD pattern of TiO₂, ZnO and ZnO/TiO₂ composites.

RESULTS AND DISCUSSION

The crystalline phase composition of the ZnO/TiO₂ nanocomposite and pure oxide samples is

verified by X-ray analysis (Fig. 1). From the XRD it is clearly seen that ZnO is crystalline, in form of hexagonal wurtzite with dominating peak (101). The titania has main peak at (101) and is in form of

anatase modification. Comparing the XRD patterns in Fig. 1 one can see that ZnO and TiO₂ are present in the composite as separate phases, there is no indication for formation of mixed compound: the main peaks of both oxides in case of composite sample do not differ in width and intensity from these in the case of pure ZnO or TiO₂ phases. The crystallites size, calculated following Sherrers equation ($k = 1.5406 \text{ \AA}$) is found to be 24 nm for ZnO and 17 nm for TiO₂. The calculation is made from the peaks (101) for ZnO and (101) for TiO₂ (relatively strong and single for the respective oxide - Fig. 1).

A comparison of the surface morphology of TiO₂ to that of ZnO/TiO₂ nanocomposite observed by SEM is shown in Fig. 2. From the micrographs is seen that the samples are uniform and homogeneous. The size of the particles grains of the samples is

calculated following the equation:

$$D_{av} = \sum_{i=1}^N (D_{i_{max}} + D_{i_{min}}) / 2N ,$$

where N is the number of observed particles, and D_{av} , D_{max} and D_{min} are the average, maximum and minimum diameter of the particles. In this case $N=350 \div 520$. The average grain size is found to be approximately 0.45 μm for ZnO and 0.02 μm for TiO₂ for all of the investigated samples.

The results from BET analysis are presented in Table 2.

As shown in the table, the surface area in the composites increases with the TiO₂ content from 23.03 m^2/g in case of 90%ZnO/10%TiO₂ to 37.89 m^2/g for the 90%ZnO/10%TiO₂ composite. The latter is greatest among all samples. The pure oxide phases have approximately equal surface area.

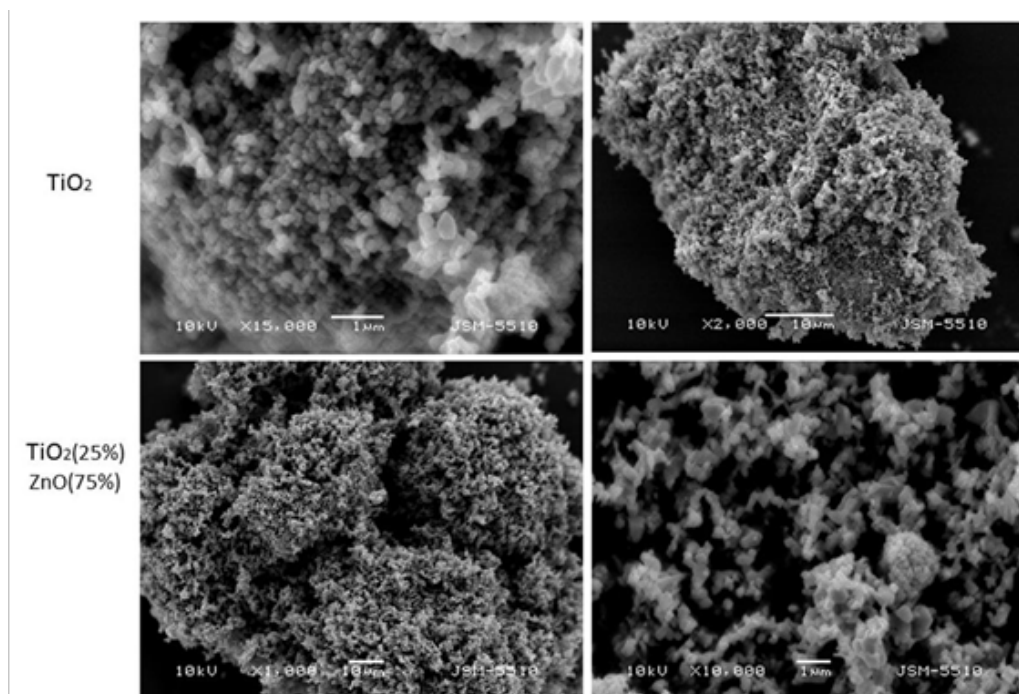


Fig. 2. SEM images of the powdered catalysts at different magnifications: (a) and (b) pure TiO₂; (c) and (d) ZnO(75%)/TiO₂(25%) composite.

Table 2. Specific surface area S of the commercial (pure ZnO and TiO₂) and prepared ZnO/TiO₂ powder catalysts

ZnO, %	TiO ₂ , %	$S, \text{m}^2/\text{g}$
100	0	35.76
90	10	23.03
75	25	26.55
60	40	30.81
50	50	31
40	60	33.45
25	75	34.35
10	90	37.89
0	100	35.52

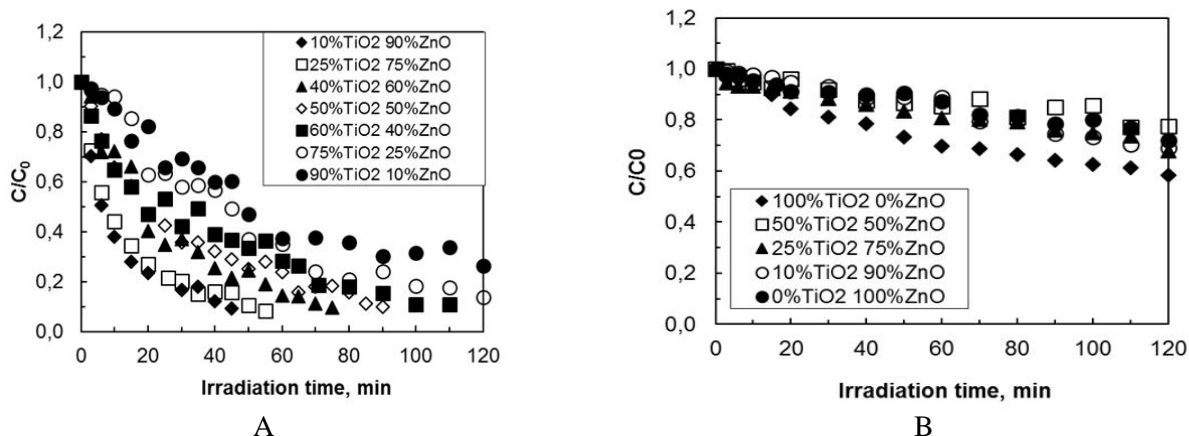


Fig. 3. Photodegradation kinetics of O II colorant from 20 ppm aqueous solutions by the different samples under: (a) UV and (b) visible light illumination.

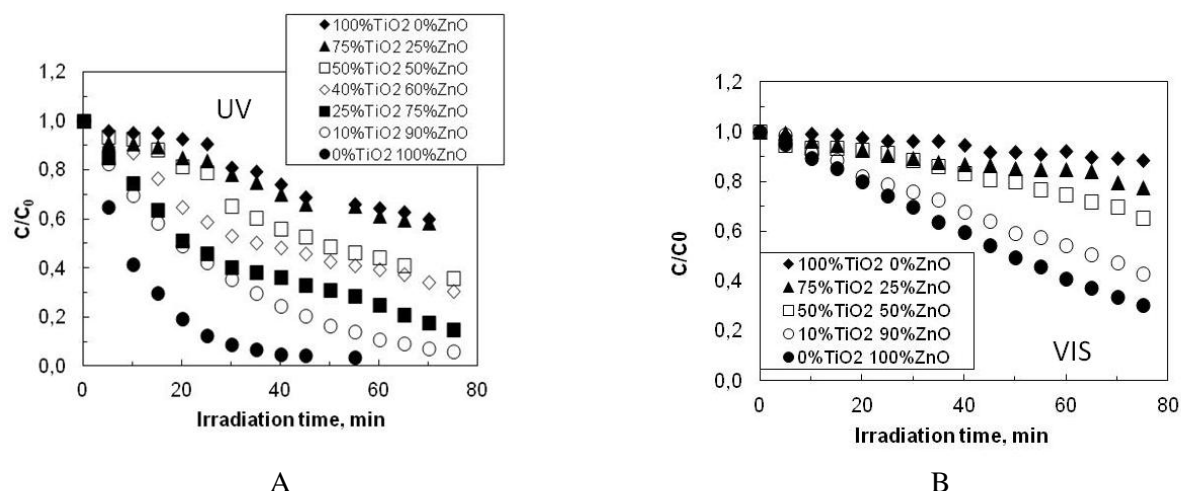


Fig. 4. Kinetics of BG colorant photodecomposition by the different powder catalysts from 20 ppm water solutions under irradiation with: (a) UV and (b) visible light.

The kinetics of colorants degradation in the photocatalytic experiments is presented in Fig. 3 for O II and in Fig 4 for BG. The colorants concentration in the water solutions is 20 ppm. Figs. 3a. and 4a show the experimental runs under UV illumination. The photocatalytic tests carried out with visible light irradiation are presented in Figs. 3b. and 4b. In general - higher rates and degrees of photodegradation under UV and visible light are achieved in case of BG in comparison to these in case of O II. The differences between the investigated heterocomposite samples are more pronounced and can be better observed also in the case of BG (Fig 4.). The experimental data in case of ZnO/TiO₂ heterocomposites show clear tendency for higher photocatalytic efficiency with the ZnO content in the sample irrespective of type of pollutant or illumination. Pure ZnO is the most efficient photocatalysts in comparison to the rest of the samples in all the photocatalytic tests. Pure TiO₂ sample always has the lowest efficiency among all tested photocatalysts.

The apparent rate constants of photocatalysis are calculated following the equation:

$$C = C_{in} \cdot e^{-Kt}$$

where C is the concentration of the contaminants solution at the moment t , C_{in} – the initial dye concentration and t is the irradiation time in minutes. The rate constants values (K), calculated by the above equation with the data, obtained from the photocatalytic experiments under both types of illumination, are plotted in Fig. 5. From the figure one can see, that highest rate constants values are observed in case of photocatalysis under UV light (Fig. 5a), where the process of photocatalysis is most effective. In comparison with O II, the BG photodegradation is always faster, irrespective of irradiation wavelength - UV or visible light.

The experimental data confirm other researchers viewpoint [16] that for some applications where the process of ZnO photocatalysis is the most effective, zinc oxide is a suitable alternative to TiO₂.

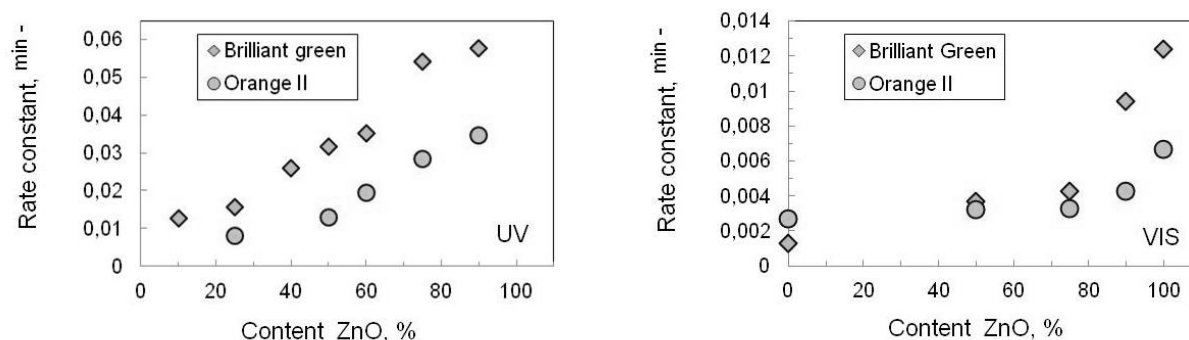


Fig. 5. Rate constant values of O II and BG photodegradation versus the ZnO content in the composite samples in case of: (a) UV and (b) visible light induced photocatalysis.

CONCLUSIONS

The photocatalytic action of the ZnO/TiO₂ samples is tested and compared to that of pure commercial oxides in UV and visible light induced purification of aqueous solutions from the organic colorants Orange II and Brilliant Green. The photocatalytic effectiveness of the composites increases regularly with the ZnO content in the powders. Most efficient colorants photodegradation is achieved in case of BG. The best photocatalyst in all the experiments is pure ZnO in comparison to the rest of the samples. The above effects are established irrespective of the type of illumination or type of purified solution. The experimental data show that in the particular purification ZnO is the suitable alternative to TiO₂.

Acknowledgements: The current study was accomplished in the frames of the project DFNI-T02/16 (№2742) and FP7 Horizon 2020.

REFERENCES

1. M.A. Henderson, *Surface Science Reports*, **66** (6-7), 185 (2011).
2. S. Rehman, R. Ullah, A. M. Butt, N. D. Gohar, *J. Hazard. Mater.*, **170** (2-3), 560 (2009).
3. A. Fujishima, T. N. Rao, D. A. Tryk, *J. Photochem. Photobiol. C*, **1**, 1 (2000).
4. M. Ladanov, M. K. Ram, G. Matthews, A. Kumar, *Langmuir*, **27** (14), 9012 (2011).
5. D. M. Fouad, M. B. Mohamed, *Journal of Nanomaterials*, **2012**, Article ID 524123, (8 pages) (2012).
6. F. Lu, W. Cai, Y. Zhang, *Advanced Functional Materials*, **18** (7), 1047 (2008).
7. M. Dahl, Y. Liu, Y. Yin, *Chem. Rev.*, **114**, 9853 (2014).
8. O. Carp, C. L. Huisman, A. Reller, *Progress in Solid State Chemistry*, **32**, 33 (2004).
9. Kian Mun Lee, Chin Wei Lai, Koh Sing Ngai, Joon Ching Juan, *Water Research*, **88**, 428 (2016).
10. N. Kaneva, S. Siuleiman, A. Bojinova, K. Papazova, D. Dimitrov, I. Gracheva, S. Karpova, V. Moshnikov, *Bulgarian Chemical Communication*, **45**, 611 (2013).
11. N. Kaneva, A. Ponomareva, L. Krasteva, D. Dimitrov, A. Bojinova, K. Papazova, G. Suchaneck, V. Moshnikov, *Bulgarian Chemical Communication*, **45**, 635 (2013).
12. A. D. Bachvarova-Nedelcheva, R. D. Gegova, A. M. Stoyanova, R. S. Iordanova, V. E. Copicia, N. K. Ivanova, I. Sandu, *Bulgarian Chemical Communications* **46** (3), 585 (2014).
13. A. Shalaby, A. Bachvarova-Nedelcheva, R. Iordanova, *Journal of Chemical Technology and Metallurgy*, **48** (6), 585 (2013).
14. A. Shalaby, A. Bachvarova-Nedelcheva, R. Iordanova, Y. Dimitriev, A. Stoyanova, H. Hitkova, N. Ivanova, M. Sredkova, *Journal of Optoelectronics and Advanced Materials* **17** (1-2), 248 (2015).
15. M. Kostadinov, P. Georgiev, A. Bojinova, C. Dushkin, in: E. Balabanova, I. Dragieva (Eds.), *Nanoscience and Nanotechnology*, **3**, Heron Press, Sofia, 2003, pp. 207–209.
16. M. D. Hernández-Alonso, F. Fresno, S. Suárez, Juan M. Coronado, *Energy Environ. Sci.*, **2**, 1231 (2009).

ZnO/TiO₂ композитни фотокатализатори

Ш. Сюлейман, Н. Кънева, А. Божинова*, Д. Димитров, К. Папазова

*Лаборатория по наука и технология на наночастици,
катедра Обща и неорганична химия, Факултет по химия и фармация,
Софийски университет, София 1164, България*

Постъпила на 11 ноември 2016 г.; приета на 20 декември 2016 г.

(Резюме)

Настоящата работа има за цел изследване на влиянието на съотношението на TiO₂ към ZnO, в състава на нанокмозитни прахове, върху тяхната ефективност като фотокатализатори в суспензия. Серия от проби, съответстващи на различно съдържание на титанов диоксид са получени от търговските марки на двата оксида. Фазовият състав и кристалността на пробите са характеризирани с рентгенова дифракция. Морфологията на повърхността на пробите е наблюдавана чрез сканираща електронна микроскопия. Фотокаталитичната активност на композитите е тествана под действието на ултравиолетова и видима светлина, при фотокаталитичното разграждане на два моделни замърсителя: азо багрилото Оранжево II (O II), използвано като козметичен оцветител CI 15510 и триарилметановото багрило, Брилянтно зелено (BG), използвано като оцветител на храни E142.

Assessment of several priority pollutants in fish from selected lakes in Bulgaria

S. K. Georgieva*, Zl. V. Peteva

Department of Chemistry, Medical University -Varna, 55 Marin Drinov Str., 9002 Varna, Bulgaria,

Received November 12, 2016; Revised December 21, 2016

The aim of the study was to assess the human health risk through fish consumption due to persistent organic pollutants like polychlorinated biphenyls (PCBs), DDT and its metabolites, hexachlorobenzene (HCB) and hexachlorobutadiene (HCBD). The present study evaluates the human daily intake of priority pollutants through consumption of freshwater fish from some lakes in Bulgaria (Varna Lake, Beloslav Lake, Burgas Lake, Mandra Lake). Concentrations of organochlorine compounds were determined in six fish species: gibel carp (*Carassius gibelio*), roach (*Rutilus rutilus*), perch (*Perca fluviatilis*), goby (*Neogobius melanostomus*), golden grey mullet (*Mugil auratus*) and silverside (*Atherina boyeri*).

The PCBs, HCB, HCBD, DDT and its metabolites DDE and DDD were determined by gas chromatography system with mass spectrometry detection. The sum of DDTs was determined from 1.81 ± 0.16 to 11.31 ± 1.26 ng/g wet weight (in perch and golden grey mullet, respectively). The other contaminants HCB and HCBD were found below the analytical detection limit. The sum of Indicator PCBs ranged from 1.00 (goby) to 5.30 ng/g ww (golden grey mullet).

The EDI of DDTs in fish from coastal lakes was calculated between 0.34 and 2.13 ng/kg body weight/ day through consumption of perch and golden grey mullet, respectively. EDI of I-PCBs in fish was between 0.19 and 1.00 ng/kg bw day through consumption of goby and golden grey mullet, respectively. The health risks were assessed using a risk quotient (RQ) of the fish consumption as the ratio of daily fish exposure level in relation to oral reference dose. All the RQ values were much lower than 1, suggesting that consumption of the fish species from coastal lakes in Bulgaria would not pose a non-cancer risk for humans.

Keywords: PCBs; DDTs, fish; risk assessment; Bulgaria

INTRODUCTION

Persistent organic pollutants (POPs) are a group of compounds, which are characterised by their ability to persist in ecosystems, their high lipid solubility and their bio-magnification in the food chain [1]. POPs accumulate in the fatty tissue of living organisms, reaching the greatest concentrations at the top of the food chain in fish, mammals and predatory birds [2]. Polychlorinated biphenyls (PCBs) and 1,1,1-trichloro - 2, 2 - bis (4-chlorophenyl) ethane (DDT) and its metabolites (DDTs) are highly lipophilic compounds and they rapidly accumulated in living organisms [3]. Although the usage for agriculture of DDTs has been banned since 1970s, DDTs are still being used in low amounts to control certain insects in tropical and subtropical countries [4]. Hexachlorobenzene (HCB) is a hydrophobic and highly persistent compound [5]. Although hexachlorobenzene is not currently manufactured, it is formed as a waste product in the production of several chlorinated hydrocarbons and is a contaminant in some pesticides [6]. The main source of HCB today is chemical industry from which this compound can be emitted as a product in high-temperature processes

[7]. Hexachlorobutadiene (HCBD) was mainly used as an intermediate in the manufacture of rubber compounds and other polymers. Other uses were in agriculture as a seed dressing, in hydraulic fluids and a number of other industrial processes [8]. HCB and HCBD are also named as priority substances under the EU Water Framework Directive [9].

These very persistent pollutants have the potential to affect the physiological functions of wildlife [10]. Although humans can be exposed to POPs through direct exposure, occupational accidents and the environment, most of the human exposure nowadays is from the ingestion of contaminated food as a result of bioaccumulation in the food chain [11, 12]. It has been reported that meat, dairy products and fish, makes up more than 90% of the intake of POPs for the general population [13, 14, 15]. Data on the presence and distribution of organohalogenated contaminants in fish and especially edible fish species are important not only from ecological, but also from human health perspective [16].

There are several lakes along Bulgarian Black Sea coast. Varna Lake is the largest by volume and deepest lake along the Bulgarian Black Sea Coast, and having an area of 17 km² and a volume of

* To whom all correspondence should be sent.

E-mail: stanislavavn@mail.bg

166 million m³. A number of rivers pour into the lake near the western shores of Beloslav Lake, which is connected to Varna Lake. Burgas Lake is located near the Black Sea, west of the Burgas city, is the largest natural lake in Bulgaria, with an area of 27.60 km². An important fish-producing reservoir in the past, Burgas Lake lost much of its economic importance after the construction of the petrochemical plant near the city, but has witnessed an increasing number of species and decreasing pollution in recent years. Mandra Lake is the southernmost of the Burgas Lakes, located in the immediate proximity of the Black Sea. Parts of Mandra Lake are designated protected areas inhabited by a number of locally and globally endangered species of fish and birds.

A lot of local fishermen consume fish from these coastal lakes. Therefore, it is very important to clarify the status of POPs in fish from these waters and the present study will provide more information on the residues of persistent organic pollutants in fish from Varna Lake, Beloslav Lake, Burgas Lake and Mandra Lake.

The aims of the present study were to evaluate the daily intake and to assess the human health risk of priority pollutants (PCBs, DDTs, HCB and HCBd) through consumption of fish from some coastal lakes in Bulgaria.

EXPERIMENTAL

Sampling

Six wild fish species: gibel carp (*Carassius gibelio*), roach (*Rutilus rutilus*) and perch (*Perca fluviatilis*), goby (*Neogobius melanostomus*), golden grey mullet (*Mugil auratus*) and silverside (*Atherina boyeri*) were sampled from some coastal lakes in Bulgaria (Varna Lake, Burgas Lake, Burgas Lake and the Mandra Lake). Samples were caught by local professional fishermen between September and November 2014. Samples were immediately transferred to the laboratory in foam boxes filled with ice and were stored in a freezer (-18°C) until analysis.

Analytical method

The method used for the preparation of the samples, clean-up and quantitative determinations of PCBs in fish samples has been previously described in details [17]. The edible tissue of each fish was homogenized using a blender; pools of about 300 g were made with fillets taken from several individual fish. Briefly, twenty grams of homogenized fish tissue were extracted with hexane / dichloromethane in Soxhlet Extractor. The extract was cleaned-up on a glass column packed with 2 g neutral silica, 4 g acid silica and 2 g neutral silica (Merck KGaA, Darmstadt, Germany). The eluates were

concentrated to near dryness and reconstituted in 0.5 ml in hexane. One micro liter of purified extract was injected into GC/MS.

Gas chromatographic analyses of PCBs were carried out by GC FOCUS (Thermo Electron Corporation, Austin, Texas, USA) using POLARIS Q Ion Trap mass spectrometer. Splitless injections of 1 µl were performed using a TR-5MS capillary column (Bellefonte, PA, USA) coated with cross-linked 5% phenyl methyl siloxane with a length of 30 m, 0.25 mm ID and a film thickness of 0.25 µm. Helium was applied as carrier gas at a flow of 1 ml/min.

Pure reference standard solutions (PCB Mix 20 - Dr. Ehrenstorfer Laboratory, Augsburg, Germany), were used for instrument calibration, recovery determination and quantification of compounds. Measured compounds were: the six Indicator PCBs (I-PCBs IUPAC No. 28, 52, 101, 138, 153 and 180) and six dioxin-like PCBs (non-ortho PCBs 77, 126, 169 and mono-ortho PCBs 105, 118, 156). Each sample was analyzed three times and was taken an average of the results obtained.

Quality control

The quality control was performed by regular analysis of procedural blanks and certified reference material BCR - 598 (DDTs in Cod liver oil) and BB350 (PCBs in Fish oil) – Institute for Reference Materials and Measurements, European Commission. Recovery of PCBs from certified reference material varied in the range 85 -109% for individual congeners. Procedural blanks and a spiked sample with standards were analyzed between each 5 samples to monitor possible laboratory contamination. Blanks did not contain traces of contaminants.

Statistical analysis

The statistical analysis of the data was based on the comparison of average values by a t-test and a significance level of $p < 0.05$ was used. When the p value was lower than 0.05, it was considered statistically significant. All statistical tests were performed using SPSS 16 software. For the purpose of statistical analysis, concentrations of contaminants reported as "not detected" were assigned as the detection limit. The data used in the present study were based on the mean concentrations of the target contaminants in the fish species.

Dietary intake estimation

Human exposure assessment of POPs through oral ingestion is generally estimated using daily intake of the contaminant. The estimated total daily intake (EDI) of the contaminants in a given fish species was calculated as follow [18]:

$$EDI = C \times \text{Intake} / BW$$

where EDI is the estimated daily intake (ng/kg body wt./day), C is the average concentration of measured POPs (ng/g wet weight), Intake is the daily food consumption of fish (13.2 g/ day for Bulgarian standard adult [19] and BW is the average consumer body weight (70 kg for adult men).

Risk assessment

Risk assessments were conducted based on the concentrations of organochlorine pesticides and PCBs compounds in fish tissues. The potential risks of non-carcinogenic effects are evaluated by the risk assessment index known as the risk quotient (RQ). RQ is defined as the ratio of daily fish exposure level (EDI) in relation to reference dose (RfD) considering non-carcinogenic effects of the contaminants. The RQ was calculated as follows [18, 20]:

$$RQ = EDI / RfD$$

where EDI is the estimated daily intake (ng/kg body wt./day); and RfD is the reference dose (ng/kg day). RfD values adopted in this study are the criteria of the USEPA (Environment Agency of the United States) [20].

RESULTS AND DISCUSSION

Indicator PCBs levels

PCBs and chlorinated pesticides have been monitored routinely in the environment and foodstuff in various countries to evaluate their potential health risk to humans [21, 22]. Consumption of contaminated food is an important route of human exposure to organochlorine compounds. The sum of the six PCBs (IUPAC № 28, 52, 101, 138, 153 and 180) comprises about half of the amount of total non dioxin-like PCBs present in feed and food [23]. They are called indicator PCBs (I-PCBs) for evaluating the risk to human health [24]. The concentration levels of individual PCBs congeners in fish from coastal lakes along Bulgarian Black Sea coast were described in our previous studies [25, 26]. Our previous studies showed that the most abundant PCB congeners in fish species were the indicator PCBs constituting more than 80% of the total amount of PCBs [25, 26].

The lipid content, mean levels of Total Indicator PCB congeners in investigated fish species from coastal lakes in Bulgaria, estimated daily intake

(EDI) and risk quotient (RQ) are shown in Table 1. The lipid percentage ranged from 0.5% (goby) to 6.1% (silverside).

The mean levels of I-PCBs ranged between 1.00 ng/g ww (goby) and 5.30 ng/g ww (golden grey mullet), calculated as the sum of 6 Indicator PCB congeners. The differences in concentrations of PCBs may be attributable to various factors such as the nature of the habitat, feeding preferences and lipid contents. The higher levels of PCBs in grey mullet compared to other fish species may be due to its nature of the habitat. These species usually inhabit muddy bottoms along the coast, and ports and estuaries, which are generally considered to be more heavily polluted than open waters. Golden grey mullet probably receive large quantities of organochlorine pollutants present in the water and in the sediments through a process of bioconcentration [27]. The European Union has recommended a maximum level of 75 ng/g wet weight, calculated as the sum of the six I-PCBs in muscle meat of fish [24]. Our results for Sum of I-PCBs in all fish species did not exceed this limit.

The pattern of indicator PCBs found in wild fish from coastal lakes showed a predominance of PCB 153 (31.9%) followed by PCB 101 (24.3%) for indicator PCBs (Table 2).

The predominance of hexachlorinated and pentachlorinated PCBs in fish species, especially PCB 153, PCB 101 and PCB 138, has been reported by several authors for different coastal areas in the Mediterranean [27] and in the Adriatic Sea [28]. The distribution of PCB congeners could be explained by the fact that the accumulative properties of PCB congeners increase with the number of chlorine atoms substituted to the hydrogen atoms in biphenyl rings and the resulting increase in their lipophilicity [29].

Estimated daily intake (EDI) of I-PCBs

Fish and seafood accounts for a small portion of human diet, but it has been proven to be one of the major routes of human exposure to organic contaminants [12]. The consumption of contaminated fat food can be a potential risk for the consumer. To comprehensively evaluate risk exposure, the mean EDIs for these harmful chemicals in each fish species were calculated. On the basis of the measured concentrations in the fish samples, the daily dietary intake of PCBs was

Table 1 Lipid content (%), levels of Total Indicator PCBs (ng/g wet weight, mean and standard deviation) determined in fish from coastal lakes in Bulgaria, Estimated daily intake (EDI) and Risk quotient (RQ).

Species	n	Lipids, %	Sum I-PCBs, ng/g ww	EDI, ng/kg bw day	RfD, ng/kg/day (USEPA)	RQ
gibel carp	8	1.3±0.4	1.60±0.37	0.30±0.08	20	0.015
roach	6	2.2±0.2	1.06±0.25	0.20±0.04	20	0.010
perch	8	0.6±0.1	1.06±0.22	0.20±0.04	20	0.010
goby	8	0.5±0.1	1.00±0.16	0.19±0.03	20	0.009
golden grey mullet	6	4.2±1.2	5.30±0.56	1.00±0.13	20	0.050
silverside	10	6.1±1.6	3.99±0.34	0.75±0.14	20	0.038

RfD – oral reference dose

Table 2 The PCB pattern (% of total indicator PCBs), estimated daily intakes of individual I-PCBs in fish (mean value) for adults (aged 15–75) in ng/ kg body weight per day.

Substance	% of total I-PCBs	Mean concentration, ng/g ww	EDI, ng/kg bw day	RfD, ng/kg/day (USEPA)
PCB 28	17.1	0.42±0.03	0.08	20
PCB 52	17.8	0.43±0.04	0.08	20
PCB 101	24.3	0.59±0.06	0.11	20
PCB 138	4.9	0.12±0.02	0.15	20
PCB 153	31.9	0.77±0.06	0.02	20
PCB 180	3.9	0.10±0.02	0.02	20

Table 3 Levels of Total DDTs (ng/g wet weight, mean and standard deviation) determined in fish collected from coastal lakes in Bulgaria, Estimated daily intake (EDI) and Risk quotient (RQ).

Species	n	Sum DDTs, ng/g ww	EDI, ng/kg bw / day	RfD, ng/kg/day (USEPA)	RQ
gibel carp	8	3.99±0.37	0.75±0.07	500	0.002
roach	6	2.45±0.25	0.46±0.06	500	0.001
perch	8	1.81±0.16	0.34±0.03	500	0.001
goby	8	2.69±0.26	0.51±0.05	500	0.001
golden grey mullet	6	11.31±1.26	2.13±0.23	500	0.004
silverside	10	6.79±0.64	1.28±0.13	500	0.003

calculated. The estimated daily intake of the Sum I-PCBs in fish species studied are shown in Table 1. The EDI was calculated on the basis of a fish consumption rate of 13.2 g/day [19] for adults with body weight of 70 kg, on the mean exposure level. The EDI of I-PCBs in fish from coastal lakes was calculated between 0.19 and 1.00 ng/kg bw day through consumption of goby and golden grey mullet, respectively and was far below recommended RfD of 20 ng/kg bw day for adults [20]. Overall, the EDIs of these POPs via fish consumption for adults in the present study were

lower than those reported in most previous studies [23, 30].

Levels and estimated daily intake (EDI) of DDTs

Because of their wide distribution in air, water, soil and food, p,p'-DDT and its metabolites (p,p'-DDD and p,p'-DDE) remain a human health concern and have been determined in edible fish tissues from investigated coastal lakes in Bulgaria [25, 26]. Summarized data of mean levels of total DDTs (like sum of p,p'-DDT, p,p'-DDD, p,p'-DDE) found in the fish samples and estimated daily intakes are present in Table 3.

The maximum level of Sum DDTs was found in golden grey mullet (11.31 ng/g ww), while the minimum value was found in perch (1.81 ng/g ww). The experimental results showed significant differences of DDTs levels between different fish species (statistical test – $p < 0.05$). The daily intake of DDTs (like sum of p,p'-DDT, p,p'-DDD, p,p'-DDE) was calculated on the basis of the measured concentration in fish species (Table 3). The mean EDI of total DDTs in fish from Varna Lake, Lake Burgas and Mandra Lake was calculated between 0.34 ± 0.03 and 2.13 ± 0.19 ng/kg body weight/ day through consumption of perch and golden grey mullet, respectively. The US Environmental Protection Agency established a Reference Dose (RfD) of 500 ng/kg body weight day [20], which corresponds to a tolerable daily intake of 0.5 µg/kg body weight from Integrated Risk Information System (IRIS) [31] for the non-carcinogenic effects. The mean EDI of 2.13 ng/kg body weight per day for adults is well below this value.

The distributions of levels PCBs, DDTs, HCB and HCBd in wild fish from Varna Lake, Beloslav Lake, Burgas Lake and Mandra Lake are summarised in Table 4.

The comparison of DDTs, PCBs, HCB and HCBd residues detected in fish collected from different coastal lakes shows that DDTs concentration are significantly higher ($p < 0.05$) in Varna Lake (10.32 ng/g ww) than those in Mandra Lake (2.20 ng/g ww). This is probably due to the influence of salty sea water in Varna Lake flowing from the Black Sea. Our previous studies have shown higher levels of organochlorine contaminants in marine fish species compared to freshwater species [32]. In term of PCBs, HCB and HCBd, no significant differences were detected between these four geographic locations.

In relation to other organochlorine compounds determined concentrations of HCB and HCBd were

all below detectable levels (Table 4) and did not exceed the European EQS of 10 µg/kg and 55 µg/kg (in biota), respectively. HCB is known as volatile and practically insoluble in water compound which leads to a low bioavailability of this contaminant in marine organisms. In a recent study of wild fish from four English rivers HCB was a maximum of 6 µg/kg in some eels [8]. In a survey of eels in Scotland [16] HCBd was only detected in one of 150 samples at detection limits of either 1 or 3 µg/kg and the authors of a French study also failed to detect any HCBd in fish [33]. The concentrations of HCB and HCBd were found below detection limit in all fish samples and daily intake was not estimated for these two chemicals.

Human health risk assessment

Many authors have revealed that high fish and seafood consumption increases the risk of POPs contamination of the human body [3, 34]. Current non-cancer risk assessment methods are usually based on the use of the Risk quotient (RQ). RQ is a ratio between the estimated dose of a contaminant and the reference dose (RfD) below which there will not be any appreciable risk [20]. The RfD is an estimate of daily exposure in humans that is likely to be without an appreciable risk of deleterious effects during a lifetime [18]. The average consumption together with the measured concentration of the contaminant are used to calculate the risk quotient RQ. RfD values adopted in this study are the criteria of the USEPA (Environment Agency of the United States) [20]. If the RQ value is less than 1, no obvious health risks due to the intake or uptake of contaminants via fish consumption would be experienced. Conversely, an exposed population of concern will experience health risks if the fish consumption rate is equal to or greater than the RfD value [18].

Table 4 Comparison of mean organochlorine levels in fish from different coastal lakes in Bulgaria (concentration, ng/g ww).

Compound	Varna Lake	Beloslav Lake	Burgas Lake	Mandra Lake
	goby, golden grey mullet	goby, golden grey mullet, silverside	gibel carp, roach	roach, perch
PCBs	4.24±2.01	2.71±1.21	1.29±0.44	1.10±0.70
DDTs	10.32±4.25	4.72±2.04	3.15±1.19	2.20±0.55
HCB	<LOD	<LOD	<LOD	<LOD
HCBd	<LOD	<LOD	<LOD	<LOD

<LOD – below limit of detection

Regarding risk assessment due to PCBs, the RQ values ranged from 0.009 to 0.050 for goby and golden grey mullet, respectively (table 2). The RQ values for DDTs in fish samples (presented in Table 3) were calculated from 0.001 (roach, perch, goby) to 0.004 (golden grey mullet). All the RQ values were much lower than 1, suggesting that consumption of the fish species would not pose a non-cancer risk.

CONCLUSION

The indicator PCB levels found in fish species from coastal lakes along Black Sea coast ranged between 1.0 ng/g ww (goby) and 5.3 ng/g ww (golden grey mullet) and did not exceed the maximum EU limit of 75 ng/g ww. The lower observed levels of PCB in fish tissues than from fish tissues of other aquatic ecosystems was potentially due to the absence of PCB manufacturing in Bulgaria. The maximum level of Sum DDTs was found in golden grey mullet (11.31 ng/g ww), while the minimum value was found in perch (1.81 ng/g ww). The estimated daily intakes of Indicator PCBs and DDTs by humans were far below RfD or the TDI for adults, recommended by US EPA and FAO/WHO, indicating that this intake would not pose a health risk. Human health risk assessment, based on RQ values much lower than one, suggesting that consumption of the fish species from coastal lakes in Bulgaria would not pose a non-cancer risk.

REFERENCES

1. D.H. Lee, I.K. Lee, Song K., M. Steffes, W. Toscano, B.A. Baker, et al., *Diabetes Care*, **29**, 1638 (2006).
2. C.J. Everett, I.L. Frithsen, V.A. Diaz, R.J. Koopman, W.M. Simpson Jr, A.G. Mainous 3rd, *Environ Res*, **103**, 413, (2007).
3. W. Masmoudi, M.S. Romdhane, S. Kherriji, M. El Cafsi, *Food Chem.*, **105**, 72, (2007)
4. X. Li, Y. Gan, X. Yang, J. Zhou, J. Dai, Muqi Xu, *Food Chem.*, **109**, 348, (2008).
5. F. Verweij, K. Booij, K. Satumalay, N. van der Molen, R. van der Oost, *Chemosphere*, **54**, 1675, (2004)
6. ATSDR 2015, Toxicological profile for hexachlorobenzene, <http://www.atsdr.cdc.gov/toxprofiles/tp90.pdf>
7. F.M. Jaward, N.J. Farrar, T. Harner, A.J. Sweetman, K.C. Jones, *Environ. Sci. and Technol.*, **38**, 34, (2004).
8. M. D. Jürgens, A.C. Johnson, K. C. Jones, D. Hughes, A. J. Lawlor, *Sci. of the Total Environ.*, **461–462**, 441, (2013).
9. EC DIRECTIVE 2013/39/EU amending Directives 2000/60/EC and 2008 /105/ EC as regards priority substances in the field of water policy (2013).

10. P. Langer, A. Kocan, M. Tajtakova, J. Petrik, J. Chovancova, B. Drobna, et al., *J. of Occup. & Environ. Med.*, **45**, 526, (2003).
11. European Commission. Assessment of dietary intake of dioxins and related PCBs by the population of EU Member States. 2000; Available from: http://www.ec.europa.eu/dgs/health_consumer/library/pub/pub08_en.pdf.
12. A.G. Smith, S. Gangoli, *Food and Chem Toxicol.*, **40**, 767, (2002).
13. A. Schecter, P. Cramer, K. Boggess, J. Stanley, J.R. Olson, *Chemosphere*, **34**, 1437, (1997).
14. J.L. Domingo, A. Bocio, G. Falcó, J.M. Llobet, *Environ. Sci. Technol.*, **40**, 4394, (2006).
15. J. Zhang, L. Feng, R. Chen, T. Feng, S. Dong & H. Shen, *Food and Chem. Toxicol.* **50**, 4285, (2012).
16. K. Macgregor, I.W. Oliver, L. Harris, I.M. Ridgway, *Environ Pollution*, **158**, 2402, (2010).
17. M. Stancheva, S. Georgieva, L. Makedonski, *Qual Assur and Safety of Foods and Crops.* **5(3)**, 243, (2013).
18. Y. Yu, X. Wang, D. Yang, B. Lei, X. Zhang, X. Zhang, *Food and Chem Toxicol.*, **69**, 86, (2014).
19. NSI (National Statistical Institute), Republic of Bulgaria, (2010), Available from: <http://www.nsi.bg/EPDOCS/HBS2010-1q.pdf>
20. USEPA (United States Environmental Protection Agency). EPA 823-B-00-008, (2000) Available from: <http://water.epa.gov/scitech/swguidance/fishshellfish/techguidance/risk/volume2index.cfm>.
21. A. Bocio, J.L. Domingo, G. Falcó, J.M. Llobet, *Environ Int.*, **33**, 170, (2007).
22. A. Törnkvist, A. Glynn, M. Aune, P. O. Darnerud, E. H. Ankarberg, *Chemosphere*, **83**, 193, (2011).
23. EFSA (European Food Safety Authority), *EFSA Journal*, **8**, 35, (2010).
24. EC. Commission Regulation (EU) No 1259/2011. *Off J of EU.* **L320**, 18, (2011).
25. S. Georgieva, M. Stancheva, L. Makedonski, *Ovidius University Annals of Chemistry*, **26** (1), 5, (2015).
26. S. Georgieva, M. Stancheva, S. Vutov, *J. of Intern. Sci. Publications*, **9**, 515, (2015).
27. B. Naso, D. Perrone, M.C. Ferrante, M. Bilancione, A. Lucidano, *Sci. of The Total Environ.*, **343**, 83, (2005).
28. M. Perugini, M. Lavalieri, A. Giammarino, P. Mazzone, V. Olivieri, M. Amorena, *Chemosphere*, **57**, 391, (2004).
29. N. Yang, M. Matsuda, M. Kawano, T. Wakimoto, *Chemosphere*, **63**, 1342, (2006).
30. R. Lavandier, N. Quinete, R.A. Hauser-Davis, P.S. Dias, S. Taniguchi, R. Montone, et al. *Chemosphere*, **90**, 2435, (2013).
31. IRIS (Integrated Risk Information System), (2004) Available: <<http://www.epa.gov/iris/>> Accessed 07.07.10
32. S. Georgieva, M. Stancheva, L. Makedonski, *Ovidius University Annals of Chemistry.* **23(1)**, 92, (2012).

- S.K. Georgieva & Z. Peteva: "Assessment of several priority pollutants in fish from selected lakes in Bulgaria"
33. C. Mieke, A. Peretti, P. Labadie, H. Budzinski, B. Le Bizec, K. Vorkamp, et al., *Anal Bioanal Chem*, **404**, 2721, (2012).
34. S. Voorspoels, A. Covaci, H. Neels, *Environ Toxicol. and Pharmacol.*, **25**, 179, (2008).

ОЦЕНКА НА НЯКОИ ПРИОРИТЕТНИ ЗАМЪРСИТЕЛИ В РИБИ ОТ ИЗБРАНИ ЕЗЕРА В БЪЛГАРИЯ

С. К. Георгиева* и Зл. В. Петева

Катедра по Химия, Медицински Университет - Варна

E-mail: stanislavavn@mail.bg

Постъпила на 12 ноември 2016 г.; приета на 21 декември 2016г.

(Резюме)

Целта на настоящото изследване беше да се оцени здравния риск чрез консумацията на риба по отношение на устойчиви органични замърсители като порихлорирани бифенили (ПХБ), ДДТ и метаболити, хексахлоробензен (ХХБ) и хексахлоробутадиен (ХХБД). Изчислен е дневен прием на приоритетните замърсители чрез консумация на сладководни риби от някои езера в България (Варненско езеро, Белославско езеро, Бургаско езеро и езеро Мандра). Концентрациите на органохлорните съединения бяха определени в шест рибни вида: каракуда (*Carassius gibelio*), бабушка (*Rutilus rutilus*), костур (*Perca fluviatilis*), кая (*Neogobius melanostomus*), платерина (*Mugil auratus*) и атерина (*Atherina boyeri*).

ПХБ, хексахлоробензен, хексахлоробутадиен, ДДТ и основните му метаболити ДДЕ и ДДД са определени чрез газова хроматография с маспектрометричен детектор. Средният дневен прием на замърсителите в риби от крайбрежните езера са изчислени между 0.34 ± 0.03 и 2.13 ± 0.19 (за ДДТ и метаболити) и между 0.19 ± 0.02 и 0.75 ± 0.08 ng/kg телесно тегло дневно (за ПХБ) чрез консумация съответно на кая и платерина. Здравният риск беше оценен чрез използване на коефициент на риск (RQ) като отношение на дневната експозиция и оралната референтна доза (RfD). Изчислените RQ са под единица, което означава, че консумацията на риба не представлява риск за човешкото здраве.

Ключови думи: ПХБ; ДДТ; риба оценка на риск; България

Basic chemical components and radical scavenging activity of tobacco extracts obtained by macroporous resin

M.H. Docheva*, M.B. Staykova, A.B. Stoilova, D. Dimanov

Tobacco and Tobacco Products Institute, Markovo 4108, Plovdiv, Bulgaria,

Received November 10, 2016; Revised December 21, 2016

The basic chemical components of tobacco extracts, containing flavonoids (E-FI) and the radical scavenging activity of E-FI was study. The extracts were prepared by using polymeric adsorbent Amberlite XAD 7. The tobaccos used in this study were selected from low to high content of nicotine, carbohydrates and polyphenols. The amount of flavonoids in extracts varied vastly depending on the content of flavonoids in the tobacco crop. The extracts contained flavonoids from $3.50 \pm 0.26 \text{ mg.g}^{-1}$ to $16.3 \pm 1.3 \text{ mg.g}^{-1}$ and phenolic acids are less than 0.6 mg.g^{-1} . The E-FI extracts showed a high radical scavenging activity (IC_{50} data varied from $9.6 \pm 0.8 \text{ }\mu\text{g.ml}^{-1}$ to $33.4 \pm 3.0 \text{ }\mu\text{g.ml}^{-1}$). In the extracts the nicotine content was less than $0.38 \pm 0.02 \text{ mg.g}^{-1}$ and depended strongly on its amount in tobacco, showing recovery mean $1.45 \pm 0.31 \%$. The content of carbohydrates in extracts E-FI was between $39 \pm 1 \text{ mg.g}^{-1}$ and $94 \pm 4 \text{ mg.g}^{-1}$ with mean recovery from tobacco 48%.

Key words: tobacco, tobacco extracts, polyphenols, nicotine, carbohydrates, radical scavenging activity

INTRODUCTION

Tobacco (*Nicotiana tabacum* L.) is a plant, containing a large number of chemical components. To date, approximately 4200 components have been identified in tobacco, which can be combined in the following large groups: alkaloids, carbohydrates, proteins, polyphenols, organic acids, essential oil, resins and etc. The type of tobacco (Virginia, Burley, Oriental) and how the tobacco is produced and cured affect the type and level of chemical compounds in tobacco leaf [1].

The chemical composition of tobaccos is a subject of extensive research in Bulgaria, especially the basic components as nicotine, carbohydrates, proteins, which are associated with processing technology, quality and the smoking properties of tobacco [2, 3, 4, 5]. In recent years, there is increasing interest on biologically active substances in tobacco - polyphenols, terpenes, alkaloids and etc [6, 7]. Tobacco leaves are rich in polyphenols, presented as phenolic acids (caffeoylquinic acids) and flavonoid glycosides. In the tobacco types Virginia and Oriental, their content can exceed 3% [8, 9, 10].

Phenolic acids possess a wide range of biological properties such as antibacterial, antioxidant, antimicrobial, anticancer and antimutagenic. Phenolic acids are active against human herpes simplex virus and adenoviruses [11]. The interest in bioflavonoids as antioxidants has been increased

remarkably over the last decade because of their protective effect against different diseases, including cardiovascular, inflammatory and neurological diseases, as well as cancers. It is known that flavonoid-rich natural products exert a wide range of pharmacological properties. Flavonoids have been associated with a reduction in the incidence of diseases such as cancer and heart diseases [12].

Recently the interest in obtain and use of natural products as supplements has been growing continuously. In view of the high content of phenolic acids and flavonoids in tobacco and their biological properties, several attempts were made to obtain tobacco extracts, enriched in phenolic acids and flavonoids [9, 13, 14, 15]. The chemical composition and the properties of the obtained products are especially important.

The aim of this study was to determine the basic chemical components of tobacco extracts, containing flavonoids (E-FI) and the radical scavenging activity of E-FI. The recovery of nicotine and carbohydrates in the extracts was evaluated.

MATERIALS AND METHODS

Plant material

Dry leaves of Oriental tobaccos (Djebel basma 1 – Db 1, Basma 79 – B 79, Muymuynovo seme - Ms, Plovdiv 380 – Pl 380) and Virginia tobaccos (Virginia 385 – V 385 and Koker 254 – K 254) were used as a material. The cultivars were provide to us by Prof. D. Dimanov from the collection of the Tobacco and Tobacco Products Institute, Plovdiv,

* To whom all correspondence should be sent.

E-mail: margarita_1980@abv.bg

Bulgaria. The tobaccos used were selected from low to high content of nicotine, carbohydrates and polyphenols.

Preparation of tobacco extracts, containing flavonoids (E-Fl)

The extracts were prepared by using polymeric adsorbent Amberlite XAD 7, according to the method described by M. Docheva with some modifications [15].

Dry tobacco powder (0.5 g) was extracted with 10 ml 60% (v/v) MeOH for 30 min on a mechanical shaker. The extract was filtered. The solution was added to 3 g macroporous resin Amberlite XAD7. The adsorption was carried out under static conditions for two hours. The flavonoids were desorbed from the resin with 65 ml 100% MeOH on a mechanical shaker for 2 hours.

Determination of polyphenols in tobacco and tobacco extracts E-Fl by HPLC analysis

0.1 g tobacco powder was sonicated for 30 min with 5 ml 60 % MeOH. The extract was filtrated under vacuum. The polyphenols were purified by passing the solution through cartridge C18 according to the method described by S. Dagnon and subjected to HPLC analysis [8].

Aliquot of the obtained extracts E-Fl was passed through a membrane filter 0.45 µm prior to HPLC analysis.

The limit of detection of the polyphenols pointed to LOQ * = 0.6 µg.ml⁻¹

Determination of nicotine in tobacco by continuous-flow analysis method

The nicotine content in tobaccos was determined according to the ISO 15152:2003 [16].

Determination of nicotine in tobacco extracts E-Fl by spectrometric analysis

The content of nicotine in the extracts was determined according to the ISO 3400:2009 with some modification [17]. Distillation of an aliquot portion of the extracts in two steps was done. Acidification of the solution with a sulfuric acid and remove the neutral and acid steam-volatile substances by distillation. By the next step were done alkalizing with sodium hydroxide solution and distillation of the alkaloids was done. The absorbance of the samples was measured at 236 nm, 259 nm and 282 nm with a spectrophotometer. The amount of tobacco was taken into account. The alkaloid content, expressed as nicotine in mg.g⁻¹ is given by formula:

$$Nic = \frac{AV_0V_2}{aV_1}$$

where:

a - absorptivity of nicotine in 0.025 mol/l sulfuric acid solution, i.e. 34.3 at the absorption maximum of 259 nm

A – corrected absorbance calculated from the absorbance measured at wavelengths of 236 nm, 259 nm and 282 nm

$$A = 1.059 \left(A_{259} - \frac{A_{236} + A_{282}}{2} \right)$$

l – optical path length of the cell, in centimetres

V₀ - the volume of extracts, in millilitres

V₁ – the aliquot of portion of V₀ used for the distillation, in millilitres

V₂ – the volume of distillate from the alkaline distillation, in millilitres

The relative standard deviation of the method (RSD) was 1.1 %. The limit of detection (LOD) of the nicotine was 0.2 µg.ml⁻¹ and the limit of quantification (LOQ) was 0.7 µg.ml⁻¹, calculated by the formulas:

$$LOD = 3s/b \text{ and } LOQ = 10s/b$$

where:

s - standard deviation of the lowest point of the calibration curve

b - slope of the calibration curve described by the equation y = a + bx

Determination of carbohydrates in tobacco and in tobacco extracts E-Fl by continuous-flow analysis method

The content of carbohydrates in tobacco was determined according to the ISO 15154:2003 [18].

Determination of radical scavenging activity of E-Fl by DPPH assay

The E-Fl extract was evaporated to dryness and its weight was measured. The dry extract was solved in 5 ml MeOH. The DPPH* assay was carried out as described by M. Docheva [15].

Statistics

All experimental procedures were done in triplicate. The quantitative data were expressed as mean ± standard deviation.

RESULTS AND DISCUSSION

Preparation of tobacco extracts, by various techniques, has already been the subject of many investigations. In the most cases, the extracts contain both phenolic acids and flavonoids [9, 13]. There have not been found enough data on the chemical composition of the tobacco extracts. Our aim was to study the content of nicotine, carbohydrates and polyphenols in tobacco extracts, obtained by macroporous resin.

Basic chemical components of tobaccos

The content of nicotine, carbohydrates and polyphenols in different varieties of tobacco is present in Table 1. The data in Table 1 show that Oriental tobaccos Db 1, B 79, Ms and P 380 contain more polyphenols (average 31.8 mg.g⁻¹) by comparing to Virginia tobaccos – average 17.9 mg.g⁻¹. Tobacco variety Ms is characterized with the highest content of polyphenols – 51 ± 4 mg.g⁻¹, followed by B 79 – 35.6 ± 2.8 mg.g⁻¹, while variety P 380 and V 385 contain lowest amount of polyphenols (approximately 15 mg.g⁻¹).

The amount of carbohydrates, as primary metabolites, varies widely in tobaccos - from 82.8 ± 3.3 mg.g⁻¹ (V 385) to 193 ± 8 mg.g⁻¹ (Db 1). The average carbohydrates amount in Oriental tobaccos is 147 mg.g⁻¹, while in Virginia tobaccos is lower - 118 mg.g⁻¹. These results confirm the established correlation between the content of carbohydrates and polyphenols [19] where tobaccos with high content of carbohydrates exert higher polyphenols content.

The content of nicotine in Oriental tobaccos Db 1, B79 and Ms is lower than 6.7 mg.g⁻¹ (0.67 %). An exception can be seen by Pl 380 - 16.3 ± 0.3 mg.g⁻¹. Virginia tobaccos V 385 and K 254 are characterized with higher nicotine content – 26.9 ± 0.5 mg.g⁻¹ and 15.4 ± 0.3 mg.g⁻¹ respectively. These

results are in accordance with the varietal characteristics of tobaccos [20, 21].

Extracts, containing flavonoids (E-Fl)

Table 2 shows the content of flavonoids, phenolic acids, carbohydrates and nicotine in tobacco extracts.

The E-Fl extracts contain flavonoids from 3.50 ± 0.26 mg.g⁻¹ (V 385) to 16.3 ± 1.3 mg.g⁻¹ (Ms). The amount of flavonoids in the extracts is proportional to the content of flavonoids in tobaccos.

The carbohydrates amounts in E-Fl extracts vary between 39 ± 1 mg.g⁻¹ (K 254) and 94 ± 4 mg.g⁻¹ (B 79) with mean recovery from tobacco about 48%.

The E-Fl extracts contain minimum amount of phenolic acids and nicotine. The nicotine content varies from ≤LOQ to 0.38 ± 0.02 mg.g⁻¹ and shows recovery maximum 2 %. The recovery of phenolic acids in these extracts is from 1.8 % to 5 % and relate to the amount of the phenolic acids in tobaccos.

The data reveal that is no correlation between the amount of carbohydrates in extracts and in tobaccos. Oriental tobacco variety B 79 and Virginia tobacco K 254 contain an equal amount of carbohydrates – 155 mg.g⁻¹ (Table 1), while their extracts show a significant difference in carbohydrates content. The extract derived from B 79 contains 94 ± 4 mg.g⁻¹ carbohydrates, whereas the extract derived from K 254 – 39 ± 1 mg.g⁻¹ (Table 2).

Table 1. Content of nicotine, carbohydrates and polyphenols in different varieties of tobacco

Tobacco varieties	Basic chemical components in tobaccos, mg.g ⁻¹			
	Flavonoids	Phenolic acids	Carbohydrates	Nicotine
Oriental tobaccos				
Djebel basma 1	12.2 ± 1.0	13.7 ± 1.1	193 ± 8	2.00 ± 0.04
Basma 79	15.5 ± 1.2	20.1 ± 1.6	156 ± 6	4.30 ± 0.09
Muymuynovo seme	23.3 ± 1.9	27.8 ± 2.2	129 ± 5	6.70 ± 0.13
Plovdiv 380	6.8 ± 0.5	8.1 ± 0.6	112 ± 5	16.3 ± 0.3
Virginia tobaccos				
Virginia 385	4.51 ± 0.36	10.4 ± 0.8	82.8 ± 3.3	26.9 ± 0.5
Koker 254	7.4 ± 0.5	13.8 ± 1.1	154 ± 6	15.4 ± 0.3

Table 2. Content of flavonoids, carbohydrates and nicotine in tobacco extracts E-Fl

Tobaccos varieties	Basic chemical components in E-Fl, mg.g ⁻¹			
	Flavonoids	Phenolic acids	Carbohydrates	Nicotine
Oriental tobaccos				
Djebel basma 1	8.1 ± 0.6	>LOQ*	55 ± 2	>LOQ**
Basma 79	13.3 ± 1.0	1.02 ± 0.08	94 ± 4	0.0500 ± 0.0033
Muymuynovo seme	16.3 ± 1.3	0.51 ± 0.04	82 ± 4	0.090 ± 0.006
Plovdiv 380	5.03 ± 0.37	0.34 ± 0.03	67 ± 3	0.32 ± 0.02
Virginia tobaccos				
Virginia 385	3.50 ± 0.26	>LOQ*	48 ± 2	0.38 ± 0.02
Koker 254	4.77 ± 0.35	>LOQ*	39 ± 1	0.15 ± 0.01

LOQ * = 0.6 µg.ml⁻¹, LOQ ** = 0.7 µg.ml⁻¹

Table 3. Radical scavenging activity of E-FI extracts

Tobaccos	Flavonoids in extracts, %	IC ₅₀ µg.ml ⁻¹
Oriental tobaccos		
Djebel basma	22.5 ± 3.0	19.8 ± 1.7
Basma 79	25.6 ± 3.1	11.3 ± 1.0
Muymuynovo seme	37 ± 4	9.6 ± 0.8
Plovdiv 380	10.9 ± 1.2	16.9 ± 1.4
Virginia tobaccos		
Virginia 385	10.2 ± 1.2	33.4 ± 3.0
Koker 254	20.3 ± 2.3	16.4 ± 1.4
Rutin		3.20 ± 0.20

The free radical scavenging activity of E-FI is presented as IC₅₀ µg.ml⁻¹ in Table 3. Lower IC₅₀ values correspond to higher radical scavenging activity of the extracts. Rutin, well-known antioxidant compounds with a structure similar to those of the tobacco flavonoids, is employed as reference compound with IC₅₀ = 3.20 ± 0.20 µg.ml⁻¹. The data in Table 3 reveal the highest scavenging activity of Ms extract (IC₅₀ = 9.6 ± 0.8 µg.ml⁻¹) which can be associated with the highest content in flavonoids – 37 ± 4 %.

The content of flavonoids in extracts, obtained from Oriental tobacco P 380 and Virginia tobacco V 385 are equal (average 10.5 ± 0.4 %), while the radical scavenging activity of V 385 extract (IC₅₀ = 33.4 ± 3.0 µg.ml⁻¹) is twice lower than P 380 extract (IC₅₀ = 16.9 ± 1.4 µg.ml⁻¹)

The obtained data coincide with the results in previous studies where, despite the lower content of flavonoids in the extract from Virginia tobacco, its radical scavenging activity is higher than that of extracts from Oriental tobaccos. This fact confirms that there are some other chemical components in the extracts, other than flavonoids, which are variety depending and influence the DPPH radical scavenging activity [15].

CONCLUSION

In this study the content of phenolic acids, flavonoids, nicotine and carbohydrates in tobacco extracts, containing flavonoids (E-FI), obtained by macroporous resin, was investigated. All extracts

were purified from phenolic acids and nicotine. The amounts of flavonoids, phenolic acids and nicotine in extracts strongly depend on their amount in tobaccos. The content of carbohydrates in extracts (E-FI) did not depend on its amount in tobaccos. E-FI showed a high radical scavenging activity.

REFERENCES

- Rodgman A., T. Perfetti: The chemical components of tobacco and tobacco smoke. CRC Press Taylor & Francis Group, New York, 2013.
- A. Stoilova, M. Docheva D. Dimanov, *Bulgarian tobacco*, **1**, 18 (2015).
- Y. Dyulgerski, *Genetics and Breeding*, **38**, 3-4, 145 (2009).
- Y. Dulgerski, *Тютюн /Tobacco* **64**, 7-12, 13 (2014).
- M. Kasheva, J. Kochev, *International scientific-practical conference "Food technology and health"*, 12 (2012).
- T. Ivanova: PhD Thesis, UHT, Plovdiv, 2014.
- V. Popova, DSc Thesis, UHT, Plovdiv, 2015.
- S. Dagnon, A. Edreva, *Contributions to Tobacco Research*, **20**, 5, 355 (2003).
- H. Wang, M. Zhao, B. Yang, Y. Jiang, G. Rao, *Food Chemistry* **107**, 1399 (2008).
- G. Xiang, H. Yang, L. Yang, X. Zhang, Q. Cao, M. Miao, *Microchemical Journal* **95**, 198 (2010).
- <http://cdn.intechopen.com/pdfs/29974.pdf>
- A. Scalbert, I. Johnson, M. Saltmarsh, *American Journal of Clinical Nutrition* **81**, 1 215 – 217 (2005).
- J. Zhang, S. Zhang, J. Wu, N. Li, J. Wang, *Journal of Medicinal Plants Research* **7**, 24, 1784 (2013).
- M. Docheva, S. Dagnon, S. Statkova-Abeghe, *Nat Prod Res.*, 1328 (2014).
- M. Docheva, S. Dagnon, *Comptes rendus de l'Académie bulgare des Sciences*, **68**, 2, 183 (2015).
- ISO 15152:2003 – "Tobacco – Determination of the content of the total alkaloids as nicotine – Continuous-flow analysis method".
- ISO 3400:2009 – "Cigarettes – Determination of alkaloids in smoke condensates – Spectrometric method".
- ISO 15154:2003 – "Tobacco – Determination of the content of reducing carbohydrates – Continuous-flow analysis method".
- J. Wooten, N. Kalengamaliro, D. Axelson, *Phytochemistry*, **70**, 940 (2009).
- D. Dimanov, R. Todorova, J. Kochev, *Scientific papers – Kardzhali*, **4**, 2, 168 (2010).
- D. Dimanov, *Тютюн/ Tobacco* **61**, 130, (2011).

ОСНОВНИ ХИМИЧНИ КОМПОНЕНТИ И РАДИКАЛ УЛАВЯЩА АКТИВНОСТ НА ТЮТЮНЕВИ ЕКСТРАКТИ ПОЛУЧЕНИ ЧРЕЗ АДСОРБЦИОННА СМОЛА

М. Х. Дочева*, М. Б. Стайкова, А. Б. Стоилова, Д. Диманов

*Институт по тютюна и тютюневите изделия, Марково 4108, Пловдив, България,
e-mail: margarita_1980@abv.bg*

Постъпила на 10 ноември 2016 г.; приета на 21 декември 2016 г.

(Резюме)

Изследвано е съдържанието на основни химични компоненти в тютюневи екстракти, съдържащи флавоноиди (Е-Фл), получени чрез използване на адсорбционна смола Amberlite XAD 7. Определена е радикал-улавящата активност на екстрактите. Тютюнните са подбрани с различно съдържание на никотин, въглехидрати и полифеноли. Количеството на флавоноидите в екстрактите варира значително и е в пряка зависимост от съдържанието им в тютюневата суровина. Съдържанието на флавоноиди в Е-Фл е между $3.50 \pm 0.26 \text{ mg.g}^{-1}$ и $16.3 \pm 1.3 \text{ mg.g}^{-1}$. Установено е по-малко от 0.6 mg.g^{-1} фенолни киселини. Екстрактите Е-Фл показват висока радикал улавяща активност (стойностите на IC_{50} варират от $9.6 \pm 0.8 \text{ }\mu\text{g.ml}^{-1}$ до $33.4 \pm 3.0 \text{ }\mu\text{g.ml}^{-1}$). Съдържанието на никотин в Е-Фл е по-ниско от $0.38 \pm 0.02 \text{ mg.g}^{-1}$ и е пропорционално на това в тютюнните. Максималният добив на никотин, изчислен спрямо съдържанието му в тютюна е до 2 %. Количеството на въглехидратите в екстрактите (Е-Фл) варира между $39 \pm 1 \text{ mg.g}^{-1}$ и $94 \pm 4 \text{ mg.g}^{-1}$. Отчетен е среден добив от 48 %.

Ключови думи: тютюн, тютюневи екстракти, полифеноли, никотин, въглехидрати, радикал-улавяща активност

Studies of the possibilities to obtain nanosized MnFe_2O_4 by solution combustion synthesis

Ts. Lazarova^{1*}, D. Kovacheva¹, Z. Cherkezova-Zheleva², G. Tyuliev²

¹*Institute of General and Inorganic Chemistry, Bulgarian Academy of Sciences,
Acad. G. Bonchev str., Bl 11, Sofia-1113, Bulgaria,*

²*Institute of Catalysis, Bulgarian Academy of Sciences,
Acad. G. Bonchev str., Bl 11, Sofia-1113, Bulgaria*

Received November 10, 2016; Revised January 3, 2017

Nanosized MnFe_2O_4 has important applications such as magnetic recording devices, ferrofluids, biosensors, catalysts, guided transport and delivery of drugs in the body and others. The possibilities to obtain nanosized MnFe_2O_4 using the method of solution combustion synthesis are studied in this work. Two systems with mixed fuels in various ratios, namely glycine-glycerol and sucrose-urea are studied. The obtained products are thermally treated at various temperatures and in various atmospheres (air, argon) to find optimal conditions for obtaining single phase nano-sized MnFe_2O_4 . Samples were studied by the methods of X-ray diffraction (XRD), X-ray photoelectron spectroscopy (XPS), low-temperature nitrogen adsorption (BET), and Mössbauer spectroscopy. Samples obtained by using pure hydrocarbons or mixtures with high content of hydrocarbons show superparamagnetic behavior due to the small size of the crystallites while samples obtained with high content of nitrogen containing fuels show magnetic ordering. It was shown that smaller particles obtained at low temperatures of thermal treatment demonstrate higher strain. Thermal treatment at higher temperatures leads to decrease of the strain without significant change of the size of the crystallites.

Keywords: *solution combustion synthesis, MnFe_2O_4 , XRD, XPS, Mössbauer spectroscopy*

INTRODUCTION

Nanoscale and nanostructured materials are among the most important priorities of modern materials science. In recent years, various technological applications based on nano-sized ferrite materials were developed using of their unique magnetic, electrical and optical properties. An important representative of the ferrite family is MnFe_2O_4 . It is well known that it is partially inverse spinel, in which about 20% of Mn^{2+} ions occupy octahedral sites (B) and 80% of them are located in tetrahedra (A). Cation distribution in spinels is very important and directly affects its physical properties [1, 2]. In recent years nano-sized MnFe_2O_4 has received increasing research interest because of its remarkable magnetic properties (low coercivity, moderate magnetization) combined with good chemical resistance, high permeability and mechanical strength [3]. The high density of MnFe_2O_4 underlies its technological applications as core materials for coils, transformers, information and communication devices and others [4]. Nanoscale MnFe_2O_4 is interesting for other practical applications, namely as contrast agent for magnetic resonance imaging, magnetic drug delivery for

cancer treatment by hyperthermia and others [5 - 7]. Another important application of nano-sized MnFe_2O_4 in the last decade is the removal of heavy metals and a variety of toxic organic pollutants from waste water [8, 9]. The use of nano-sized manganese ferrite as a sensor for monitoring the environment is based on its high specific surface area. The same fact lies at the basis of the use of this material as a catalyst [10, 11] and as electrode material in asymmetric supercapacitors [12, 13]. Physical and chemical properties of MnFe_2O_4 are strongly dependent on its structural and micro-structural characteristics that are directly related to and can be controlled during the synthesis process [14]. Various methods for preparing nano-sized MnFe_2O_4 have been developed, such as sol-gel [15], co-precipitation [16], hydrothermal method [17], solid state reaction [18, 19], thermal decomposition [20], solution combustion synthesis [21, 22], mechanochemical reaction [23], etc. Among them solution combustion synthesis is considered as very appropriate for preparation of nano-sized materials due to the fact that this method is simple, fast, versatile, and cost-effective [24]. In our previous study concerning the preparation of nano-sized NiFe_2O_4 using the solution

* To whom all correspondence should be sent.
E-mail: cveti_ura@abv.bg

combustion method was found that the type of the fuel component has an influence both on structural characteristics (cation distribution) and on the morphological characteristics (size and shape of the particles, aggregation ability, etc.) [25]. The aim of this work was to study the influence of mixing of different types of fuel (nitrogen-containing and hydrocarbons) at different ratios in the systems of fuels: sucrose-urea and glycine-glycerol for preparing a single phase $MnFe_2O_4$ and to study the influence of mixing of different types of fuels on structural and morphological characteristics of the obtained powders.

MATERIALS AND METHODS

The method of solution combustion synthesis was used to obtain nano-sized $MnFe_2O_4$. Metal nitrates (oxidizers) and fuels sucrose, urea, glycine, and glycerol in various ratios were used. The ratio of the amounts of oxidant and fuel was based on the proposed by Jain *et al* theory [26]. Stoichiometric amounts of the starting reagents were dissolved in an appropriate amount of deionized water. The resulting solutions were heated on a magnetic stirrer. Initially, the solution was dehydrated, and then the residue reaches its point of ignition and ignites. The obtained powders were then thermally treated at various temperatures from 400 to 700°C for one hour in a different atmosphere (air, argon). Structural characteristics of all samples were studied with powder X-ray diffractometer Bruker D8 Advance with $Cu-K\alpha$ radiation and LynxEye detector. Powder diffraction patterns were collected in the range from 10 to 90 deg. 2θ with a step 0.03 deg. 2θ rotating the sample with 15 rpm. Phase analysis was performed with the software package Diffracplus EVA using the database ICDD-PDF2 (2014). The unit cell parameters and mean crystallite sizes were determined with the program Topas - 4.2 [27]. The specific surface areas (SSA) was determined by low temperature nitrogen adsorption (BET) method in an equipment Quantachrome Instruments NOVA 1200e (USA). The particle size and morphology were studied by a transmission electron microscopy (TEM) with a TEM JEOL 2100 at 200 kV. The XPS measurements were carried out in the analysis chamber of the electron spectrometer Escalab-MkII (VG Scientific) with a base pressure of $\sim 5 \times 10^{-8}$ Pa. The C1s, O1s, Mn2p, Fe2p and Mn3s photoelectron lines were evaluated by using the normalized photoelectron intensities [28]. Mössbauer spectra were recorded on electromechanical spectrometer

(Wissenschaftliche Elektronik GMBN, Germany) operating under constant acceleration at room temperature. As a source $^{57}Co/Cr$ was used (Activity >50 mCi). The standard material was α -Fe. The spectra were processed using a program based on the least squares method.

RESULTS AND DISCUSSION

The possibilities for obtaining nano-sized $MnFe_2O_4$ were studied when as a fuel were used mixture of sucrose-urea or glycin-glycerol in various ratios, namely: 1:0, 0.75:0.25; 0.5:0.5, 0.25:0.75 and 0:1. All samples were thermally treated for one hour at a temperature ranging between 400 and 700°C in air and in argon atmosphere. The obtained materials were analyzed by powder X-Ray diffraction. Table 1 and Table 2 show the results for phase composition of these samples. As can be seen from Table 1 single-phase product was obtained when using only sucrose as a fuel and for the sucrose-urea fuel mixtures, for fuel compositions with higher sucrose content. Preparation of single-phase product using urea as a fuel was not observed. In the second fuel system, the formation of single phase nano-sized $MnFe_2O_4$ was observed when using glycerol as fuel and for fuel compositions with higher glycerol content. Formation of single phase $MnFe_2O_4$ using only glycine as a fuel was not observed. In all the samples thermally treated at a temperatures above 600°C in both atmospheres (air, argon) a decomposition of the spinel phase to the individual oxides (Fe_2O_3 -hematite and Mn_2O_3 -bixbite) was observed. It deserves commenting that samples prepared with high content of nitrogen-containing fuels show impurity phase of oxides of divalent ions (Fe^{2+} , Mn^{2+}) which indicates that synthesis reaction proceeds at high temperatures and with the release of gases that promote the reduction of metal ions. These observations leads to the conclusion that single-phase nano-sized $MnFe_2O_4$ can be synthesized using either pure hydrocarbons (sucrose, glycerol) as a fuel or having fuel mixtures with high content of hydrocarbons.

From the data presented in Table 1 and Table 2 it may be concluded that single phase spinel product can be obtained at temperatures below 600°C from fuel mixtures containing high content of hydrocarbons. In Fig. 1 (a-d) are presented powder diffraction patterns of some $MnFe_2O_4$ synthesized using a mixture of fuels (a, b) sucrose-urea, (c, d) glycine-glycerol. All diffraction lines can be indexed within the cubic Space group $Fd-3m$.

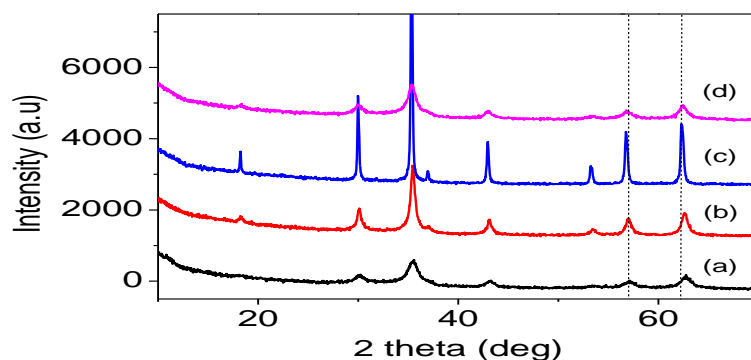


Fig. 1. XRD patterns of nanosized MnFe₂O₄ synthesized by (a) sucrose-urea 0.75:0.25 at 500°C, (b) sucrose-urea 0.25:0.75 at 500°C, (c) glycine-glycerol 0.75:0.25 at 400°C (Ar) and (d) glycine-glycerol 0.25:0.75 at 500°C (Ar).

Table 1. Phase composition of samples synthesized with mixture of sucrose and urea at different ratios, thermally treated at 400 to 700°C in Air and Argon atmosphere. Identified phases were manganese ferrite spinel-MnFe₂O₄, bixbite-Mn₂O₃, hematite-Fe₂O₃ and wustite (Fe,Mn)O.

Air		Argon	
Fuel/Temperature	Identified phases	Fuel/Temperature	Identified phases
<i>sucrose</i>		<i>sucrose</i>	
400°C	spinel	400°C	spinel
500°C	spinel	500°C	spinel
600°C	bixbite + hematite	600°C	spinel + wustite
700°C	bixbite + hematite	700°C	spinel + wustite
<i>sucrose and urea</i> <i>0.75:0.25</i>		<i>sucrose and urea</i> <i>0.75:0.25</i>	
400°C	spinel	400°C	spinel
500°C	spinel	500°C	spinel
600°C	bixbite + hematite	600°C	spinel + bixbite + hematite
700°C	bixbite + hematite	700°C	Traces of spinel + bixbite + hematite
<i>sucrose and urea</i> <i>0.5:0.5</i>		<i>sucrose and urea</i> <i>0.5:0.5</i>	
400°C	spinel	400°C	spinel
500°C	spinel	500°C	spinel
600°C	bixbite + hematite	600°C	spinel + hematite
700°C	bixbite + hematite	700°C	spinel + bixbite + hematite
<i>sucrose and urea</i> <i>0.25:0.75</i>		<i>sucrose and urea</i> <i>0.25:0.75</i>	
400°C	spinel	400°C	spinel
500°C	spinel	500°C	spinel
600°C	bixbite + hematite	600°C	traces of spinel + hematite
700°C	bixbite + hematite	700°C	traces of spinel + bixbite + hematite
<i>urea</i>		<i>urea</i>	
400°C	spinel + bixbite	400°C	spinel
500°C	spinel + bixbite + hematite	500°C	spinel + hematite
600°C	bixbite + hematite	600°C	spinel + hematite
700°C	bixbite + hematite	700°C	spinel + hematite

Table 2. Phase composition of samples synthesized with mixture of glycine and glycerol at different ratios, thermally treated at 400 to 700°C in Air and Argon atmosphere. Identified phases were manganese ferrite spinel-MnFe₂O₄, bixbite-Mn₂O₃, hematite-Fe₂O₃ and wustite (Fe,Mn)O.

Air		Argon	
Fuel/Temperature	Identified phases	Fuel/Temperature	Identified phases
glycine		glycine	
400°C	spinel + wustite	400°C	spinel + wustite
500°C	traces of spinel+ bixbite+ hematite	500°C	spinel + wustite
600°C	traces of spinel + bixbite + hematite	600°C	spinel + hematite
700°C	bixbite + hematite	700°C	spinel + hematite
glycine and glycerol 0.75:0.25		glycine and glycerol 0.75:0.25	
400°C	three unknown spinels	400°C	spinel
500°C	three unknown spinels	500°C	spinel+ hematite + maghemite
600°C	bixbite + hematite	600°C	traces of spinel+ bixbite + hematite
700°C	bixbite + hematite	700°C	traces of spinel + bixbite + hematite
glycine and glycerol 0.5:0.5		glycine and glycerol 0.5:0.5	
400°C	spinel	400°C	spinel
500°C	spinel	500°C	spinel + hematite
600°C	bixbite + hematite	600°C	traces of spinel+ bixbite + hematite
700°C	bixbite + hematite	700°C	traces of spinel bixbite + hematite
glycine and glycerol 0.25:0.75		glycine and glycerol 0.25:0.75	
400°C	spinel	400°C	spinel
500°C	spinel	500°C	spinel
600°C	bixbite + hematite	600°C	traces of spinel+ bixbite + hematite
700°C	bixbite + hematite	700°C	traces of spinel+ bixbite + hematite
glycerol		glycerol	
400°C	spinel	400°C	spinel
500°C	spinel + traces of hematite	500°C	spinel
600°C	bixbite + hematite	600°C	traces of spinel+ bixbite + hematite
700°C	bixbite + hematite	700°C	traces of spinel + bixbite + hematite

Diffraction patterns indicate the formation of single-phase spinels, but also reveal that materials, obtained with different fuel mixture differ strongly by their mean crystallite size and unit cell parameters. This fact indicates that the mixture of fuels produces different synthesis conditions thus leading to the production of materials with different structural and morphological characteristics.

A significant difference in particles morphology can be seen from the TEM-photographs of the materials synthesized with the use of different fuel

mixtures. Fig. 2 represents the TEM images of MnFe₂O₄ synthesized using a mixture of sucrose-urea (a, b) and glycine-glycerol (c, d) fuels. TEM images show poorly shaped particles with an average size smaller than 10 nm for the materials obtained with the use fuel mixture of sucrose-urea and glycine-glycerol with high hydrocarbons content. The exception is the sample from glycine-glycerol fuel system with high content of glycine (Fig. 2c), where the average size is about 50 nm.

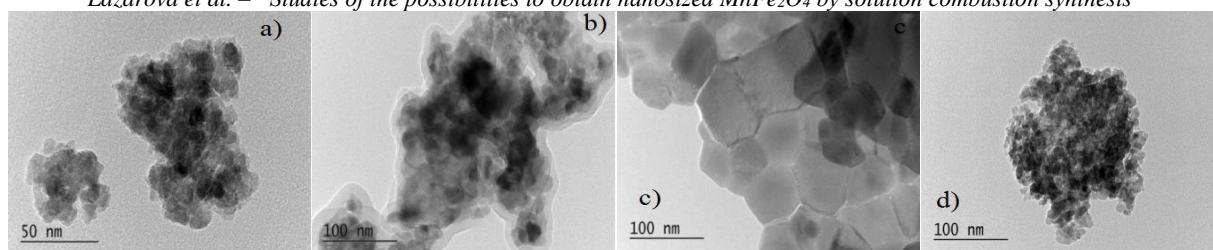


Fig. 2. TEM image of nano-sized MnFe₂O₄ synthesized by using a mixture of fuels: (a) sucrose-urea 0.75:0.25 at 500°C, (b) sucrose-urea 0.25: 0.75 at 500°C, (c) glycine-glycerol 0.75: 0.25 at 400°C (Ar) and (d) glycine-glycerol 0.25:0.75 at 500°C (Ar).

Table 3. Structural parameters determined by XRD analysis of nano-sized MnFe₂O₄ synthesized by using mixture of sucrose and urea fuels in different ratio and thermally treated in Air or Argon atmosphere.

fuel	temperature °C	unit cell parameter (Å)	mean crystallite size, nm	SSA, m ² /g / mean size derived from BET, nm	Strain x10 ⁻⁴
<i>sucrose</i>	400 °C	8.35	5.7		69.17
	500 °C	8.34	6.4	88/12.7	56.82
<i>sucrose and urea 0.75:0,25</i>	400 °C	8.35	6.9		52.46
	500 °C	8.379	19.1	85/13.15	13.96
<i>sucrose and urea 0,5:0,5</i>	400 °C	8.38	15.8	44 /25.4	18.94
	500 °C	8.379	20.04	39/28.66	16.32
<i>sucrose and urea 0.25:0.75</i>	400 °C	8.38	20.57		17.99
	500 °C	8.352	6.6	40/27.9	44.92
<i>sucrose (Argon)</i>	400 °C	8.439	5.9	85/13.15	51.39
	500 °C	8.5142	14.2	44/25.4	25.76
<i>sucrose and urea 0.75:0.25 (Argon)</i>	400 °C	8.387	6.8		44.83
	500 °C	8.401	7.8	98/11.5	37.07
<i>sucrose and urea 0.5:0.5 (Argon)</i>	400 °C	8.500	13.3		15.06
	500 °C	8.499	26.1	54/20.7	33.97
<i>sucrose and urea 0.25:0.75 (Argon)</i>	400 °C	8.456	7.2		30.7
	500 °C	8.461	6.8	82/13.63	61.3

Table 4. Structural parameters determined by XRD analysis of nanosized MnFe₂O₄ synthesized by using mixture of glycine and glycerol fuels in different ratio and thermally treated in air or argon atmosphere.

fuel	temperature °C	unit cell parameter Å	mean crystallite size, nm	SSA, m ² /g / mean size derived from BET, nm	Strain x10 ⁻⁴
<i>glycine and glycerol 0.5:0.5</i>	400 °C	8.37	11		19.33
	500 °C	8.38	12		11.44
<i>glycine and glycerol 0.25:0.75</i>	400 °C	8.37	12		8.06
	500 °C	8.38	15	60 /18.63	7.85
<i>glycerol</i>	400 °C	8.37	11		13.03
<i>glycine and glycerol 0.75:0.25 (Argon)</i>	400 °C	8.4208	59	11/102	6.04
<i>glycine and glycerol 0.5:0.5 (Argon)</i>	400 °C	8.38	10		36.19
<i>glycine and glycerol 0.25:0.75 (Argon)</i>	400 °C	8.45	9.7	96/11.64	37.42
	500 °C	8.41	10.4	86/13	11.52
<i>Glycerol (Argon)</i>	400 °C	8.44	13		45.32
	500 °C	8.40	13		13.05

Table 3 and Table 4 show the unit cell parameters, mean coherent domain sizes and microstrains for all single-phase samples, and for some of them the specific surface areas. Samples obtained from both fuel systems and thermally treated in argon atmosphere show spinel phase with higher unit cell parameters and higher specific surface areas than those thermally treated in air atmosphere. At the same time the mean crystallite domain sizes of the samples treated in different atmospheres show similar values.

The data presented in Table 3 and Table 4 show correlation between unit cell parameters, mean crystallite sizes and residual microstrains. In general, samples with small unit cell parameters have also small mean crystallite size and high values of lattice strain. Thermal treatment at higher temperatures leads to

decrease of the strain without significant change of the size of the crystallites. The differences in unit cell parameters can be due to differences of oxidation state of cations, as well as to different cation distributions into two cation sublattices in the spinel structure (tetrahedral and octahedral).

The Mn2p and Fe2p photoelectron lines are shown on Fig. 3. The Mn2p_{3/2} binding energy value of 642.0 eV is slightly higher than expected for Mn²⁺ i.e. 641.3 eV [29, 30]. In addition, the absence of satellite at ~ 647 eV is an indication for the possible presence of Mn in oxidation state higher than 2+ due to air exposure after samples preparation. The Fe2p_{3/2} main line has maximum at 711.0 eV, a value characteristic of Fe³⁺ as in Fe₂O₃ [31].

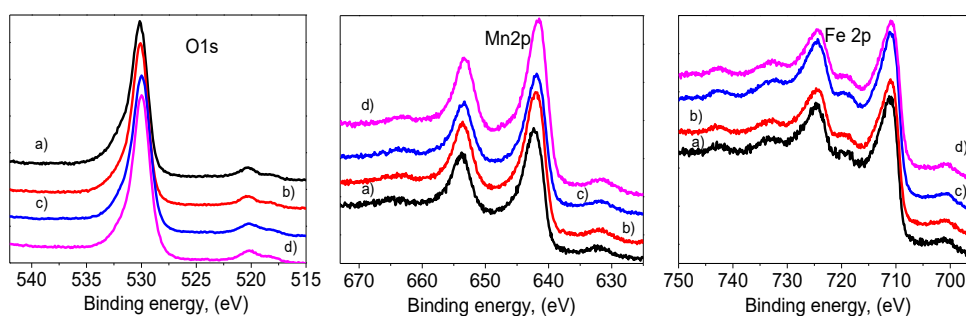


Fig. 3. O1s, Mn2p and Fe2p photoelectron lines for MnFe₂O₄ samples synthesized by (a) sucrose-urea 0.75:0.25 at 500°C, (b) sucrose-urea 0.25: 0.75 at 500°C, (c) glycine-glycerol 0.75: 0.25 at 400°C (Ar) and (d) glycine-glycerol 0.25:0.75 at 500°C (Ar).

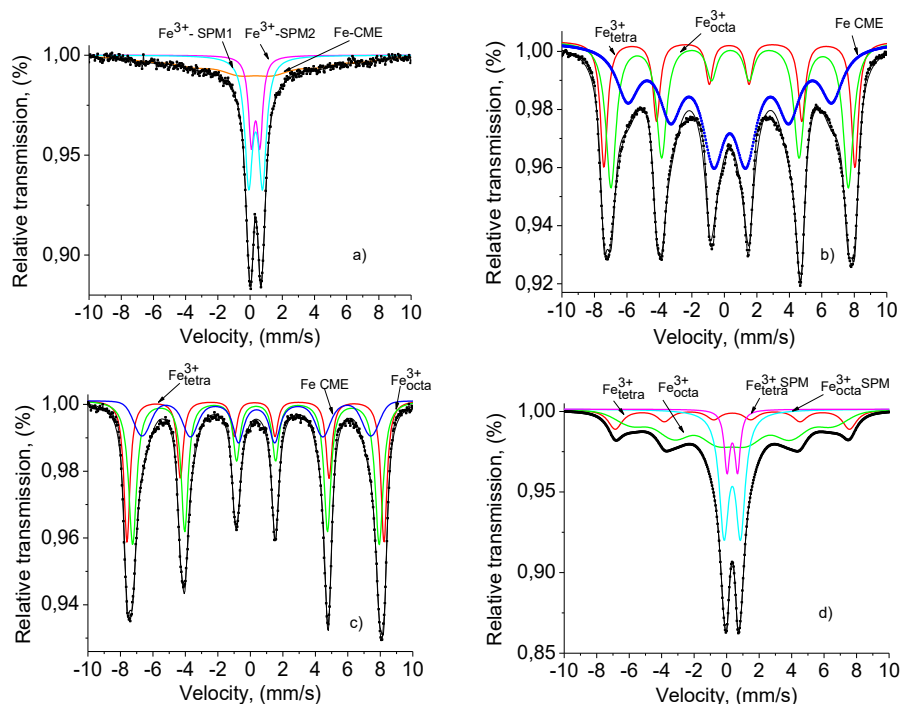


Fig. 4. The Mössbauer spectra of MnFe₂O₄ synthesized by (a) sucrose at 500°C (Ar), (b) sucrose-urea 0.5:0.5 at 500°C, (c) glycine-glycerol 0.75: 0.25 at 400°C (Ar) and (d) glycine-glycerol 0.25:0.75 at 500°C (Ar).

The Fe³⁺ ions can be distinguished also by the small satellite appearing at higher binding (~8.5 eV above the main line). The position of O1s peak practically does not change for all samples and has a binding energy of 530.0 eV, a value typical for lattice oxygen in transition metal oxides. The higher binding energy shoulder is usually assigned to species adsorbed on surface defect structures, OH group and/or adsorbed water.

The Mössbauer spectra at room temperature of some of synthesized samples are shown on Fig. 4. It can be seen that all the experimental spectra are complicated and include unresolved components. Two of materials, MnFe₂O₄ synthesized by sucrose-urea 0.5:0.5 and glycine-glycerol 0.75:0.25 (Ar), have only sextet components i.e. magnetic structure. The spectra of MnFe₂O₄ synthesized by sucrose (Ar) and glycine-glycerol 0.25:0.75 (Ar), contain both doublet and sextet components. The calculated hyperfine parameters IS and QS suggest the presence of spinel ferrite material with critically small particle size. This leads to registration of relaxation effects as superparamagnetism (SPM) and collective magnetic excitation behavior (CME) [32, 33].

CONCLUSION

Single phase nanosized spinel manganese ferrites were prepared by solution combustion method using two mixtures of fuels urea-sucrose and glycine-glycerol in different ratios. The type of fuel has a strong influence on the possibilities to obtain single-phase product. The analyses indicate that single-phase product was obtained using pure hydrocarbons as fuel or fuel mixtures with high content of hydrocarbons. The spinel phase decomposes to individual oxides at temperatures above 600°C despite the atmosphere of thermal treatment. Samples obtained by using pure hydrocarbons or mixtures with high content of hydrocarbons show superparamagnetic behaviour due to the small size of the crystallites while samples obtained with high content of nitrogen containing fuels show magnetic ordering. It was shown that smaller particles obtained at low temperatures of thermal treatment demonstrate higher strain. Thermal treatment at higher temperatures leads to decrease of the strain without significant change of the size of the crystallites.

Acknowledgment: This work is performed with the financial support of the Program for career development of young scientists, BAS and

National Science Fund of Bulgaria under the contract DFNI E02/18.

REFERENCES

1. M.Y. Rafique, P.L.Qing, Q. Javed, M.Z. Iqba, Q.H. Mei, M.H. Farooq, G.Z.Gang, M. Tanveer, *Chin. Phys. B* **22** (10), 107101 (2013).
2. N.M. Deraz, A. Alarifi, *Int. J. Electrochem. Sci.* **7**, 5534 (2012).
3. A. Goldman, *Modern Ferrite Technology*, Marcel Dekker, New York 54, (1993).
4. D. Shi, B. Aktas, L.Pust, F. Mikailov, *Nanostructured Magnetic Materials and Their Applications* **593**, (2002).
5. S. Seifikar, B. Calandro, E. Deeb et al., *Journal of Applied Physics* **112**, 12391 (2012).
6. S. Seifikar, A. Tabei, E. Sachet et al., *Journal of Applied Physics* **112**, 063908, (2012).
7. S. Shafiu, R. Topkaya, A. Baykal, M.S. Toprak, *Materials Research Bulletin* **48**, 4066 (2013).
8. L. X. Yang, F. Wang, Y. F. Meng, Q. H. Tang, Z. Q. Liu, *J. Nanomater.* 263 (2013).
9. N. Mahmoodi, *J Environ Eng.* **139** (11), 1382 (2013).
10. N. M. Mahmoodi, M. Arabloo, J. Abdi, *Water Res.* **67**, 216 (2014).
11. T. V. Solis, P. Tartaj, G. Marban, A. B. Fuertes, *Catal Commun* **8**, 2037 (2007).
12. S. L. Kuo, N. L. Wu, *Electrochem. Solid-State Lett.* **8**, A495 (2005).
13. S. L. Kuo, J. F. Lee, N. L. Wu, *J. Electrochem. Soc.* **154**, A34 (2007).
14. J. Wang, Q. Chen, B. Hou, Z.Peng, *J. Inorg Chem.* **6**, 1165 (2004).
15. L. Jianjun, Y. Hongming, L. Guodong, L. Yanju, L. Jinsong, *J. Magn. Magn Mater* **322**, 3396 (2010).
16. J. Amighian, M. Mozaffari, B. Nasr, *Phys. Status Solidi C3*, 3188 (2006).
17. P. A. Seema Verma, Y. B. Joy, H. S. Kholam, S.B. Potdar, *Mater.Lett.* **58**, 1092 (2004).
18. H. H. Kedesdy, A. Tauber, *J Am Ceram Soc.* **39**, 425 (1956).
19. T. K. Kundu, S. Mishra, *Bull Mater Sci.* **31**, 507 (2008).
20. H. Yang, C. Zhang, X. Shi, H. Hu, X. Du, Y. Fang, Y. Ma, H. Wu, S. Yang, *Biomaterials* **31**, 3667 (2010).
21. K. Suresh, N. R. S. Kumar, K. C. Patil, *Adv. Mater.* **3**, 148 (1991).
22. S. Sam, A. Samson Nesaraj, *International Journal of Applied Science and Engineering* **9**, (4) 223 (2011).
23. P. Osmokrovi, C. Jovaleki, D. Manojlovi, M. B. Pavlovi, *Journal of optoelectronics and advanced materials* **8**, 312 (2006).
24. K.C. Patil, S. T.Aruna, S. Ekambaram, *Solid State &Materials Science* **2**, 158 (1997).
25. Ts. Lazarova, M. Georgieva, D. Tzankov, D. Voykova, L. Aleksandrov, Z. Cherkezova-

- T.S. Lazarova et al.: "Studies of the possibilities to obtain nanosized MnFe₂O₄ by solution combustion synthesis"*
Zheleva, D. Kovacheva, *Journal of Alloys and Compounds*, in press.
26. S. R. Jain, K. C. Adiga, V. R. Pai Vernekar, *Combustion and Flame* **40**, 71 (1981).
27. Bruker TOPAS, Version 4.2, Bruker AXS, Karlsruhe, Germany (2007).
28. J. H. Scofield, *Journal of electron spectroscopy and related phenomena* **8**, (2) 129 (1976).
29. M. A. Langell, C. W. Hutchings, G. A. Carson, M. H. Nassir, *J. Vac. Sci. Technol. A* **14**, 1656 (1996).
30. D. Kovacheva, T. Trendafilova, K. Petrov A. Hewat, *Journal of Solid State Chemistry*, **169**, 44 (2002).
31. T. Yamashita, P. Hayes, *Applied Surface Science* **254**, 2441 (2008).
32. F. L. Deepak, M. Bañobre-López, E. Carbo-Argibay, M. Cerqueira, Y. Piñeiro-Redondo, J. Rivas, C. M. Thompson, S. Kamali, C. Rodriguez-Abreu, K. Kovnir, Y. V. Kolen'ko, *J. Phys. Chem. C* **119**, (21) 11947 (2015).
33. A. Yang, C. N. Chinnasamy, J. M. Greneche, Y. Chen, S. D. Yoon, Z. i Chen, K. Hsu, Z. Cai, K. Ziemer, C. Vittoria, V. G. Harris, *Nanotechnology* **20**, 185704 (2009).

ИЗСЛЕДВАНЕ НА ВЪЗМОЖНОСТИТЕ ЗА ПОЛУЧАВАНЕ НА НАНОРАЗМЕРЕН MnFe₂O₄ ПРИ СИНТЕЗ ПО МЕТОДА НА ИЗГАРЯНЕ ОТ РАЗТВОР

Цв. Лазарова¹, Д. Ковачева¹, З. Черкезова-Желева², Г. Тюлиев²

¹Институт по обща и неорганична химия, Българска академия на науките,
ул. акад. Г. Бончев, Бл 11, София-1113, България, sveti_ura@abv.bg

²Институт по катализ, Българска академия на науките,
ул. акад. Г. Бончев, Бл 11, София-1113, България

Постъпила на 10 ноември 2016 г.; приета на 3 януари 2017 г.

(Резюме)

Наноразмерният MnFe₂O₄ има важни приложения в устройства за магнитен запис, ферофлуиди, биосензори, катализатори, направляван транспорт на лекарства в организма и др. В работата се изучават възможностите за получаване на наноразмерни MnFe₂O₄ по метода на синтез чрез изгаряне от разтвор. Изучени са две системи със смесени горива в различни съотношения, а именно глицин-глицерол и захароза-урея. Получените продукти са подложени на термична обработка при различни температури и в различни среди (въздух, аргон), за да се намерят оптималните условия за получаване на монофазен наноразмерен MnFe₂O₄. Образците са изследвани с методите на рентгеновата дифракция, нискотемпературна адсорбция на азот (БЕТ), фотоелектронна и Мьосбауерова спектроскопия. Образците, получени чрез използване на чисти въглеродороди или смеси с високо съдържание на въглеродороди показват суперпарамагнитно поведение поради малкия размер на кристалите, докато тези, получени с високо съдържание на азотсъдържащи горива показват магнитно подреждане. Показано е, че по-малките частици, получени при ниски температури на термична обработка имат по-високи стойности на решетъчните напрежения. Термична обработка при високи температури води до намаляване на напреженията без значителна промяна на размера на кристалите.

Ключови думи: синтез чрез изгаряне от разтвор, MnFe₂O₄, XRD, XPS, Мьосбауерова спектроскопия.

Synthesis and stability of zinc hydroxide nitrate nanoparticles

K. I. Ivanov*, E. N. Kolentsova, N. Cao Nguyen, A. B. Peltekov, V. R. Angelova

Department of Chemistry, Agricultural University, 4000 Plovdiv, Bulgaria

Received October 24, 2016; Revised January 3, 2017

The nanosized zinc hydroxide nitrate has been recently estimated as prospective foliar fertilizer, possessing improved zinc solubility, but low phytotoxicity, in comparison with ZnO and other Zn-containing compounds. The main problem is obtaining stable particles with dimensions less than 100 nm. This work studies the effect of preparation conditions on the chemical compositions and particle size of the zinc hydroxide nitrates prepared by precipitation. $\text{Zn}(\text{NO}_3)_2 \cdot 6\text{H}_2\text{O}$ and NaOH were used with concentrations ranging from 0.4 to 3.2 M and the initial OH/Zn ratio of 1.6 at temperatures from 20 to 60°C. All samples were characterized in detail by X-ray diffraction, scanning electron microscopy, thermal analysis, and inductively coupled plasma (ICP). Stability and distribution of the zinc hydroxide nitrate particles were estimated too.

Keywords: Zinc hydroxide nitrate, nanoparticles, preparation, foliar fertilizer.

INTRODUCTION

The layered double hydroxides (LDH) family of materials are important compounds with the general formula of $[\text{M}^{\text{II}}_{1-x}\text{M}^{\text{III}}_x(\text{OH})_2]^{x+}[\text{A}^{n-}]_{x/n} \cdot m\text{H}_2\text{O}$ where M^{II} and M^{III} are di- and trivalent metals, and A^{n-} is an anion (e.g. nitrate) [1]. As modified form of LDH, hydroxide double salts (HDS) with a general formula of $[\text{M}^{\text{II}}_{1-x}\text{M}^{\text{II}}_{2x}(\text{OH})_2]^{2x+}[\text{A}^{n-}]_{2x/n} \cdot m\text{H}_2\text{O}$ exist, which contain two divalent cations. In case the cations in HDS are the same, the salts are known as “basic salts” [2]. They are precursors for useful materials such as UV absorbents in sunscreen formulations [3] and matrices for immobilization of metal complexes and dyes [4]. Recently, HDS have been intensively studied as potential long-term foliar fertilizers [5, 6]. Zinc hydroxide nitrate ($\text{Zn}_5(\text{OH})_8(\text{NO}_3)_2 \cdot 2\text{H}_2\text{O}$) seems to be the most promising in this respect. The crystal suspension maintains a Zn^{2+} concentration of 30–50 mg/l which is enough for suffusion leaf uptake without phytotoxicity [7]. Four forms of zinc hydroxide nitrate are known in the scientific literature: $\text{Zn}_5(\text{OH})_8(\text{NO}_3)_2 \cdot 2\text{H}_2\text{O}$, $\text{Zn}_5(\text{OH})_8(\text{NO}_3)_2$, $\text{Zn}_3(\text{OH})_4(\text{NO}_3)_2$ and $\text{Zn}(\text{OH})(\text{NO}_3)_2 \cdot \text{H}_2\text{O}$. The last one is not layered [8]. Many efforts are devoted to the preparation of free of impurities nanosized $\text{Zn}_5(\text{OH})_8(\text{NO}_3)_2 \cdot 2\text{H}_2\text{O}$. It is generally accepted that zinc hydroxide nitrate with the ideal composition $\text{Zn}_5(\text{OH})_8(\text{NO}_3)_2 \cdot 2\text{H}_2\text{O}$ can be prepared by precipitation from a solution of $\text{Zn}(\text{NO}_3)_2 \cdot 6\text{H}_2\text{O}$ with NaOH (OH/Zn ratio 0.5) at room temperature with vigorous stirring. It was found that increasing the OH/Zn ratio, or the reaction temperature, resulted in the formation of ZnO or $\text{Zn}(\text{OH})(\text{NO}_3)_2 \cdot \text{H}_2\text{O}$, in addition to the desired product [7, 8]. The main misadventure of the procedure is the limitation of the

OH/Zn ratio, which predicts substantial concentration of Zn^{2+} in the mother liquor. Therefore, the main objective of this research is to develop and optimize the preparation of zinc hydroxide nitrate, $\text{Zn}_5(\text{OH})_8(\text{NO}_3)_2 \cdot 2\text{H}_2\text{O}$, with nanosized dimensions and to evaluate the shelf life of prepared crystals in suspension.

EXPERIMENTAL

Preparation procedure

Materials: Zinc nitrate hexahydrate $\text{Zn}(\text{NO}_3)_2 \cdot 6\text{H}_2\text{O}$ and NaOH reagent grade were used in the present experiments.

Synthesis: Preparation of zinc hydroxide nitrate ($\text{Zn}_5(\text{OH})_8(\text{NO}_3)_2 \cdot 2\text{H}_2\text{O}$) was performed by pouring NaOH solution into $\text{Zn}(\text{NO}_3)_2 \cdot 6\text{H}_2\text{O}$ under vigorous stirring. The initial OH/Zn molar ratio was 1.6 (corresponding to stoichiometric OH/Zn molar ratio) and the time of precipitation was 10 minutes in all cases (to prevent transformation of the synthesized zinc hydroxide nitrate to ZnO). Five series of samples (Table 1) were synthesized under the following conditions: a solution containing 120 mmol of NaOH with concentration ranged from 0.4 M to 3.2 M was poured in a solution containing 75 mmol of $\text{Zn}(\text{NO}_3)_2 \cdot 6\text{H}_2\text{O}$ with concentration ranged from 0.4 M to 3.2 M under vigorous stirring.

In order to evaluate the influence of the temperature on the parameters of the resulting zinc hydroxide nitrate, more experiments were performed under different conditions, including increasing the temperature to 70 °C and monitoring the precipitate in the mother liquor for one month. The white precipitate was filtered, washed with deionized water and dried at 65°C for 24 h. The scheme of the experiments is presented in Table 1.

* To whom all correspondence should be sent.
E-mail: kivanov1@abv.bg

Powder X-Ray Diffraction (XRD)

The XRD patterns were recorded on a Philips PW 1050 diffractometer, equipped with Cu K α tube and a scintillation detector. Data for cell refinements was collected in θ -2 θ , step-scan mode in the angle interval from 10 to 90° (2 θ) at counting time of 3 s/step and steps of 0.03° (2 θ).

Scanning Electron Microscopy (SEM)

SEM images were recorded in a JSM 6390 electron microscope (Japan) in conjunction with energy dispersive X-ray spectroscopy (EDS, Oxford INCA Energy 350) equipped with ultrahigh resolution scanning system (ASID-3D) in a regime of secondary electron image (SEI) and backscattered electrons (BEC). The samples were coated with gold before imaging.

Chemical Analysis

ICP-AES (Prodigy 7, Leeman) was applied to quantify the zinc content in the solid products and filtrates. The pH values were monitored by a pH meter WTW inoLab® pH 7110 (Germany).

RESULTS

The Influence of the main parameters of the synthesis on the chemical composition and morphology of the resulting samples were monitored.

Influence of initial concentration

Chemical Composition

Twenty five samples were prepared according to the scheme presented in Table 1, and zinc content and weight loss (ΔG , %) were determined for each of them. The weight loss was calculated after calcination of the samples for 2 hours at 450°C. The results are presented in Table 2.

The theoretical value of zinc content in the dried at 65°C zinc hydroxide nitrate, calculated for the formula $Zn_5(OH)_8(NO_3)_2 \cdot 2H_2O$, is 52.47%. According to the data of [9] complete decomposition of $Zn_5(OH)_8(NO_3)_2 \cdot 2H_2O$ to ZnO ends at 300°C with the weight loss of 34.7%.

A weight loss less than this and zinc content more than 52.47% indicates the presence of impurities with a higher content of zinc (ZnO, $Zn_3(OH)_4(NO_3)_2$ or $Zn(OH)(NO_3) \cdot H_2O$). The results presented in Table 2 correspond very closely to the theoretical ones and suggest the formation of $Zn_5(OH)_8(NO_3)_2 \cdot 2H_2O$ in all cases. This suggestion was verified by X-ray and SEM analysis of the fresh samples after filtration and washing with distilled water. Some of these results are shown in Figs. 1-4.

Table 1. Scheme of the experiment

Series	S-1	S-2	S-3	S-4	S-5
Zn(NO ₃) ₂ ·6H ₂	0.4	1.2	1.6	2.4	3.2
O, mol/l	M	M	M	M	M
	0.4	0.4	0.4	0.4	0.4
	M	M	M	M	M
	1.2	1.2	1.2	1.2	1.2
NaOH, mol/l	M	M	M	M	M
NaOH, mol/l	1.6	1.6	1.6	1.6	1.6
NaOH, mol/l	M	M	M	M	M
NaOH, mol/l	2.4	2.4	2.4	2.4	2.4
NaOH, mol/l	M	M	M	M	M
	3.2	3.2	3.2	3.2	3.2
	M	M	M	M	M

Table 2. Chemical composition (Zn, %) and weight loss at 450°C (ΔG ,%) of the samples synthesized at room temperature

Series	S-1	S-2	S-3	S-4	S-5
Zn,%	52.3±0.8	51.3±0.9	52.7±0.5	53.1±0.8	52.4±0.6
ΔG ,%	34.48	34.57	34.63	34.3	34.8
Zn,%	53.1±0.8	53.4±0.8	51.9±0.8	52.3±0.9	52.7±0.7
ΔG ,%	34.53	34.66	34.34	34.85	34.95
Zn,%	52.6±0.8	53.3±0.9	51.9±0.4	52.1±0.6	52.3±0.7
ΔG ,%	34.11	34.7	34.87	34.54	34.25
Zn,%	53.3±0.9	51.8±0.8	52.4±0.5	53.1±0.7	53.6±0.8
ΔG ,%	34.28	34.02	33.98	34.11	33.73
Zn,%	52.4±0.8	52.9±0.8	52.2±0.7	53.4±0.6	53.8±0.7
ΔG ,%	34.46	34.00	34.25	33.60	33.62

Fig. 1 presents the X-ray pattern of the sample synthesized at 25°C and concentration of sodium hydroxide and zinc nitrate 1.6 M. The strongest peak at $2\theta = 9.2^\circ$ and other characteristic peaks at $2\theta = 18.4, 34.6, 35.4, 46.8,$ and 47.4° identified formation of pure well crystallised zinc hydroxide nitrate ($Zn_5(OH)_8(NO_3)_2 \cdot 2H_2O$, JCPDS card 24-1460).

The results for all other samples were identical except for the last two from series S5. In these cases, a new set of very weak peaks appears at $2\theta = 31.8^\circ, 34.5^\circ$ and 47.4° . These peaks are identical to the JCPDS card 36-1451 for ZnO and indicate the presence of insignificant amounts of zinc oxide and $Zn_3(OH)_4(NO_3)_2$ ($2\theta = 26.1^\circ$, JCPDS card 70-1361). The presence of the last one is not fully clarified (Fig. 2).

Fig. 3 presents the SEM images of the sample synthesized at 25°C and concentration of sodium hydroxide and zinc nitrate 1.6 M. As it can be seen, the sample is composed of sheet-like particles, the typical morphology of zinc hydroxide nitrate. These images are typical for all other samples, prepared according to the scheme presented in Table 1 except for the last two from series S5. The result is consistent with the observation from XRD pattern, presented in Fig. 1 and confirm the obtaining of pure $Zn_5(OH)_8(NO_3)_2 \cdot 2H_2O$.

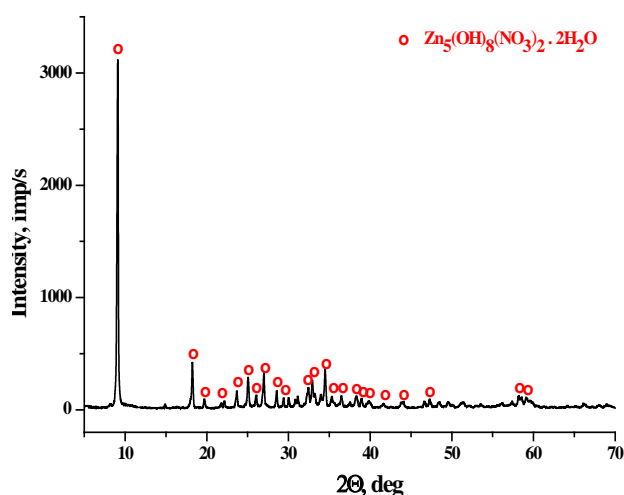


Fig. 1. X-ray pattern of the sample synthesized at 25°C and concentration of NaOH and Zn(NO₃)₂ 1.6 M

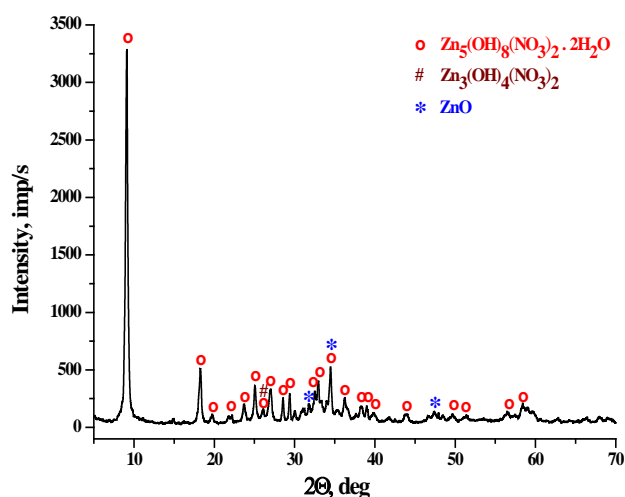
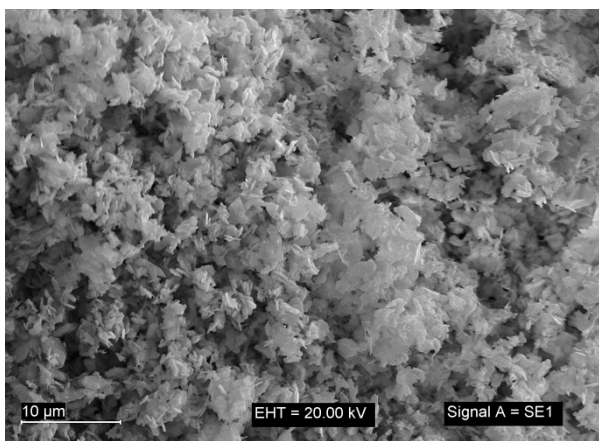
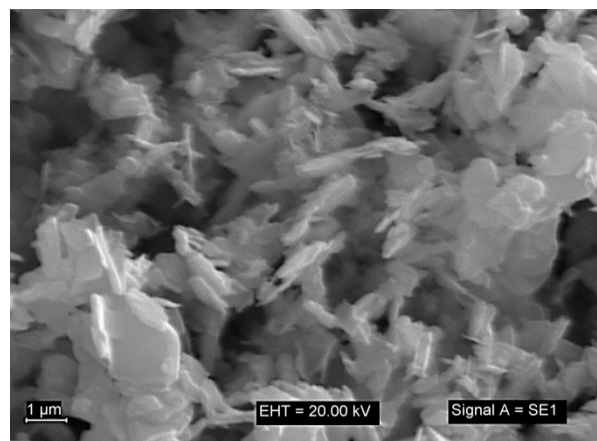


Fig. 2. X-ray pattern of the sample synthesized at 25°C and concentration of NaOH and Zn(NO₃)₂ 3.2 M



A



B

Fig. 3. SEM images of samples synthesized at 25°C with initial OH/Zn molar ratio 1.6 and concentration of zinc nitrate and sodium hydroxide 1.6 M. Scale bar: **A:** 10 μm; **B:** 1.0 μm

Fig. 4 presents the SEM images of the sample synthesized at 25°C and concentration of NaOH and Zn(NO₃)₂ 3.2 M. The results presented suggest two easily noticeable differences, concerning particle size and sample composition. Fig. 4 (a) demonstrates the same morphology of the resulting precipitate but a visible decrease of the particle size, more often smaller than 1 μm.

A slight morphology change can be seen after careful examination of the image presented in Figs. 4 (b) and (c). Obvious domination of the sheet-like particles with thickness less than 100 nm, belonging to $(\text{Zn}_5(\text{OH})_8(\text{NO}_3)_2 \cdot 2\text{H}_2\text{O})$ can be seen. Furthermore, although few in number, a new type of

particles appears. Probably ZnO crystals or the intermediates to ZnO, as suggested by the weak characteristic peaks of ZnO in the X-ray pattern, presented in Fig. 2.

Influence of temperature and storage time in the mother liquor

Except the concentration of the solutions used in the synthesis, the temperature and acidity of the medium are essential for the composition and stability of the resulting precipitates. Takada [10] investigated the effect of pH on the formation of the zinc compound, including $\text{Zn}_5(\text{OH})_8(\text{NO}_3)_2 \cdot 2\text{H}_2\text{O}$.

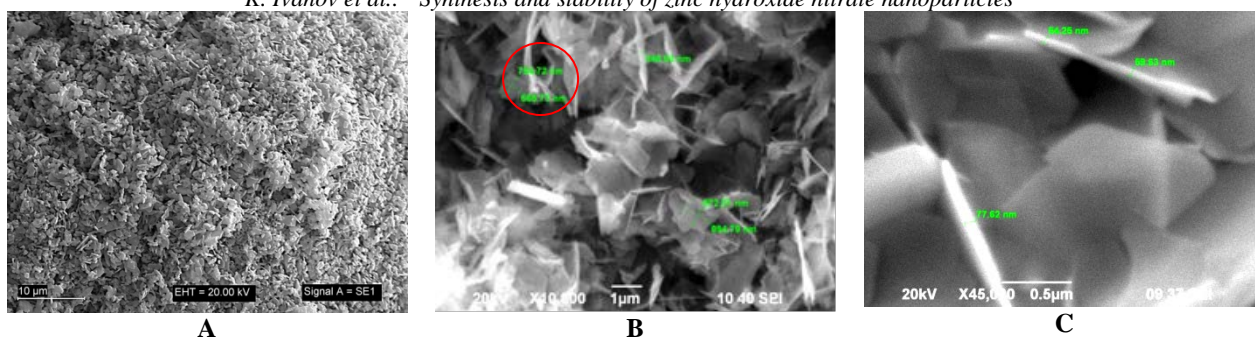


Fig. 4. SEM images of samples synthesized at 25°C with initial OH/Zn molar ratio 1.6 and concentration of zinc nitrate and sodium hydroxide 3.2 M. Scale bar: A: 10 µm; B: 1.0 µm; C: 0.5 µm

In order to accelerate hydrolysis, suspensions containing 0.15 or 0.5 M $\text{Zn}(\text{NO}_3)_2$ and 1.0 M NaOH with $2\text{OH}/\text{Zn}^{2+}$ (R) from 0.01 to 2.0 are subjected to ageing on a rotating drum for 100-120 h at 25, 50 and 70°C. The authors found that a zinc hydroxide nitrate and/or ZnO are formed depending on the $2\text{OH}/\text{Zn}^{2+}$ value. Impurities of zinc oxide are found at R close to 1.0 and pure ZnO is formed after this point. According to the results presented, increasing the temperature up to 70°C does not affect the composition of the precipitate obtained.

Similar results are obtained in [7], [11] and [12], which studied in detail the preparation of zinc hydroxide nitrate nanocrystals and their chemical and structural stability. These authors found that this compound can be synthesized by quick precipitation of zinc nitrate and sodium hydroxide solution under various conditions. Transformation in the composition and morphology of the precipitate along the ageing is monitored. It was concluded that zinc hydroxide nitrate crystals are very stable when isolated and then dispersed in aqueous solution.

In our opinion, isolation and drying of the precipitate is not the best approach for the successful preparation of foliar fertilizer. The main reason is the sintering of the particles, leading to a rapid decrease in its affectivity. This is why the shelf life of the precipitate in the mother liquor after synthesis is extremely important in terms of the use of the basic zinc nitrate as foliar fertilizer. Therefore, we changed the method of investigating the stability of the synthesized samples by limiting the time of synthesis to 10 minutes. The precipitates obtained at higher temperatures were cooled rapidly to room temperature and ongoing processes in the thus obtained suspensions were monitored for 30 days.

Figs. 5 and 6 show the temperature influence on the samples prepared at 70°C, initial OH/Zn molar ratio 1.6 and concentration of the NaOH and $\text{Zn}(\text{NO}_3)_2$ 3.2 M.

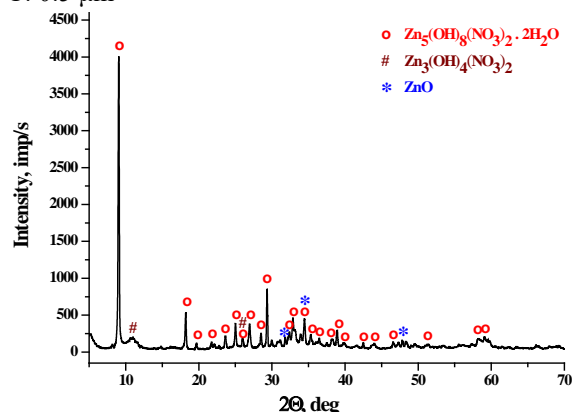


Fig. 5. XRD patterns of sample prepared at 70°C, initial OH/Zn molar ratio 3.2 and concentration of the zinc nitrate and sodium hydroxide 3.2 M

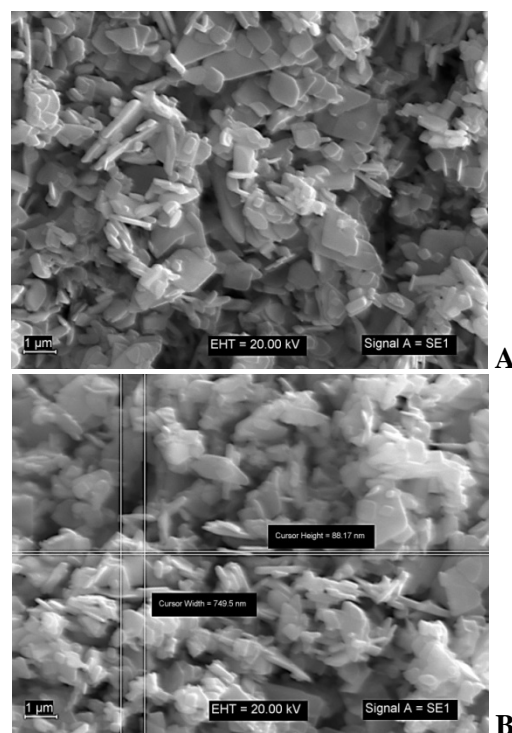


Fig. 6. SEM images of sample synthesized at 70°C, initial OH/Zn molar ratio 3.2 and concentration of the zinc nitrate and sodium hydroxide 3.2 M. Scale bar: A: 1.0 µm; B: 1.0 µm.

No substantial change in the composition and morphology of the resulted sample can be observed. The sheet-like particles of $Zn_5(OH)_8(NO_3)_2 \cdot 2H_2O$ dominate and traces of $Zn_3(OH)_4(NO_3)_2$ are also present. This result confirms the suggestion that increasing the temperature to 70°C slightly affects the crystal phase and morphology of the precipitate. The shelf life in the mother liquor of the precipitate obtained at 25 and 75°C was monitored. The results are presented in Tables 3 and 4.

The results presented in Tables 3 and 4 correspond very closely to the theoretical ones and suggest no change in the composition and morphology of the precipitate. This suggestion was confirmed by the results of X-ray and SEM analysis, which are similar to the results presented above. Obviously the crystal phase does not undergo detectable change along the storage in the mother liquor (up to 30 days).

Table 3. Chemical composition (Zn, %) and weight loss at 450°C (ΔG , %) of the samples synthesized at room temperature, OH/Zn molar ratio 1.6 and NaOH and $Zn(NO_3)_2$ concentration 1.6 M after 30 days storage in mother liquor

No	Time	Zn, %	ΔG , %	pH
1	Immediately	53.4 ± 0.8	34.61	5.98
2	1 hour	52.0 ± 1.0	34.12	6.01
3	3 hours	53.1 ± 0.9	34.00	6.01
4	5 hours	52.6 ± 0.7	33.84	6.00
5	8 hours	53.2 ± 0.8	34.65	6.00
6	1 day	51.2 ± 0.9	34.13	6.00
7	10 days	52.0 ± 0.6	35.12	6.02
8	20 days	51.3 ± 1.0	34.53	6.03
9	30 days	53.2 ± 0.8	33.91	6.06

Table 4. Chemical composition of the samples synthesized at 70°C, OH/Zn molar ratio 1.6 and NaOH and $Zn(NO_3)_2$ concentration 3.2 M after 30 days storage in mother liquor at room temperature

No	Time	Zn, %	ΔG , %	pH
1	immediately	52.0 ± 0.8	34.22	6.10
2	1 hour	52.8 ± 1.0	34.81	6.15
3	3 hours	53.1 ± 0.8	33.52	6.14
4	5 hours	52.9 ± 0.8	33.81	6.18
5	8 hours	52.2 ± 0.8	34.90	6.18
6	1 day	53.2 ± 0.9	34.10	6.17
7	10 days	53.0 ± 1.0	35.11	6.15
8	20 days	53.1 ± 0.9	34.53	6.10
9	30 days	52.8 ± 0.8	35.62	6.10

The essential difference between the results obtained by us and those of other authors can be explained with the very low speed of hydrolysis processes at room temperature, leading to the transformation of the $Zn_5(OH)_8(NO_3)_2 \cdot 2H_2O$ to ZnO. The minor change in pH values is noteworthy, which also confirms the absence of significant processes in the frame of the investigated time period.

CONCLUSIONS

Zinc hydroxide nitrate has been synthesized by precipitation of zinc nitrate in sodium hydroxide solution under various conditions. The phase transformation from zinc hydroxide nitrate to ZnO or other intermediate compounds has been examined. A long-term stability of the crystal phase in the mother liquor was found which identifies the zinc hydroxide nitrate suspension as a promising feedstock for the preparation of foliar fertilizer.

REFERENCES

1. J. He, M. Wei, B Li, Y. Kang, D. Evans, X. Duan, *Layered double hydroxides*, Springer, Berlin, Heidelberg, 89 (2006).
2. M. Rajamathi, G. Thomas, P. Kamath, *J. Chem. Sci.*, **113**, 671 (2001).
3. A. Cursino, J. da Costa Gardolinski, F. Wypych, F. J. *Colloid Interf. Sci.*, **347**, 49 (2010).
4. R. Marangoni, L. Ramos, F. Wypych, *J. Colloid Interf. Sci.*, **330**, 303 (2009).
5. P. Li, L. Li, Y. Du, M. Hampton, A. Nguyen, L. Huang, Z. Xu, *J. Nanopart. Res.* **16**, 1 (2014).
6. D. Vu, L. Huang, L., A. Nguyen, Z. Du, Z. Xu, M. Hampton, V. Rudolph, *J. Plant Nutr. Soil Sci.*, **176**, 764 (2013).
7. P. Li, Z. Xu, M. Hampton, D. Vu, L. Huang, V. Rudolph, A. Nguyen, *J. Phys. Chem. C*, **116**, 10325 (2012).
8. S. Newman, W. Jones, *J. Solid State Chem.*, **148**, 26 (1999).
9. J. Auffredic, D. Louër, *J. Solid State Chem.*, **46**, 245 (1983).
10. T. Takada, M Kiyama, H. Torii, T. Asai, M. Takano, N. Nakanishi, *Bull. Inst. Chem. Res., Kyoto Univ.*, **56**, 242 (1978).
11. P. Li, Z. Xu, M. Hampton, D. Vu, L. Huang, A. Nguyen, V. Rudolph, *Chemeca 2011: Engineering a Better World: Sydney Hilton Hotel, NSW, Australia, 18-21 September 2011*, 375 (2011).
12. H. Longbin, A. Nguyen, V. Rudolph, Z. Xu, *CA Patent 2865911 A1* (2012).

СИНТЕЗ И СТАБИЛНОСТ НА НАНОКРИСТАЛИ ОТ ЦИНКОВ ХИДРОКСИНИТРАТ

К. И. Иванов*, Е. Н. Коленцова, Н. Као Нгуен, А. Б. Пелтеков, В. Р. Ангелова

Катедра „Обща химия“, Аграрен университет, 4000 Пловдив, България

Постъпила на 24 октомври 2016 г.; приета на 3 януари 2017 г.

(Резюме)

Наноразмерният цинков хидрокси нитрат се оценява като перспективен листен тор с по-добра разтворимост от ZnO и с по-ниска фитотоксичност в сравнение с други цинк-съдържащи съединения. Основният проблем е получаването на стабилни кристали с размери под 100 nm. Това изследване има за цел да оцени влиянието на условията на получаване върху химическия състав и големината на частиците на цинковия хидрокси нитрат, синтезиран чрез съутаяване на $Zn(NO_3)_2 \cdot 6H_2O$ и NaOH с концентрация на изходните разтвори от 0.4 до 3.2 M и молно отношение OH/Zn 1.6 при температури на синтез от 20 до 60°C. Всички образци са детайлно охарактеризирани чрез рентгеноструктурен анализ, сканираща електронна микроскопия, термичен и елементарен (ICP) анализ. Изследвана е също стабилността на кристалите от цинков хидрокси нитрат при престой в маточния разтвор до 30 дни.

Ключови думи: *цинков хидрокси нитрат, наночастици, синтез, листен тор.*

Assessment of organic pollutants in sediments from Maritsa River basin (Bulgaria)

V.M. Genina^{1,2*}, G.M. Gecheva¹, I.G. Velcheva¹, M.I. Marinov³

¹ University of Plovdiv, Faculty of Biology, 24 Tsar Asen Str., Plovdiv 4000, Bulgaria

² Executive Environmental Agency, branch Plovdiv, 1 Perushtitsa Str., Plovdiv 4000, Bulgaria

³ East Aegean River Basin Directorate Plovdiv, 35 Yanko Sakazov Str., Plovdiv 4000, Bulgaria

Received November 13, 2016; Revised January 5, 2017

Sediments were sampled from 5 sites from the Maritsa River basin in the period 2013–2014 with the aim to assess effects of the anthropogenic pressure caused by the pesticides production and by the intensive agriculture. Sites were located in the middle part of the Maritsa River basin (near Plovdiv city) and the watersheds of Chepelarska and Stryama rivers. Methods for analysis of certain priority substances and specific pollutants were applied in order to establish trends in the accumulation in sediments, as required by the Directive 2000/60/EC and Directive 2008/105/EC. The reported data for organic pollutants are the first for the studied river basin.

Key words: sediments, Maritsa River, PCBs, OCPs, PAHs

INTRODUCTION

The Maritsa is the largest river on the Balkan Peninsula; it is the biggest river in terms of discharge volume and the third longest river in Bulgaria. It emerges from springs in the Rila mountain range and its basin is a cross-border watershed for Bulgaria, Greece and Turkey. The number of the tributaries of Maritsa River is about 100. The most significant among them are the rivers Chepinska, Topolnitsa, Luda Yana, Vacha, Chepelarska, Stryama, Sazliyka, Arda, Tundzha, Ergene.

Sediments are by far less variable in time, but much more heterogeneous than waters. Determining organic compounds in river sediments enables the identification of the contaminant origin in local regions. Polychlorinated biphenyls (PCBs) are toxic chemicals, which precipitate in soil and water. They are mixtures of synthetic and organic chemical substances which share similar chemical structure. PCBs had been derived for their very high flash points and were widely deployed as fire-extinguishing agents, electrical insulators and plasticizers mainly in electrical apparatuses. Most often they are introduced into the environment through defective equipment, illegal discharge, scavenge oil from electrical equipment, as well as hazardous waste. They are a family of 209 synthetic molecules composed of a biphenyl nucleus with chlorine at any, or all, of the 10 available sites [1]. The ortho-, meta- and para positions are important in determining the chemical properties of PCB, such as high dielectric constants, nonflammability, hydrophobic quality and chemical stability. The usefulness of these properties led PCBs to be used in

mixtures for a wide range of applications from the 1930s onwards [2,]. However, after their toxicity became recognized, PCBs were progressively banned in most developed countries during the 1980s [4]. Due to their large-scale production, extensive use and environmental persistence, these compounds have accumulated in many ecosystems all over the world; in aquatic environments they are trapped in sediments. PCB contamination continues to be a problem as compounds can be transferred from the sediment to the lower trophic levels of an ecosystem through microbial and bottom-feeder uptake.

Organochlorine pesticides (OCPs) have been widely used in the past, but because of their high persistency in environment and accumulation in the food chain, they can still arouse topical concerns about human health.

Polyaromatic hydrocarbons (PAHs) are a large group of organic substances with two or more benzene cores. They are characterized by low solubility in water, but high solubility in fats. The polycyclic aromatic hydrocarbons are produced mainly by incomplete combustion of coal and diesel fuel. There are several hundred PAHs. These compounds are absorbed by organisms mainly through the respiratory system, but may also be assimilated together with water and food. The most thorough study of the carcinogenic effect is that of inhaled benzo[a]pyrene (BaP), essential source of which is tobacco smoke.

The aim of the research was to identify the extent of accumulation of organic pollutants in “sediment” matrix in selected river valleys and monitoring stations along the Maritsa River basin. The study for

* To whom all correspondence should be sent.
E-mail: vgenina@abv.bg

the first time provided information about the organic pollutants and could be a basis for initial examination of the level of pollution in the surveyed water bodies and identification of the sources of anthropogenic pressure. The selection of indicators (priority substances and specific pollutants) provides particular guidelines for planning future monitoring for assessment of their chemical and ecological status. The data from the analysis conducted may be used for the purpose of monitoring the tendencies in the pollution of water bodies in terms of the examined indicators.

EXPERIMENTAL

The monitoring of sediments was accomplished in accordance with Guidance document No. 25 on chemical monitoring of sediment and biota to the common implementation strategy for the Water Framework Directive (WFD) 2000/60/EC.

The research was conducted at 5 monitoring stations located in the Maritsa River basin and two of its major tributaries – Chepelarska River and Stryama River (Fig 1). The selection of the stations was made in compliance with the key criteria and the best practices of the strategy for sampling of sediments specified in Guidance document No. 7 [5] of the WFD. Thus, stations were selected upon a preliminary analysis of the information about the

anthropogenic pressure from point and diffuse sources of organic pollutants, the typological characteristics of the rivers, the composition of the bottom substrate (pebbles, gravel, sand, slime, clay), the hydrological characteristics (water runoff, water level) and accessibility for sampling. The geographic characteristics of the monitoring stations (watershed, river, location, geographic coordinates) were specified below.

Stryama river, the village of Slatina (42.6902; 24.56917) has been selected as a potential reference site for national type R5 Semi-mountain rivers in Ecoregion 7, slightly influenced by anthropogenic pressure and limited impact on the quality elements: extensive agriculture and forestry in the vicinity of the monitoring station; low pressure from domestic discharges in the catchment area of the site (the town of Klissura); limited automobile traffic; good chemical and good to high ecological status identified as a reference point for type R5 in the RBMP of East Aegean River Basin district. Substratum was consisted mainly by pebbles, gravel and sand, and organic slime where the current is sluggish. Moderate to significant water runoff, moderate to high current velocity, water level was 0.2-0.4 m.

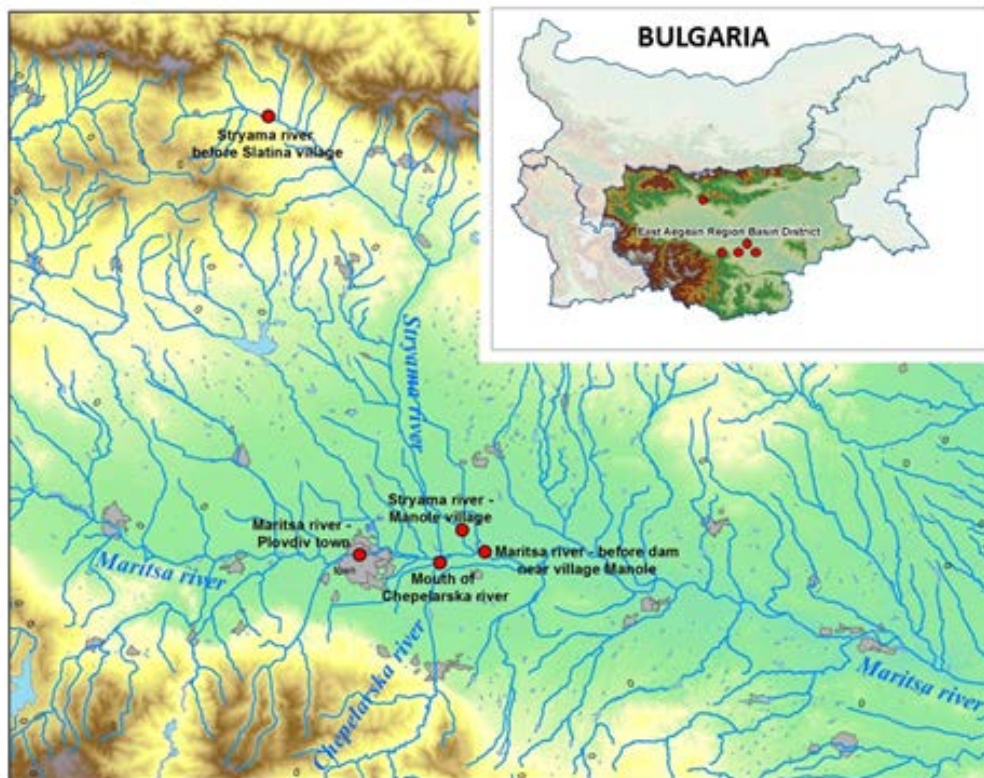


Fig. 1. Map of the studied region.

Stryama river, the village of Manole (42.1871; 24.91314) – type R13 Small and medium-sized

lowland rivers in Ecoregion 7, located in a region with settlements in the catchment area of the of

monitoring station; intensive agriculture; cumulative pressure from small settlements (<2000 p.e.); automobile traffic; good chemical and moderate ecological status; substrate – mostly sand and at places where the current is sluggish – organic slime. Moderate to significant water runoff, moderate to low current velocity, water level was 0.3-0.6 m.

Mouth of Chepelarska river, Kemera bridge area (42.1457; 24.87722) – type R5 Semi-intensive rivers in Ecoregion 7, a site of significant anthropogenic pressure from industrial plants producing pesticides and metals (Agria AD, KCM AD); discharge of untreated waste water from large settlements (Assenovgrad >1000 p.e.); intensive agriculture; automobile traffic; poor chemical status (metals) and poor ecological status; substrate – mostly gravel and sand, and where the current is sluggish – organic slime. Moderate to significant water runoff, moderate to low current velocity, water level: 0.3-0.5 m.

Maritsa river upstream of Plovdiv city (42.1608; 24.95124)– type R12 Large lowland rivers in Ecoregion 7, site of combined point and diffuse pressure from the upper and middle part of the catchment area of the Maritsa river, before discharge of waste water from the city of Plovdiv; discharge of treated waste water from large settlements in the catchment area on the monitoring station (Pazardzhik >1000 p.e., Stamboliyski town 2000-10000 p.e.); advanced industry (pulp and paper, food and flavor industry); intensive agriculture; intensive automobile traffic; good chemical and moderate to good ecological status; substrate – mostly sand and gravel with depositions of organic slime at places of sluggish current; significant water runoff, moderate to low current velocity, water level: 0.4-1.2 m.

Maritsa river, dam near the village of Manole (42.1529; 24.74322)– type R12 Large lowland rivers in Ecoregion 7; a monitoring station of significant cumulative anthropogenic pressure from all the sources in the catchment area of the other monitoring stations (discharge of waste water from large settlements, industrial enterprises and intensive agriculture; discharge of treated waste water) from large settlements in the catchment area of the monitoring station (Plovdiv – 300000 p.e., Assenovgrad >10000 p.e., a large number of settlements <2000 p.e.); combined pressure from developed industry (industrial zones of the city of Plovdiv, Agria AD, KCM AD); intensive agriculture in the catchment areas of the surveyed rivers – the Maritsa, Stryama and Chepelarska rivers; limited automobile traffic; good chemical and moderate ecological status; substrate – massive deposition of organic slime in the area of the monitoring station

before the dam near the village of Manole, sand; significant water runoff, low velocity of the current, water level: 1.0-3.0 m.

Samples were collected from their upper layer, which indicates the actual materials deposited and the actual extent of pollution. Furthermore, the sediment topmost layer forms the habitat of the benthic organisms, which are part of the biological quality elements for the assessment of the status of water bodies. The sediments are composed of particles varying from very fine clay (< 2 µm) to larger pebbles and stones with a size of several mm. Their surface is often covered with organic substances which have the effect of binding element for many pollutants and other compounds. The smaller the particle is, the greater the relative surface area is, which means that the majority of monitored substances are contained in the fine fractions of the sediments, which are the main source of nutrients for the biota. The size of the particle is one of the most important factors, which controls the distribution of natural and anthropogenic components in sediments, along with the content of organic substances. The clay-silt fraction of particle size < 63 µm was analyzed. Volume (quantity) of sample for analysis was 200 mL.

The sampling was done in compliance with the ISO 5667-12:2002 standard [6]. Stainless steel blades were used in order to minimize contamination.

Transportation and sieving

In order to minimize the possibility of disturbing the sediment/water equilibrium, wet sieving was done at the point of sampling with water from the environment. The samples (upon sieving) were transferred into preliminary cleaned brown glass containers for organic pollutants. The containers for samples were filled up to the brim (allowing a minimum space for the stopper), in order to minimize the probability of oxidation and loss of acid-volatile sulfide during transportation. The samples were transported in a cooled state to the laboratory (at T 4°C) within a period not exceeding 6 hours. Cooling was accomplished by using cool boxes and freezer block inserts.

Storage

Temperature is the most important factor concerning samples from the time of sampling, throughout their handling and processing to the moment of final analysis. Another source of contamination is the adsorption of pollutants from the laboratory air. Decomposition and evaporation of contaminants might also be a source of analysis error. The sifted samples of sediments were kept in

containers freeze dried in accordance with the EN ISO 16720:2007 standard [7] and deep frozen at -20°C.

Analytical methods

Validated standardized methods as per: ISO 18287-1; EN 16167; SD/CEN/TS 16181; EN 16179 were used for the analyses [8-11].

Sample preparation

A 10 g sample was extracted with organic solvent Hexane:Acetone (1:1), by microwave decomposition under a programmed furnace temperature of 120°C detainment time 25. The extract obtained was concentrated, then subjected to a purification procedure with silica gel and again concentrated. The sample was analyzed using Gas chromatography – mass spectrometry (GC-MS) equipment.

Quality control

The procedures for quality assurance include validation of the methods by routine in-house procedures and independent external procedures (participation in inter-laboratory tests). Use was made of certified reference materials: Certified Reference Material PAHs, PCBs, and Pesticides in Fresh Water Sediment CNS391, Fluka and Standard Reference Material NIST- SRM 1944.

Period and frequency of sampling

As a result from the limited rate of deposition (typically within the range of 1-10 mm/year) and the physical и biological blending of surface sediments, the composition of sediments is usually quite stable in comparison to the concentration of the pollutants

in the aquatic ecosystem. The sediment sampling was accomplished three times in the period 2013-2014 and corresponded to the expected changes in the sediments, taking into account the seasonal changes in the hydrological regimes of the rivers.

Selection of organic pollutants to be monitored

Analysis of synthetic compounds was made (pesticides, medicinal preparations, industrial pollutants), dissociated in the event of pollution from point and diffusive sources, atmospheric depositions, which are taken into account in the assessment of the chemical and ecological status of the water bodies (e.g. priority substances according to Directive 2008/105/EO and Directive 2013/39/EC), and specific pollutants in compliance with the approved list and the EQS of the Bulgarian legislation [12].

RESULTS AND DISCUSSION

All six PCBs (PCB 28, PCB 52, PCB 101, PCB 138, PCB 153, PCB 180) studied were below the limit of quantification (<0.001 mg kg⁻¹) at all monitoring stations, probably due to the ban imposed on the manufacture thereof for decades.

Results for 17 OCPs showed that exceeding the limit of quantification have been detected for chlorbenzene, α-HCH, β-HCH, α-Endosulfane, endrine, o,p-DDE, p,p-DDE, o,p-DDD (Table 1). The lowest concentrations were detected in the Stryama River, Slatina village – a site slightly influenced by anthropogenic pressure.

Table 1. Detected minimum, maximum and average values of studied OCPs in sediments, mg kg⁻¹ d.w.

OCP	min (n=15)	max	average
Pentachloro benzene	<0.001	-	-
ChBenzene	0.001	0.0023	
α-HCH	0.002	0.05	0.0093
β-HCH	0.002	0.015	0.0028
γ-HCH	<0.002	-	-
α-Endosulfane	0.003	0.068	0.0388
β-Endosulfane	<0.003	-	-
Aldrin	<0.002	-	-
Dieldrin	0.002	0.024	0.0106
Endrin	<0.002	-	-
Heptachlor	<0.001	-	-
o,p-DDE	0.001	0.035	0.0113
p,p-DDE	0.002	0.047	0.0192
o,p-DDT	<0.001	-	-
p,p-DDT	<0.001	-	-
o,p-DDD	0.001	0.007	0.0034
p,p-DDD	<0.003	-	-

Table 2. Minimum, average and maximum concentrations of 16 measured PAH in sediments, mg kg⁻¹ d.w.

PAH	min (n=15)	max	average
Naphthalene	0.01	0.03	0.02
Acenaphthene	<0.01		
Acenaphthylene	<0.01		
Fluoranthene	<0.02		
Phenanthrene	0.02	0.046	0.014
Anthracene	0.002	0.008	0.002
Flurene	0.002	0.05	0.015
Pyrene	0.001	0.038	0.013
Benzo(a)anthracene	0.001	0.022	0.002
Chrysene	0.001	0.022	0.004
Benzo(b)fluoranthene	0.001	0.09	0.013
Benzo(k)fluoranthene	0.001	0.08	0.012
Benzo(a)pyrene	0.001	0.04	0.009
Indeno(1,2,3cd)pyrene	<0.003		
Dibenz(a,h)anthracene	<0.003		
Benzo(g,h,i)perylene	<0.003		

Exceeding the limit of quantification for 16 PAHs analyzed was recorded for Naphthalene, Phenanthrene, Anthracene, Flurene, Pyrene, Benzo(a)anthracene, Chrysene Benzo(b)fluoranthene, Benzo(k)fluoranthene, Benzo(a)pyrene (Table 2).

The lowest concentrations were ascertained again in the Stryama River, Slatina village, while the highest concentrations were in the Chepelarska River, Kemera village – a site of significant anthropogenic pressure due to discharge of waste waters from settlements (Assenovgrad) and industrial enterprises (KCM AD and Agria AD).

CONCLUSION

At none of the monitoring stations PCBs (used in the past as pesticides in agriculture) have been detected since production thereof has been discontinued for decades. At all monitoring stations OCPs and PAHs above the LOQ have been detected, which was probably due to diffuse and point pollution in the area of the surveyed river sections.

Eight substances from the group of OCPs were established (persistent organic pollutants used as pesticides in agriculture and forestry). Moreover, six of them were found constantly in all five monitoring stations (α -HCH, α -Endosulfane, Dieldrin, o,p-DDE, p,p-DDE, o,p-DDD).

Nine substances from the group of PAH were also established (pressure from industry and traffic). The lowest number of substances were found in sediments from provisionally selected reference point of Stryama River before Slatina (Naphthalene and Anthracene), in concentrations close to the limit of quantification (LOQ). In the rest of the stations they were detected continuously in different

concentrations depending on the anthropogenic pressure.

The highest concentrations of OCPs and PAHs were detected just upstream of the mouth of Chepelarska River, which are in consequence of the combined pollution caused by industry, intensive agriculture and automobile traffic.

The results from the conducted for the first time survey of organic pollutants in sediments from Maritsa River basin could be used for the purpose of monitoring the trends in pollution of water bodies in terms of the examined indicators in accordance with the requirements of Directive 2008/105/EC.

REFERENCES

1. V.A. McFarland, J.U. Clarke. *Environ. Health Perspect.*, **81**, 225 (1989).
2. A. Beyer, M. Biziuk M. *Rev. Environ. Contam. Toxicol.*, **201**,137 (2009).
3. Breivik et al., *Science of The Total Environ.*, **290**, 199 (2002)
4. G. Letz. *West J. Med.*, **138**, 534 (1983).
5. Guidance documents No. 7, Monitoring under the Water Framework Directive, EC, 2003.
6. ISO 5667-12:2002 Water quality - Sampling - Part 12: Guidance on sampling of bottom sediments, 2002.
7. ISO 16720:2007 Soil quality - Pretreatment of samples by freeze-drying for subsequent analysis.
8. ISO 18287-1 Soil quality -- Determination of polycyclic aromatic hydrocarbons (PAH) -- Gas chromatographic method with mass spectrometric detection (GC-MS)
9. EN 16167 Sludge, treated biowaste and soil - Determination of polychlorinated biphenyls (PCB) by gas chromatography with mass selective detection
10. (GC-MS) and gas chromatography with electron-capture detection (GC-ECD), 2012

11. CEN/TS 16181 Sludge, treated biowaste and soil - Determination of polycyclic aromatic hydrocarbons (PAH) by gas chromatography (GC) and high performance liquid chromatography (HPLC).
12. EN 16179:2012 Sludge, treated biowaste and soil - Guidance for sample pretreatment.
13. Ordinance H-4 of 2012 concerning characterization of surface water, SG 22, 2013.

ОЦЕНКА НА ОРГАНИЧНИ ЗАМЪРСИТЕЛИ В СЕДИМЕНТИ ОТ БАСЕЙНА НА РЕКА МАРИЦА (БЪЛГАРИЯ)

В.М. Генина^{1,2*}, Г. М. Гечева¹, Ил. Г. Велчева¹, М.Ив. Маринов³

¹ Пловдивски университет, Биологически факултет, ул. „Цар Асен“ 24., Пловдив 4000, България

² Изпълнителната агенция по околна среда, клон Пловдив, ул. „Перуцица“ 1., Пловдив 4000, България

³ Източнобеломорски район Басейнова дирекция Пловдив, ул. „Янко Сакъзов“ 35., Пловдив 4000, България

* E-mail: vgenina@abv.bg

Постъпила на 13 ноември 2016 г.; приета на 5 януари 2017 г.

(Резюме)

В периода 2013-2014 е извършено пробовземане от седименти в 5 мониторингови станции в басейна на река Марица с цел оценка на ефектите от антропогенния натиск, причинен от производството на пестициди и интензивно земеделие. Станциите са разположени с средната част на басейна на река Марица (в района на гр.Пловдив) и водосборите на р.Чепеларска и р.Стряма. Използвани са методи за анализ на приоритетни вещества и специфични замърсители за установяване на тенденции при акумулацията в седименти в съответствие с изискванията на Директива 2000/60/ЕС и Директива 2008/105/ЕС. Представените данни за органични замърсители са първите за изследвания речен басейн.

Ключови думи: седименти, река Марица, PCBs, OCPs, PAH

Microwave assisted carbon modification of magnetite nanoparticles, used for solid phase extraction of trace elements

D. H. Sánchez¹, D. L. Georgieva^{2*}, V. J. Kmetov², V. M. Stefanova²

¹University of Alicante; PO Box 99, 03080 Alicante, Spain

²Department of Analytical chemistry and computer chemistry, University of Plovdiv, 24 "Tzar Assen" Str., Plovdiv 4000, Bulgaria

Received November 14, 2016; Revised December 14, 2016

The carbon encapsulated magnetic nanoparticles (MNPs) have high potential as a sorbent for solid phase extraction (SPE) of organic and inorganic compounds. Carbon is an excellent material for MNPs core-shell modification due to its chemical stability, biocompatibility, and possibility for further surface modification. This coating improves the stability of magnetic nanoparticles and introduces new surface properties that could facilitate their application.

A new microwave-assisted procedure for carbon coating of magnetite nanoparticles by hydrothermal route is presented. The Fourier transform infrared spectroscopy with attenuated total reflection (ATR-FTIR) was used for surface characterization of produced Fe₃O₄@C NPs.

The carbon coated nanoparticles were tested as sorbent for SPE of V, Cr, Co, Ni, Cu, Zn, Cd, Tl and Bi from model solutions.

The inductively coupled plasma quadrupole mass spectrometer (ICP-MS) was used for SPE optimization studies.

Key words: magnetic nanoparticles, MW-assisted carbon coating, SPE Introduction

The magnetic nanoparticles MNPs are attractive new material as a sorbent for solid phase extraction of different compounds [1, 2]. Compared to other nano-sized materials the use of MNPs allows to simplify the extraction process and saves time as a result of their isolation from the sample matrix by an external magnetic field. For the purpose of magnetic assisted SPE, iron oxides nanoparticles (Fe₃O₄ and Fe₂O₃ [2]) or different types of ferrites (MnFe₂O₄ [3], CoFe₂O₄ [4]) are commonly used. The application of bare MNPs for extraction of trace elements is limited, due to their instability in acidic solutions [3]. One approach to overcome this drawback is to protect the magnetic core with resistant layer (commonly SiO₂) [5]. Carbon is also excellent material for MNPs core-shell modification due to its chemical stability, biocompatibility, and possibility of further surface modification. Carbon coating improves the stability of magnetic nanoparticles, but also introduces new surface properties, that could facilitate their application or further modification.

Carbon encapsulated magnetic materials were previously used for SPE of trace elements [6, 7], organophosphorus pesticides [8], polycyclic aromatic hydrocarbons (PAHs) [9, 10], etc.

The synthesis of MNPs@C is attracting a lot of attention and interests from scientists and a few strategies were reported to prepare MNPs@C [1]. Different synthesis routes of carbon-coating, are

reported including arc discharge [11], thermal chemical vapour condensation (TCVC) [12], pyrolysis [13], and hydrothermal reactions [14–17]. The latter does not require special reagents (the carbon precursor usually is glucose), but a special equipment (autoclaves) is needed and it consumes time (3 to 14h) and energy.

According to Wang *et al* [17] for effective construction of carbon layer on magnetite nanoparticles, a preliminary modification with oleic acid is required. The authors compared TEM images of the products from classical hydrothermal reaction with glucose where Fe₃O₄ nanoparticles were added in absence of any additional surface modification and after oleic acid treatment. Authors declare that according to TEM characterization Fe₃O₄ nanoparticles without any surface modification cannot be incorporated into carbon sphere and the final product mainly consists two kinds of particles, ones is carbon nanospheres and the others are free Fe₃O₄ nanoparticles [17].

In the present work, a new route for MW assisted hydrothermal synthesis of carbon-coated Fe₃O₄ nanoparticles is investigated. Two types of magnetic cores (bare and oleic acid stabilised) were studied as precursors for Fe₃O₄@C NPs production.

MATERIALS AND METHODS

Reagents

All reagents were analytical or suprapur reagent-grade. Ferric chloride (FeCl₃·6H₂O), ferrous

* To whom all correspondence should be sent.
E-mail: georgieva@uni-plovdiv.net

D.H. Sánchez et al.: "Microwave assisted carbon modification of magnetite nanoparticles, used for solid phase extraction ..."
chloride ($\text{FeCl}_2 \cdot 4\text{H}_2\text{O}$), were used for NPs synthesis, as well as Glucose monohydrate ($\text{C}_6\text{H}_{12}\text{O}_6 \cdot \text{H}_2\text{O}$), Oleic acid and 2-(2,4-Dihydroxy-phenylazo) thiazole (TAR), were used for surface modification. All were purchased from Sigma Aldrich Company (Milwaukee, WI, USA). Other reagents, including ammonia solution (25%) for magnetic NPs precipitation; KCl for pH zero charge determination; and HNO_3 (65%) for model solution conservation and carbon encapsulated NPs stability test, were from Merck (Darmstadt, Germany). Double distilled water was used for the preparation of all solutions.

After appropriate dilution, ICP multi-element standard solution 28 elements 100 mg L^{-1} (CPA, Bulgaria), was used for SPE procedure optimization. Single element solution of Rh 10 mg L^{-1} (Fluka Chemie GmbH, Buchs, Switzerland) was used as internal standard during ICP-MS determination.

Instrumentation

An inductively coupled plasma quadrupole mass spectrometer ICP-MS Agilent 7700 (Tokyo, Japan) with octopole reaction system (He collision gas flow 4.0 mL min^{-1}) was used for SPE optimization studies. The instrumental parameters were as follow: RF power 1.5 kW; plasma, auxiliary and nebulizer Ar gas flow rates: 15 L min^{-1} ; 0.9 L min^{-1} and 0.95 L min^{-1} respectively; sample flow rate 0.34 mL min^{-1} ; MicroMist nebulizer. Fifteen isotopes: ^{51}V , ^{53}Cr , ^{59}Co , ^{60}Ni , $^{63,65}\text{Cu}$, $^{66,68}\text{Zn}$, $^{111,114}\text{Cd}$, ^{205}Tl , $^{206,208}\text{Pb}$, ^{209}Bi and ^{103}Rh (as internal standard) were monitored at 1 point per mass peak with 100 ms acquisition time with five replicates for each measurement.

For characterization of carbon coated magnetic NPs, ATR-FT-IR Bruker Vertex 70 (Bruker Corporation, Germany) and FAAS Perkin Elmer 4000 were used. A microwave system MDS ETHOS One (Milestone Inc.) was used for magnetite nanoparticles carbon encapsulation.

A permanent NdFeB magnet, N45, Ni-Cu-Ni (P188/5-45-30-N) was used for phase separation during SPE tests.

Magnetic NPs synthesis

The magnetic NPs were produced by co-precipitation of a mixture containing Fe^{2+} ion and Fe^{3+} in basic media according previously optimised procedure [3]. Produced nanoparticles were stored as suspensions in double distilled water ($10 \text{ g L}^{-1} \text{ Fe}_3\text{O}_4$ NPs)

Magnetic NPs modification

1. Oleic acid modification

The modification with oleic acid was used as preliminary step before the carbon coating according to the modified procedure proposed from Zhang *et al.* [17]. Briefly into 30 mL of magnetite

nanoparticles suspension, 0.5 mL of oleic acid and 0.3 mL of ammonia solution (25%) were added dropwise at 80°C under vigorous stirring for 30 min. The oleic acid-stabilized Fe_3O_4 nanoparticles were separated by centrifugation (6000 rpm, 2 hours) and washed with water three times and once with ethanol.

2. Preparation of carbon encapsulated magnetite nanoparticles ($\text{Fe}_3\text{O}_4@\text{C}$)

Both type magnetite nanoparticles (bare and oleic acid modified) were tested as a precursor for carbon modified magnetic material production. Modification procedure was based on microwave assisted hydrothermal reaction in aqueous solution of glucose. The reaction mixtures were prepared by suspending 0.3 g of magnetite nanoparticles (bare or oleic acid modified) in 10 mL, 5 mol L^{-1} glucose solution in water. Prepared suspensions were subjected to microwave treatment under the following conditions: MW power 180 W; reaction mixture heated in 4 steps - 100°C , 130°C , 170°C and 200°C . For the first three steps, 2 min were set to reach the specified temperature and 2 min to hold on. For the last step (200°C) 5 min were set as ramp time, and the samples were treated at for one hour. After cooling, the carbon modified nanoparticles were washed with double distilled water and stored as water suspension.

Estimation of pH zero charge of the carbon coated magnetite nanoparticles

The pH zero charge of the produced $\text{Fe}_3\text{O}_4@\text{C}$ NPs was determined by pH drift method [7]. For this estimation 30 mL of 0.1 mol L^{-1} KCl solution was used and initial pH_i was adjusted from 2-10 by addition of diluted HNO_3 or NaOH solutions. The adjusted pH solutions were transferred to conical test tube containing 0.1 g of carbon coated NPs. The suspensions were shaken and allowed to equilibrate for 24 h. After treatment the MNPs were separated by permanent magnet and the pH in supernatant solution (pH_f) were measured again. The difference between initial and final pH values (ΔpH) was plotted against pH_i . The pH point zero charge (pH_{PZC}) was identified as the cross point of the fitted line with the abscissa.

Evaluation the potential of new carbon coated magnetite nanoparticles as sorbents for SPE of elements

The solid phase extraction procedure was performed in a batch mode. The optimization of SPE was carried out using model solutions ($10 \mu\text{g L}^{-1}$), prepared by dilution of multi-element standard.

Approximately 200 mg of the modified nanoparticles were transferred into a conical test tube. Afterwards the model solution of tested

elements was added and pH was adjusted to 8. The extraction of metal ions was performed by continuous shaking for 30 min.

The carbon modified MNPs with adsorbed analytes were separated by a permanent magnet for 5 min and the supernatant solution was decanted. The obtained solution was then stabilised with HNO₃ (0.1% v v⁻¹) and was subjected to ICP-MS analysis.

RESULTS AND DISCUSSION

Characterisation of carbon modified Fe₃O₄ nanoparticles

The ATR-FT-IR technique was employed for characterisation of carbon modified nanoparticles. The spectra obtained for unmodified and carbon encapsulated (with and without oleic acid modification) dried Fe₃O₄ nanoparticles are presented on Fig. 1

The intensive peaks at 1700 cm⁻¹ and 1060 cm⁻¹ observed on Figure 1 illustrate the presence of C=O in modified samples. The peaks from 2800 to 2980 cm⁻¹ are ascribed to C-H vibration. The region at 1000–1300 cm⁻¹ is assigned to O-H bending and C=O stretching vibrations. The broad band at 3100–3700 cm⁻¹ comes from the stretching vibrations of O-H. The obtained results are consistent with those reported by Zhang *et al* [10] for carbon coated magnetite nanoparticles obtained by classical hydrothermal reaction. The ATR-IR examination proved the presence of carbon as a result from MW assisted modification procedure, but results are not indicative for a formation of compact carbon layer surrounding the magnetic core.

One indirect test for the efficiency of encapsulation of Fe₃O₄ nanoparticles with a protective carbon layer is to examine their stability in acidic medium. All produced MNPs (bare and modified) were exposed to the action of nitric acid (1 mol L⁻¹) for 15 min and then the content of dissolved iron was determined by FAAS. The results presented as mass of dissolved iron per gram sorbent are given in Table 1.

From the results presented in Table 1, it can be concluded that preliminary modification with oleic acid is necessary for successful encapsulation of magnetic core with carbon. The Fe₃O₄@C produced after modification of magnetite with oleic acid show the best stability in acidic medium.

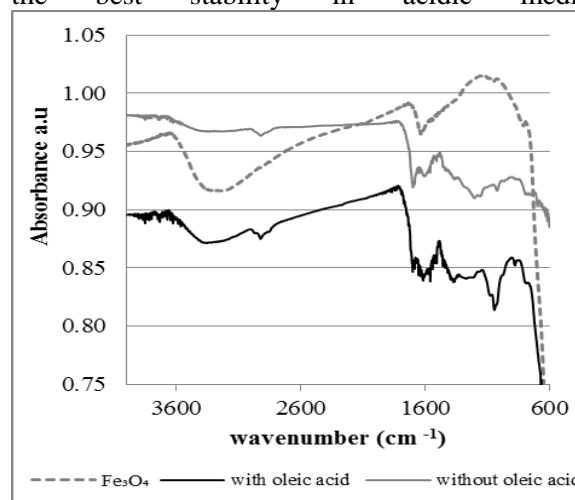


Fig. 1 ATR-FTIR spectra of unmodified and modified Fe₃O₄@C NPs

Table 1. Stability of nanoparticles in acidic medium

Sample	mass dissolved Fe in mg per 1g nanoparticles mg g ⁻¹
Unmodified Fe ₃ O ₄ NPs	117
Fe ₃ O ₄ @C without oleic acid modification	84
Fe ₃ O ₄ @C with oleic acid modification	18

The mass of dissolved Fe reduced by factors of 6.5 to 4.66, compared to the bare material and directly carbonised nanoparticles respectively. The observed positive effect of oleic acid on the stabilisation of carbon layer is in agreement with the results reported by Wang *et al* [17]. All further experiments were performed with Fe₃O₄@C produced after MNPs treatment with oleic acid.

The pH zero charge (pH_{PZC}) of studied Fe₃O₄@C NPs was found to be 4.8. This result additionally proves the successful formation of carbon layer because the obtained here value is close to the reported by Pyrzynska *et al* (pH_{PZC} ~ 4 for carbon

composites [7]). While the existing data of bare Fe₃O₄ NPs indicate the pH_{PZC} ~7 [2].

Evaluation of Fe₃O₄@C NPs applicability as a sorbent for SPE of elements

The evaluation of new Fe₃O₄@C NPs as a potential sorbent for magnetic assisted SPE of elements was accomplished varying two parameters: (i) pH of the extraction medium and (ii) quantity of nanoparticles used for the extraction.

The extraction degree E% (Eq. 1) was used as an estimator for the sorption effectiveness. For calculation of E%, model solutions (with 10 µg L⁻¹

initial analyte concentrations) were subjected to solid phase extraction with Fe₃O₄@C NPs and the residual concentration of elements in the aqueous phase after extraction were measured by ICP-MS.

$$E (\%) = \frac{Q_i (\text{initial}) - Q_s (\text{residual})}{Q_i (\text{initial})} \cdot 100 \quad (1)$$

where: E% is the extraction degree; Q_{initial} is the analyte quantity in the model solution; Q_{residual} is the final analyte quantity in residual aqueous phase after SPE.

Study of the pH influence on extraction degree

The solution pH is a parameter influencing on NPs surface charge and affects the sorption capabilities of carbon. At pH values above pH_{PZC}, the negative charge of carbon layer promotes the adsorption process due to the electrostatic attraction between metallic cations and nanoparticles, and vice versa when the pH of the solution is less than corresponding pH_{PZC} - repulsion between positively charged NPs and metal ions is expected to decrease the extraction degree.

The effect of pH on the extraction degree of target metal ions was assessed in the pH range from 4 to 10 (Fig. 2).

As it is seen from Fig. 2, at pH=4 the extraction is not effective for most of the studied elements with exception of Bi and Tl. The extraction of Cr is slightly favourable at pH=4 and decreases at higher pH values. An explanation of this phenomenon is the possibility used multi-elemental standard to contain chromium in its highest oxidation state (6+) which under the specified experimental conditions could form an oxo-anion. Unfortunately the documentation, provided by the producer, includes certified values for concentrations of the elements with corresponding uncertainties, but the certificate does not contain information about the oxidation state of elements.

For the whole tested pH range the extraction degrees for V and Pb are below 45%. Best performance for all other studied element is obtained when pH of the model solution was set in the pH interval from 6 to 8. Lowering of the extraction degrees for all elements (with an exception of Tl) were observed at pH=10. Considering the fact, that all studied metal ions (except Tl) are able to form stable negatively charged complexes with hydroxide, the observed trend can be explained with an electrostatic repulsion between M(OH)_{xn}⁻ and the negatively charged MNPs.

Optimization of the sorbent amount

In comparison to classical sorbents used in SPE, the nanoparticles possess significantly higher surface, therefore the amount needed for extraction of analytes should be much lower. The quantity of

Fe₃O₄@C NPs was varied at levels 5, 10, 20 and 30 mg (Fig. 3).

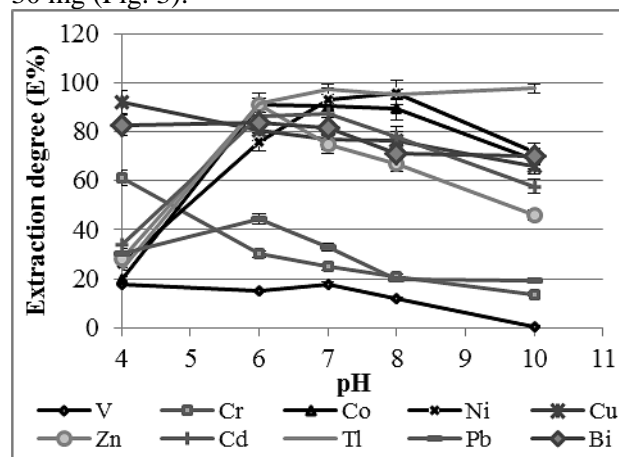


Fig. 2 Effect of solution pH on the extraction degree of metal ions collected on Fe₃O₄@C NPs. Other conditions: 200 mg NPs; C_A = 10 µg L⁻¹; V_A = 50 mL.

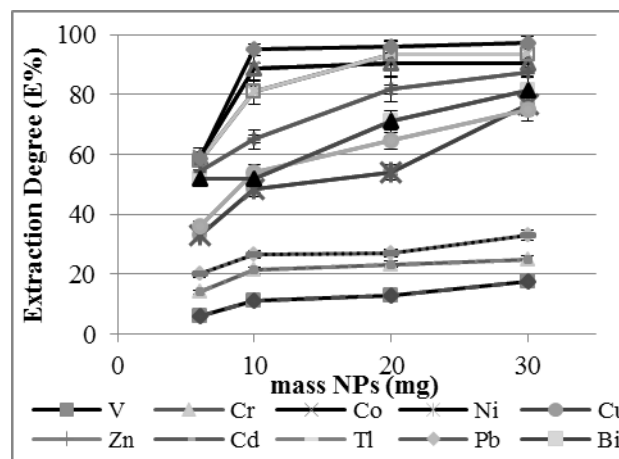


Fig. 3 Effect of the amount of sorbent on the extraction degree of analytes on Fe₃O₄@C NPs. Other conditions: pH=7; C_A = 10 µg L⁻¹; V_A = 50mL.

Extraction degrees higher than 80% were achieved only for Ni, Co and Tl using at least 10 mg of NPs. Further increase of the mass of sorbent leads to an improvement of E% for all elements with exception of Tl, Co and Cr. For most of the elements (except from Cu, Zn and Bi) a uniform extraction is reached when mass of carbon modified NPs is above 20 mg. The mass of carbon modified nanoparticles needed for SPE of studied elements is at least twice higher compared to quantity of unmodified Fe₃O₄ NPs (10 mg) used for group extraction of 9 elements as APDC complexes [3]. This can be explained by the extensively increase of nanoparticles size during carbon modification which reduces the surface/mass ratio.

CONCLUSIONS

A new MW assisted procedure with a hydrothermal reaction with glucose was developed

D.H. Sánchez et al.: "Microwave assisted carbon modification of magnetite nanoparticles, used for solid phase extraction ..." for production of carbon encapsulated magnetite nanoparticles (Fe₃O₄@C). The preliminary modification of magnetite cores with oleic acid leads to improvement of modification procedure. Further development of the modification procedure in the direction of formation of thin and thick carbon layer, respectively, would reduce the consumption of sorbent.

In comparison with classical hydrothermal route, the proposed procedure is fast, simple and easy for implementation.

The synthesised Fe₃O₄@C NPs are promising sorbent for magnetically assisted dispersive SPE of Co, Ni, Cu, Zn, Cd, Tl and Bi.

Acknowledgments: DHS is thankful to the Erasmus+ program for the possibility to be an exchange master student in University of Plovdiv. The authors are thankful to NI15-HF-001 (NPD, University of Plovdiv) for financial support.

REFERENCES

1. J. González-Sálamo, A.V. Herrera-Herrera, C. Fanali, J. Hernández-Borges, *LC-GC Eur.* **29** (2016).
2. M. Faraji, Y. Yamini, M. Rezaee, *J. Iran. Chem. Soc.* **7** (2010) 1–37.
3. V. Stefanova, D. Georgieva, V. Kmetov, I. Roman, A. Canals, *J. Anal. At. Spectrom.* **27** (2012) 1743.
4. I.P. Román, Chisvert Alberto, A. Canals, *J. Chromatogr. A.* **1218** (2011) 2467–2475.
5. G. Giakisikli, A.N. Anthemidis, *Anal. Chim. Acta.* **789** (2013) 1–16.
6. M. Bystrzejewski, K. Pyrzyńska, A. Huczko, H. Lange, *Carbon N. Y.* **47** (2009) 1201–1204.
7. K. Pyrzyńska, M. Bystrzejewski, *Colloids Surfaces A Physicochem. Eng. Asp.* **362** (2010) 102–109.
8. B. Maddah, S. Alidadi, M. Hasanzadeh, *J. Sep. Sci.* **39** (2016) 256–263..
9. L. Bai, B. Mei, Q.-Z. Guo, Z.-G. Shi, Y.-Q. Feng, *J. Chromatogr. A.* **1217** (2010) 7331–6.
10. S. Zhang, H. Niu, Z. Hu, Y. Cai, Y. Shi, *J. Chromatogr. A.* **1217** (2010) 4757–64.
11. F. Zhang, L. Cui, K. Lin, F.-M. Jin, B. Wang, S.-X. Shi, et al., *J. Alloys Compd.* **553** (2013).
12. H. Bakhshi, A. Shokuhfar, N. Vahdati, *Int. J. Miner. Metall. Mater.* **23** (2016).
13. C. Ma, B. Luo, H. Song, L. Zhi, *New Carbon Mater.* **25** (2010) 199–204.
14. S. Xuan, L. Hao, W. Jiang, X. Gong, Y. Hu, Z. Chen, *Nanotechnology.* **18** (2007).
15. N.Y. He, Y.F. Guo, Y. Deng, Z.F. Wang, S. Li, H.N. Liu, *Chinese Chem. Lett.* **18** (2007) 487–490.
16. Z. Wang, P. Xiao, N. He, *Carbon N. Y.* **44** (2006) 3277–3284.
17. Z. Wang, H. Guo, Y. Yu, N. He, *J. Magn. Magn. Mater.* **302** (2006) 397–404.

НОВА МИКРОВЪЛНОВО ПОДПОМОГНАТА ПРОЦЕДУРА ЗА ПОЛУЧАВАНЕ НА ВЪГЛЕРОД-МОДИФИЦИРАНИ МАГНЕТИТНИ НАНОЧАСТИЦИ С ЦЕЛ ПРИЛОЖЕНИЕТО ИМ ЗА ТВЪРДОФАЗНА ЕКСТРАКЦИЯ НА ЕЛЕМЕНТИ

Д. Санчес¹, Д. Георгиева^{2*}, В. Кметов², В. Стефанова²

¹ Университет Аликанте, Испания, PO Box 99, 03080 Аликанте, Испания

² Пловдивски Университет „Паисий Хилендарски“, Катедра аналитична химия и компютърна химия, ул. Цар Асен, 24, 4000 Пловдив, *E-mail: georgieva@uni-plovdiv.net

Постъпила на 14 ноември 2016 г.; приета на 14 декември 2016 г.

(Резюме)

Предложен е нов подход за получаване на въглерод модифицирани магнетитни наночастици, чрез хидротермична реакция с глюкоза, проведена в лабораторна микровълнова система. Изследвана е възможността за изграждане на въглероден слой върху немодифицирани и на третиран с олеинова киселина Fe₃O₄ наночастици. Получените нови материали са охарактеризирани с инфрачервена спектроскопия с пълно вътрешно отражение (ATR FTIR), изследвана е стабилността им в кисела среда. Установено е че за успешно изграждане на защитен слой от въглерод върху магнетитното ядро е необходима предварителна модификация с олеинова киселина.

Изследван е потенциала на получените нови материали за магнетно подпомогната твърдофазна екстракция на V, Cr, Co, Ni, Cu, Zn, Cd, Tl, Pb и Bi от моделни разтвори. Проследено е влиянието на киселинността на разтворите и количеството на наночастиците върху ефективността на екстракцията на изследваните елементи.

Ключови думи: въглерод-модифицирани магнетитни наночастици, МВ подпомогната модификация, твърдофазна екстракция

Understanding the degradation processes of the electrolyte of lithium ion batteries by chromatographic analysis

E. Rosenberg^{1*}, C. Kanakaki¹, A. Amon², I. Gocheva², A. Trifonova²

¹Vienna University of Technology, Institute of Chemical Technologies and Analytics, Getreidemarkt 9/164 AC, A-1060 Vienna, Austria

²Austrian Institute of Technology, Mobility Department, Electric Drive Technologies, Giefinggasse 2, A-1210 Vienna, Austria

Received November 29, 2016; Revised December 20, 2016

The electrolyte of lithium ion batteries (LIBs) degrades both under normal operation – e.g. in the formation of the solid electrolyte interphase (SEI) – and in particular under conditions of extreme temperature, voltage or current flow. Degradation products of the electrolyte (typically a mixture of organic carbonates such as ethylene carbonate (EC), ethylmethyl carbonate (EMC), dimethyl carbonate (DMC) or diethyl carbonate (DEC) with a suitable conducting salt such as LiPF₆) can be volatile or permanent gases, e.g. H₂, CO, CO₂ and the low hydrocarbons (C1-C3) and are thus ideally determined by gas chromatography. GC with various detectors can be used, accounting for the vastly different detectability of the degradation products with common GC detectors like flame ionization, thermal conductivity or mass spectrometric detection. Evolved gas analysis is complemented by the direct analysis of the electrolyte which requires careful opening of the cell for post mortem analysis. In the presence of the conducting salt LiPF₆, but also in the presence of water or air, condensed or more polar degradation products are formed which are more easily separated in liquid phase by RP-HPLC or ion chromatography. These include carbonate oligomers (with varying number of ethoxy moieties resulting from the ring-opening reaction of the ethylene carbonate) and organic phosphates and monofluorophosphates, resulting from the degradation and (partial) hydrolysis of the conducting salt and its reaction with the organic solvent. Chromatographic techniques, in particular with mass spectrometric detection, are indispensable tools to characterize the wide spectrum of degradation products, and to better understand the processes leading to electrolyte degradation. This forms the basis for the improvement of lithium ion battery safety and performance.

Keywords: lithium-ion battery, electrolyte; degradation products, gas chromatography, liquid chromatography

INTRODUCTION

Lithium ion batteries (LIBs) are nowadays indispensable sources and storage devices for electric energy. They are widely used in industry, transport and telecommunication, and have become essential in many applications of our daily life such as portable computers, mobile phones, devices and instruments, and all sorts of consumer electronics [1]. LIBs are the currently preferred technology, as they are lighter than other rechargeable batteries for a given capacity; the Li-ion chemistry delivers a high open-circuit voltage; LIBs are characterized by a low self-discharge rate (about 1.5% per month) and they do not suffer from battery memory effect (i.e. loss of capacity upon repeated charging/discharging cycles) [2]. They have a large environmental impact as they are rechargeable and thus reduce toxic landfill [3]. This advantage is contrasted by a number of shortcomings. These are: poor cycle life, particularly in high current applications; rising internal resistance with cycling and age; and the need for Li-

ion batteries with even higher capacity for high-power applications [4]. Finally, but of highest relevance, are to be mentioned the safety concerns in case of overheating or overcharging or internal short circuit of the battery. A number of incidents have attracted public attention to the safety of lithium ion batteries, such as the recent recall of Samsung Galaxy Note 7 mobile phones due to potentially defective lithium ion batteries [5], three car fires involving the battery electric vehicle Tesla Model S that occurred in 2013, or the Boeing 787 Dreamliner Li-ion battery fire incidents in 2013–2014, as well as serious accidents on cargo airplanes involving Li-ion batteries in the cargo hold, that have increased the awareness of the safety risks associated with this type of battery [6].

One of the most important fields of application of LIBs is in electric vehicles (both hybrid and full electric vehicles). It is anticipated that by 2020, 12.9 million electric vehicles will exist, which would represent approx. 3% of the global car stock [7]. With both the number and the size of lithium ion battery packs increasing (the battery pack of a full

* To whom all correspondence should be sent.
E-mail: erosen@mail.zserv.tuwien.ac.at

electrical vehicle may weigh up to 250 kg), the aspect of battery safety becomes crucial. Lithium ion batteries contain by mass ca. 10-12% of an organic electrolyte [8]. This is a highly flammable solvent that has the Li salt dissolved while the Li ions cycle between cathode and anode. Electrochemical, thermal and hydrolysis reactions lead to the partial decomposition of the electrolyte and the formation of even more volatile reaction products. When these are vented upon overheating of the LIB, there is the risk of fire or explosion of the entire battery pack. As the degradation of the LIB electrolyte is a continuously proceeding process, it can be followed by monitoring the formation of volatile degradation products, as well as the composition of the electrolyte itself [9]. This provides important diagnostic information, both on the actual state (of charge, SOC, and of health, SOH) of the battery, as well as on its preceding charging history, and can thus be used to better understand electrode and electrolyte processes to eventually increase battery safety and performance. This review will therefore discuss chromatographic techniques that allow the analysis of the organic electrolyte and its reaction or degradation products (Figure 1)

Electrolytes used in lithium ion batteries must fulfill a variety of conditions: They must withstand the extreme redox environment at both cathode and anode side and the voltage range during electrochemical cycling without decomposition. Second, they should be stable at typical cell operating temperatures which may range up to 60-70°C. Third, they must be good solvents for the lithium salts dissolved at relatively high concentrations (1 M typically). Furthermore, they should have favorable physicochemical properties such as low viscosity, high flash and boiling point, and ideally be non-toxic, environmentally benign and can be produced at low cost. It is evident that none of the currently used solvents satisfies all requirements to the same extent. For this reason, solvent mixtures are used in the electrolytes of commercial LIBs: Polar aprotic solvents, such as the organic carbonates have high dielectric constant and are selected to solvate the lithium salts at the high concentrations (1 M) in which they are present.

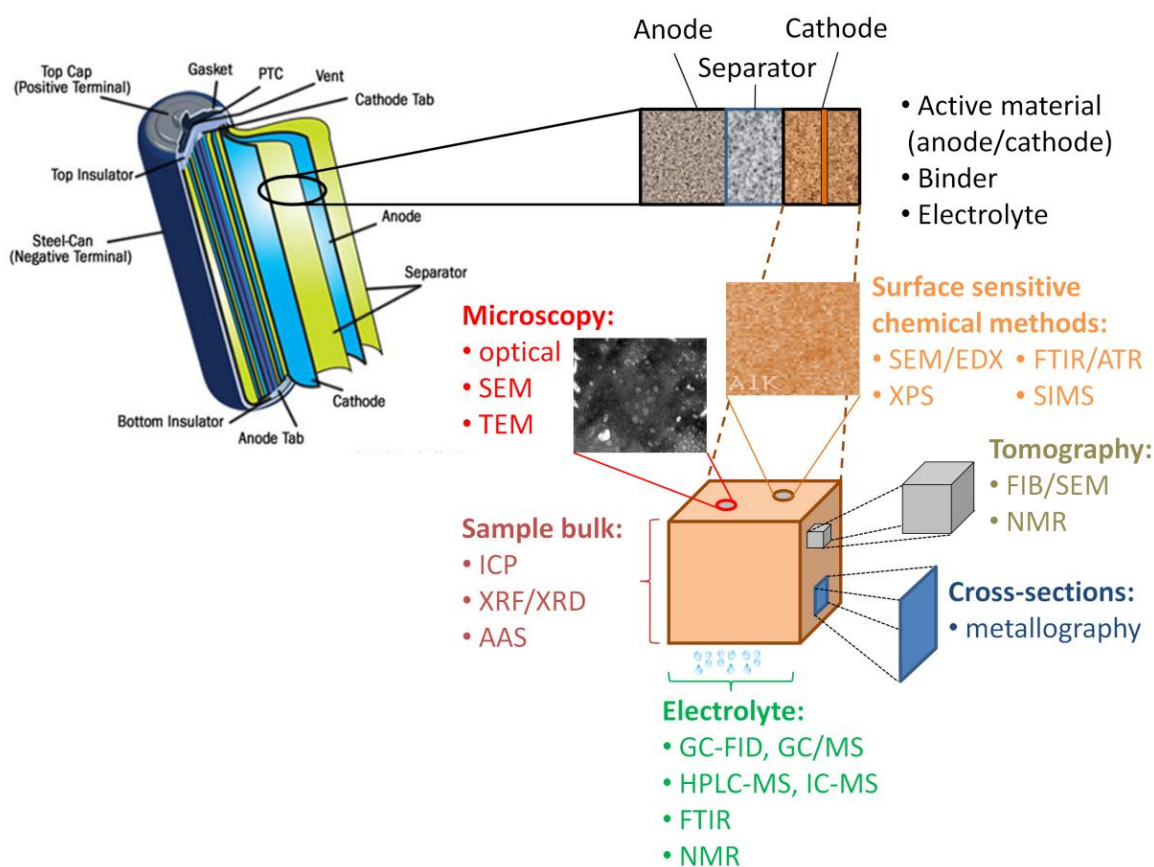


Figure 1 Overview of components inside a Li-ion battery and physico-chemical methods for their characterization after post-mortem analysis (after Waldmann *et al.* [21]).

On the contrary, solvents with low viscosity and low melting point are used to meet the requirements of high ion mobility in the temperature range considered. A variety of solvents has been investigated for this purpose, including dimethyl carbonate (DMC), diethyl carbonate (DEC), ethyl methyl carbonate (EMC), propylene carbonate (PC), ethylene carbonate (EC), diethoxyethane, dioxolane, γ -butyrolactone, and tetrahydrofuran (THF) [10]. More recently, also heteroatom-containing organic solvents have been suggested [11], as well as ionic liquids [12], however, the investigations presented in this review will concentrate on the former group of substances whose properties are presented in Table 1. A great variety of conducting salts has been investigated, including LiPF_6 , LiBF_4 , LiAsF_6 , LiClO_4 and LiCF_3SO_3 . The most characteristic properties of these conducting salts are summarized in Table 2. Only those conducting salts can be used whose anions are stable under typical operating

conditions of the LIB, avoiding the possibility of oxidation at the anode. This rules out the use of simple anions such as Cl^- , Br^- or I^- . The most commonly used conducting salt is LiPF_6 which excels in view of its safety, conductivity and the balance between conductivity and the balance between ionic mobility and the dissociation constant. The only, although significant disadvantage of LiPF_6 is its reactivity with water in the presence of which it forms the highly toxic and corrosive HF. For this reason, humidity must be minimized when handling a LiPF_4 -containing electrolyte.

Since no single solvent has all desired properties for safe and efficient LIB operation, electrolytes are typically formulated and solvents combined to produce the desired viscosity, conductivity and stability and to dissolve easily the particular Li-ion salt.

Table 1. Properties of the most important organic solvents used in LIB electrolytes. (Data compiled from Amon [13] and the PubChem database [14].)

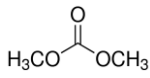
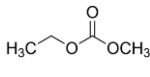
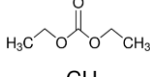
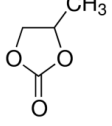
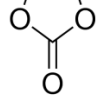
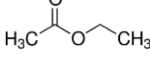
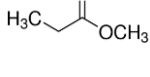
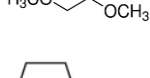
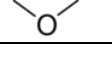
Electrolyte Components	CAS Registry No.	Structure	Melting / Boiling Point (°C)	Dielectric constant ϵ (25°C)	Viscosity η (cP, 25°C)	Vapor Pressure (torr)	Flash Point (°C)	Auto-Ignition Temperature (°C)
Dimethyl carbonate (DMC)	616-38-6		2 / 91	3.1	0.59	18 at 21°C	18	458
Ethyl methyl carbonate (EMC)	623-53-0		14 / 107	3.0	0.65	27 at 25°C	25	440
Diethyl carbonate (DEC)	105-58-8		-43 / 126	2.8	0.75	10 at 24°C	25	445
Propylene carbonate (PC)	108-32-7		-49 / 242	65	2.53	0.13 at 20°C	135	455
Ethylene carbonate (EC)	96-49-1		36 / 248	90 (at 40°C)	1.9 (at 40°C)	0.02 at 36°C	145	465
Ethyl acetate (EA)	141-78-6		-83 / 77	6.0	0.45	93 at 25°C	-4	4
Methyl propionate (MP)	554-12-1		-84 / 102	5.6	0.60	64 at 20°C	11	469
Ethyleneglycol dimethylether (DME)	110-71-4		-58 / 84	7.2	0.46	48 at 20°C	0	202
Tetrahydrofuran (THF)	109-99-9		-108 / 65...66	7.4	0.46	143 at 20°C	-17	321

Table 2. Properties of the most important conducting salts used in Li ion batteries [13, 17].

Salt	T _{Decomp.} in solvent [°C]	Al-corrosion	Conductivity (1.0 M, EC/DMC, 25°C)	Electrochemical stability until	Characteristics
LiClO ₄	>100	No	8.4 mS/cm	4.5 V vs. Li ⁺ /Li	Not sensitive to hydrolysis; no formation of HF; explosive
LiAsF ₆	>100	No. Passivates Al current collector.	11.1 mS/cm	4.5 V (cathodic) / 6.3 V anodic vs. Li ⁺ /Li	Good SEI formation. Toxic degradation products.
LiBF ₄	>100	No	4.9 mS/cm		Strong Lewis base; decomposes and forms HF
LiPF ₆	>70	Effectively suppresses Al corrosion	10.7 mS/cm	4.8 V vs. Li ⁺ /Li	Very sensitive to hydrolysis
LiCF ₃ SO ₃	>100	Yes	>10 mS/cm		
LiN(SO ₂ F) ₂	>100	Yes: Insufficient passivation of Al electrode	>10 mS/cm	4.8 V vs. Li ⁺ /Li	Not sensitive to hydrolysis, no formation of HF; expensive production

As an example, high dielectric solvents with a high viscosity are typically mixed with solvents of low viscosity to produce an electrolyte that is sufficiently conductive and liquid in the temperature window of operation. Some commonly used electrolytes are 1 M LiPF₆ in 50:50 w/w mixtures of EC with DMC, DMC or EMC (known under trade names LP30, LP40 and LP50 electrolytes, respectively). EC can stabilize Li⁺ ions more effectively than DEC or DMC [15]. The resulting electrolyte offers a reasonable stability over a wide potential range. In order to improve the formation of a stable solid-electrolyte interphase (SEI) which is of crucial importance for cell stability, various additives such as vinylene carbonate (VC) are added to the electrolyte [16, 17].

In addition to liquid electrolytes [18], other forms of electrolytes exist such as polymer [19], gel and ceramic electrolytes [20]; however, these will not be discussed in this context

METHODS FOR THE ANALYSIS OF LITHIUM ION BATTERY ELECTROLYTES

When studying LIB electrolyte decomposition only as an effect of temperature, humidity or oxidation, simulation experiments can be performed under laboratory conditions with the isolated electrolyte, without the need of using a commercial

electrochemical cell or a laboratory cell set-up. As soon as electrochemical reactions are to be considered as well, it is inevitable to have either a commercial battery or a laboratory-type electrochemical cell to be able to go through various charging / discharging cycles, or to subject the electrochemical cell to defined stress conditions. For fundamental studies, laboratory-made electrochemical cells are often favorable, as the fraction of electrolyte relative to the other cell components is typically larger, and also can easier be extracted. Commercial cells require a very careful disassembly (under inert atmosphere), the separation into its components, and the partially tedious extraction of the electrolyte prior to analysis (Figure 2). A very comprehensive description of cell disassembly procedures has been given by Waldmann *et al.* [21]. It shall be noted that chromatographic analysis not necessarily has to take place *ex situ* and *post mortem*. *In situ* chromatographic analysis is also possible and meaningful when targeting the volatile products of LIB electrolyte degradation: Since most of the LIBs have a gas vent valve in order to avoid pressure build-up due to the formation of gaseous degradation products, they would release volatiles to the environment during operation which can be analyzed by gas chromatography.

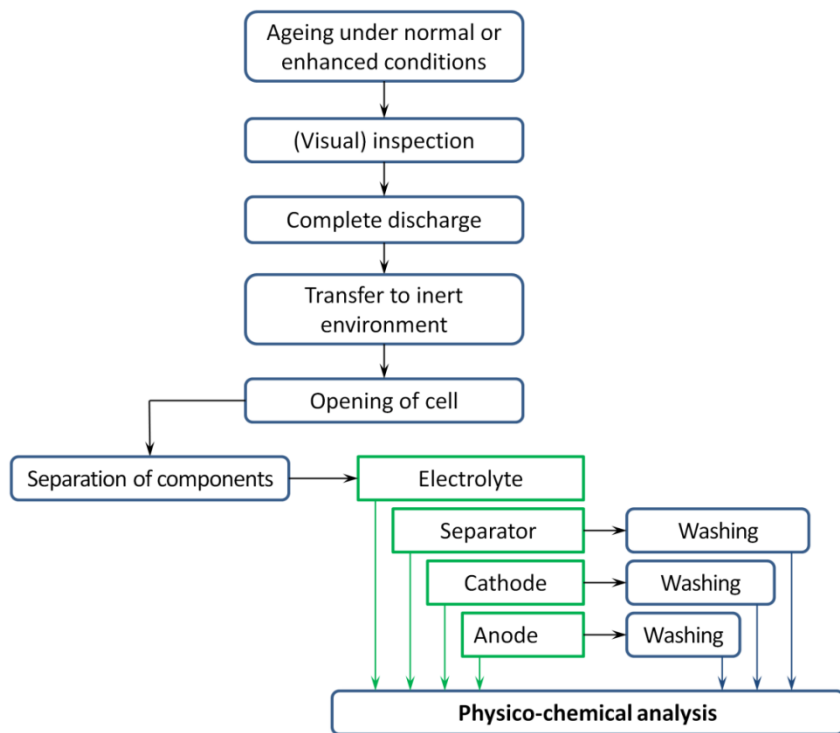


Figure 2 Flow chart for the disassembly of Li-ion batteries prior to the analysis of individual cell components (after Waldmann et al. [21])

Analysis of the LIB electrolyte provides information on the degradation products and allows modeling of the (electrochemical, thermal, oxidative or hydrolytic) reaction mechanisms leading to these products. Spectroscopic methods (particularly UV/Vis [22], FTIR [23, 24, 36], NMR [25] and mass spectrometry [26]) are widely used and are at advantage when measuring electrolyte composition and degradation *in situ* in laboratory set-ups, as they offer high time resolution and they do not necessarily require sampling. Chromatographic methods, on the contrary, do require sampling, but at the same time provide more information as they are capable of resolving and quantifying even more complex mixtures.

For the analysis of the electrolyte mixture, both liquid and gas chromatographic techniques can be used: Gas chromatography offers high separation power, positive identification capabilities (when mass spectrometric (MS) detection is used), good quantification and a high dynamic range, making it possible to detect even minor constituents in the mixture, such as electrolyte additives or degradation products. Liquid chromatography is used to investigate the less or non-volatile constituents of the electrolyte and particularly its polar degradation compounds; the technique often results in a less efficient separation than GC, and identification is more difficult even with mass spectrometric

detection due to the lack of spectral libraries. Confirmation of tentative structures is therefore either based on high-resolution MS measurements which allow the calculation of the elemental composition of the particular analyte, or the use of MS/MS detection, in which a selected precursor ion is fragmented and the fragments are detected, thereby providing increased structural information.

Gas chromatographic analysis

Gas chromatography with flame-ionization detection (GC-FID) and thermal conductivity detection (GC-TCD) was used for the analysis of volatile products generated during long cycling of a LIB [27]. The use of two GC setups is necessary due to the fact that the FID does not respond to fixed gases and oxidized compounds, such as N₂, O₂, or CO₂ which have to be determined by TCD, although with lower sensitivity. The authors developed a device in which they could quantitatively collect the volatiles formed in the degradation of the electrolyte and establish a mass balance. It was found that during normal cycling, the volume of gaseous products formed is between 1 and 2 ml for a standard 18,650 (Boston Power) cell, and that the low hydrocarbons (CH₄, C₂H₆, C₃H₈ and C₃H₆) represent the largest fraction of this. Under overcharging conditions, the gas volume formed is drastically increased (to ca. 10 cm³) of which CO₂ forms the by

far largest fraction with about 75%, whereas overdischarge conditions will lead to the formation of an even larger gas volume (of about 40 cm³), with the appearance of CO as a major product and the virtual disappearance of the lowest alkanes (Table 3).

Analyzing the neat electrolyte by GC/FID or GC/MS is straightforward: Medium polarity columns (such as DB-17 ((50%-phenyl)-methylpolysiloxane), DB-1701 ((14%-Cyanopropyl-phenyl)-methylpolysiloxane) or DB-200 ((35% Trifluoropropyl)-methyl-polysiloxane) and equivalent) of dimensions 30 m x 0.25 mm ID can

be used with relatively large film thickness (up to 1 μm) in order to provide sufficient capacity to avoid column overload by the main constituents of the electrolyte. Direct liquid injections of the undiluted electrolyte or after dilution in a suitable solvent (e.g. methanol or acetonitrile) are performed with a suitable high split ratio (e.g. 100:1). Under these conditions, the main volatile constituents of a commercial LIB electrolyte can be determined and identified on the base of their mass spectra as well as the additives present at the low and sub-percent level [28, 29] (Figure 3).

Table 3. Composition of gases generated in the nominal operating voltage range 4.2 V–2.5 V, and during overcharging and overdischarging (relates to a standard 18650 Li ion cell with 1 Ah capacity). (Reprinted from [26], with permission of Elsevier)

Test no.	Test conditions		Cycle number	Capacity at end cycle (Ah)	Composition of detected gases (%)							Total volume (ml)	
	Charge current	Discharge current			O ₂	N ₂	CO ₂	CO	CH ₄	C ₂ H ₆	C ₃ H ₈		C ₃ H ₆
R1	Before cycle test				5.3	42.5	1.7		40	4.2	0.4		0.95
R2		100 mA	2043	0.6	2.7	8.5	2.2		72	6.7	7.2	0.4	2.23
R3	200 mA	125 mA	2397	0.6	1.7	5.9	4.1		73	7.0	7.9	0.4	2.42
R4		200 mA	2331	0.5	1.5	6.5	7.2		61	7.6	15.6	0.8	2.63
R5		500 mA	2301	0.5	2.3	11.0	4.0		62	9.2	10.4	0.6	1.73
R6	125 mA		1915	0.6	2.1	7.7	1.3		75	7.8	6.2	0.2	2.01
R7	200 mA	125 mA	2570	0.5	3.2	6.6	3.2		72	8.3	7.2	0.4	2.78
R8	500 mA		3111	0.6	6.1	25.4	2.5		51	6.2	8.5	0.4	1.75
R9	200/200 mA, overcharge		880	0.6	1.3	5.3	75.6		12	2.6	2.7		10.57
R10	200/200 mA, over-discharge		880	0.0	0.3	1.5	71.2	0.6	21	3.2	0.8	1.0	40.21

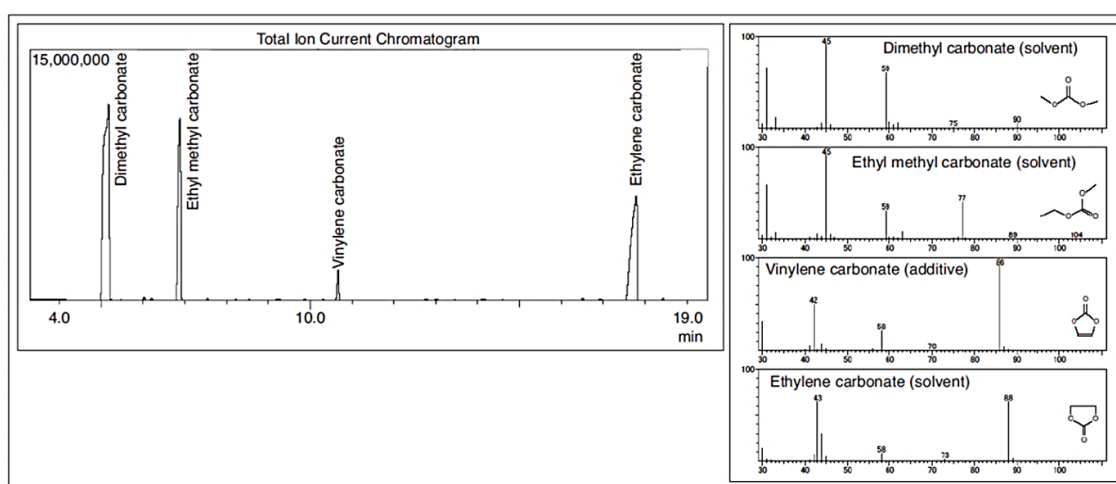


Figure 3: GC/MS chromatogram of a mixture of common electrolyte compounds (DMC, EMC and EC) and an electrolyte additive (VC) and mass spectra of the individual constituents [29].

In a study of the thermal stability of the organic electrolyte, various electrolyte mixtures were exposed to elevated temperature in the presence and absence of oxygen [30]. Even in the presence of oxygen and humidity, the carbonate solvents are

remarkably stable up to a temperature of ca. 70°C which is often considered a normal operating temperature for LIBs. When this temperature is exceeded, then the electrolyte rapidly starts decomposing, leading to the formation of a large

number of aliphatic and cyclic degradation products (Figure 4). A similar study was performed by Nowak and co-workers [31] who have thermally aged commercial LP50 electrolyte for 21 days at 80°C. The formation of the organic phosphates diethyl- (DEFP), dimethyl- (DMFP), and methyl-ethylfluorophosphate (MEFP) as well as triethyl- (TEFP) and trimethylphosphite (TEP) was detected by GC/MS [32], and also confirmed by ion chromatography with electrospray-MS detection (IC-ESI-MS). In a further extension of this work, the same group of authors used GC/MS with chemical ionization to elucidate the structure of LP50 thermal degradation products [33]. The authors were able to confirm the formation of various cyclic and (dominantly) aliphatic (poly)ethers and carbonate esters as illustrated in Table 4.

The most interesting finding of these authors was that, when the electrolyte was kept at elevated temperature (90°C) for a longer period of time (21 days), degradation commenced to a larger extent only after an induction period of ca 5-10 days. After this period of time, the formation of linear polyethylene glycol ethers increased continuously, while the concentration of carbonate esters with a monoethylene glycolether moiety appeared to reach equilibrium, and the formation of carbonate esters with di- and presumably also triethyleneglycol ether moieties further increased. This appears plausible, as this would explain some of the reaction mechanisms observed within the commercial Li electrolytes.

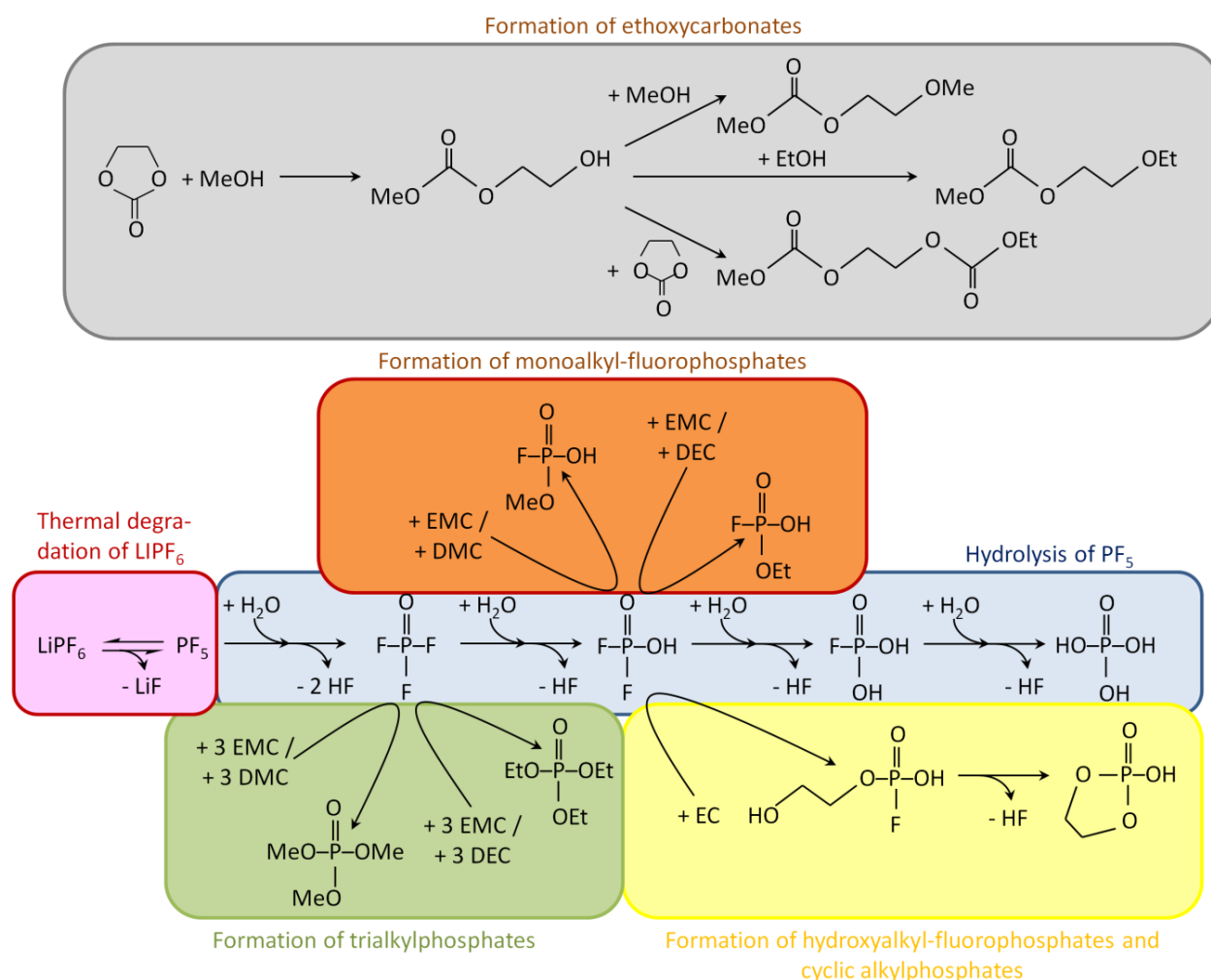
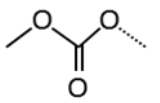
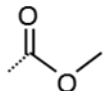
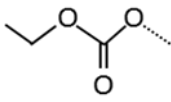
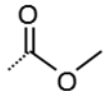
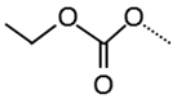
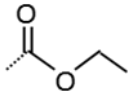
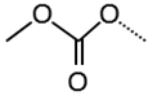
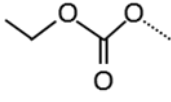
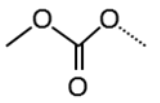
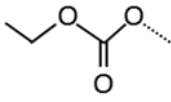


Figure 4. Reaction schemes proposed for the degradation of commercial electrolytes containing EC, EMC, DEC or DMC and LiPF₆ as conductive salt. After Grützkke *et al.* [32].

Table 4. Thermal degradation products of LP50 electrolyte identified by GC-MS with gas- and liquid chromatographic methods [9, 32].

$R^1 \left(\text{---} \left[\text{---} \text{CH}_2 \text{---} \text{CH}_2 \text{---} \text{O} \right]_n \text{---} R^2 \right)$	R^1	R^2	n	Sum Formula	Molecular mass
Series 1			1	C ₆ H ₁₀ O ₆	178.047740
			2	C ₈ H ₁₄ O ₇	222.073955
Series 2			1	C ₇ H ₁₂ O ₆	192.063390
			2	C ₉ H ₁₆ O ₇	236.089605
Series 3			1	C ₈ H ₁₄ O ₆	206.079040
			2	C ₁₀ H ₁₈ O ₇	250.105255
Series 4		CH ₃	1	C ₅ H ₁₀ O ₄	134.057910
			2	C ₇ H ₁₄ O ₅	178.084125
Series 5		CH ₃	1	C ₆ H ₁₂ O ₄	148.073560
			2	C ₈ H ₁₆ O ₅	192.099775
Series 6	CH ₃ O	CH ₃	1	C ₄ H ₁₀ O ₂	90.068080
			2	C ₆ H ₁₄ O ₃	134.094295
Series 7		H	1	C ₄ H ₈ O ₄	120.042260
			2	C ₆ H ₁₂ O ₅	164.068475
Series 8		H	1	C ₅ H ₁₀ O ₄	134.057910
			2	C ₇ H ₁₄ O ₅	178.084125
Series 9	HO	CH ₃	1	C ₃ H ₈ O ₂	76.052430
			2	C ₅ H ₁₂ O ₃	120.078645
Series 10	HO	H	1	C ₂ H ₆ O ₂	62.036780
			2	C ₄ H ₁₀ O ₃	106.062995

It was already observed earlier that the degradation of the LIB electrolyte is dependent on the water content and also the container material [34]. The authors speculated that in glass containers the reaction of hydrofluoric acid with the silicon oxide from the glass leads to the formation of SiF₄ and H₂O which itself can induce further electrolyte decomposition.

Very similar results were obtained when the electrolyte and gaseous emissions from commercial cells were investigated: Looking at the volatile emissions, Dahn and co-workers remarked that the emission of gaseous components takes place in two distinguishable steps, namely at 3.7 and 4.3 V charging voltage [35], the first step being attributable to reactions mainly at the cathode, while

the second step was attributed to the anodic reaction, distinguished by a stronger formation of CO₂ and a decreased production of the low hydrocarbons (C₂H₆, C₂H₄ and C₃H₈) compared to the first gas evolution step.

More recently, three further hyphenated GC techniques were used to identify volatile emissions from degraded LIB electrolytes. In the first study, Laruelle and co-workers used gas chromatography with Fourier-transform infrared spectrometric detection (GC/FTIR) to complement GC/MS analyses, thereby confirming the presence of degradation products such as acetaldehyde whose chromatographic peak coincides with that of ethylene oxide [36]. Schug and co-workers [37] used GC with vacuum UV detection (GC-VUV) for the

determination of degradation products in the off-gassing from three different lithium-ion battery samples. Gas samples collected from LiCoO₂, LiMn_{0.33}Ni_{0.33}Co_{0.33}O₂, and LiMnNi 18,650 cells (LCO, NMC, and MN cells, respectively) showed similar qualitative and somewhat diverging quantitative patterns with the confirmation of the production of acetaldehyde and traces of propionaldehyde. Kanakaki *et al.* [30] have used gas chromatography with a dielectric barrier-discharge ionization detector (GC-BID) for the analysis of volatile degradation products. The particular advantage of this plasma ionization detector is that it responds to virtually all compounds, including the permanent gases (N₂, O₂) and highly or fully oxidized compounds (as CO, CO₂ and HCHO) which give a very poor or no FID response at all. While most of the studies so far have been of qualitative nature, aiming to identify the volatile degradation products from the decomposition of the electrolyte under thermal aging or overcharge conditions, few authors only reported quantitative results. Among these are Ohsaki and co-workers who report the formation of volatile compounds from the degradation of an EC/EMC electrolyte in a 633,048 type prismatic cell [38]. Dahn *et al.* [35] have investigated initial gas formation in Li[Ni_{0.4}Mn_{0.4}Co_{0.2}]O₂ (NMC442) pouch cells with three different electrolytes: 3:7 ethylene carbonate : ethyl methyl carbonate (EC:EMC) with 1 M LiPF₆ as the control, control + 2% prop-1-ene-1,3-sulfone (PES) and control + 2% vinylene carbonate (VC). *In situ* volume measurements revealed three main features of gas evolution, namely an initial gas step, gas absorption, and a second gas step at higher voltage. In addition to identification by GC/MS, the authors also determined the gas volumes formed. These results compare well with the findings of Kumai and co-workers [27] who have determined quantitatively the gases evolving during charging cycles of Li_xC₆/Li_{1-x}CoO₂ cells using electrolytes such as 1 M LiPF₆ in propylene carbonate (PC), dimethyl carbonate (DMC), ethyl methyl carbonate (EMC), and diethyl carbonate (DEC). A further study also reported quantitative results for the gases liberated in the thermal abuse of high-power lithium cells [39]. The commercial cell used in this study (a high-power 18,650 cell) contained an electrolyte consisting of ethylene carbonate/ethyl methyl carbonate (EC:EMC, 3:7 by wt.) solvent with 1.2M LiPF₆ as conducting salt. Most interesting was the observation that the profile of volatile emissions (mainly H₂, CO, CO₂ and C1-C3 hydrocarbons) from the cell for which thermal runaway was induced by heating to a temperature of >84°C

differed, depending on whether the cell housing was punctuated to vent the evolved gases or not.

Liquid chromatographic analysis

Somewhat less frequent than GC methods, liquid chromatography has been used for the analysis of degradation products. LC separation addresses the less volatile degradation products, including the analysis of the conducting salt and its degradation/reaction products with the organic solvents. For the latter task, ion chromatography is preferably used, as ions show little retention on reversed phase stationary columns. The probably first use of chromatographic techniques to identify LIB degradation products was reported by Yoshida *et al.* [40] who used hyphenated HPLC-FTIR to elucidate the degradation mechanism of electrolytes in a lithium-ion cell with LiCoO₂ and graphite electrodes during initial charging. The solvents used in this work were EC, DMC, EMC and DEC with LiPF₆ as conducting salt. In addition to transesterification products, diethyleneglycol dicarbonate methyl- and ethyl esters were further products identified in the electrolyte. In their seminal work [36], Laruelle and co-workers used electrospray-high resolution-MS (ESI-HR-MS) to elucidate the structure of degradation products. They concluded that at least six series of degradation products of varying ethoxylate chain length and different end groups (H-, methyl- and methyl carbonate-terminated) are formed. Subsequent work from the group of Nowak used ion chromatography to detect monofluorophosphate and organic substituted phosphates in the aged commercial LP50 electrolyte in LMNO/Li half cells after performing about 50 electrochemical cycles [41]. In a follow-up work of the same group [42], a larger number of organic phosphates (including organic monofluorophosphates) was detected by IC-ES-MS in the electrolyte under thermal ageing conditions. The study was slightly extended to report the influence of the electrolyte volume and the temperature on the formation of organophosphates, and the influence of the separator materials and the storage container materials on the thermal ageing, as well as to provide quantitative results on the degradation products [31]. Earlier obtained results were repeatedly reported by the group in other papers using ESI-MS/MS and ESI-time of flight (TOF)-MS [43, 44] as well as HPLC-DAD and HPLC with ESI- and APCI-MS detection (Figure 5) [45]. Osaka and co-workers [46] used HPLC-Q-TOF-MS which would allow elucidation of the deterioration mechanism. The analysis results showed that the degradation products contain multiple components, including polymers of

carbonate compounds and – detected for the first time –also (polymeric) phosphate esters, which are formed via electrochemical and chemical reactions, resulting in remarkably reduced capacity. Altogether, this demonstrates the versatility that HPLC has – particularly with MS detection – as a complementary analytical tool to GC/MS, providing information on the polar, ionic and oligomeric compounds that are not amenable to GC analysis.

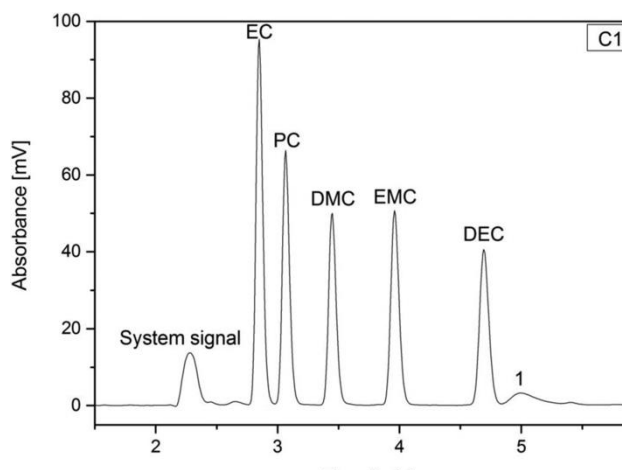


Figure 5. Separation of the electrolyte components EC, PC, DMC, EMC and DEC by HPLC-UV/VIS using a C18 column (Thermo Fisher Scientific Acclaim 120 C18, 250 mm x 4.6 mm ID, 5 μ m particle size). Reproduced from [44] with permission.

SUMMARY AND CONCLUSION

Chromatographic methods have been shown to be valuable tools to gain insight into the thermal, electrochemical, hydrolytic and oxidative processes leading to the formation of degradation products. GC/MS is the method of choice to identify and quantify volatile degradation products ranging from permanent gases (e.g. H₂, CO, CO₂ and the low hydrocarbons) to higher and oxygenated hydrocarbons (linear and cyclic ethers, esters and ethylene glycol derivatives). The amount and relative fractions in the evolved gas are indicative for the dominant degradation reaction. The polar, ionic and polymeric degradation products are more advantageously detected by HPLC, particularly with MS detection. Since the soft ionization mechanisms in LC/MS with single-quadrupole MS detection provide only simple mass spectra with hardly any structural information, more sophisticated mass spectrometers, such as MS/MS, TOF-MS or Q-TOF-MS instruments are required to increase the structural information by providing either high mass accuracy (and thus the ability to calculate elemental formulae), or fragmentation. In this way both the degradation products of the conducting salt (most often LiPF₆), as well as its numerous reaction products with the organic solvent of the electrolyte

can be identified. The identification of degradation products of LIB electrolytes is an important step in understanding the degradation mechanisms of LIB electrolytes, and in being able to improve battery safety and performance.

Acknowledgments: Financial support of this work by the Austrian Research Promotion Agency (FFG) in the frame of the Project "SiLithium" (Proj. No. 835790) is gratefully acknowledged.

REFERENCES

1. D. Deng, *Energy Sci & Eng.*, **3**, 385 (2015).
2. N. Nitta, F. Wu, J.T. Lee, G. Yushin, *Materials Today*, **18**, 252 (2015).
3. J.F. Peters, M. Baumann, B. Zimmermann, J. Braun, M. Weil, *Renewable Sust. Energy Rev.* **67**, 491 (2017).
4. O. Gröger, H.A. Gasteiger, J.-P. Suchsland, *J. Electrochem. Soc.*, **162**, A2605 (2015).
5. New York Times, *Samsung's Recall: The Problem With Lithium-Ion Batteries* (03.09.2016), online available at: http://www.nytimes.com/2016/09/03/technology/samsungs-recall-the-problem-with-lithium-ion-batteries.html?_r=0
6. F. Larsson, P. Andersson, B.-E. Mellander, *Batteries* **2**, 9 (2016), doi:10.3390/batteries2020009.
7. International Energy Agency, Paris (www.iea.or) Global EV Outlook 2016: Beyond one million electric cars (2016).
8. J.B. Dunn, L. Gaines, M. Barnes, J. Sullivan, M. Wang, *Material and Energy Flows in the Materials Production, Assembly, and End-of-Life Stages of the Automotive Lithium-Ion Battery Life Cycle*. Argonne National Laboratories ANL/ESD/12-3 (2012). Available online at: <http://www.ost.gov/bridge>
9. G. Gachot, P. Ribière, D. Mathiron, S. Grugeon, M. Armand, J.-B. Leriche, S. Pilard, S. Laruelle, *Anal. Chem.*, **83** (2011) 478.
10. T.R. Jow, K. Xu, O. Borodin, M. Ue (eds.), *Electrolytes for Lithium and Lithium-Ion Batteries*. Springer, Heidelberg (2014).
11. K. Xu, *Chem. Rev.*, **114**, 11503 (2014).
12. A. Lewandowski, A. Świdarska-Mocek, *J. Power Sources*, **194**, 601 (2009).
13. A. Amon, *Master Thesis*, University of Vienna (2015).
14. PubChem Compound Database; <https://pubchem.ncbi.nlm.nih.gov/> (accessed Nov. 21, 2016).
15. V. Tarnopolskiy, J. Kalhoff, M. Nádherná, D. Bresser, L. Picard, F. Fabre, M. Rey, S. Passerini, *J. Power Sources*, **236**, 39 (2013).
16. D. Aurbach, K. Gamolsky, B. Markovsky, Y. Gofer, M. Schmidt, U. Heider, *Electrochim. Acta*, **47**, 1423 (2002).
17. C. Hartnig, M. Schmidt, in: R. Korthauer (Hrsg.), *Handbuch Lithium-Ionen-Batterien*, pp. 61-77, Springer, Berlin, Heidelberg (2013).
18. S. Zhang and T. Jow, *J. Power Sources*, **109**, 458 (2002).

19. E. Cho, J. Mun, O.B. Chae, O.M. Kwon, H. -T. Kim, J. H. Ryu, Y.G. Kim, S.M. Oh, *Electrochem. Commun.*, **22**, 1 (2012).
20. E. Sarasketa-Zabala, F. Aguesse, I. Villarreal, L.M. Rodriguez-Martinez, C.M. López, P. Kubiak, *J. Phys. Chem. C*, **119**, 896 (2015).
21. T. Waldmann, A. Iturrondobeitia, M. Kasper, N. Ghanbari, F. Aguesse, E. Bekaert, L. Daniel, S. Genies, I. Jiménez Gordon, M.W. Löble, E. De Vito, M. Wohlfahrt-Mehrens, *J. Electrochem. Soc.*, **163**, A2149 (2016).
22. M.U.M. Patel, R. Dominko, *ChemSusChem*, **7**, 2167 (2014).
23. F. Shi, H. Zhao, G. Liu, P.N. Ross, G.A. Somorjai, K. Komvopoulos, *J. Phys. Chem. C*, **118**, 14732 (2014).
24. K. Hongyou, T. Hattori, Y. Nagai, T. Tanaka, H. Nii, K. Shoda, *J. Power Sources*, **243**, 72 (2013).
25. C. L. Campion, W. Li, and B. L. Lucht, *J. Electrochem. Soc.*, **152**, A2327 (2005).
26. B. Vortmann, S. Nowak, C. Engelhard, *Anal. Chem.*, **85**, 3433 (2013).
27. K. Kumai, H. Miyashiro, Y. Kobayashi, K. Takei, R. Ishikawa, *J. Power Sources*, **81–82**, 715 (1999)
28. L. Terborg, S. Weber, S. Passerini, M. Winter, U. Karst, S. Nowak, *J. Power Sources* **245**, 836 (2014).
29. *Application Note M264, Analysis of Electrolyte Solution in Lithium Ion Rechargeable Battery (LIRB) and Evolved Gas from LIRB*, Shimadzu, Kyoto (2011).
30. C. Kanakaki, PhD thesis, Vienna University of Technology, in preparation (2017).
31. V. Kraft, W. Weber, M. Grützke, M. Winter, S. Nowak, *RSC Adv.*, **5**, 80150 (2015).
32. M. Grützke, V. Kraft, B. Hoffmann, S. Klamor, J. Diekmann, A. Kwade, M. Winter, S. Nowak, *J. Power Sources*, **273**, 83 (2015).
33. M. Grützke, W. Weber, M. Winter, S. Nowak, *RSC Adv.*, **6**, 57253 (2016).
34. P. Handel, G. Fauler, K. Kapper, M. Schmuck, C. Stangl, R. Fischer, F. Uhlig, S. Koller, *J. Power Sources* **267**, 255 (2014).
35. J. Self, C.P. Aiken, R. Petibon, J.R. Dahn, *J. Electrochem. Soc.*, **162**, A796 (2015)
36. G. Gachot, S. Grugeon, I. Jimenez-Gordon, G. Gebresilassie Eshetu, S. Boyanov, A. Lecocq, G. Marlair, S. Pilard, S. Laruelle, *Anal. Methods*, **6**, 6120 (2014).
37. L. Bai, J. Smuts, P. Walsh, H. Fan, Z. Hildenbrand, D. Wong, D. Wetz, K.A. Schug, *J. Chromatogr. A*, **1388**, 244 (2015).
38. T. Ohsaki, T. Kishi, T. Kuboki, N. Takami, N. Shimura, Y. Sato, M. Sekino, A. Satoh, *J. Power Sources* **146**, 97 (2005).
39. D.P. Abraham, E.P. Roth, R. Kostecky, K. McCarthy, S. MacLaren, D.H. Dougherty, *J. Power Sources* **161**, 648 (2006).
40. H. Yoshida, T. Fukunaga, T. Hazama, M. Terasaki, M. Mizutani, M. Yamachi, *J. Power Sources* **68**, 311 (1997).
41. W. Weber, R. Wagner, B. Streipert, V. Kraft, M. Winter, S. Nowak, *J. Power Sources* **245**, 836 (2014).
42. V. Kraft, M. Grützke, W. Weber, M. Winter, S. Nowak, *J. Chromatogr. A*, **1354**, 92 (2014).
43. C. Schultz, S. Vedder, M. Weber, S. Nowak, *Spectrosc. Europe*, **28**, 21 (2016).
44. C. Schultz, S. Vedder, M. Weber, S. Nowak, *Anal. Chem.*, **88**, 11160, (2016).
45. C. Schultz V. Kraft, M. Pyschik, S. Weber, F. Schappacher, M. Winter, S. Nowak, *J. Electrochem. Soc.*, **162**, A629 (2015).
46. M. Tochihara, H. Nara, D. Mukoyama, T. Yokoshima, T. Momma, T. Osaka, *J. Electrochem. Soc.*, **162**, A2008 (2015).

ИЗЯСНЯВАНЕ ПРОЦЕСА НА РАЗПАД НА ЕЛЕКТРОЛИТА ОТ ЛИТИЕВО-ЙОННИ БАТЕРИИ ЧРЕЗ ХРОМАТОГРАФСКИ АНАЛИЗИ

Е. Розенберг^{1*}, Н. Канакаки¹, А. Амон², Ир. Гочева², Ат. Трифонова²

¹Технически университет във Виена, Институт по химични технологии и анализи,
Виена, Австрия, Email: erosen@mail.zserv.tuwien.ac.at

²Австрийски технологичен институт, Департамент "Мобилност, електро технологии", Виена, Австрия

Постъпила на 29 ноември 2016 г.; приета на 20 декември 2016 г.

(Резюме)

Електролитът от литиево-йонните батерии се разпада както при нормални експлоатационни условия - например формиране на твърда междинна електролитна фаза, така и при екстремни условия, като висока температура, напрежение, електрически ток. Продуктите на разпад на електролита (обикновено смес от органични карбонати, като етиленкарбонат, етилметил карбонат, диметилкарбонат или диетилкарбонат с различни електропроводими соли като LiPF_6) могат да бъдат летливи или постоянни газове като H_2 , CO , CO_2 , или късоверижни въглеводороди (C1-C3), които са подходящи за определяне чрез газова хроматография GC.

Предвид многообразието на продуктите на разпад, могат да бъдат подбирани газови хроматографи с различни детектори, които да регистрират продуктите чрез пламъчно-йонизационни детектори, детектори по топлопроводност (катарометъри), мас спектрометри. Като допълнение на предложените GC анализи, могат да се приложат директни анализи на електролита, след внимателно разрязване на батерията за *post mortem* анализ.

В присъствието на електропроводимата сол LiPF_6 , както и в присъствието на вода или въздух, се образуват кондензирани или силно полярни продукти, които могат да бъдат по-лесно определени в течна фаза чрез високо ефективна течна хроматография с обърнати фази RP-HPLC, или чрез йонна хроматография IC. Това включва карбонатни олигомери (с различен брой на етоксигрупите, получени след разкъсване на етилен карбонатния пръстен) и органофосфати и монофлуорофосфати, които са продукти на реакциите на разпад и (частична) хидролиза на електропроводимата сол и нейното взаимодействие с органичния разтворител.

Хроматографските техники, особено тези с масспектрометрична детекция са незаменимо средство за охарактеризиране на широкия спектър от разпадни продукти, и за изясняването на процесите, водещи до деградация на електролита. Това формира основата за подобряване на безопасността и ефективността на литиево-йонните батерии.

Ключови думи: литиево-йонни батерии, електролит; разпадни продукти, газова хроматография, течна хроматография

BULGARIAN CHEMICAL COMMUNICATIONS

Instructions about Preparation of Manuscripts

General remarks: Manuscripts are submitted in English by e-mail or by mail (in duplicate). The text must be typed double-spaced, on A4 format paper using Times New Roman font size 12, normal character spacing. The manuscript should not exceed 15 pages (about 3500 words), including photographs, tables, drawings, formulae, etc. Authors are requested to use margins of 3 cm on all sides. For mail submission hard copies, made by a clearly legible duplication process, are requested. Manuscripts should be subdivided into labelled sections, e.g. **Introduction, Experimental, Results and Discussion**, etc.

The title page comprises headline, author's names and affiliations, abstract and key words.

Attention is drawn to the following:

a) **The title** of the manuscript should reflect concisely the purpose and findings of the work. Abbreviations, symbols, chemical formulas, references and footnotes should be avoided. If indispensable, abbreviations and formulas should be given in parentheses immediately after the respective full form.

b) **The author's** first and middle name initials, and family name in full should be given, followed by the address (or addresses) of the contributing laboratory (laboratories). **The affiliation** of the author(s) should be listed in detail (no abbreviations!). The author to whom correspondence and/or inquiries should be sent should be indicated by asterisk (*).

The abstract should be self-explanatory and intelligible without any references to the text and containing not more than 250 words. It should be followed by key words (not more than six).

References should be numbered sequentially in the order, in which they are cited in the text. The numbers in the text should be enclosed in brackets [2], [5, 6], [9–12], etc., set on the text line. References, typed with double spacing, are to be listed in numerical order on a separate sheet. All references are to be given in Latin letters. The names of the authors are given without inversion. Titles of journals must be abbreviated according to Chemical Abstracts and given in italics, the volume is typed in bold, the initial page is given and the year in parentheses. Attention is drawn to the following conventions:

a) The names of all authors of a certain publications should be given. The use of “*et al.*” in

the list of references is not acceptable.

b) Only the initials of the first and middle names should be given.

In the manuscripts, the reference to author(s) of cited works should be made without giving initials, e.g. “Bush and Smith [7] pioneered...”. If the reference carries the names of three or more authors it should be quoted as “Bush *et al.* [7]”, if Bush is the first author, or as “Bush and co-workers [7]”, if Bush is the senior author.

Footnotes should be reduced to a minimum. Each footnote should be typed double-spaced at the bottom of the page, on which its subject is first mentioned.

Tables are numbered with Arabic numerals on the left-hand top. Each table should be referred to in the text. Column headings should be as short as possible but they must define units unambiguously. The units are to be separated from the preceding symbols by a comma or brackets.

Note: The following format should be used when figures, equations, etc. are referred to the text (followed by the respective numbers): Fig., Eqns., Table, Scheme.

Schemes and figures. Each manuscript (hard copy) should contain or be accompanied by the respective illustrative material as well as by the respective figure captions in a separate file (sheet). As far as presentation of units is concerned, SI units are to be used. However, some non-SI units are also acceptable, such as °C, ml, l, etc.

The author(s) name(s), the title of the manuscript, the number of drawings, photographs, diagrams, etc., should be written in black pencil on the back of the illustrative material (hard copies) in accordance with the list enclosed. Avoid using more than 6 (12 for reviews, respectively) figures in the manuscript. Since most of the illustrative materials are to be presented as 8-cm wide pictures, attention should be paid that all axis titles, numerals, legend(s) and texts are legible.

The authors are asked to submit **the final text** (after the manuscript has been accepted for publication) in electronic form either by e-mail or mail on a 3.5” diskette (CD) using a PC Word-processor. The main text, list of references, tables and figure captions should be saved in separate files (as *.rtf or *.doc) with clearly identifiable file names. It is essential that the name and version of

the word-processing program and the format of the text files is clearly indicated. It is recommended that the pictures are presented in *.tif, *.jpg, *.cdr or *.bmp format, the equations are written using "Equation Editor" and chemical reaction schemes are written using ISIS Draw or ChemDraw programme.

The authors are required to submit the final text with a list of three individuals and their e-mail addresses that can be considered by the Editors as potential reviewers. Please, note that the reviewers should be outside the authors' own institution or organization. The Editorial Board of the journal is not obliged to accept these proposals.

EXAMPLES FOR PRESENTATION OF REFERENCES

REFERENCES

1. D. S. Newsome, *Catal. Rev.–Sci. Eng.*, **21**, 275 (1980).
2. C.-H. Lin, C.-Y. Hsu, *J. Chem. Soc. Chem. Commun.*, 1479 (1992).
3. R. G. Parr, W. Yang, *Density Functional Theory of Atoms and Molecules*, Oxford Univ. Press, New York, 1989.
4. V. Ponec, G. C. Bond, *Catalysis by Metals and Alloys* (Stud. Surf. Sci. Catal., vol. 95), Elsevier, Amsterdam, 1995.
5. G. Kadinov, S. Todorova, A. Palazov, in: *New Frontiers in Catalysis* (Proc. 10th Int. Congr. Catal., Budapest, 1992), L. Guzzi, F. Solymosi, P. Tetenyi (eds.), Akademiai Kiado, Budapest, 1993, Part C, p. 2817.
6. G. L. C. Maire, F. Garin, in: *Catalysis. Science and Technology*, J. R. Anderson, M. Boudart (eds), vol. 6, Springer-Verlag, Berlin, 1984, p. 161.
7. D. Pocknell, *GB Patent 2 207 355* (1949).
8. G. Angelov, PhD Thesis, UCTM, Sofia, 2001.
9. JCPDS International Center for Diffraction Data, Power Diffraction File, Swarthmore, PA, 1991.
10. *CA* **127**, 184 762q (1998).
11. P. Hou, H. Wise, *J. Catal.*, in press.
12. M. Sinev, private communication.
13. <http://www.chemweb.com/alchem/articles/1051611477211.html>.

CONTENTS

Preface.....	4
L. Dospatliev, M. Ivanova, Determination of heavy metals in mushroom samples by atomic absorption spectrometry.....	5
V. Y. Zapryanova, K. K. Simitchiev, E. N. Piskova, Determination of Cd, Cr, Cu, Ni, Pb and Zn in compost: evaluation of different approaches for sample preparation and instrumental analysis (MP-AES as an alternative to ICP-OES).....	10
G. Toncheva, K. Nikolova, D. Boyadziev, G. Antova, Z. Jeleu, Mathematical analysis of the trace element content of Bulgarian fruits.....	16
N. S. Yantcheva, I. N. Vasileva, P. N. Denev, P. V. Lutova, S. E. Mitov, Z. A. Iordanova, M. A. Galabova, I. N. Panchev, A. M. Slavov, Valorization of waste of <i>Calendula officinalis</i> - obtaining of ethanol extracts.....	21
D.V. Markova, I.N. Vasileva, N.S. Yancheva, A.M. Slavov, Comparison of physicochemical parameters of pectic polysaccharides from different plant materials.....	26
Y. Stremiski, S. Statkova-Abeghe, D. Georgiev, P. Angelov, I. Ivanov, Synthesis and antibacterial activity of 2-substituted benzothiazoles.....	32
K. Peycheva, L. Makedonski, M. Stancheva, Human exposure to some toxic and essential elements through freshwater fish consumption in Bulgaria.....	37
T.R. Tasheva, V.V. Dimitrov, Synthesis, structure and nonlinear optical properties of tellurium oxide – bismuth oxide – boron oxide glasses	43
E. K. Varbanova, P. A. Angelov, K. K. Simitchiev, L. I. Kaynarova, V. M. Stefanova, Cloud point extraction of lanthanides with 3-ethylamino-but-2-enoic acid phenylamide from water samples prior to ICP-MS determination.....	49
G. A. Antova, M. I. Angelova – Romova, Zh. Y. Petkova, O. T. Teneva, M.P. Marcheva, Lipid composition of mustard seed oils (<i>Sinapis alba</i> L.).....	55
P. N. Penchev, S. H. Tsoneva, S. R. Nachkova, Spectral similarity versus structural similarity: Raman spectra.....	61
S.M. Momchilova, S.P. Taneva, M.D. Zlatanov, G.A. Antova, M.J. Angelova-Romova, E. Blagoeva, Fatty acids, tocopherols and oxidative stability of hazelnuts during storage.....	65
S.M. Bakalova, J. Kaneti, Theoretical insights regarding the electronic spectra and proton transfers in a sensor molecule.....	71
A. V. Terzieva, R. Z. Vrancheva, N. D. Delchev, Antioxidant activity of different extracts of dried and frozen fruits of <i>Schisandra chinensis</i> (Turcz.) Baill	78
D. K. Chakarova-Dimitrova, V. J. Kmetov, Compatibility of measurement results for the active substance Zineb, determined by CIPAC and ICP-OES methods.....	83
M. Panova, V. Kmetov, D. Davcheva, T. Tomova, D. Tomov, Optimizing the determination of mercury in human urine by ICP-MS with a collision cell mode.....	88
M. Katsarova, S. Dimitrova, L. Lukanov, F. Sadakov, P. Denev, E. Plotnikov, I. Kandilarov, I. Kostadinova, Antioxidant activity and nontoxicity of extracts from <i>Valeriana officinalis</i> , <i>Melissa officinalis</i> , <i>Crataegus monogyna</i> , <i>Hypericum perforatum</i> , <i>Serratula coronata</i> and combinations Antistress 1 and Antistress 2	93
I. D. Yordanova, S. Zh. Todorova, H. G. Kolev, Z. P. Cherkezova-Zheleva, Co-Mn mixed oxide catalysts for purification of waste gases from <i>n</i> -hexane.....	99
M. Penkova, S. Nikolova, Application of aziridines for the synthesis of isoquinoline derivatives	105
D.A. Dobрева, V.Z. Panayotova, R.S. Stancheva, M. Stancheva, Simultaneous HPLC determination of fat soluble vitamins, carotenoids and cholesterol in seaweed and mussel tissue.....	112
D.A. Dobрева, A. Merdzhanova, L. Makedonski, Fat soluble nutrients and fatty acids in skin and fillet of farmed rainbow trout.....	118
D. Bojilov, S. Dagnon, I. Ivanov, Constituent composition of <i>Chenopodium botrys</i> essential oil	124
H.N. Panajotova, H.N. Strinska, V. D. Gandova, V.T. Dobрева, B.J. Zhekova, G.T. Dobrev, Purification of lipase from <i>Aspergillus carbonarius</i> NRRL369 by ATPS PEG/potassium phosphate.....	130

<i>H.N. Strinska, D.N. Petrov, H.N. Panajotova, V.T. Dobрева, B.J. Zhekova, G.T. Dobrev,</i> Isolation and purification of lipase from <i>Rhizopus arrhizus</i> by ultrafiltration and fractional precipitation.....	137
<i>H. Karabulut, İ. Pekgözlü, A.S. Başak, A. Mergen,</i> Synthesis and characterization of $\text{Sr}_2\text{Be}_2\text{B}_2\text{O}_7$ by XRD and FTIR.....	144
<i>K. Ivanov, P. Zapryanova, V. Angelova, L. Dospatliev,</i> Application of X-ray and SEM–EDS evaluation of the main digestion methods for determination of macroelements in soil.....	147
<i>N.S. Velitchkova, S.V. Velichkov, M.G. Karadjov, N.N. Daskalova,</i> Optimization of the operating conditions in inductively coupled plasma optical emission spectrometry.....	152
<i>V.I. Kircheva, J.Ts. Zaharieva, I. Manolov, M.M. Milanova,</i> Synthesis and characterization of lanthanoid complexes with 3, 3'- [(4-bromophenyl)methylene]bis (4-hydroxy-2h-1-benzopyrane-2-one).....	160
<i>M. Spassova, S. Angelova, M. Kandinska, A. Vasilev, S. Kitova, J. Dikova,</i> Molecular design of electron-donor materials for fullerene-based organic solar cells.....	166
<i>N.V. Kaneva, A. S. Bojinova, K. I. Papazova, D. Tz. Dimitrov, A. E. Eliyas,</i> Investigation of photocatalytic properties of pure and Ln (La^{3+} , Eu^{3+} , Ce^{3+}) – modified ZnO powders synthesized by thermal method.....	172
<i>T.M. Dodevska, N. D. Dimcheva, E. G. Horozova, Y. L. Lazarova,</i> Electrochemically modified with osmium graphite: catalytic activity and application to the amperometric detection of hydrogen peroxide.....	177
<i>P.E. Marinova, I.D. Nikolova, M.N. Marinov, S.H. Tsoneva, A.N. Dimitrov, N.M. Stoyanov,</i> Ni(II) complexes of 4- and 5- nitro-substituted heteroaryl cinnamoyl derivatives.....	183
<i>M.K. Stoyanova, St.G. Christoskova, D.N. Petrov, V.V. Ivanova,</i> Catalytic oxidation of formaldehyde in aqueous solutions over $\text{NiO}_x/\text{CeO}_2$	188
<i>L. H. Yoanidu, Y. I. Uzunova, I. D. Stefanova,</i> Recent applications of polymer materials in biomedical sciences.....	194
<i>S. Siuleiman, N. Kaneva, A. Bojinova, D. Dimitrov, K. Papazova,</i> ZnO/TiO ₂ coupled semiconductor photocatalysts.....	199
<i>S.K. Georgieva, Zl. . Peteva,</i> Assessment of several priority pollutants in fish from selected lakes in Bulgaria.....	205
<i>M.H. Docheva, M.B. Staykova, A.B. Stoilova, D. Dimanov,</i> Basic chemical components and radical scavenging activity of tobacco extracts obtained by macroporous resin.....	212
<i>Ts. Lazarova, D. Kovacheva, Z. Cherkezova-Zheleva, G. Tyuliev,</i> Studies of the possibilities to obtain nanosized MnFe_2O_4 by solution combustion synthesis.....	217
<i>K.I. Ivanov, E.N. Kolentsova, N.Cao Nguyen, A.B. Peltekov, V.R. Angelova,</i> Synthesis and stability of zinc hydroxide nitrate nanoparticles.....	225
<i>V.M. Genina, G.M. Gecheva, I.G. Velcheva, M.I. Marinov,</i> Assessment of organic pollutants in sediments from Maritsa River basin (Bulgaria).....	231
<i>D.H. Sánchez, D.L. Georgieva, V.J. Kmetov, V.M. Stefanova,</i> Microwave assisted carbon modification of magnetite nanoparticles, used for solid phase extraction of trace elements...	237
<i>E. Rosenberg, C. Kanakaki, A. Amon, I. Gocheva, A. Trifonova,</i> Understanding the degradation processes of the electrolyte of lithium ion batteries by chromatographic analysis.....	242
<i>Instruction to the authors</i>	254

СЪДЪРЖАНИЕ

Предговор.....	4
Л. Доспатлиев, М. Иванова, Определяне количеството на тежки метали в проби от гъби чрез атомна абсорбционна спектроскопия.....	9
В. Й. Запрянова, К. К. Симитчиев, Е. Н. Пискова, Определяне на Cd, Cr, Cu, Ni, Pb и Zn в компост: оценка на различни подходи за предварителна подготовка на пробите и инструментален анализ (MP-AES като алтернатива на ICP-OES).....	15
Г. Тончева, К. Николова, Д. Бояджиев, Г. Антова, З. Желев, Математически анализ на съдържанието на микроелементи в български плодове.....	20
Н.С. Янчева, И.Н. Василева, П.Н. Денев, П.В. Лютова, С.Е. Митов, З.А. Йорданова, М.А. Гълъбова, И.Н. Панчев, А.М. Славов, Оползотворяване на отпадъци от <i>Calendula officinalis</i> – получаване на етанолни екстракти.....	25
Д. В. Маркова, И. Н. Василева, Н. С. Янчева, А. М. Славов, Сравнително изследване на физико-химични параметри на пектинови полизахариди от различни растителни източници.....	31
Й. Стремски, С. Статкова-Абебхе, Д. Георгиев, П. Ангелов, И. Иванов, Синтез и антибактериална активност на 2-заместени бензотиазоли.....	36
К. Пейчева, Л. Македонски, М. Станчева, Оценка на приема на някои токсични и есенциални елементи чрез консумация на сладководни риби в България.....	42
Т.Р. Ташева, В.В. Димитров, Синтез, структура и нелинейни оптични свойства на телур-бисмут-бор оксидни стъкла.....	48
Е.К. Върбанова, П.А. Ангелов, К.К. Симитчиев, Л.И. Кайнарова, В.М. Стефанова, Екстракция при температура на коагулация на лантаниди от водни проби с 3-етиламино-бут-2-енова киселина фениламид и ICP-MS анализ.....	54
Г.А. Антова, М.Й. Ангелова-Ромова, Ж.Ю. Петкова, О.Т. Тенева, М.П. Марчева, Липиден състав на семена от синап (<i>Sinapis alba</i> L.).....	60
П.Н. Пенчев, С.Х. Цонева, С.Р. Начкова, Връзка между спектралното подобие и структурното подобие за Раман спектри.....	64
С.М. Момчилова, С.П. Танева, М.Д. Златанов, Г.А. Антова, М.Й. Ангелова-Ромова, Е. Благоева, Масни киселини, токофероли и окислителна стабилност на лешници по време на съхранението им.....	70
Сн. Бакалова, Х. Канети, Теоретични виждания за електронните спектри и преноси на протон в молекулата на един сензор.....	77
А.В. Терзиева, Р.З. Вранчева, Н.Д. Делчев, Антиоксидантна активност на различни екстракти от изсушени и замразени плодове от <i>Schisandra chinensis</i> (Turcz.) Baill.....	82
Д.К. Чакърова-Димитрова, В.Й. Кметов, Съвместимост на резултатите от анализ на активната субстанция Цинеб, определена чрез CIPAC и ICP-OES методи.....	87
М. Панова, В. Кметов, Д. Давчева, Т. Томова, Д. Томов, Оптимизиране определянето на живак в човешка урина чрез ICP-MS в режим с колизионна клетка.....	92
М. Кацарова, С. Димитрова, Л. Луканов, Ф. Садъков, П. Денев, Е. Плотников, И. Кандиларов, И. Костадинова, Антиоксидантна активност и нетоксичност на екстракти от <i>Valeriana officinalis</i> , <i>Melissa officinalis</i> , <i>Crataegus monogyna</i> , <i>Hypericum perforatum</i> , <i>Serratula coronata</i> и комбинации Антистрес 1 и Антистрес 2.....	98
И.Д. Йорданова, С.Ж. Тодорова, Х.Г. Колев, З.П. Черкезова-Желева, Со-Mn смесени оксидни катализатори за пречистване на отпадъчни газове от <i>n</i> -хексан.....	104
М. Пенкова, С. Николова, Приложение на азиридины за синтез на изохинолинови производни.....	111
Д.А. Добрева, В.З. Панайотова, Р.С. Станчева, М. Станчева, Съвместно ВЕТХ определяне на мастноразтворими витамини, каротеноиди и холестерол в тъкан на водорасли и миди.....	117
Д.А. Добрева, А. Мерджанова, Л. Македонски, Масно-разтворими нутриенти и масни киселини в кожа и филе на култивирана дъгова пъстърва.....	123
Д. Божилков, С. Данъон, И. Иванов, Състав на етеричното масло от <i>Chenopodium botrys</i>	129

<i>Х.Н. Панайотова, Х.Н. Стринска, В.Д. Гандова, В.Ц. Добрева, Б.Й. Жекова, Г.Т. Добрев,</i> Пречистване на липаза от <i>Aspergillus carbonarius</i> NRRL369 с двуфазни водни системи полиетилен гликол/калиев фосфат.....	136
<i>Х.Н. Стринска, Д.Н. Петров, Х.Н. Панайотова, В.Ц. Добрева, Б.Й. Жекова, Г.Т. Добрев,</i> Изолитране и пречистване на липаза от <i>Rhizopus arrhizus</i> с ултрафилтрация и фракционно утаяване.....	143
<i>Х. Карабулут, И. Пекгьозлу, А.С. Башак, А. Мерген,</i> Синтез и охарактеризиране на $Sr_2Ve_2V_2O_7$ посредством XRD и FTIR.....	146
<i>К.И. Иванов, П.А. Запрянова, В.Р. Ангелова, Л.К. Доспатлиев,</i> Приложение на рентгеноструктурния анализ и електронната микроскопия при оценката на основните методи за подготовка на почвени проби за анализ на макроелементи.....	151
<i>Н.С. Величкова, С.В. Величков, М.Г. Караджов, Н.Н. Даскалова,</i> Оптимизиране на работните условия при оптичната емисионна спектрометрия с индуктивно свързана плазма.....	159
<i>В.И. Кирчева, Й.Цв. Захариева, И. Манолов, М.М. Миланова,</i> Синтез и охарактеризиране на лантаноидни комплекси с 3,3'- (4-бромофенилметиле)бис(4-хидрокси-2Н-1- бензопиран-2-он).....	165
<i>М. Спасова, С. Ангелова, М. Къндинска, А. Василев, С. Китова, Ю. Дикова,</i> Молекулен дизайн на електрон-донорни материали за фулерен-базирани слънчеви клетки.....	171
<i>Н.В. Кънева, А.С. Божинава, К.И. Папазова, Д.Ц. Димитров, А.Е. Елиас,</i> Изследване фотокаталитичните свойства на чисти и Ln (La^{3+} , Eu^{3+} , Ce^{3+}) – модифицирани ZnO прахове, синтезирани чрез термален метод.....	176
<i>Т.М. Додевска, Н.Д. Димчева, Е.Г. Хорозова, Я.Л. Лазарова,</i> Електрохимично модифициран с осмий графит: каталитична активност и приложение за амперометрична детекция на водороден пероксид.....	182
<i>П.Е. Маринова, И.Д. Николова, М.Н. Маринов, С.Х. Цонева, А.Н. Димитров, Н.М. Стоянов,</i> Комплекси на Ni(II) с 4- и 5- нитро-заместени хетероарил цинамоилни производни.....	187
<i>М. Стоянова, Ст. Г. Христоскова, Д. Н. Петров, В. В. Иванова,</i> Каталитично окисление на формалдехид във водни разтвори върху NiO_x/CeO_2	193
<i>Л. Х. Йоаниду, Й. И. Узунова, И. Д. Стефанова,</i> Съвременни приложения на полимерните материали в биомедицинските науки.....	198
<i>Ш. Сюлейман, Н. Кънева, А. Божинава, Д. Димитров, К. Папазова,</i> ZnO/TiO ₂ композитни фотокаталитизатори.....	204
<i>С.К. Георгиева, Зл.В. Петева,</i> Оценка на някои приоритетни замърсители в риби от избрани езера в България.....	211
<i>М.Х. Дочева, М.Б. Стайкова, А.Б. Стоилова, Д. Диманов,</i> Основни химични компоненти и радикал-улавяща активност на тютюневи екстракти получени чрез адсорбционна смола.....	216
<i>Цв. Лазарова, Д. Ковачева, З. Черкезова-Желева, Г. Тюлиев,</i> Изследване на възможностите за получаване на наноразмерен $MnFe_2O_4$ при синтез по метода на изгаряне от разтвор.....	224
<i>К.И. Иванов, Е.Н. Коленцова, Н. Као Нгуен, А.Б. Пелтеков, В.Р. Ангелова,</i> Синтез и стабилност на нанокристали от цинков хидроксинитрат.....	230
<i>В.М. Генина, Г.М. Гечева, Ил.Г. Велчева, М.Ив. Маринов,</i> Оценка на органични замърсители в седименти от басейна на река Марица (България).....	236
<i>Д. Санчес, Д. Георгиева, В. Кметов, В. Стефанова,</i> Нова микровълново подпомогната процедура за получаване на въглерод-модифицирани магнетитни наночастици с цел приложението им за твърдофазна екстракция на елементи.....	241
<i>Е. Розенберг, Н. Канакаки, А. Амон, Ир. Гочева, Ат. Трифонова,</i> Изясняване процеса на разпад на електролита от литиево-йонни батерии чрез хроматографски анализи.....	253
<i>Инструкция за авторите.....</i>	254